POST ELASTIC BEHAVIOUR

OF

REINFORCED CONCRETE BEAM-COLUMN JOINTS

A thesis submitted in partial fulfilment of the requirements for the degree of Doctor of Philosophy in Civil Engineering at the University of Canterbury, Christchurch, New Zealand

by

Charles Walter Beckingsale

August 1980

ABSTRACT

Three cyclic loading tests on interior reinforced concrete beam-column joints from plane frame and one from a space frame are described. Mechanisms of joint shear resistance are postulated and recommendations are made for the aseismic design of beam-column joints. The effect of joint behaviour on overall structural response to earthquake loading is considered.

An analysis of reinforced concrete column sections subject to biaxial bending and axial load is presented. The effect of biaxial bending on the uniaxial bending strength of columns is considered.

ACKNOWLEDGEMENTS

The research described in this thesis was carried out in the Department of Civil Engineering of the University of Canterbury. Professor H.J. Hopkins was Head of Department until 1977, and Professor R. Park from 1978 onwards.

The project was carried out under the supervision of Professors R. Park and T. Paulay, and their continual guidance and encouragement is gratefully acknowledged. Other members of the academic staff and other postgraduate students in the Department have also helped with constructive criticism and discussion of the project from time to time.

The project involved a large amount of experimental research, and expert assistance with this phase of the work was provided by the technical staff of the Department, under the supervision of Technical Officers, K. Marrion, N.W. Prebble, and the late Mr. H.T. Watson. Technicians closely associated with the project were J.M. Adams, G.E. Hill, A. Robinson and G.C. Clarke, who carried out the construction and assisted with the testing of the test specimens in the laboratory. Their work was always carried out with great care and efficiency, and their contribution to the success of the test program is humbly acknowledged.

Test data reduction and analytical work was carried out at the Computer Centre of the University of Canterbury, and the assistance of the staff with programming and with data preparation is acknowledged.

Great work has been done by Mrs. A. Watt in typing my manuscript, mostly at long distance, and I acknowledge her great patience and efficiency in this task.

Financial assistance for the author was provided initially by a University Grants Committee Post-Graduate Scholarship, and later by a Teaching Fellowship from the University of Canterbury. The New Zealand Ministry of Works and Development contributed a grant towards the cost of materials and a technician's salary for the test program.

I would like to thank my own, and my wife's, parents who helped us both financially and in many other ways throughout the period of my postgraduate study. Their patient support is gratefully acknowledged.

Finally I would like to express my heartfelt thanks to my wife, Kathie, who traced most of the diagrams for my thesis, and who has unflinchingly supported and encouraged me throughout my doctoral study.

TABLE OF CONTENTS

NOTATION

A_b = gross area of individual reinforcing bar

A_c = area of core of column or joint section, measured to outside of confining reinforcement

A_{eff} = effective area of individual reinforcing bar

A_g = gross area of column section

A_{sb} = area of flexural reinforcement in bottom of beam

A_{sc} = lesser area of column flexural reinforcement in tension or compression face at joint

A'_{sc} = greater area of column flexural reinforcement in tension or compression face at joint

A_{sh} = total area of horizontal reinforcement crossing diagonal plane from corner to corner of joint between top and bottom layers of beam flexural reinforcement

A_{si} = area of steel at the ith reinforcement location

A_{st} = area of flexural reinforcement in top of beam

A_{sv} = area of joint vertical reinforcement

A_v = area of shear reinforcement within spacing s

b' = effective width of joint to outside of ties

b_c = breadth of column section

b_j = effective breadth of joint

b_w = breadth of beam section

C_{bi} = compressive force in concrete of the ith beam adjacent to the joint

C_{colt}, C_{colb} = compressive force in column concrete immediately above, below the joint

C_i = compressive force in reinforcement at the ith location

d_b = nominal diameter of reinforcing bar

d = distance from extreme compression fibre to centroid of tension reinforcement in beam

d'_b = distance from extreme compression fibre to centroid of compression reinforcement in beam

D = length of joint diagonal

D_c = diagonal compressive force in joint concrete due to direct strut mechanism

D_s = diagonal compressive force in joint concrete due to joint truss mechanism

e_x, e_y = eccentricity of loading about X,Y axis

E_c = Modulus of Elasticity for concrete

E_s = Modulus of Elasticity for steel

f = relative lever arm at which reinforcement is placed in column section (Fig. A.1)

f_c = compressive stress in concrete

f'_c = compressive cylinder strength of concrete

f_h = stress developed in reinforcing bar by standard hook

f_s = steel stress

f_{si} = stress in steel at ith reinforcement location

f_y = yield strength of steel

f_{yb} = yield strength of beam reinforcement

f_{yh} = yield strength of joint horizontal reinforcement

f_{yv} = yield strength of joint vertical reinforcement

f_u = ultimate tensile strength of steel

F_{ACI} = concrete compressive force in ACI rectangular stress block

F_{cb} = derived concrete compressive force in beam at joint face

F_i = concrete compressive force in ith assumed stress block

F_{ib} = force in ith layer of column reinforcing at bottom of joint

F_{it} = force in ith layer of column reinforcing at top of joint

g = relative lever arm at which reinforcement is placed in column section (Fig. A.1)

h_b = overall depth of beam

h_c = overall depth of column

k = instantaneous elastic stiffness

k_e = initial 'elastic' stiffness of idealised load-displacement curve

k_n = stiffness for negative loading

k_p = stiffness for positive loading

k_x, k_y = relative depth of neutral axis of column section in X,Y directions

k_l = 'strain-hardening' stiffness of idealised load-displacement curve

K = tangent of specific angle of loading

l_B = span of beam from centre-to-centre of columns

l_c = storey height above joint

l'_c = storey height below joint

l_d = development length of reinforcing bar

l_h = length of leg of confining reinforcement

$l_{\phi max}$ = distance from column face at which maximum beam curvature observed

m_x, m_y = specific moment strength of column section about X,Y axis

m_θ = resultant specific moment strength of column section

M_{bi} = moment in ith beam adjacent to joint core

M_{colb}, M_{colt} = moment in column section immediately below, above joint core

M_{cx}, M_{cy} = moments about X,Y axes due to concrete actions only

M_Q = moment calculated using quadratic stress-strain function for concrete

$\bar{M}_Q$ = mean of calculations for M_Q

M_R = moment calculated using rectangular stress-block for concrete

$\bar{M}_R$ = mean of calculations for M_R

M_{sx}, M_{sy} = moments about X,Y axes due to reinforcement actions only

M_{ux}, M_{uy} = ultimate moment about X,Y axes

M_{ux0} = ultimate moment about X axis when moment about Y axis is zero

N = column axial load

N_b = column axial load to cause balanced failure

N_c = number of discrete concrete elements into which column section is divided

N_s = number of discrete elements into which reinforcement of column section is divided

N_u = ultimate axial load on column section

N_o = ultimate concentric column axial load capacity

P_{Bi} = load applied to end of ith beam

P_c = axial load in column due to concrete actions only

P_s = axial load in column due to reinforcement actions only

P_{yn}, P_{yp} = theoretical beam end load at which yield strain is just attained in all tension reinforcement at column face for negative,positive loading

P_{un}, P_{up} = beam end load at which theoretical ultimate flexural strength is attained at column face for negative,positive loading

s = spacing between sets of ties

s_h = spacing between sets of confining hoops

T_i = tension force in reinforcement at the ith location

T_1 = fundamental period of vibration of structure

v_{jh} = average nominal shear stress on joint core

V_{bi} = shear force in ith beam at column face

V_c = net column shear

V'_c = gross column shear observed in test

V_{ch} = horizontal shear resisted by joint concrete direct strut mechanism

V_{colt}, V_{colb} = column shear above,below joint

V_{cv} = vertical shear resisted by joint concrete mechanisms

V_{jh} = horizontal shear applied to joint core

V_{jv} = vertical shear applied to joint core

V_{sh} = horizontal shear resisted by joint truss mechanism

V_{shl} = horizontal shear resisted by joint truss mechanism formed with long legs of joint horizontal reinforcement

V_{sh2} = horizontal shear resisted by joint truss mechanism formed with short legs of joint horizontal reinforcement

V_{sv} = vertical shear resisted by joint vertical reinforcement

V_u = column shear associated with beam end loads P_u

V_y = column shear associated with beam end loads P_y

$\bar{x}_b, \bar{x}_t$ = depth of centroid of concrete compression force from compressed edge of column section immediately below,above joint core

x_i, y_i = coordinates of ith discrete element of column section

X_i, Y_i = relative coordinates of ith discrete element of column section

Z = slope of falling branch of concrete stress strain curve (Equation 8-6)

α = overstrength factor applied to beam reinforcement nominal yield strength

α = index for determination of instantaneous elastic stiffness (Equation 6-9)

α = angle in plan between centreline of tie and centreline of beam

α_i = proportion of concrete cylinder strength carried by ith discrete concrete element of column section

β = joint type factor

β = index for determination of instantaneous elastic stiffness (Equation 6-10)

β_c = inclination of direct concrete strut to horizontal

β_J = inclination of joint diagonal to horizontal

β_T = inclination of applied joint shear to horizontal

β_1 = proportion of neutral axis depth over which uniform compressive stress is assumed

γ = shear strain

γ = joint confinement factor

γ_1, γ_2 = components of joint shear strain

Δ_{Bi} = end displacement of ith beam

Δ_C = interstorey drift of column

$\Delta F_b, \Delta F_t$ = force transferred from beam bars to joint core by bond at bottom,top of joint

ΔF_i = force transferred to joint core by bond from column bars adjacent to ith face of joint

Δ_y = experimental yield displacement of beam ends

Δ_γ = beam end displacement due to shear distortion of joint core

$\Delta_{\gamma Bl}$ = shear displacement of beam in gauge length between column face and half of beam effective depth away from face

$\Delta_{\gamma B2}$ = shear displacement of beam in gauge length between half and one times beam effective depth away from column face

$\Delta_{\theta B1}$ = beam end displacement due to rotation of beam in gauge length between column face and half of beam effective depth away from column face

$\Delta_{\theta B2}$ = beam end displacement due to rotation of beam in gauge length between half and one times beam effective depth away from column face

Δ_1, Δ_2 = displacements along joint diagonals

ε_c = concrete strain

ε_{cmax} = maximum concrete strain

ε_{sh} = strain at which strain-hardening of steel commences

ε_y = strain at first yield of steel

ε_o = concrete compressive strain at which maximum stress is carried

ε_{50u} = strain at which stress has fallen to half of maximum value for unconfined concrete

ε_{50h} = additional concrete strain at half of maximum stress due to presence of confining reinforcement

θ = specific angle of loading on column

θ_{b1} = rotation of beam in gauge length between column face and half of beam effective depth away from column face

θ_{b2} = rotation of beam in gauge length between one half and one times beam effective depth away from column face

θ_{by} = rotation of beam in gauge length between column face and half of beam effective depth away from column face corresponding to theoretical beam yield load

ϕ = angle between neutral axis and Y-axis of column section under biaxial bending

ϕ_j = strength reduction factor for joint design

ϕ_{max} = maximum observed beam curvature

ϕ_y = beam curvature corresponding to theoretical beam yield load

ϕ_1 = beam curvature measured at 76 mm away from column face

ρ_b = reinforcement content to cause balanced failure of beam section

ρ_B = bottom reinforcement content of beam

ρ_s = volumetric confining reinforcement content

ρ_t = reinforcement content of column

ρ_T = top reinforcement content of beam

Σ_μ = cummulative displacement ductility factor

$\Sigma\varepsilon_{pl}$ = cummulative plastic strain

μ = beam end displacement ductility factor

ω = dynamic magnification factor

ω_p = dynamic magnification factor for plane frames

ω_s = dynamic magnification factor for space frames

REFERENCES

1. NZS4203 : 1976, "Code of Practice for General Structural Design and Design Loadings for Buildings", Standards Association of New Zealand, Wellington, 1976, 80p.

2. SEAOC, "Recommended Lateral Force Requirements and Commentary", Seismology Committee, Structural Engineers' Association of California, San Francisco, 1973, 146p.

3. Park, R. and Paulay, T., "Reinforced Concrete Structures", John Wiley and Sons, New York, 1975, 769p.

4. ACI Committee 318, "Building Code Requirements for Reinforced Concrete (ACI 318-77)", American Concrete Institute, Detroit, 1977, 102p.

5. DZ3101 (Draft New Zealand Standard) "Code of Practice for the Design of Concrete Structures", Standards Association of New Zealand, Wellington, 1978.

6. Jury, R.D., "Seismic Load Demands on Columns of Reinforced Concrete Multi-storey Frames", Research Report 78-12, University of Canterbury, Department of Civil Engineering, February 1978, 109p.

7. ACI-ASCE Committee 352, "Recommendations for Design of Beam-Column Joints in Monolithic Reinforced Concrete Structures", Journal of the American Concrete Institute, Proceedings V.73, No. 7, July 1976, pp375-393.

8. Paulay, T., Park, R. and Priestley, M.J.N., "Reinforced Concrete Beam-Column Joints Under Seismic Actions", Journal of the American Concrete Institute, Proceedings V.75, No. 11, Nov. 1978, pp.585-593.

9. Ogura, K., "Outline of Damage to Reinforced Concrete Structures", Proceedings of the U.S.-Japan Seminar on Earthquake Engineering With Emphasis on the Safety of School Buildings, September 1970, pp.38-48.

10. Hanson, N.W. and Conner, H.W., "Seismic Resistance of Reinforced Concrete Beam-Column Joints", Proceedings of the Structural Division, American Society of Civil Engineers, Vol. 93, No. ST5, October 1967, pp.533-560.

11. Hanson, N.W., "Seismic Resistance of Concrete Frames with Grade 60 Reinforcement", Proceedings of the Structural Division, American Society of Civil Engineers, Vol. 97, No. ST6, June 1971, pp.1685-1700.

12. Hanson, N.W. and Conner, H.W., "Tests of Reinforced Concrete Beam-Column Joints Under Simulated Seismic Loading", Portland Cement Association Research and Development Bulletin, RD012.01D, 1972.

13. Higashi, Y. and Ohwada, Y., "Failing Behaviour of Reinforced Concrete Beam-Column Joints Under Cyclic Loading", Memoirs of the Faculty of Technology, No. 19, Tokyo Metropolitan University, 1969, pp.91-101.

14. Umemura, H., Aoyama, H. and Noguchi, H., "Experimental Studies on Reinforced Concrete and Composite Steel and Reinforced Concrete Members", Vol. 2, Faculty of Engineering, Department of Architecture, University of Tokyo, December 1977, pp.140-225.

15. Park, R. and Paulay, T., "Behaviour of Reinforced Concrete External Beam-Column Joints under Cyclic Loading", Proceedings, Fifth World Conference on Earthquake Engineering, Paper 88, Vol. 1, Session 2D, Rome, June 1973, pp.772-781.

16. Patton, R.N., "Behaviour Under Seismic Loading of Reinforced Concrete Beam-Column Joints With Anchorage Blocks", Master of Engineering Report, University of Canterbury, February 1972, 103p.

17. Blakeley, R.W.G., Megget, L.M. and Priestley, M.J.N., "Seismic Performance of Two Full Size Reinforced Concrete Beam-Column Joint Units", Bulletin of the New Zealand National Society for Earthquake Engineering, Vol. 8, No. 1, March 1975, pp.38-69.

18. Fenwick, R.C. and Irvine, H.M., "Reinforced Concrete Beam-Column Joints for Seismic Loading", Bulletin of the New Zealand National Society for Earthquake Engineering, Vol. 10, No. 4, December 1977, pp.174-185.

19. Thompson, K.J. and Park, R., "Ductility of Concrete Frames Under Seismic Loading", Research Report No. 75-14, Department of Civil Engineering, University of Canterbury, 1975, 442p.

20. Yeoh, S.K., "Prestressed Concrete Beam-Column Joints", Research Report No. 78-2, Department of Civil Engineering, University of Canterbury, 1978, 71p.

21. Uzumeri, S.M. and Seckin, M., "Behaviour of Reinforced Concrete Beam-Column Joints Subjected to Slow Load Reversals", Publication 74-05, University of Toronto, Department of Civil Engineering, March 1974, 85p.

22. Seckin, M. and Uzumeri, S.M., "Examination of Design Criteria for Beam-Column Joints", European Conference on Earthquake Engineering, Dubrovnik, September 1978.

23. Lee, D.L.N., "Original and Repaired Reinforced Concrete Beam-Column Subassemblages Subjected to Earthquake Type Loading", Ph.D. Thesis, University of Michigan, 1976, 206p.

24. Meinheit, D.F. and Jirsa, J.O., "The Shear Strength of Reinforced Concrete Beam-Column Joints", CESRL Report No. 77-1, University of Texas at Austin, Department of Civil Engineering, Structures Research Laboratory, January 1977, 271p.

25. Fenwick, R.C. and Paulay, T., "Mechanisms of Shear Resistance of Concrete Beams", Journal of the Structural Division, American Society of Civil Engineers, Vol. 94, No. ST10, October 1968, pp.2325-2350.

26. Untrauer, R.E. and Henry, R.L., "Influence of Normal Pressure on Bond Strength", Journal of the American Concrete Institute, Vol. 62, No. 5, May 1965, pp.577-586.

27. Birss, G.R., "The Elastic Behaviour of Earthquake Resistant Reinforced Concrete Interior Beam-Column Joints", Research Report 78-13, Department of Civil Engineering, University of Canterbury, February 1978, 96p.

28. Bull, I.N., "The Shear Strength of Relocated Plastic Hinges", Research Report 78-11, Department of Civil Engineering, University of Canterbury, February 1978,

29. Bresler, B. and Bertero, V.V., "Behaviour of Reinforced Concrete Under Repeated Load", Journal of the Structural Division, American Society of Civil Engineers, Vol. 94, No. ST6, June 1968, pp.1567-1589.

30. Ismail, M.A.F. and Jirsa, J.O., "Behaviour of Anchored Bars Under Low Cycle Overloads Producing Inelastic Strains", Journal of the American Concrete Institute, Vol. 69, No. 7, July 1972, pp.433-438.

31. NZS1900, Chapter 8, "Basic Design Loads", New Zealand Standard Model Building Bylaw, Standards Association of New Zealand, Wellington, 1965.

32. Erasmus, L.A. and Pussegoda, L.N., "Strain Age Embrittlement of Reinforcing Steels", New Zealand Engineering, Vol. 32, No. 8, August 1977, pp.178-183.

33. Spurr, D.D., "The Post-Elastic Response of Frame - Shear Wall Assemblies Subjected to Simulated Seismic Loading", Ph.D. Thesis in preparation, Department of Civil Engineering, University of Canterbury, 1979.

34. Renton, G.W., "The Behaviour of Reinforced Concrete Beam-Column Joints Under Cyclic Loading", Master of Engineering Thesis, Department of Civil Engineering, University of Canterbury, 1972, 181p.

35. Bertero, V.V., "Experimental Studies Concerning Reinforced, Prestressed, and Partially Prestressed Concrete Structures and Their Elements", Introductory Report for Theme IV, Symposium on Resistance and Ultimate Deformability of Structures Acted on by Well Defined Repeated Loads, International Association for Bridge and Structural Engineering, Lisbon, 1973, pp.67-99.

36. Paulay, T., "A Consideration of P-Delta Effects in Ductile Reinforced Concrete Frames", Bulletin of the New Zealand National Society for Earthquake Engineering, Vol. 11, No. 3, September 1978, pp.151-160.

37. Clough, R.W., "Effects of Stiffness Degradation on Earthquake Ductility Requirements", Report No. 66-16, Structural Engineering Laboratory, University of California at Berkeley, October 1966, 67p.

38. Chopra, A.K. amd Kan, C., "Effects of Stiffness Degradation on Ductility Requirements for Multistorey Buildings", Earthquake Engineering and Structural Dynamics, Vol. 2, No. 1, July-September 1973, pp.35-45.

39. Imbeault, F.A., and Nielsen, N.N., "Effect of Degrading Stiffness on the Response of Multistorey Frames Subjected to Earthquakes", Proceedings of the Fifth World Conference on Earthquake Engineering, Rome 1973.

40. Anderson, J.C. and Townsend, W.H., "Models for Reinforced Concrete Frames with Degrading Stiffness", Journal of the Structural Division, American Society of Civil Engineers, Vol. 103, No. ST12, December 1977, pp.2361-2376.

41. Park, R. and Yeoh Sik Keong, "Tests on Structural Concrete Beam-Column Joints with Intermediate Column Bars",Bulletin of the New Zealand National Society for Earthquake Engineering, Vol. 12, No. 3, September 1979, pp.189-203.

42. Anderson, P. and Lee, H.N., "A Modified Plastic Theory of Reinforced Concrete", Bulletin No. 33, University of Minnesota Vol. LIV, No. 19, April 1951.

43. Bresler, B., "Design Criteria for Reinforced Concrete Columns Under Axial Load and Biaxial Bending", Journal of the American Concrete Institute, Vol. 57, No. 5, November 1960, pp.481-490.

44. Ramamurthy, L.N., "Investigation of the Ultimate Strengths of Square and Rectangular Columns under Biaxially Eccentric Loads", Paper No. 12, Symposium on Reinforced Concrete Columns, American Concrete Institute Special Publication SP-13, 1966, pp.263-298.

45. Hsu, C-T., "Behaviour of Structural Concrete Subjected to Biaxial Flexure and Axial Compression", Structural Concrete Series No. 74-2, Ph.D. Thesis, McGill University, Montreal, August 1974, 479p.

46. Paulay, T., "Columns - Evaluation of Actions", Bulletin of the New Zealand National Society for Earthquake Engineering, Vol.10, No. 2, June 1977, pp.85-94.

47. ACI Committee 340, "Ultimate Strength Design Handbook", Vol. 2, ACI Special Publication No. 17A, American Concrete Institute, Detroit, 1970, 226p.

48. Parme, A.L., Nieves, J.M. and Gouwens, A., "Capacity of Reinforced Rectangular Columns Subject to Biaxial Bending", Journal of the American Concrete Institute, Vol. 63, No. 9, September 1966, pp.911-923.

49. Meek, J.L., "Ultimate Strength of Columns with Biaxially Eccentric Loads", Journal of the American Concrete Institute, Vol. 60, No. 8, August 1963, pp.1053-1064.

50. Weber, D.C., "Ultimate Strength Design Charts for Columns with Biaxial Bending", Journal of the American Concrete Institute, Vol. 63, No. 11, November 1966, pp.1205-1230.

51. Row, D.G., "The Effects of Skew Seismic Response on Reinforced Concrete Frames", Master of Engineering Report, University of Canterbury, Department of Civil Engineering, February 1973, 101p.

52. Moran, F., "Design of Reinforced Concrete Sections Under Normal Loads and Stresses in the Ultimate Limit State", Bulletin d'Information No. 83, Comité Européen du Béton, Paris, April 1972, 134p.

53. Mattock, A.H. and Kriz, L.B., "Ultimate Strength of Nonrectangular Structural Concrete Members", Journal of the American Concrete Institute, Vol. 57, No. 7, January 1961, pp.737-766.

54. Mattock, A.H., Kriz, L.B. and Hognestad, E., "Rectangular Concrete Stress Distribution in Ultimate Strength Design", Journal of the American Concrete Institute, Vol. 57, No. 8, February 1961, pp.875-926.

55. CEB-FIP., "International Recommendations for the Design and Construction of Concrete Structures", Comité Européen du Béton - Fédération Internationale de la Précontrainte, Paris, 1970 (English translation from Cement and Concrete Association, London, 88p.)

56. Hognestad, E., "A Study of Combined Bending and Axial Load in Reinforced Concrete Members", University of Illinois Engineering Experimental Station Bulletin No. 399, 1951, 128p.

57. Kent, D.C. and Park, R., "Flexural Members with Confined Concrete", Journal of the Structural Division, American Society of Civil Engineers, Vol. 97, No. ST7, July 1971, pp.1969-1990.

58. Iyengar, K.T.R.J., Desai, P. and Reddy, K.N., "Stress-Strain Characteristics of Concrete Confined in Steel Binders", Magazine of Concrete Research Vol. 22, No. 72, September 1970, pp.173-184.

59. Sargin, M., Ghosh, S.K. and Handa, V.K., "Effects of Lateral Reinforcement upon the Strength and Deformation Properties of Concrete", Magazine of Concrete Research, Vol. 23, No. 75-76, June-September 1971, pp.99-110.

60. Kriz, L.B. and Lee, S.L., "Ultimate Strength of Over-Reinforced Beams", Journal of the Engineering Mechanics Division, American Society of Civil Engineers, Vol. 86, No. EM3, June 1960, pp.85-105.

61. Hildebrand, F.G., "Introduction to Numerical Analysis", 2nd Edition, McGraw-Hill, New York, 1974, 672p.

CHAPTER 1

INTRODUCTION

1.1 The Joint Problem

Designers of multistoreyed buildings in countries prone to earthquake attack have long recognised the need to provide substantial lateral resistance to seismic ground motions by means of a rational structural form. In New Zealand reinforced concrete is the most commonly used material for structures of this type, while the choice of structural form lies between moment-resisting frames, shear wall structures, or some combination of these two types. The commonly accepted philosophy of aseismic design recognises that elastic response will be exceeded under moderately severe earthquake attack in structures designed to the base shear coefficients specified by building codes[1,2]. A number of structures are then required to possess sufficient ductility, that is ability to deform plastically without losing significant strength, to dissipate earthquake energy in a controlled and predictable fashion. In reinforced concrete frames this ductility is usually achieved by inelastic rotation of plastic hinges located in the beams, normally adjacent to the column faces as shown in Fig. 1.1. Both the philosophy and the means of achieving ductility in beam plastic hinges are well understood[3], and designers and codes[4,5] take care to achieve this by, for example, limiting the ratio of top to bottom reinforcement in the beams, and by providing generous stirruping in the critical regions to carry the shear and to confine the flexural bars.

Having provided in the beam hinges the capacity to undergo the necessary plastic deformation in order to achieve efficient energy dissipation, the designer must further ensure the integrity of the structure by eliminating the possibility of significant inelastic behaviour at other less desirable locations. The philosophy of capacity design has been developed to assist in accomplishing this aim. This approach utilizes the maximum possible flexural strengths (or capacities) of the beam sections, which are calculated and used as input in the design for beam shear, column, and joint reinforcement.

The distribution of the beam capacity moments to the column above and below a joint is uncertain because of the influence of higher modes of vibration on the column bending moment pattern. However results of computer-based inelastic dynamic analyses of frames under earthquake

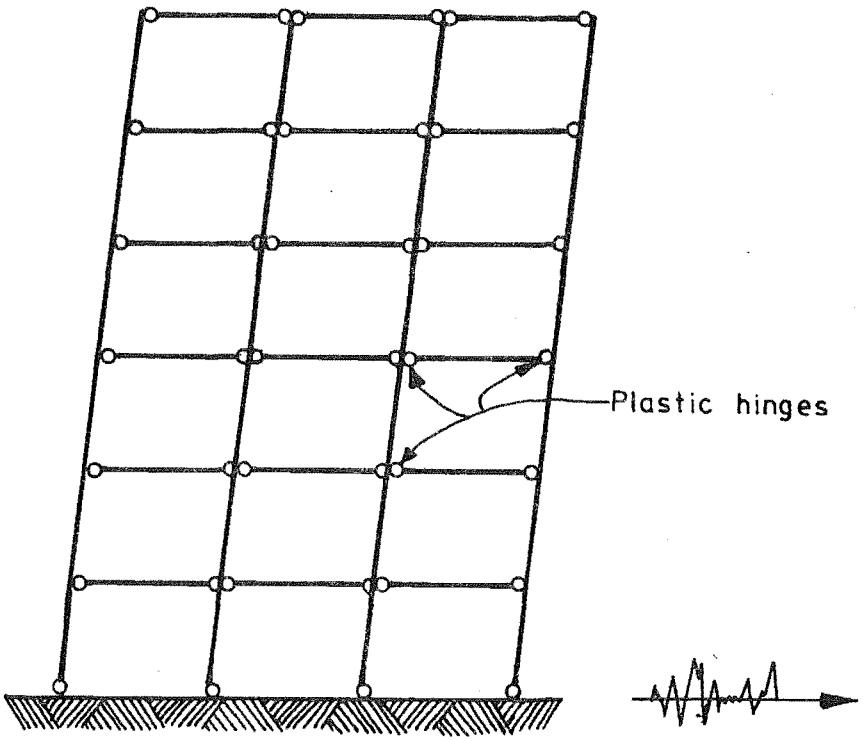

FIG.1.1 :BEAM SIDESWAY MECHANISM FOR FRAME UNDER SEISMIC LOADING

acceleration records[6] show that by adopting rational design procedures inelastic behaviour in columns can readily be limited to brief yield excursions, having negligible ductility demand at either top or bottom of a particular column in a limited number of columns in a given bent. If a particular column yields, the sidesway deformation is limited by the stiffness of the remaining unyielded columns, and the ductility demand for the column can never be large. These observations are limited to uniaxial frames such as the perimeter frames of a tube-frame structure. When the columns of a space frame have beams framing into both sides of the column, the probability of concurrent beam moment input must be considered by the designer. The possible loading on the column is then much more severe, while the column section design for biaxial bending is not as well defined as for uniaxial bending, where reliable design charts are readily available. Inelastic dynamic frame analysis for checking the actual response of space frames to earthquake attack is also much more difficult, and is usually accomplished by analysing the frames in the two directions separately, and checking the columns afterwards for possible yielding under concurrent loading.

The design of beam-column joints has generally been based on the horizontal shear input from the yield strength of the beam reinforcement at the column face, less the shear in the column above[5,7]. Following the philosophy of capacity design, the nominal yield strength of the beam bars is increased by a multiplier to give the maximum likely force input. Opinion as to the manner in which this shear is resisted within the joint is varied amongst researchers and designers. Consideration of the effect of vertical joint shear, and the need to provide resistance for this component have only recently been recognised[8] as significant to the problem of joint design. Besides the difficulties of providing resistance to the high shears within the joint core, beam-column joints face the additional problem of accommodating the very high bond stresses required to be developed by the flexural reinforcement across the joint, due to the change in the sense of the moments in the flexural members at the joint under lateral loading. These problems are discussed in more detail in Section 1.3.

In terms of configuration, joints may be classified principally as plane frame or space-frame types. Fig. 1.2 shows that plane frame joints, i.e. those in which the column is bent about one principal axis only, may be further subdivided into interior joints, in which beams

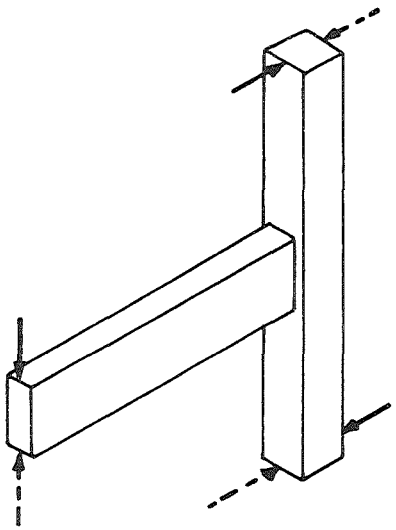

Plane frame exterior joint

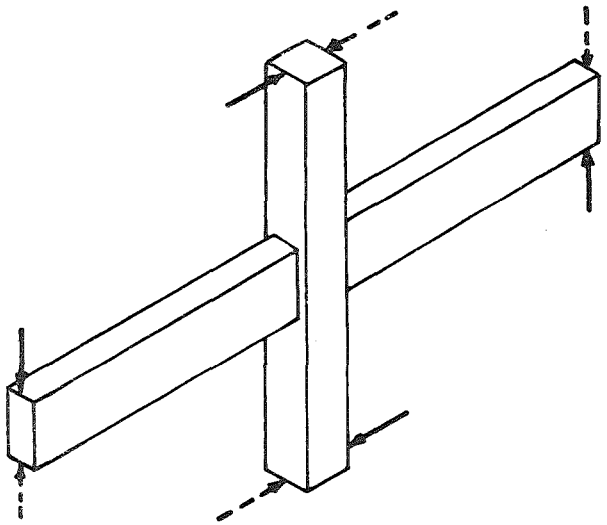

Plane frame interior joint

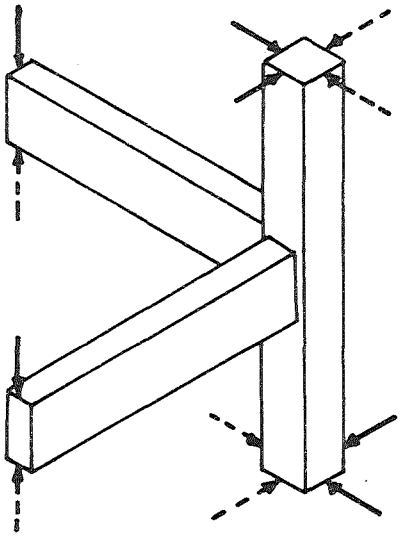

Space frame corner joint

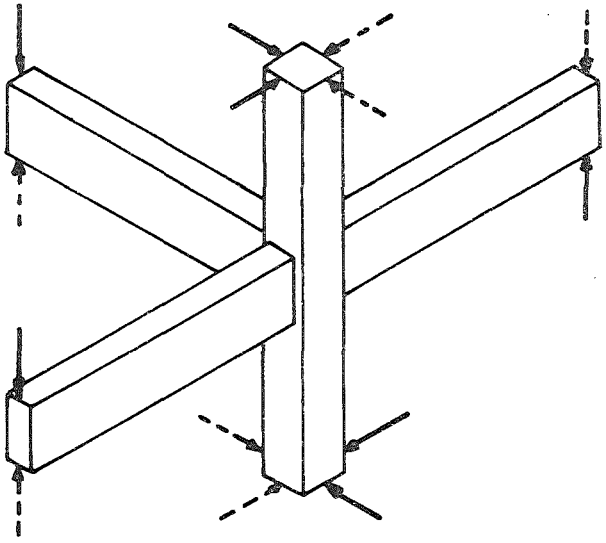

Space frame edge joint

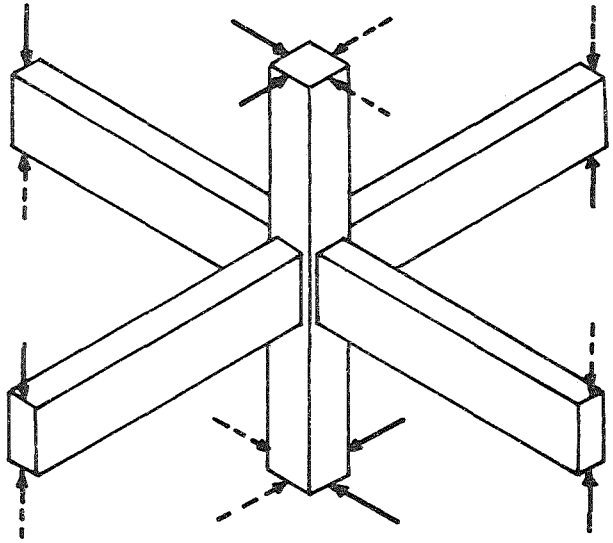

Space frame interior joint

FIG.1.2 :CLASSIFICATION OF JOINTS

frame into two opposite faces of the column, and exterior joints, in which a beam frames into one column face only. Space frame joints, where the column is in bending about both principal axes, may be categorised as corner joints, edge joints, or interior joints, according to the number of beams.

A wide variety of tests on plane frame joints of both interior and exterior types has been undertaken since about 1967, as discussed in the following section, but interpretation of the results varies widely. In the present study the results of three tests on plane-frame interior joints, and one test on a space frame interior joint are reported. In the case of space frame joints, the problems of analysis and of postulating appropriate mechanisms of resistance are compounded, while the physical configuration of an appropriate unit makes realistic testing of such a joint much more difficult, both in terms of manufacture and of test loading than is the case for an equivalent plane frame unit. For these reasons published information on these joints to date has been largely speculative, while the writers of codes have been reluctant to make any recommendations.

It is a somewhat paradoxical situation that the occurrence of joint distress in framed structures in recent destructive earthquakes has seldom been reported, whereas the joint has frequently been found to be the weakest component of beam-column subassemblages tested under cyclic loading in the laboratory. The principal reason for this anomaly appears to be that very few framed structures have formed a very convincing beam sidesway mechanism (see Fig. 1.1) under actual earthquake attack, as postulated by the capacity design approach, with destructive non-ductile failures occurring elsewhere in the structure limiting the load applied to the joints. In typical events brittle behaviour has been caused by premature shear failure of beams or columns, compression failures of columns, or anchorage failures in various locations, due to either inadequate design or faulty workmanship. One notable case of joint failure occurred during the Tokachi-Oki earthquake in Japan in 1968[9], where brittle joint failure was apparent in several cases; however these joints were somewhat unusual in having quite large eccentricities between beam and column centrelines, which would have caused torsions not apparent in joints of conventional geometry.

1.2 Review of Previous Tests

A wide variety of tests on beam-column joint units from reinforced concrete frames has been undertaken since the tests conducted by the Portland Cement Association were reported by Hanson and Connors[10,11,12].

This series of sixteen tests showed that the joint problem is critical for both interior and exterior plane frame joints in the endeavour to achieve ductile frame behaviour under cyclic loading. The need to provide reinforcement to resist joint shear was clearly illustrated, although the design approach suggested by the authors was, perhaps because of the lack of a suitable structural model, derived directly from the current equations for beam shear which, as will be shown in Section 1.3, are quite inappropriate. The joints tested all suffered either bond failure or shear failure in the joint panel before the tests were completed. Moreover the loading sequence used could not be considered to represent a severe earthquake. The maximum ductility factor imposed was only 5.0 in terms of the beam rotation within the first half-beam depth from the column face. The performance of some of the units was enhanced by the use of beam stubs to represent the transverse beams of a space frame. Although these stubs were cracked before the testing began, the validity of their inclusion is questionable because in the prototype situation both sets of beams may be loaded concurrently at some stages of response to earthquake loading, and this would tend to negate the advantage observed as a result of the confining action of the beam stubs. In most cases a relatively heavy column axial load (one-third of the column concentric axial load capacity, N_o) was applied to the test units, and this would also have improved their performance.

Because the P.C.A. test units all showed an unsatisfactory failure mode, either shear or bond, in spite of the moderate ductility demand, and because of the need for a better understanding of joint behaviour to give a more suitable design approach, further tests were undertaken by various workers.

A series of seventeen tests was undertaken by Higashi and Ohwada[13], with both interior and exterior plane frame joints being included. Ordinary and lightweight concrete units were tested, with relatively light column axial loads, but shear failures in the joint panel, or bond failures of the beam bars were predominant, and the results showed unsatisfactory behaviour. Significant strength and stiffness degradation was observed in most of the tests.

More recent tests on interior plane-frame joints, reported by Umemura, Aoyama, and Noguchi[14], demonstrated the response of test units for which the ratio of column depth to beam bar diameter was relatively small (between 12 and 20). The response of the units was unsatisfactory in that bond failure of the beam bars occurred across the joint, and

plastic action in the beam hinges was very limited.

A series of thirteen tests on exterior uniaxial joints was undertaken at the University of Canterbury[15] with quite severe values of section curvature ductility being required of the test units. Deficiencies were demonstrated in both the shear resistance of the joint panel, and in the anchorage of the flexural reinforcement. The principal conclusion from these tests was that, for low axial loads at least, the critical joint crack forms along the joint diagonal, rather than at the 45° angle usually assumed for beam shear resistance, while the contribution of joint concrete to shear resistance was assessed as negligible under severe cyclic loading. Patton[16] provided a solution to the anchorage problem for exterior joints by demonstrating the advantage of using a beam stub extending beyond the outer face of the column as the location for the anchorage of the beam flexural reinforcement.

More recent tests in New Zealand have been conducted by the Ministry of Works and Development[17]. One exterior and one interior plane frame joint was tested, with joint design based on the recommendations of Park and Paulay[15]. The test units were built to full scale and the column axial load level was small. The results of the tests were very encouraging with inelastic joint behaviour and anchorage problems eliminated, although the joint reinforcement needed to achieve these results was heavy. The two-thirds inefficiency factor suggested by Park and Paulay for the design of exterior joints was shown to be unnecessary.

Four tests on interior plane frame joints conducted by Fenwick and Irvine[18] at the University of Auckland were undertaken to investigate the feasibility of using steel plates welded to the flexural reinforcement to eliminate the bond problem, and to improve the joint concrete shear resisting mechanism. The results showed that this was indeed a valid approach to the problem in that the unit with bond plates behaved considerably better than those without, although the control units were deficient in having no intermediate column bars passing through the joint. However, the welded bond plate detail would appear to be expensive for actual construction, while the desirability of heavy welding of the flexural bars immediately adjacent to the plastic hinge must be questionable in terms of the introduction of secondary shrinkage stresses and alteration of the steel properties in the critical region.

Thompson[19] conducted a series of ten tests on plane frame interior joints having beams all of similar strength, with either mild steel reinforcement, partial prestressing, or fully prestressed, principally in

order to investigate the behaviour of the beam plastic hinges with these different configurations of flexural reinforcement. However, joint failure occurred in several of the tests, and prestressing of the beams was shown to improve the joint behaviour significantly. Three supplementary tests by Yeoh[20] showed conclusively that inclusion of intermediate column bars largely remedied the deficient joint performance observed in the earlier tests.

Uzumeri and Seckin[21] reported a series of eight tests on plane frame exterior joints with heavy column axial loads (about 40% of the column capacity, N_o). Joint reinforcement was included in only five of the test units, and most of these failed in the joint region, with extensive yielding of joint ties. An arbitrary criterion for 'satisfactory performance' is that given in the New Zealand "Code of Practice for General Structural Design and Design Loadings for Buildings"[1], where it is suggested that structural elements of buildings should be able to withstand four complete cycles of loading to a displacement ductility factor of four in each direction, with no more than 30% loss in strength. Only specimen 6 of the units tested by Uzumeri and Seckin approached this level of performance. The heavy column load was shown to be beneficial to joint performance by providing good bond conditions for the beam flexural reinforcing, and by reducing the bond demand on the column flexural reinforcement, but it is felt that a typical exterior joint under critical seismic loading is unlikely to encounter this condition of constant heavy axial load, and that the test conditions were therefore optimistic.

A later unit tested by Uzumeri and Seckin[22] was subjected to a relatively light column axial load, with the somewhat surprising result that the response was not significantly inferior to that observed for the comparable unit with heavy axial load. Possible reasons for this result are discussed in the light of the present test results in Chapter 6.

Lee[23] has described a series of six tests on plane frame exterior joints which behaved well under cyclic loading, largely because the sum of the column flexural strengths above and below the joint was up to 4.3 times greater than the beam flexural capacity. The bond requirement for the column reinforcement down the joint was therefore moderate, while the elastic state of the column above and below allowed the joint concrete to develop a satisfactory strut mechanism for shear transfer, and thus reduced the demand on the joint reinforcement. Again it seems that the test conditions were not representative of typical prototype structures under actual earthquake attack, where columns will probably be highly stressed, possibly to the extent of occasional brief yield excursions.

Some useful results were given for repaired units, showing that repair involving replacement of damaged concrete by stronger material may result in beam sections stronger than the original, both because of the stronger compression material, and also perhaps because of strain-aging of the yielded beam reinforcement. Thus the demand on the joint and the column could be increased in subsequent earthquakes, possibly to the extent of shifting the failure location, as happened in one of the reported tests.

Finally, a series of tests that was examined is that reported by Jirsa and Meinheit[24], in which fourteen plane frame interior test units were tested with a wide variation in parameters. Unfortunately the beams reached their yield strength simultaneously on both sides of the column in only three of the fourteen specimens, and this could only be sustained for at most one and half post-elastic cycles. The reason for this was that in most cases only nominal joint reinforcing was provided, while quite large bars were used as beam flexural reinforcement. Hence the joint panel failed in shear in most cases before yield load was attained, and in the remaining cases bond failure led to rapid loss of strength. Because yield strength was seldom attained in the beam reinforcement the shear was introduced to the joint in a significantly different manner to that observed for a prototype joint, where the integrity of the joint should be maintained while extensive yielding of the beam reinforcement occurs in the plastic hinges. Hence the conclusions drawn from these tests in respect of the shear strength of the joint concrete cannot be considered to have much relevance to seismic criteria. In particular the reduction factor proposed for cyclic loading cannot possibly be justified, because the number of significant cycles imposed on the test units was minimal.

1.3 Mechanisms of Joint Shear Resistance

1.3.1 Actions on Plane Frame Joints

In order to study the strength of a beam-column joint, it is necessary firstly to define the forces acting on the joint under severe seismic loading. For an interior joint of a plane frame having plastic hinges located in the beams adjacent to the column faces, the horizontal shear force acting on the joint may be derived from the forces in the beam flexural bars, less the shear force in the column above or below the joint, as demonstrated below.

Using the notation shown in Fig. 1.3, the horizontal shear force acting above a horizontal plane passing across the beam-column joint between the layers of top and bottom bars is

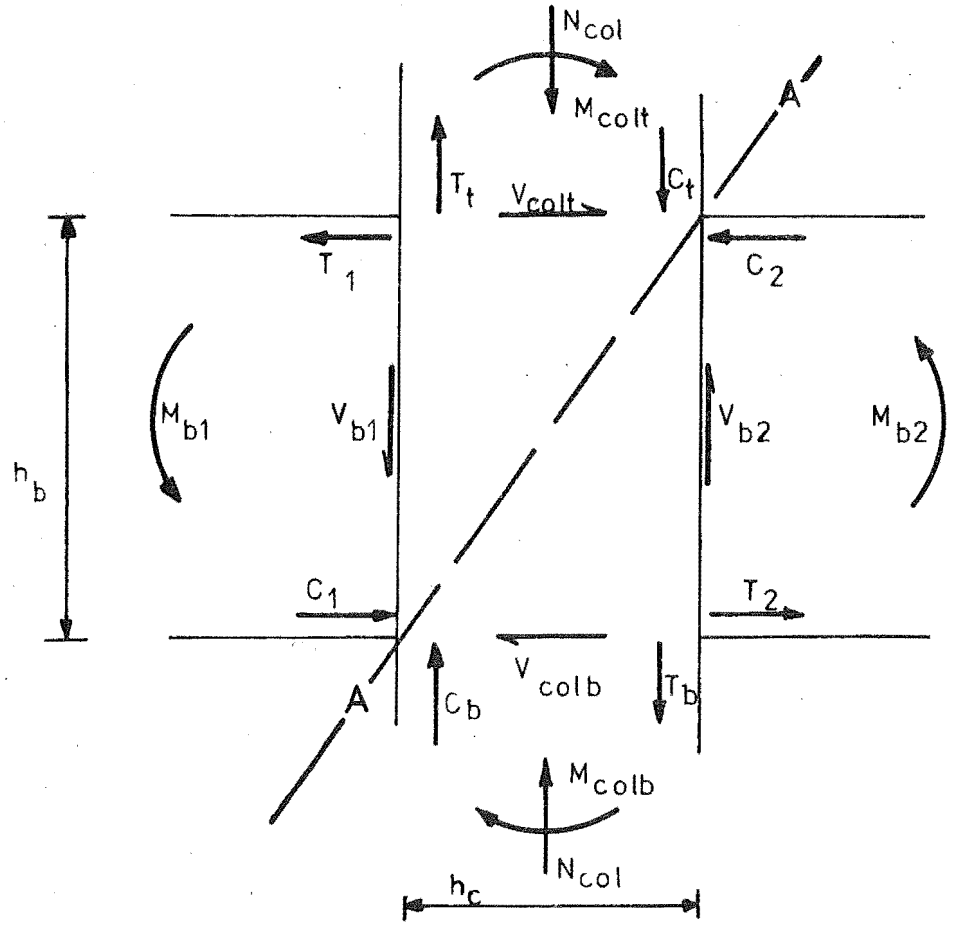

FIG.1.3 : ACTIONS ON JOINT

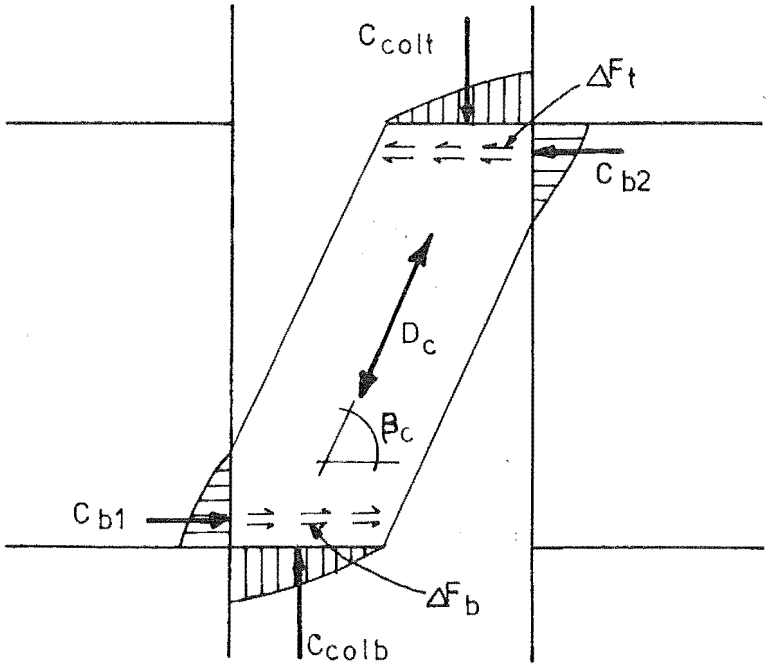

FIG.1.4 : CONCRETE DIRECT STRUT MECHANISM FOR JOINT SHEAR RESISTANCE

$$V_{jh} = T_1 + C_2 - V_{col\,t} \tag{1-1}$$

The tension force T_1 at the top of the left-hand beam in Fig. 1.3 is

$$T_1 = A_{s1}.f_{s1} \tag{1-2}$$

where A_{s1} is the area of top reinforcement in the beam, including any slab reinforcement which may act in conjunction with the principal beam top bars, and f_{s1} is the tensile stress in the top reinforcement.

From equilibrium of the beam section to the right of the joint, the total compression force C_2 at the top of the right-hand beam (in both steel and concrete) is equal to the tensile force T_2 at the bottom of that beam.

$$C_2 = T_2 = A_{s2}.f_{s2} \tag{1-3}$$

where A_{s2} is the area of bottom reinforcement, and f_{s2} is the stress in it. This is based on the assumption that $V_{col\,t} = V_{col\,b}$.

Under severe seismic loading the beam reinforcement will yield, and if the ductility demand on the plastic hinges is sufficient, some strain-hardening can also be expected. To allow for possible strain-hardening, and also for the likelihood that the actual yield strength of the bars will exceed the ideal yield strength, f_y, it is prudent that the input shear for joint design should be based on a design strength for the beam bars greater than the specified yield strength. This may be achieved by applying an overstrength factor α to the specified yield strength.

$$f_{s1} = f_{s2} = \alpha.f_y \tag{1-4}$$

For New Zealand mild steel of specified yield strength 275 MPa a suitable value[5] for the overstrength factor is $\alpha = 1.25$. Once an appropriate value of α has been applied, the maximum likely action of the beam flexural bars on the joint is well defined. The value of the column shear $V_{col\,t}$ or $V_{col\,b}$ is less precisely defined. Under dynamic loading the bending moment patterns in the columns of a frame may not be regular, and the distribution of beam input moments to the column sections above and below the joint is uncertain. The column shear in a particular storey depends on the moments at top and bottom of the column, but for the purposes of joint design a reasonable approximation[8] for the column shear in a regular frame is given with the notation of Fig. 1.3.

$$V_{col\,t} = V_{col\,b} = \frac{M_{b1} + M_{b2} + 0.5(V_{b1} + V_{b2})h_c}{0.5(l_c + l_c')} \qquad (1\text{-}5)$$

where l_c and l_c' are the storey heights from centre to centre of the beams above and below the joint, and h_c is the column depth.

Concurrently with the horizontal joint shear, a vertical shear, V_{jv}, is imposed on the joint due to the change in the sense of the column moments above and below the joint. This may be assessed by considering the column bar forces, the concrete compression force in the column, and the appropriate beam shear force to one side or other of the column centreline.

The actions on a plane frame exterior joint are similar to those derived for an interior joint, but since moment is applied at one face of the joint only, the horizontal joint shear is given by the overstrength tensile force in the top or bottom beam reinforcement only, less the appropriate column shear force.

1.3.2 Direct Concrete Strut Mechanism

The shear applied to a beam column joint under lateral loading of a building frame may be resisted in a variety of ways, depending on the condition of the joint and the adjacent flexural members at any given stage of loading. Fig. 1.4 shows that if sufficient horizontal and vertical forces are available at the appropriate corners of the joint, then shear may be transferred across the joint by a direct concrete strut, which carries a compressive force, D_c. This mechanism does not require any joint reinforcement apart from confining reinforcement to ensure that the concrete strut can sustain the compressive stresses. Consideration of the boundary conditions necessary to sustain this mechanism shows that the vertical forces from the column are readily available, since the column is designed to remain essentially elastic throughout seismic loading. Concrete compression forces $C_{col\,t}$ and $C_{col\,b}$ within the column section due to flexure and axial load should therefore remain viable, and loss of bond strength of the column bars will be negligible. In the beams, however, the expected inelastic response of the hinges adjacent to the column faces means that the horizontal actions necessary to provide viable end conditions for the action of a concrete strut will not be so readily available once severe seismic loading has been imposed on the structure.

In elastic conditions, that is before the occurrence of significant yielding in the beam reinforcement, the concrete compression forces in the beams, C_{b1} and C_{b2}, and the forces ΔF_b and ΔF_t transferred from the beam bars by bond within the compressed area of the column section,

will be a significant fraction of the total horizontal force to be transferred across the joint. Thus in this situation the direct diagonal strut mechanism may resist a significant proportion of the total applied horizontal joint shear, V_{jh}. However, after reversed inelastic loading has been applied, the concrete compression forces in the beams, C_{b1} and C_{b2}, are likely to be small (due to permanent elongation of the reinforcement leaving full depth cracks) while penetration of strains in excess of yield strain in the beam bars into the joint core means that bond strength will be lost close to the corners of the joint panel, and the total horizontal force available to combine with the vertical forces to allow a diagonal strut to act will therefore be small.

The inclination β_c of the strut to the horizontal may be approximated by that of the line between the centroids of concrete compression in the beam and column at diagonally opposite corners as shown in Fig. 1.4. When reversed inelastic loading occurs the location of the centre of effective compression in the beams may be somewhat uncertain, and the appropriate horizontal forces may be considered to act at the centroid of the beam bars.

1.3.3 Joint Truss Mechanism

A second mechanism by which joint shear may be resisted in shown in Fig. 1.5. This mechanism consists of a truss, comprising joint horizontal reinforcement, diagonal concrete struts, and a vertical reaction supplied either by concrete compressive forces in the column, and/or by vertical joint reinforcing. The horizontal reinforcement may consist of either horizontal joint stirrups or bars running through the joint and anchored in the beams beyond. Vertical reinforcement may consist of either vertical stirrups or column intermediate bars. In most cases it is impractical because of construction difficulties to place stirrups in both vertical and horizontal directions, and the most common configuration for joint reinforcing consists of horizontal stirrups with intermediate column bars used as vertical reinforcing. Note that the diagonal compression force D_s carried by the concrete is additive to the diagonal force (D_c) caused by the direct compression strut mechanism of resistance.

Study of Fig. 1.5 shows that the horizontal and vertical input shears may be introduced to the truss mechanism at any location around the joint perimeter. For this reason the mechanisms may be expected to provide shear resistance throughout the loading history of the structure. It should also be noted that inclusion of horizontal joint reinforcing alone is insufficient to ensure the satisfactory performance of this mechanism.

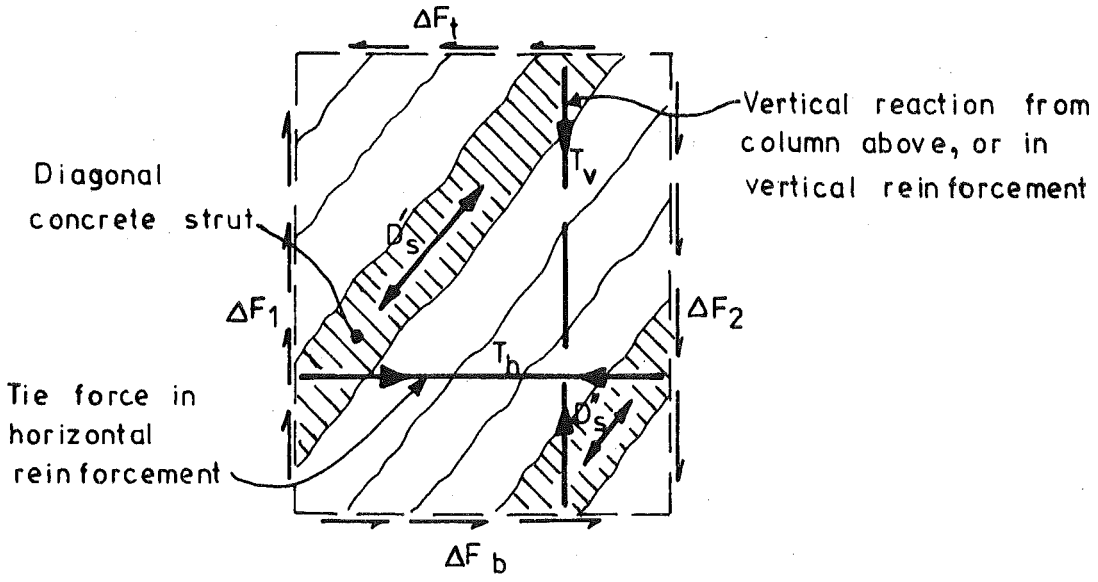

FIG.1.5 :TRUSS MECHANISM FOR JOINT SHEAR RESISTANCE

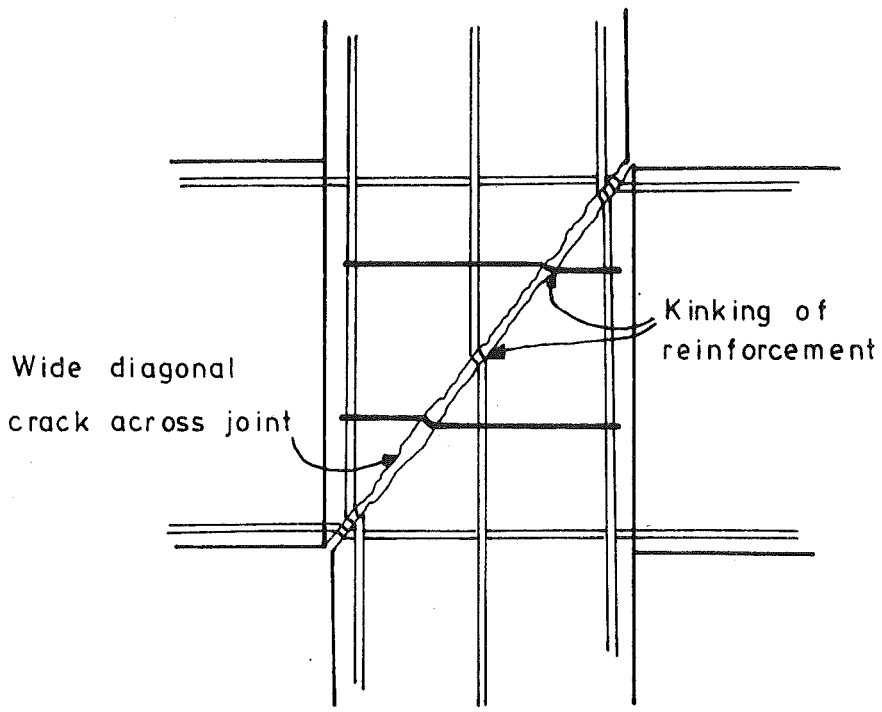

FIG.1.6 : DOWEL ACTION IN BEAM COLUMN JOINT

Vertical compression components must be supplied, and this is particularly important in the design of joints for which the column axial load is small, where vertical reinforcement must be provided across the joint.

1.3.4 Other Mechanisms of Joint Shear Resistance

It is possible that other sources of shear strength for joints may lie in the mechanisms of aggregate interlock and dowel action of the reinforcing, both of which are known to be sources of shear strength for beams[25]. However joint test results[15,19] show conclusively that the expected direction of cracking in the joint panel is parallel to the joint diagonals. Since there cannot be significant shear displacement along the diagonal cracks it does not seem that aggregate interlock will be a significant source of shear strength for joints. Also, since the joint is required to remain essentially elastic it seems unlikely that shear deformations within the joint will be large enough to permit significant dowel action to be mobilized under normal circumstances. It is possible that dowel action could provide a useful source of reserve strength should extensive yielding of conventional joint reinforcement occur. However this would require large joint deformations, as shown in Fig. 1.6, and it cannot be regarded as a primary source of joint shear strength.

1.3.5 Allocation of Applied Joint Shear to Mechanisms of Resistance

It is postulated that the primary means of resistance to joint shear will be the direct concrete strut (Fig. 1.4) and the truss mechanism (Fig. 1.5), with the proportion of the input shear resisted by each mechanism depending on the boundary conditions.

The shear V_{jh} applied to the joint in the horizontal direction may be derived from Eqs. (1-1) to (1-5). The concrete direct strut will carry part of this horizontal shear, V_{ch}, and the truss mechanism can then be designed to carry the remaining shear V_{sh}.

$$V_{jh} = V_{ch} + V_{sh} \tag{1-6}$$

Fig. 1.4 shows that for joints for which reversible plastic hinges are expected to form in the beams immediately adjacent to the joint (i.e. where C_{b1} and C_{b2} are small), and for which the column axial load is small, the direct strut mechanism may not be very effective[18] under inelastic cyclic loading, and hence it is postulated that in this case the horizontal shear resisted by the joint concrete should be taken as zero

$$V_{ch} = 0 \tag{1-7}$$

When heavier axial loads are applied to the column, and where the column neutral axis is therefore relatively deep in the section, some bond forces may be picked up within the compressed area of the column, so that some diagonal compression may be transferred directly by the strut mechanism. In this case some horizontal shear resistance will be provided by the concrete strut mechanism, and Fig. 1.4 shows that it may be defined as

$$V_{ch} = D_c \cos\beta_c \qquad (1\text{-}8)$$

The relationship between column axial load and the shear resistance of the strut mechanism is discussed further in Chapter 6, in the light of the test results.

The horizontal reinforcing required in the joint to form the required truss mechanism is

$$A_{sh} = \frac{V_{sh}}{f_{yh}} \qquad (1\text{-}9)$$

where A_{sh} is the total area of horizontal reinforcement crossing the diagonal plane from corner to corner of the joint (Plane A-A in Fig. 1.3) between the top and bottom layers of beam bars, and f_{yh} is the yield strength of the joint horizontal reinforcement.

Considering the vertical shears applied to the joint, a similar equation to Eq. (1-6) may be written

$$V_{jv} = V_{cv} + V_{sv} \qquad (1\text{-}10)$$

However concrete compression forces may be expected to be available in the column throughout the loading history, due to the absence (or very limited occurrence) of yielding in the column reinforcement. The term V_{cv} therefore includes not only the vertical component of the direct strut mechanism, $D_c \sin\beta_c$, but also part of the necessary vertical action for the truss mechanism. The vertical actions, T_v, shown in Fig. 1.5, can be provided both as tensile forces in vertical joint reinforcement within the joint panel, and as compressive forces acting in the column concrete at the top and bottom edges of the joint panel. Thus the availability of appropriate forces in the column sections can reduce the vertical joint reinforcement required to complete the truss, so that the total value of V_{cv} can also be expected to depend on the column axial load. This will be discussed further in Chapter 6. The necessary vertical joint reinforcement to be placed between the outer layers of column bars is

$$A_{sv} = \frac{V_{sv}}{f_{yv}} \qquad (1\text{-}11)$$

where f_{yv} is the yield strength of the vertical joint reinforcement.

For design purposes a strength reduction factor ϕ_J is often[5] applied when determining the required reinforcement in both horizontal and vertical directions, given by Eqs. (1-9) and (1-11).

1.3.6 Mechanisms of Resistance for Space Frame Joints

When skew loading is applied to a space frame joint, the horizontal shears on the joint in each principal direction may be derived on the same basis as the horizontal shear for a plane frame joint (Equations 1-1 to 1-5). The vertical shear may be calculated by assessing the forces to one side of a vertical plane through the plan diagonal of the joint.

The mechanisms of resistance in a space frame joint under skew loading are similar to those described for plane frame joints except that the critical planes are differently oriented. A direct diagonal strut may be expected to form between opposite diagonal corners of the joint core if the boundary conditions are favourable, but the exact nature of the strut is complex. Fig. 1.7 shows that the expected compression fields in the adjacent beam and column members do not extend over the same widths of joint core. Thus stress concentrations will occur at each end of the compression strut which acts between diagonally opposite corners of the joint core. Note that there is some similarity here to the way in which a diagonal strut will form across a plane frame joint where the column breadth is greater than the beam breadth.

A truss mechanism may also be postulated by means of which horizontal and vertical reinforcement may be utilized to combine with concrete struts acting in planes oriented between diagonally opposite corners of the joint core, to resist joint shear introduced around the exterior surface of a space frame joint. However Fig. 1.8 shows that the orientation of critical planes between opposite corners of the joint cuboid means that conventional joint ties will only be approximately half as effective in resisting a component of skew joint shear, applied along the joint diagonal, as they are for plane frame shear. Only one leg of each tie in each principal direction will be crossed by the critical plane, whereas both legs of a tie will be crossed by the critical plane for plane frame action. Ties placed diagonally (that is with a diamond-shaped orientation relative to the joint cross section) will tend to carry skew shear more efficiently.

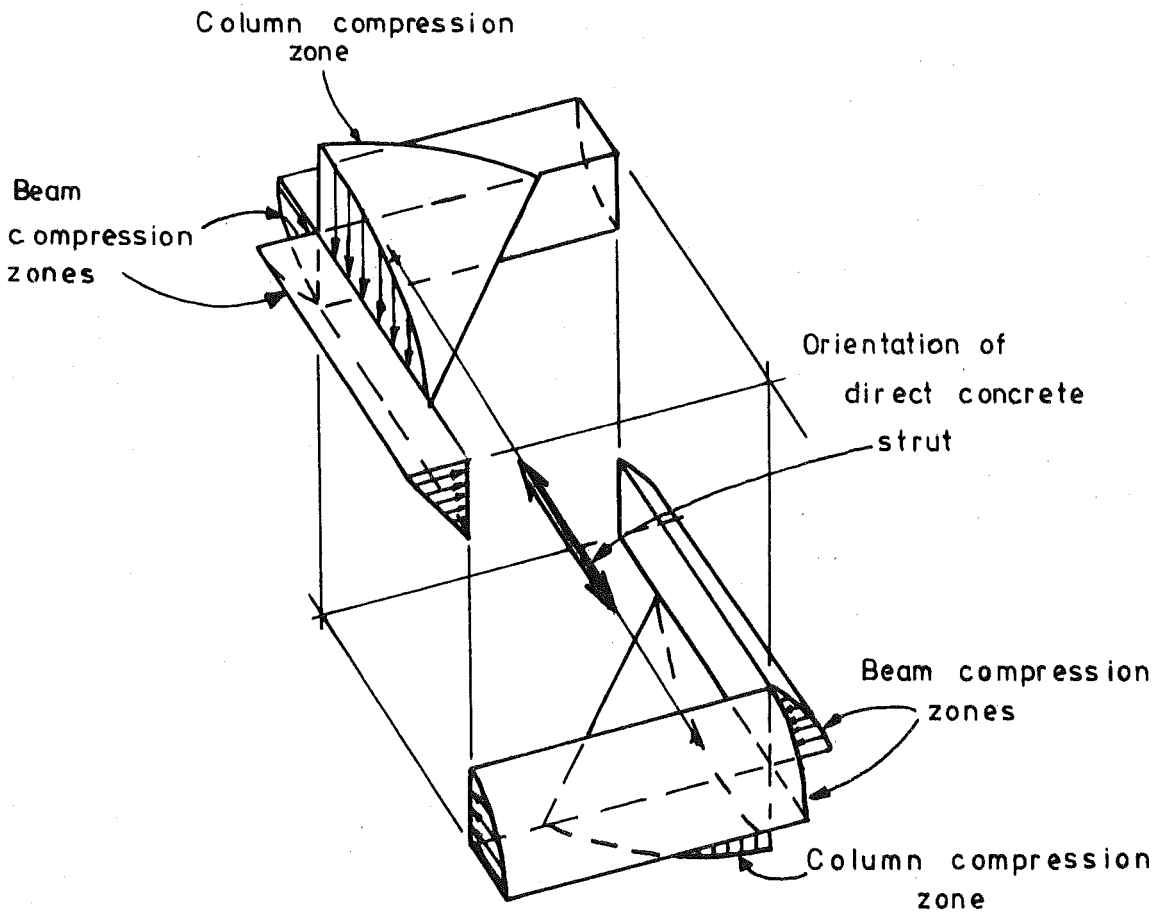

FIG.1.7:END CONDITIONS FOR DIRECT STRUT IN SPACE FRAME JOINT

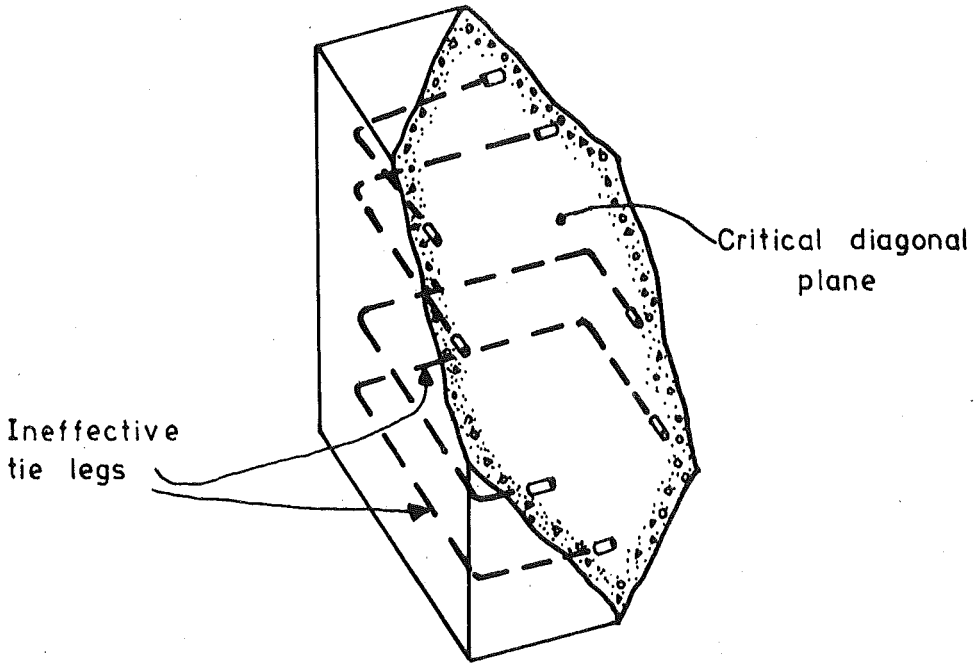

FIG.1.8:CRITICAL PLANE FOR SPACE FRAME JOINT

For joint cores with square columns, with square ties placed parallel to the core sides, the horizontal shear force which can be carried by the ties diagonally is only $1/\sqrt{2}$ of the horizontal shear force which can be carried by the ties along either principal axis of the column section. If the beams in the two directions form plastic hinges adjacent to the joint core simultaneously due to skew loading, and if the beams are similar, it is evident that the applied horizontal shear force along the diagonal is $\sqrt{2}$ times that which is applied along a principal axis of the section if plane frame action only occurs. Thus, in the limit, if the shear carried by the direct concrete strut mechanism is zero, consideration of space frame action on the joint core could require twice as much horizontal joint reinforcement as would plane frame action only.

The critical diagonal plane crosses all the vertical joint reinforcement, and hence the only requirement for additional reinforcement in this direction due to skew loading arises if the applied vertical joint shear is greater for skew loading than for unidirectional loading.

1.4 Parameters Affecting Joint Response to Seismic Loading

1.4.1 General Comments

The resistance of beam-column joints to the high shear forces generated by severe seismic loading has been postulated to be resisted by joint concrete acting as a direct compression strut mechanism, and by joint reinforcement acting with the concrete to form a truss mechanism. The total shear to be resisted by a joint must be limited to prevent overstressing the concrete, which is required to carry diagonal compression in both principal mechanisms of resistance. Since the joint concrete will become extensively cracked in both diagonal directions under cyclic loading, it is obvious that the maximum stress that can be carried safely will be considerably less than the cylinder strength of the concrete. A limit may be set by restricting the maximum nominal horizontal shear stress within the joint[5,7].

The shear to be resisted by the truss mechanism is normally limited by the congestion of the necessary joint reinforcement. The resistance of the truss mechanism to joint shear depends only on the quantity of joint reinforcement and the yield strength of the reinforcing steel, as shown by Eq. (1-9), unless skew loading of the joint must be considered as described in the previous section.

It is therefore apparent that the assessment of the strength of the direct concrete strut mechanism is critical for the efficient design of

beam-column joints to resist seismic loading. If more shear resistance can be allocated to this mechanism then the requirement for joint reinforcement will be reduced. The strength and viability of the mechanism depends on a variety of parameters, and these are discussed individually in the following sections.

1.4.2 Concrete Strength

Since the concrete strut is expected to carry load at stresses considerably less than the crushing strength of the concrete, the compressive strength has no direct influence on the amount of joint shear strength which can be allocated to this mechanism. The viability of the concrete strut mechanism depends on the availability of appropriate end conditions rather than on the material strength of the strut. The only significant effect of concrete strength on these end conditions lies in its influence on the bond strength of the flexural bars, which provide input shear to the joint. If the penetration of yield strain in beam bars into the joint can be reduced by greater bond strength, then a greater contribution to joint shear resistance may be expected from the direct strut mechanism. However greater concrete strength will also tend to reduce the neutral axis depths in the flexural members adjacent to the joint, and this may counteract any enhancement of the strength of the strut mechanism caused by greater bond strength and reduced yield penetration.

1.4.3 Column Axial Load

Clearly the level of column axial load may be expected to have a significant effect on the effectiveness of the direct strut mechanism. As the compressed area of concrete in the column section above or below a joint increases due to increasing axial load, so the amount of horizontal input shear transferred by bond within the compression zone will increase. This means that horizontal shear is available to combine with the vertical compression forces, so that the strut will be effective regardless of the presence or otherwise of concrete compression forces in the beam sections. The other expected benefit of axial compression lies in the probability that the bond environment for the beam bars should be improved in joints with heavier axial loads[26], so that yield penetration should be reduced. The minimum axial compression load to be expected on a joint during seismic loading is likely to provide the critical load case for design.

1.4.4 Flexural Reinforcement

Although the quantity and strength of the beam flexural reinforcement provides the input shear forces for joint design, the composition of the

beam reinforcement may also have some influence on the resistance of the joint to the applied shear. The size of the flexural bars relative to the column depth influences the bond stresses in the bars across the joint, and if yield penetration can be reduced by using smaller diameter bars, then the direct strut mechanism may be expected to carry more shear.

The distribution of applied joint shear between the two principal mechanisms of resistance may also be influenced by the ratio of the beam tension to compression reinforcement. If this ratio is greater than unity then some compression force must be carried by the beam concrete in the beam under negative (hogging) moment, and this might improve the end conditions for the concrete strut. However since the concrete compression force in the other beam under positive (sagging) moment must always be zero after one complete inelastic cycle of loading, the end conditions for the strut at the top of the joint will not be favourable, and the net effect is unclear. This problem is discussed in more detail in Chapter 3 and Chapter 6.

The distribution and amount of column flexural reinforcement will affect the concrete strut mechanism so far as the depth of compression in the column section is affected. It has already been noted in Section 1.3.3 that vertical reinforcing is required through the joint to ensure that the truss mechanism functions properly.

The use of post-tensioned prestressing tendons in place of ordinary mild steel reinforcing bars in beams of equivalent ultimate strength has been demonstrated in the tests of Thompson[19] to significantly enhance joint performance. This is due to the presence of larger concrete compression forces in the prestressed beams, and this would be expected to benefit the strut mechanism for joint shear resistance. Extensive inelastic straining of the prestressing tendons will reduce the effective prestress. Hence only tendons located near the mid depth of the beam can be relied upon[5] to supply effective concrete compression forces after severe seismic loading, since during rotation of the beam hinge these will undergo less plastic strain, if any, than tendons located near the extremities of the beam hinge. Some benefit may also be gained by prestressing of columns to increase the area of compressed concrete at the periphery of the joint, particularly for columns of low rise buildings, or for the upper storey columns of higher buildings, where the axial load due to gravity is small.

1.4.5 Geometric Parameters

The aspect ratio of the joint h_c/h_b (see Fig. 1-3), may have some influence on the joint performance, since if the column depth h_c is

made greater while the beam depth h_b remains constant, the depth of compression in the column is likely to increase, and hence more force can be acquired from the beam bars within the compressed area of the column. However the average compressive stress in the larger column is likely to be smaller and it is possible that the bond strength of the beam bars may thus be reduced sufficiently to negate the benefit gained by the larger depth of compression.

A second geometric parameter which may have some influence on the effectiveness of the joint direct strut mechanism is the ratio of the beam breadth b_w to the column breadth b_c. Since the column forces are not critical in forming the concrete strut, joints for which the beam breadth is less than the column breadth should perform satisfactorily. However it seems likely that efficient operation of the strut mechanism will be reduced in joints for which the column breadth is significantly less than the beam breadth.

The draft New Zealand Concrete Code[5] makes recommendations for the effective joint width, b_j, to be used in assessing nominal joint stresses as follows:

Where $b_c \geq b_w$

$$\text{either } b_j = b_c \qquad \text{or } b_j = b_w + 0.5h_c \qquad (1\text{-}12)$$

whichever is the smaller,

and where $b_c < b_w$

$$\text{either } b_j = b_w \qquad \text{or } b_j = b_c + 0.5h_c \qquad (1\text{-}13)$$

whichever is the smaller.

These equations imply equal limitations on the effectiveness of the joint for the case of narrow beam-wide column (Eq. 1-12), and for the case of narrow column-wide beam (Eq. 1-13), whereas it could be postulated that the former situation may be more favourable to efficient joint response.

Further problems will arise in joints in which the beam and column centrelines do not intersect. Additional stresses due to torsional moments will be caused in joints of this type due to the eccentricity at which the horizontal shear is applied to the joint.

1.4.6 Location of Beam Plastic Hinges

Study of the postulated mechanisms of resistance to joint shear shows that two features are required to allow efficient joint shear transfer by the direct concrete strut mechanism. These are firstly the presence of significant concrete compression forces in all beams adjacent to the joint, and secondly limitation or elimination of the penetration of yield strain in the beam flexural bars into the joint core. It has been suggested[8] that this might be achieved efficiently by reinforcing the beams so that the plastic hinges form at some distance away from the column faces, rather than immediately adjacent to the faces, as happens in conventionally reinforced beams. This relocation of the plastic hinges will result in the sections adjacent to the column faces remaining essentially elastic, so that beam concrete compression forces can be sustained in this location, and penetration of yield strain into the joint core does not occur. Thus at some cost in reinforcing of the beam, the concrete strut mechanism can be made much more efficient than for conventionally reinforced beams, and the joint reinforcing can be significantly reduced. Tests conducted by Birss[27] in parallel with the present series, but using this concept of 'elastic' joint resistance, showed that this approach could result in significant improvements in joint response and savings in joint reinforcement. These tests and their implications are discussed in more detail in Chapter 6.

1.4.7 Joint Type

It was postulated in Section 1.3.6 that the direct strut mechanism would apply to space frame joints as well as to plane frame joints considering the appropriate end conditions. It has been suggested[4] that the presence of beams on all four sides of a joint should confine the joint core and thus strengthen the joint concrete in shear resistance. However post-elastic loading of the beams in both directions will cause open flexural cracks at all column faces, and the confinement is therefore unlikely to be completely effective, except in the case of beams with plastic hinges located away from the column face, as described in the previous section.

It is expected that the mechanisms of shear resistance for exterior joints will be similar to those postulated for interior joints, provided that adequate provision is made for the anchorage of the beam flexural reinforcement. The relationship of the strength of exterior joints to that of interior joints is discussed in more detail in Chapter 6.

1.5 Scope of This Project

1.5.1 Necessity for Testing

The mechanisms of joint shear resistance postulated in Section 1.3 are quite simple, and tentative assumptions about their responses to seismic loading and about the interaction between the two principal mechanisms can be made on the basis of the known behaviour of reinforced concrete under cyclic loading. However the interaction of the postulated mechanisms in an actual joint may be rather more complicated than first study of the postulates suggests. It has been shown, for example, that the bond strength of the beam bars across the joint is a critical feature with respect to joint performance, and while the bond strength of deformed bars under cyclic loading has been studied in various tests[28,29], the bond environment for the beam bars in the joint situation is somewhat more complex and adverse than most bond test situations can model. Hence the bond strength of beam bars across joints, and complete joint response can only be effectively studied by testing of complete beam-column joint subassemblages.

1.5.2 Scope of Experimental Work

Three beam-column joint test units representing interior plane frame joints for a multistoreyed structure were tested in the present series. Variables which were studied were the beam reinforcement configuration, and the column axial load level. The background to the design, manufacture and testing of the plane frame units is given in Chapter 2, while the results of the individual tests are reported in Chapters 3, 4, and 5. A summary of the test results and design recommendations are given in Chapter 6. A further test was carried out on an interior space frame joint, which was able to be loaded simultaneously in both principal directions, and the results of this test are reported in Chapter 7.

1.5.3 Origin of Test Units

The origin of the plane frame test units is shown in Fig. 1.9. The beam of the test unit extends from mid-span in one bay of a frame to mid-span in the next bay, while the column is taken from the mid-height of one storey to the mid-height of the next storey. These mid-span and mid-height points correspond approximately to the expected points of contra-flexure in a regular frame under lateral load. Where gravity loads on the beams are relatively high, or where higher mode response of the frame to dynamic loading affect the column bending moment pattern, then the points of contraflexure may shift from these assumed locations, but the mid-span points can be expected to represent the mean locations. The performance of

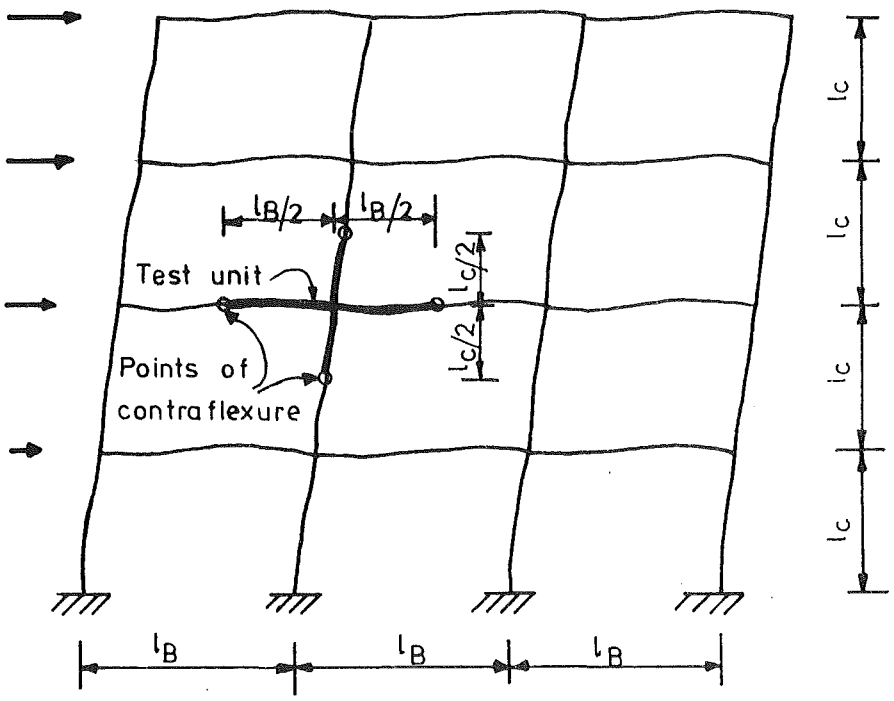

FIG.1.9 : ORIGIN OF TEST UNIT

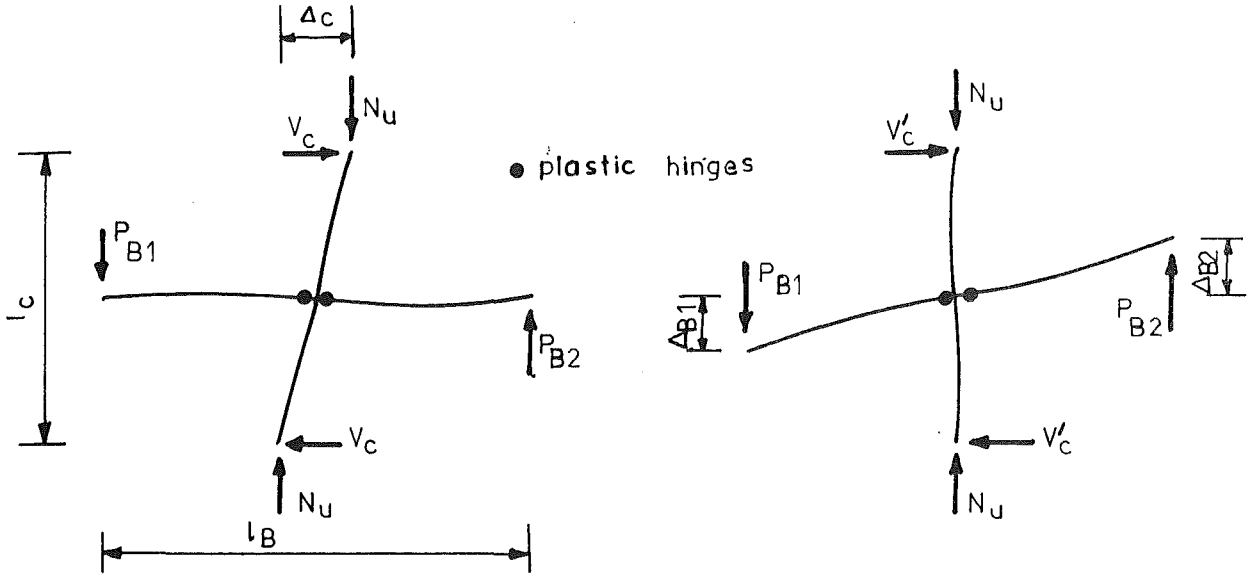

(a) In displaced frame

(b) In test rig.

FIG.1.10 : BEAM COLUMN SUB-ASSEMBLY

the joint panel should not be greatly affected by the exact location of the points of contraflexure in the adjacent members.

Lateral load on a frame causes interstorey drift, Δ_c, which means that the points of contraflexure in the columns above and below a given joint do not remain vertically above one another, as shown in Fig. 1.10(a). To apply equivalent load to a joint in a test rig, it is most convenient to apply loads P_{B1} and P_{B2} to the beam ends, and to supply reaction points for the column shears V_c', keeping the column vertical, and measuring the total displacement of the unit in terms of the beam end displacements Δ_{B1} and Δ_{B2}, as shown in Fig. 1.10(b). The equivalent column sidesway Δ_c is easily obtained by considering the geometrical relationships between the two loading situations, as shown in Fig. 1.10:

$$\frac{\Delta_c}{\ell_c} = \frac{0.5(\Delta_{B1} + \Delta_{B2})}{0.5\ell_B} \qquad (1\text{-}14)$$

$$\therefore \quad \Delta_c = (\Delta_{B1} + \Delta_{B2}) \frac{\ell_c}{\ell_B} \qquad (1\text{-}15)$$

Retaining the column in a vertical position in the test rig means that the P-delta effect is not included in the observed response. However a suitable correction can easily be applied during the reduction of the test data. The procedure followed to achieve this is outlined in Section 3.2.

The derivation of the interior joint test unit from a space frame is similar to that of the plane frame units, with the beams being taken between mid-span points in adjacent bays in each principal direction. The test was again carried out with the column vertical, and P-delta corrections were made to give the net column shear in both principal directions.

Note that no attempt was made in the tests to simulate the floor slab, which would normally form a wide top flange for the beams. This ommission is common practice[10,13,15] in the design of beam-column joint test units, due to the difficulties inherent in manufacture and testing of units including a portion of the slab. It is felt that while the slab will have a significant effect on the beam response, the effect on the joint core will be slight. For prototype joint design, some slab reinforcement must of course be included with the beam top reinforcement[5] in assessing

the input horizontal joint shear according to Eqs. (1-1) to (1-3).

1.5.4 Analytical Study of Biaxial Column Bending

As a corollary to the experimental study of a space frame joint, a further effect of the skew seismic loading of space frames was studied analytically. The strength of reinforced concrete columns under biaxial bending was examined with a view to finding the most appropriate stress-strain relationships for concrete for use in the biaxial bending analysis or design for columns. The effect of biaxial bending on the uniaxial bending strength of columns was also studied to illustrate the possibilities of designing columns for uniaxial actions only. This study is described in Chapter 8, while the conclusions drawn from the whole project are presented in Chapter 9.

CHAPTER 2

THE PLANE-FRAME INTERIOR JOINT TEST UNITS

2.1 Design of the Test Units

A series of three plane-frame interior beam-column joint test units, of the form described in Section 1.5, was designed to investigate the effects on joint performance of the beam reinforcing steel configuration and of column axial load. The size of the test units was limited by the capacity of the test rig in that the maximum axial load that could be applied to the column was 2990 kN (300 T) . It was desired to have this axial load level correspond to the maximum load level ever likely to be encountered as an extreme case for a prototype structure, so that the effect of a wide range of axial load levels could be studied. The maximum average compressive stress over the column section required during the test series was set at fifty percent of the design concrete cylinder strength of 28 MPa, and the test rig constraint thus resulted in a column size of 457 mm square (18 in square).

The beam size was selected as 610 x 356 mm, and the resulting configuration (Fig. 2.1) was felt to represent an approximately two-thirds scale model of an element of a typical frame building in the range of 10 to 15 storeys, built according to current New Zealand code requirements [31]. The two-thirds scale factor was applied to reinforcing bar sizes, to the depth of concrete cover, and to the maximum aggregate size, in order to enhance the validity of the scale model, especially in relation to the bond conditions for flexural bars across the joint. It was not expected that the scale effect would be significant in relation to general joint performance; hence the tests were expected to give valid results as full-size models for smaller buildings.

The flexural bars in the beams were chosen so that the quantity of joint ties resulting from the design procedure outlined below would not cause excessive congestion, thus allowing concrete to be placed and compacted effectively, even with extensive instrumentation included. This constraint resulted in quite lightly reinforced beams, as shown in Fig. 2.2, and Table 2.3.

Column steel and transverse steel in the flexural members were designed conservatively to ensure that failure would occur either in the beam plastic hinges, or within the joint. Generous stirruping was

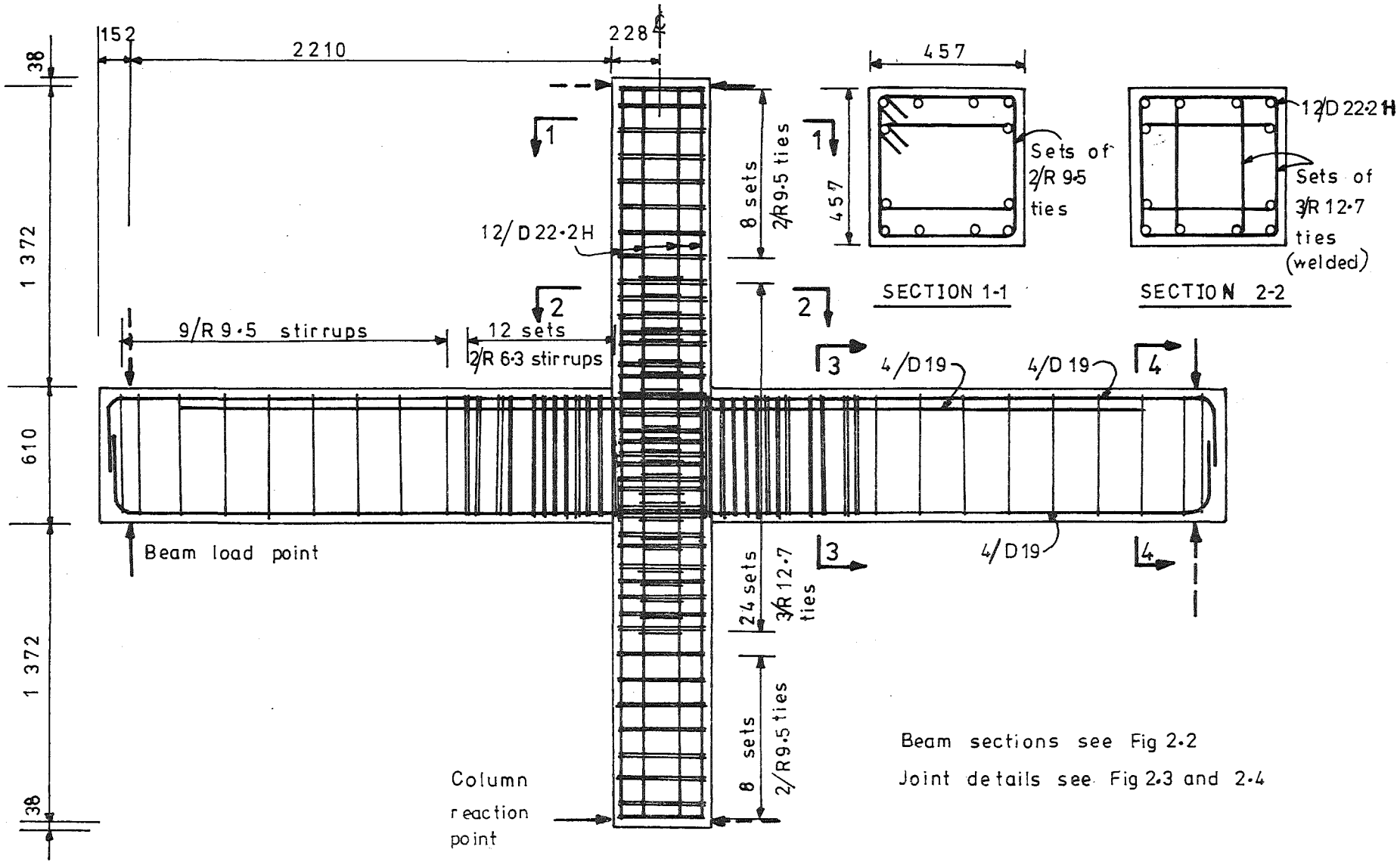

FIG. 2·1 : TEST UNIT REINFORCING UNIT B 11

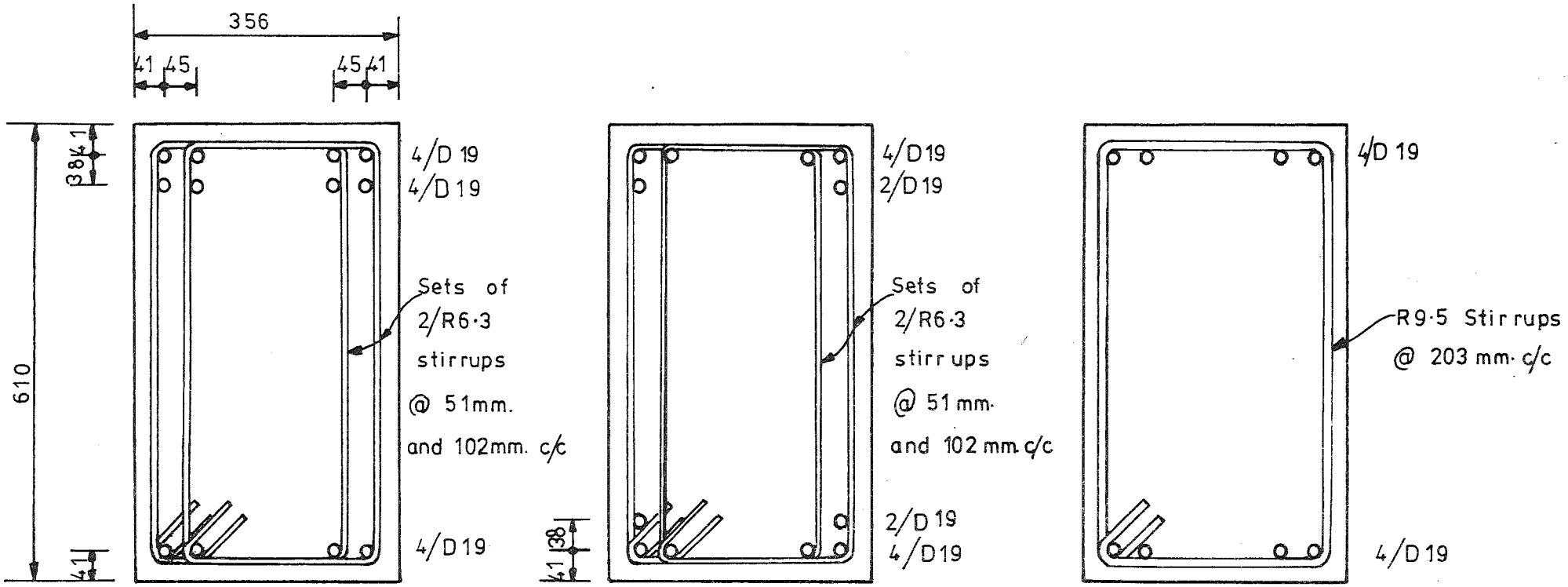

BEAM SECTION 3-3
FOR UNIT B 11 ONLY

BEAM SECTION 3-3
FOR UNITS B 12 AND B13

BEAM SECTION 4-4
ALL UNITS.

FIG. 2·2 : BEAM DETAILS.

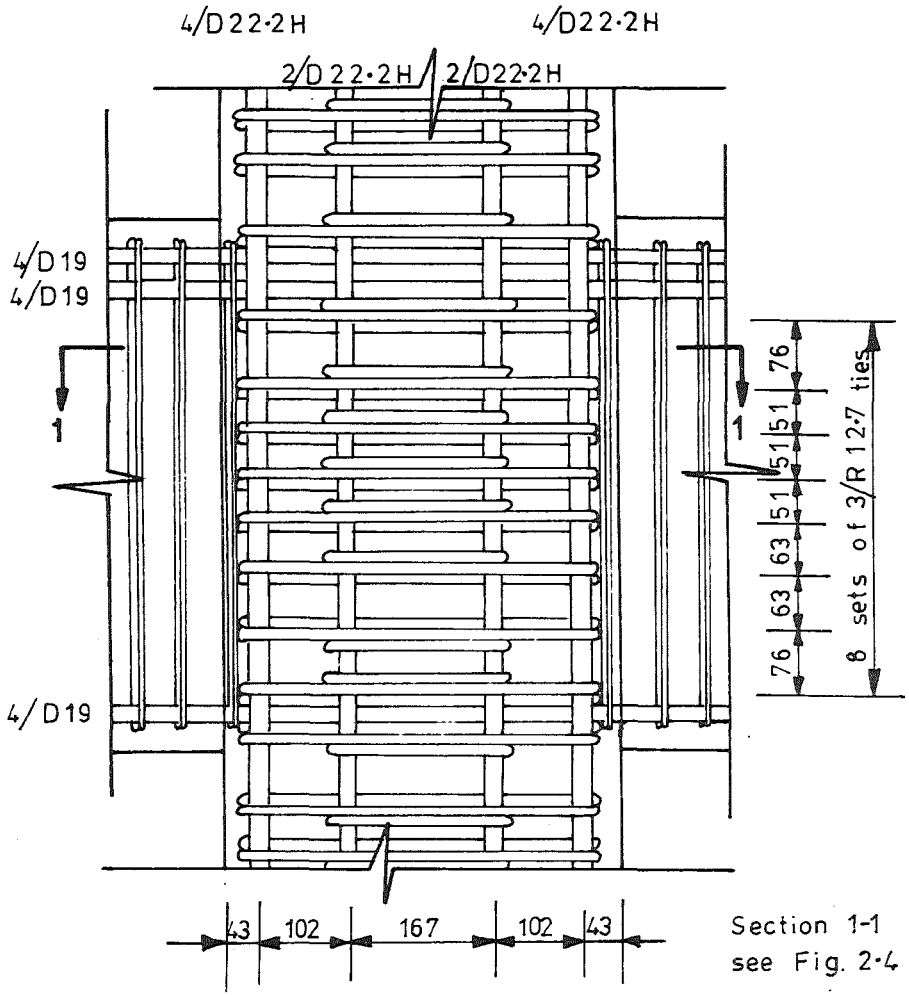

TEST UNIT B11 (B12 SIMILAR)

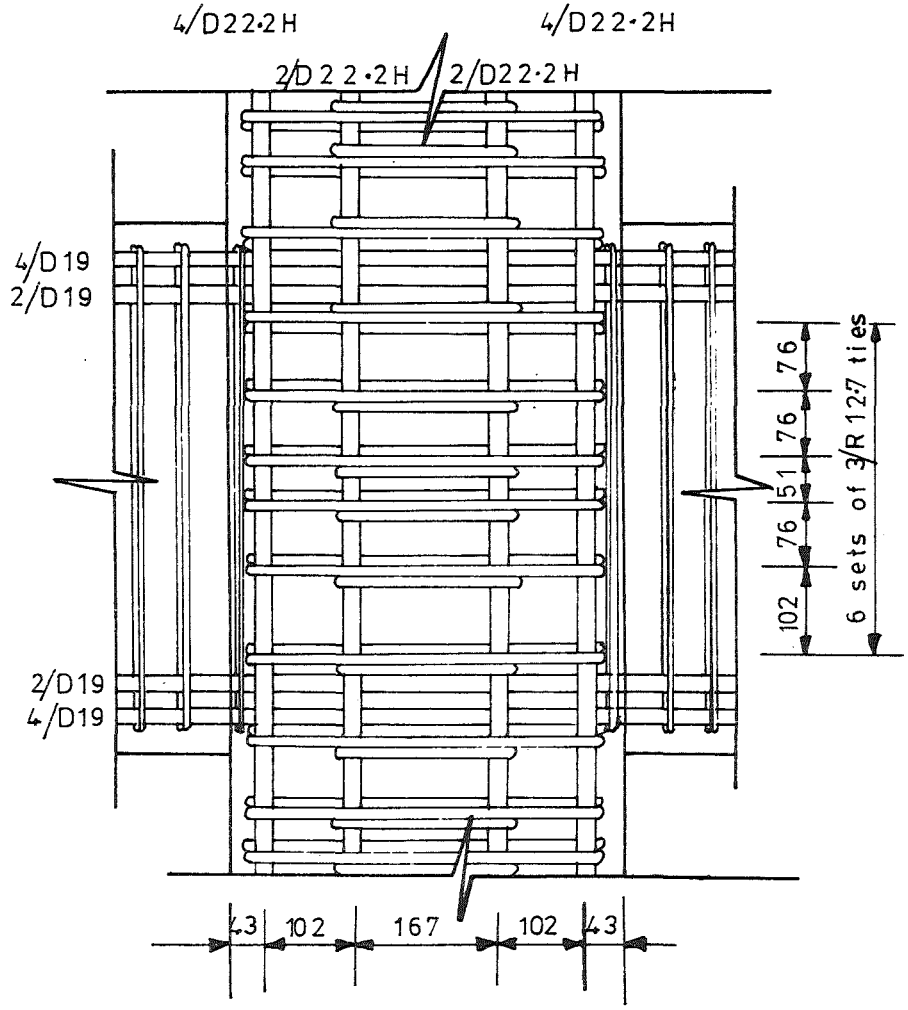

TEST UNIT B13

FIG.2·3 : JOINT REINFORCING DETAILS.

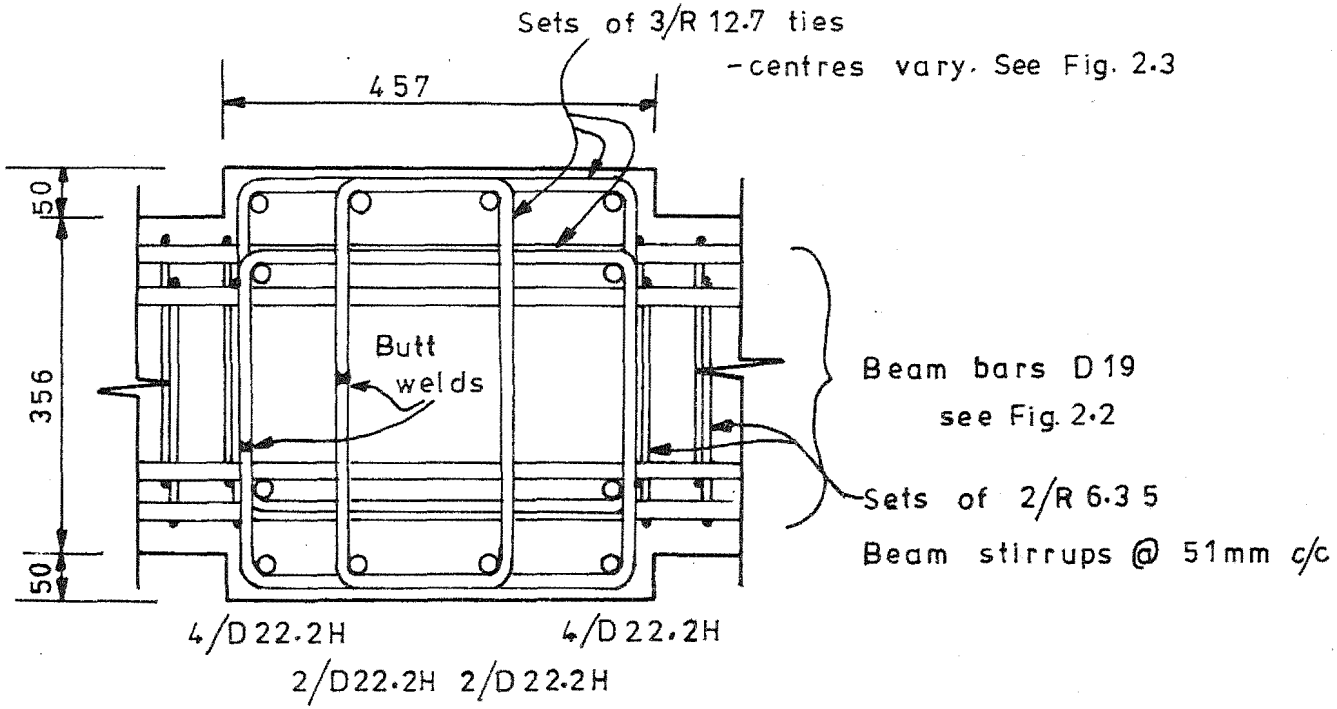

FIG 2.4: JOINT SECTION

provided in the beam plastic hinge regions in an effort to minimize strength or stiffness degradation not relevant to the immediate problem of joint behaviour.

The axial load level for the first two test units B11 and B12 was very low ($0.05f'_c A_g$). For these units the contribution of joint concrete to the resistance of horizontal joint shear was taken to be zero.

$$V_{ch} = 0 \tag{2-1}$$

The horizontal joint ties were designed as a prototype joint might be, on the basis of the nominal material properties (i.e. yield strength f_y = 275 MPa for beam and joint steel). An overstrength factor of $\alpha = 1.25$ was applied to the nominal yield strength for the beam steel to allow for an actual yield strength greater than nominal. All joint ties were assumed to be effective in resisting horizontal joint shear, but a capacity reduction factor, $\phi_j = 0.85$, was employed to reduce the likelihood of individual ties reaching yield strain because of non-uniform shear resistance down the depth of the joint.

The design equations for these joints were then as follows:

$$V_{jh} = (A_{sb} + A_{st}) . \alpha . f_{yb} - V_{col} \tag{2-2}$$

$$V_{sh} = V_{jh} - V_{ch} \tag{2-3}$$

$$V_{sh} = \phi_j \Sigma A_{sh} . f_{yh} \tag{2-4}$$

where

V_{jh} = applied joint shear in the horizontal direction
A_{st}, A_{sb} = areas of top and bottom flexural reinforcement in beam
V_{col} = column shear above joint
V_{sh} = shear resisted by reinforcement in the horizontal direction
ΣA_{sh} = total area of horizontal joint reinforcement.

Joint ties were placed in sets of three as shown in Fig. 2.4, but only long stirrup legs, i.e. those between corner column bars, were assumed to be effective in resisting shear. No shear resistance was assigned to the shorter stirrup legs between inner column bars.

For the third test unit, B13, a large column axial load ($0.50f'_cA_g$) was applied. In this case an arbitrary reduction in the joint steel content was made in the light of the preceding test results (See Section 5.1), and hence the shear assigned to the concrete was also arbitrary.

No specific design was undertaken for vertical joint shear, but the twelve column bars were distributed around the perimeter of the column section in order to provide, together with the axial load, some vertical component of shear resistance.

The quantity of joint reinforcement used in the test units was also checked against the requirements of ACI 318-77[4], Equations 10-5 and A.2 for confinement of the concrete core, but these were not found to be critical, i.e.

$$\rho_s > 0.45 \left(\frac{A_g}{A_c} - 1\right) \frac{f'_c}{f_{yh}} \qquad (2\text{-}5)$$

$$\Sigma A_{sh} = \rho_s l_h (d_b - d'_b)/2 \qquad (2\text{-}6)$$

where

ρ_s = ratio of volume of joint reinforcing to total volume of joint core.

2.2 Test Unit Dimensions and Details

The height of the test units between points of application of column shear was 3.354 m, while the length between beam end loads was 4.877 m. Details of the first unit B11 are shown in Fig. 2.1. The beam reinforcement for this unit consisted of eight D19 (No. 6)* top bars in two layers of four bars each, with four D19 bottom bars in a single layer. The cut-off lengths for the second layer of top steel were conservative, as were the quantities of stirrups provided. Stirrups in the plastic hinge regions of the beam were to scale size, while those in non-critical regions were made larger to minimize fabrication time. Spacings for stirrups in the hinge regions were somewhat irregular in order to fit around the Demec studs required for instrumentation of the beam flexural steel strains (see Section 2.5.3).

The beam sections of the other two test units were symmetrically reinforced, with six D19 bars top and bottom, arranged with four bars in the outer layer and two bars in the inner layer as shown in Fig. 2.2.

* $\frac{3}{4}$ inch diameter.

Beam and column ties in the critical regions were placed in sets of two and three respectively, to provide maximum confinement to individual flexural bars. The first set of ties in each member adjacent to the joint was placed directly against the joint ties.

Detailed drawings of the joint reinforcing are shown in Figs. 2.3 and 2.4. In order to allow instrumentation to be included, while still maintaining a density of reinforcement consistent with current prototype joints, it was necessary to utilize butt-welded ties in the joint. The drawings show that spacing of ties through the depth of the joint was not exactly uniform. This was because of interference with the instrumentation; the irregularity of spacing is probably not significantly more than that which occurs in a prototype joint without instrumentation, where ties with 135° hooked ends were used.

For unit B13 the joint steel content was reduced from eight to six sets of ties. This implied a slightly less congested joint, but welded ties were used again for consistency with the preceding units, while the spacing of tie sets within the joint could still not be made uniform because of the presence of Demec studs welded to the column bars.

2.3 Test Rig

Because the laboratory did not have a compression machine capable of accommodating a column with the desired height, it was necessary to design and build a test rig to apply the required loads to the test units. An overall view of the test set-up is shown in Fig. 2.5. The test rig comprised two separate parts, axial load being applied to the test unit column by one component, while lateral load was applied to the structure by the other component acting independently.

The axial load part of the rig utilized a 1495 kN (150 T) hydraulic ram operating on a two to one lever arm within a self-contained system to apply up to 2990 kN load to the ends of the test unit column, as shown in Fig. 2.6. The horizontal members were built-up steel box-girders, the bottom one being bolted to the strong floor of the laboratory, while the upper member was located by tubular braces. The vertical members consisted of double universal beams acting as tension ties.

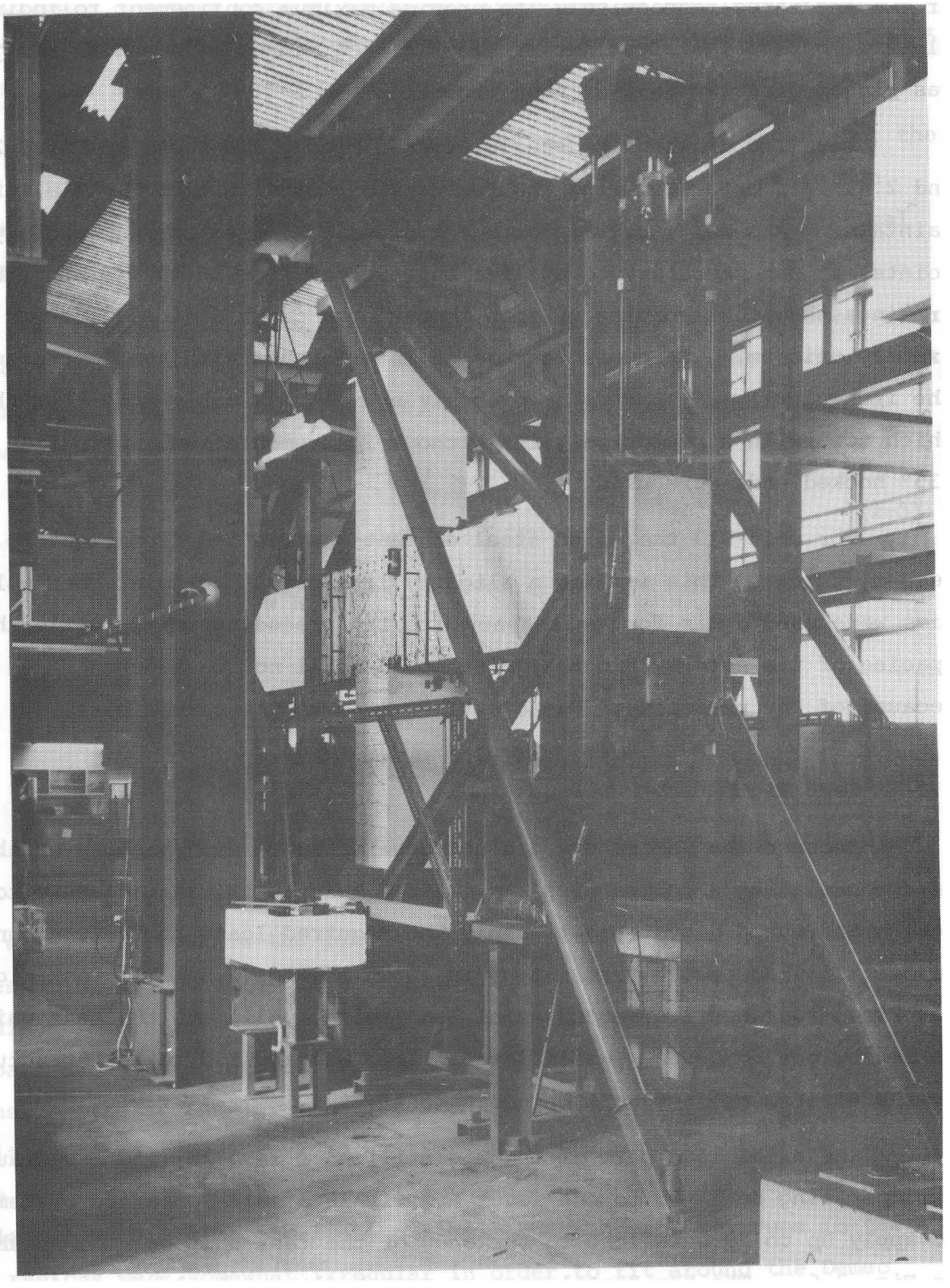

FIG. 2.5 : TEST UNIT B 11 IN TEST RIG.

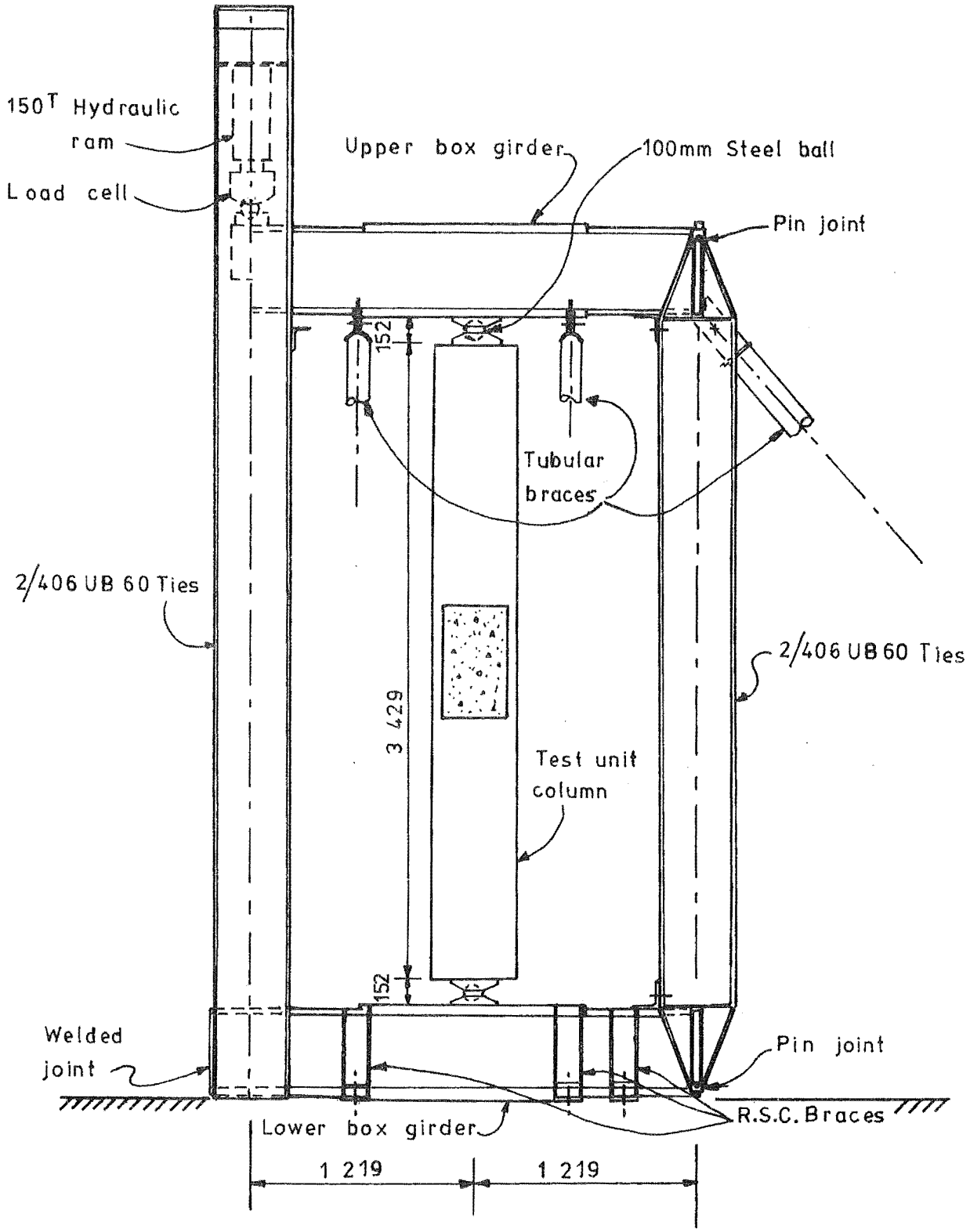

FIG.2.6 : TEST RIG - AXIAL LOADING SYSTEM

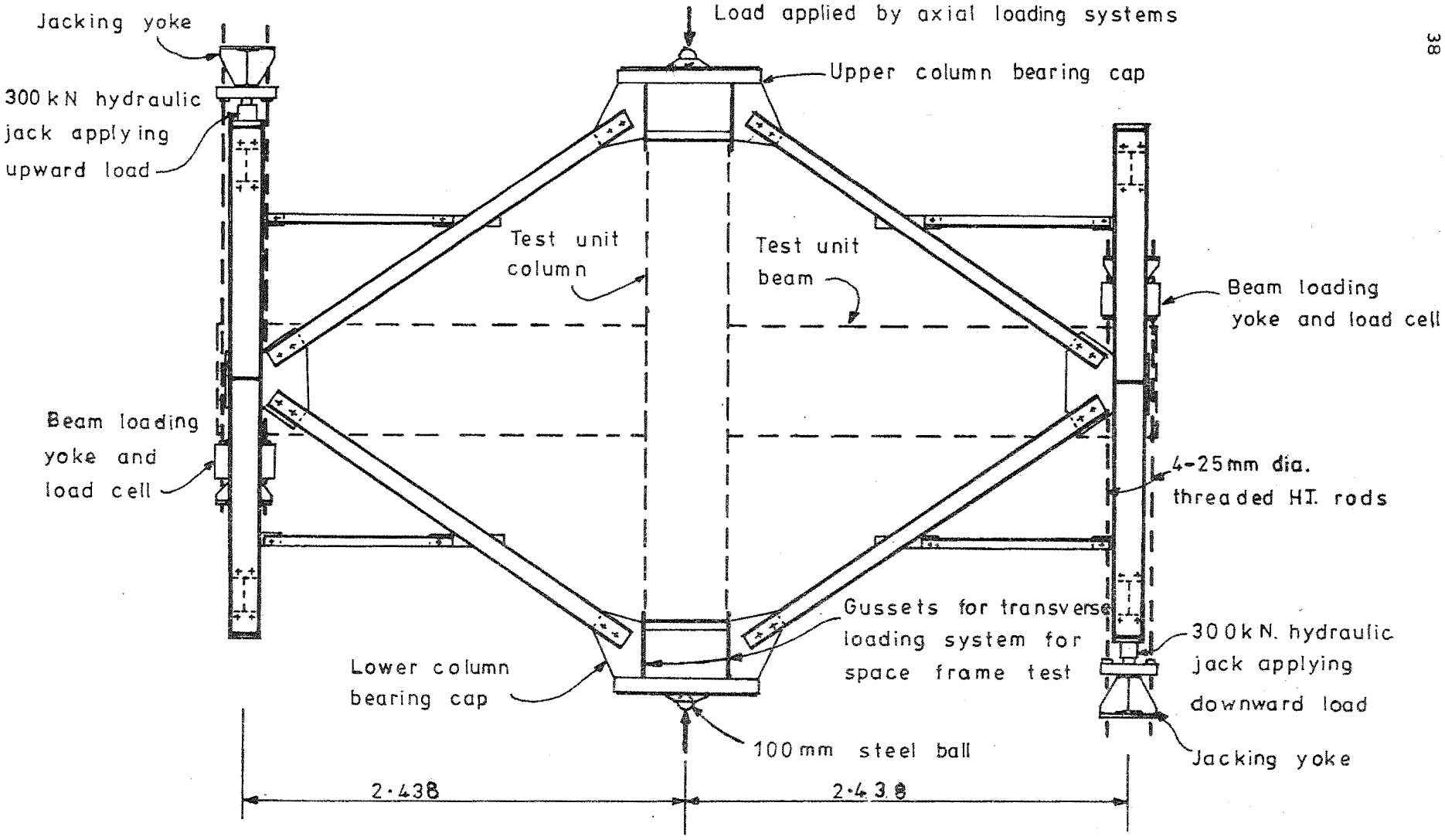

FIG. 2.7 : TEST RIG LATERAL LOADING SYSTEM

Lateral loading was introduced to the test unit as beam end loads (see Section 1.5). The rig shown in Fig. 2.7 allowed 300 kN loads to be applied to each beam end using hydraulic rams, high-tensile rods, and transverse yokes. The reactions from the hydraulic rams were transferred by diagonal members to resist the shears at top and bottom of the column. By this means the lateral loading system was made self-contained, and did not need to rely upon the strong floor for the reactions. With the axial load introduced via a 100 mm diameter steel ball top and bottom, the test unit and lateral loading system could be rotated as required so that two lateral systems could operate on the unit for the two-directional test. The bearing caps to the column were in this case the only common component of the loading systems in the two directions. The column shear was introduced in the caps by plates 75 mm in depth bearing steel to steel around the column perimeter, a reusable steel insert being built into the test unit when the reinforcing cage was assembled. The beam loads were introduced via 50 mm steel balls seated in steel bearing plates plastered against the face of the concrete above and below the beam.

To reverse the direction of lateral loading on the structure at the end of each load run, the transverse yokes, high tensile rods, hydraulic ram, and load cell had to be stripped and replaced to act in the opposite direction at each end of the beam. Various devices were attached to the rig to facilitate this operation.

A consequence of the test configuration was that the implied point of contraflexure in the members remained constant. In particular the point of contraflexure occurred at the same position under both positive and negative bending of the beams throughout the loading history. This does not occur in a prototype structure where the position of the point of contraflexure differs in the two cases, and varies throughout the loading history, depending on the relative magnitude of gravity and seismic loadings. Hence the curvature distributions measured in the plastic hinges of the test units were representative only for a structure with minimal gravity loading, but the performance of the joint itself should not have been much affected by this discrepancy. It is considered that this set-up has adequately represented the behaviour of a wider range of structures.

2.4 Manufacture of the Test Specimens

The test units for the plane frame test series were all cast on the flat, i.e. with beam and column both horizontal, and then lifted into the column-vertical position for testing. Since the maximum depth of concrete with the unit in this horizontal position was only 457 mm, it was not expected that significant gradation of concrete properties across the section would occur due to sedimentation.

A reusable mould was made from 18 mm plywood supported on a steel frame. Instrumentation was attached to the reinforcing bars and stirrups as described in Section 2.6, and the cage was then assembled in the mould, using 1.6 mm black wire ties at all accessible corners of stirrups to impart maximum rigidity to the cage. Accuracy in the placement and tying of steel was very good with a tolerance of ± 2mm being achieved in virtually all places. After building of the cage was complete it was lifted out to allow the mould to be cleaned and oiled before concreting. The completed cage for unit B12 is shown in Fig. 2.8, while Fig. 2.9 shows the relatively congested steel in the joint area.

Concrete for the test units was obtained from a commercial ready-mix plant, with properties as described in Section 2.5.2. Concrete was placed in the mould, vibrated using an internal 'spud' vibrator, and screeded off. Twelve test cylinders, 150 mm diameter by 300 mm, were made for each pour, and a slump test was also taken. After the top surface of the unit had been floated off to a smooth finish it was cured under damp sacking and polythene for seven days, the sides of the mould being also left in place for this period.

When the units were stripped, the concrete was painted with a flat white paint, and sundry items of instrumentation were added. The units were lifted at fourteen days, using hooks built into the beams, and positioned on the lower box-girder of the test rig. The remaining components of the rig were then assembled about the test body, along with the miscellaneous paraphernalia required for access, instrumentation, and communication, before the test could begin.

2.5 Material Strengths and Member Properties

2.5.1 Reinforcing steel.

The majority of the reinforcing steel used in the test series was obtained from a single delivery so that properties were consistent

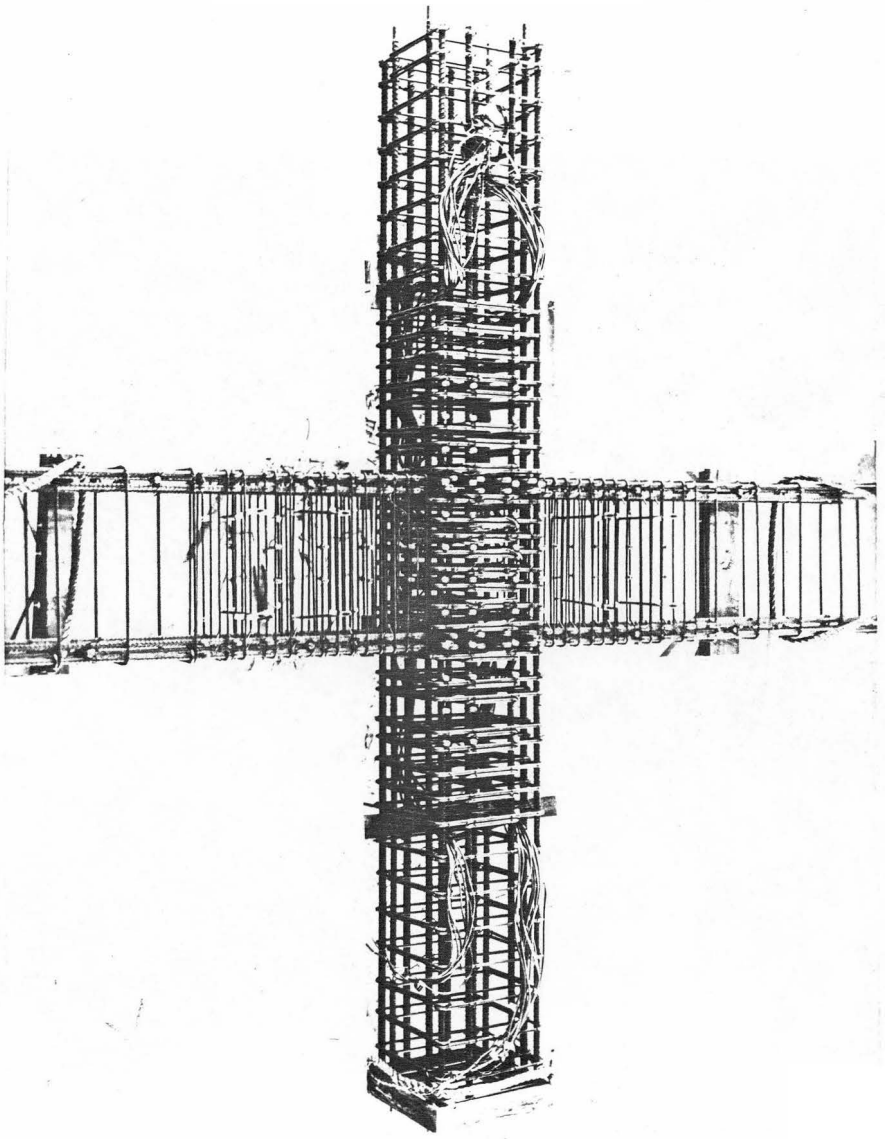

FIG. 2.8 : REINFORCING CAGE FOR UNIT B 12.

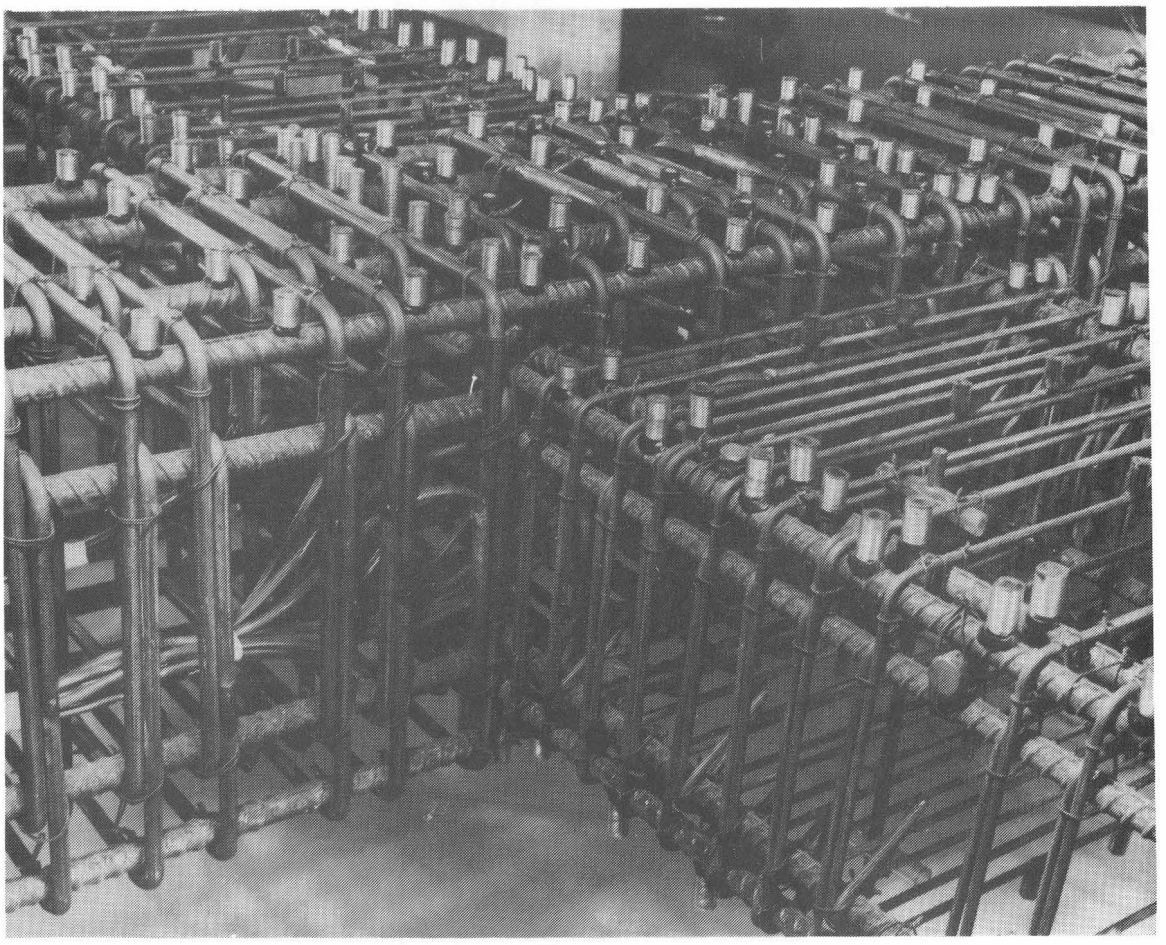

FIG. 2.9 : CLOSE UP OF REINFORCING STEEL IN JOINT AREA (UNIT B 13)

throughout. This was the case for the D19 (No. 6) deformed mild steel bar used for flexural steel in the beams, and also for all the plain round mild steel bars (R12.7, R9.5 and R6.35)* used for the ties and stirrups. The D22.2 (No. 7) deformed high yield strength bar used as longitudinal reinforcing in the columns was obtained separately for each test because the pattern of column load was not decided upon before the series began. The tensile properties of the various bars were obtained by testing under monotonic loading in a 1100 kN Avery Universal Testing Machine using a Bàty mechanical extensometer of 51 mm gauge length to monitor strain. These properties are summarised in Table 2.1, while Fig. 2.10 shows typical stress-strain curves obtained for D19, D22.2 and R.12.7 bar used in test unit B11.

TABLE 2.1 : PROPERTIES OF REINFORCING STEEL

Bar	D19.05 Grade 275 (No. 6)	R12.7 Grade 275 ($\frac{1}{2}$" ϕ)	R9.5 Grade 275 ($\frac{3}{8}$" ϕ)	R6.35 Grade 275 ($\frac{1}{4}$" ϕ)	D22.2 - Grade 380 (No.7)		
					B11	B12	B13
f_y (MPa)	297.6	336.2	331.9	329.2	422.8	422.3	397.8
f_u (MPa)	461.1	447.6	468.5	429.9	678.4	699.2	655.1
$\frac{\varepsilon_{sh}}{\varepsilon_y}$	12.90	10.84	Not measured		6.91	4.17	5.16

Since the testing of each unit extended over a significant period of time (seven weeks for units B11 and B13; four weeks for unit B12), it was necessary to check the strain ageing properties of the D19 bar, which was loaded plastically over several weeks. This was achieved by taking some samples of the bars and applying an initial plastic strain, then unloading the bars and leaving them for a fortnight. A further strain increment was then applied and the process repeated at fortnightly intervals up to eight weeks. The results of a typical test are shown in Fig. 2.11. The strain ageing phenomenon did not occur until the tensile strain in the steel was greater than the strain hardening value. When load was reapplied in this range after a time interval, the strength of the bar was found to be greater than the strength of a bar loaded monotonically or that of a bar unloaded and reloaded immediately. The stress-strain curve for the strain-aged bar tends to show another

* $\frac{1}{2}$", $\frac{3}{8}$" and $\frac{1}{4}$" diameter.

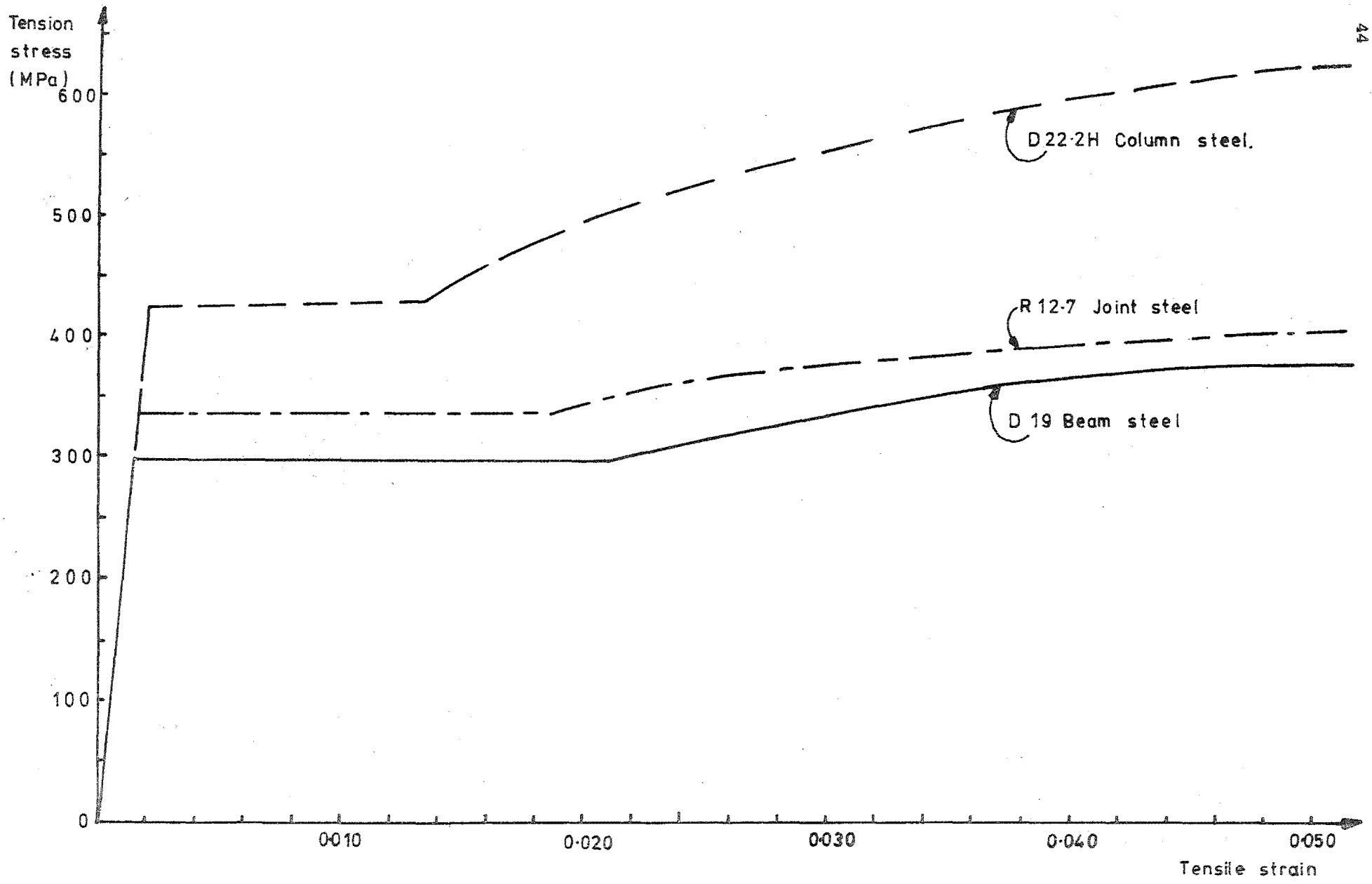

FIG. 2.10 : STRESS-STRAIN PROPERTIES OF REINFORCING STEEL

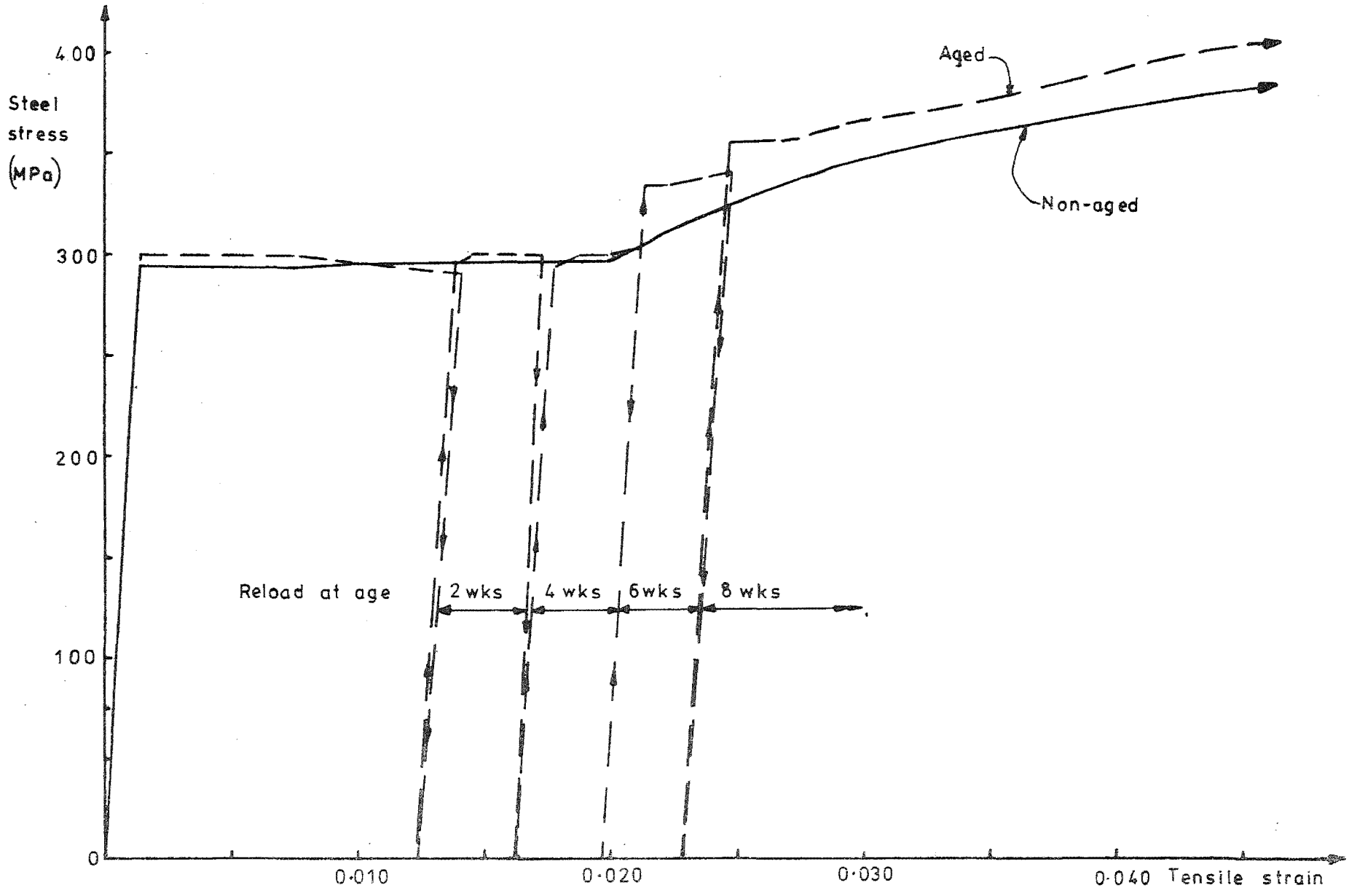

FIG. 2.11 : STRAIN AGING BEHAVIOUR FOR D19 MILD STEEL

shorter yield plateau so that the increase in strength compared to that of a non-aged bar is not uniform because the shapes of the curves are dissimilar. These results are similar to those described by Erasmus and Pussegoda[32]. The range of increase in strength found in these tests was five to nine per cent, which was quite significant in relating calculated beam steel stresses from experimental strain histories to the applied loads. Conversion of steel strain data to stresses was achieved using a computer program developed by Spurr[33] to represent the Bauschinger effect in mild steel under cyclic loading. The envelope of stresses used by the program was the monotonic stress-strain curve for the steel, so that the increase in available strength due to strain ageing would have led to some discrepancy. This feature is discussed further in Section 3.3.

2.5.2 Concrete.

Concrete for the test units was obtained from a commercial ready-mix plant. The specified guaranteed crushing strength at twenty eight days was 24 MPa, while a 75 mm slump and 12.5 mm maximum aggregate size were specified to ensure efficient compaction. The actual properties are listed in Table 2.2. Cylinder strengths were obtained from 150 x 300 mm cylinders tested in a 2600 kN Avery Universal Testing Machine, taking the mean result for six cylinders at twenty eight days, and again at the beginning of the actual test for each unit. Stress-strain properties were obtained for the cylinders at the time of testing, using two Demec strain gauges (see Section 2.6) on 202 mm (8 in.) gauge lengths diametrically opposite on the mid-depth of the cylinder. A typical stress-strain curve obtained for concrete used in unit B11 is given in Fig. 2.12.

2.5.3 Member Properties.

The theoretical strengths and properties of the members of the test units are listed in Table 2.3. The theoretical beam yield loads P_y are such as to cause yield strain in all the tension steel of the appropriate beam section at the column face, assuming a linear strain profile over the depth of the section, a linear stress-strain relationship for the concrete, and zero tensile strength in the concrete. The beam ultimate loads P_u are such as to cause the ultimate flexural strength of the section to be attained at the column face, assuming a linear strain profile, steel stress not greater than the measured yield strength, and

TABLE 2.2 : CONCRETE PROPERTIES

Unit	B11	B12	B13
Slump (mm)	80	120	90
f'_c 28 days (MPa)	34.7	34.2	28.9
Age at test (days)	47	31	57
f'_c at test (MPa)	35.9	34.6	31.4
ε_o	0.0025	0.0025	0.0020

using a conventional equivalent rectangular stress block to represent the stress distribution in the compressed concrete, with a maximum strain in the concrete of 0.003, as recommended by ACI 318-71[4], Clause 10.2.7. The difference between the externally applied upward and downward loads for the symmetrically reinforced beams is due to the dead load (self weight), for which allowance has been made.

The properties of the respective column sections are given in Table 2.3 both for the nominal material properties, on which the design was based and by which the axial load levels were set, and also for the actual material properties.

Both the design and the actual quantities are given in Table 2.3 for the joint properties. The design quantities are derived using the nominal material properties, with a stress multiplier, $\alpha = 1.25$, being applied to the beam steel yield strength to give the input shear. However, the input shear given for the actual case is based only on the measured beam steel yield stress, with $\alpha = 1.0$, no account being taken in the calculation of possible excursions into the strain-hardening range. During the course of the tests the beam steel did in fact enter the strain-hardening range when the units were under maximum displacement. Hence the input shears given in Table 2.3 are less than the maximum shears actually imposed during the tests.

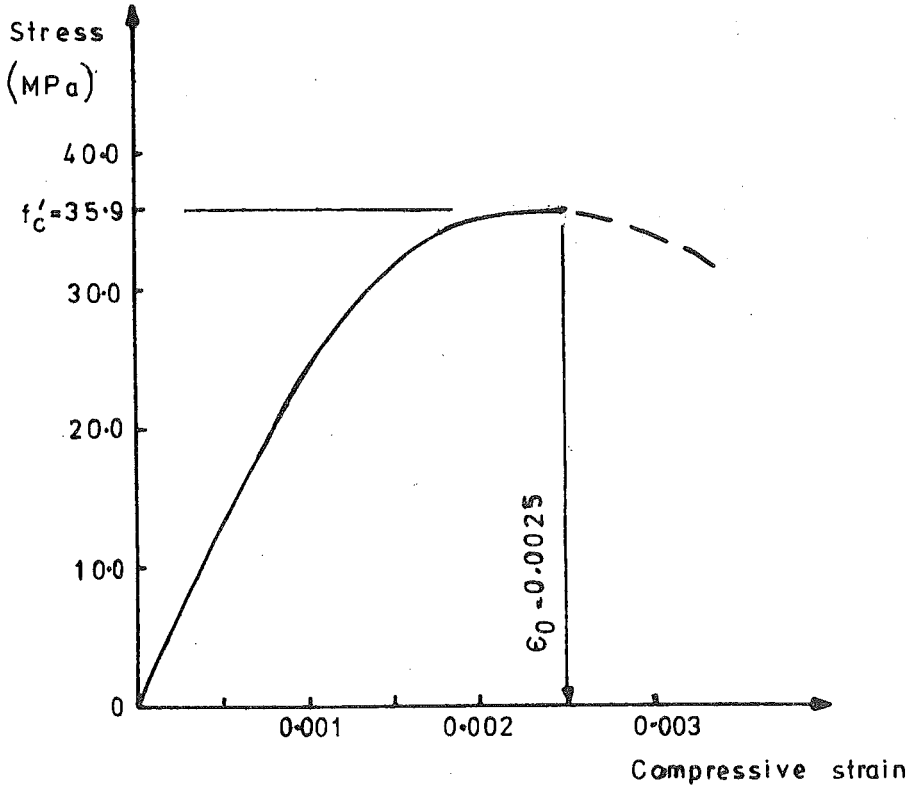

FIG. 2.12 : STRESS-STRAIN CURVE FOR CONCRETE UNIT B11

TABLE 2.3 BEAM, COLUMN, AND JOINT PROPERTIES AND THEORETICAL STRENGTHS*

	Unit	B11	B12	B13A	B13B
	Beam top bars	8/D19(#6)	6/D19	6/D19	
	ρ_T	0.0112	0.0086	0.0086	
	ρ_T/ρ_b	0.228	0.175	0.175	
	Beam bottom bars	4/D19(#6)	6/D19	6/D19	
	ρ_B	0.0056	0.0086	0.0086	
	ρ_B/ρ_b	0.114	0.175	0.175	
	P_y(up) (kN)	86.82	122.98	122.66	
	P_y(down) (kN)	145.93	110.08	109.76	
	P_u(up) (kN)	96.22	130.72	129.33	
	P_u(down) (kN)	153.04	117.83	116.44	
	Column bars	12/D22.2 (#7)	12/D22.2	12/D22.2	
	ρ_T	0.022	0.022	0.022	
	N_{col} (kN)	311	311	2890	1677
Based on actual material properties	N_{col}/N_b	0.115	0.117	1.130	0.655
	N_{col}/N_o	0.038	0.039	0.396	0.230
	$N_{col}/f'_c A_g$	0.043	0.044	0.441	0.255
Based on design material properties	N_{col}/N'_b	0.135	0.135	1.258	0.730
	N_{col}/N'_o	0.046	0.046	0.430	0.250
	$N_{col}/(f'_c A_g)'$	0.054	0.054	0.501	0.290
	Joint Reinforcement	8 sets x 3 ties R12.7($\frac{1}{2}$")	8 sets x 3 ties R.12.7	6 sets x 3 ties R12.7	
	A_{vj} (mm^2)	4130	4130	3097	
Based on actual material properties	V_{jh} (kN)	844.8	844.7	844.7	
	v_{jh} (MPa)	5.31	5.31	5.31	
	$v_{jh}/\sqrt{f'_c}$ **	0.89	0.90	0.95	
	V_{sh} (kN)	1178.3	1178.3	883.7	
	V_{ch} (kN)	0	0	0	
Based on design material properties	V'_{jh} (kN)	978.6	978.5	978.5	
	v'_{jh} (MPa)	6.15	6.15	6.15	
	$v'_{jh}/\sqrt{f'_c}$ **	1.17	1.17	1.17	
	V'_{sh} (kN)	967.9	967.9	725.9	
	V'_{ch} (kN)	10.7	10.6	252.6	

* See notes on page 50. ** $\sqrt{f'_c}$ in MPa units.

Notes to Table 2.3

$\rho_T = \frac{A_{ST}}{b.d}$ = top reinforcement content of beam

$\rho_B = \frac{A_{SB}}{b.d}$ = bottom reinforcement content of beam

ρ_b = reinforcement content to cause balanced failure of beam

P_y = calculated beam end load to cause the measured yield strain to be attained in all beam tension reinforcement at the column face

P_u = calculated beam end load to cause ultimate flexural strength of beam section to be attained at column face, assuming steel stress does not exceed the measured yield strength, maximum concrete strain = 0.003

$\rho_t = \frac{A_{st}}{b.h}$ = total reinforcement content of column section

N_{col} = axial load applied to column (compression)

N_b = calculated axial load to cause balanced failure of column, i.e., concrete reaching maximum strain of 0.003, simultaneously with tension reinforcement reaching yield strain

$N_o = 0.85f'_c A_g + A_{st} f_y$ = calculated ultimate axial load capacity of column

f'_c = cylinder crushing strength of concrete

A_g = gross area of column section

A_{vj} = total area of joint reinforcement in the shear direction

V_{jh} = joint horizontal shear

v_{jh} = average nominal shear stress on joint core

V_{sh} = horizontal joint shear resisted by joint reinforcement mechanism

V_{ch} = horizontal joint shear resisted by joint concrete mechanism

2.6 Instrumentation

2.6.1 Measurement of Loads.

The major divisions of instrumentation employed in the tests may be taken as measurement of load and measurement of deformation. The loads measured were the column axial load and the two beam end loads. The column axial load was measured by a 1500 kN load cell placed directly beneath the loading ram. Therefore the load at the column head was obtained by multiplying the load cell reading by two and by adding a correction for the weight of that part of the test rig above the column which was not measured by the load cell.

Load cells of 500 kN capacity were used to measure the beam end loads. These load cells had strain gauges arranged in double circuits to give two outputs. One output from each load cell was read directly using a Budd Strain Indicator against which it had been calibrated in a testing machine. The second load cell output was used to drive the Y-axis of a Hewlett-Packard X-Y Pen Recorder, of which the X-axis was driven by the signal from a Linear Variable Displacement Transducer, fixed to measure the appropriate beam end displacement. By this means an instantaneous plot of beam load vs end displacement was obtained for each beam as the test progressed. This was very useful in controlling and monitoring the overall progress of the test. All load cell outputs were calibrated against a testing machine both before and after each test, in order to check for possible drift in their characteristics; however this was never found to be significant.

2.6.2 Measurement of Displacements.

Because of the time and expense required for the manufacture of each test unit, it was desirable to extract the maximum possible information from each test, and hence the instrumentation for measurement of deformation was extensive. Nineteen 50 x 1.00 Mitutoyo dial gauges were employed to measure the displacement of the test body as shown in Fig. 2.13. Small brass plates were fixed to the concrete surface to provide smooth surfaces for the dial gauge stems to butt against. Because of the interference of the loading yokes, dial gauges could not be placed directly beneath the beam ends, and thus displacement was therefore transferred inwards towards the column by a system of cables and pulleys. Corrections for the horizontal component of the cable movement were applied during reduction of the data.

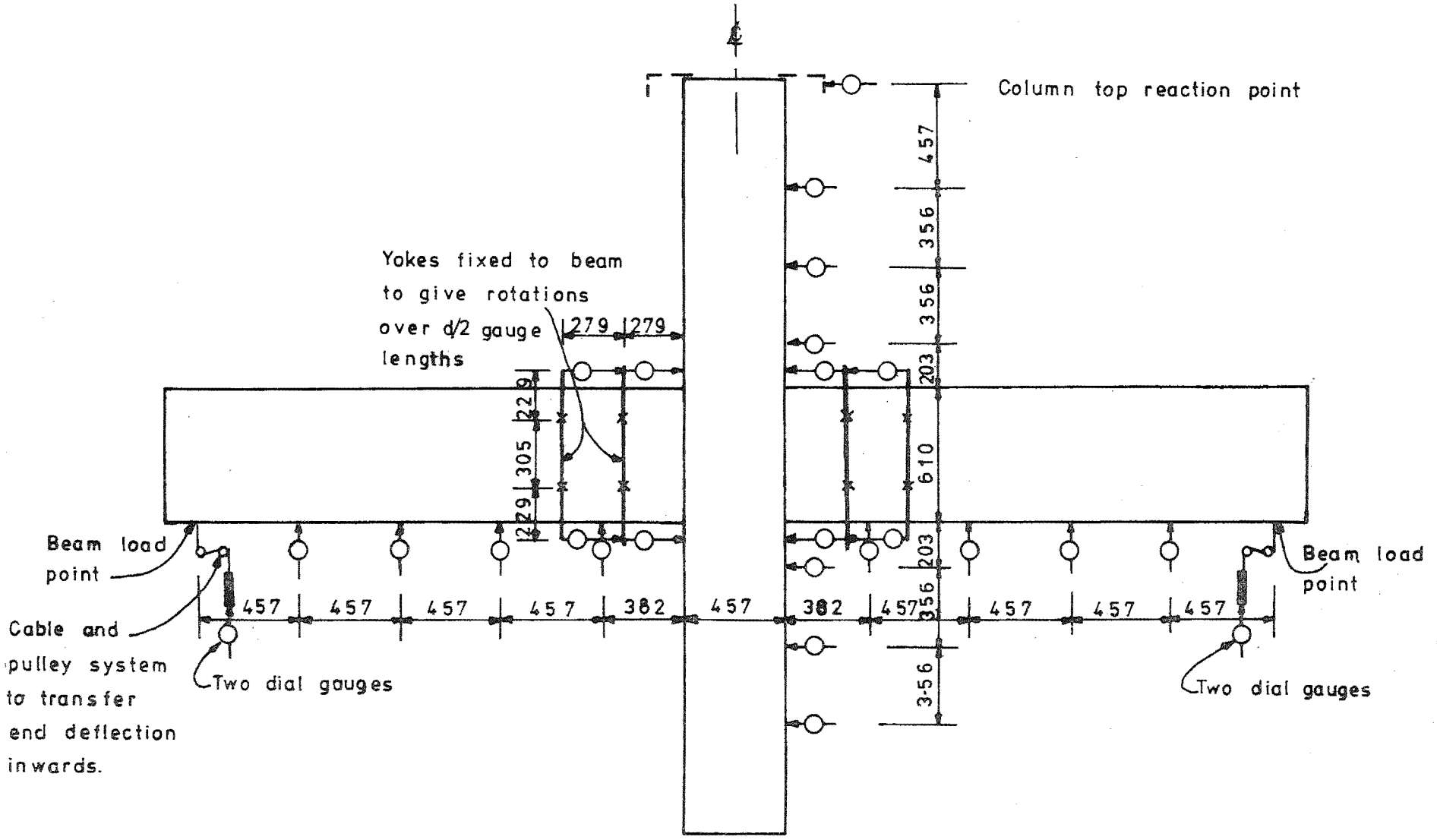

FIG. 2.13: POSITIONING OF DIAL GAUGES

Eight further dial gauges were used to measure the rotation of the beam in the plastic hinge region. These dial gauges were fixed to steel yokes attached to the beam at 280 mm intervals from the column face. This gauge length was equal to half of the effective depth of the beam section. The rotations measured in the inner gauge lengths, i.e. those immediately adjacent to the column, included a component due to joint distortion. An appropriate correction was therefore subtracted from these results when the data was reduced. When slip of the beam flexural steel through the joint occurred this also contributed to the apparent rotation measured in the inner gauge length.

2.6.3 Measurement of Steel Strains.

Steel strain results were obtained by a variety of means. Strains for beam flexural steel, column flexural steel, and beam stirrups were obtained using 100 mm Demountable Mechanical (Demec) strain gauges which gave strain results accurate to within 20×10^{-6}. To obtain these readings it was necessary to project the strains in the outer bars of the members to the face of the concrete. This was achieved by welding 10 mm diameter studs to the outer bars, and by fixing the drilled Demec points to the ends of these studs after the formwork had been stripped from the concrete. To allow for unrestricted differential movement between the concrete cover and the reinforcing steel, an annular space was provided around each stud using a length of 16 mm plastic tubing and a soft wire spiral. These were withdrawn after stripping. A channel-shaped extension to the stud was used to provide readings across the 50 mm step at the column face resulting from the difference in breadth of the members. Strains from the beam bars were recorded simultaneously from both faces of the beam, and the average of these results was used. Because of the congestion of reinforcement in the joint and the necessity to provide Demec studs at fixed 100 mm intervals, it was impossible to incorporate studs on both faces for the column bars through the joint, and hence these strains were recorded from one face only. The locations of Demec studs for unit B12 are shown in Fig. 2.14. Other units were similar.

Because of the possibility of extensive yielding of the joint reinforcement, allowing the joint to bulge outwards and thus to cause outward bending of the ties, Demec studs fixed to the tie legs could not be relied upon to provide accurate strain information for the joint ties. (This phenomenon is explained by Renton[34].) It was desired

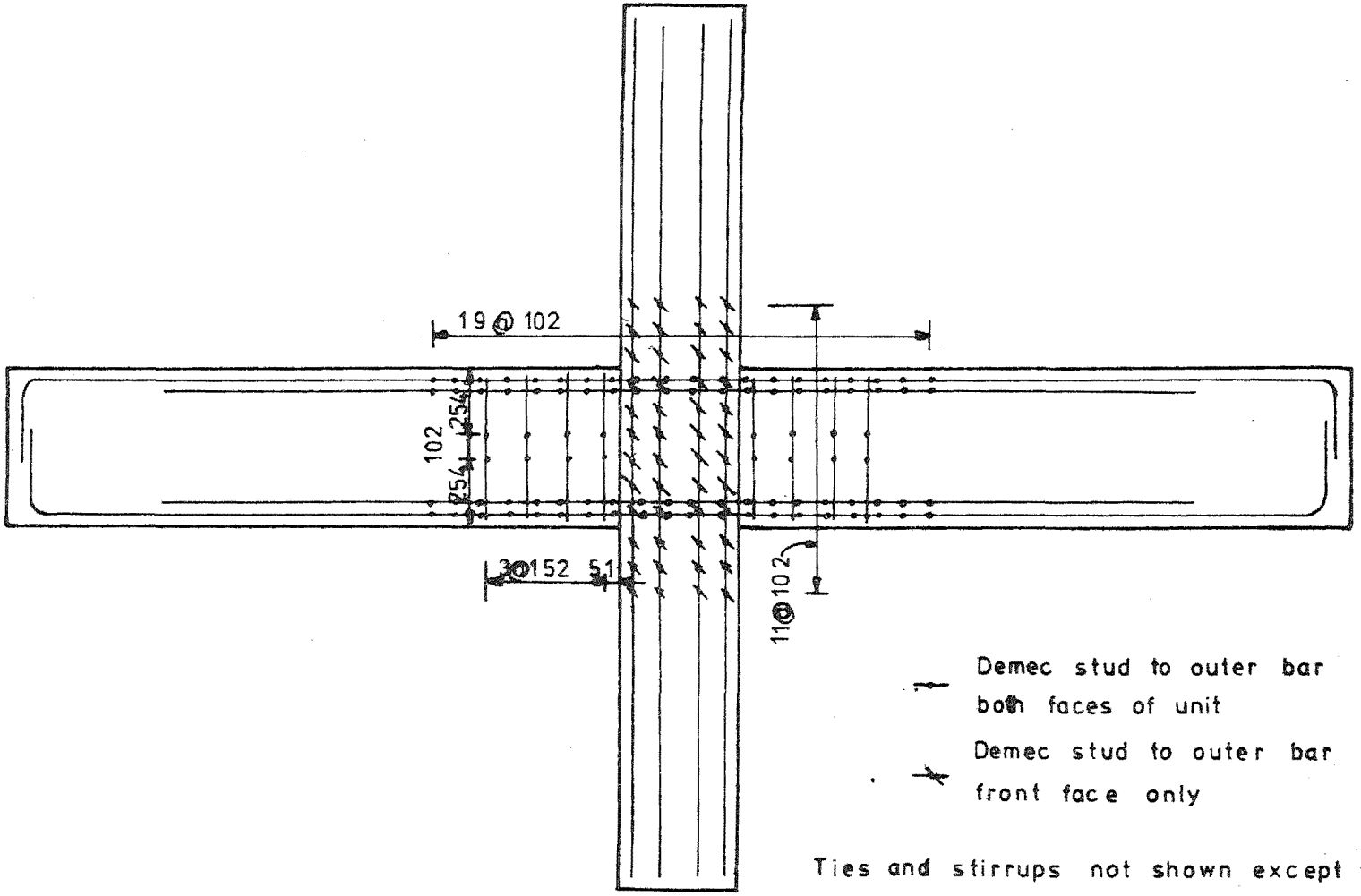

FIG.2.14 : LOCATION OF DEMEC STUDS FOR TEST UNIT B12

to obtain strain information at different points along the length of at least some tie legs, but since it was expected that the fixing of electrical resistance strain gauges at several points would disrupt the bond characteristics of the bar while the large number of leads to be carried through the joint core concrete could significantly reduce its strength, this was not regarded as a suitable method. The instrument used to provide this information was a Pfender Contact strain gauge. This is a mechanical strain gauge with a 100 mm gauge length, utilizing 1.6 mm diameter steel balls punched into the outer surface of the tie. Holes to provide access for the legs of the instrument to fit onto the balls were formed by short lengths of 12 mm I.D. steel tubing tack-welded to the ties. The Pfender gauge provided three strain readings at 100 mm intervals for each of four tie legs in each test unit. Side cover to the tie steel was reduced to 12 mm to improve the accessibility for the instrument.

To provide further information on the strains in the tie legs, especially those away from the concrete surface, electrical resistance strain gauges were employed. The number and distribution of these varied somewhat between the different units as shown in Fig. 2.15. The strain gauges used were Shinkoh Fl24-8-Tll 120 ohm foil gauges of 25 mm gauge length with a gauge factor of 2.19, fixed to the bars with Eastman 910 strain gauge cement after the bar had been polished smooth with fine emery cloth. Various precautions were taken to protect the gauges against the impact of aggregate during placing of the concrete, and to provide sufficient resistance to earth in the concrete environment. The primary protection in all cases was two applications of Shinkoh SN4 synthetic rubber waterproofing compound. For unit Bll this was covered by a block of Araldite epoxy placed in a mould over the strain gauge and terminal strip, but it was subsequently felt that this method provided too rigid a projection from the surface of the steel so that the Araldite block could be displaced by movement of the concrete cover. Hence the protection for the next two units was made more flexible. The covering used was Phillips PR9258 strain gauge sealing compound, covered with Expandite '5-Minute Epoxy' to harden and smooth the interface of the concrete. This system of protection was found to be both more reliable and easier to apply than the Araldite. In all cases it was endeavoured to minimize the area of the stirrups covered by the waterproofing so as to reduce the resultant disruption of bond. The leads from the strain gauges were encased in

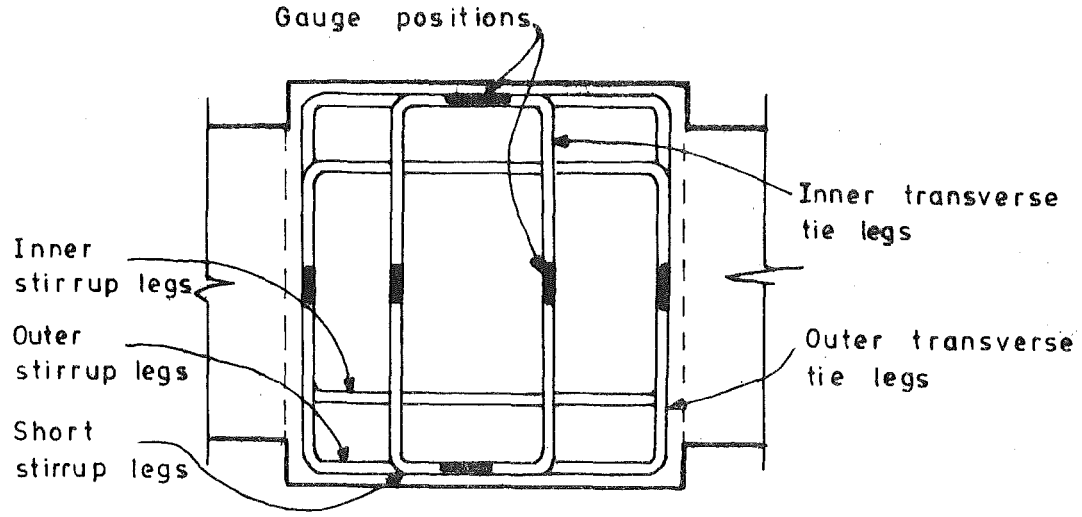

Unit	B 11	B 12	B 13
No. of instrumented tie sets	10	10	8
No. of strain gauges -on inner stirrup legs	10	10	8
-on outer stirrup legs	6	6	4
-on short stirrup legs	0	4	4
-on inner transverse tie legs	10	6	6
-on outer transverse tie legs	8	10	10

FIG. 2.15 : DISTRIBUTION OF ELECTRICAL RESISTANCE STRAIN GAUGES

plastic 'spaghetti' for extra insulation, and routed out of the concrete via the column above and below the joint, emerging from the face of the concrete about 700 mm away from the joint.

For the tests of units B11 and B12 the strain gauge results were recorded on an EDAC 200 channel strain logger which gave results accurate to 10 microstrains. Between the tests of units B12 and B13 the logger developed a fault which could not be repaired immediately so a 50-way manual switchbox and a Budd Strain Indicator were used instead.

2.6.4 Other Measurements

In order to assess the shear distortion of the joint panel, a 202 mm Demec gauge was modified to allow the deformations of the joint diagonals to be measured over a gauge length of 600 mm. This device was used successfully, although some measurements were not available during the test of unit B11 because the range required of the instrument was greater than expected. This limitation was rectified for the subsequent tests. By referring to Fig. 2.16 it may be seen that the shear strain γ is derived from the diagonal displacements Δ_1 and Δ_2 as follows:

$$\gamma_1 = \frac{0.5\Delta_1 \cdot \sin\theta + 0.5\Delta_2 \cdot \sin\theta}{D \cos\theta} \qquad (2\text{-}7)$$

$$\gamma_2 = \frac{0.5\Delta_2 \cdot \cos\theta + 0.5\Delta_2 \cdot \cos\theta}{D \sin\theta} \qquad (2\text{-}8)$$

$$\gamma = \gamma_1 + \gamma_2 = \frac{\Delta_1 + \Delta_2}{2D} \left(\tan\theta + \frac{1}{\tan\theta}\right) \qquad (2\text{-}9)$$

where θ = inclination of the joint diagonal to the horizontal

D = length of the joint diagonal.

During the test of unit B12 the shear distortions in the beam plastic hinges were observed visually from a grid pencilled on the concrete surface. For the test of unit B13 these quantities were measured by taking further readings of diagonal displacements along the beam.

Cracks on one face of each test unit were marked on the white painted surface with felt-tip pens as they were observed. Photographs of the unit were taken at the maximum displacement of each run, and at other increments as required. Because of the interference of the test rig it was necessary to take the photographs in sets of three to provide a full coverage of the unit. Crack widths were measured as required using an

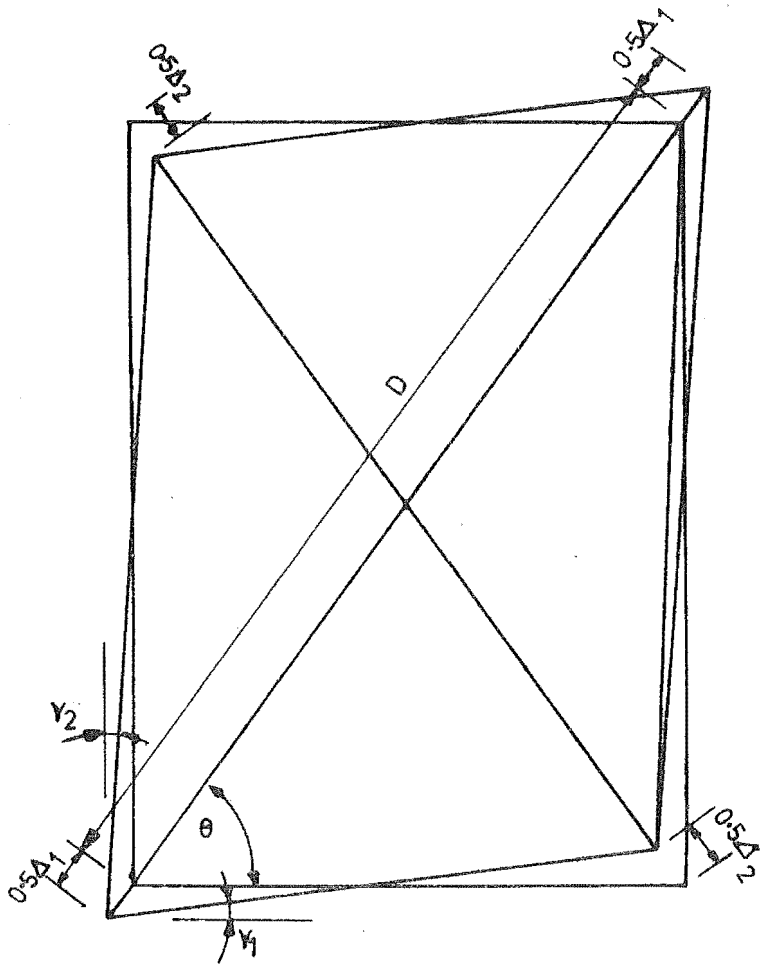

FIG. 2·16: SHEAR DISTORTION OF JOINT PANEL

Ultra-Lomara crack microscope, with particular attention being paid to the cracks in the joint panel.

2.7 Test Loading Sequence and Procedure

2.7.1 Definition of Displacement Ductility Factor.

In order to simulate seismic loading on the structure, one beam of the test unit was loaded upwards and the other downwards for one load run, the loads were released when the prescribed maximum load or displacement was attained, and the loads were then reapplied in the reverse directions, to complete a full cycle. The loading sequence for the tests consisted of four initial load runs to three quarters of the theoretical yield loads P_y for each beam (see Table 2.3), followed by a series of post-elastic load runs controlled in terms of the beam end displacements to prescribed displacement ductility factors determined as described below.

Beam displacements in all cases were applied symmetrically about the original zero line. It is recognised that this represents a somewhat artificial situation as several computer-based studies[6,35] of the inelastic behaviour of reinforced concrete structures under actual earthquake attack have shown the tendency for structures to develop a permanent set during the first major inelastic excursion of the structure's response, and for subsequent oscillations to occur about an off-centre position. However, for comparison with other test programs, and because of the uncertainty inherent in deciding what would be a representative zero shift at any given level of cyclic displacement, it was decided not to incorporate this feature in the loading program.

The displacement ductility factors for the post-elastic cycles were defined in terms of an experimentally derived yield deflection of the beam ends, Δ_y, obtained by extrapolating the mean of the observed deflections, Δ_1, under $0.75P_y$ in the first load run, to that at $1.0P_y$, as illustrated in Fig. 2.17.

$$\Delta_y = \frac{4}{3} (\Delta_{1\,up} + \Delta_{1\,down}) /2 \qquad (2\text{-}10)$$

This extrapolation procedure was adopted because of the difficulties inherent in searching for an experimental yield deflection during the first inelastic load run. The presence of two layers of tension reinforcement in most cases caused some rounding of the load-deflection curves in the vicinity of the 'yield point', while the

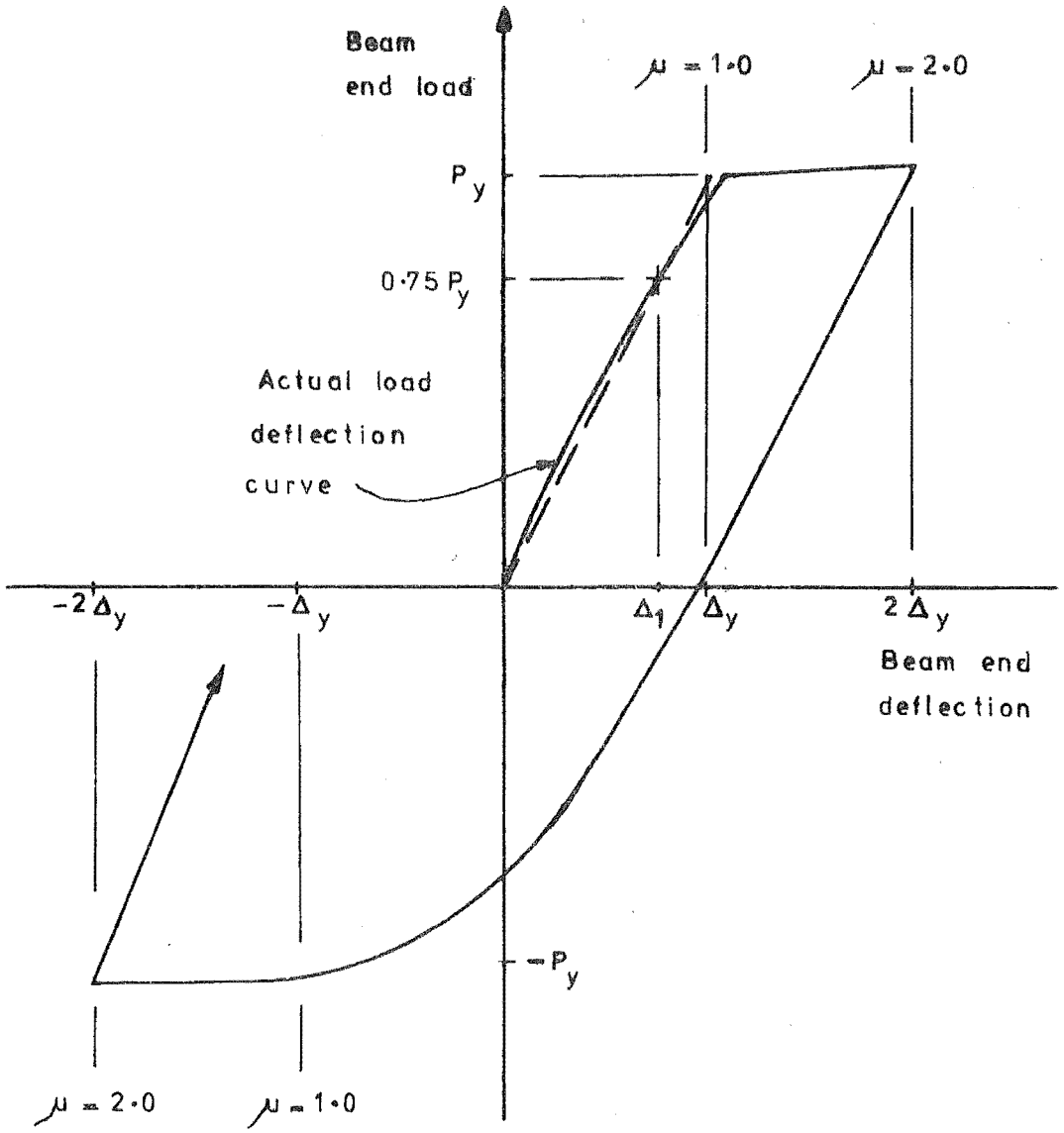

FIG.2·17: DEFINITION OF DISPLACEMENT DUCTILITY FACTOR

different properties under positive and negative bending of the beams of unit B11, due to the unequal reinforcing configuration, would have made the direct determination of a yield deflection for the unit very approximate. Also, since the test set-up did not allow continuous monitoring of beam steel strains, and because of possible differences between the strains in individual bars, it was not considered that the definition of yield displacement from these strain results would be a satisfactory alternative.

The displacement ductility factor for any stage of post-elastic loading was then:

$$\mu = \Delta/\Delta_y \qquad (2\text{-}11)$$

Under reversed loading the displacement ductility factor was defined with respect to the original zero displacement axis, rather than from the point of residual deflection at zero load, as shown in Fig. 2.17. This definition of ductility imposed quite severe demands on the test units in that a complete reversal of the displacement ductility factor from say +4.0 to -4.0 would seldom, if ever, occur in an actual structure under earthquake attack. However, the cyclic loading pattern used was not intended to simulate any particular earthquake, but rather to provide a suitable performance test in a manner that conforms with the New Zealand loading code[1], and with other tests undertaken in this country[15,17]. Consistent use of such a loading pattern should assist greatly in making meaningful comparisons between the results of various tests on reinforced concrete subassemblages.

2.7.2 Cyclic Loading Sequence.

The loading sequence for the tests of units B11 and B12 is illustrated in Fig. 2.18. After the two initial elastic cycles, inelastic cycles were applied at progressively larger displacement ductility factors, with two full cycles being imposed at each level of ductility. The object of progressively increasing the ductility demand on the structure was to define as closely as possible the ductility demand at which a failure in the unit might occur, and to observe the behaviour both before and after any such failure. The intermediate cycles to displacement ductility factor $\mu = 0.75$ were included on the basis that cyclic behaviour under actual seismic attack would not consist merely of increasingly larger post-elastic cycles. The smaller

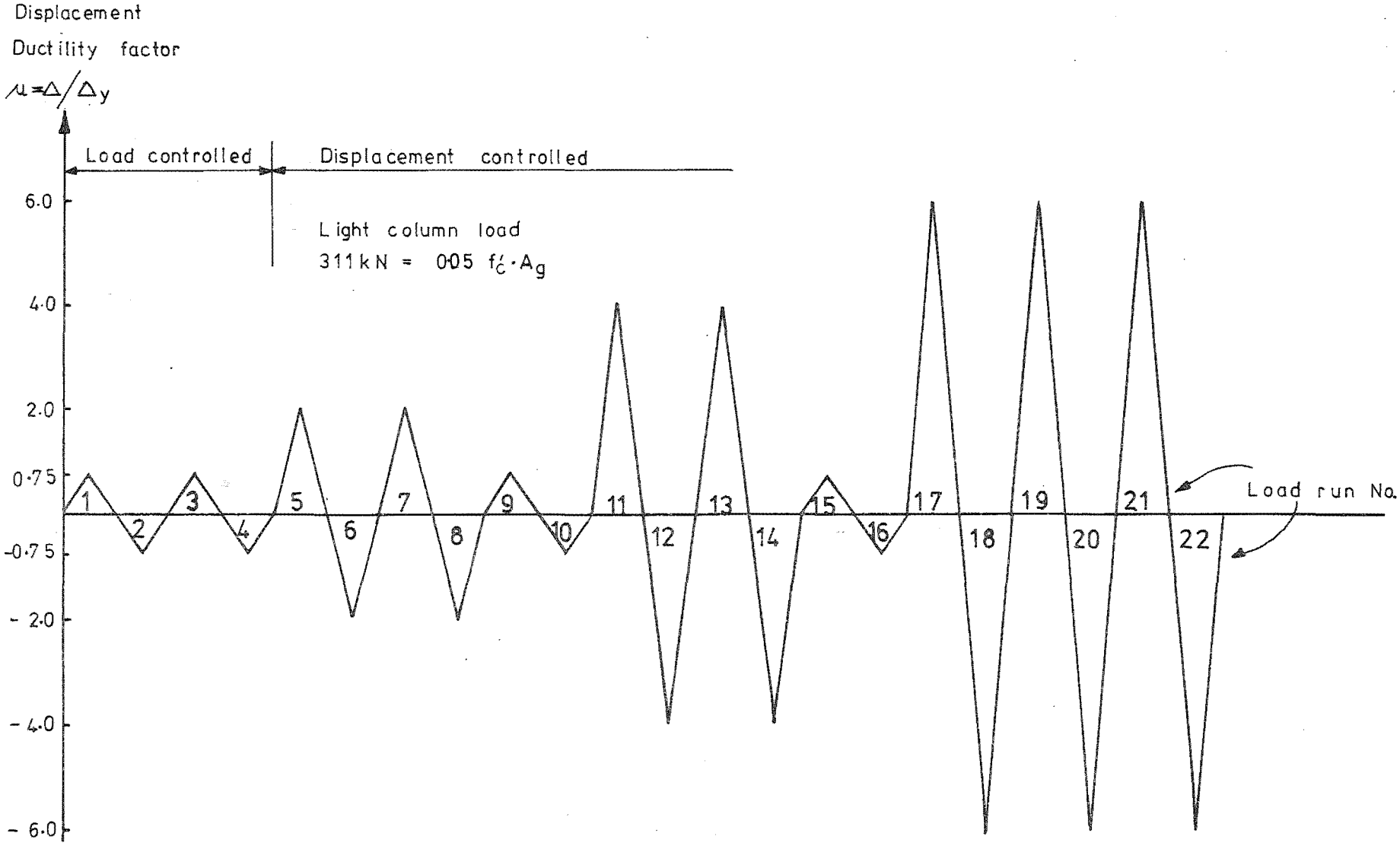

FIG.2.18:CYCLIC LOADING SEQUENCE FOR TEST UNITS B 11 & B12

cycles were included to allow stiffness degradation resulting from the previous inelastic cycles to be measured.

When the test units B11 and B12 underwent a severe but not catastrophic bond failure during load runs 17 to 20 it was felt that little would be gained by imposing higher ductility requirements, but an extra cycle at the existing ductility level, $\mu = 6.0$, was applied in order to observe the degree of stiffness degradation. An overall displacement ductility requirement for buildings of $\mu = 4.0$ is suggested by several loading codes [1,2], and the value achieved in these tests would have allowed the local demand for a given element to exceed the overall building requirement by fifty percent, which was considered to be a satisfactory margin.

For the test of unit B13 the same loading pattern was followed initially but at the conclusion of load run 20 the unit was still in a very sound condition, and it was decided that more could be learned by changing the test parameters than by imposing greater ductility demands under the existing conditions. Hence the axial load was reduced and the test was continued as B13B as shown in Fig. 2.19. The displacement ductility factors describing this part of the test were still defined in terms of the original yield displacement obtained for B13A, since obviously the yield displacement for the new conditions could not be determined in any consistent manner. Since the lower axial load would have allowed more column and joint cracking, the actual yield displacement for B13B would be slightly greater than that used and hence the actual ductility factors achieved were somewhat less than given in Fig. 2.19. Nevertheless it is considered that the total cumulative ductility applied ($\Sigma\mu = 104$ in terms of the original yield displacement) was quite sufficient to demonstrate effectively the performance of the unit.

2.7.3 Test Procedure.

Before the test proper was commenced, several sets of zero readings were taken, to check repeatability. The column axial load was then set to its required level, and left for about a week to allow the major part of stress redistribution due to creep in the column to occur prior to the actual testing. Unit B13 with its heavy axial load was left under axial load only for a longer time.

Load runs were applied in the sequence described above at the

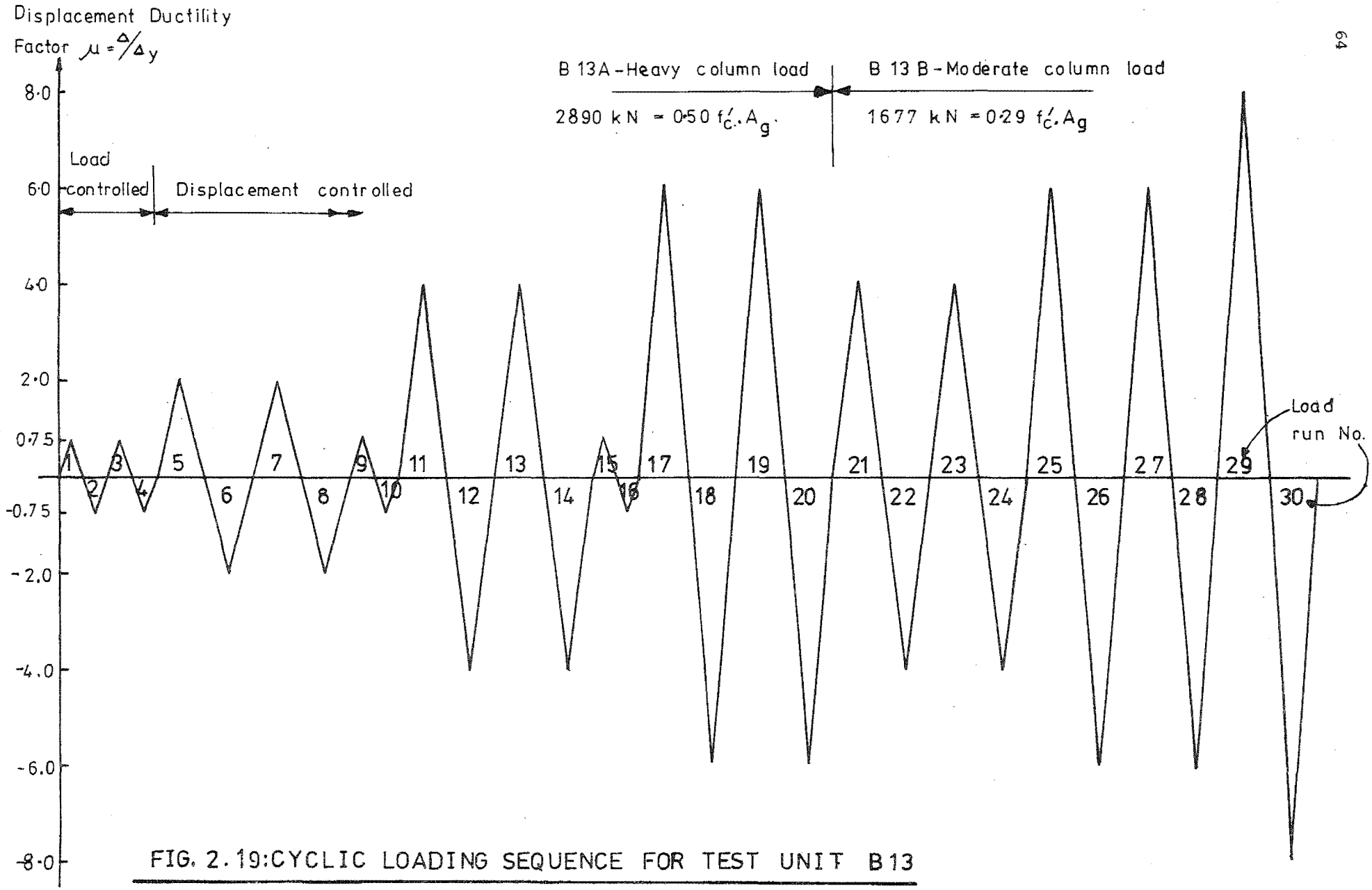

FIG. 2.19: CYCLIC LOADING SEQUENCE FOR TEST UNIT B13

rate of one or two load runs per day. The application of load at the two beam ends was co-ordinated manually, to give equal proportions of beam yield load in the initial load-controlled cycles, or equal beam displacements in the displacement controlled cycles. Unloading of the beams after maximum load or displacement was attained was accomplished under load control, removing equal proportions of the maximum load for that load run from each beam. Where the residual deflections of the two beams were not equal at the commencement of a load run, the imbalance was corrected in the initial stages of the load run by applying more displacement to the beam having the greater residual deflection (usually twice the displacement applied to the beam having the smaller residual deflection) until the two beam deflections were equal.

When a set of readings was required the displacements were fixed by closing the valves of the hydraulic hand pumps, allowing the loads to diminish slowly under the influence of creep, until the next increment of load was to be applied. At each increment the beam loads were recorded, the column axial load was adjusted to the correct level, and measurements of deflection and strain were made. A full set of data was recorded only at maximum displacement and at zero load for each load run, selected data only being taken at intermediate increments.

CHAPTER 3

TEST OF UNIT B11

3.1 Introduction

Plane frame test unit B11 was the first specimen to be built and tested, and was designed according to the philosophy described in Chapter 2. The intended column axial load was small, causing a compressive stress of $0.05f'_c$ over the column section; the ratio of top to bottom steel areas for the beams was 2.0, and the joint reinforcement was designed to resist all the horizontal shear arising from an overstrength of 1.25 times the nominal yield strength of the beam flexural bars, with no contribution to horizontal joint shear resistance from the joint concrete. Specimen details and material properties were given in Chapter 2, as was the idealized seismic loading sequence used in the test. (See Fig. 2.18.)

The scheduled loading sequence for the test was disrupted in load run 13 when load on the western beam was reduced suddenly when the test rig became unstable. This situation necessitated removal of the loads from both beams so that the fault could be rectified, and the interrupted load run was then completed by reloading to the required displacement. The axial load actually applied to the column varied a little from the intended constant value, because of an error in calculation of the correction necessary to compensate for unequal upward and downward beam loads. This resulted in axial loads at the maximum displacement of each cycle being an average of 7% less than the intended value, with a maximum difference of 9%. Because bending was the dominant action on the column, the small variation in axial load would not have affected the area of concrete in compression in the column sections above and below the joint very greatly. Hence it is unlikely that the joint response observed in the test was significantly affected.

The overall performance of the test unit was satisfactory in that the design aim of restricting inelastic behaviour to the beam hinges was largely achieved. The integrity of the joint throughout the test is illustrated by the photographs (Figs. 3.1 to 3.4) in which the cracks have been marked with a felt-tip pen to show their positions more clearly. Although the density of the crack pattern in the joint increased, crack widths in the joint never became excessive, the maximum crack width

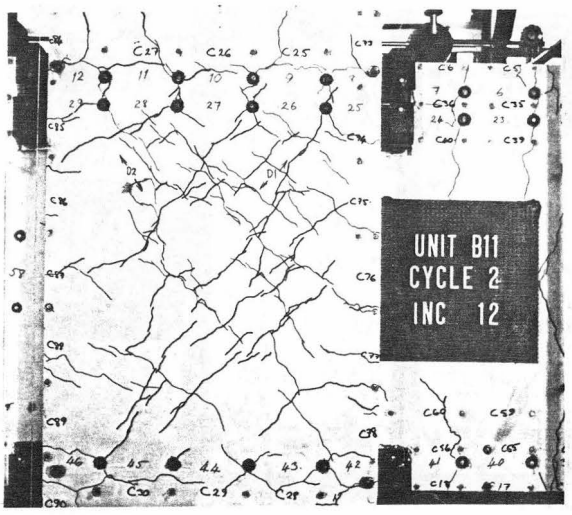

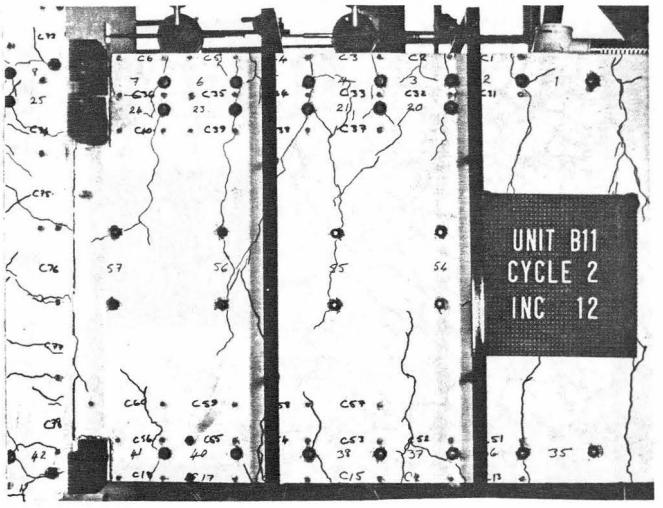

(a) JOINT (b) WESTERN BEAM

FIG.3.1: TEST UNIT AT MAX. LOAD, RUN 2. ($P = 0.75 P_y$)

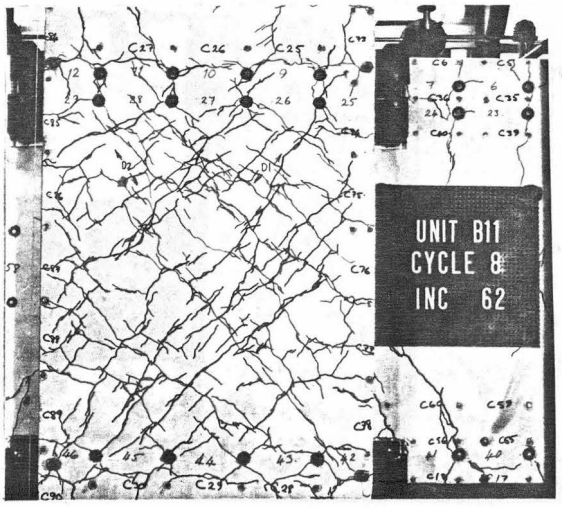

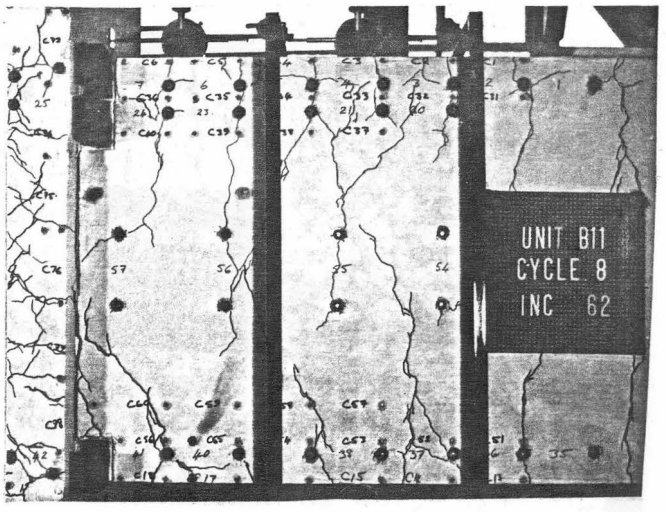

(a) JOINT (b) WESTERN BEAM

FIG. 3.2: TEST UNIT AT MAX. DISPLACEMENT, LOAD RUN 8 ($\mu = 2.0$)

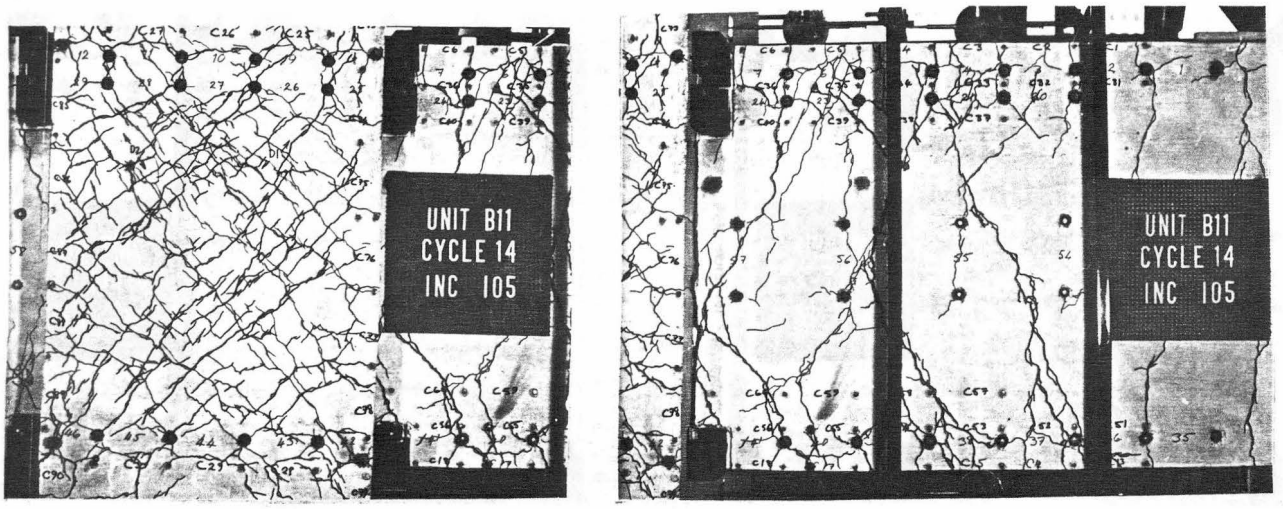

(a) JOINT (b) WESTERN BEAM

FIG. 3.3 : TEST UNIT AT MAX. DISPLACEMENT, LOAD RUN 14 (μ = 4.0)

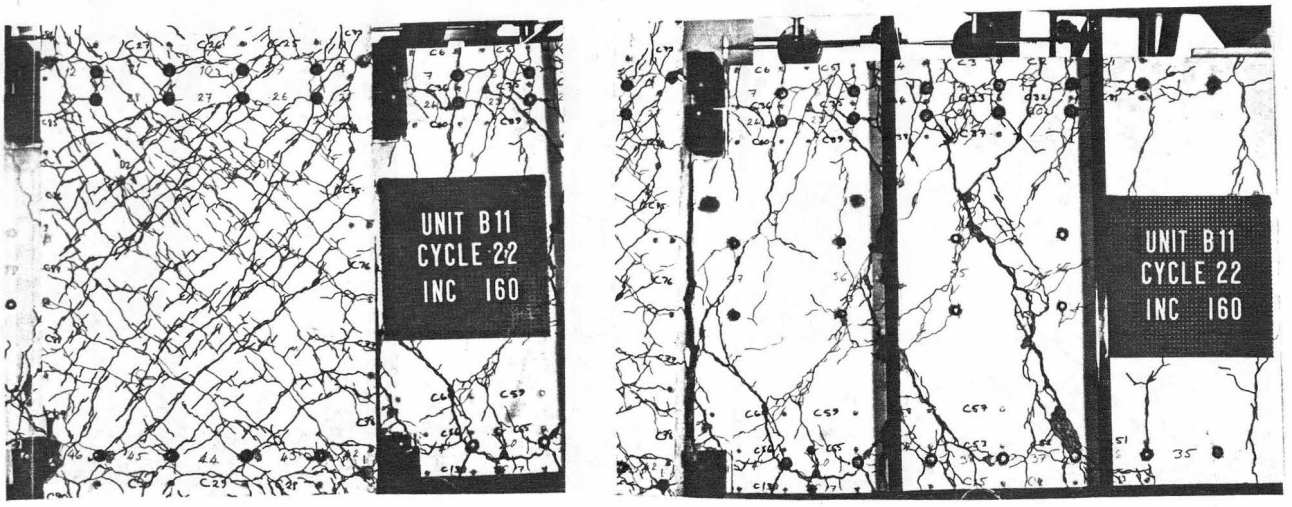

(a) JOINT (b) WESTERN BEAM

FIG. 3.4 : TEST UNIT AT MAX. DISPLACEMENT, LOAD RUN 22 (μ = 6.0)

observed being 0.55 mm. A small amount of yielding of joint reinforcement occurred, but only towards the end of the test, and apparently in a well-controlled manner. Of more serious consequence was the slip failure of the bottom bars of the beams through the joint. This phenomenon occurred relatively late in the test but its affect on the behaviour of the unit was then serious, causing severe pinching of the load-deflection loops, and consequent loss of energy dissipating capacity.

Data from the test was analysed and found to give a good fit to the mechanisms of concrete diagonal strut action and truss action postulated in Chapter 1 for concrete and reinforcement resistance to applied joint shear.

3.2 Load-Displacement Response

The beam end load vs end displacement curves for the western and eastern beams are given in Figs. 3.5 and 3.6 respectively. Positive beam loads and positive beam end displacements are those associated with sagging bending moments, while negative loads and displacements are associated with hogging moments.

The first cycle to three-quarters of yield load showed some hysteresis because of energy dissipated in cracking, but the repeated cycles (load runs 3 and 4) showed relatively little hysteresis since little further cracking occurred.

When the first inelastic cycle was applied, first yield in the beams was observed at loads slightly less than those predicted by theory, but these loads were exceeded when maximum displacement ($\mu = 2.0$) was reached.

During the second cycle to displacement ductility factor of 2.0 (load runs 7 and 8) the stiffness under negative bending degraded significantly, although this did not occur to the same extent under positive bending. The difference in stiffness degradation at this stage would appear to be due to the loss of concrete compression area when cracks remained open in the early part of the load run. This had a more significant effect on the section with the smaller area of compression steel, i.e. the section under negative bending. Penetration of beam steel yield strain into the joint, shear distortion of the joint panel, and shear sliding displacement along open flexural cracks in the beam hinges also contributed to the stiffness degradation.

In the subsequent cycles to displacement ductility factors of 4.0 and 6.0, the theoretical ultimate loads, calculated assuming a maximum concrete strain of 0.003 and the steel stress at the measured yield strength, were exceeded by as much as 19% (see Table 3.1). This

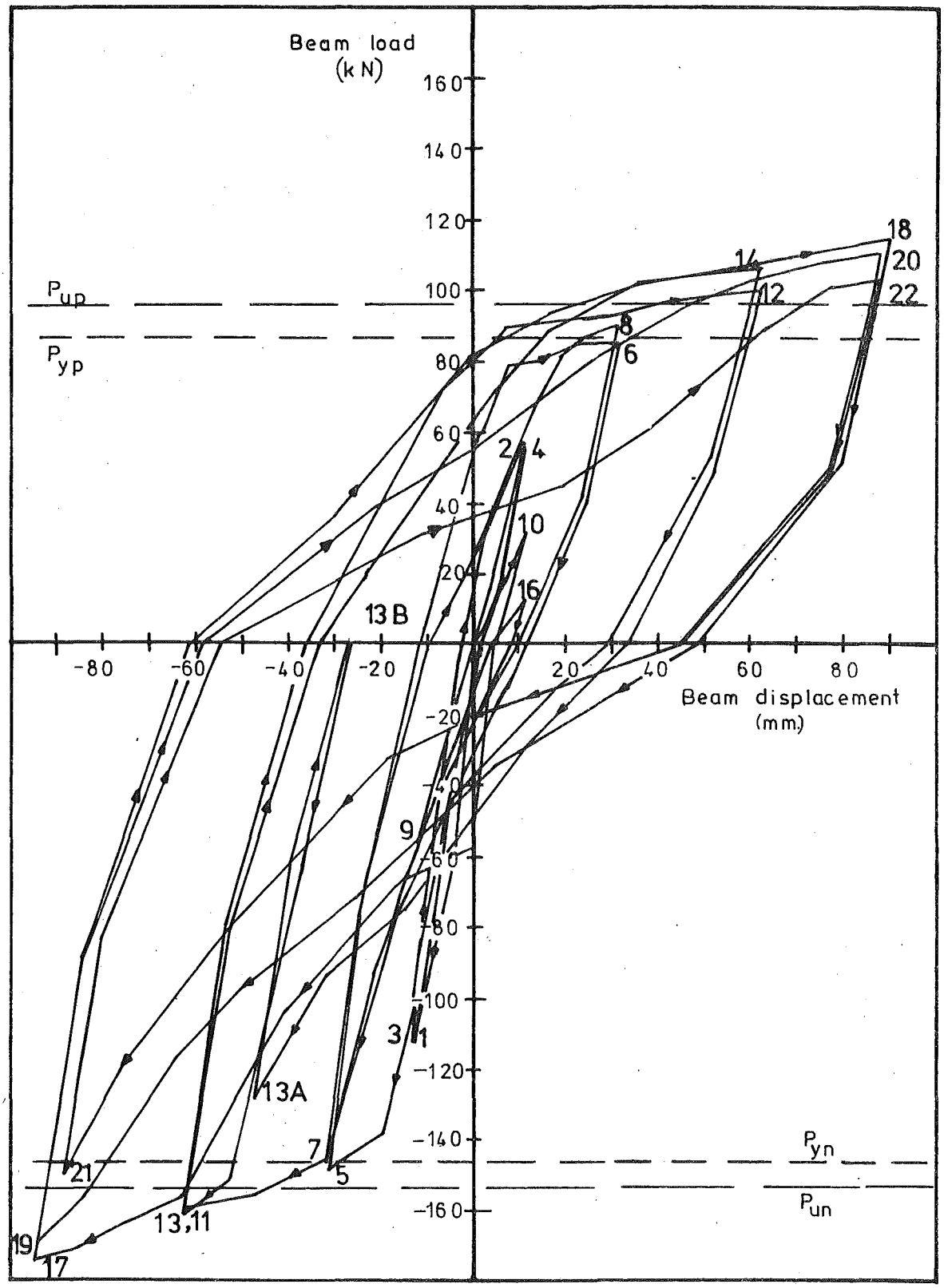

FIG. 3.5 :LOAD-DISPLACEMENT RESPONSE, WESTERN BEAM

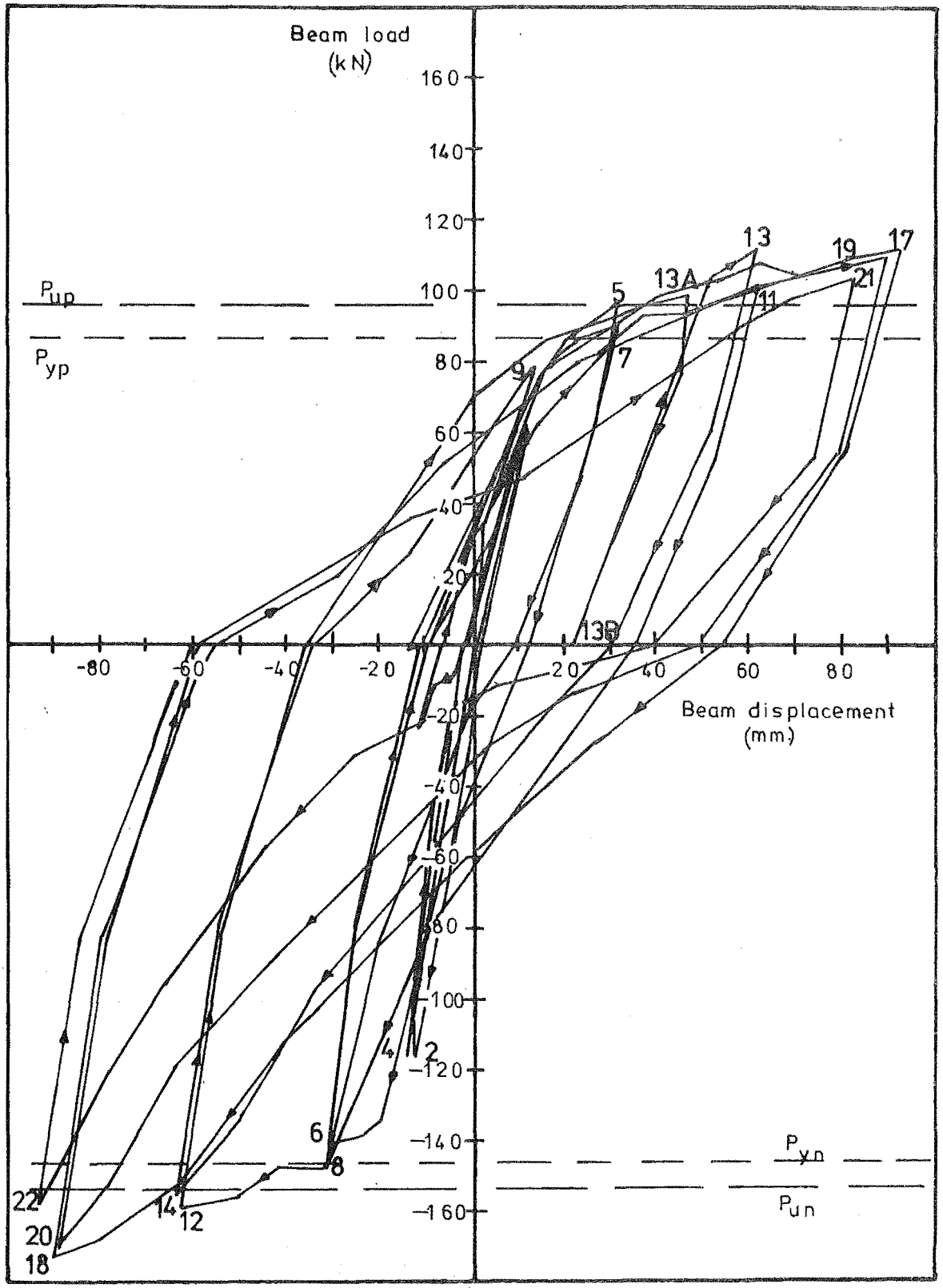

FIG.3.6 : LOAD-DISPLACEMENT RESPONSE FOR EASTERN BEAM

TABLE 3.1 : BEAM END LOADS

Load Run No.	μ (i)	Beam West			Beam East		
		P (kN) (ii)	P/P_y (iii)	P/P_u (iv)	P (kN)	P/P_y	P/P_u
1	0.75	-112.92	0.774	0.738	63.96	0.737	0.665
2		58.11	0.669	0.604	-116.90	0.801	0.764
3		-110.96	0.760	0.725	61.63	0.710	0.640
4		57.73	0.665	0.600	-116.37	0.797	0.760
5	2.0	-148.88	1.020	0.973	97.30	1.121	1.011
6		85.18	0.981	0.825	-141.55	0.970	0.925
7		-144.16	0.988	0.942	90.01	1.037	0.935
8		89.83	1.035	0.934	-146.17	1.002	0.955
9	0.75	-54.19	0.371	0.354	57.29	0.660	0.595
10		32.42	0.373	0.337	-23.77	0.163	0.155
11	4.0	-159.76	1.095	1.044	101.74	1.172	1.057
12		100.21	1.154	1.042	-158.82	1.088	1.038
13		-160.72	1.101	1.050	112.46	1.295	1.169
14		106.30	1.224	1.105	-155.09	1.063	1.013
15	0.75	-56.04	0.384	0.366	77.89	0.897	0.809
16		13.72	0.158	0.143	-1.51	0.010	0.010
17	6.0	-173.60	1.190	1.134	112.01	1.290	1.164
18		114.62	1.320	1.191	-172.60	1.183	1.128
19		-169.13	1.159	1.105	110.12	1.268	1.144
20		111.00	1.278	1.154	-169.83	1.163	1.110
21		-150.41	1.031	0.983	104.32	1.202	1.084
22		103.75	1.195	1.078	-159.07	1.090	1.039

Notes: (i) $\mu = \Delta_B/\Delta_y$ = applied beam end displacement ductility factor (See Section 2.7)

(ii) P = observed beam end load

(iii) P_y = calculated beam end load to cause yield strain in all beam tension reinforcement at the column face

(iv) P_u = calculated beam end load to cause ideal ultimate strength to be attained in beam at column face, assuming steel stress not to exceed the measured yield strength, and ultimate concrete strain $\varepsilon_c = 0.003$

(v) P_y, P_u are listed in Table 2.3

overstrength was due to strain hardening and strain ageing of the beam reinforcing steel. The cycles to ductility factor of 4.0 showed further stiffness degradation, especially under negative bending.

Because of the unsymmetrical beam reinforcing configuration, flexural cracks remained open at the top of the beams throughout the inelastic part of the test, since the bottom bars in tension could never cause yielding in all the top bars in compression. However the flexural cracks closed up at the bottom of the beams during negative bending load runs when the bottom bars yielded in compression and the conditions for dowel action and in particular for aggregate interlock to resist beam shear were therefore most favourable during the later stages of negative load runs and during the initial stages of positive load runs. By the time the flexural cracks opened up over the full depth of the beam during positive load runs, the stiffness of the section was decreasing due to the Bauschinger effect in the steel, and stiffness degradation due to shear sliding deformation was therefore not obvious. Visual observations of the sliding along the cracks indicated that the total shear displacement under positive and negative bending were similar at maximum displacements, but that shear displacement was greater under negative bending during the early part of the load run.

When a displacement ductility factor of 4.0 was first exceeded in load run 17, the bottom beam bars started to slip through the joint. This phenomenon continued in the subsequent cycles to ductility factor of 6.0 and caused severe stiffness degradation and pinching of the load-displacement loops under both positive and negative bending. Because the Demec studs welded to the outer bars came into bearing on the sides of their holes in the cover concrete (see Section 3.3.5 and Fig. 3.24), the loss of stiffness was perhaps not as severe as might be expected in a prototype structure that would not have the benefit of this extra bar anchorage. However, it is likely that a prototype would still be able to sustain near full load at maximum displacement, as did the test unit.

Fig. 3.7 shows the column shear versus sidesway curves, derived for the unit by combining the two previous graphs, and by taking into account the P-Δ effect. The relevant actions and deformations are shown in Fig. 1.10. The sidesway Δ_c is derived from the applied beam end displacements Δ_{B1} and Δ_{B2} to give the displacement equivalent in a prototype structure to those imposed on the test unit.

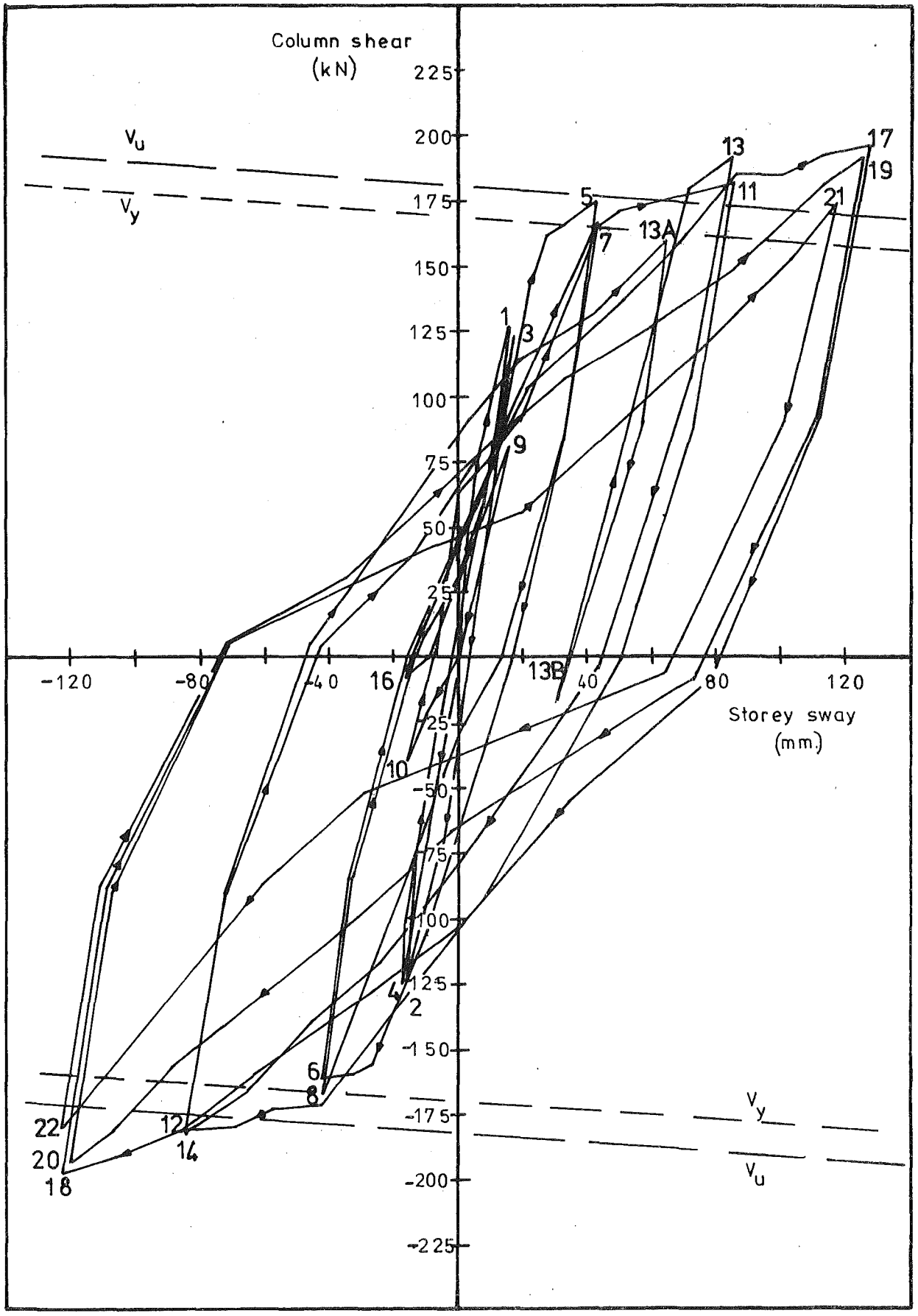

FIG. 3. 7 :COLUMN SHEAR-STOREY SWAY RESPONSE.

$$\Delta_c = (\Delta_{B1} - \Delta_{B2}) \times l_c/l_B \quad (3.1)$$

where l_c = storey height of column = 3.353 m

l_B = length of beam from mid-span one bay to the next = 4.875 m

The column shear V_c is derived from the beam loads P_{B1} and P_{B2} and the column axial load N

$$V_c = (P_{B1} - P_{B2})l_B/2l_c - N \times \Delta_c/l_c \quad (3.2)$$

The graph shows the features mentioned in relation to the beam load displacement curves, with the different degrees of stiffness degradation in the beams under positive and negative bending combined to an intermediate level of stiffness degradation characterising the behaviour of the whole unit. The P-Δ effect was found to be insignificant for this unit because of the small axial load. Within the displacements applied in this test the net column shear did not decrease as displacement was increased, since the strain-hardening effect was greater than the P-Δ effect. The maximum reduction in column shear due to the P-Δ effect was 5.6% in load run 22.

3.3 Beam Behaviour

3.3.1 Components of Beam End Displacement

The contribution of various sources of deformation to the beam end displacements throughout the course of the test is depicted in Figs. 3.8 and 3.9. These figures show that for most of the test the beam rotation in the gauge length from the column face to half the effective beam depth from the face, θ_{b1}, contributed the major component of displacement. Displacements due to rotations in the second half beam depth gauge length from the face, θ_{b2}, were significant in load runs 11 to 18, but this component diminished later as the bottom steel slip increased.

Since the rotations θ_{b1} were obtained by dial gauges above and below the beam reading against the column face (see Fig. 2.13), the resulting displacement components included the effect of beam bar slip and yield penetration.

Significant rotations in the second gauge lengths of the beams occurred predominantly in the direction of first loading, i.e. during the odd-numbered load runs, where additional deformation of the test unit caused additional yielding of the tension reinforcement further along the beam. Under reversed loading the open flexural cracks and yield

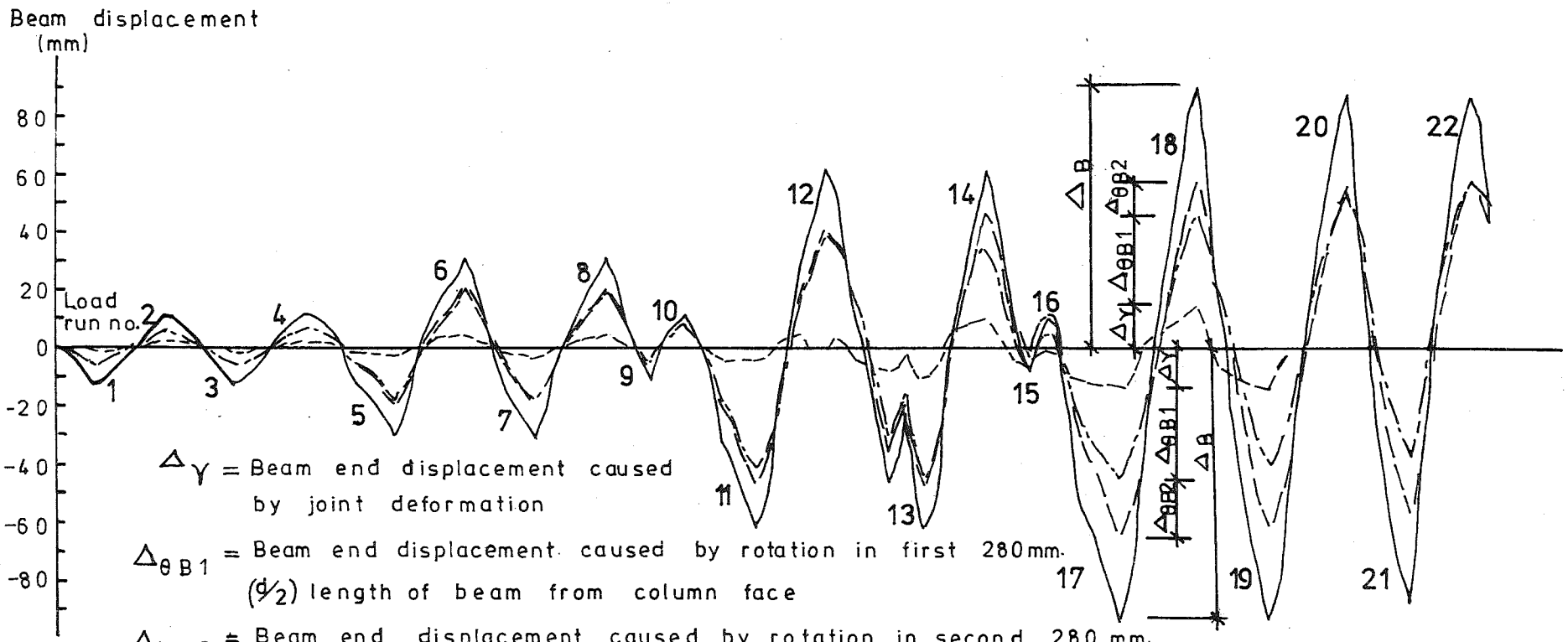

FIG. 3·8 : COMPONENTS OF BEAM DISPLACEMENT FOR WESTERN BEAM

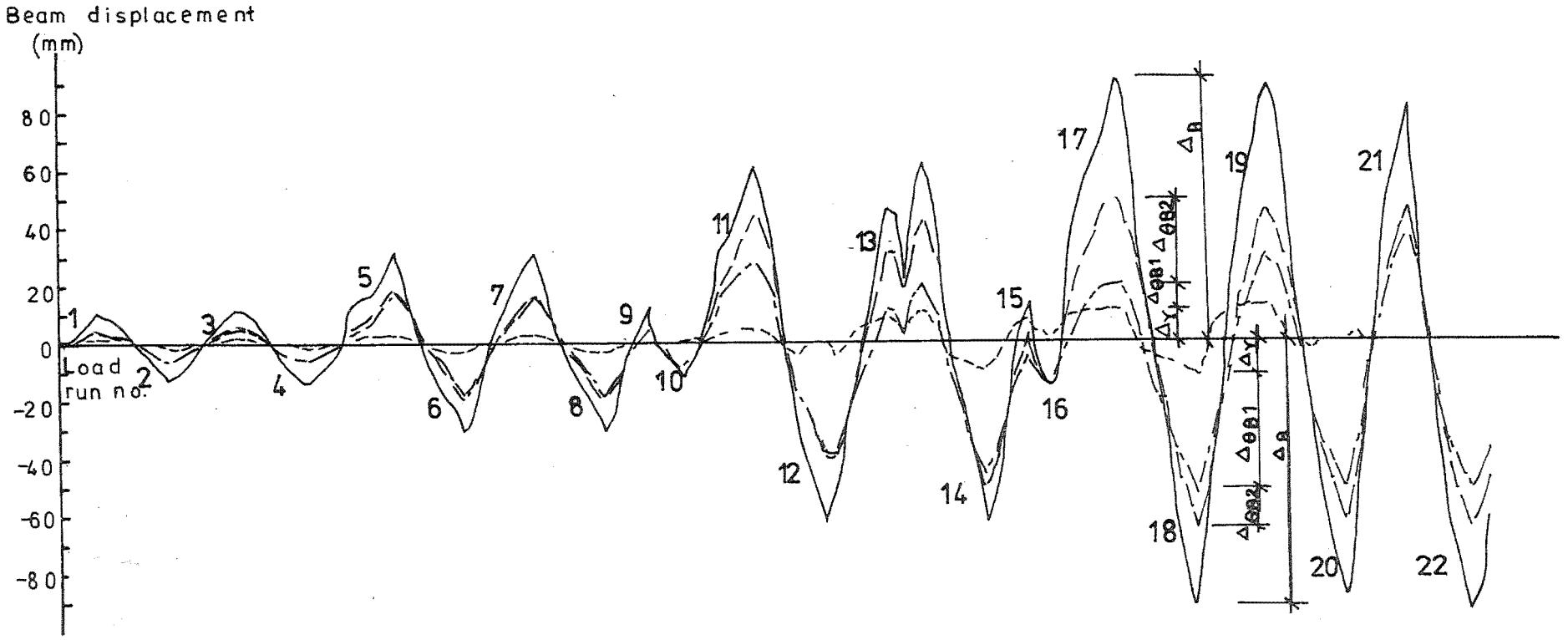

FIG.3·9 : COMPONENTS OF BEAM DISPLACEMENT FOR EASTERN BEAM

penetration into the joint allowed other sources of displacement such as beam shear displacement and slip to be more dominant. This was particularly the case for the eastern beam, which was under negative moment loading when reversed loading was applied, since the reversed loads in this case were of greater magnitude than the (positive) loads applied in the direction of first loading. Although beam end displacements were applied symmetrically about the original zero positions throughout the test, the resistance of the test unit was not symmetrical, and the rotations in the second gauge length consequently occurred about an off-centre position.

Shear distortion of the joint panel caused a significant contribution to the beam end displacements. Data for the joint panel rotation was not obtained in load runs 12, 20, 21 and 22 because the device used to measure this quantity did not function. As a proportion of the total beam end displacements the component caused by the joint panel rotation was a maximum in load run 8 when this component comprised 27% of the total displacement. Since the joint deformation was basically elastic it did not increase as much as the plastic beam rotations in the subsequent larger cycles, although some increase was observed. The maximum joint deformation occurred in load run 18, when it caused 16% of the total beam end displacement.

Figs. 3.8 and 3.9 illustrate how beam deformation lagged behind joint deformation. At the beginning of each major cycle the displacement components due to joint distortion and beam rotation were of opposite sign, because the joint behaved elastically and thus followed the sense of the load quite closely. The plastic nature of the beam hinge rotation, however, meant that substantial loads had to be applied before this component of displacement was of the same sign as the load.

The remainder of the beam end displacement was caused by elastic bending in the remainder of the beam (i.e. beyond the rotation gauge lengths); shear deformation in the beams; and bending of the column.

3.3.2 Beam Rotational and Curvature Ductility Factors

Beam rotations and curvatures measured during the post-elastic cycles are listed in Tables 3.2a and 3.2b for the western and eastern beams respectively. The rotations θ_{bl} are those measured in the first 280 mm length of beam from the column face. This gauge length was equal to half the effective beam depth, and the rotations were those which caused the beam displacement components $\Delta_{\theta_{bl}}$ in Figs. 3.8 and 3.9. The curvatures

TABLE 3.2a : ROTATIONAL AND CURVATURE DUCTILITY FACTORS - BEAM WEST

Load Run No.	μ	θ_{bl} rad. x 10^4	$\frac{\theta_{bl}}{\theta_{by}}$	ϕ_1 rad/mm x 10^6	ϕ_{max} rad/mm x 10^6	$^1\phi_{max}$ mm	ϕ_1/ϕ_y	ϕ_{max}/ϕ_u
5	2.0	-73.82	2.89	-11.98	-11.98	76	2.77	2.77
6		75.06	3.70	25.70	25.70	76	8.40	8.40
7		-68.11	2.67	-12.96	-12.96	76	3.00	3.00
8		71.88	3.55	21.47	21.47	76	7.02	7.02
9	0.75	-15.45	0.61	6.29	-2.29	279	-1.46	0.53
10		32.44	1.60	11.81	11.81	76	3.86	3.86
11	4.0	-177.10	6.93	-35.66	-49.94	178	8.25	11.56
12		186.48	9.20	23.23	38.85	381	7.59	12.70
13		-144.40	5.65	-30.00	-40.68	178	6.94	9.42
14		115.51	5.70	17.86	35.60	584	5.84	11.64
15	0.75	3.26	-0.13	3.14	-6.36	178	-0.73	1.47
16		31.28	1.54	7.03	26.51	584	2.30	8.67
17	6.0	-214.30	8.38	-42.65	-54.36	178	9.87	12.58
18		222.44	10.98	34.04	34.04	76	11.13	11.13
19		-190.55	7.46	-15.74	-45.05	178	3.64	10.43
20		249.61	12.32	33.03	33.03	76	10.79	10.79
21		-175.72	6.88	-0.58	-37.96	483	0.13	8.79
22		278.61	13.75	26.77	26.77	76	8.75	8.75

Note: Terms as defined in text.

TABLE 3.2b : ROTATIONAL AND CURVATURE DUCTILITY FACTORS - BEAM EAST

Load Run No.	μ	θ_{bl} rad. x 10^4	$\frac{\theta_{bl}}{\theta_{by}}$	ϕ_1 rad/mm x 10^6	ϕ_{max} rad/mm x 10^6	$^1\phi_{max}$ mm	ϕ_1/ϕ_y	ϕ_{max}/ϕ_y
5	2.0	66.08	3.26	16.04	16.04	76	5.24	5.24
6		-70.60	2.76	-19.03	-19.03	76	4.41	4.41
7		59.58	2.94	22.88	22.89	76	7.48	7.48
8		-67.02	2.62	-14.01	-14.01	76	3.24	3.24
9	0.75	9.68	0.48	-1.13	2.79	381	-0.37	0.91
10		-32.31	1.26	-6.46	-6.46	76	1.49	1.49
11	4.0	114.90	5.67	38.55	38.55	76	12.60	12.60
12		-183.73	7.19	-37.22	-45.31	178	8.61	10.49
13		42.69	2.11	21.48	30.63	483	7.02	10.01
14		-169.58	6.64	-31.29	-38.36	178	7.24	8.88
15	0.75	-57.20	-2.82	-11.85	4.59	483	-3.87	1.50
16		-79.96	3.13	-14.92	-24.49	178	3.45	5.67
17	6.0	96.06	4.74	29.08	51.26	584	9.51	16.75
18		-250.52	9.80	-32.86	-46.66	178	7.60	10.80
19		143.18	7.06	23.06	31.03	584	7.54	10.14
20		-246.19	9.63	-9.69	-38.26	279	2.24	8.86
21		182.55	9.01	22.95	22.95	76	7.50	7.50
22		-247.24	9.67	2.39	-32.47	381	-0.55	7.51

listed in the tables were obtained from top and bottom reinforcement strains measured by Demec gauges over a 102 mm gauge length. The curvature ϕ_1 was the value observed at the closest available location to the column face, i.e. 76 mm from the face, while the curvature ϕ_{max} was the maximum value of those observed at seven positions between 76 mm and 686 mm from the column face. Signs of both rotations and curvatures were defined with respect to the original zero-displacement position at the commencement of the test. The length $l_{\phi_{max}}$ was the distance from the column face at which the maximum curvature was observed. Ductility factors were calculated in terms of both rotation and curvature, and these are also listed in Tables 3.2a and 3.2b. The yield rotation θ_y and the yield curvature ϕ_y were obtained by extrapolation from the appropriate measurements in the initial elastic cycles in a similar manner to that in which the experimental yield deflection was obtained (see Section 2.7 and Fig. 2.17)

The curvature ductility demand at a section was normally greater than the overall rotational ductility demand, especially during the first inelastic cycles to displacement ductility factor of 2.0, where yield strain in the beam flexural steel did not extend over the complete length of the rotational measurement. (See Figs. 3.10 - 3.11). The apparent rotational demand was greater than the curvature demand only in the final cycles where the slip contribution became predominant. An estimate of the portion of the beam rotation resulting from beam curvature alone was obtained by summing the curvatures measured over the rotational gauge length. This calculation showed that up to load run 17 the curvature within the rotational gauge length accounted for an average of 55% of the total rotation, the remainder being caused by yield penetration and resultant slip of the beam bars within the joint core. During load runs 18 to 22 the corresponding proportion was only 27%, showing that slip had become the primary source of deformation.

The location of the section with maximum curvature demand varied throughout the test, depending on the interaction of flexural and diagonal cracking and the stress-strain history of the reinforcing steel at any given stage.

The low values of rotational ductility observed in load run 9 and the negative values in load run 15 arose because the beam hinge deformation was lagging behind load and total deformation as explained

in Section 3.2.1. For load run 15 the lag of beam rotation behind load was so great that at maximum displacement (ductility factor = 0.75), the beam rotation still had the sense of the previous major load run. Similar effects were apparent with respect to the curvature ϕ_1 measured at 76 mm from the column face.

3.3.3 Beam Reinforcement Strain Profiles

Strain profiles measured along the beam flexural reinforcement during alternate major inelastic load runs are presented in Figs. 3.10 to 3.16. The strains plotted are the mean of those measured in the outer two bars of each layer of four. The strain profiles show clearly the lengthening of the plastic hinge as ductility demand was increased. During load run 5, the first inelastic run, the steel yield strain was exceeded initially close to the column face, and spread to about 150 mm from the face in both top and bottom steel. Yield penetration into the joint core was significant even at this early stage of the test, to within 150 mm of the column centreline. In the subsequent cycles to displacement ductility factor of 2.0, yield did not spread much further along the beams but penetration into the joint increased to about 100 mm from the column centreline by load run 8. The exact extent of yield penetration into the joint at any stage is difficult to determine because the Demec gauge length of 102 mm is quite large relative to the total column depth of 457 mm.

In load runs 11 to 14 the yielding spread along the beam to 400 mm and later to 550 mm from the column face for the top reinforcement, while yield in the bottom bars spread to 400 mm in load run 11, and eventually to 650 mm. Yield strain in the top bars penetrated into the joint to within about 50 mm from the centreline, while bottom steel yield strain penetrated to about 30 mm from the centreline.

During the cycles to displacement ductility factor of 6.0, the yield spread in the top bars to 700 mm from the column face, and in the bottom bars to more than 700 mm (this being as far as readings were taken). Yield penetration in the top bars increased to within about 30 mm from the column centreline. In the bottom bars yield penetration reached the column centreline in load run 17 and the bars began to slip through the joint. From load run 18 onwards no strain readings were available for the bottom bars across the joint since the slip caused the Demec studs to come into bearing against the cover concrete around the holes, and consequently to bend and render any readings meaningless.

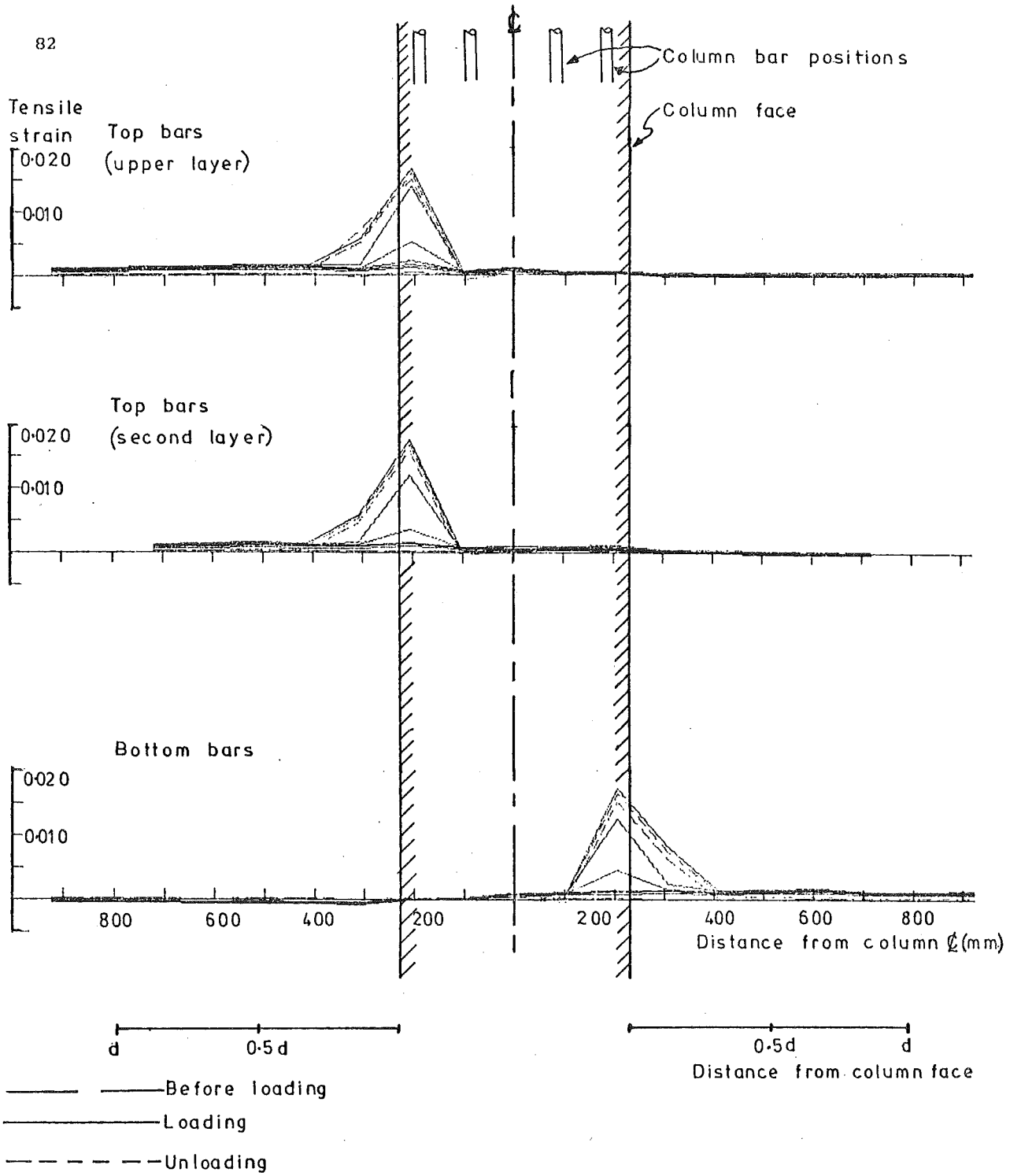

FIG.3.10 : BEAM BAR STRAINS, LOAD RUN 5

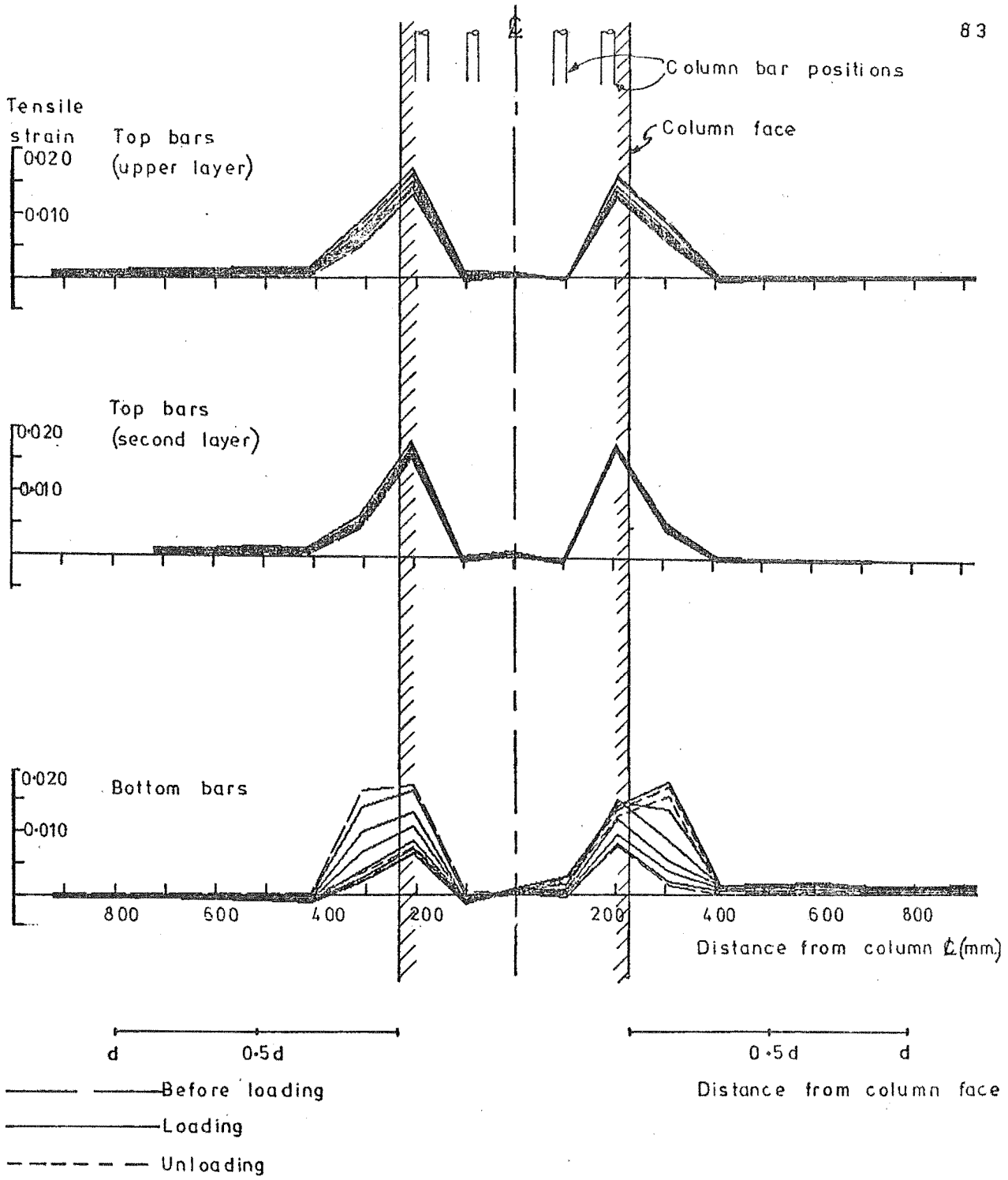

FIG.3.11 :BEAM BAR STRAINS, LOAD RUN 7

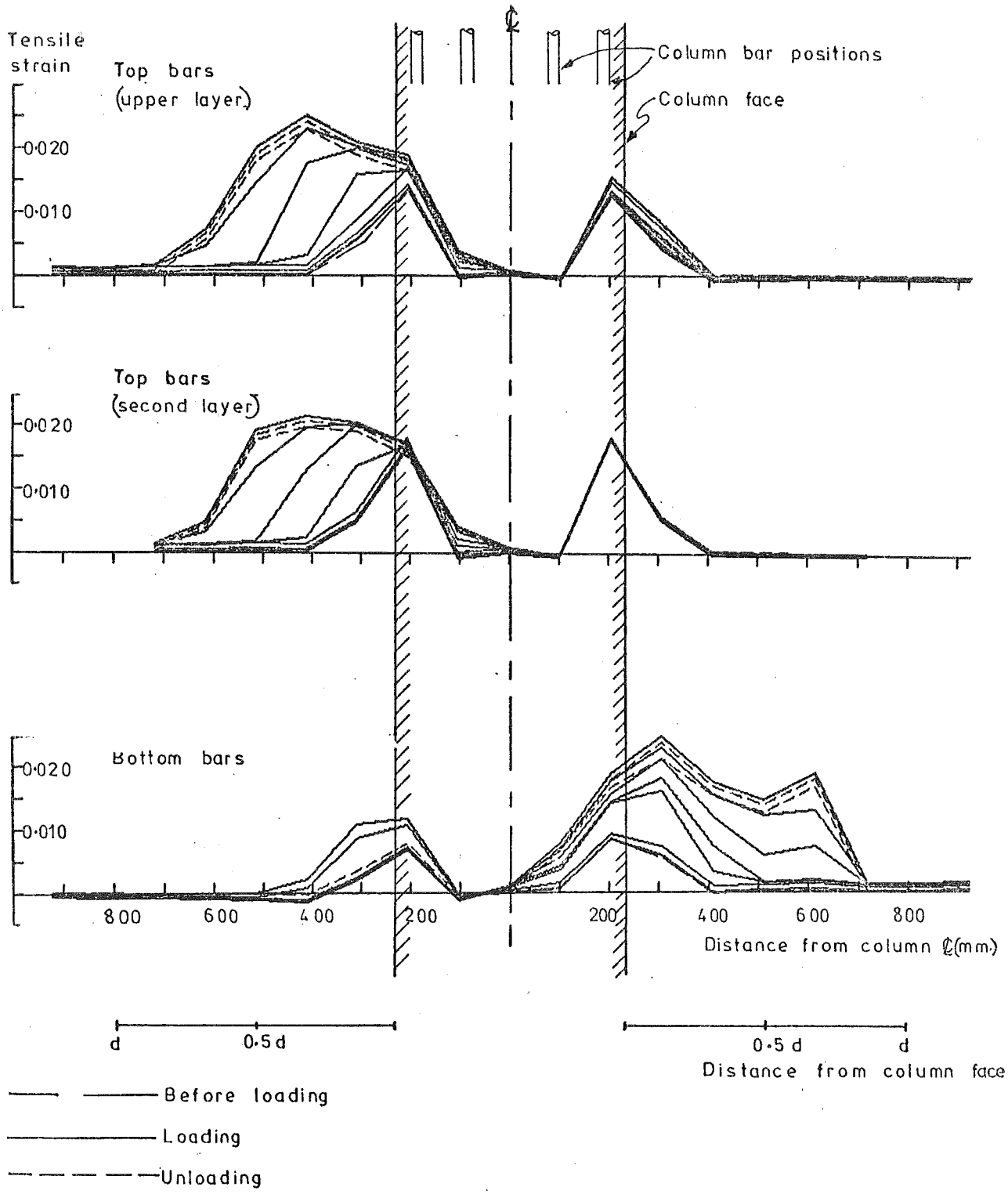

FIG. 3.12 : BEAM BAR STRAINS, LOAD RUN 11

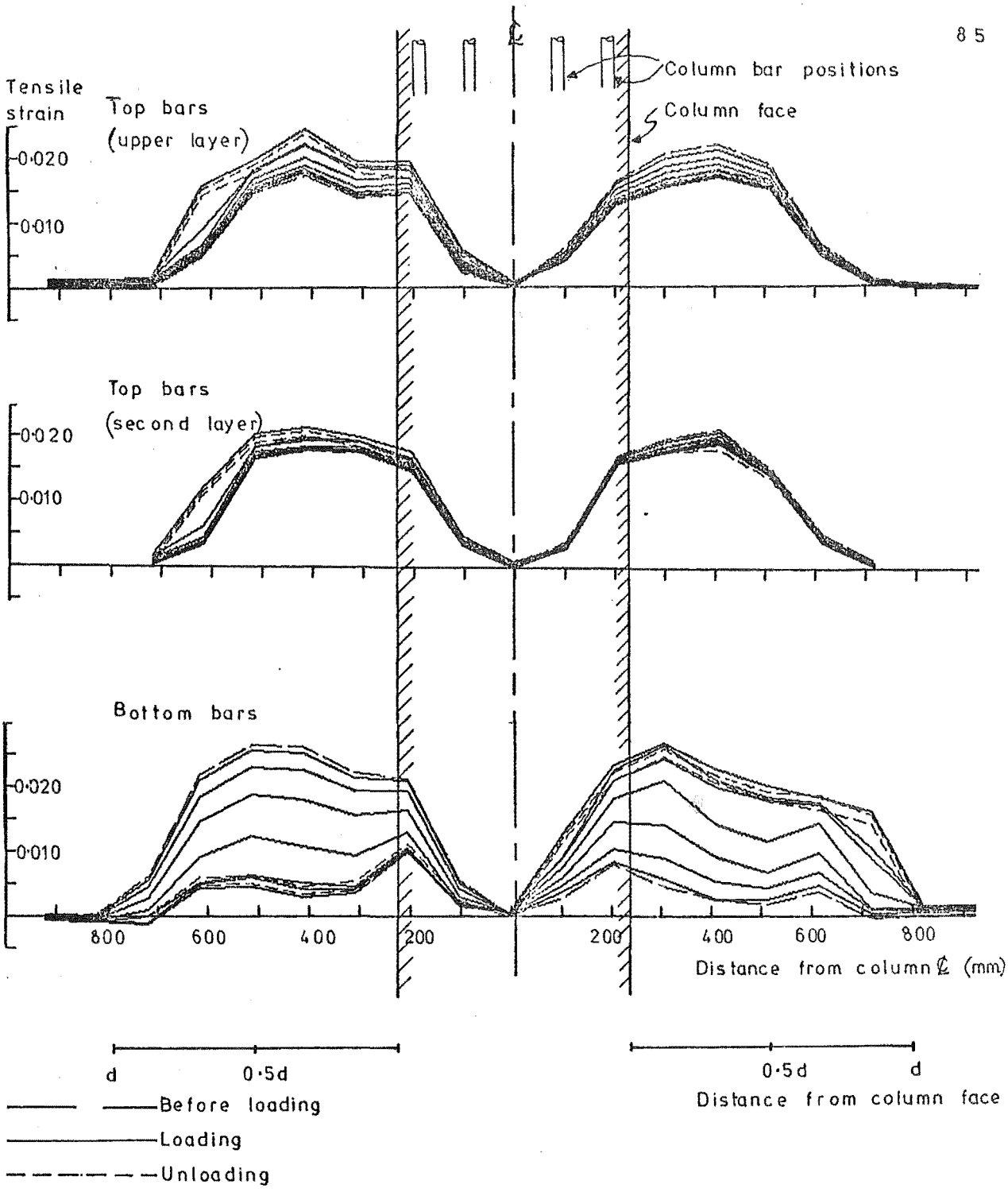

FIG.3.13 : BEAM BAR STRAINS, LOAD RUN 13

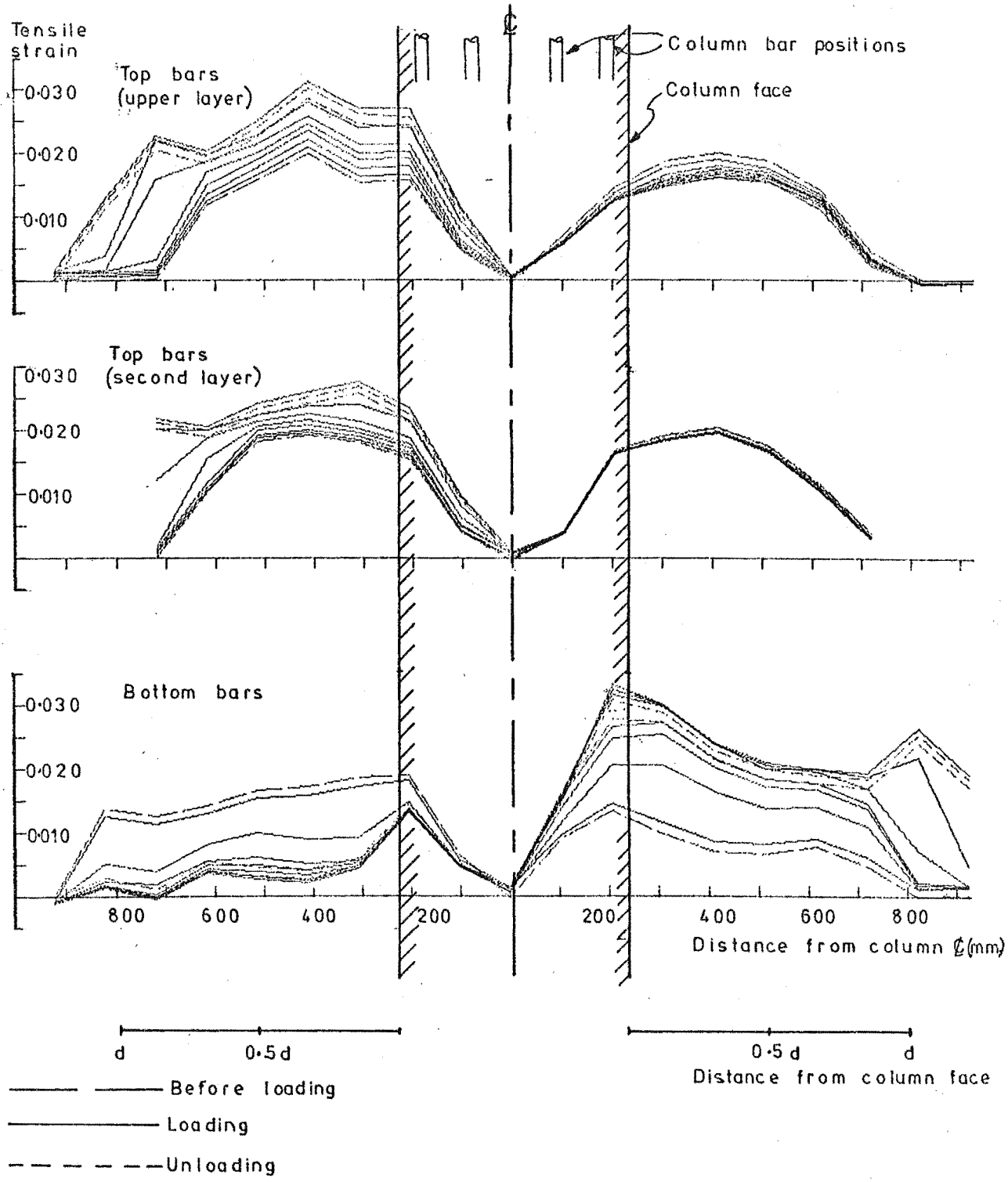

FIG. 3.14 : BEAM BAR STRAINS, LOAD RUN 17

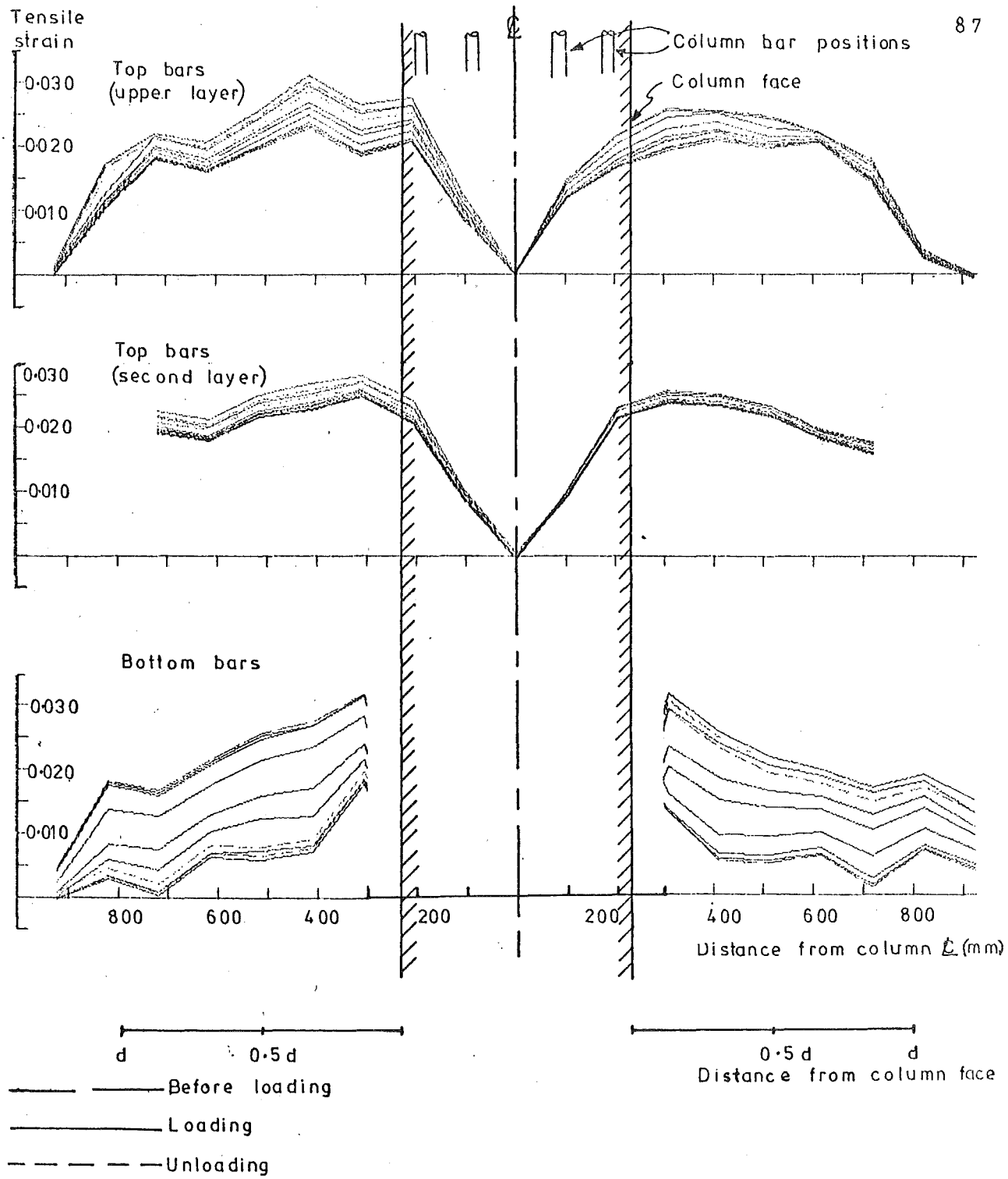

FIG.3.15 : BEAM BAR STRAINS, LOAD RUN 19

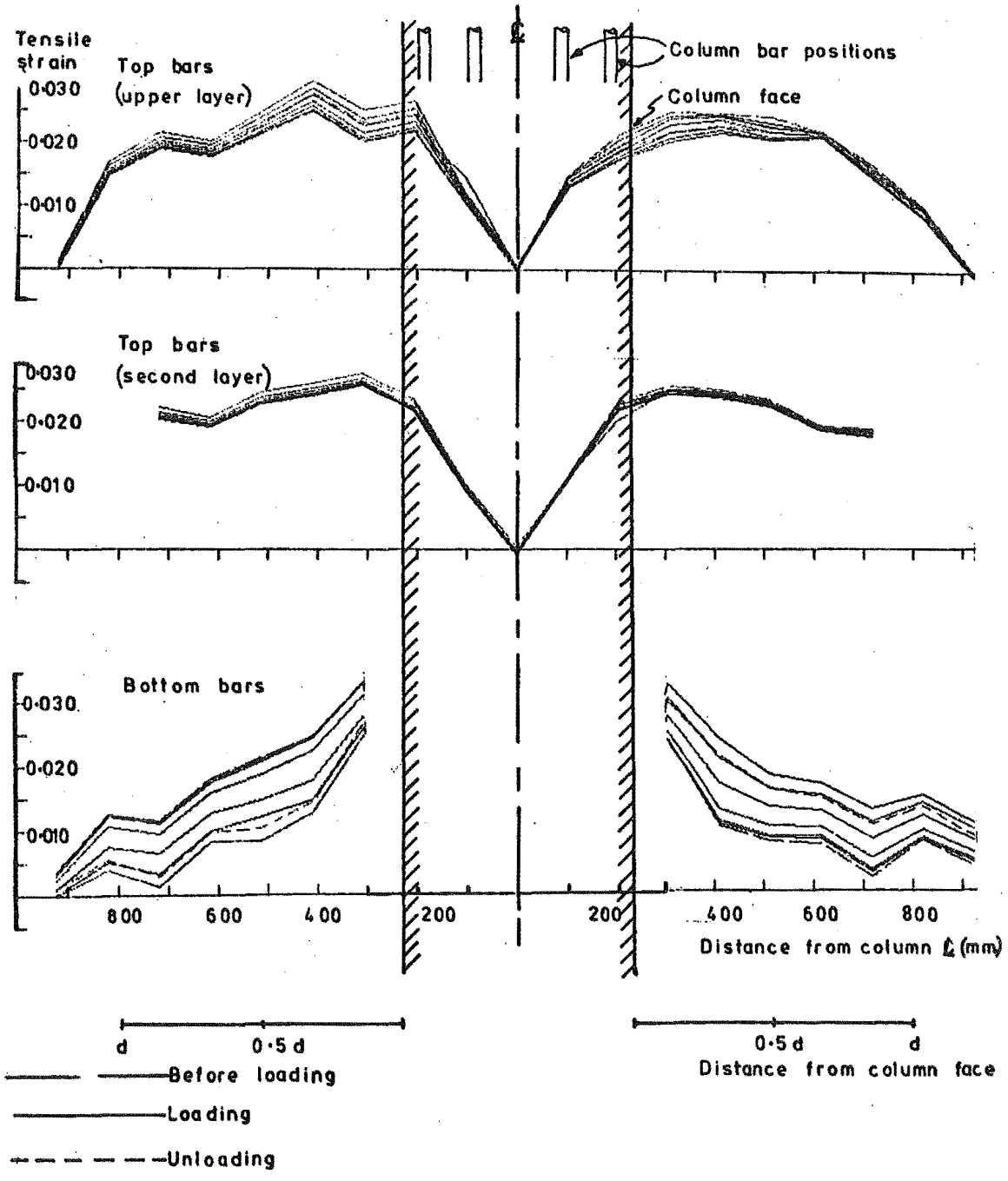

FIG·3.16 : BEAM BAR STRAINS, LOAD RUN 21

The magnitude of tensile strains measured in the beam reinforcement exceeded the strain at the commencement of strain-hardening from load run 11 onwards. This accounts for most of the overstrength noted in Table 3.1. It also partly accounts for the spread of yielding along the beam bars described above, since the greater the overstrength moment at the column face, the larger the distance from the column face at which the first yield moment was attained in the beam. The spread of yielding was also affected by slip of the beam bars in the concrete.

Figs. 3.12 to 3.16 show that maximum strains in the flexural reinforcement did not occur across the column face crack, but at the next crack, which was 100 to 200 mm away from the column face. This feature was more pronounced for the top bars, and the reason for it was interaction between shear and flexural resistance of the beam hinge. Diagonal cracking under negative loading affected the rotational demands from load run 11 onwards, and the strain profiles reflect this characteristic.

The bar strain profiles show that after the first cycle to each successively larger ductility factor, the bottom reinforcement provided most of the plastic deformation, whether positive or negative loading was being applied. Under positive moment loading the neutral axis was close to the second layer of top bars, so that strain-hardening of the bottom bars caused compression yielding of the top layer of top bars, and small elastic compression strains in the second layer. Under repeated negative moment loading the top bars just reached yield stress, and the bottom bars again provided most of the inelastic deformation, this time in compression. Only when a larger displacement demand was made did the top reinforcement undergo significant plastic deformation. Obviously this implies that the flexural steel content of the beam hinge was poorly utilized, as the bottom reinforcement (i.e. only one third of the total steel content) was required to dissipate most of the input energy, and this apparently contributed to the eventual slip failure of the bottom bars.

3.3.4 Beam Reinforcement Stresses

The strain histories measured from the beam bars during the test were analysed using a cyclic loading program for reinforcing steel developed by Spurr[33] to give an estimate of beam steel stresses in the vicinity of the joint during the test. Plots of stress-strain histories are given in Figs. 3.17 to 3.19 for bars in each of the three layers of reinforcement at a section 75 mm from the column face in the western beam. Equilibrium

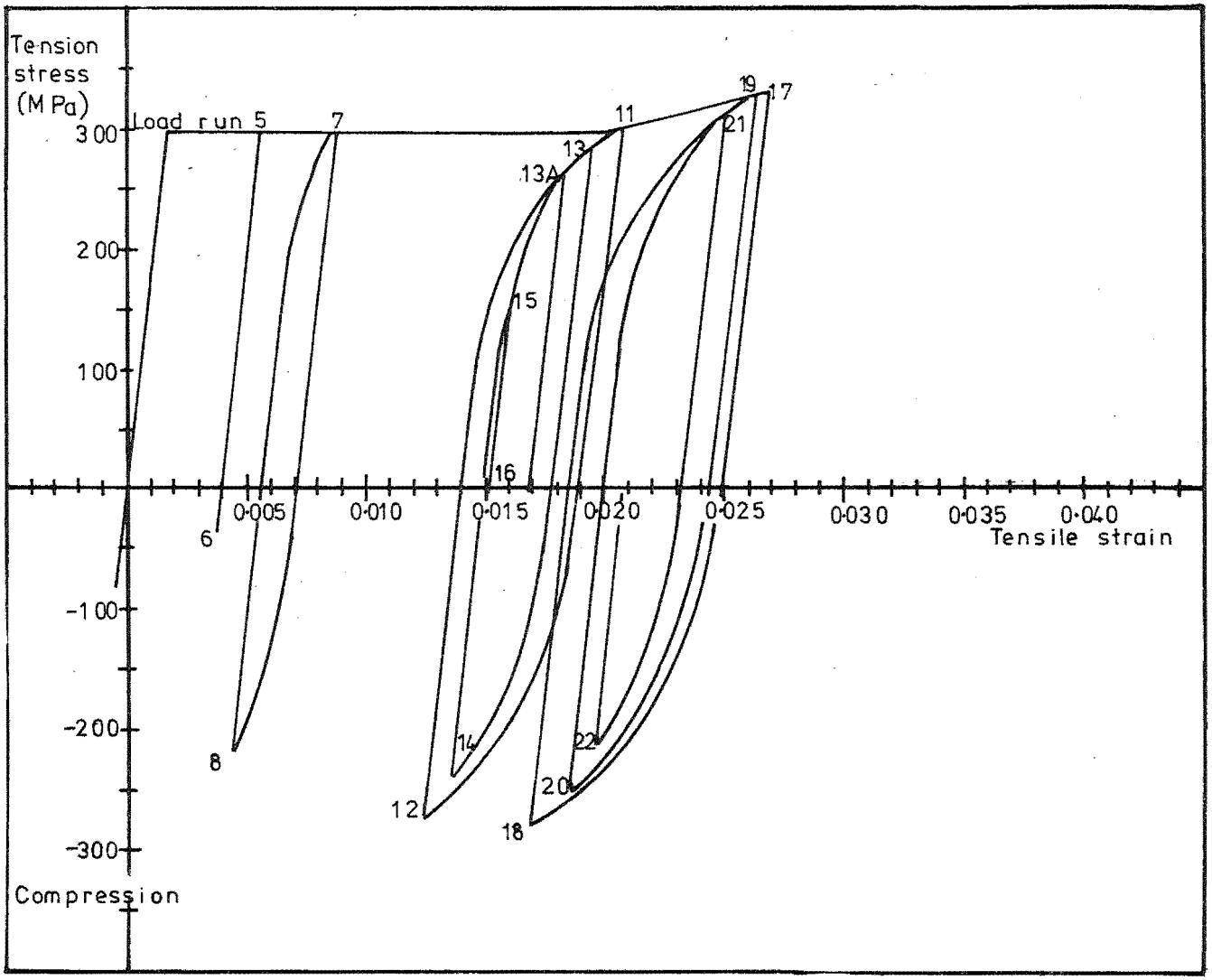

FIG.3.17:STRESS-STRAIN HISTORY FOR UPPER LAYER OF TOP REINFORCING AT 76MM. AWAY FROM COLUMN FACE IN WESTERN BEAM

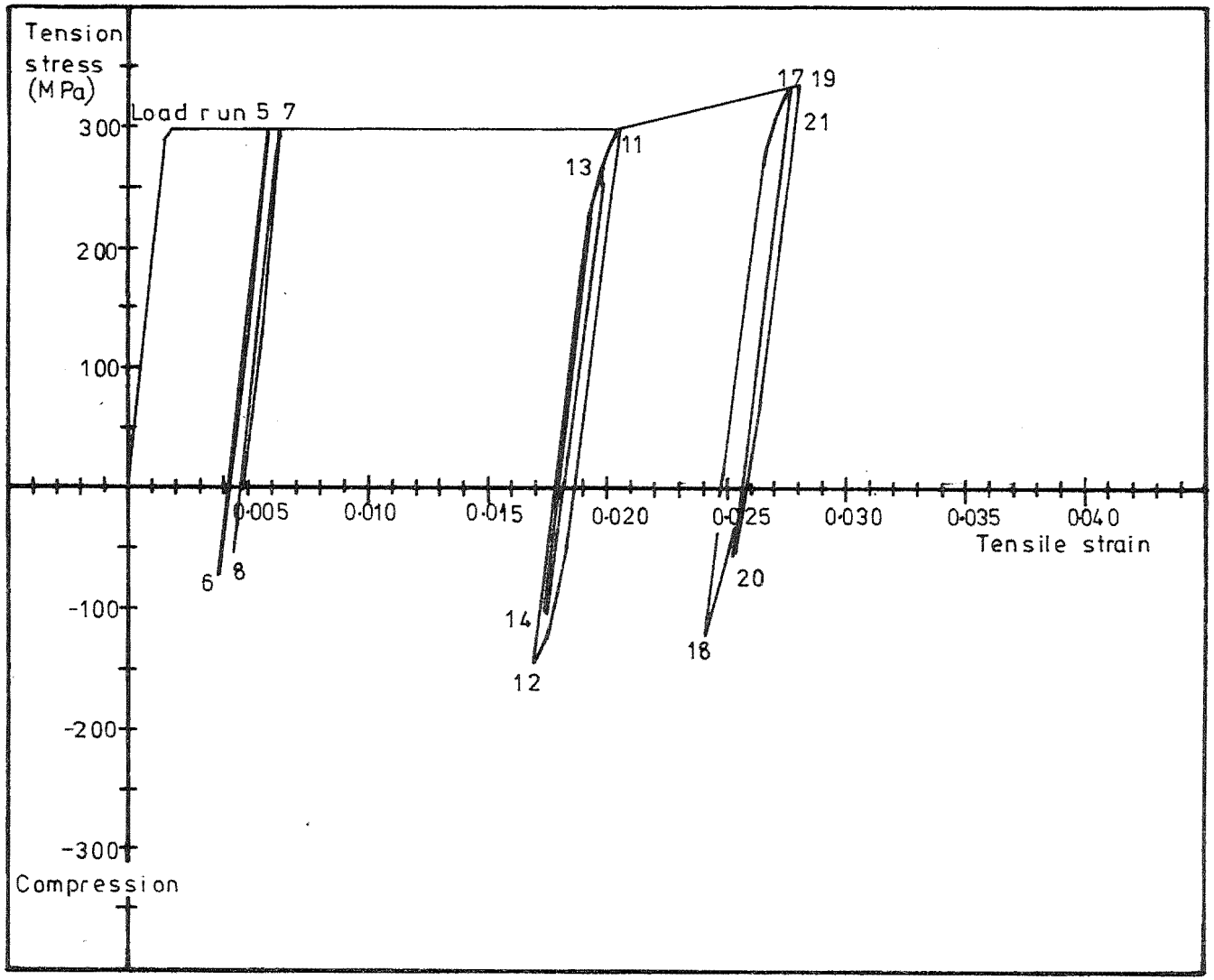

FIG.3.18 : STRESS-STRAIN HISTORY FOR SECOND LAYER OF TOP REINFORCEMENT AT 76 MM. AWAY FROM COLUMN FACE IN WESTERN BEAM.

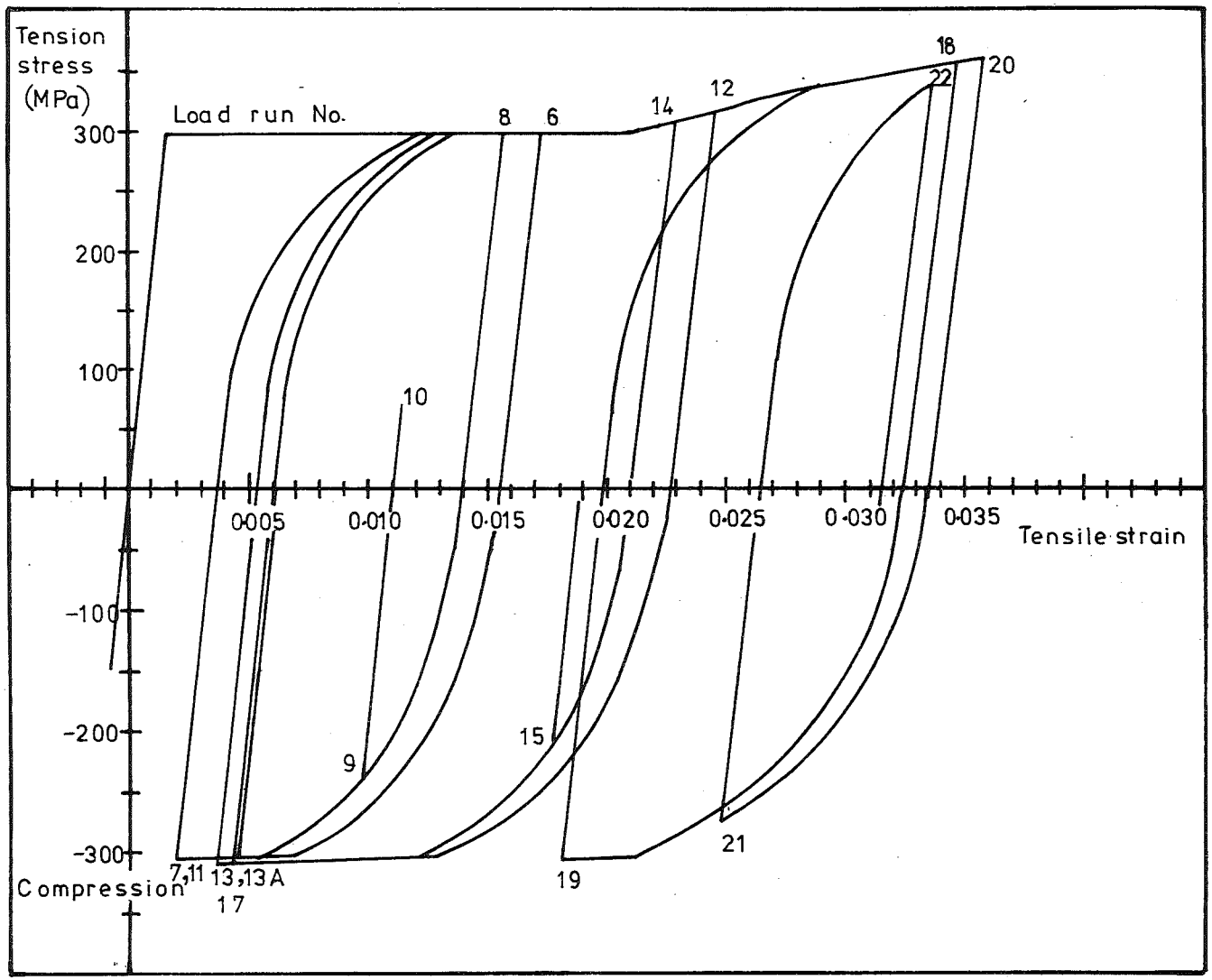

FIG. 3.19 : STRESS-STRAIN HISTORY FOR BOTTOM REINFORCEMENT AT 76 MM. AWAY FROM COLUMN FACE IN WESTERN BEAM

checks for this section and the corresponding section in the eastern beam show that force balance at maximum displacement under positive moment loading is generally within 15%. This is considered acceptable in this case where the compression stress in the second layer of top bars is in the elastic part of the curve, and is very sensitive to the experimental strain values, both for maximum tension strain in the previous load run, and for the compression reading in the positive load run. A force balance check is not possible for negative bending since the concrete takes some compression and must be assumed to carry the difference between the tension and compression forces calculated for the reinforcement. If the calculated bar forces are taken as correct in this case the location of the centroid of concrete compression may be obtained by calculating the beam internal lever arm, since the internal forces and the applied moment are known. However these calculations resulted in a range of answers for the depth of the centroid of concrete compression from 5 mm to 126 mm away from the compressed edge, and this was considered too wide a range for particular results to be used with confidence.

To allow a moment balance check to be made the concrete compression forces were assumed to be acting in all cases at the level of the compression reinforcement. Comparisons of moment values from the derived bar forces and from the applied load then indicate that the derived stresses on average underestimate the applied bending moments by 3%. The greatest discrepancies occur in the latter part of the test where strains were in the strain-hardening range. The stress envelope used by the analysis included the virgin strain-hardening curve for the steel, but tests done on samples of the beam steel indicated that at two weeks after first yielding the stresses in the strain hardening range could have increased by up to 8% due to strain ageing. Since the test took four weeks from first yield to completion, it would seem that strain ageing could account for the difference in moment values.

The very different stress-strain histories obtained for top bars and bottom bars illustrate again the inequality of energy dissipation. The area within the curve for a given cycle represents the work done by the steel at that location, and this was evidently relatively large for the bottom bars but quite small for the top layer of top bars, and almost zero for the second layer of top bars.

Figs. 3.20 to 3.22 give plots of stress distributions along the beam steel in the vicinity of the joint, as derived from analyses of strain results similar to those shown in Figs. 3.17 to 3.19. The increasingly severe bond requirement across the joint core is clearly shown by the increasing slope of the stress distributions close to the column centreline. In particular the difference between the plots at load run 5 and at run 7 show the effect on this requirement of cyclic loading as opposed to monotonic loading. As the test progressed and beam displacements were increased, yield penetration resulted in severe bond requirements, especially for the bottom steel. The second layer of top bars had a much less severe requirement because full compression yield was never reached. The graphs indicate that within the limits of experimental and analytical accuracy the bond stress may be assumed to be uniform, i.e. the stress profiles are approximately linear. The critical feature for the determination of the magnitude of bond stresses is the extent of yield penetration

Calculations based on uniform bond stresses along the beam bars through the joint from the steepest parts of the stress profiles in Figs. 3.20 to 3.23 gave the results plotted in Fig. 3.23. The differences in the bond requirements for the bars in the various layers of reinforcement are clearly shown. The maximum bond stress derived for the bottom bars was over five times that at ultimate for bars in tension allowed by the development lengths given in ACI 318-77, Section 12.2.2[4]. The bond stress for the upper layer of top bars also approached this value in load run 18, although the variation in these values from load runs 17 to 22 is considerable. Evidently large bond stresses can be sustained in these situations, although not without limits.

3.3.5 Slip of Bottom Bars

As noted above the bond stresses imposed on the bottom bars exceeded the available bond strength, and slip of the bars through the joint commenced in load run 17. The magnitude of the slip increased with successive cycles, and this resulted in severe loss of stiffness of the unit and pinching of the load-displacement loops, although the ability to attain full load at maximum displacement was not greatly impaired. The slip of outer bars was made visibly obvious by the movement of Demec studs to an off-centre position in their holes in the cover concrete, as shown in Fig. 3.24. The inner bars may not have started slipping at exactly the same stage as the outer bars, but they must certainly have slipped with the

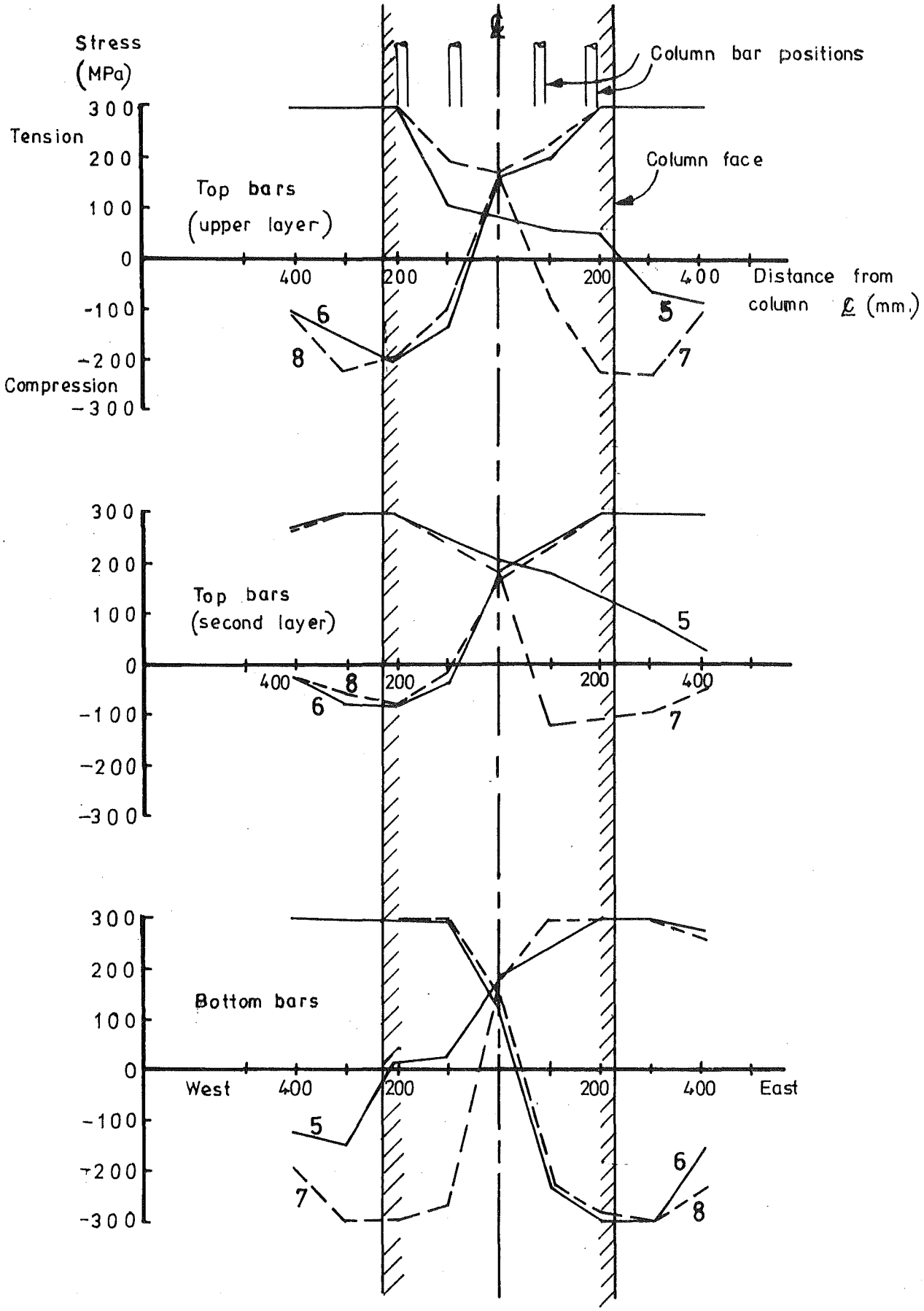

FIG. 3.20; BEAM STEEL STRESSES ACROSS JOINT, LOAD RUNS 5 TO 8.

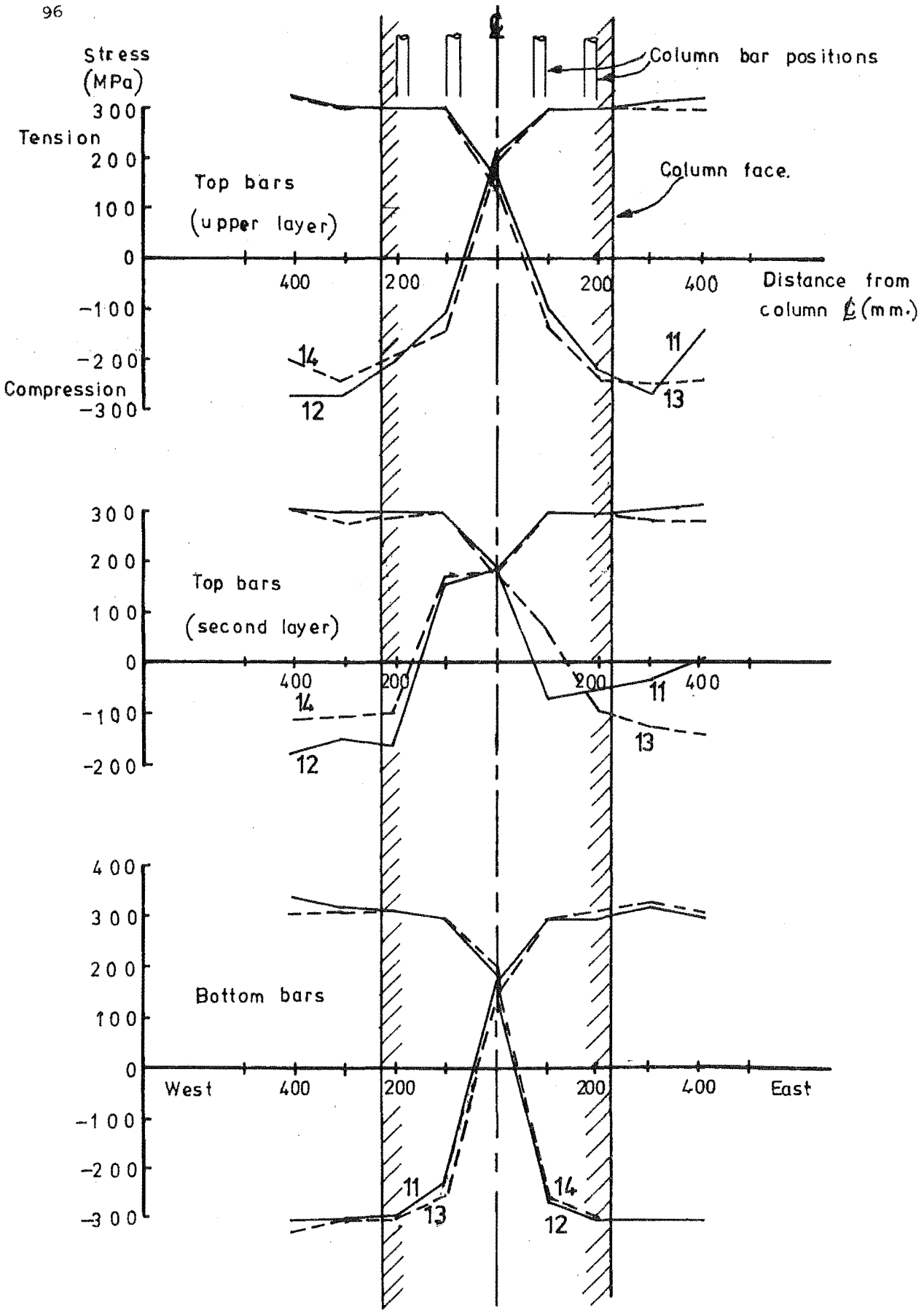

FIG. 3.21 : BEAM STEEL STRESSES ACROSS JOINT, LOAD RUNS 11 TO 14.

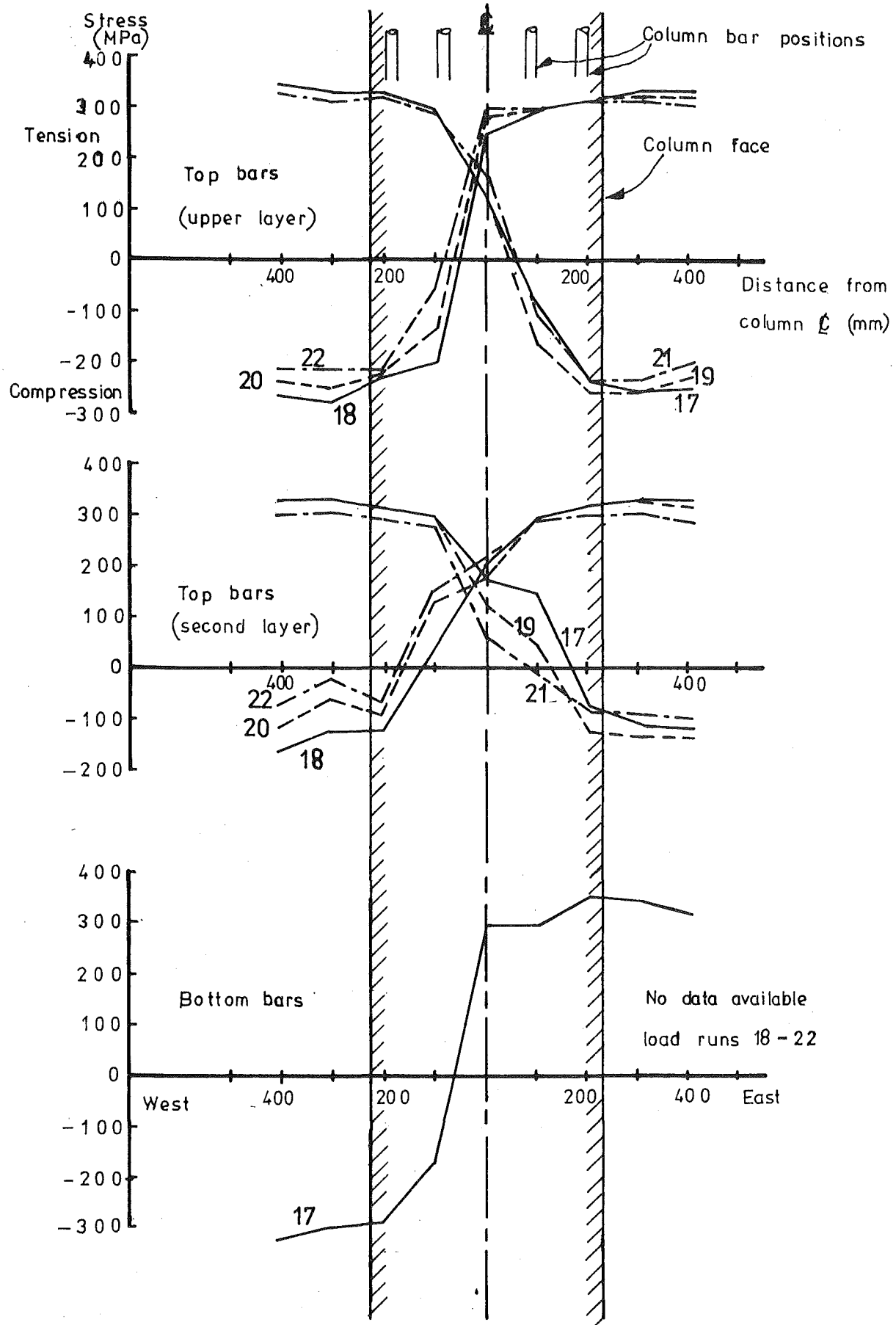

FIG.3.22 : BEAM STEEL STRESSES ACROSS JOINT, LOAD RUNS 17 TO 22

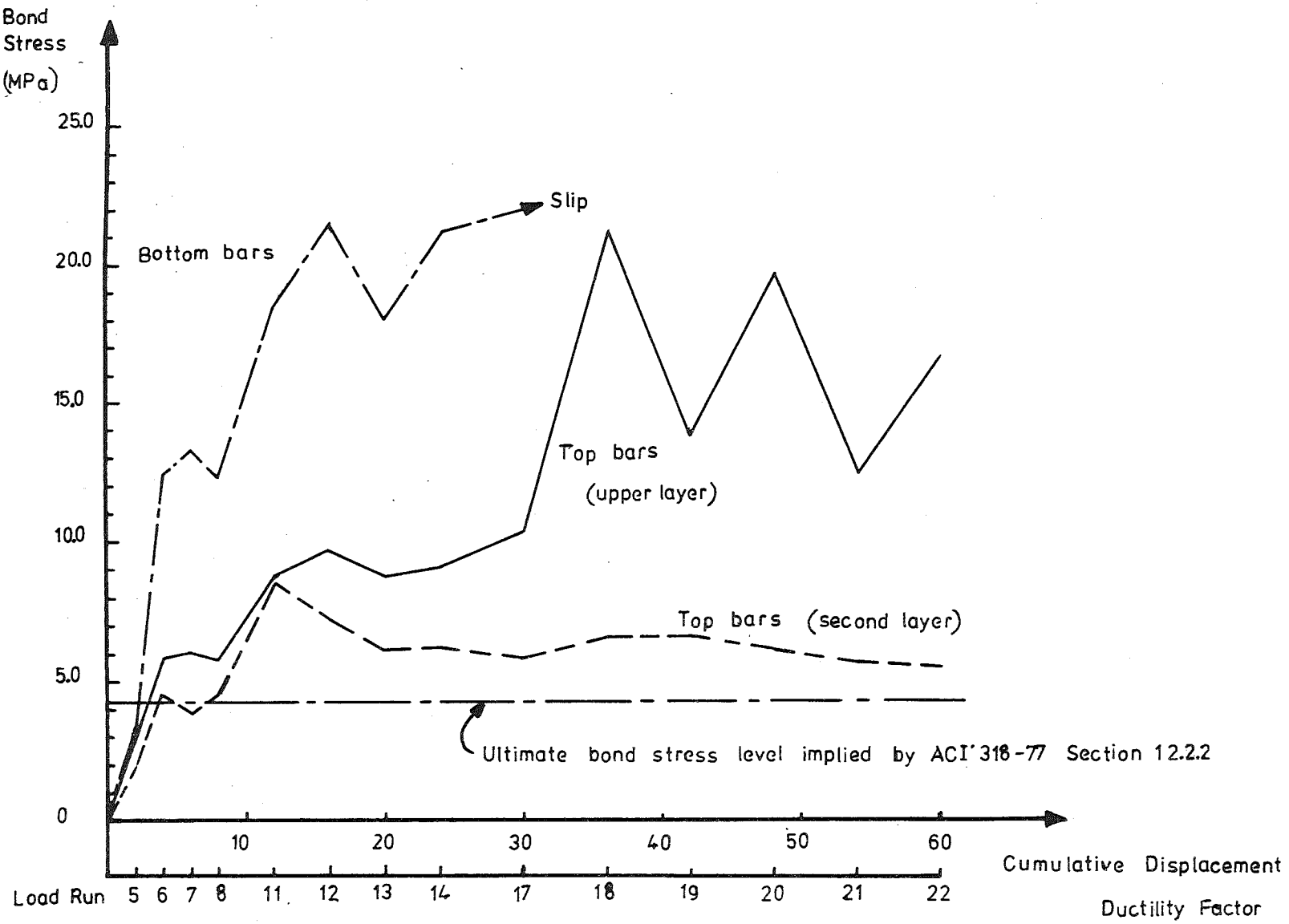

FIG. 3.23 : BOND STRESS IN BEAM BARS ACROSS JOINT.

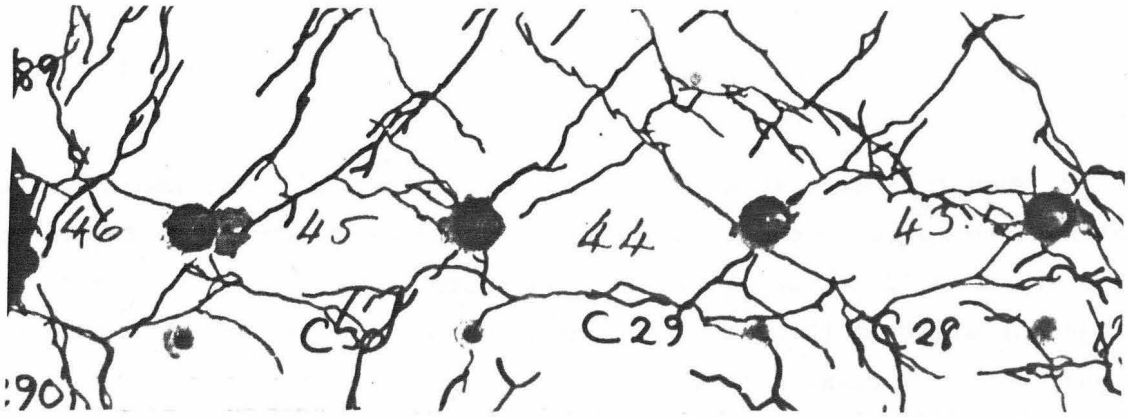

FIG. 3.24: MOVEMENT OF DEMEC STUDS TO BOTTOM BEAM BARS THROUGH JOINT TO OFF-CENTRE POSITIONS IN THEIR HOLES IN THE COVER CONCRETE.

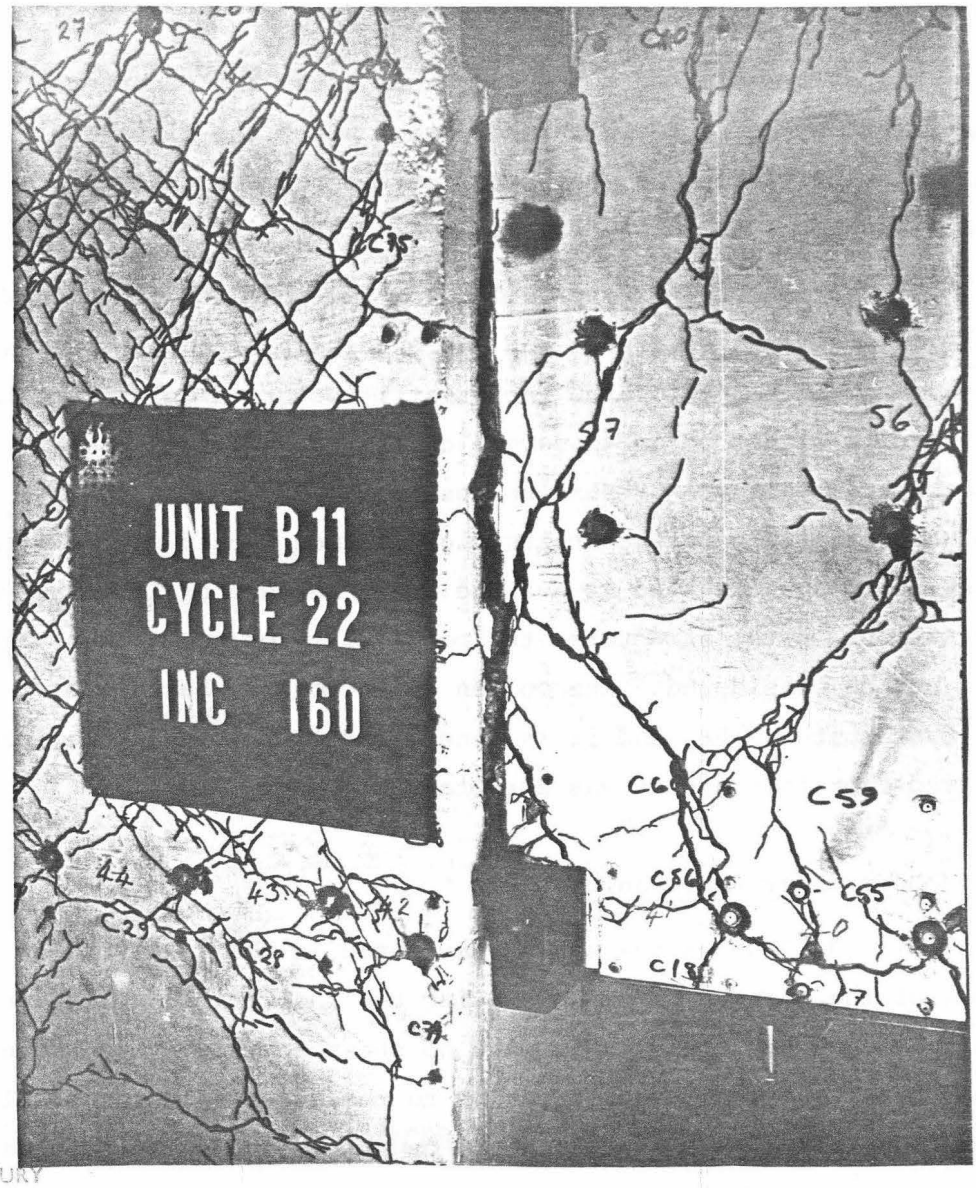

FIG. 3.25: WIDE CRACK AT COLUMN FACE CAUSED BY SLIP OF BOTTOM BARS THROUGH JOINT

outer bars in later cycles, as evidenced by the wide crack which developed at the column face (Fig. 3.25).

When the Demec studs moved in their holes they came into bearing against the cover concrete, and thus provided extra anchorage for the outer bars which would not be available in a prototype structure. In the early stages of slippage this stud bearing combined with bar friction to develop significant compression in the steel at the first available strain measurement position (75 mm from the column face), although maximum compression in the steel was not developed until further along the beam. However this anchorage evidently diminished in efficiency as the test progressed since by load run 21 comparatively little compression was developed near the column face (compare Fig. 3.14 to Fig. 3.16). Probably this was due to less effective friction bond with successive cycles and increased local crushing of the cover concrete under bearing of the Demec studs.

The deformation of the Demec studs after the occurrence of slips is illustrated in Fig. 3.26 which shows that after the first cycle in which significant slip occurred, the studs were effective throughout the load run in providing some anchorage capability.

The effect of the slip failure on the response of the test unit was severe in so far as stiffness and energy dissipation capacity was concerned. However, having regard of the fact that it occurred only after the unit had successfully withstood quite severe cyclic loading, and that it did not cause brittle failure nor serious loss of load-carrying ability at maximum displacement, it is felt that its significance should not be overrated. Serious slippage occurred at a stage when, because of large permanent deformations in the structure, the possibility of post-earthquake repair would not be considered. The column depth to beam bar diameter ratio for this test unit was 24, and it is considered that the bond performance achieved from this design was acceptable.

3.3.6 Beam Shear Resistance

Fig. 3.27 shows the strains measured in beam stirrups at various stages of the test. The lines showing the theoretical stirrup strains predicted by a 45° truss model with no shear carried by concrete obviously gave only a very rough approximation to the observed strains, although the maximum nominal shear stress imposed on the beams during the test was only

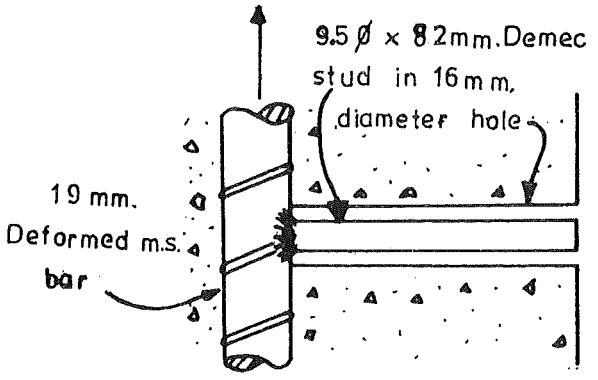

(a) No slip - Demec stud central.

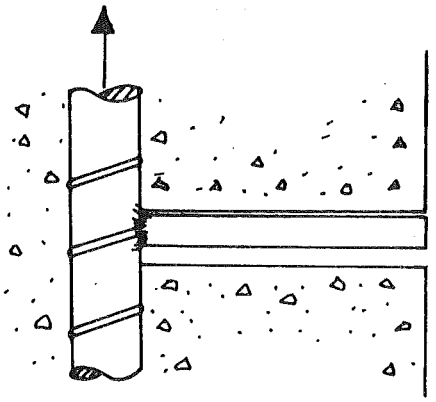

(b) First slip - stud moves in direction of load.

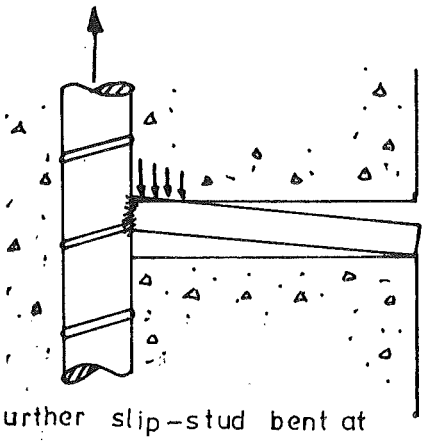

(c) Further slip - stud bent at base; visible end moves to side of hole opposite load.

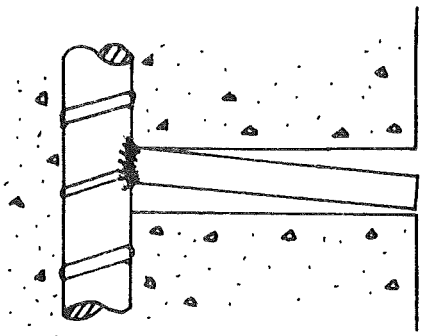

(d) Zero load - elastic recovery of stud.

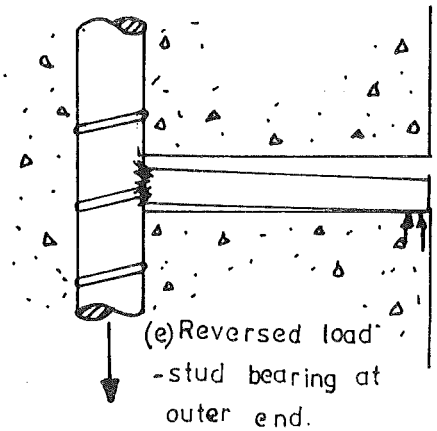

(e) Reversed load - stud bearing at outer end.

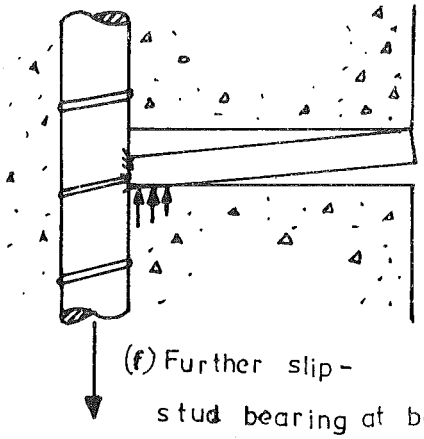

(f) Further slip - stud bearing at base.

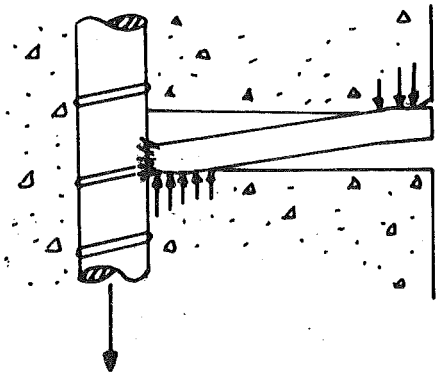

(g) Further slip - stud bearing at base and end

FIG. 3.26: MECHANISM OF ANCHORAGE PROVIDED BY DEMEC STUDS TO SLIPPING BEAM BARS.

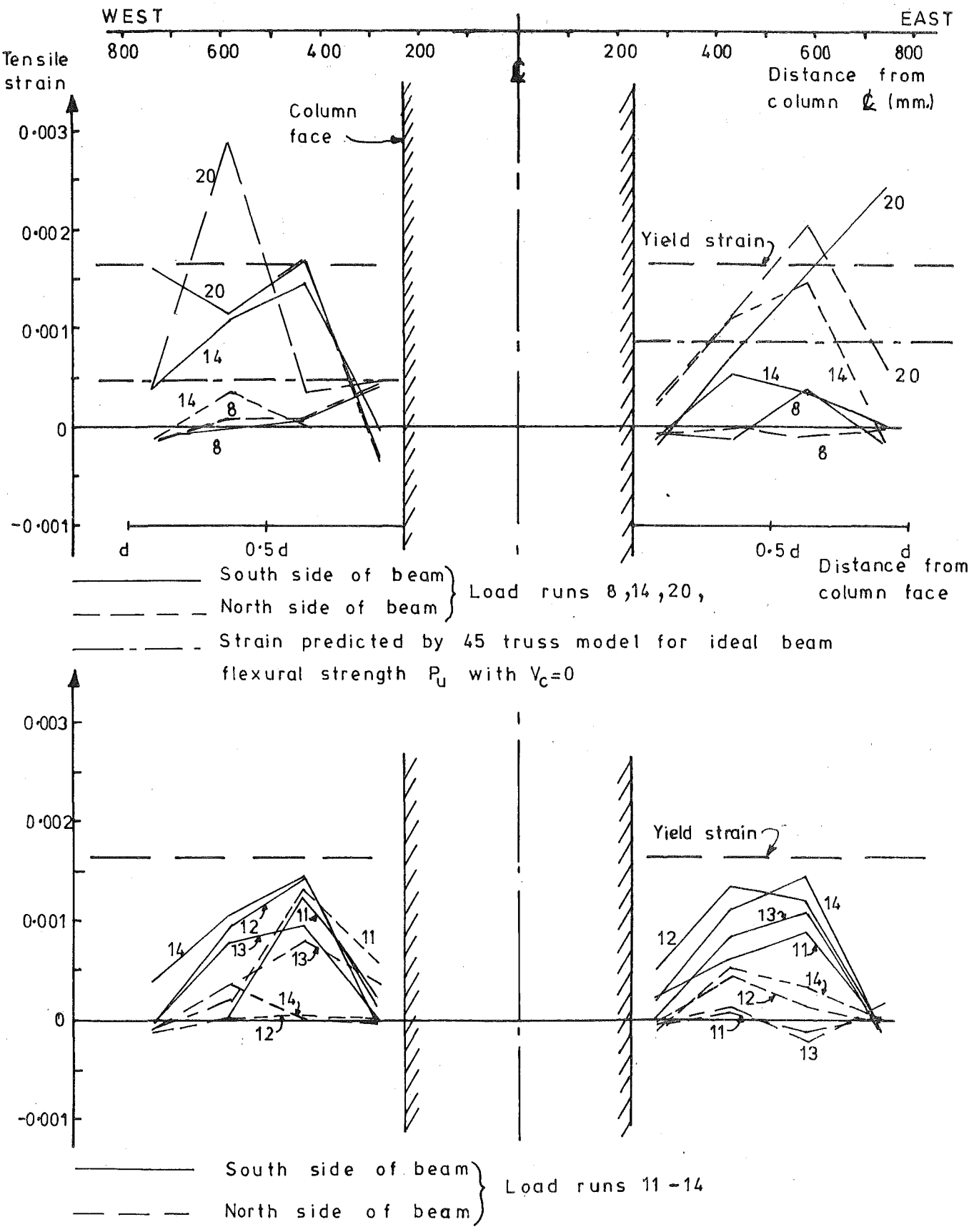

FIG. 3·27: BEAM STIRRUP STRAINS

0.94MPa (or $0.157\sqrt{f'_c}$ MPa). The photographs (Figs. 3.1 to 3.4) show that diagonal cracking was pronounced, especially under negative moment loading, while the tendency for the holes provided for the Demec studs on the beam stirrups to act as crack initiators is also shown. Thus the stirrup strain data recorded was not representative, and was insufficient to support any more elaborate model of shear resistance.

Shear deformation in the beam hinges caused significant stiffness degradation throughout the test (see Section 3.2) especially for negative moment loading where flexural cracks were initially open over the full depth of the beam. This deformation was apparent as sliding displacement along the cracks; this was estimated to be approximately equal for both directions of loading, although the measurements were not precise. A contributing factor towards the magnitude of these displacements was the tendency for flexural cracks to be well distributed and narrow near the beam flexural bars, but to combine into relatively few wider cracks in the mid-depth of the beam. The inclusion of small longitudinal crack control bars at mid-depth might have improved this situation considerably.

3.4 Column Behaviour

When ultimate loads were applied to the beams the column became extensively cracked above and below the joint with the major cracks forming at the level of the beam top and bottom surfaces (see photographs - Figs. 3.2 to 3.4).

Strains measured on the longitudinal column bars in the south face of the column at the maximum displacement of the major cycles are plotted in Figs. 3.28 to 3.30. Some irregularities are apparent in the strains measured in the vicinity of the beam top bars. The expected strain pattern due to flexure and axial load was disrupted at this level by the large bond forces that were transferred from the beam bars in this locality. The apparent strains measured in the column bars were affected by (a) bending of the column bars under the action of the beam bar forces, and (b) confinement of the radial bursting forces in the concrete arising from the high bond stresses. The strains in the column bars were measured by Demec gauges from studs producing the reading to the column face, but since the strains observed in the transverse ties were not excessive (see Section 3.5.5 below), it seems unlikely that any tendency for the column bars to bulge out of the face was sufficient to cause exaggerated readings from the Demec studs. Extra tensile strains were

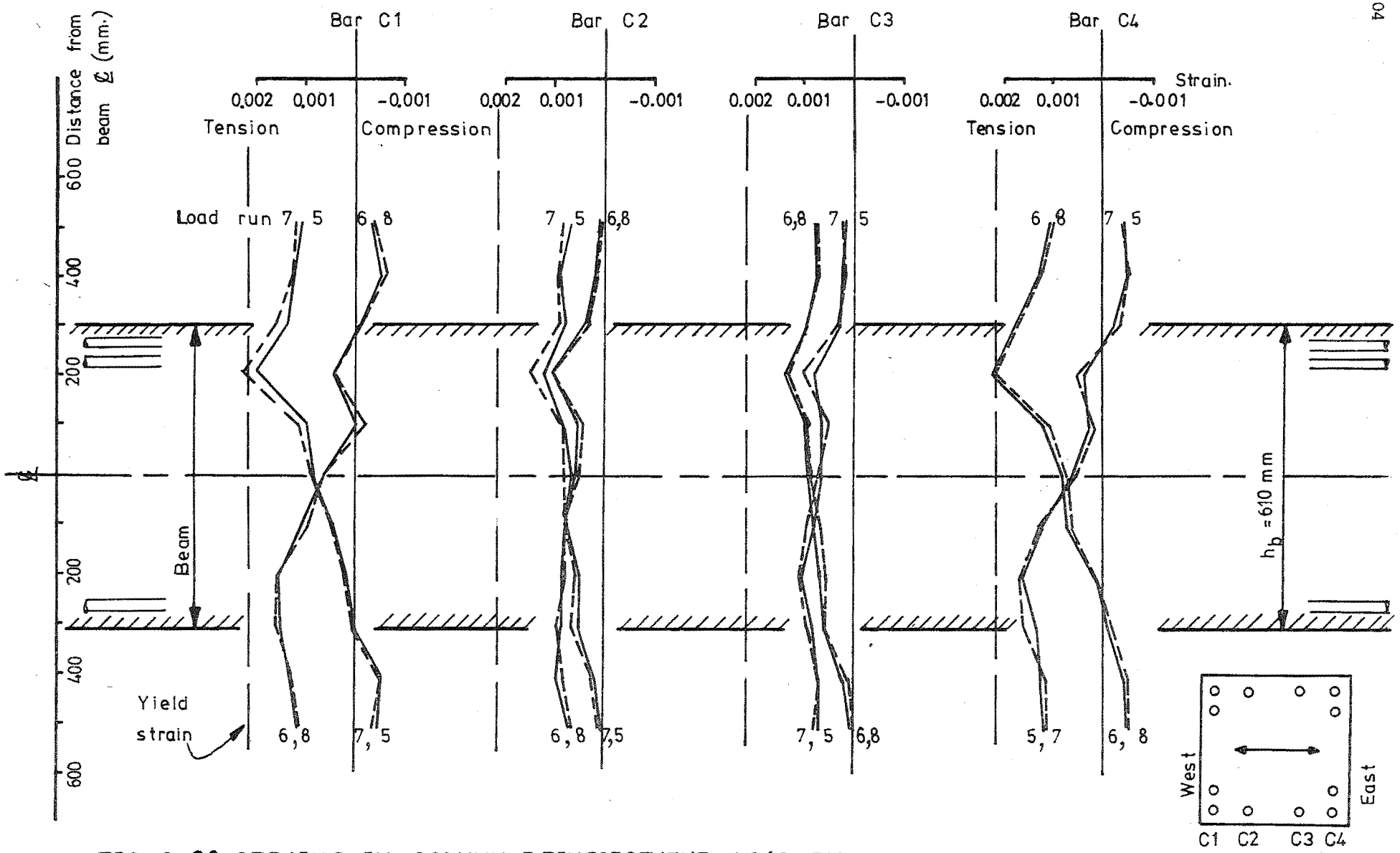

FIG. 3.28: STRAINS IN COLUMN REINFORCEMENT - LOAD RUNS 5-8

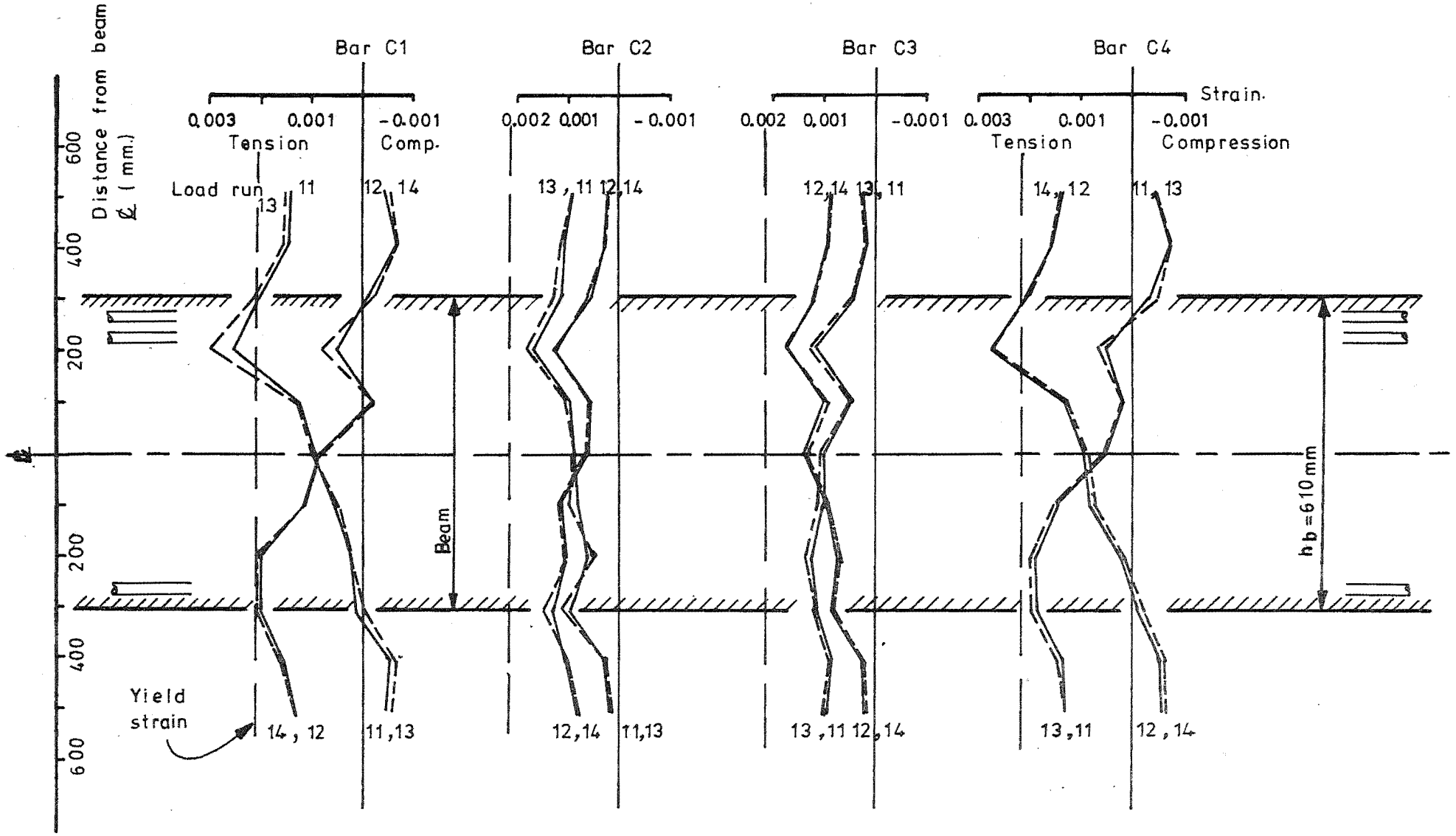

FIG. 3·29: STRAINS IN COLUMN REINFORCEMENT - LOAD RUNS 11–14

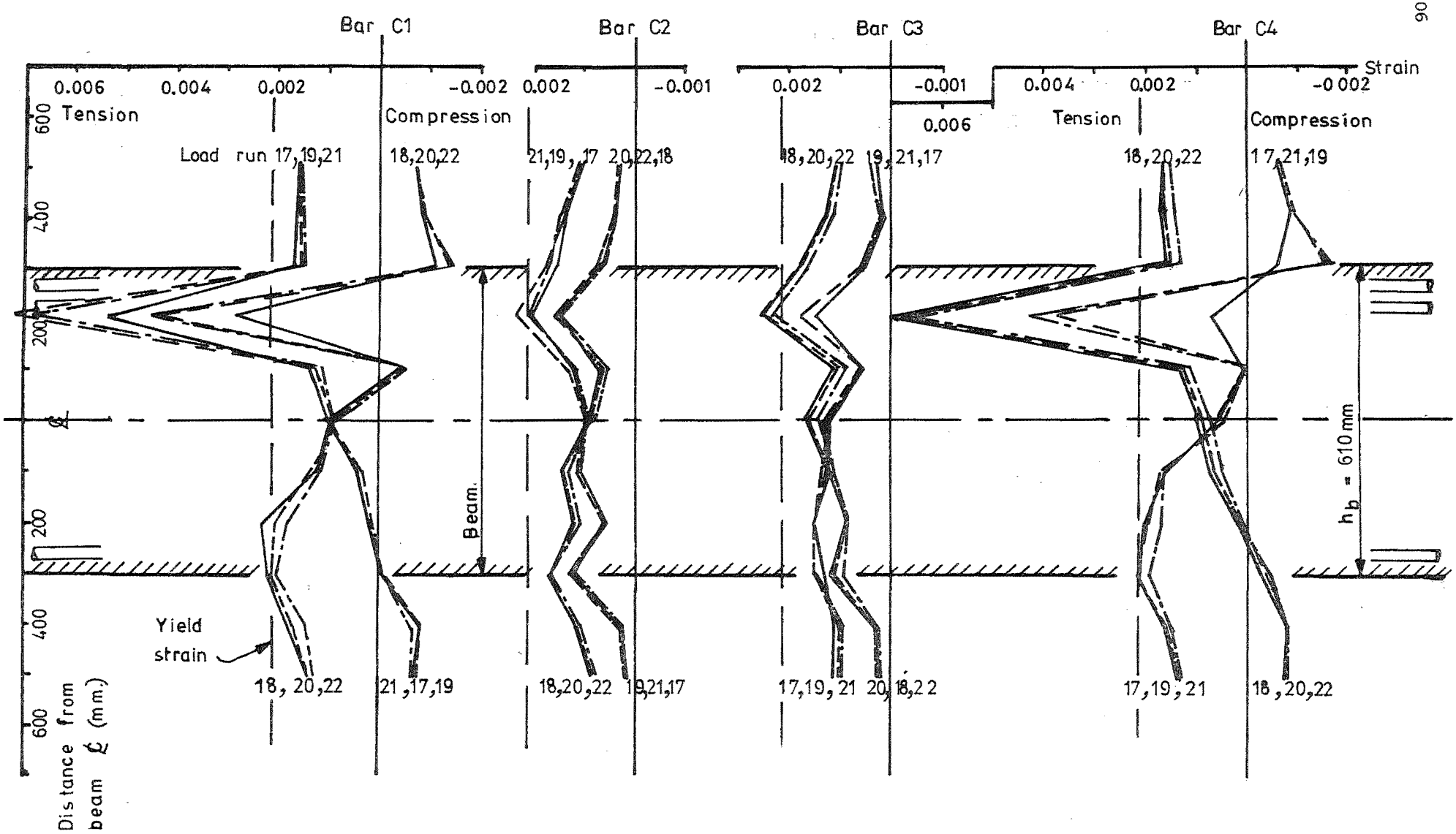

FIG.3.30:STRAINS IN COLUMN REINFORCEMENT - LOAD RUNS 17 -22.

also apparent in the column bars in the mid-depth region of the joint. These were caused by the action of the column bars in providing (together with the axial load) the vertical component of the joint shear resistance mechanism (see Section 3.5.4).

3.5 Joint Behaviour

3.5.1 Joint Cracking

The pattern of joint cracking during the test is shown in the photographs (Figs. 3.1 to 3.4). The cracks were well distributed across the joint throughout the test, with no concentration in a single major corner to corner crack as had been observed in some previous tests [10,15,27], since in this test yielding of the joint ties was limited. The inclination of the cracks was close to 45° to the vertical, although analysis of the data showed that in the major cycles the joint shear was resisted at a steeper angle close to the joint diagonal angle (see Section 3.5.4). The cracks at 45° would be as predicted by the direction of principal tensile stresses in the uncracked body, since the applied axial load was small.

The maximum crack widths observed in the joint panel were 0.30 mm in cycles to displacement ductility factor of 2.0 ; 0.40 mm in cycles to ductility 4.0 ; and 0.55 mm in the final cycles to ductility 6.0 . Cracks closed up to about 0.20 mm at zero load, even in the final stages of the test. Some sliding shear displacement along the joint cracks was observed, with a maximum of about 0.25 mm.

Towards the end of the test the cover to the joint was observed to be separating from the core in some areas, especially near the top of the joint. This was determined by tapping the cover with a screwdriver handle and noting the extent of the hollow sound. No cover concrete was actually lost, but it was estimated that separation had occurred over perhaps 30% of the area of cover concrete.

3.5.2 Joint Deformation

Opening of joint cracks and sliding along them led to shear deformation of the joint panel, and this deformation was a significant source of beam end displacement as noted in Section 3.3.1 and Figs. 3.8 and 3,9, Because yielding of joint shear reinforcement was limited, the joint distortion did not become excessive and it followed the load in a basically elastic manner. As a proportion of total beam end displacement

the component caused by joint rotation was a maximum of 27% in load run 8, while the maximum absolute contribution to beam end displacement was 14.3 mm in load run 18 (16% of the total).

3.5.3 Strains in the Horizontal Joint Shear Reinforcement

Fig. 3.31a shows the increasing strains in the horizontal joint shear reinforcing during the course of the test. The strains plotted are those measured in the inner legs of sets of ties. Strains were distributed rather unevenly down the depth of the joint, with yield strain exceeded in two positions during load run 20, while other ties carried less than half of yield strain. The strain pattern does not correlate well with an assumption of uniform strain distribution resulting from a single diagonal crack. Strains tended to increase as the ductility demand on the unit was increased, although this was not so for the strains in the ties close to the bottom beam bars during load run 20 relative to those observed in load run 14. This was because the shear input by means of bond stress along the bottom bars had been decreased due to the onset of slip. More shear was being introduced as concrete compression which could be resisted by direct diagonal strut action in the lower part of the joint, so that the joint reinforcement strains were decreased in this vicinity.

Fig. 3.31b gives an envelope of the maximum strains observed in the joint shear reinforcement throughout the test. Yield strain was exceeded at three stirrup positions, with a maximum strain observed of 19% greater than yield strain in the first tie set below the beam top bars at the maximum displacement of load run 19. Evidently the yielding was well controlled and did not seem to affect the performance of the joint in resisting the input shear, so that this extent of yielding would appear to be quite acceptable. Some redistribution of strain in the vicinity of the yielded ties was apparent, with adjacent ties taking greater load after given ties had yielded.

The inner legs of tie sets carried more strain than the outer legs at all levels. This was because (a) the corners of the inner legs were more firmly located in the core concrete than those of the outer legs, (b) the inner stirrup legs were physically closer (in the transverse direction) to the beam bars providing the input shear, and (c) the inner legs had to balance a greater width of the concrete compression struts of the truss mechanism (see Section 1.3.3), and would therefore be expected to carry more load.

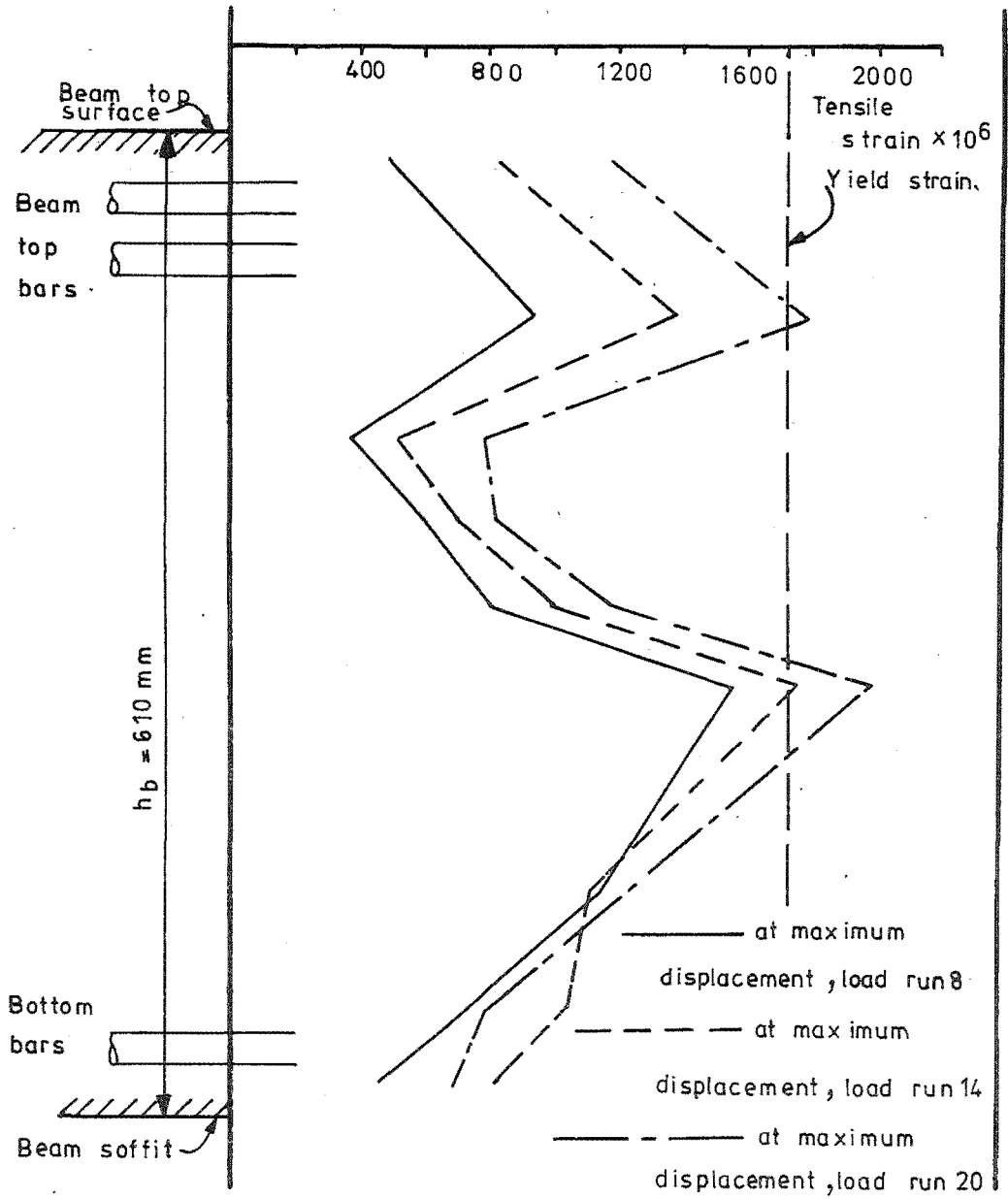

FIG. 3.31: (a) DEVELOPMENT OF STRAINS IN INNER STIRRUP LEGS OF JOINT REINFORCEMENT.

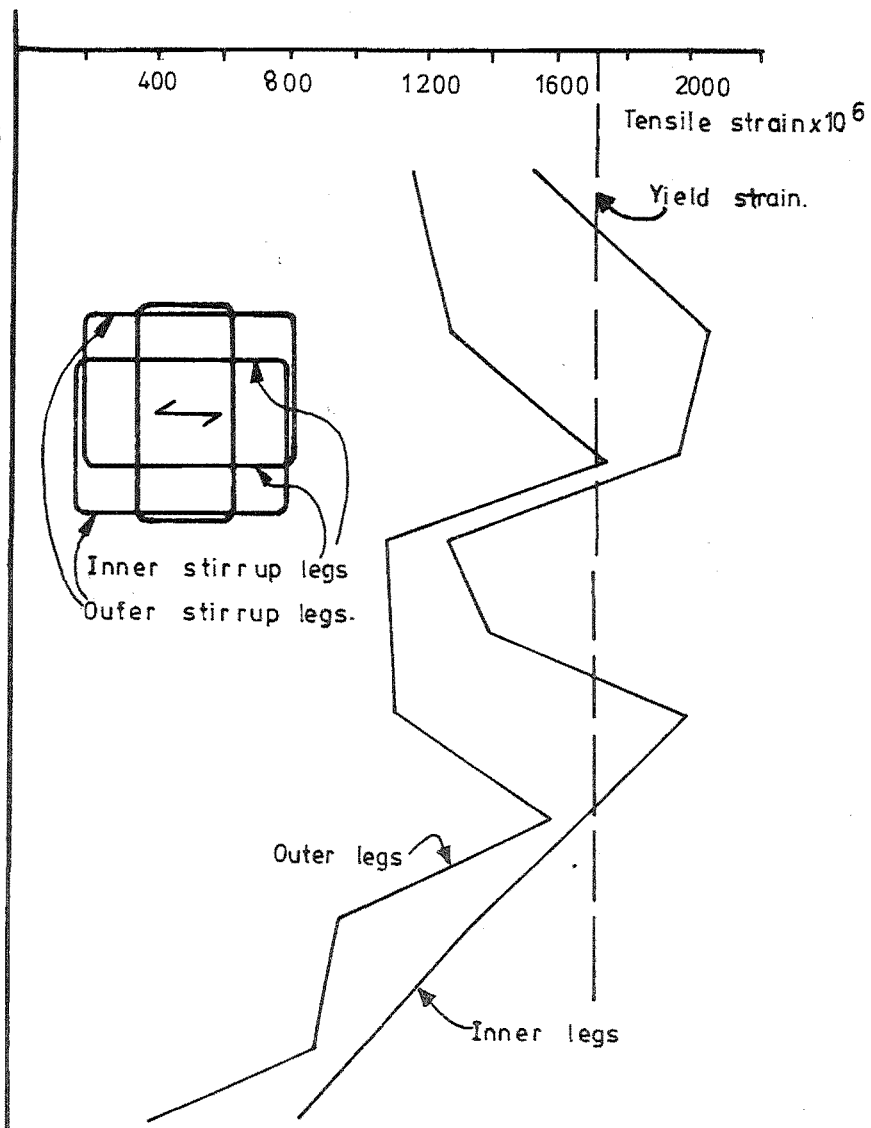

(b) ENVELOPE OF MAXIMUM STRAINS IN STIRRUP LEGS.

The distribution of strains along joint ties in four out of the eight tie sets was measured at the top of each load run, and these results are shown in Fig. 3.32 for load runs 5, 6, 19 and 20. The strains were clearly greater close to the critical diagonal failure plane of the joint, and a strain gradient along the ties is evident, especially near the top and bottom of the joint. Thus some bond transfer from ties to concrete occurs.

A history of strain versus joint shear is presented in Fig. 3.33 for the inner stirrup leg of tie set 4, which was just below the mid depth of the joint. The increasing strain demand as the applied ductility was increased is evident, as is the consistent elastic recovery of the strains when load was released. This was reflected in the elastic nature of joint deformation, and the closing of the joint cracks.

3.5.4 Mechanism of Joint Shear Resistance

The measured strains in the stirrup legs of the horizontal joint shear reinforcement at the maximum displacement of each load run were converted to stresses and summed to give the total shear V_{sh} carried by the joint shear reinforcing in the horizontal direction across a diagonal crack.

$$V_{sh} = \Sigma A_{shi} . f_{shi} \tag{3.3}$$

This quantity was then subtracted from the input joint shear V_{jh} derived from the beam end loads to give the shear carried by the concrete mechanism in the horizontal direction.

$$V_{ch} = V_{jh} - V_{sh} \tag{3.4}$$

These values are tabulated in Table 3.3 and presented in histogram form in Fig. 3.34 (Note: no strains were measured in this test to give the shear resisted by the short stirrup legs of the joint stirrup ties; data from the later tests indicates that this would have been in the order of 5% of the input shear in the final stages).

The ability of the concrete to resist a significant proportion of the input shear clearly diminished rapidly as the test progressed. From resisting an average of 61% of the shear during the initial elastic cycles the contribution of the concrete decreased to 5.6% at the maximum displacement of load run 18. As expected the reinforcing was required

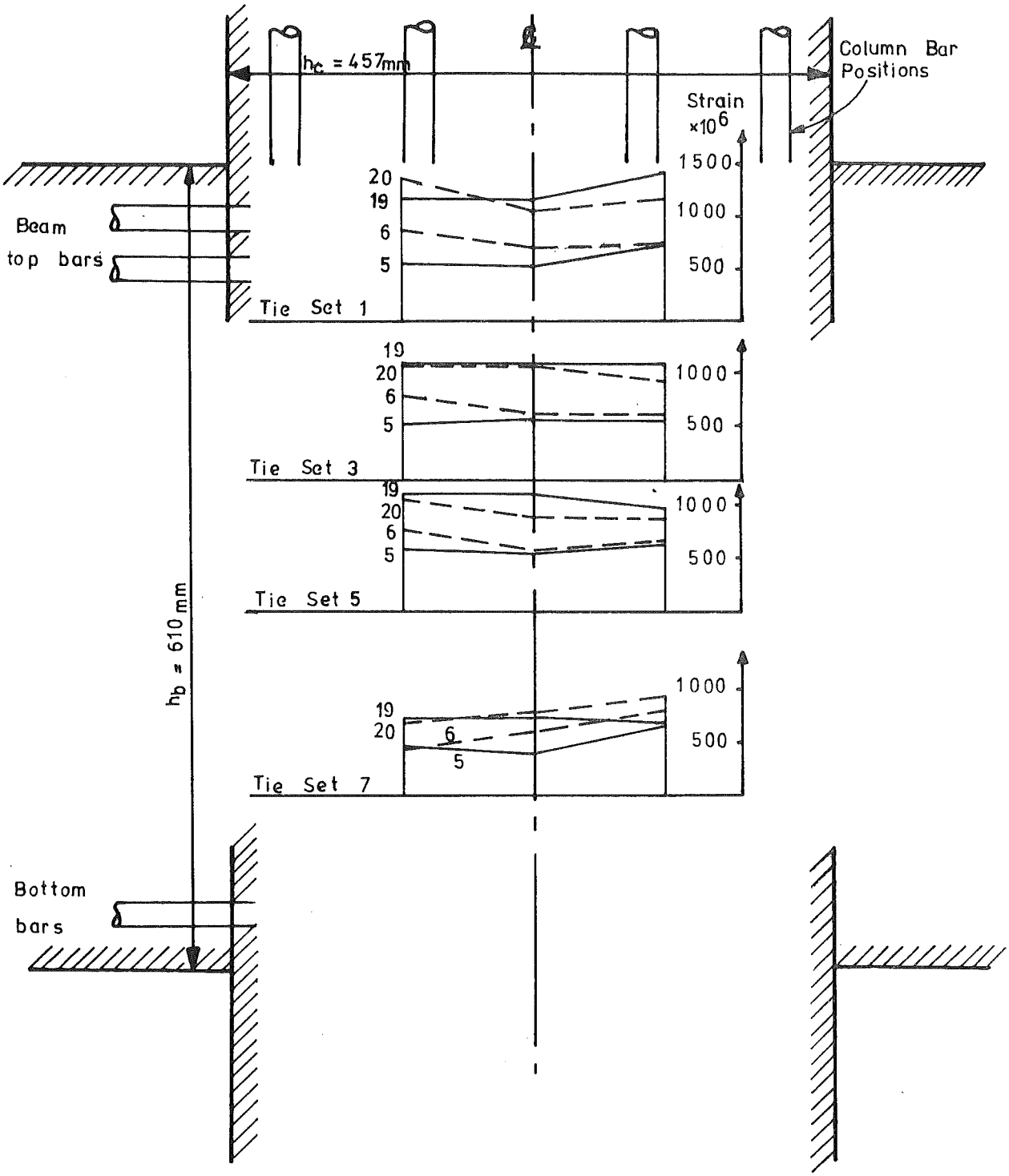

FIG. 3. 32: TENSILE STRAINS ALONG STIRRUP LEGS OF JOINT TIES

LOAD RUNS 5, 6, 19 AND 20.

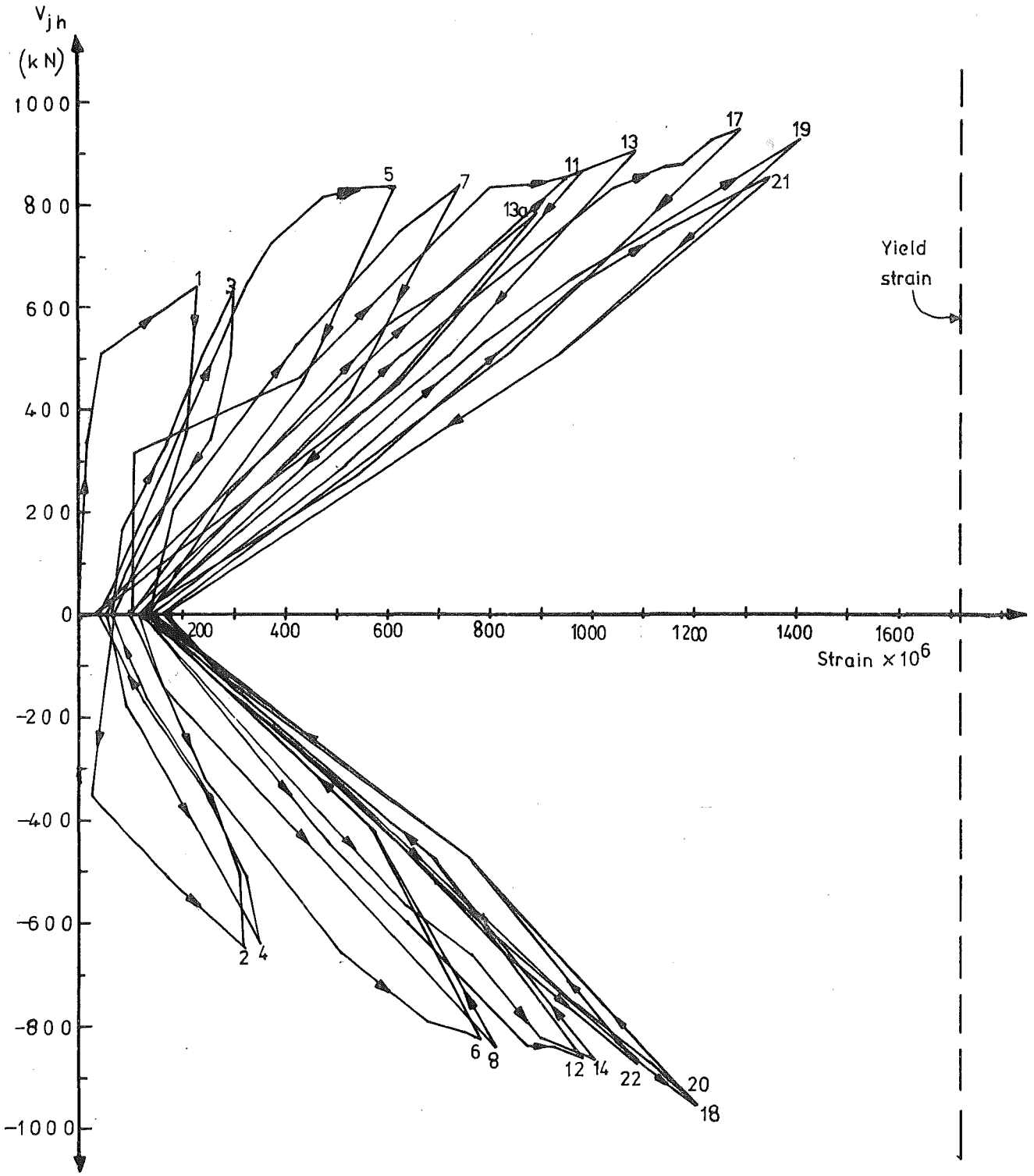

FIG. 3.33: TENSILE STRAIN vs. JOINT SHEAR FOR INNER STIRRUP LEG OF TIE AT MID-DEPTH OF JOINT.

TABLE 3.3 : MECHANISM OF RESISTANCE TO JOINT SHEAR

Load Run No.	V_{jh} (kN)	V_{sh} (kN)	V_{sh}/V_{jh}	V_{ch} (kN)	V_{ch}/V_{jh}	V_{jv}	$\tan\beta_T$	$\tan\beta_c$
1	639.7	222.9	0.348	416.8	0.652	765.8	1.197	-
2	636.0	235.7	0.371	400.3	0.629	892.8	1.404	1.468
3	624.5	255.7	0.409	368.8	0.591	899.0	1.440	1.512
4	623.6	276.5	0.437	356.1	0.563	897.6	1.419	1.493
5	843.2	528.6	0.627	314.6	0.373	1278.5	1.517	1.493
6	818.0	630.4	0.771	187.6	0.229	1497.1	1.830	2.205
7	833.4	639.2	0.767	194.2	0.233	1502.9	1.803	2.116
8	840.1	619.8	0.738	220.3	0.262	1519.1	1.808	2.125
11	880.7	737.6	0.837	143.1	0.163	1714.8	1.947	2.205
12	873.2	809.0	0.927	64.2	0.073	1827.0	2.092	2.395
13	915.5	785.2	0.858	130.3	0.142	1819.4	1.987	2.311
14	876.8	796.4	0.908	80.4	0.092	1857.2	2.118	2.558
17	961.1	851.0	0.855	110.1	0.115	1838.7	1.913	2.091
18	965.3	911.4	0.944	53.9	0.056	1937.2	2.007	2.252
19	939.3	861.4	0.917	77.9	0.083	1856.8	1.977	2.311
20	944.9	803.0	0.850	141.9	0.150	1889.7	2.000	2.322
21	863.6	783.4	0.907	80.2	0.093	1774.7	2.055	2.716
22	883.8	753.5	0.853	130.3	0.147	1779.9	2.014	2.301

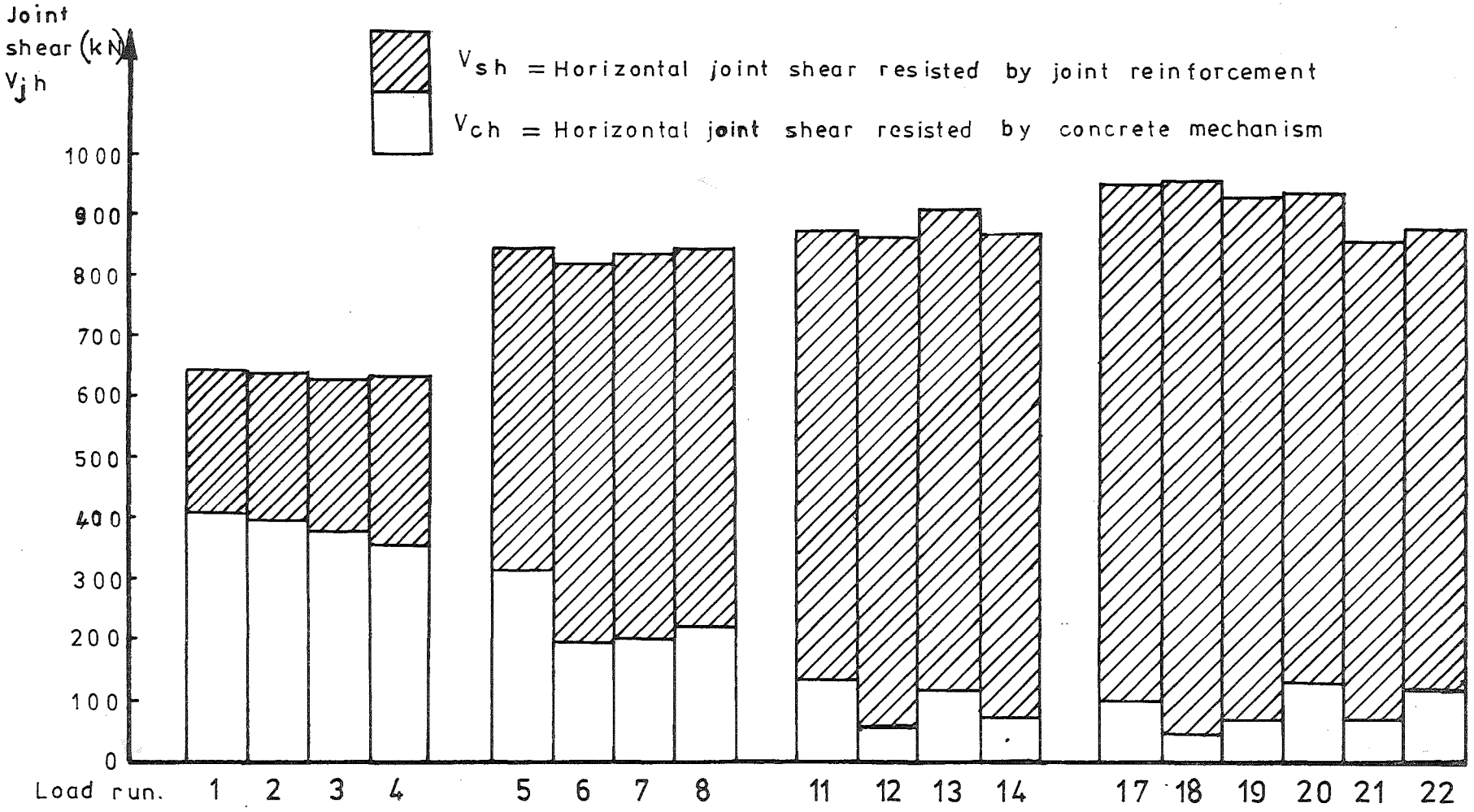

FIG·3·34: MODE OF RESISTANCE TO JOINT SHEAR.

to provide the major element of resistance to horizontal joint shear once inelastic cycles commenced. This was because (a) column axial load level was light and (b) permanently open cracks across the beams at the column face led to all shear being transferred by bond from the beam flexural reinforcement at the top of the joint. These factors did not favour the direct diagonal strut action by which it was postulated that joint concrete would transfer shear (Section 1.3.2) since the effectiveness of this mechanism depends upon the presence of concrete compression forces in the flexural members.

Some longitudinal shear could be transferred by concrete compression at the bottom of the joint where the face crack was closed at maximum displacement, but the direct strut action could not be fully effective because of the lack of an equilibrating system at the top of the joint. Hence more strain tended to accumulate in ties near the top of the joint, as is shown in Fig. 3.31.

Having allocated shear to the reinforcement and concrete in the horizontal direction, it was desired to resolve the forces in the vertical direction in order to assess the total mechanism of joint shear resistance. This was achieved by determining the input shear in the vertical direction from the column bars and concrete. Referring to Fig. 3.35, which shows the actions of the various forces on the joint, the vertical joint shear is

$$V_{jv} = F_{1t} + F_{2t} + F_{1b} + F_{2b} + F_{cb} - V_{BW} \qquad (3\text{-}5)$$

where the column bar forces F_{1t}, etc, were obtained by converting the experimental column strain readings to stresses, and the column concrete compression force F_{cb} was derived by taking the difference between the applied column axial load and the sum of the column bar forces.

The vertical and horizontal shear forces acting on the joint may then be related by the angle β_T

$$\tan \beta_T = \frac{V_{jv}}{V_{jh}} \qquad (3\text{-}6)$$

Values of V_{jv} and $\tan \beta_T$ at maximum displacement of the major load runs are included in Table 3.3.

It was then assumed that the shear resisted by the joint concrete was carried by a direct diagonal strut acting along the line between adjacent centroids of concrete compression in beam and column (see Section

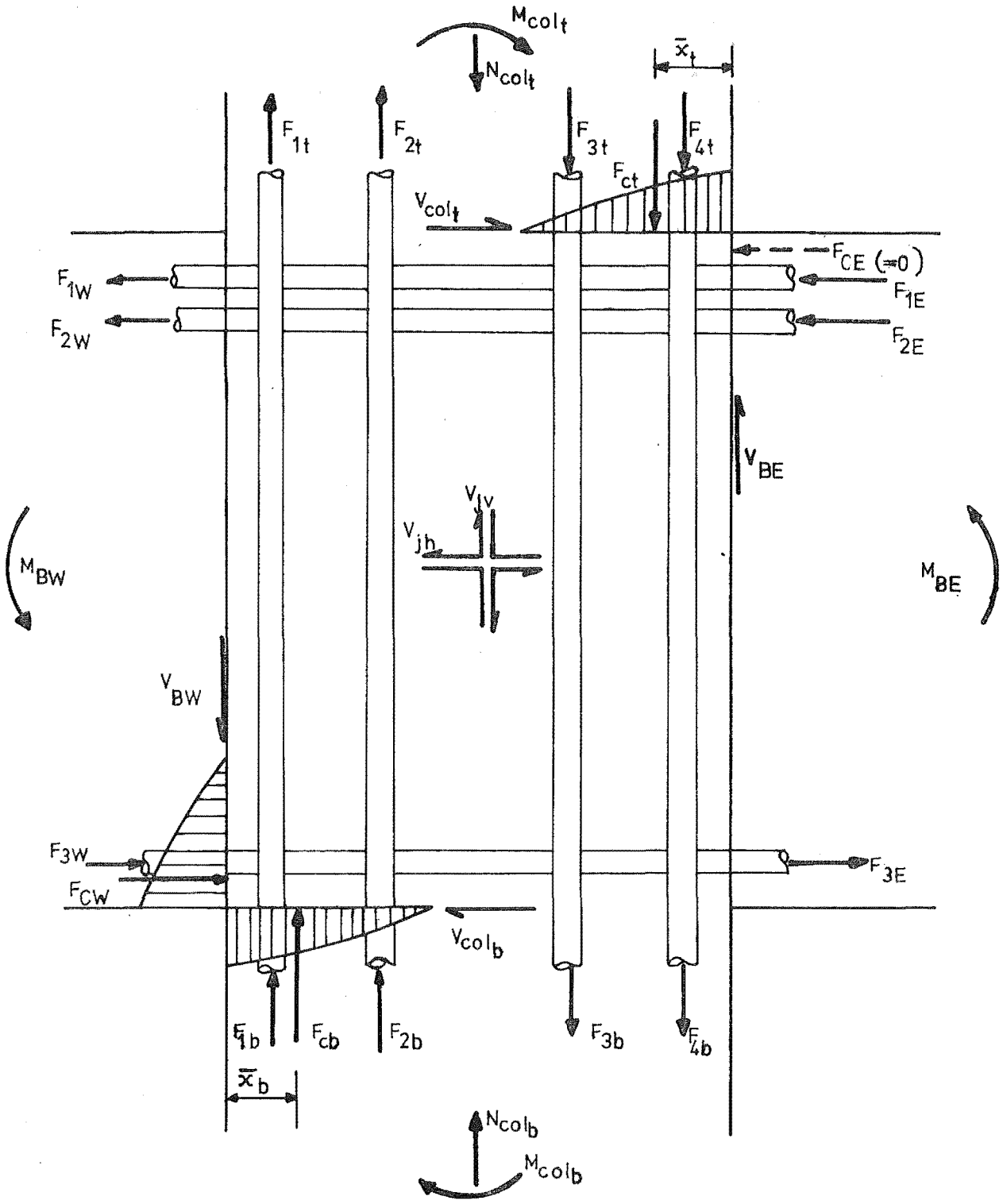

FIG.3.35: ACTIONS ON JOINT CORE

1.3.2, Fig. 1.4). The centroid of column concrete compression at the joint face was determined by converting the column steel strain results to bar forces, and hence computing the magnitude and location of concrete compression necessary to maintain force and moment equilibrium with the applied loads. The location of the concrete compressive force in the beams could not be derived exactly because of the relative uncertainty of the beam steel stress results; hence it was assumed that concrete compression would act at the level of the outer layers of beam reinforcing. Thus the inclination of the direct concrete strut is given by

$$\tan \beta_C = \frac{(d - d')_B}{h_c - \bar{x}_t - \bar{x}_b} \qquad (3.7)$$

Values of $\tan\beta_T$ and $\tan\beta_C$ as given by equations (3.6) and (3.7) are tabulated in Table 3.3 and shown graphically in Fig. 3.36. No value is given for $\tan\beta_C$ in load run 1 because concrete tensile stresses in the uncracked column sections made determination of $\bar{x}_t$ and $\bar{x}_b$ uncertain.

The angle of shear transfer across the joint became steeper as the test progressed. This occurred because penetration of beam bar strains in excess of yield strain into the joint core caused shear to be introduced closer to the column centreline, thus requiring the steeper angle of shear resistance indicated by the calculations.

The angle of resistance of the concrete strut, β_C, was close to the angle of applied joint shear, β_T, during the initial elastic and monotonic inelastic load runs only (i.e. up to load run 5). This was as expected, since only during these runs did the concrete strut carry a significant proportion of the total horizontal joint shear (see Fig. 3.35). In subsequent load runs the angle of applied joint shear was not as steep as the inclination of the direct concrete strut. The angle of total shear resistance was closer to the joint diagonal angle ($\beta_J = 54°$) than was the inclination of the concrete strut, throughout cyclic inelastic loading.

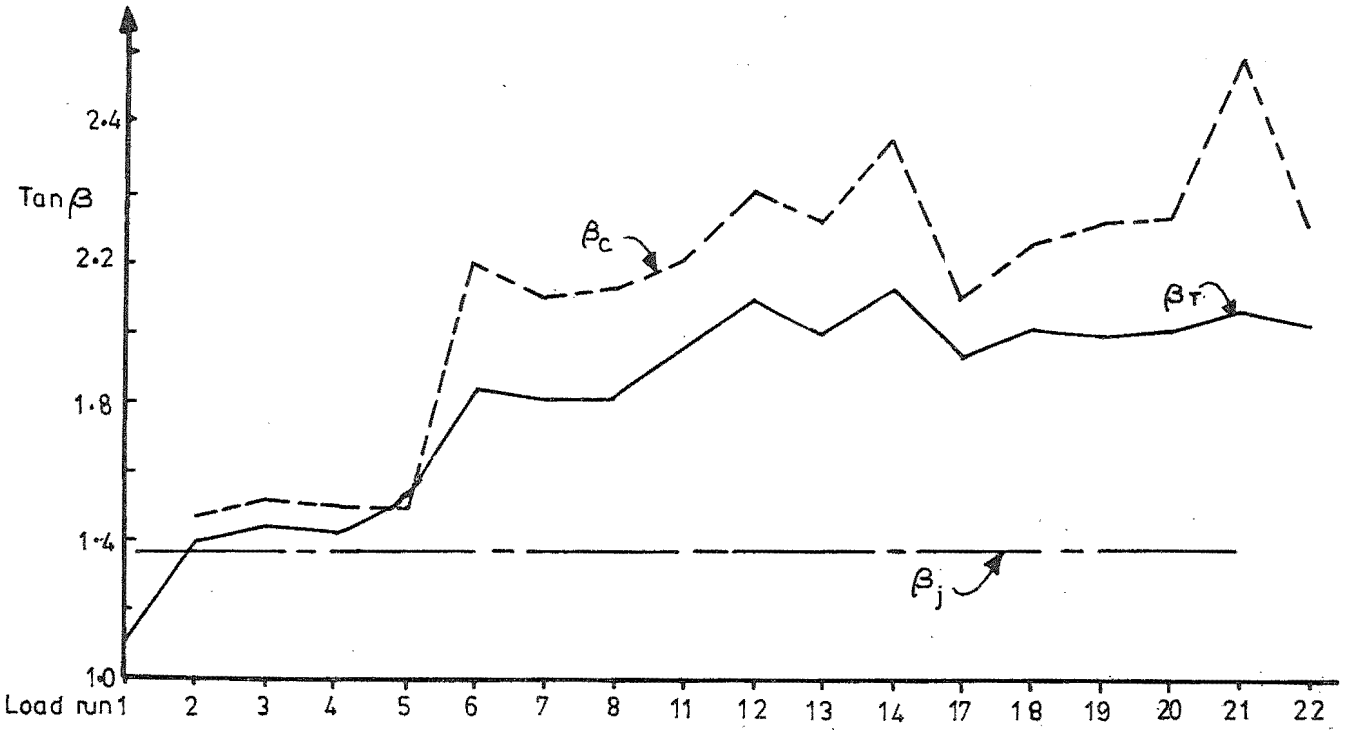

FIG.3.36:ANGLE OF RESISTANCE TO JOINT SHEAR

3.5.5 Strains in the Horizontal Joint Transverse Tie Reinforcement

The development of strain in the transverse legs of joint ties is shown in Fig. 3.37a ,) and the envelope of the maximum strains observed throughout the test in Fig. 3.37b. Most strain measurements were taken from the inner tie legs, but the strains observed close to the beam flexural bars indicate that those in the outer tie legs may have been more critical. Bursting effects of bond forces from the beam bars caused the greatest strains in the transverse tie reinforcement to be concentrated at the top and bottom of the joint. For this unit with its light axial load the confinement of bond forces was apparently more significant in stressing the transverse ties than was confinement of the compression members of the shear resisting mechanisms near the mid-depth of the joint.

3.6 SUMMARY

The primary object of this test was achieved in that satisfactory performance of a beam-column joint under severe cyclic loading was obtained. Joint cracking and deformation were well controlled, and the test result showed that some yield in joint reinforcing can be accommodated without serious repercussions on the overall response. Analysis of the data showed that resistance to joint shear in the post-elastic cycles could be modelled quite effectively by assuming that shear resisted by the concrete was carried by direct strut action in the direction of the joint diagonal, while shear resisted by the reinforcement was carried by a truss mechanism having the joint ties as horizontal members, column bars and axial load to provide the vertical component, and compression struts acting approximately parallel to the joint diagonal.

The design basis of assuming a 25% overstrength on the nominal yield strength of the beam steel resulted in satisfactory performance for this unit. It should be noted that the assumed strength of the beam flexural steel (1.25 x the specified yield strength) for joint design was 345 MPa and its actual yield strength was 298 MPa, whereas the assumed strength of the joint reinforcement was 275 MPa and its actual yield strength was 336MPa. Thus the possible margin between design and actual strengths of beam and joint steel could be much worse in a prototype structure. However analysis of the beam steel strain results showed that the maximum stress attained by the bottom bars in the test was 361 MPa after strain

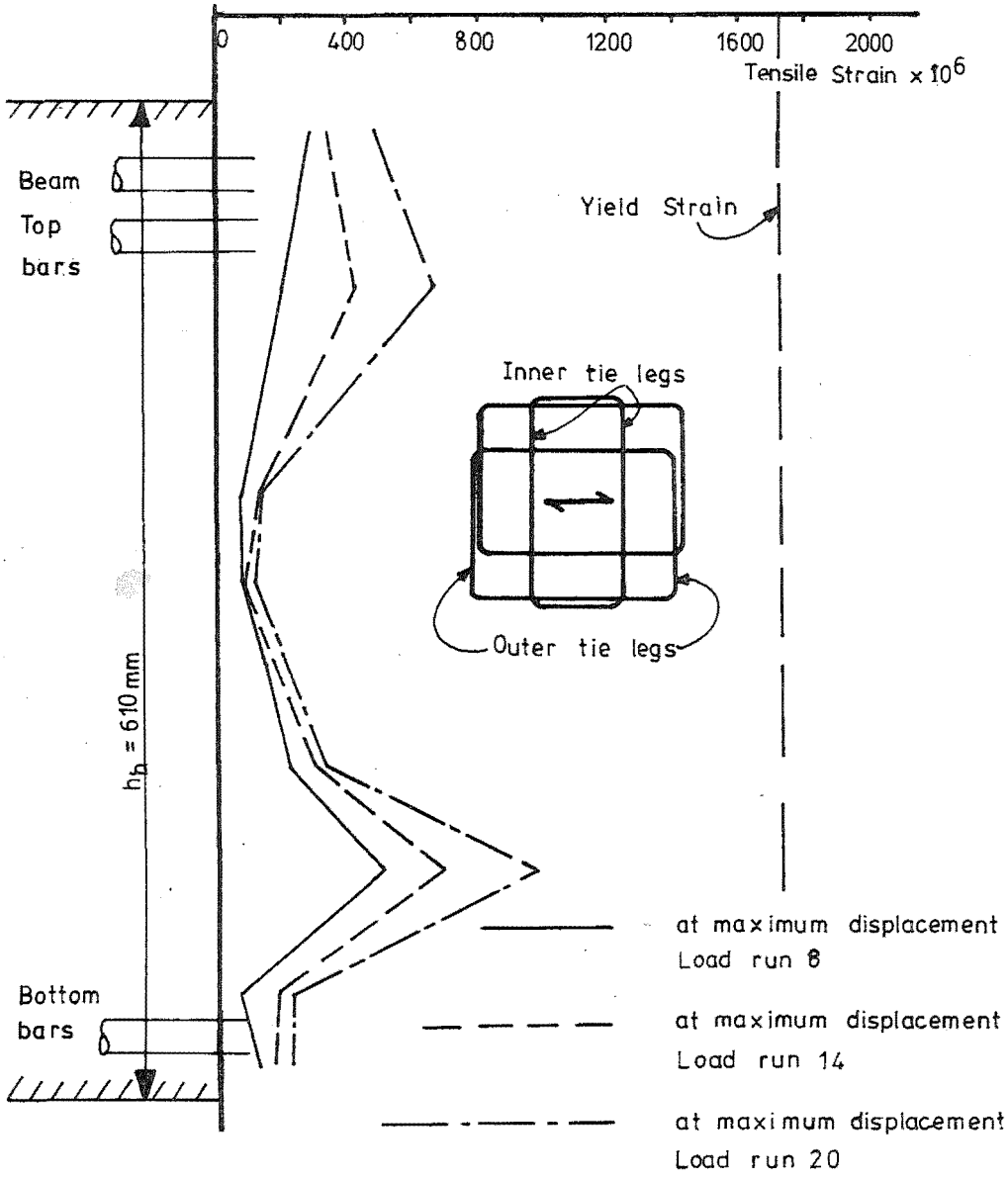

FIG.3·37:(a) DEVELOPMENT OF STRAIN IN INNER TIE LEGS OF JOINT REINFORCEMENT

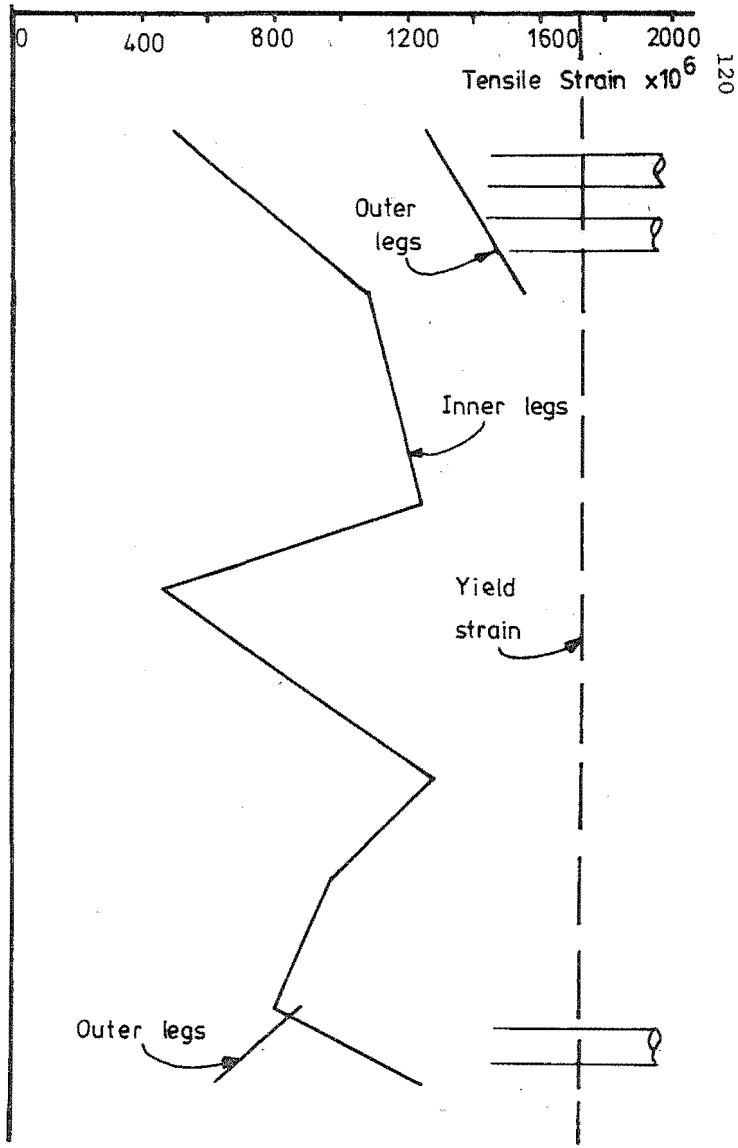

(b) ENVELOPE OF STRAINS IN TRANSVERSE TIE LEGS

hardening, while the top bars reached 347 MPa. These values were possibly increased by a further 3 to 8% due to strain-ageing effects which would not occur under actual earthquake loading. Thus the difference between the design and actual shear input values is less than is at first apparent. The ability of the joint ties to redistribute strains suggests that the extra load could probably be carried even under the most unfavourable combination of possible material strengths, so that the present design basis may be considered satisfactory.

The slip failure of the bottom bars through the joint caused a significant loss of stiffness and of energy dissipating capacity of the structure, but it did not occur until quite late in the test after several severe post-elastic reversals had already been resisted satisfactorily. Although a failure of this type is not desirable in an element of a structure under seismic loading, it is not a brittle failure and should not be catastrophic. Such a slip failure even at several joints of a multistorey building would reduce the overall stiffness, and hence the seismic response of the structure, so that the likelihood of a majority of joints reaching this stage is remote. One would recommend, however, that no joints should contain beam bars of a size implying any greater bond stress across the joint than was appropriate in this case. Bars in the second layer of the larger steel area in an unsymmetrically reinforced beam section could be larger than those in the outer layers since they do not carry large compression stresses under positive bending.

The test showed that beams with unequal top to bottom reinforcement ratios do not utilize their total reinforcement content very efficiently. In repeated cycles of loading the majority of the plastic rotation was due to plastic straining in the bottom bars and this resulted in greater yield penetration for the bottom bars and the eventual slip failure. It seems from this result that a steel configuration at interior beam-column joints closer to equal top and bottom reinforcement would perform more efficiently.

CHAPTER 4

TEST OF UNIT B12

4.1 Introduction

Test unit B12 was tested under the simulated seismic loading described in Chapter 2, in which the dimensions, details and material properties for the test units were also given. The test variable for unit B12 was the beam flexural reinforcement configuration. Equal top and bottom reinforcement contents (6/D # 19 bars, $\rho_T = \rho_B = 0.0086$) were used because it was felt that (a) this change might alleviate the problem of beam bar slip through the joint encountered in the previous test, and also give better beam plastic hinge performance, (b) this configuration might be closer to what is often required in current designs, where spans may be small, and hence the gravity load contributions to beam design moments are small, and moment redistribution is used in design to make the positive and negative beam design moments similar. The unit was identical to the preceding unit B11 in all other respects.

Although the difference in the performance observed during the test compared to that of unit B11 was not as great as had been hoped, the result of the test was nonetheless satisfactory. The condition of the unit during the course of the test is illustrated in the photographs (Figs. 4.1 - 4.3), which show well-controlled joint cracking, and plastic action restricted mainly to the beam hinges. Significant degradation in the stiffness of the unit was again apparent, but load capacity at maximum displacement was maintained. Severe slip of the beam bars through the joint occurred towards the end of the test as in the previous test. Yielding of joint reinforcement was observed in one tie only.

Reduction of the test data showed that the proportion of horizontal joint shear resisted by the strut mechanism decreased throughout the test as the ductility demand on the unit was increased, following closely the pattern displayed by Unit B11.

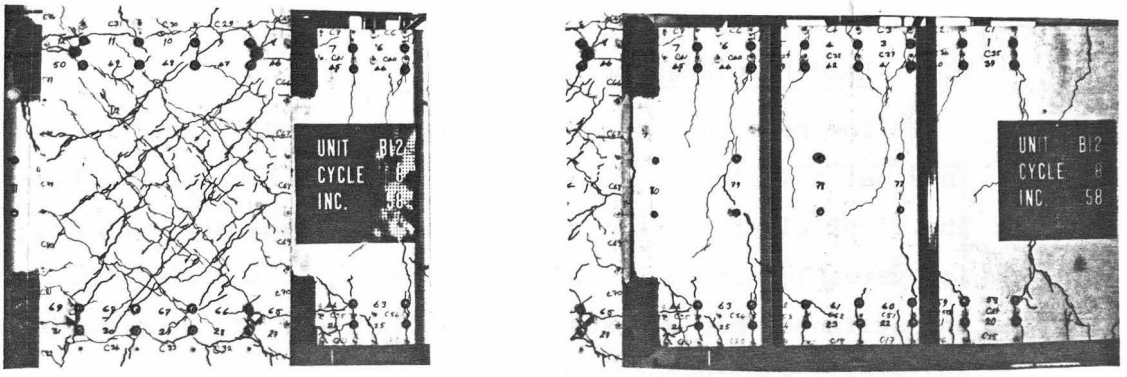

(a) JOINT (b) WESTERN BEAM

FIG·4.1: TEST UNIT AT MAX. DISPLACEMENT, LOAD RUN 8 (μ=2·0)

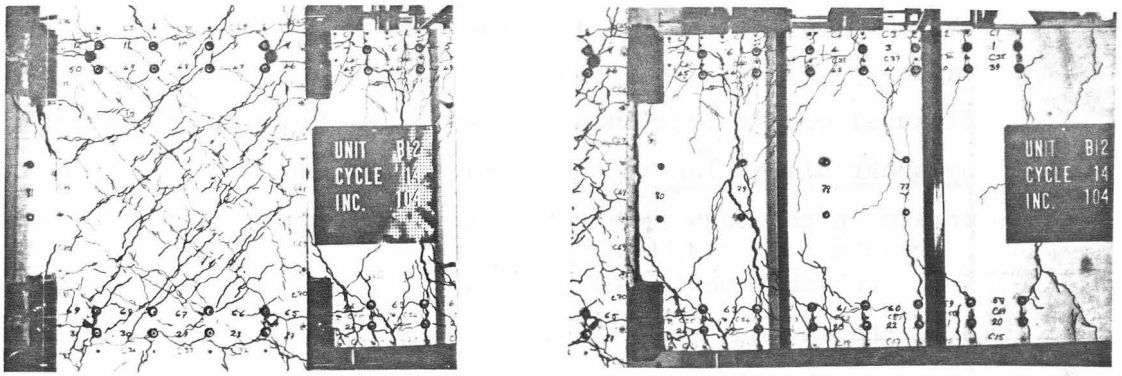

(a) JOINT (b) WESTERN BEAM

FIG·4.2: TEST UNIT AT MAX. DISPLACEMENT, LOAD RUN 14 (μ=4·0)

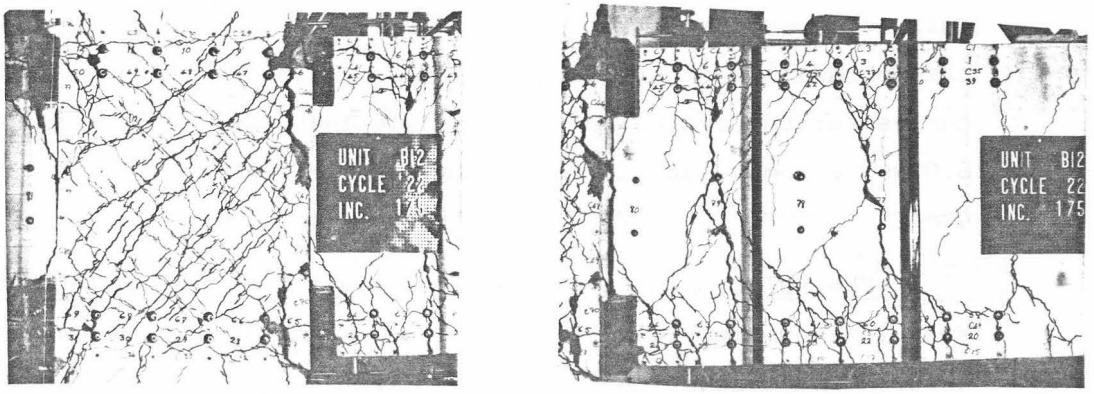

(a) JOINT (b) WESTERN BEAM

FIG·4.3: TEST UNIT AT MAX. DISPLACEMENT, LOAD RUN 22 (μ=6·0)

4.2 Load-Displacement Response

The beam end-load versus end-displacement relationships are shown in Figs. 4.4 and 4.5 for the West and East beams respectively. During the first elastic cycle slight hysteresis was apparent due to the irreversible nature of concrete cracking, but during the second cycle the stiffness had degraded to the stiffness of the cracked unit, and hysteresis was therefore negligible.

During the first post-elastic cycle to displacement ductility factor of 2.0 (load runs 5 and 6), the beams yielded at loads fairly close to the theoretical value. A slight rounding of the curve was apparent due to the presence of two layers of reinforcing bars. During the repeated cycle to displacement ductility factor 2.0 (load runs 7 and 8), the stiffness of the test unit degraded significantly, so that the area of the second load-displacement loop was only sixty per cent of the area of the initial loop, implying a considerable loss in energy dissipating capacity. The degradation was caused by shear displacement along the flexural cracks left open at the column face during the previous cycle, by shear distortion of the joint panel, and by penetration of yield strain in the beam bars into the joint core.

In subsequent cycles to displacement ductility factors of 4.0 and 6.0, the maximum beam end-loads exceeded the theoretical ultimate loads based on the yield strength of the steel by up to 17% as shown in Table 4.1, mostly because of steel strains entering the strain hardening range. Further stiffness degradation occurred in these cycles, and from load run 17 onwards slip of the beam bars through the joint caused more severe degradation. As explained in Section 3.3 bearing of the Demec studs welded to the outer beam bars provided additional anchorage for these bars, so that the load-displacement loops observed in the test were rather fuller than would be the case for a prototype structure. Full load could still be carried at maximum displacement in spite of the degradation of stiffness. Some rounding of the load-displacement curves for the cycles to displacement ductility factors of 4.0 and 6.0 was evident, due to the Bauschinger effect in the beam reinforcing steel.

The relationships between the applied column shear and the storey sway is shown in Fig. 4.6, which gives the overall response of the test unit. The derivation of the net column shear V_{col} and the storey sway Δ_c from the beam end loads and displacements, and the column axial load was outlined in Section 3.2. As in the test of unit B11,

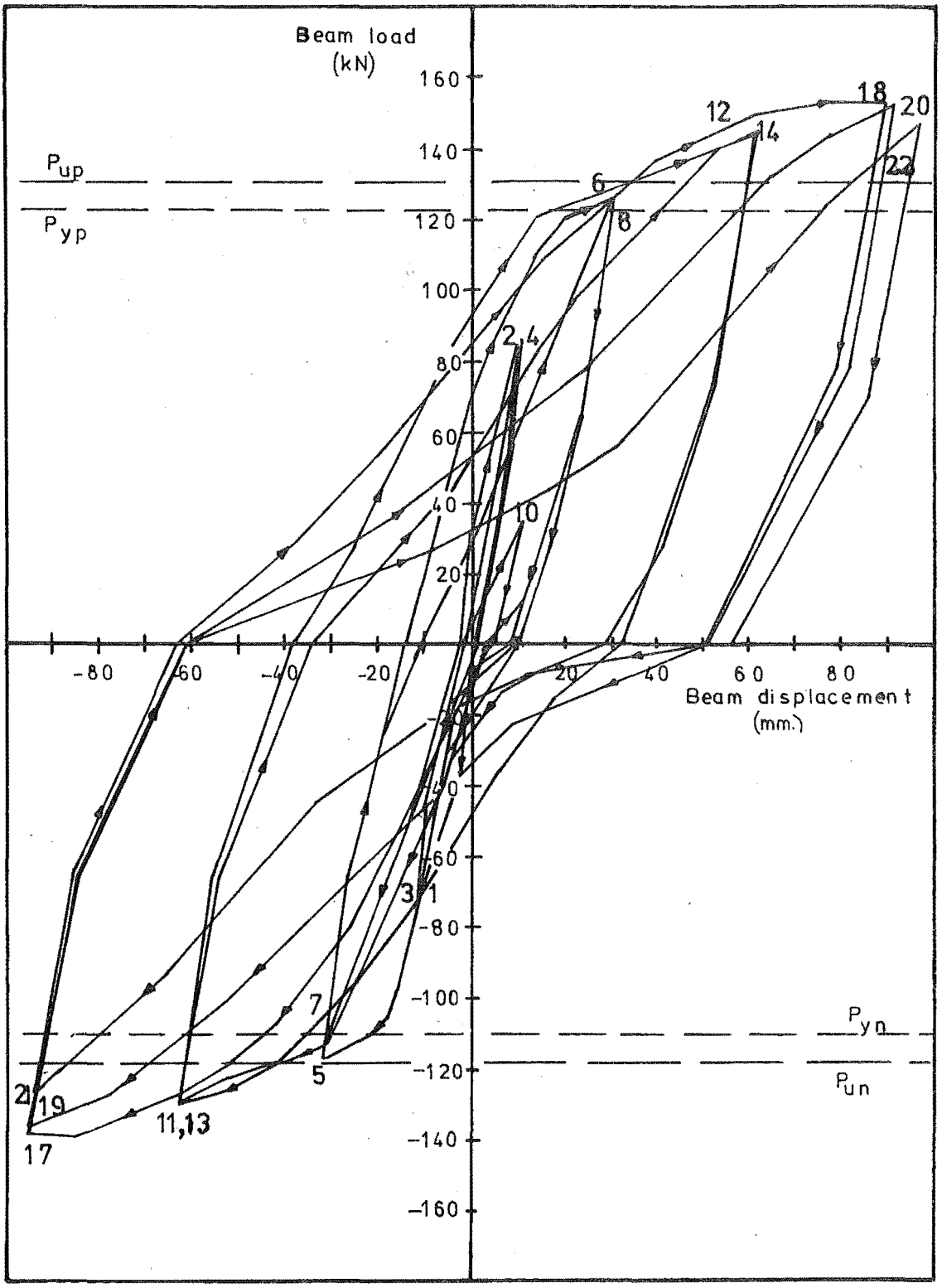

FIG.4.4 :BEAM LOAD-DISPLACEMENT RESPONSE-WESTERN BEAM

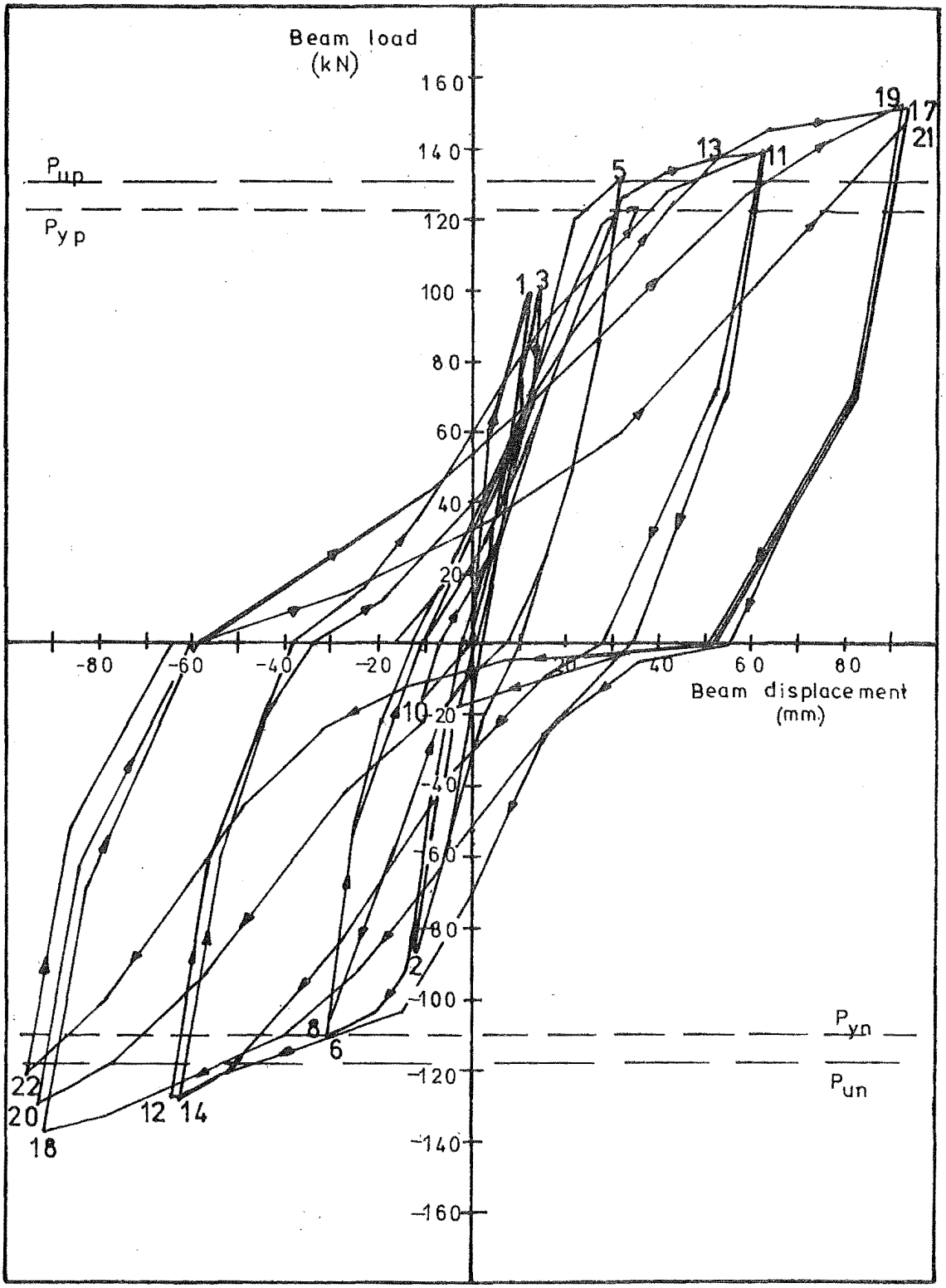

FIG.4.5 :BEAM LOAD-DISPLACEMENT RESPONSE-EASTERN BEAM

TABLE 4.1 : BEAM END LOADS

Load Run No.	μ	Beam West			Beam East		
		P (kN)	P/P_y	P/P_u	P (kN)	P/P_y	P/P_u
1	0.75	-73.13	0.664	0.621	86.70	0.705	0.663
2		85.26	0.693	0.652	-75.92	0.690	0.644
3		-72.75	0.661	0.617	87.59	0.712	0.670
4		83.94	0.683	0.642	-75.03	0.682	0.637
5	2.0	-118.09	1.073	1.002	132.30	1.076	1.012
6		126.99	1.033	0.971	-111.55	1.013	0.947
7		-113.45	1.031	0.963	123.00	1.000	0.941
8		127.23	1.035	0.973	-108.27	0.984	0.919
9	0.75	-42.09	0.382	0.357	56.84	0.462	0.435
10		35.36	0.288	0.270	-18.28	0.166	0.155
11	4.0	-129.54	1.177	1.099	138.49	1.126	1.059
12		145.01	1.179	1.109	-127.99	1.163	1.086
13		-130.00	1.181	1.103	140.19	1.140	1.072
14		144.79	1.177	1.108	-128.24	1.165	1.088
15	0.75	-49.69	0.451	0.422	60.23	0.490	0.461
16		11.12	0.090	0.085	0.00	0.0	0.0
17	6.0	-138.26	1.256	1.173	152.04	1.236	1.163
18		152.71	1.242	1.168	-137.93	1.253	1.171
19		-136.29	1.238	1.157	153.03	1.244	1.171
20		152.34	1.239	1.165	-130.51	1.186	1.108
21		-127.18	1.155	1.079	145.92	1.187	1.116
22		147.30	1.198	1.127	-120.75	1.097	1.025

Note: 1. For definition of terms, refer to Table 3.1.

2. P_y and P_u are given in Table 2.3.

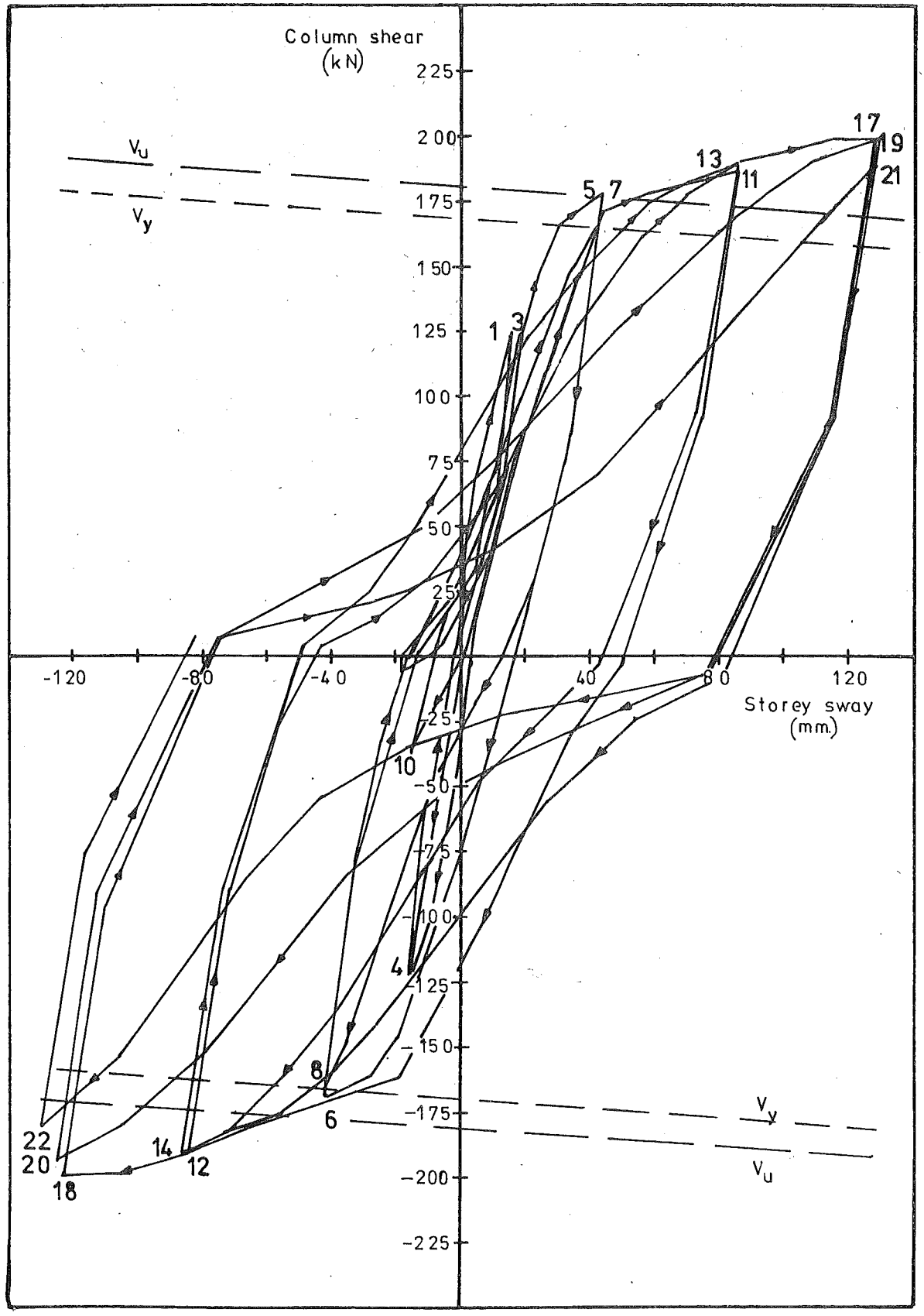

FIG.4.6 : COLUMN SHEAR-STOREY SWAY RESPONSE

the axial load was small at $0.05f'_cA_g$, and the P-delta effect was therefore slight. The net column shear carried did not decrease within the displacements applied during the test, due to the compensating effects of strain hardening of the beam reinforcing on the end loads. The maximum reduction in the shear carried due to the P-delta effect was observed in load run 22 when the shear resistance of the unit was reduced by 6.3%.

4.3 Beam Behaviour

4.3.1 Components of Beam End Displacement

Components of the beam end displacement measured in the Western beam during the test are plotted in Fig. 4.7. Corresponding measurements taken for the Eastern beam were similar throughout the test. The plot shows clearly that the rotation, θ_{b1}, measured in the first gauge length extending over half the effective beam depth (d/2) away from the column face, caused the major component of beam end displacement throughout the test. As noted in Section 3.3.1 the method of obtaining this measurement implied that the apparent rotation included the effect of beam bar slippage through the joint, and this is apparent in the results illustrated in Fig. 4.7. As a proportion of the total beam end displacement the component caused by rotation θ_{b1} was greatest in load run 11, when it comprised 62% of the total. In the subsequent cycles this proportion decreased as yielding spread along the beam, and the rotation θ_{b2} in the second d/2 gauge length of the beam became more significant. However in the final stages of the test severe slip of the beam reinforcement through the joint caused the apparent rotation measured in the first gauge length to increase again, and the resulting component of beam end displacement again approached 60% of the total. As a corollary to this increase, the displacement component caused by the rotation θ_{b2} decreased from a maximum value of 23% of the end displacement in load run 17 to only 2% in load run 22.

Since the response of the joint remained essentially elastic throughout the test, the component of beam end displacement caused by the shear distortion of the joint did not increase in proportion to the total beam displacement demand. Thus only a 90% increase in joint distortion was noted between load runs 8 and 22, whereas the corresponding increase in total beam displacement demand was 200%. The proportion of total beam end displacement caused by joint

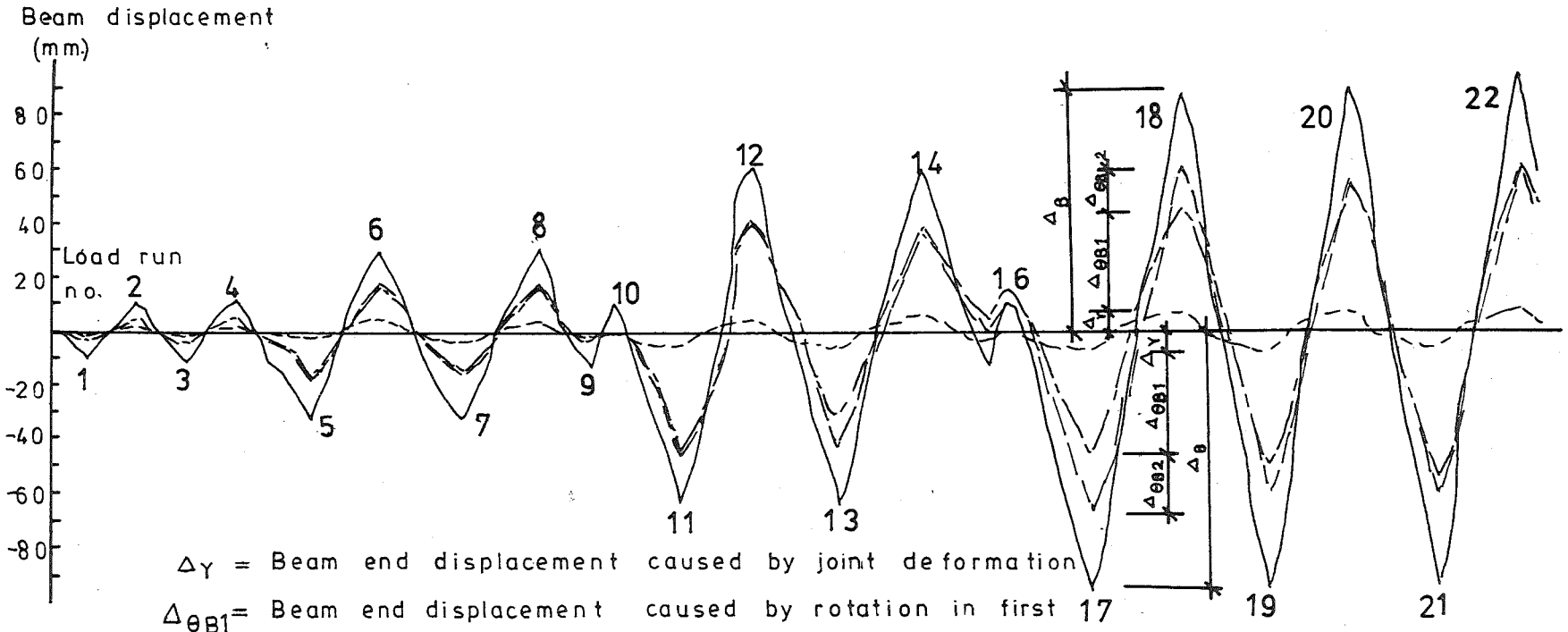

Δ_Y = Beam end displacement caused by joint deformation

$\Delta_{\theta B1}$= Beam end displacement caused by rotation in first 280(d/2) length of beam from column face

$\Delta_{\theta B2}$= Beam end displacement caused by rotation in second 280 (d/2) length of beam from column face

Δ_B = Total beam end displacement

FIG. 4.7 : COMPONENTS OF BEAM END DISPLACEMENT FOR WESTERN BEAM

distortion was a maximum in load runs 5 to 8 when the average proportion was 24%. In load runs 11 to 14 the average proportion was 18%, and in load runs 17 to 22 the average value was 15%.

The elastic nature of joint deformation compared to the plastic beam rotations was also illustrated by the relative lag of the displacement components due to rotation behind the component caused by joint shear distortion. The component of displacement due to joint distortion decreased to zero much more quickly following the reversal of load than did the displacement components due to beam rotation.

The portions of the beam end displacement in Fig. 4.7 not caused by beam rotations and joint shear distortion were caused by column deformation, shear deformation of the beam, and flexural deformation of the beam in the area beyond the two rotational gauge lengths.

4.3.2 Rotational and Curvature Ductility Factors

Values of beam rotations and curvatures measured during the test are listed in Tables 4.2a and 4.2b for the Western and Eastern beams respectively. The beam rotations θ_{bl} were measured over the first d/2 gauge length of the beam away from the column face as shown in Fig. 2.13 while the curvatures were derived from strain readings over gauge lengths of 102 mm in the outer layers of beam flexural reinforcing. The curvatures ϕ_1 were the values determined at 76 mm away from the column face, while the values ϕ_{max} were the maximum curvatures observed at intervals of 102 mm up to 686 mm away from the face. The length $l\phi_{max}$ was the distance from the column face at which maximum curvature was observed. Rotational and curvature ductility factors were determined in terms of experimental yield values extrapolated from the appropriate measurements in load run 1, in accordance with the procedure outlined in Section 2.7.1 for defining the displacement ductility factor. From load run 19 onwards the curvatures ϕ_1 could not be measured at maximum displacement because the slippage of beam bars through the joint pulled Demec studs in the compression side of the beams too close to the column face, so that there was insufficient clearance for the Demec gauge to be used in this position. As noted in the previous section the measurement of the rotation θ_{bl} included the effect of beam bar slip, and this is reflected in the large rotational ductility factors derived in the final stages of the test. In the earlier cycles the maximum curvature ductility demand exceeded the rotational ductility demand as

TABLE 4.2a : BEAM ROTATIONAL AND CURVATURE DUCTILITY FACTORS - BEAM WEST

Load Run No.	μ	θ_{bl} rad. x 10^4	$\frac{\theta_{bl}}{\theta_{by}}$	ϕ_1 rad./mm x 10^6	ϕ_{max} rad./mm x 10^6	$^1\phi_{max}$ mm	$\frac{\phi_1}{\phi_y}$	$\frac{\phi_{max}}{\phi_y}$
5	2.0	-69.21	3.01	-15.60	-15.60	76	4.50	4.50
6		71.74	3.12	8.59	8.59	76	2.48	2.48
7		-59.77	2.60	-9.94	-9.94	76	2.87	2.87
8		69.08	3.01	20.92	20.92	76	6.03	6.03
9	0.75	-13.10	0.57	8.68	-2.25	279	-2.50	0.65
10		33.62	1.46	13.52	13.52	76	3.90	3.90
11	4.0	-189.35	8.24	-38.78	-45.17	178	11.18	13.03
12		183.41	7.98	28.13	38.53	178	8.11	11.11
13		-135.79	5.91	-23.86	-32.21	381	6.88	9.29
14		173.21	7.54	23.00	33.94	178	6.63	9.79
15	0.75	29.55	-1.29	10.24	-2.52	483	-2.95	0.73
16		72.94	3.18	13.36	23.18	178	3.85	6.69
17	6.0	-205.82	8.96	-33.17	-42.17	483	9.57	12.16
18		206.02	8.97	15.15	35.40	584	4.37	10.21
19		-220.96	9.62	-19.42	-24.42	279	5.60	7.04
20		243.41	10.60	*	26.14	178	*	7.54
21		-242.39	10.55	*	-16.97	279	*	4.89
22		279.84	12.18	*	20.85	178	*	6.01

Note: Terms as defined in text. * No reading available

TABLE 4.2b : BEAM ROTATIONAL AND CURVATURE DUCTILITY FACTORS - BEAM EAST

Load Run No.	μ	θ_{bl} rad. x 10^4	$\frac{\theta_{bl}}{\theta_{by}}$	ϕ_1 rad./mm x 10^6	ϕ_{max} rad./mm x 10^6	$^1\phi_{max}$ mm	$\frac{\phi_1}{\phi_y}$	$\frac{\phi_{max}}{\phi_y}$
5	2.0	62.78	2.73	7.39	7.39	76	2.13	2.13
6		-69.77	3.04	-14.00	-14.00	76	4.04	4.04
7		55.44	2.41	8.19	8.19	76	2.36	2.36
8		-68.29	2.97	-22.16	-22.16	76	6.39	6.39
9	0.75	14.02	0.61	-10.21	3.30	279	-2.94	0.95
10		-19.05	0.83	-15.35	-15.35	76	4.43	4.43
11	4.0	182.26	7.93	38.99	43.00	178	11.24	12.40
12		-184.46	8.03	-30.02	-39.42	178	8.66	11.37
13		134.87	5.87	24.14	28.57	381	6.96	8.24
14		-165.73	7.21	-25.36	-29.34	178	7.31	8.46
15	0.75	-23.38	-1.02	-12.32	1.81	584	-3.55	0.52
16		-68.48	2.98	-15.73	-19.08	178	4.54	5.50
17	6.0	179.84	7.83	26.07	43.37	381	7.52	12.51
18		-216.92	9.44	-23.36	-32.41	178	6.74	9.35
19		214.53	9.34	*	28.82	381	*	8.31
20		-243.67	10.61	*	-22.47	178	*	6.48
21		244.36	10.64	*	23.03	381	*	6.64
22		-272.36	11.86	*	-13.40	178	*	3.86

* No reading available

expected, due to the integral nature of the rotational measurement, but from load run 18 onwards the effect of slip resulted in greater apparent values of ductility for rotation than for curvature. As in the test of unit B11 the visual observation of slip of beam bars across the joint was verified by increasing differences between the measured rotations and the sum of curvatures over the rotational gauge length, as the test progressed.

The position of maximum curvature in the beams was at the closest position to the column face during the first two inelastic cycles only (load runs 5 to 8). In subsequent cycles the position of maximum curvature shifted further along the beams, but tended to be found in different locations for positive and negative bending, depending on the location of diagonal and flexural cracks in each case.

As described in the previous section, plastic beam rotation lagged behind the applied loads and the elastic deflections during the early part of each load run. Thus at displacement ductility factor of 0.75 in load run 15 (following previous cycles to displacement ductility factor of 4.0), the beam rotations still had the sense of the previous load run, and negative values of rotational ductility factor resulted. The same type of behaviour caused the small values of θ_{b1}/θ_{by} derived for load run 9, although the phenomenon was not as pronounced at this stage due to the smaller ductility demand in the preceding major cycles.

4.3.3 Beam Reinforcement Strain Profiles

The spreading of plastic action along the beams as the ductility demand on the test unit was increased is shown clearly in the photographs (Figs. 4.1 to 4.3), and also in the strain profiles for the beam longitudinal reinforcement during major inelastic load runs (Figs. 4.8 to 4.10). The strains plotted in these profiles were the mean of those measured in the outer two bars of each layer of reinforcing.

During the first inelastic load runs to a displacement ductility factor of 2.0 (Fig. 4.8), the tension reinforcement yielded initially close to the column face. After two full cycles of loading at this displacement level, strains in excess of yield strain in the beam bars spread to approximately 250 mm outward from the column face, but penetration of yield strain into the joint was not great at this stage. This was difficult to determine with great accuracy because of the large interval between readings, i.e. 102 mm, relative to the total

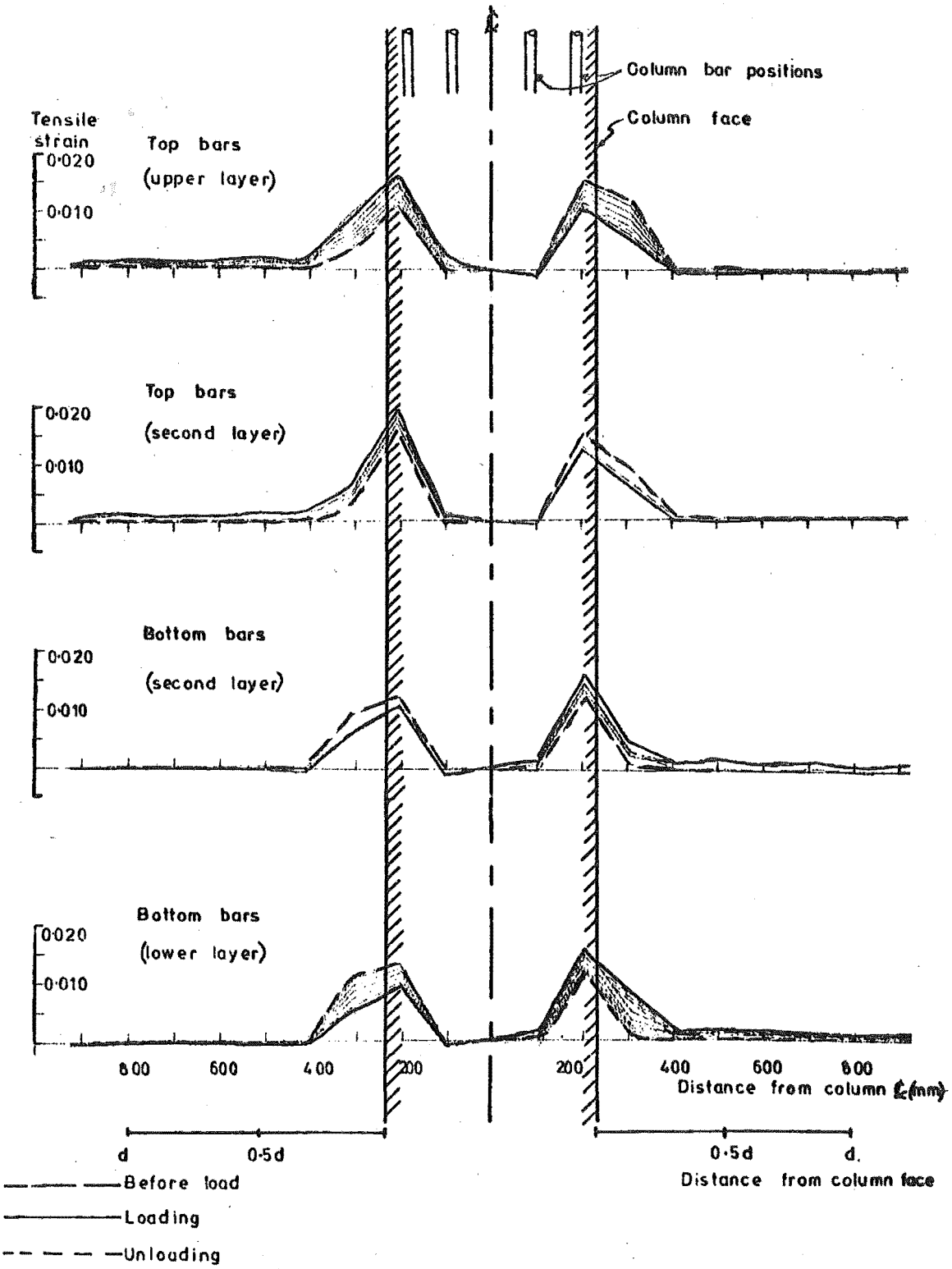

FIG. 4.8 :BEAM BAR STRAINS, LOAD RUN 7

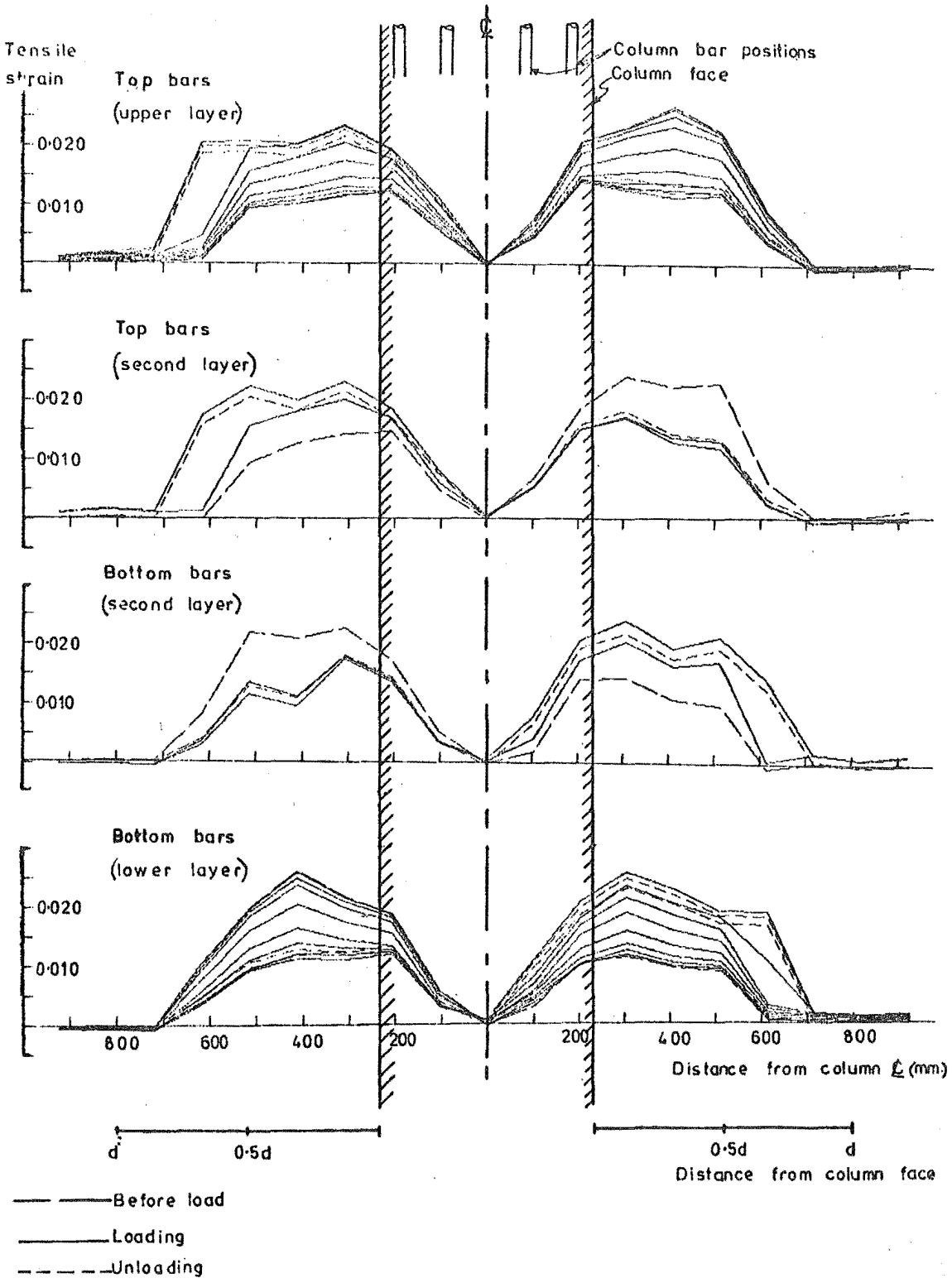

FIG.4.9 :BEAM BAR STRAINS, LOAD RUN 13

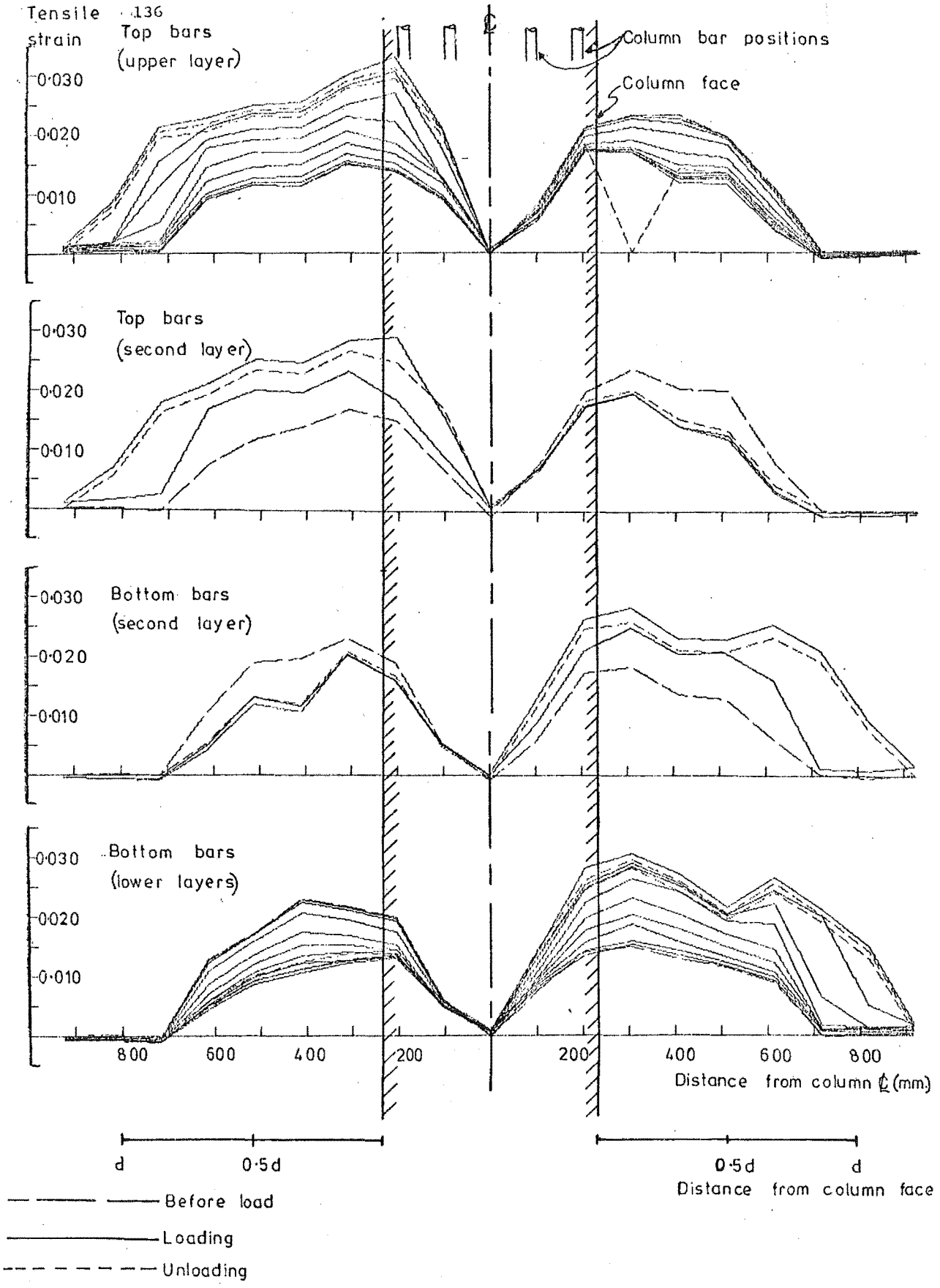

FIG.4.10 : BEAM BAR STRAINS, LOAD RUN 17

column breadth of 457 mm. Strains in the compression reinforcement indicated that cracks in the compression zone were not completely closed, but since the inner layer of bars was carrying compression at less than the yield stress, the concrete must nonetheless have been carrying some small compression forces. The equal configuration of beam reinforcement used in this test unit resulted in equal participation of top and bottom bars in plastic action, which was a desirable feature in terms of the efficiency of energy dissipation.

When displacements were applied to a ductility factor of 4.0 (Fig. 4.9), yield strain spread much further along the beams, and also penetrated significnatly into the joint core. The hinge length from the column face increased to about 350 mm during load run 11, and then to about 450 mm from load run 12 onwards. Strains in the tension reinforcement were now well into the strain-hardening range. Reduction of strain data to steel stresses as discussed in the following section showed that the tensile strain hardening was reflected in yielding of both layers of compression reinforcement, although the cracks still did not close completely. Penetration of yield strain into the joint increased so that only on the centre gauge length was a strain less than yield strain measured. However the unit was still able to carry full load and the bars could apparently transfer full tension plus full compression yield stress over the remaining bond length.

When a displacement ductility factor of 6.0 was first applied in load run 17, the plastic hinge length increased further to 650 mm, as shown in Fig. 4.10. With further yield penetration into the joint at this stage the available bond length was inadequate, and slippage of the bars through the joint commenced. As a consequence of this failure the Demec studs welded to the bars came into bearing against the sides of their holes in the corner concrete, and no strain readings were available from the bars across the joint in the subsequent cycles. However strain readings from the beam bars were still available, and these showed reduced differences in the strains required of the reinforcing bars between zero load and maximum displacement during the later cycles. This was due to the diminishing importance of plastic deformation of the flexural reinforcement as a means of accommodating the applied displacements, compared to the displacements caused by slip.

4.3.4 Beam Reinforcement Stresses

The strain histories obtained experimentally from the beam bars in the joint region were analysed using a computer program based on the cyclic loading algorithm for reinforcing steel given by Spurr[33], to give the stresses in the reinforcement at various stages of the test. Typical stress-strain histories are shown in Figs. 4.11 and 4.12 for points on the top two layers of beam reinforcement at 76 mm away from the western column face. Corresponding histories computed for the bottom two layers of reinforcing bars were quite similar to those shown for the top bars. Equilibrium checks with the applied loads for the sections closest to the column face indicated correlation within 3% during load runs 5 to 8, but in later cycles stresses were underestimated by an average of 5%. Strain ageing again affected the experimental loads in the later cycles, although not as severely as in the test of unit B11, since the present test was completed in four weeks. However the preliminary tests on reinforcing steel described in Section 2.5.1 that strain-ageing could cause discrepancies of this magnitude, even for this relatively shorter duration of post-elastic loading. As in the analysis of the results for unit B11 (Section 3.3.4), the compression force resisted by the beam concrete could not be located with any certainty, and it was therefore assumed to act at the level of the outer layer of compression reinforcement. The concrete compression force was too small for reasonable changes in its location to affect the equilibrium calculations significantly.

Stresses derived from analyses of the type shown in Figs. 4.11 and 4.12 are shown in Figs. 4.13 to 4.15 for the four layers of bars at the maximum displacement of the major cycles. The penetration of yield stress into the joint, and the increasingly severe bond conditions for the bars at the column centreline, as the test progressed, are clearly shown.

From load run 17 onwards meaningful readings of strain from the beam bars across the joint became unavailable as mentioned in the previous section. The plots of bar stresses given in Fig. 4.15 for the final cycles are therefore incomplete, but the increasing severity of the bond conditions leading to slip failure is nonetheless apparent in the increasing slope of the available bar stress gradients across the joint. Where stress results were available for repeated cycles of

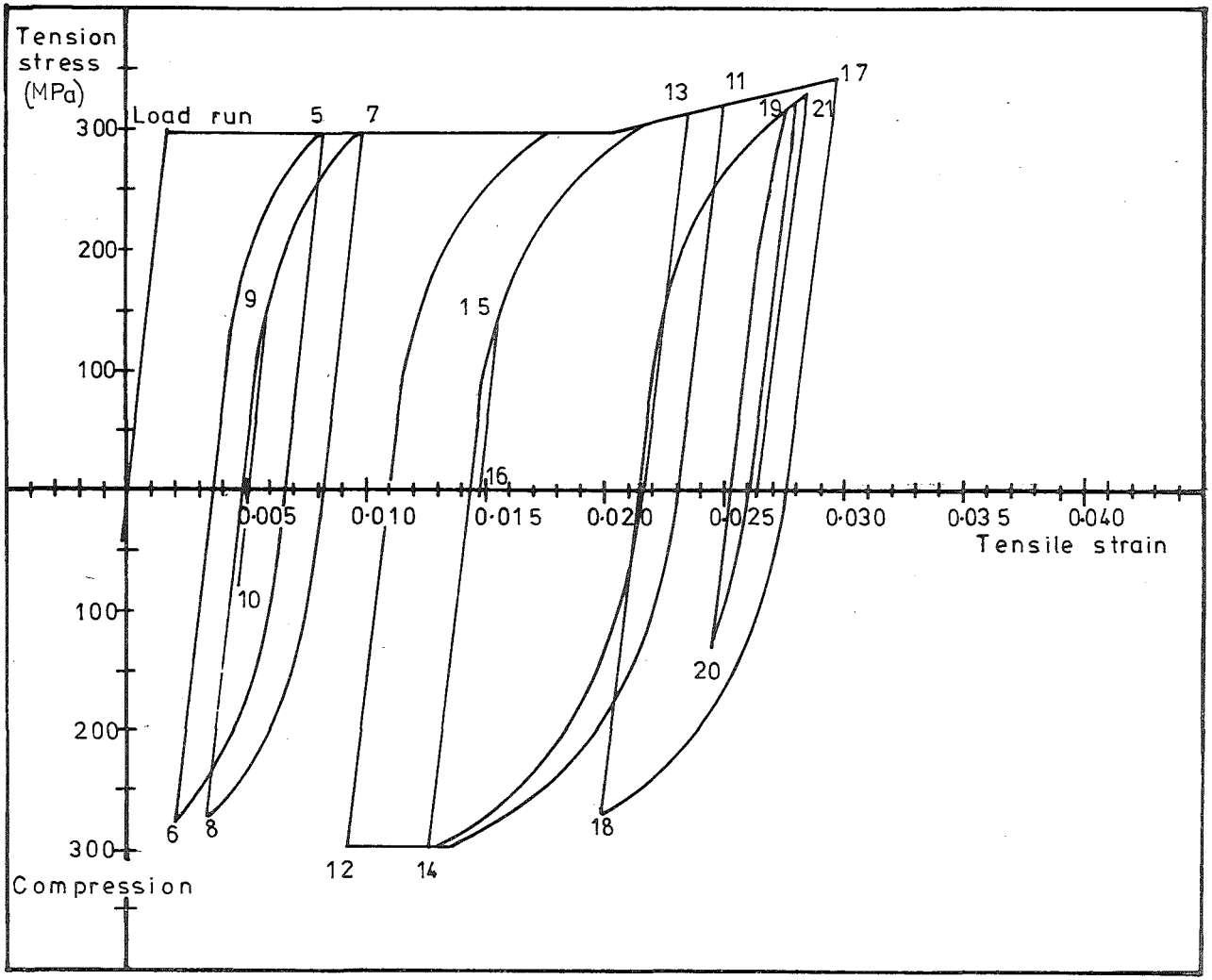

FIG.4.11 : STRESS-STRAIN HISTORY FOR UPPER LAYER OF TOP REINFORCEMENT AT 76MM. AWAY FROM COLUMN FACE IN WESTERN BEAM

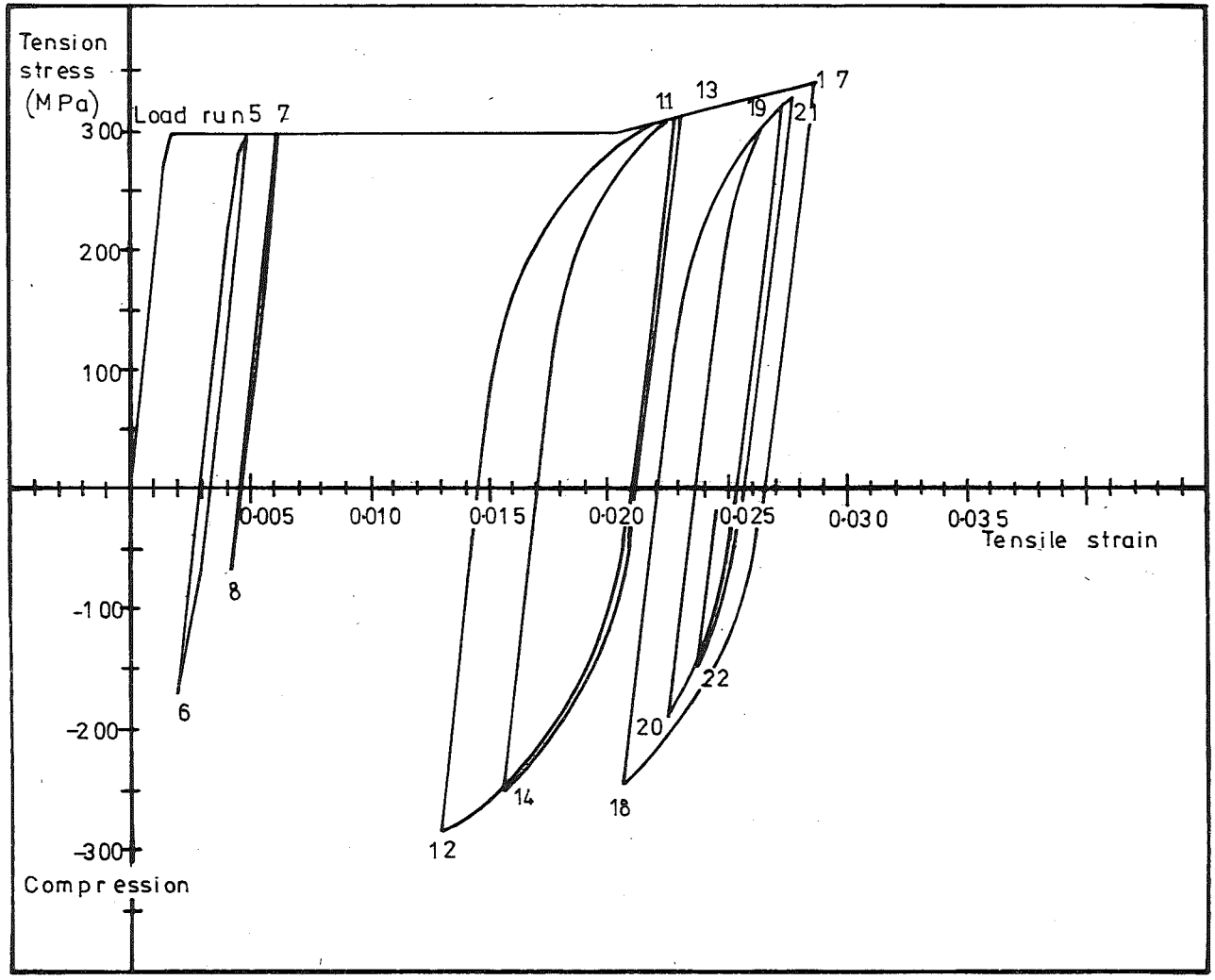

FIG. 4.12 : STRESS-STRAIN HISTORY FOR SECOND LAYER OF TOP REINFORCEMENT AT 76 MM. AWAY FROM COLUMN FACE IN WESTERN BEAM

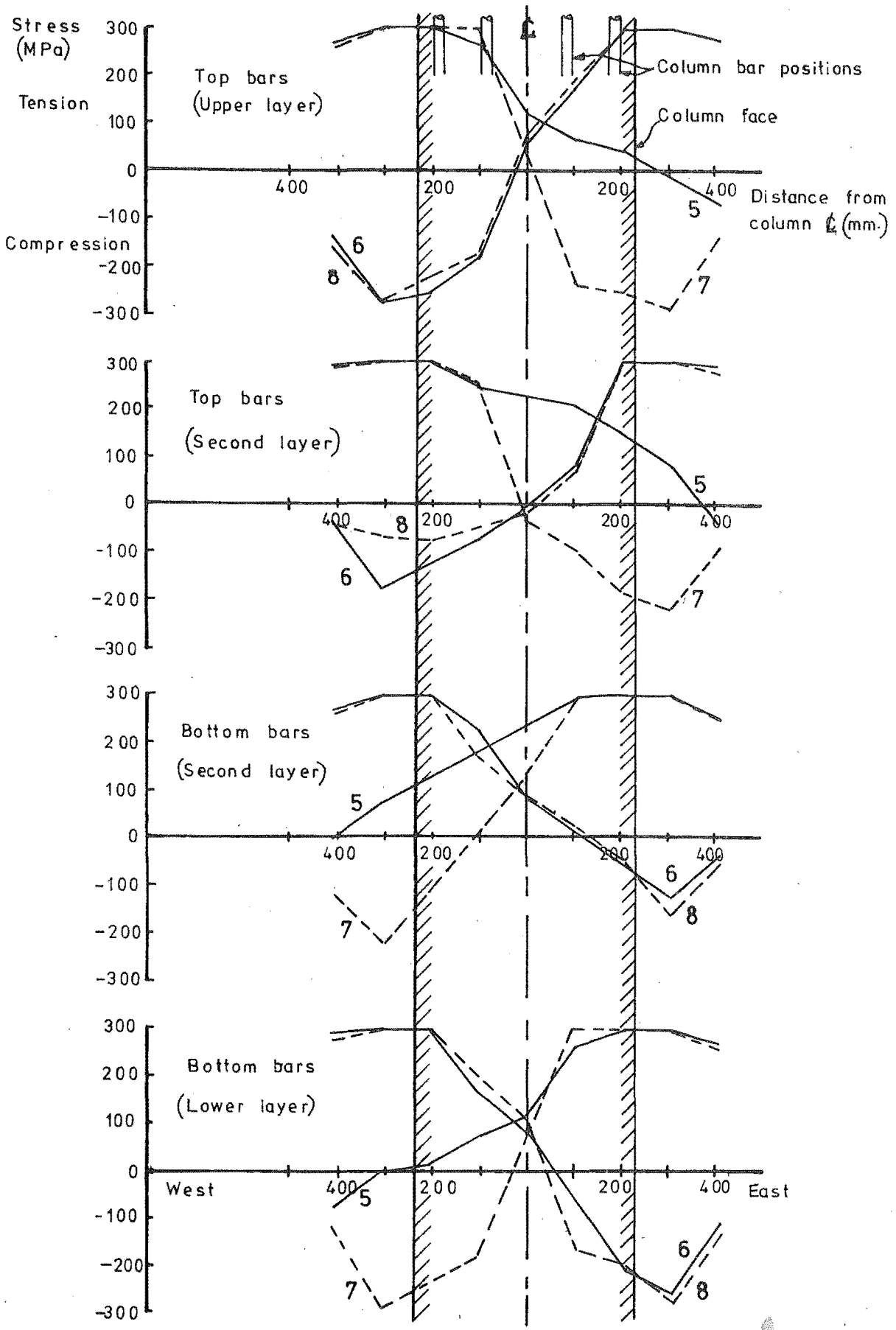

FIG.4.13 : BEAM STEEL STRESSES ACROSS JOINT, LOAD RUNS 5 TO 8

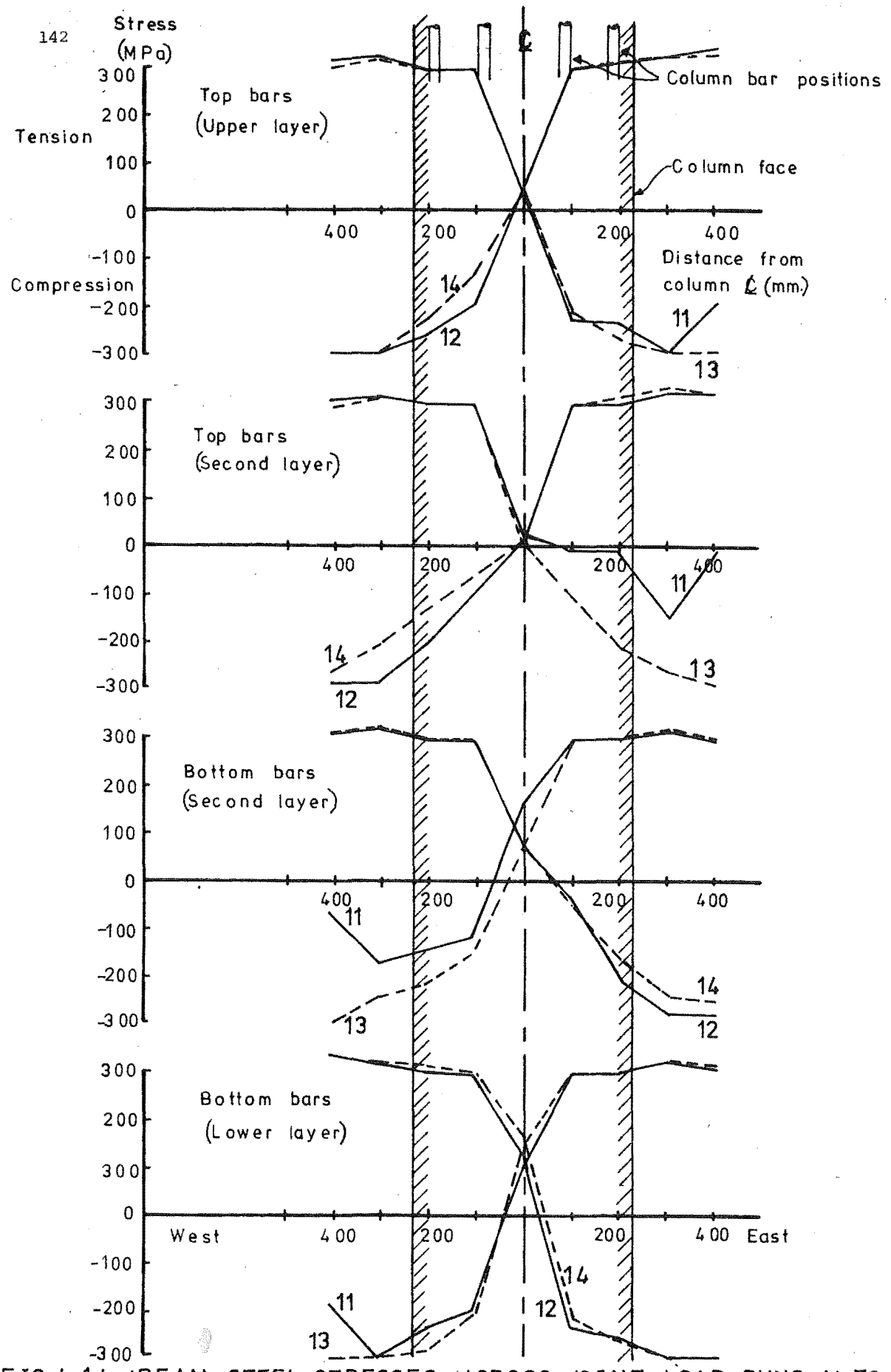

FIG.4.14 :BEAM STEEL STRESSES ACROSS JOINT, LOAD RUNS 11 TO 14

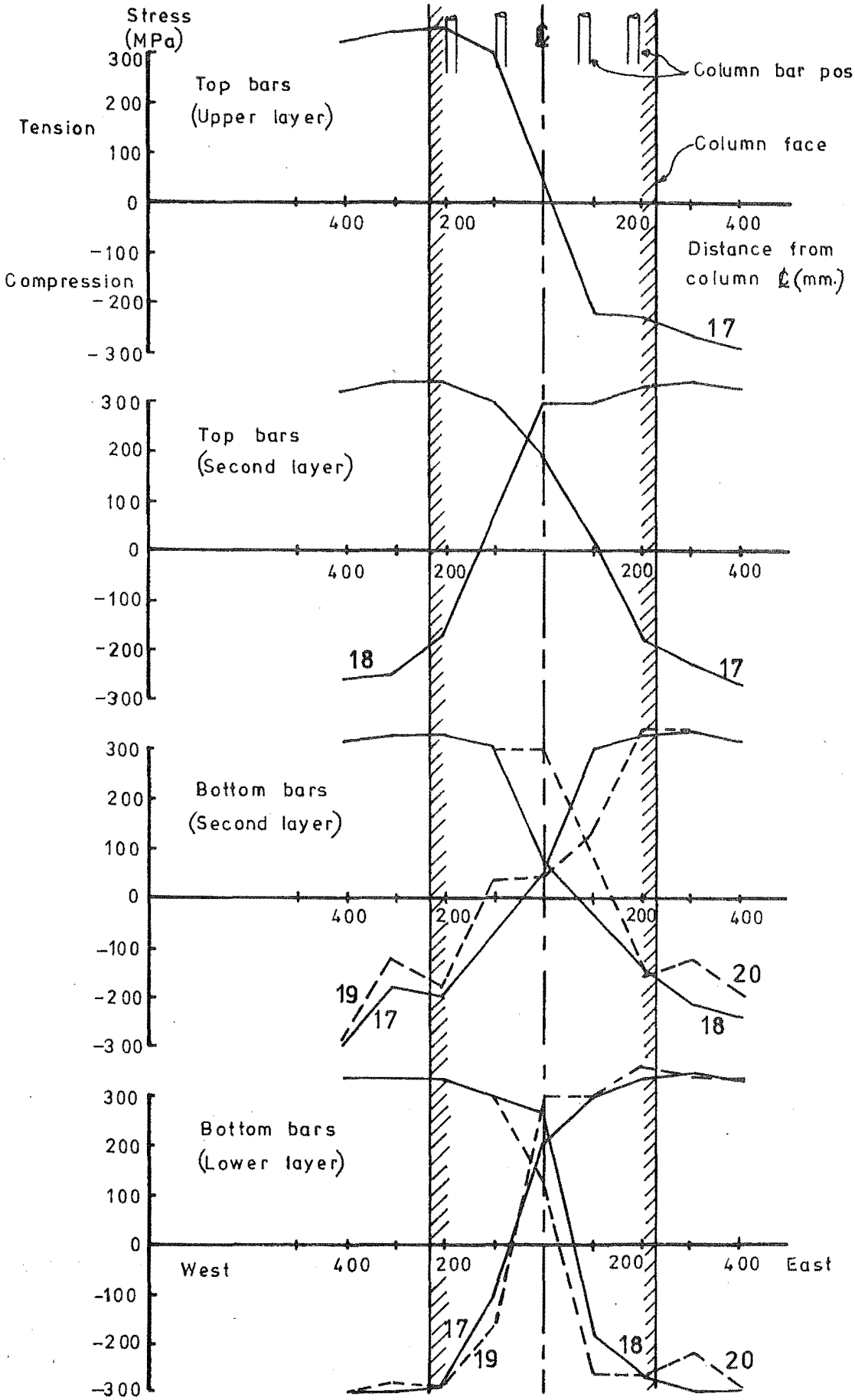

FIG.4.15 : BEAM STEEL STRESSES ACROSS JOINT, LOAD RUNS 17 TO 20

displacement ductility factor of 6.0 (i.e. for both layers of bottom bars in Fig. 4.15), the compression stresses at or just outside the column face were smaller in the repeated cycle than in the initial cycle, due to the progressive loss of bond strength across the joint. This is in contrast to the situation in Figs. 4.13 and 4.14, where,with the bond strength of the bars maintained, greater compressive stresses were carried in the repeated cycle than in the initial cycle.

Bond stresses for the various layers of bars derived from the steepest gradients of the stress profiles in Figs. 4.13 to 4.15 are shown in Fig. 4.16. The bond strength required of the bars across the joint increased as the ductility demand on the unit was increased, and bond stresses considerably in excess of the ultimate values implied in codes[4,5] were sustained before failure. No clear reason was apparent for the more severe bond stress demands on the top bars as compared to the demand for the bottom bars. Possibly the range of results indicated in the stress-strain curves show that the energy dissipated in both layers of beam bars was approximately equal in this test, in contrast to the response observed in unit B11, where the unsymmetrical reinforcing configuration resulted in unequal energy dissipation for the different layers of bars. The symmetrical reinforcing configuration used in the beams of unit B12 resulted in a much more efficient utilization of the reinforcing steel for plastic action. Slip of the bars from load run 17 onwards resulted in reduced differences in the strains imposed at the maximum displacement of alternate load runs, so that the area of the stress-strain loops decreased in the subsequent cycles. This response was also observed at other locations of the beam reinforcing, and the reduced area of the beam steel stress-strain loops was reflected in the reduced area of beam end-load versus displacement loops (Figs. 4.4 and 4.5), showing the reduced energy dissipation capacity of the unit as a whole after slippage of the beam bars became a significant factor in the response.

Fig. 4.16 merely represents the scatter of experimental values, since the gauge length for strain measurements in the bars was relatively coarse, and the computation of bond stresses involved two stages of data reduction, firstly from the mean strain values over the 102 mm gauge length to bar stresses, and secondly from the gradients of the stress distributions to bond stresses.

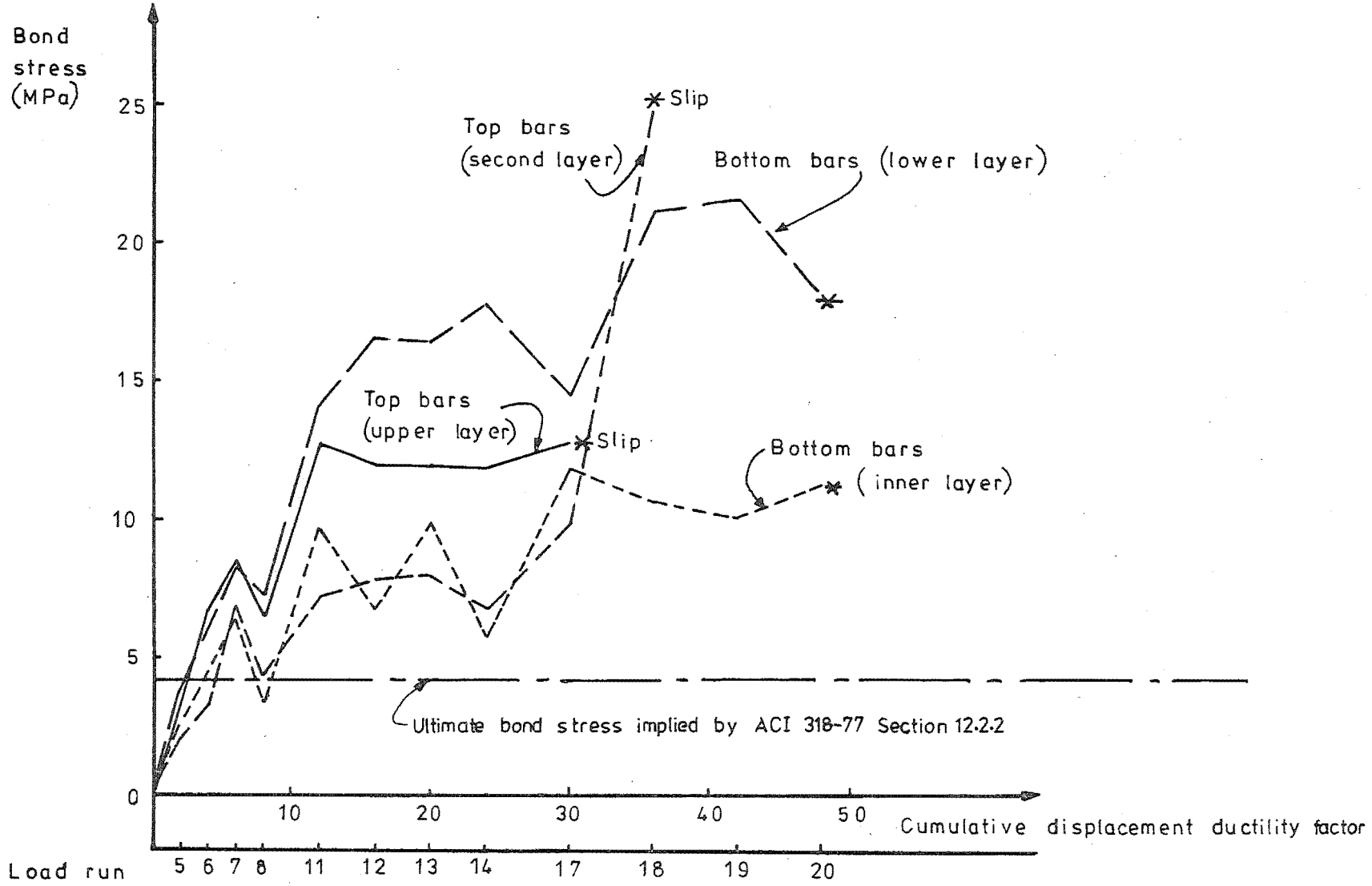

FIG.4.16 : BOND STRESSES DERIVED FOR BEAM BARS ACROSS JOINT

4.3.5 Slip of Beam Bars Through the Joint

As described in the previous chapter (Section 3.3.5) severe slip of the beam bars through the joints of the test units became obvious when the Demec studs moved across their holes in the cover concrete, and became visibly off-centre. For unit B12 (as for B11), this phenomenom was first observed across the full breadth of the column when maximum displacement was approached in load run 17 (the first load run to a displacement ductility factor of 6.0). Top bars slipped more than bottom bars initially, but by load run 19 all the beam bars were slipping. This resulted in severe loss of stiffness and pinching in the load-displacement loops, and reduced plastic deformation of the beam bars in the plastic hinge region. Although the inner beam bars could not be seen it seems likely from the width of the beam crack at the column face, and from the pinching of the load-displacement loops, that these bars must have slipped as well. Possibly slip failure of these inner bars did not occur simultaneously with that observed in the outer bars, but from the evidence it seems certain to have occurred soon afterwards.

As for unit B11, the bearing of Demec studs against the sides of their holes provided additional anchorage for the outer beam bars in the test which would not be available for a prototype structure. By the end of the test the welds of four studs had broken, indicating that considerable loads were carried by them. Without the additional anchorage provided by the studs the load-displacement loops would presumably have been more severely pinched, and the capacity to approach full load at maximum displacement should not have been affected.

After the test was completed the beam bars through the joint were exposed as shown in the photographs (Figs. 4.17 and 4.18) by carefully chipping away the cover concrete. Examination of the bars showed a distinct failure surface on the cylinder containing the bar deformations, with the cover concrete able to be lifted off leaving the concrete between the deformations adhering to the bars. Some crushing of the concrete was evident immediately in front of the ribs, but the principal failure mechanism appeared to be a shear failure as shown in Fig. 4.19.

4.3.6 Beam Shear Behaviour

During the course of the test approximate measurements of sliding shear deformation along the flexural cracks in the beams were taken, using

FIG. 4.17: SLIPPED BEAM BARS EXPOSED IN CONCRETE AFTER TEST

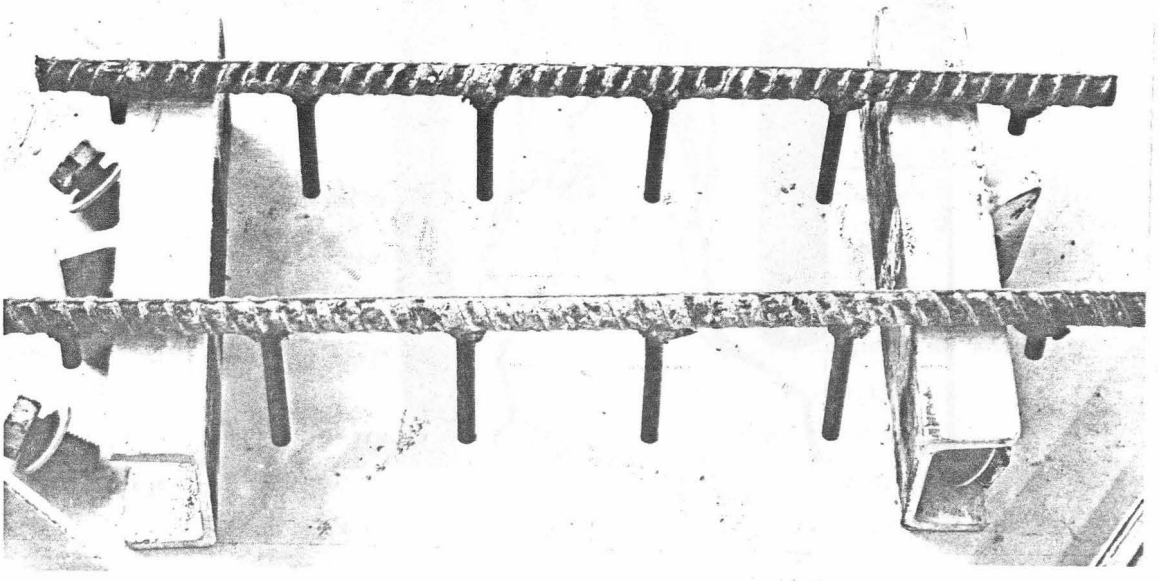

FIG. 4.18: BARS REMOVED FROM CONCRETE

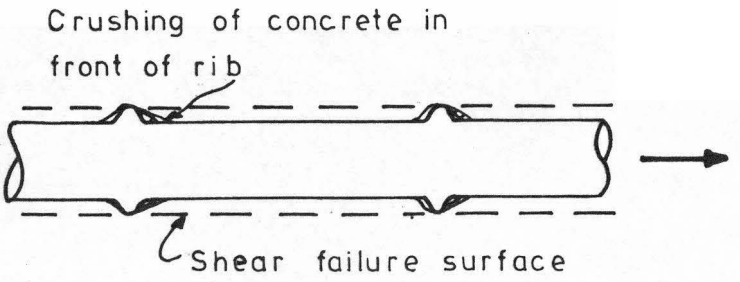

FIG.4.19 :SLIP FAILURE OF BEAM BARS THROUGH JOINT

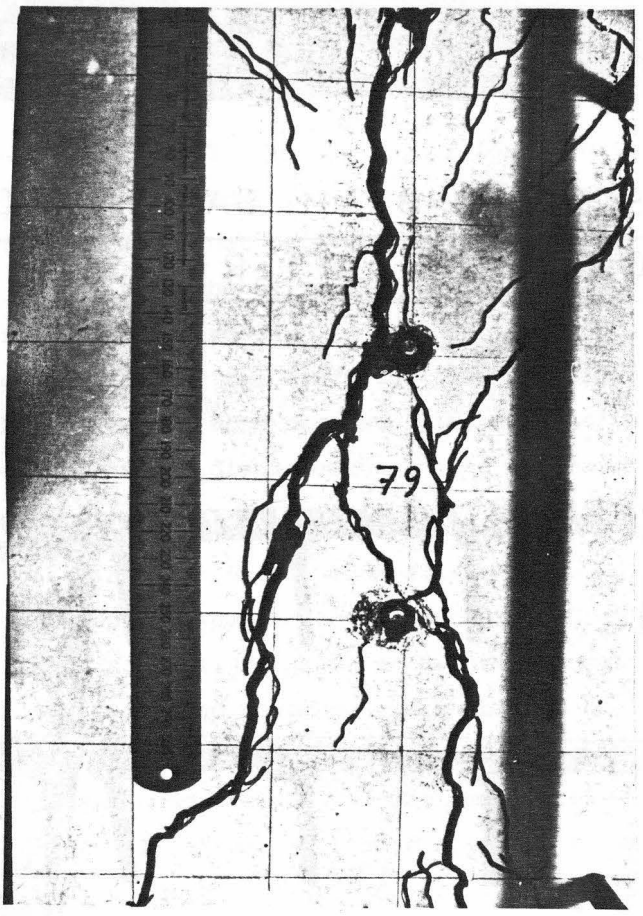

FIG.4.20: SLIDING SHEAR DISPLACEMENT ALONG FLEXURAL CRACK

a grid pencilled on the concrete surface for reference. A typical example of the deformation is shown in Fig. 4.20. As a maximum, these displacements totalled about 8 mm for each beam, or 9% of the total displacement at a displacement ductility factor of 6.0, but they provided a greater proportion of the displacement in the early part of each load run. The tendency for well distributed flexural cracks at the level of the longitudinal reinforcement to combine into relatively few large cracks in the mid-depth region of the beam was obviously disadvantageous with respect to this behaviour.

Stirrup strains measured at the mid-depth of every third stirrup along the beams away from the column face at various stages of the test are shown in Fig. 4.21. As in the test of unit B11 the observed strains were distorted somewhat by the tendency for the holes provided for the Demec studs to act as crack initiators. This phenomenon may be seen in the photographs (Figs. 4.2 and 4.3), and it resulted in a wide scatter of observed strains, both along the beam and between the North and South faces of the beam. The beam stirrups provided were significantly in excess of the reinforcement necessary to resist the applied shears, assuming a 45° truss mechanism of shear resistance, and the maximum nominal shear stress in the beams was only 0.76 MPa. The observed strains were quite different from those predicted using the 45° truss mechanism, assuming no resistance to be provided by beam concrete in the plastic hinges. However the data obtained was too scattered and too sparse to support any alternative mechanism of shear resistance.

4.4 Column Behaviour

The pattern of column cracking outside the joint was strongly influenced by the positions of column ties and vertical bars. Only the cracks immediately above and below the joint (at the level of the beam surface) opened to significant widths, and these closed up under reversed loading.

Strains measured from column vertical bars in the South face of the column are plotted in Figs. 4.22 to 4.24. Analysis of the column section using elementary elastic theory with the known material properties showed that whereas the strains measured at 100 mm above and below the beam surfaces were in good agreement with theoretical values, the strains measured in the vicinity of the beam bars indicated much larger tension forces in all column bars than would be expected from flexural response. Evidently the apparent strain pattern was disrupted by the large bond forces from the beam bars acting transversely to the column bars. However

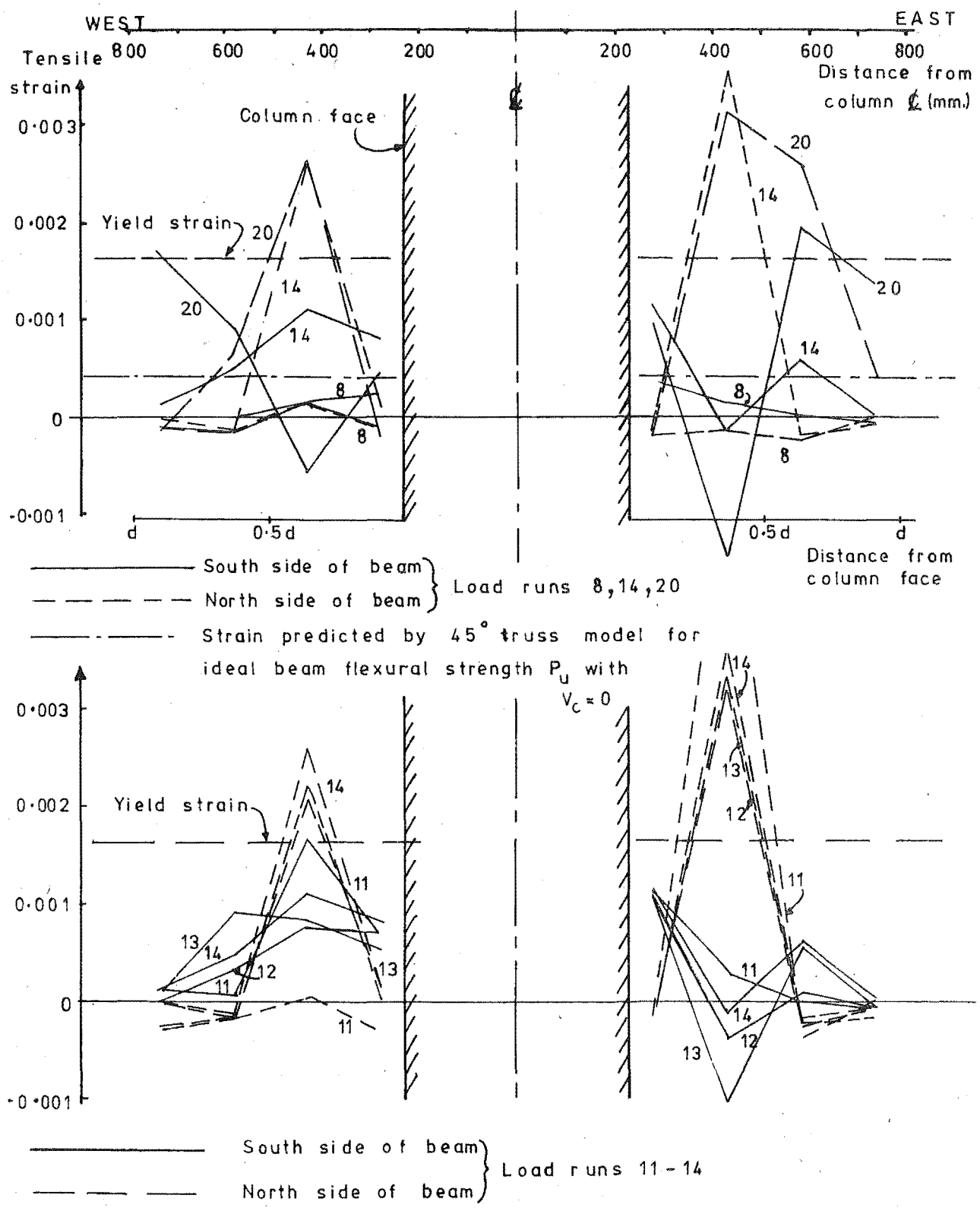

FIG . 4 · 21 : BEAM STIRRUP STRAINS

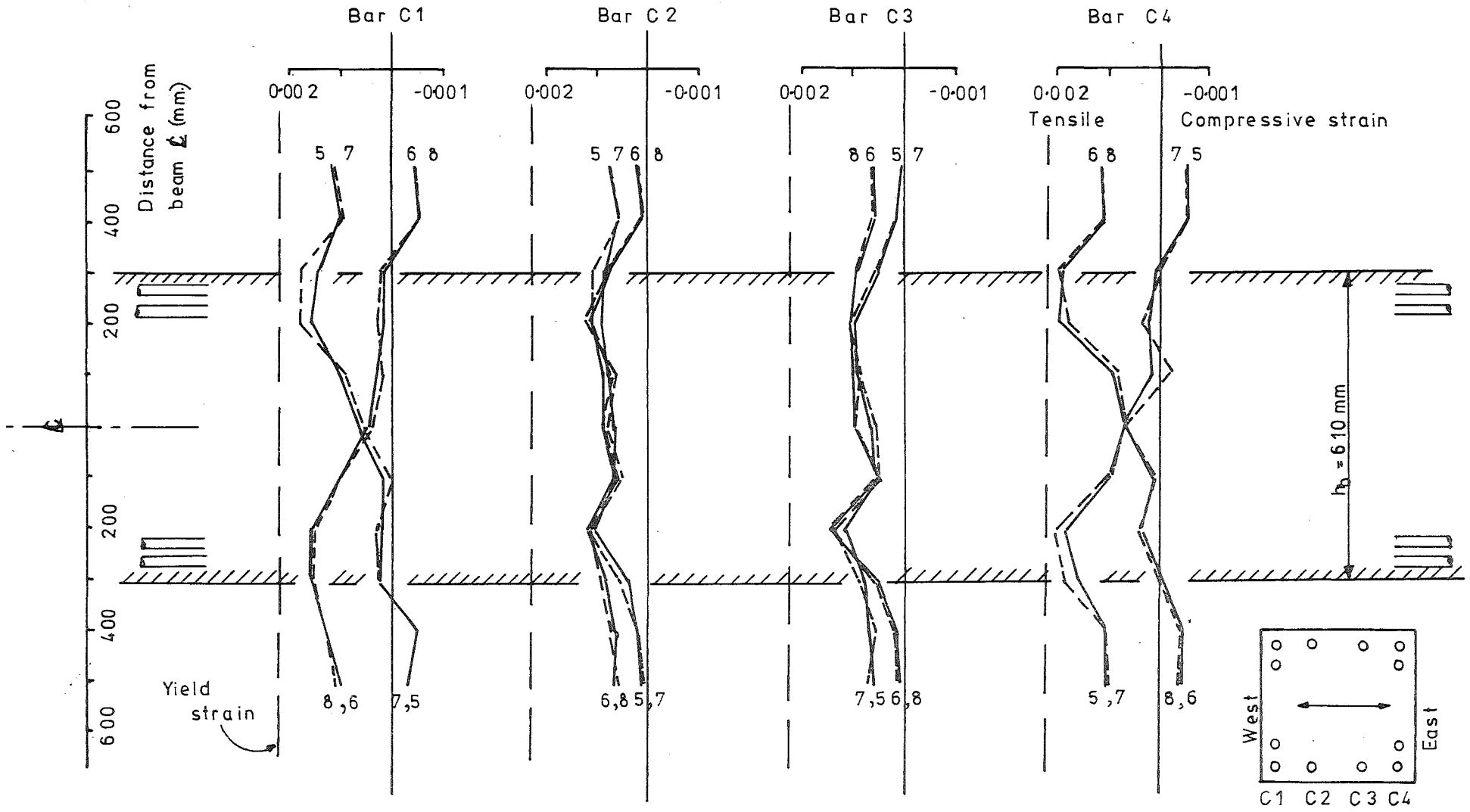

FIG.4.22: COLUMN STEEL STRAINS, LOAD RUNS 5 TO 8

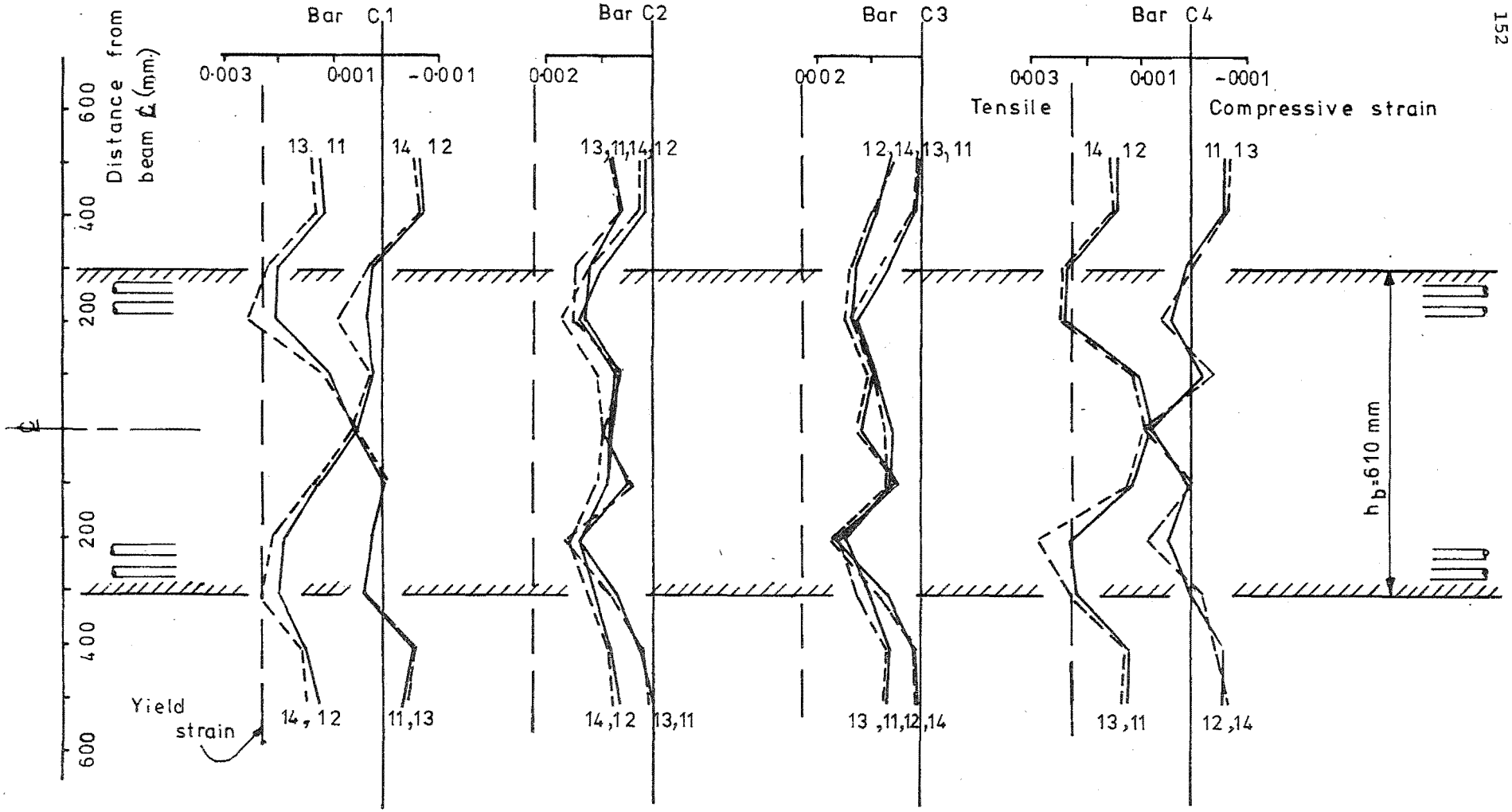

FIG. 4.23 : COLUMN STEEL STRAINS, LOAD RUNS 11 TO 14

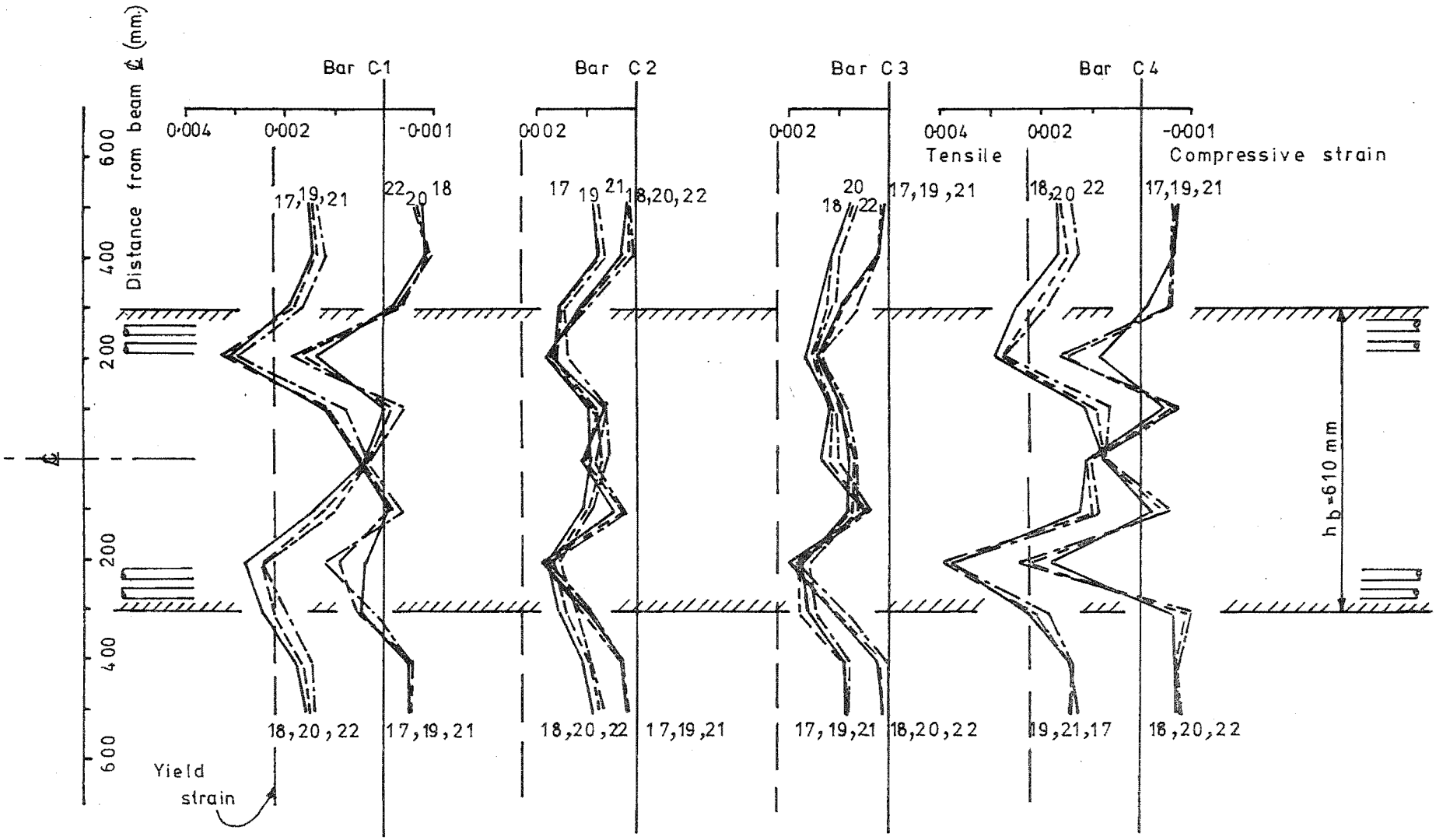

FIG.4.24 :COLUMN STEEL STRAINS, LOAD RUNS 17 TO 22

the effect was not so great as was observed in the test of unit B11, where the bond forces from the greater quantity of top bars were larger than in this case.

The action of the column vertical bars in providing the vertical component of the truss mechanism by means of which joint reinforcement was postulated to resist joint shear caused the extra tension forces apparent in the column bars at the mid-depth of the joint. A detailed discussion of the mechanism of joint shear resistance is given below in Section 4.5.4.

4.5 Joint Behaviour

4.5.1 Joint Cracking

Although joint cracks formed at an early stage of the test, they were well distributed throughout, and did not become excessively wide. The maximum crack width observed in the joint panel was 0.55 mm. Cracks formed generally parallel to the joint diagonals, eventually making a very fine mesh pattern. (See Fig. 4.3). Evidence of sliding along the joint cracks was very limited; such sliding as was observed corresponding to the shear distortions measured in the joint panel as a whole.

From load run 18 onwards, tapping the cover of the joint panel resulted in a hollow sound over some of the panel area, indicating that separation of the cover from the core had occurred. By the completion of the test it was estimated that perhaps 30% of the cover had separated from the joint core, although none had actually fallen off.

4.5.2 Joint Distortion

The shear distortion of the joint panel was measured throughout the test by measuring the deformations along the joint diagonals. The component of beam end displacement caused by this distortion of the joint is shown in Fig. 4.7. Although the joint distortion was essentially elastic in nature, the extensive joint cracking meant that the resulting displacements were quite large, and 26% of the total beam end displacements in load run 8 were due to this source of deformation. Since the loads in subsequent cycles did not increase as much as the displacement demand, the proportion of total displacement caused by joint rotation decreased to a minimum value of 14% in load run 17, although the absolute magnitude of the joint deformation increased, owing to increased cracking.

4.5.3 Strains in Stirrup Legs of Joint Reinforcement

The development of strains in the stirrup legs of joint reinforcement (i.e. those whose primary function was to resist the applied joint shear), is shown in Fig. 4.25(a). The stirrup leg strains increased throughout the test, except for the strain in stirrup legs adjacent to the beam bars, which decreased at load run 20. This was as would be expected, since with the beam bars slipping the bond forces picked up by these stirrups decreased. The largest strains tended to occur at the mid-depth of the joint. The short legs of stirrups carried significant strains, and these increased throughout the test in a similar manner to those in the long legs.

Fig. 4.25(b) shows the envelope of stirrup leg strains throughout the test, i.e. the maximum strain observed in each location at any stage. Only one tie was observed to exceed yield strain during the test, and then by the small margin of only 5%. Inner stirrup legs carried larger strains than outer legs, because (a) they were physically closer to the beam bars providing the input shear, (b) they were more tightly located within the joint core, and (c) they had to resist a larger width of the diagonal compression struts that formed part of the truss mechanism of joint shear resistance.

Fig. 4.26 gives distributions of strain along the outer stirrup legs for four out of the eight sets of joint ties, at the maximum displacement of load runs 5, 6, 19 and 20. The positions of the ties are plotted to approximately the correct vertical scale. The tendency for greater strains to develop on the joint diagonal is shown by the reversal in slope of the strain profiles with the reversal of loading, especially for the tie sets closer to the beam bars. The reversal of slope was more marked between load runs 5 and 6 than in the later cycle, because of the relatively light cracking in the joint in load run 5, a feature which does not recur.

A history of the strain measured in the inner stirrup leg of the fourth tie set from the top of the joint, plotted against the applied joint horizontal shear, is presented in Fig. 4.27. The recovery of joint tie strain at zero load is clearly shown, and this was reflected in the elastic recovery of joint deformation throughout the test, as noted in Section 4.3.1.

4.5.4 Mechanism of Joint Shear Resistance

The horizontal joint shear $V_{sh\,l}$ resisted by the long stirrup legs of the joint reinforcement was determined as described in Section 3.5.4 by summing the tie leg forces derived from strain measurements over the depth

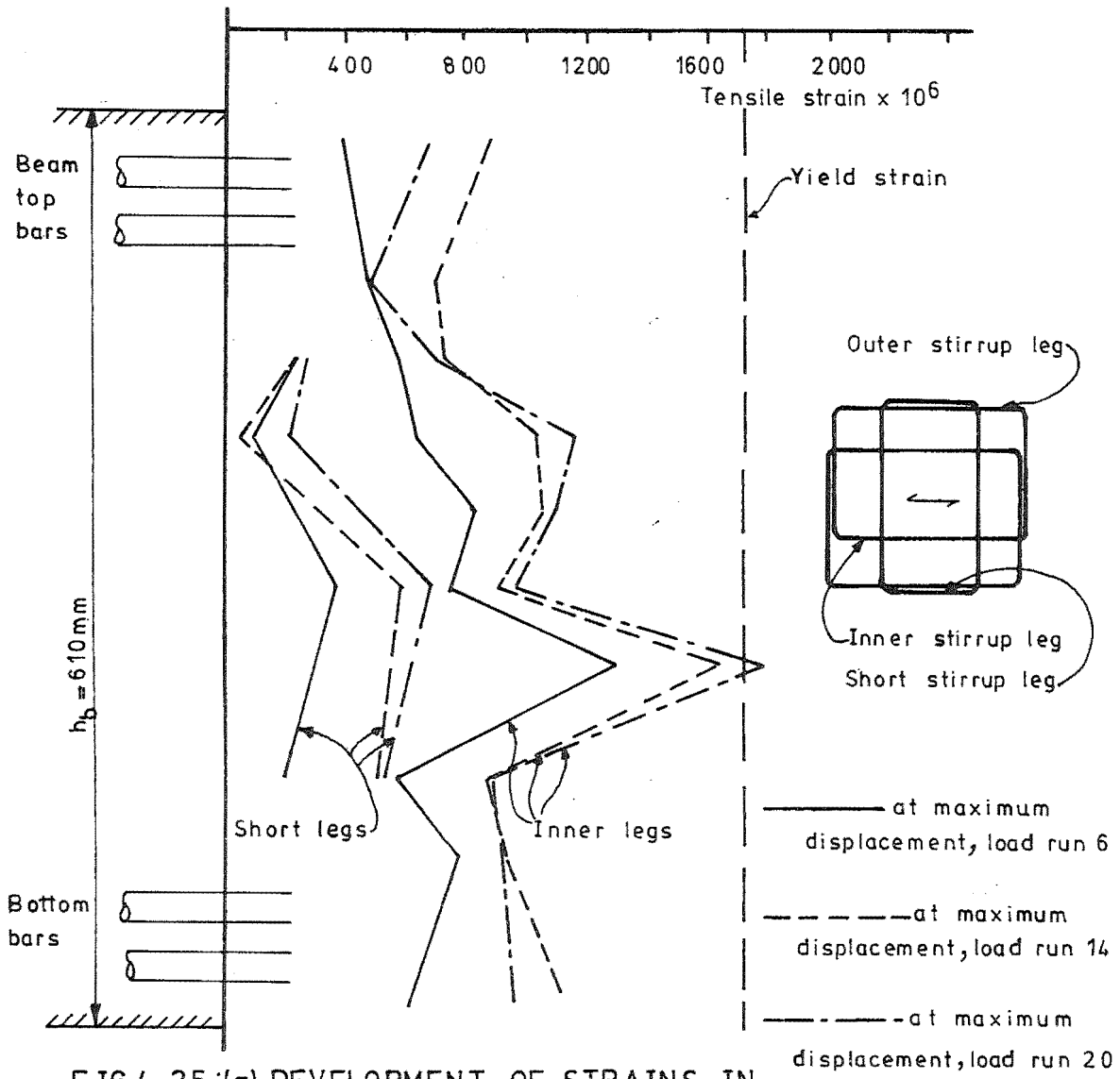

FIG·4·25 :(a) DEVELOPMENT OF STRAINS IN INNER STIRRUP LEGS OF JOINT REINFORCEMENT

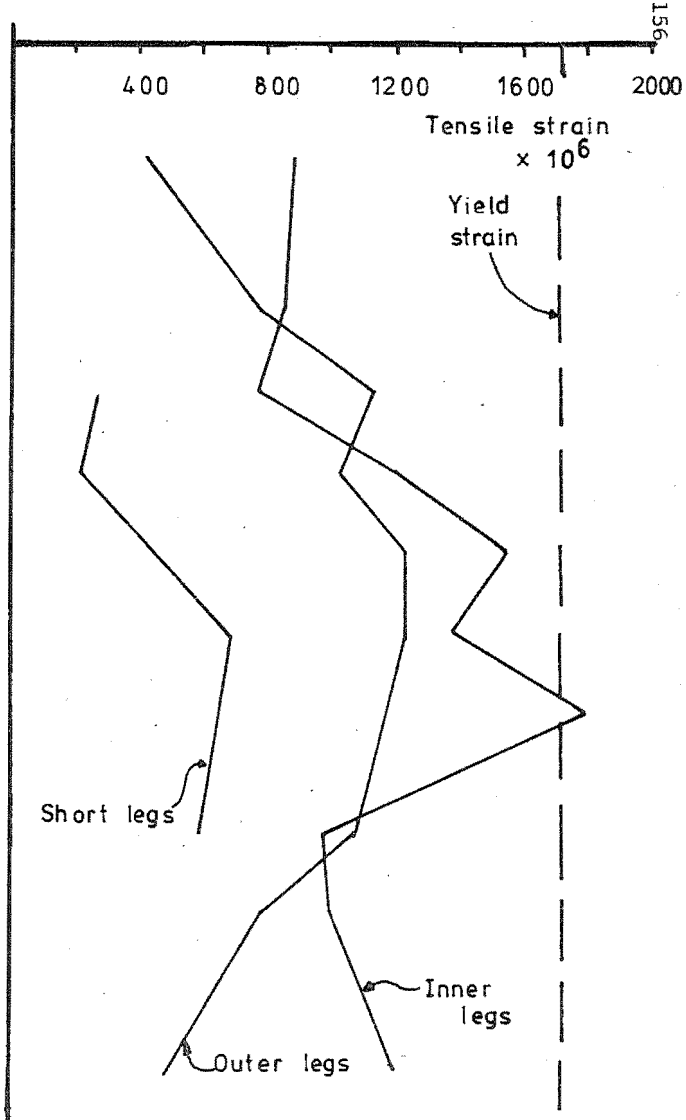

(b) ENVELOPE OF MAXIMUM STRAINS IN STIRRUP LEGS

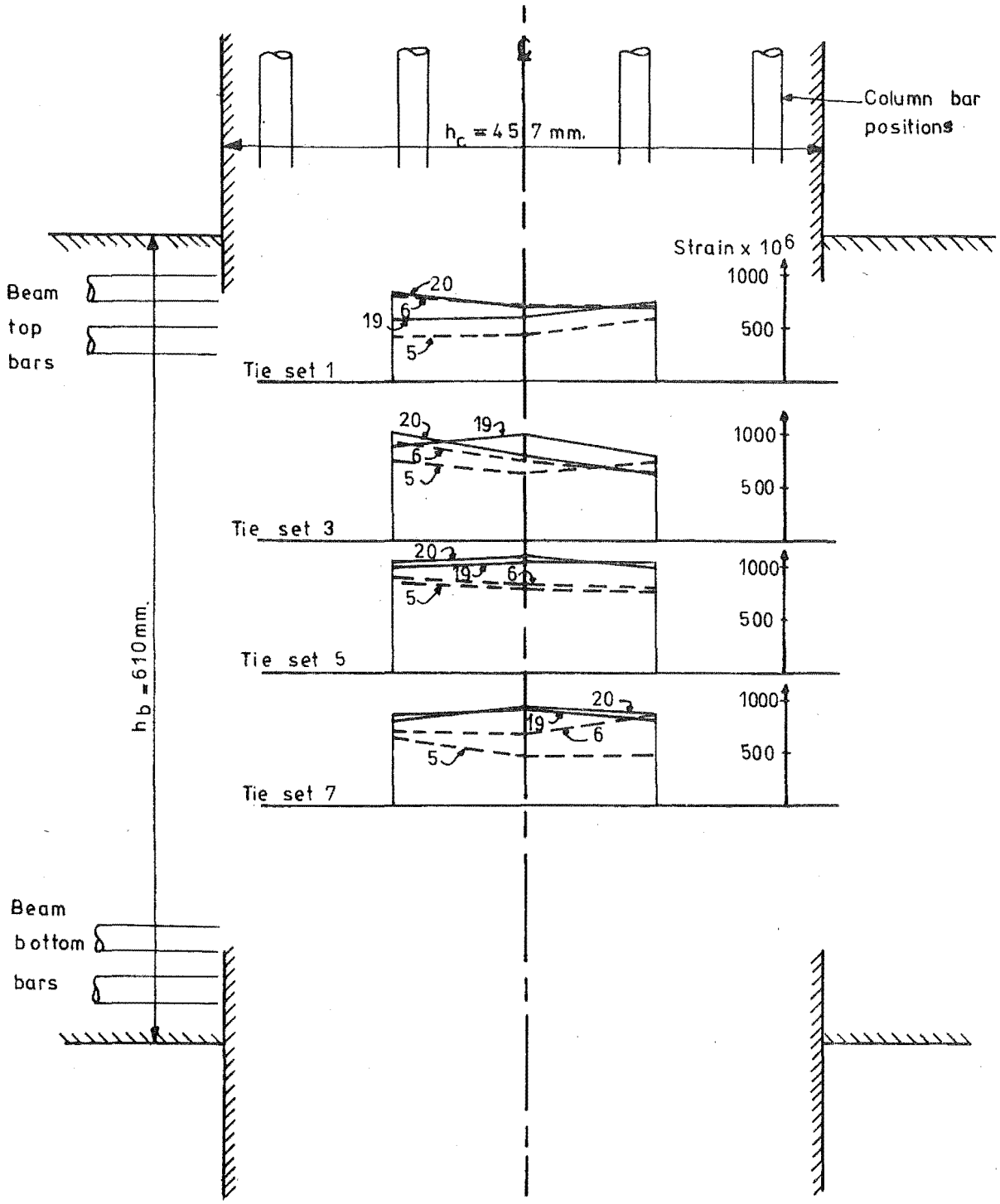

FIG.4.26: DISTRIBUTION OF STRAIN ALONG JOINT TIES AT TOP OF CYCLES 5,6,19&20.

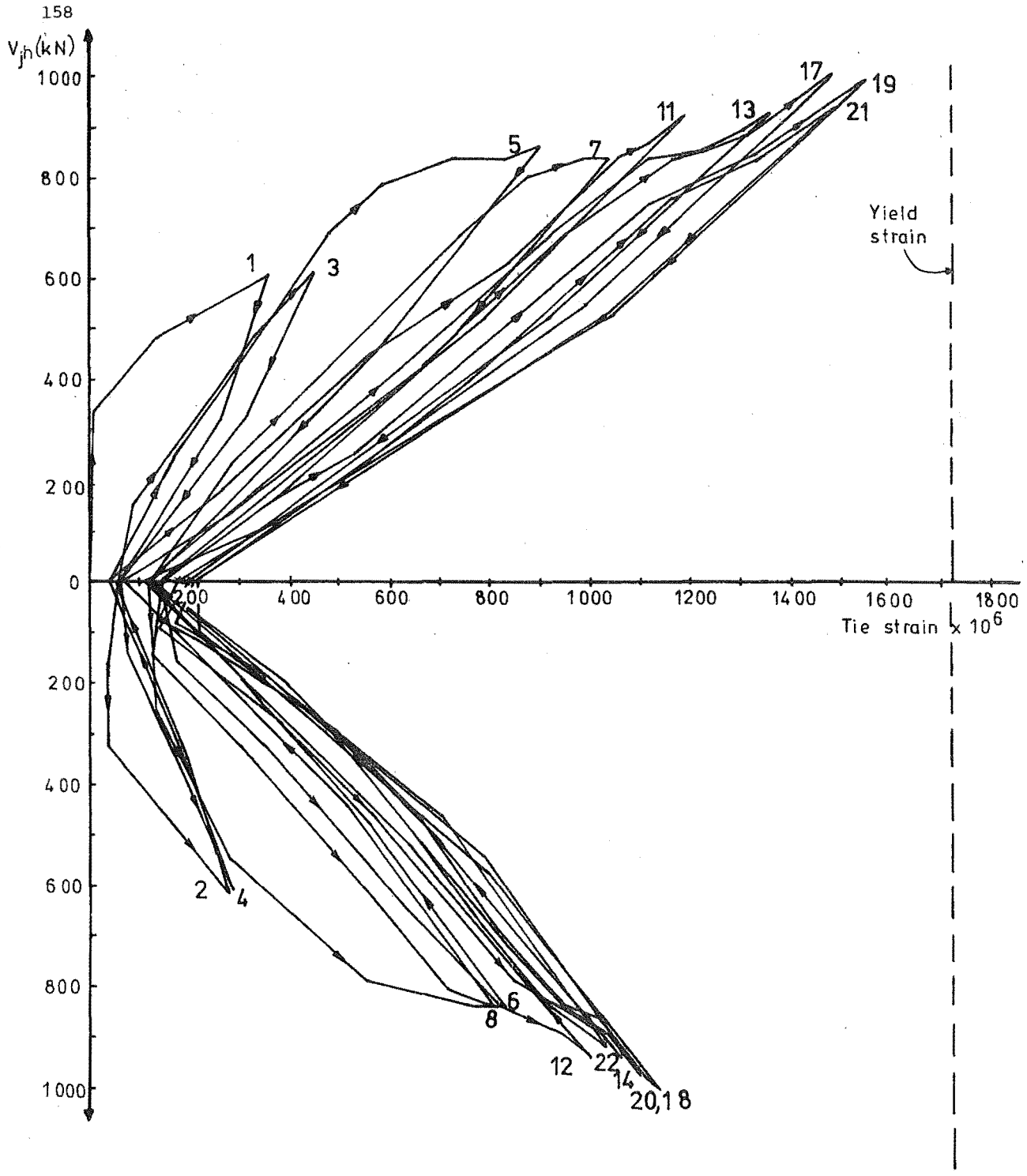

FIG. 4.27 : TENSILE STRAIN vs. JOINT SHEAR FOR INNER STIRRUP LEG OF TIE AT MID DEPTH OF JOINT

of the joint. In this test measurements of strain in the short stirrup legs of the joint reinforcement were taken, in four out of the eight tie sets, and the resulting contribution to horizontal joint shear resistance $V_{sh\,2}$ was assessed by extrapolating these results. This was done by assuming that the critical surface would be inclined in accordance with the observed direction of joint cracking, and would not therefore cross the short tie legs contained in the tie sets closest to the top and bottom beam bars. Thus the short tie legs from only six sets of joint ties were assumed to be effective, and the total horizontal shear resisted by them was taken as 1.5 times the sum of the forces in the four instrumented short tie legs. The difference between the applied horizontal joint shear V_{jh} and the shear resisted by the long and the short stirrup legs of joint reinforcement was termed the horizontal shear resisted by the joint concrete, V_{ch}. The values calculated for the various modes of resistance to horizontal joint shear at the maximum displacement of the major load runs are listed in Table 4.3, and shown in histogram form in Fig. 4.28.

During the initial elastic cycles the joint concrete resisted an average of 48% of the applied horizontal shear, but this proportion decreased rapidly to 30% in the first post-elastic load run (load run 5), and eventually to apparently zero contribution in load run 18. The resistance of joint concrete to horizontal shear tended to be greater whenever conditions were more favourable for the action of a direct concrete strut as described in Section 1.3.2. This occurred in the initial load run of each series to greater ductility demand, where the column face cracks in the beams closed up at the compressed edge more than in repeated cycles, and hence more of the shear was introduced to the joint as concrete compression forces from the beams. This criterion also applied from load run 19 onwards, where reduced bond strength for the beam bars across the joint meant that increasing amounts of horizontal joint shear were introduced as concrete compression at the column faces, and the shear resistance of the joint concrete mechanism increased.

The calculation of the horizontal joint shear resisted by short stirrup legs of joint ties showed that they supplied an average of 9% of the total horizontal joint shear resistance. However the results for individual load runs appeared to be rather sensitive to the direction of loading, particularly towards the end of the test, and the individual values given for $V_{sh\,2}$ must therefore be assumed to be somewhat approximate.

TABLE 4.3 : MECHANISM OF RESISTANCE TO JOINT SHEAR

Load Run No.	V_{jh} (kN)	V_{sh1} (kN)	$\frac{V_{sh1}}{Vjh}$	V_{sh2} (kN)	$\frac{V_{sh2}}{Vjh}$	V_{ch} (kN)	$\frac{V_{ch}}{V_{jh}}$	V_{jv} (kN)	$\tan\beta_T$	$\tan\beta_c$
1	560.6	256.0	0.457	32.6	0.058	272.0	0.485	774.9	1.382	1.298
2	566.6	248.7	0.439	19.2	0.034	298.7	0.527	825.1	1.456	1.402
3	562.1	309.3	0.550	31.4	0.056	221.4	0.394	865.9	1.540	1.510
4	559.3	259.3	0.464	19.8	0.035	280.2	0.501	908.6	1.625	1.652
5	846.1	543.4	0.642	45.8	0.053	256.9	0.304	1362.3	1.610	1.472
6	840.1	624.6	0.743	68.6	0.082	146.9	0.175	1529.0	1.820	1.869
7	840.1	631.9	0.752	58.2	0.069	150.0	0.179	1614.5	1.922	2.067
8	833.2	617.0	0.741	70.8	0.085	145.4	0.175	1545.0	1.854	1.930
11	906.8	698.1	0.770	61.2	0.067	147.5	0.163	1795.4	1.980	1.996
12	922.3	754.8	0.818	88.4	0.096	79.1	0.086	1815.9	1.969	1.989
13	913.9	791.2	0.866	74.6	0.082	48.1	0.053	1916.9	2.097	2.205
14	922.4	714.6	0.775	104.3	0.113	103.5	0.112	1892.7	2.052	2.187
17	981.5	864.7	0.881	78.4	0.080	38.4	0.039	1866.9	1.902	1.882
18	982.4	852.3	0.868	130.1	0.132	0.0	0.0	1927.8	1.962	2.134
19	977.6	842.5	0.862	80.7	0.083	54.4	0.056	1826.3	1.868	1.824
20	954.8	784.8	0.822	129.7	0.136	40.3	0.042	1685.0	1.765	1.799
21	922.3	754.5	0.818	69.2	0.075	98.6	0.107	1628.2	1.765	1.684
22	903.8	707.7	0.783	121.9	0.135	74.2	0.082	1504.5	1.665	1.587

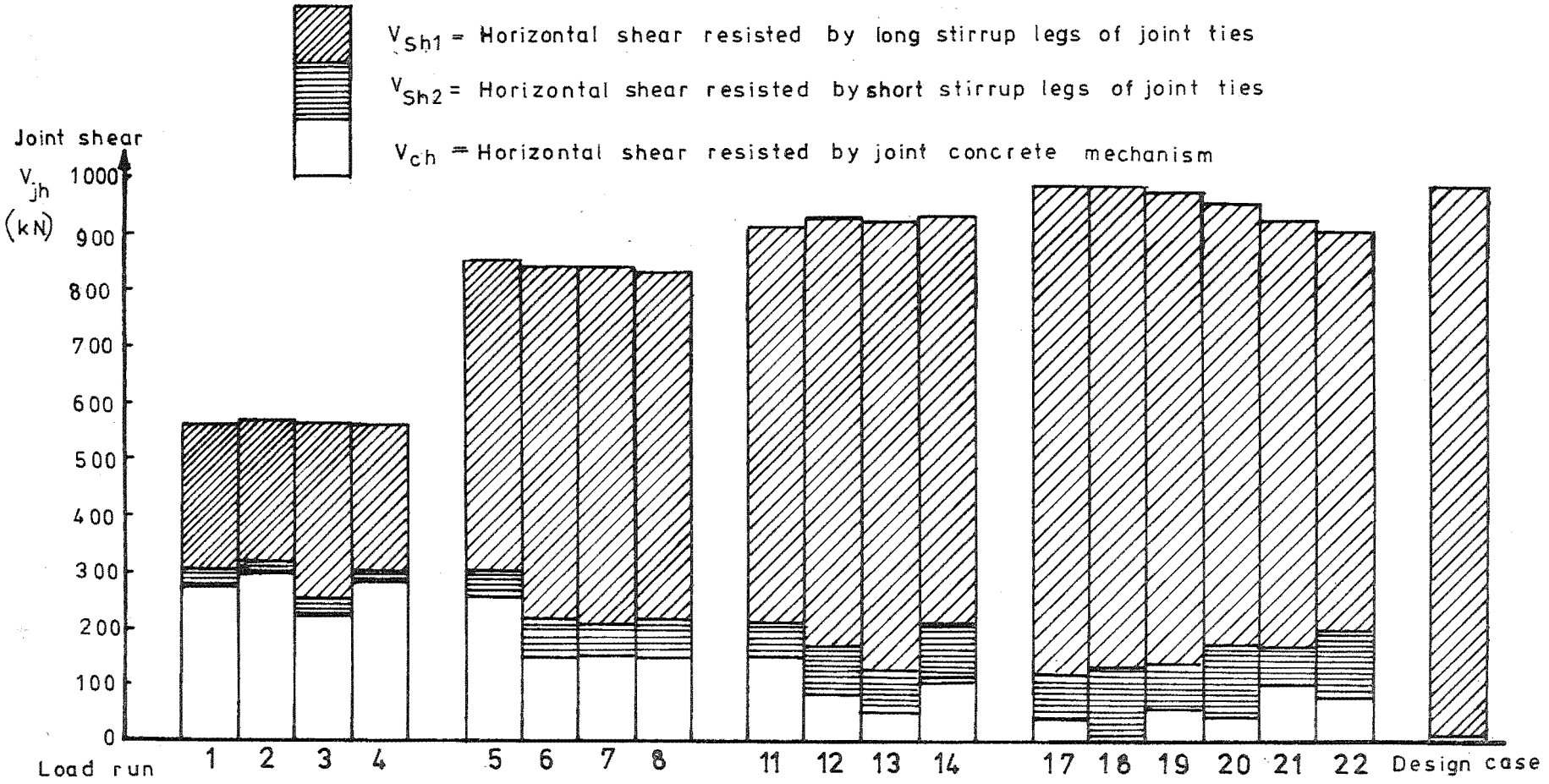

FIG.4.28:MODE OF RESISTANCE TO HORIZONTAL JOINT SHEAR

Comparison of the design assumptions for the resistance of horizontal joint shear as shown in Fig. 4.28 with the experimental observations at the maximum displacement of load runs 17 to 22 shows that the design assumption was accurate after significant cyclic loading had been applied.

The vertical joint shear V_{jv} was calculated as described in Section 3.5.4 from the experimental column bar forces, the concrete compression forces in the column sections above and below the beam, and the beam shear forces. The resulting values of V_{jv} are listed in Table 4.3, together with the tangent of the angle of applied joint shear, $\tan \beta_T = V_{jv}/V_{jh}$. Also listed in Table 4.3 is the tangent of the angle β_c between the centroids of concrete compression in the beam and column sections at diagonally opposite corners of the joint panel. The centroid of concrete compression in the columns was calculated to satisfy moment equilbrium considering the internal forces, and the applied moments and axial load. The centroid of concrete compression in the beams could not be accurately located from the experimental results, and it was therefore assumed to be at the level of the outer layer of beam bars. Values of $\tan\beta_T$ and $\tan\beta_C$ are plotted in Fig. 4.29, and both values were similar throughout the test. After the initial elastic cycles (load runs 1 to 4), the applied shear was resisted at angles steeper than the joint diagonal β_J. Up to load run 14 the angle of resistance gradually increased as penetration of yield strain in the beam bars into the joint increased, and the horizontal shear was thus applied closer to the column centreline. From load run 17 onwards the onset of slip of the beam bars through the joint changed the mode of introduction of horizontal shear into the joint, and the angle of resistance thus decreased significantly.

4.5.5 Strains in Transverse Tie Legs of Joint Reinforcement

The development of strains in the inner transverse tie legs of the joint reinforcement and the envelope of the maximum strains for inner and outer tie legs are given in Fig. 4.30. The strains were well below yield strain, except in the tie sets closest to the beam bars, where bursting stresses in the concrete due to bond forces from the beam bars caused the higher values. In this vicinity the difference in the strain measured in inner and outer tie legs was also greatest, because the bond effects from the beam bars were more severe towards the edges of the column. Evidently the confinement of bond stresses from the beam bars was more critical with respect to the stressing of the transverse tie reinforcement than was the confinement of the direct compressive forces.

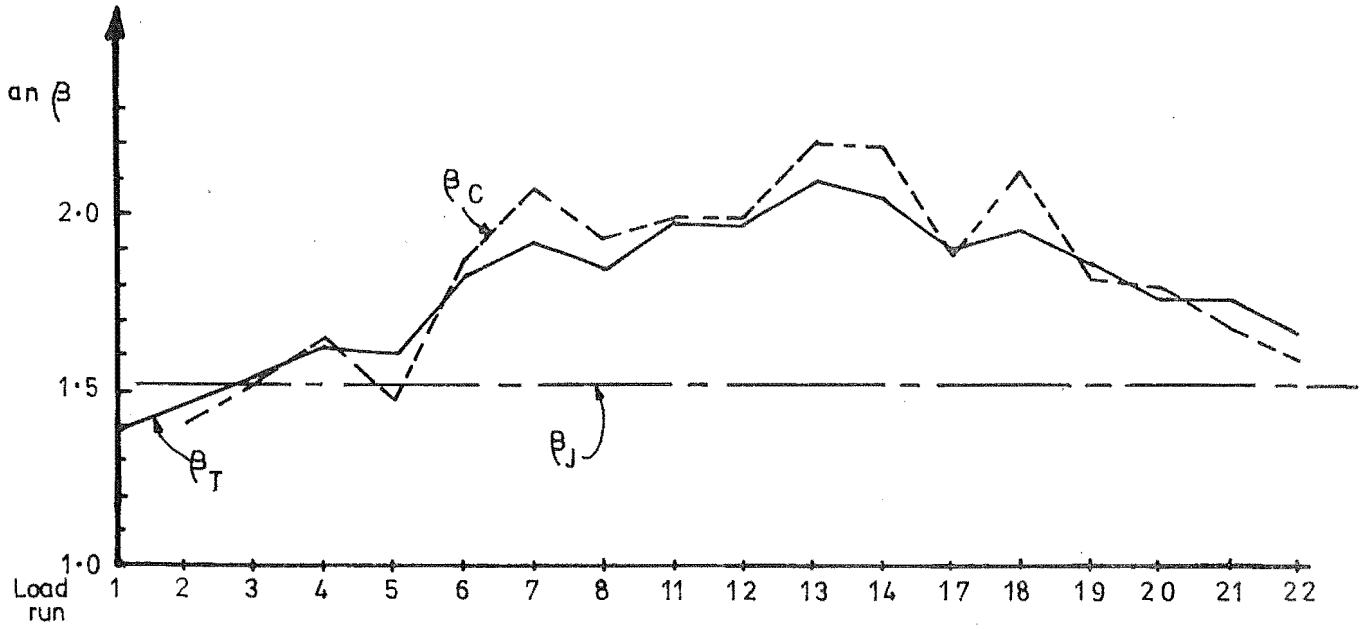

FIG.4.29 :ANGLE OF RESISTANCE TO JOINT SHEAR

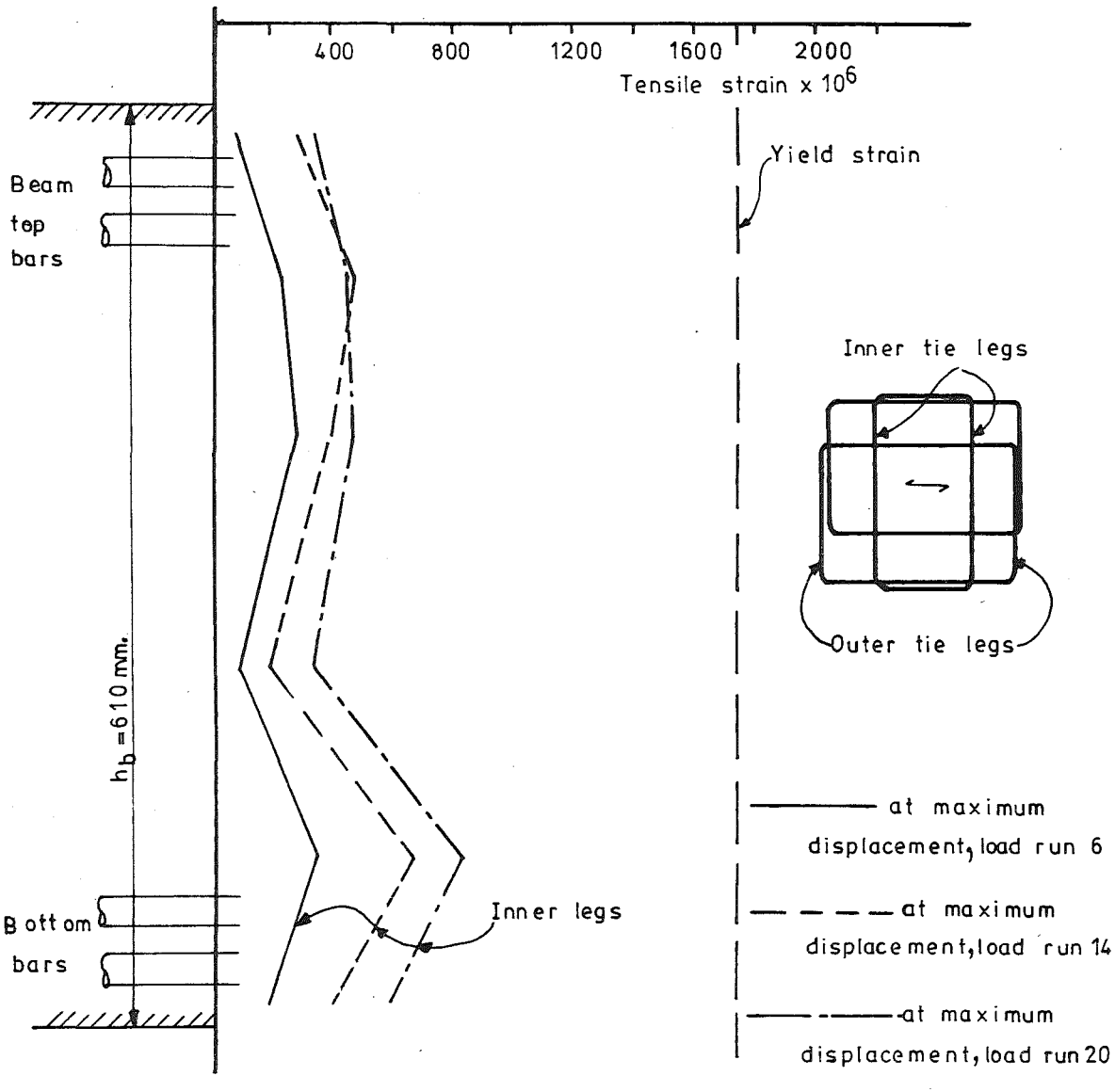

FIG. 4.30: (a) DEVELOPMENT OF STRAIN IN INNER TIE LEGS OF JOINT REINFORCEMENT

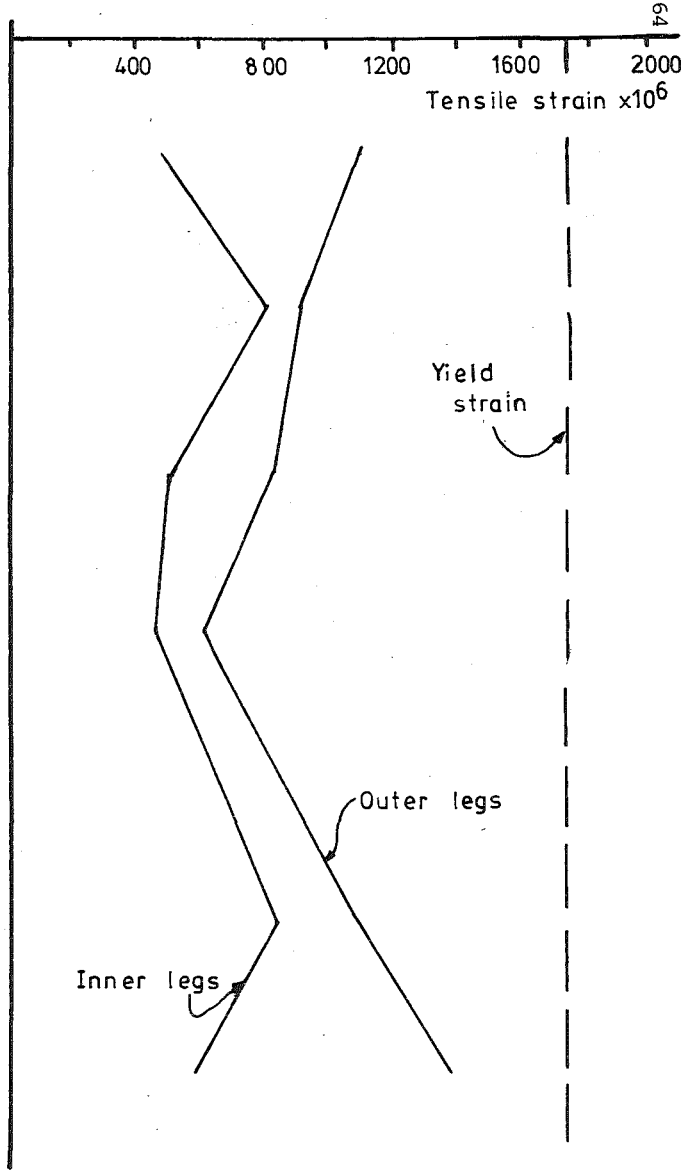

(b) ENVELOPE OF STRAINS IN TRANSVERSE TIE LEGS

For the low axial load used in the test, it is considered that the confining ties could have been of a smaller size (R10), at least in the mid-depth of the joint, without compromising the integrity of the joint in any way.

4.6 Summary

The primary object of this test, namely to achieve a satisfactory joint performance, was achieved. Joint cracks were kept narrow and well distributed; joint distortion was well controlled; and strain in the joint reinforcement exceeded yield in one location only. The secondary object of the test was to assess the benefits and limitations of a beam flexural reinforcement configuration of equal contents of top and bottom bars, and the outcome of this study was disappointing in that slip of beam bars through the joint was not suppressed. Some benefits did accrue from the equal beam reinforcement configuration however, principally in so far as top and bottom bars were approximately equally utilised for plastic deformation, and hence the layout of reinforcement could be considered more efficient than was the unequal reinforcement case, as illustrated in the preceding test of unit B11. The occurrence of sliding shear deformation along open flexural cracks in the beam hinges was not suppressed. Evidently intermediate longitudinal bars in the mid-depth region of the beam would be necessary to limit this distortion by distributing the flexual cracks over the full depth of the beams.

The implications of the slip of the beam bars through the joint were serious where the response of the test unit was concerned, but the same response would not necessarily be as serious for an element of a complete structure. It should be noted that this failure occurred only after severe pseudo-seismic loading had already been imposed and resisted satisfactorily. The probability of all or even a majority of joints in a multistoreyed building reaching this state under real earthquake loading is considered to be low, especially as the stiffness of the building as a whole will be reduced if slip does occur at some joints. However the ratio of column breadth to beam bar diameter, h_c/d_b, for prototype joints should not exceed the value of 24 used in this test unit.

It is felt that the performance of the unit would not have been adversely affected to any great degree if the eight sets of joint ties used had been reduced to seven sets. More yielding of the joint reinforcement would have been encountered, but it is felt that redistribution of stresses would have prevented seriously deleterious effects. However for an

arbitrary design case it should be remembered that the beam steel strength for joint design was taken as 345 MPa, whereas the bars used in the test unit had a yield strength of only 298 MPa, and reached about 336 MPa under strain hardening. The design steel strength for the joint ties on the other hand was 276 MPa, while their actual yield strength was 336 MPa. Thus the differences in assumed, actual, and possible reinforcing steel properties could easily take up a margin of joint strength somewhat greater than that implied by the reduction of joint reinforcing suggested above. However even the combination of all quantities having their most unfavourable values would appear unlikely to overtax a joint designed on the same basis as the test unit.

The symmetrically reinforced beams of unit B12 resulted in a more uniform distribution of strain in joint ties down the depth of the joint than was observed in the test of unit B11. This resulted in less yield excursions being noted in the joint reinforcement for unit B12 than for unit B11, but the difference in performance was insufficient to warrant any recommendation that the beam reinforcement configuration should be a factor in the design of joint horizontal reinforcement. The only plausible recommendation is that a greater volume of the required joint reinforcement should be placed closer to the greater area of beam reinforcement where the beams are not symmetrically reinforced, rather than at the uniform spacing usually used.

Reduction of the strain data obtained from the joint reinforcement showed that very little horizontal shear was resisted by joint concrete after severe cyclic loading had been imposed. However the increase in the beam concrete compression forces resulting from the slip failure of beam bars across the joint was shown to cause a small increase in the horizontal shear resisted by joint concrete. The slip failure was also shown to significantly affect the angle at which joint shear resisted. Both these observations lend validity to the mechanisms of joint shear resistance proposed in Section 1.3.

CHAPTER 5

TEST OF UNIT B13

5.1 INTRODUCTION

The test unit B13, being identical in most respects with the preceding unit B12, was intended to demonstrate by comparison with unit B12 the effect of column axial load on joint performance. The axial load applied to the column of unit B13 was 2890 kN, which resulted in a uniform stress over the gross area of the column of fifty percent of the specified crushing strength of the concrete, f'_c, whereas the applied axial load on the column of unit B12 represented only five percent of $f'_c.A_g$. This high level of column load was chosen as an extreme value of the compressive axial load likely to act on a column during a severe earthquake, considering the combined effects of gravity loading, earthquake induced beam shears in the floors above, and vertical ground motions. It was intended that the large difference in the axial load levels employed in the two tests would make any differences in joint response quite obvious, although ideally more tests at intermediate levels of column load would have been desirable to define more exactly the effect of this parameter. Beam and column reinforcement configurations for test unit B13 were identical to those used in unit B12. However, joint steel content was arbitrarily reduced by 25% (i.e. six sets of three R12.7 ties were used instead of eight sets). It follows from the mechanisms of shear resistance postulated in Section 1.3 that significant horizontal joint shear would be resisted by the concrete strut mechanism, because of the better bond conditions for the beam flexural reinforcement across the joint due to the greater depth of compression in the more heavily loaded column.

After the standard loading sequence had been applied up to load run 20 (i.e. to displacement ductility factor of six), the performance of the unit had been entirely satisfactory, with no evidence of compromising secondary failures in joint shear nor in anchorage of the beam flexural reinforcement. It was then decided that further useful information might be gained by decreasing the column load and applying further cycles of lateral loading. The load was therefore reduced to 1677 kN ($0.29\ f'_c A_g$), and further cycles were imposed as described in Section 2.7. The first and second parts of the test under different levels of column axial load are referred to as tests B13A and B13B respectively.

The response of the test unit was very good in both parts of the test, with plastic action restricted to the beam hinges, and well controlled joint cracks and deformations, while yielding of the joint reinforcement was

limited. The photographs taken during the test (Figs. 5.1 to 5.5) show that cracking of the joint and column was much less extensive than was observed in the test of unit B12 (compare Figs. 4.1 to 4.3), especially during test B13A. In the final cycle of the test, slip of the beam flexural reinforcement across the joint was observed, but this failure was not considered to be significant nor representative, since the total number of severe inelastic cycles imposed on the unit was then excessive. The total cumulative displacement ductility applied during the major cycles was 104, and since conditions were then unrealistic the final cycle was not repeated.

Analysis of the test data showed that the ability of the joint concrete to resist shear decreased as the test progressed, with the smaller axial load in test B13B causing further reduction. The inclination of the concrete struts of the joint shear resisting mechanisms was also shown to depend on the axial load level.

5.2 Load-Displacement Response

5.2.1 Response During Test B13A

Beam end load-displacement relationships measured during test B13A with heavy column axial load ($0.50f'_cA_g$) applied are presented in Figs. 5.6 and 5.7 for the Western and Eastern beams respectively. The stiffnesses of the unit observed during the initial elastic cycles were approximately 50% greater than those observed in the test of unit B12, because of the absence of cracking in the joint panel and throughout the column. This resulted in a smaller yield deflection (as defined in Section 2.7) than was observed in previous tests, so that the actual beam end displacements corresponding to given ductility factors in the post-elastic cycles were about two-thirds of those applicable to the other units.

Comparisons of the measured beam end loads with the theoretical loads at yield of the beam tension reinforcement and at the ultimate flexural strengths for the beams are listed in Table 5.1a. Maximum beam end loads during the first inelastic cycles to displacement ductility factor of two were typically between the theoretical yield and ultimate loads, but during subsequent cycles with greater ductility demand the theoretical section strength was exceeded by as much as nineteen percent. The excess of strength was due mainly to the strain-hardening and strain-aging of the beam flexural reinforcement.

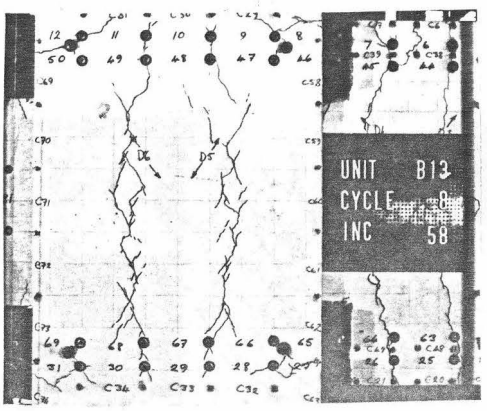

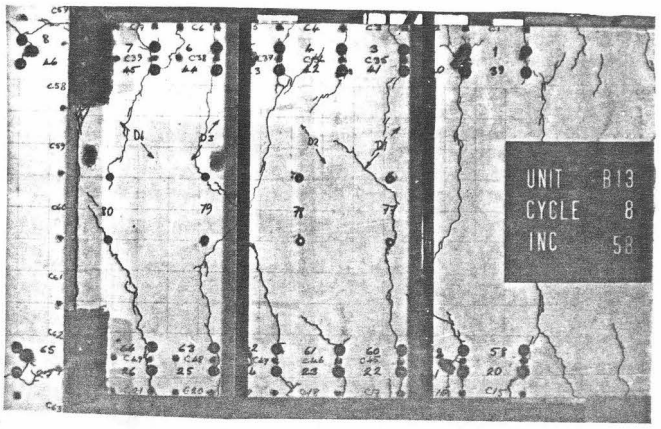

(a) JOINT (b) WESTERN BEAM

FIG. 5.1: TEST UNIT AT MAX. DISPLACEMENT, LOAD RUN 8 (μ=2·0)

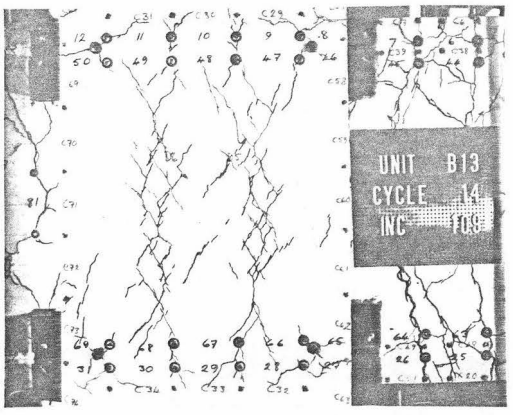

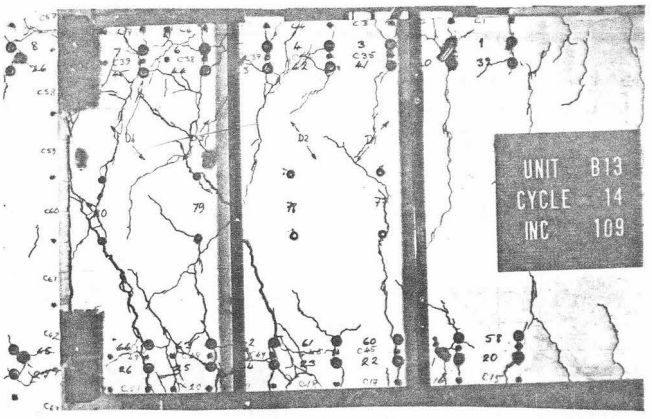

(a) JOINT (b) WESTERN BEAM

FIG. 5.2: TEST UNIT AT MAX. DISPLACEMENT, LOAD RUN 14 (μ=4·0)

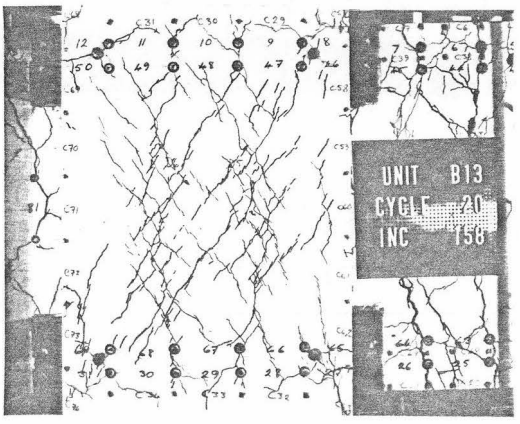

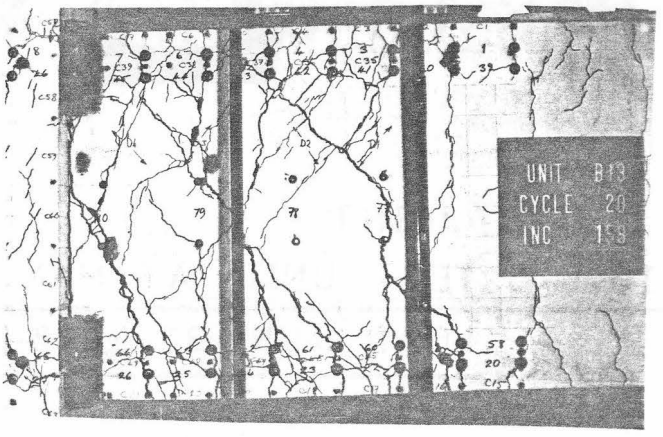

(a) JOINT (b) WESTERN BEAM

FIG. 5.3: TEST UNIT AT MAX. DISPLACEMENT, LOAD RUN 20 (μ=6·0)

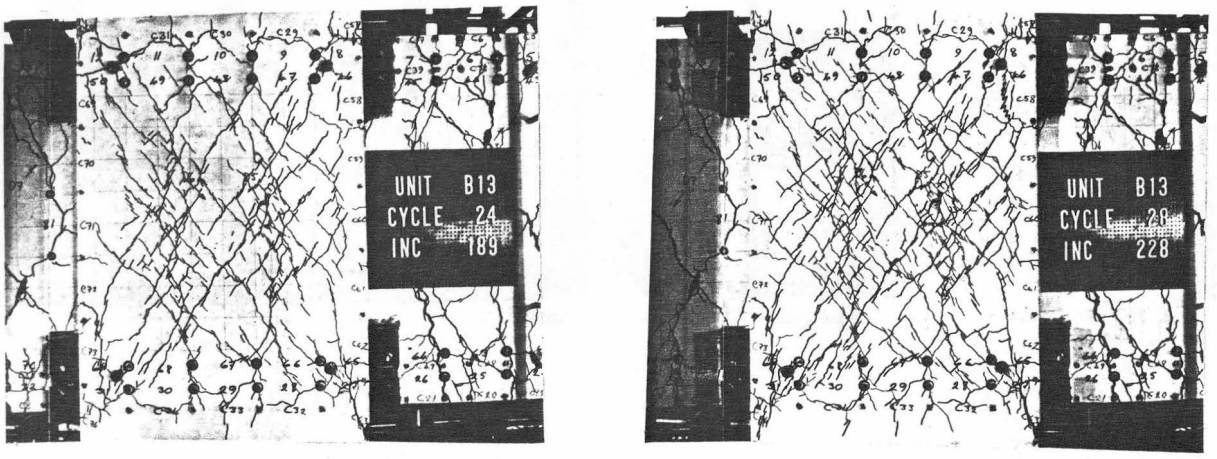

(a) LOAD RUN 24 (μ=4·0) (b) LOAD RUN 28 (μ=6·0)

FIG. 5.4 : TEST UNIT JOINT DURING TEST B13B

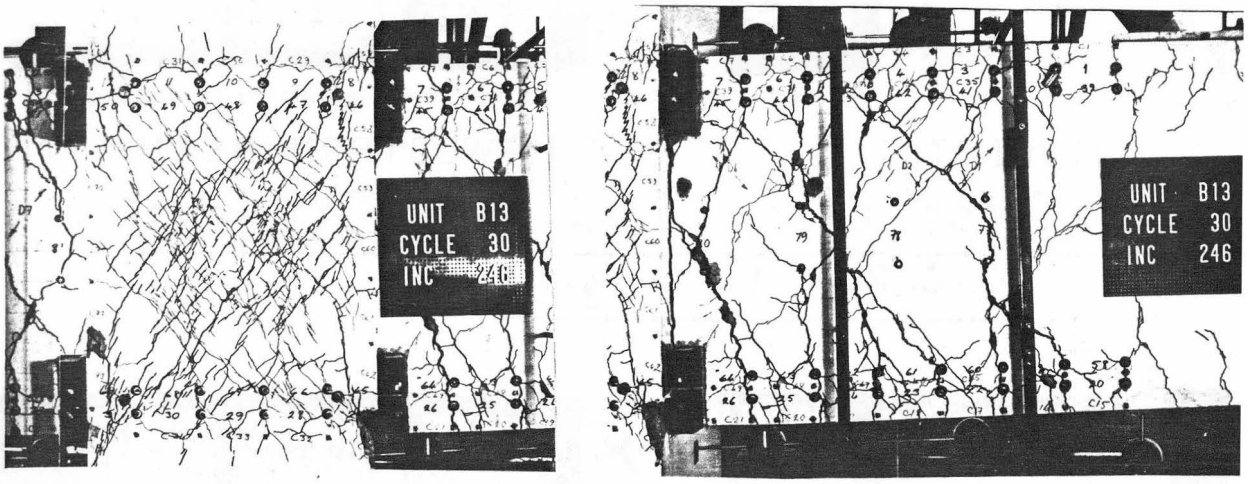

(a) JOINT (b) WESTERN BEAM

FIG. 5.5 : TEST UNIT AT MAX. DISPLACEMENT, LOAD RUN 30 (μ=8·0)

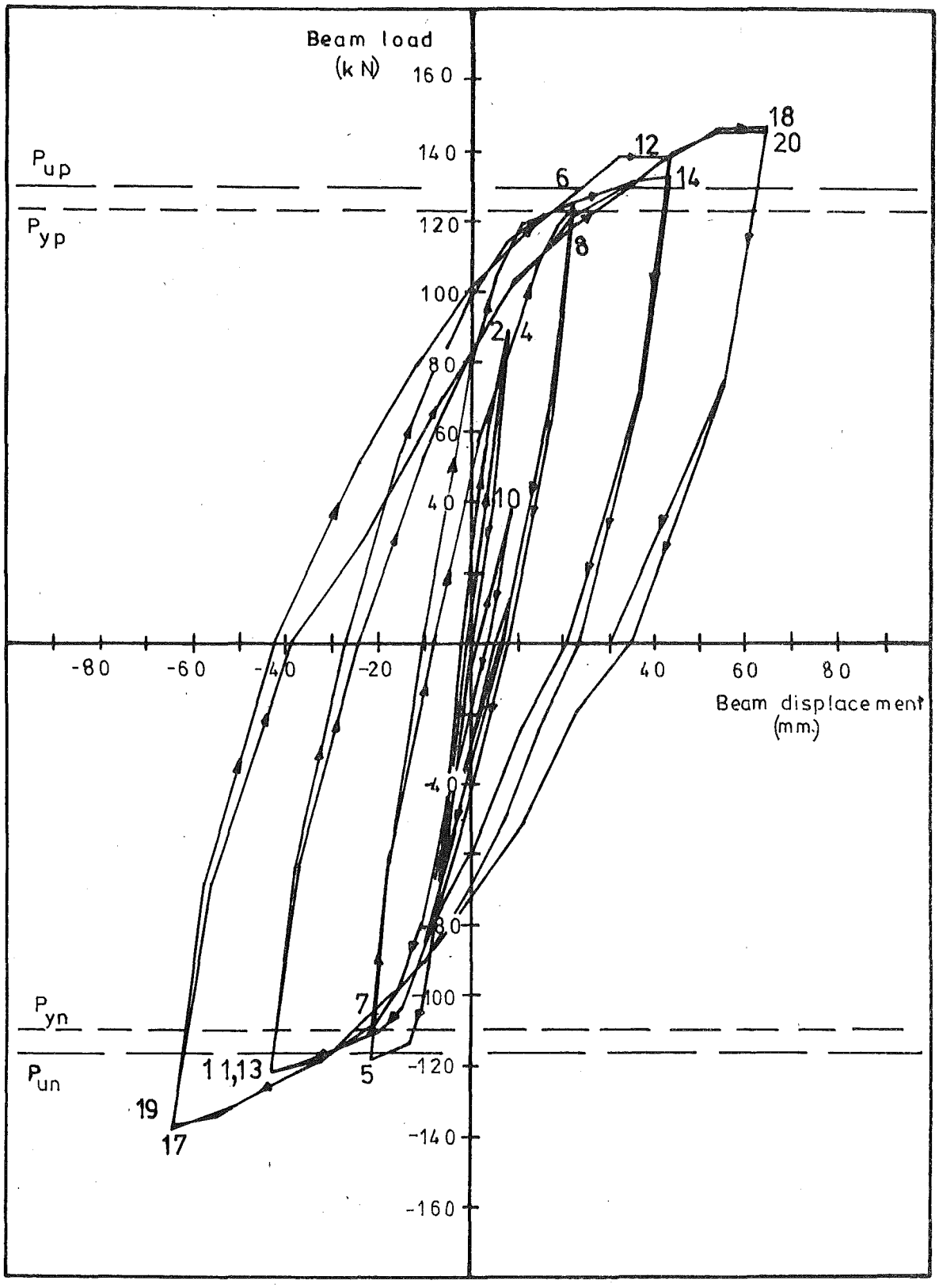

FIG. 5. 6 : BEAM LOAD-DISPLACEMENT RESPONSE - WESTERN BEAM TEST B13A

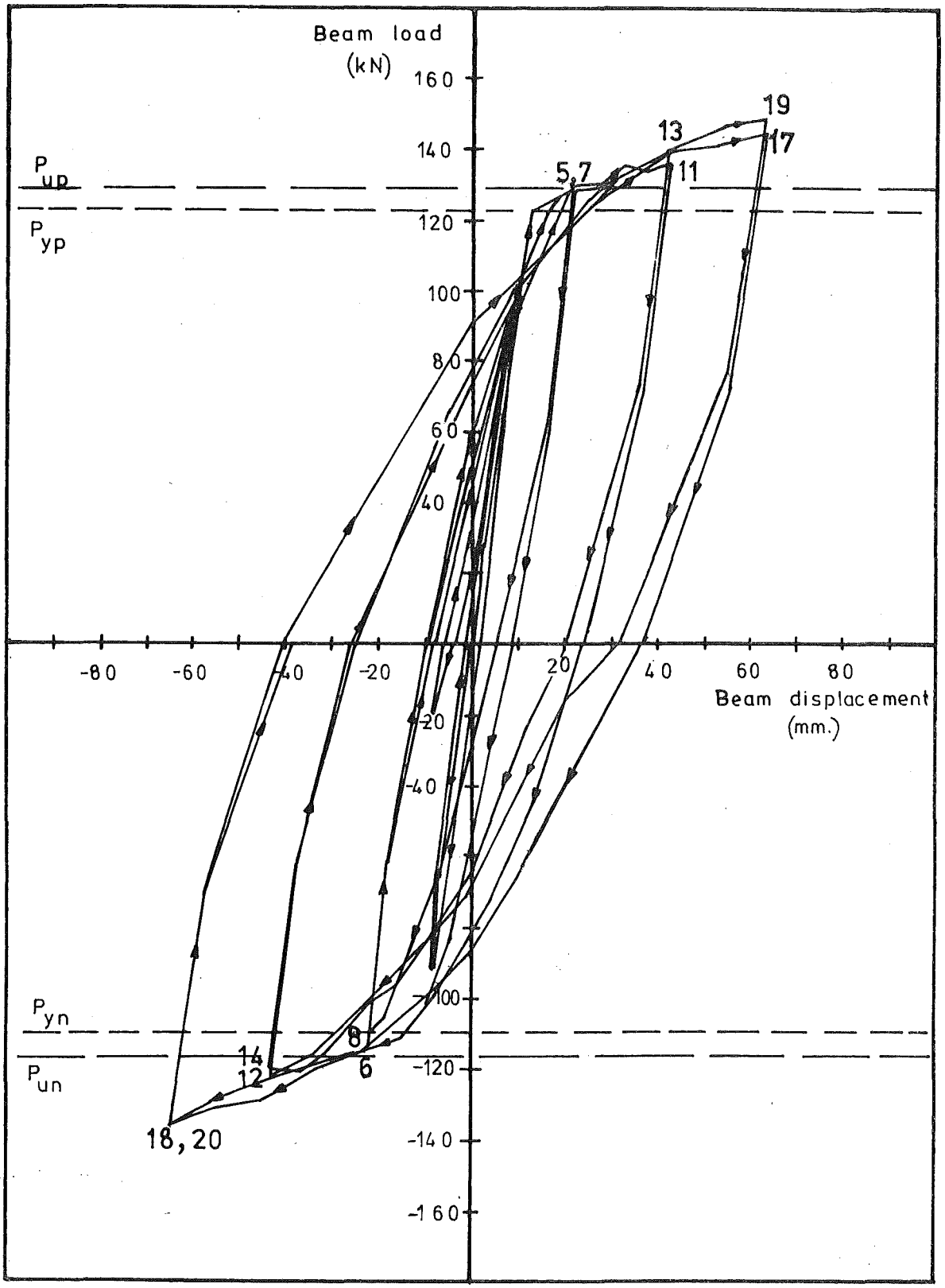

FIG·5.7 :BEAM LOAD-DISPLACEMENT RESPONSE—
EASTERN BEAM TEST B13A

TABLE 5.1a : BEAM END LOADS - TEST B13A

Load Run No.	μ	Beam West			Beam East		
		P (kN)	P/P_y	P/P_u	P (kN)	P/P_y	P/P_u
1	0.75	-80.07	0.729	0.688	86.27	0.703	0.667
2		89.51	0.730	0.692	-79.68	0.726	0.684
3		-81.07	0.739	0.696	88.37	0.721	0.683
4		89.52	0.730	0.692	-79.02	0.720	0.678
5	2.0	-118.70	1.081	1.019	129.10	1.053	0.998
6		125.37	1.022	0.969	-113.17	1.031	0.972
7		-111.07	1.012	0.954	128.55	1.048	0.994
8		123.50	1.007	0.955	-110.07	1.003	0.945
9	0.75	-68.54	0.624	0.589	84.66	0.690	0.655
10		38.26	0.312	0.296	-20.24	0.184	0.174
11	4.0	-122.13	1.113	1.049	136.11	1.110	1.052
12		132.21	1.078	1.022	-122.69	1.118	1.054
13		-122.07	1.112	1.048	140.01	1.141	1.083
14		138.27	1.127	1.069	-120.14	1.095	1.032
15	0.75	-82.14	0.748	0.705	94.72	0.772	0.732
16		12.40	0.101	0.096	0.00	0.0	0.0
17	6.0	-138.36	1.261	1.188	145.46	1.186	1.125
18		146.39	1.193	1.132	-136.44	1.243	1.172
19		-137.32	1.251	1.179	148.62	1.212	1.149
20		144.99	1.182	1.121	-136.33	1.242	1.171

TABLE 5.1b : BEAM END LOADS - TEST B13B

Load Run No.	μ	Beam West			Beam East		
		P (kN)	P/P_y	P/P_u	P (kN)	P/P_y	P/P_u
21	4.0	-121.94	1.111	1.047	133.47	1.088	1.032
22		106.50	0.868	0.823	-100.65	0.917	0.864
23		-117.33	1.069	1.008	125.23	1.021	0.968
24		107.14	0.873	0.828	-98.45	0.897	0.845
25	6.0	-135.81	1.237	1.166	149.13	1.216	1.153
26		144.95	1.182	1.121	-133.39	1.215	1.146
27		-132.68	1.209	1.139	140.47	1.145	1.086
28		138.02	1.125	1.067	-128.09	1.167	1.100
29	8.0	-144.34	1.315	1.240	152.15	1.240	1.176
30		152.88	1.246	1.182	-140.91	1.284	1.210

Note: 1. For definition of terms, refer to Table 3.1

2. P_y and P_u are given in Table 2.3

The load-displacement loops recorded in the inelastic cycles of this test were much fuller than those determined in the previous tests, implying a more effective energy dissipation capability in this case. Some stiffness degradation was apparent between consecutive cycles due to penetration of yield strain in the beam flexural bars into the joint, joint distortion, and beam shear deformation. Rounding of the loops due to the Bauschinger effect in the flexural steel was evident in all of the major cycles.

The column shear versus sidesway response for the unit is given in Fig. 5.8. The derivation of this response from the two beam load displacement curves, and the method of incorporating the P-delta effect was explained in Section 3.2. In this test the effect of the column axial load on the overall response of the unit was severe in that the P-delta effect caused the net column shear to decrease as the applied displacement was increased. Maximum net column shear was carried at only 20 mm. sidesway in each direction (in load run 5 for positive shear, and in load run 12 for negative shear). The P-delta effect led to reductions in column shear of 15% at displacement ductility factor of two, 27% at ductility four, and 36% at ductility six. Due to the partial compensation for these reductions by strain hardening, etc, the column carried 89% of the maximum observed shear at ductility four, and 85% of the maximum at ductility six. Evidently for a joint in a real structure under a sustained load of the magnitude applied in this test, plastic instability would be possible. However in a real structure under seismic loading the column axial loads will fluctuate, and the level of load applied to the test unit column was approaching the upper limit of load likely to be considered in design. Thus only one (or very few) columns in a bent would be subjected to axial loads of this magnitude at any instant during seismic loading of the structure. The P-delta effect is however the result of the response of the entire bent, so that the loss in the total storey shear is much less than was apparent in this extreme case. If the total P-delta effect nonetheless becomes significant during the response of a bent, then it would be vital that stiffness and energy dissipation ability should be maintained by the structure to prevent the displacement demand becoming excessive[36]. The test results show that these criteria were met in the test because the joint maintained its integrity, and non-ductile modes of energy dissipation were suppressed.

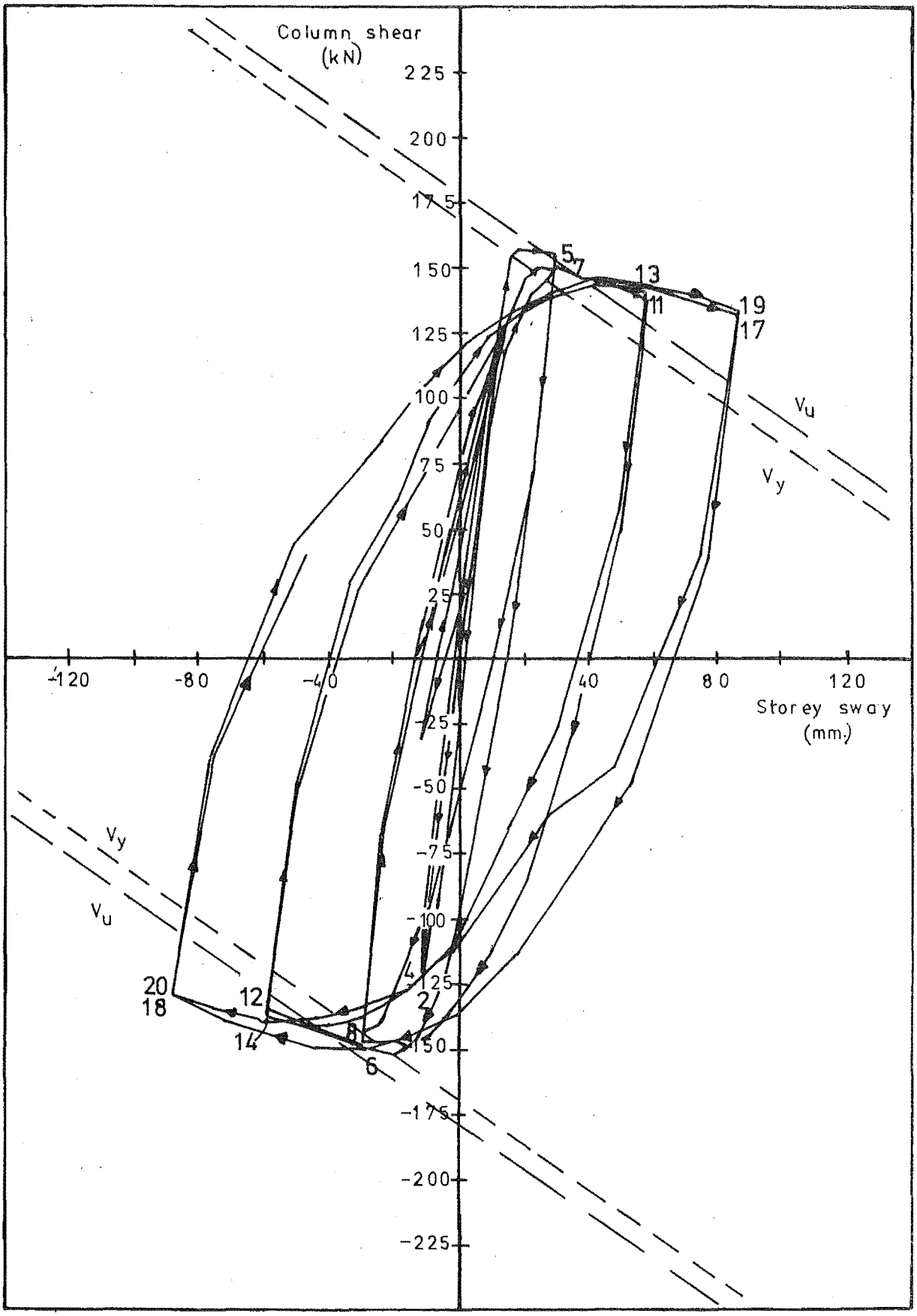

FIG.5.8 COLUMN SHEAR—STOREY SWAY RESPONSE TEST B13A

5.2.2 Response During Test B13B

Beam end load-displacement relationships measured during test B13B, when the column load was reduced to 1677 kN ($0.29f'_cA_g$) are presented in Figs. 5.9 and 5.10. A significant reduction in the stiffness of the unit compared to that observed during test B13A was apparent. This occurred because of increased penetration of yield strain in the beam flexural bars into the joint, and because of more extensive cracking in the joint and column. Because the displacements applied in load runs 21 to 24 were less than the previous maximum, and because the stiffness had degraded somewhat, the response in the first two cycles was unsymmetrical, with the residual deflections from the previous test requiring a greater displacement increment for the odd-numbered load runs than for the even-numbered ones. This resulted in smaller loads being applied in load runs 22 and 24 as shown in Table 5.1b. When displacement was again applied up to the previous limits (i.e. load run 25 onwards) symmetrical response was obtained again, and the theoretical ultimate strength of the unit was exceeded in all subsequent cycles. At the maximum displacement applied in the final cycle to displacement ductility factor of eight, the ideal ultimate loads were exceeded by up to 24%, the overstrength being caused by strain-hardening and strain-aging of the beam flexural reinforcement.

The effectiveness of the load-displacement loops in terms of energy dissipation ability was rather less than in the first part of the test, with some pinching resulting from the stiffness degradation described above. However in view of the total number of severe inelastic cycles applied, stiffness degradation at this stage of response could nonetheless be considered quite acceptable.

The column shear versus storey sway relationship for test B13B is presented in Fig. 5.11. The P-delta effect was smaller with the reduced column load, but nonetheless the net column shear available in the final cycle was 4% less than the maximum, which was observed at maximum displacement in load run 25. In the load cycles to displacement ductility factors of four, six, and eight, the average reductions in column shear due to the P-delta effect were 18%, 22% and 27% respectively. Without the additional strengthening provided by strain-aging of the beam flexural reinforcement, not available under actual earthquake loading, the reduction in net strength of the assembly would have been even more severe. Although these reductions were apparently of more than secondary importance, it should be pointed out that, as noted in the previous section, the average axial load to be carried by all columns of a bent is unlikely to be as high

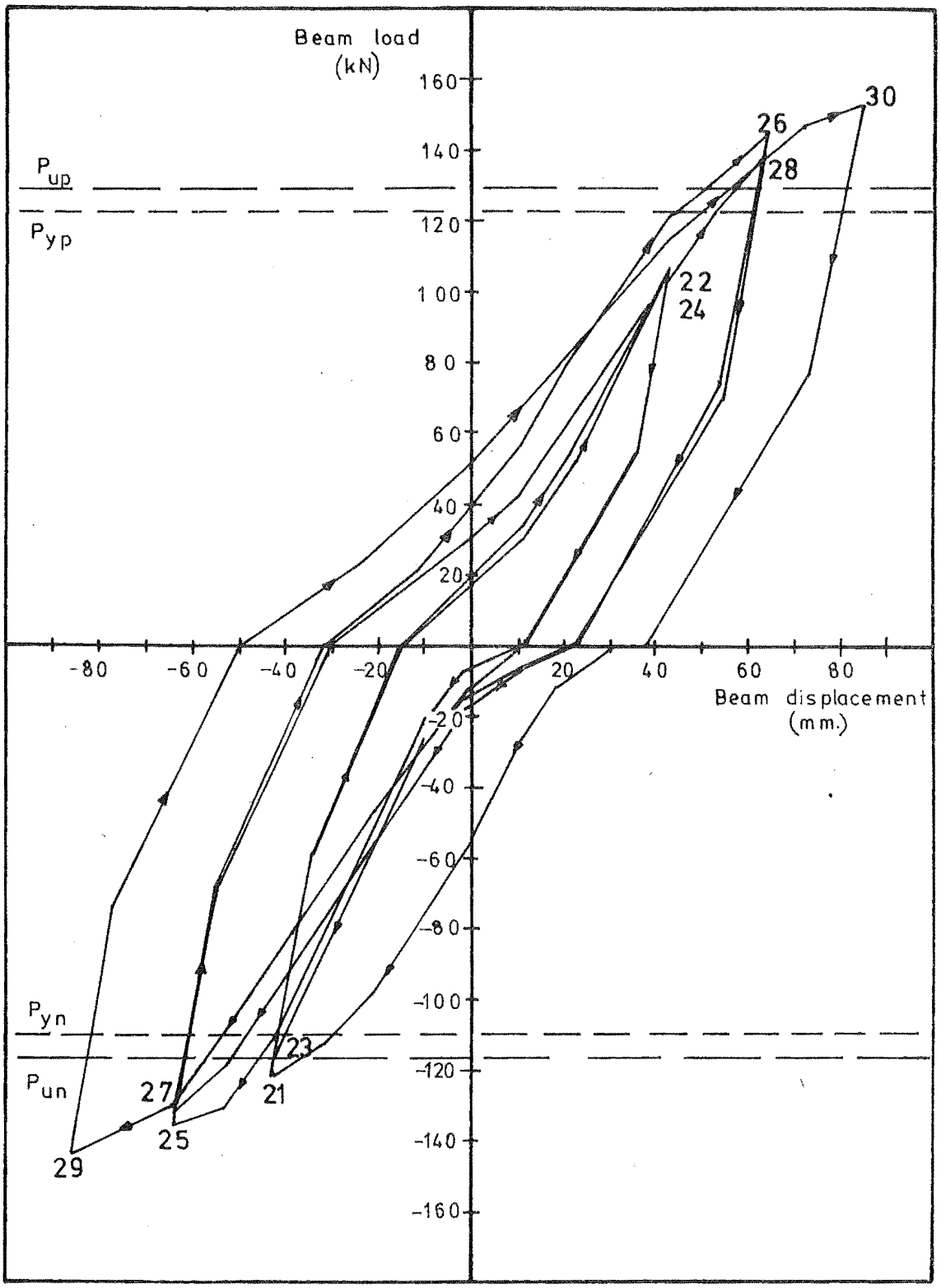

FIG.5.9 :BEAM LOAD-DISPLACEMENT RESPONSE - WESTERN BEAM TEST B13B

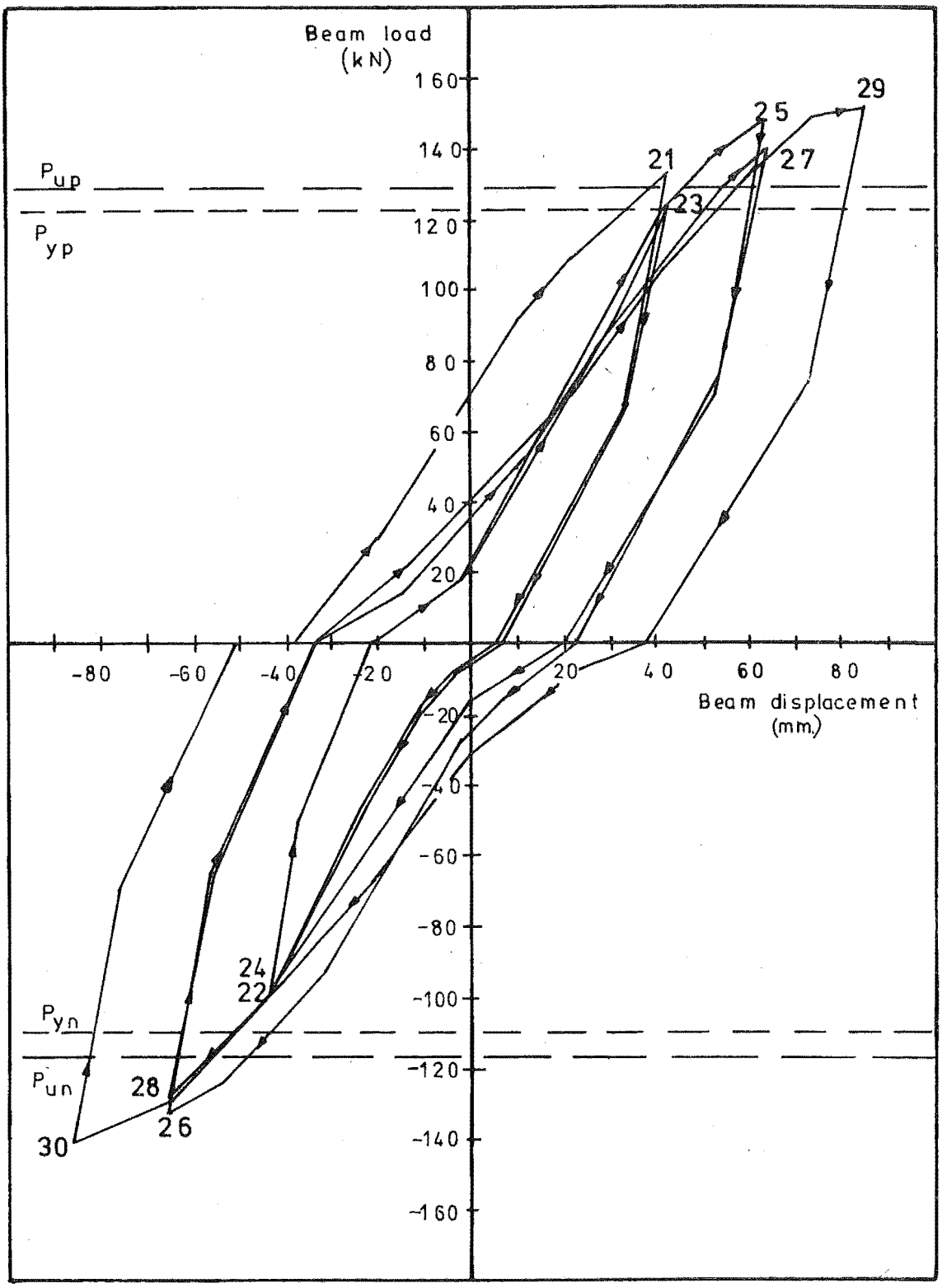

FIG.5.10 :BEAM LOAD-DISPLACEMENT RESPONSE - EASTERN BEAM TEST B 13 B

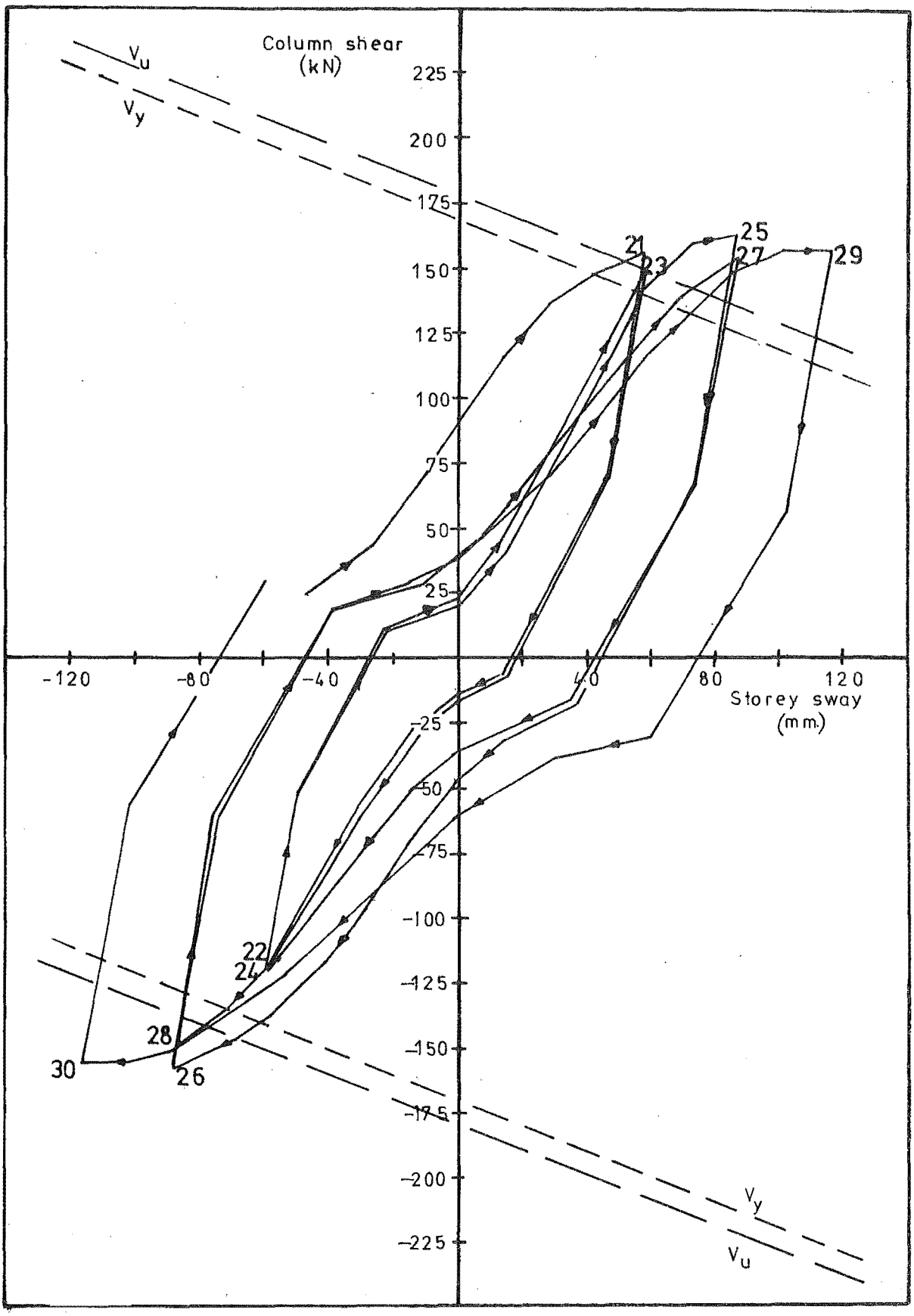

FIG.5.11 :COLUMN SHEAR-STOREY SWAY RESPONSE TEST B13B

as was imposed on the test unit column, even in this second part of the test. Hence the net effect is much less serious for the whole structure than for the test unit.

5.3 Beam Behaviour

5.3.1 Components of Beam End Displacement

The major components of beam end displacement throughout the test are shown in Figs. 5.12 for the Western beam of the test unit. A corresponding record obtained of the components of displacement for the Eastern beam was very similar to that shown for the Western beam. During test Bl3A, where the column axial load was heavy, the component of beam end displacement caused by shear deformation of the joint panel was relatively small, being in the range of 8 to 12% of the total displacement at maximum, up to load run 20. The joint shear deformation was small due to the limited extent of joint cracking and the absence of yielding in the joint reinforcement in this test. When the column load was reduced for test Bl3B the deformation of the joint increased in consequence of the more extensive joint cracking and a limited amount of yielding of joint reinforcing. The resulting component of beam end displacement ranged between 20 and 25% of the total at maximum displacement during this part of the test.

As noted in the previous tests the major component of beam end displacement was that caused by rotation measured over a gauge length of half the effective beam depth from the column face. These rotations caused proportions of the total beam end displacements varying between 30 and 65%. As noted in the previous chapters the means of obtaining this measurement meant that rotation due to yield penetration and slip through the joint was included. An estimate of the proportion of the measured rotations caused by yield penetration and slip was obtained by subtracting the sum of the curvatures derived from beam steel strain measurements over the 280 mm length from the column face. These calculations showed that during the major cycles of test Bl3A yield penetration and slip caused between 30 and 40% of the total measured rotations, while in test Bl3B the corresponding proportion was between 60 and 70%, due to the less favourable bond conditions for the beam bars under the reduced column load, with slip failure occurring in the final cycle.

Rotation was also measured over a second d/2 gauge length of the beam, and the corresponding component of beam end displacement became

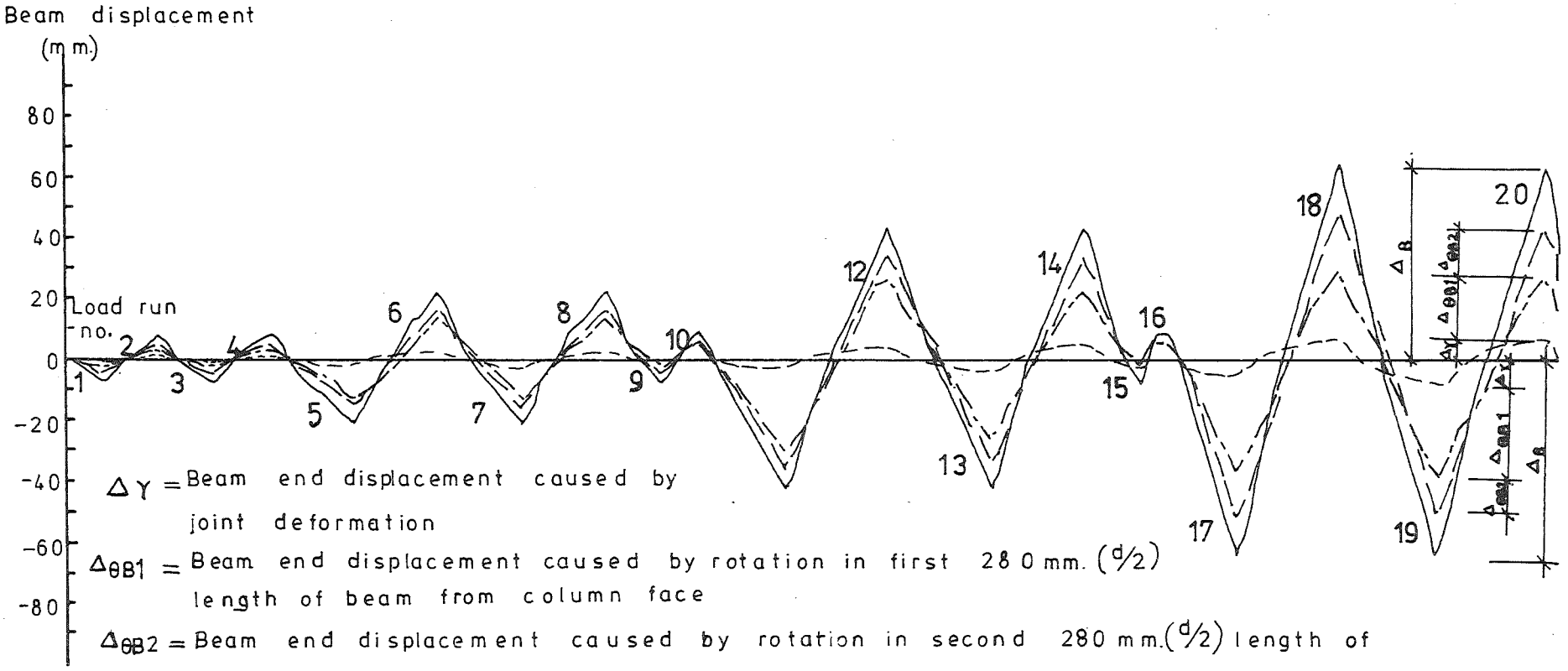

FIG. 5.12: COMPONENTS OF BEAM END DISPLACEMENT FOR WESTERN BEAM

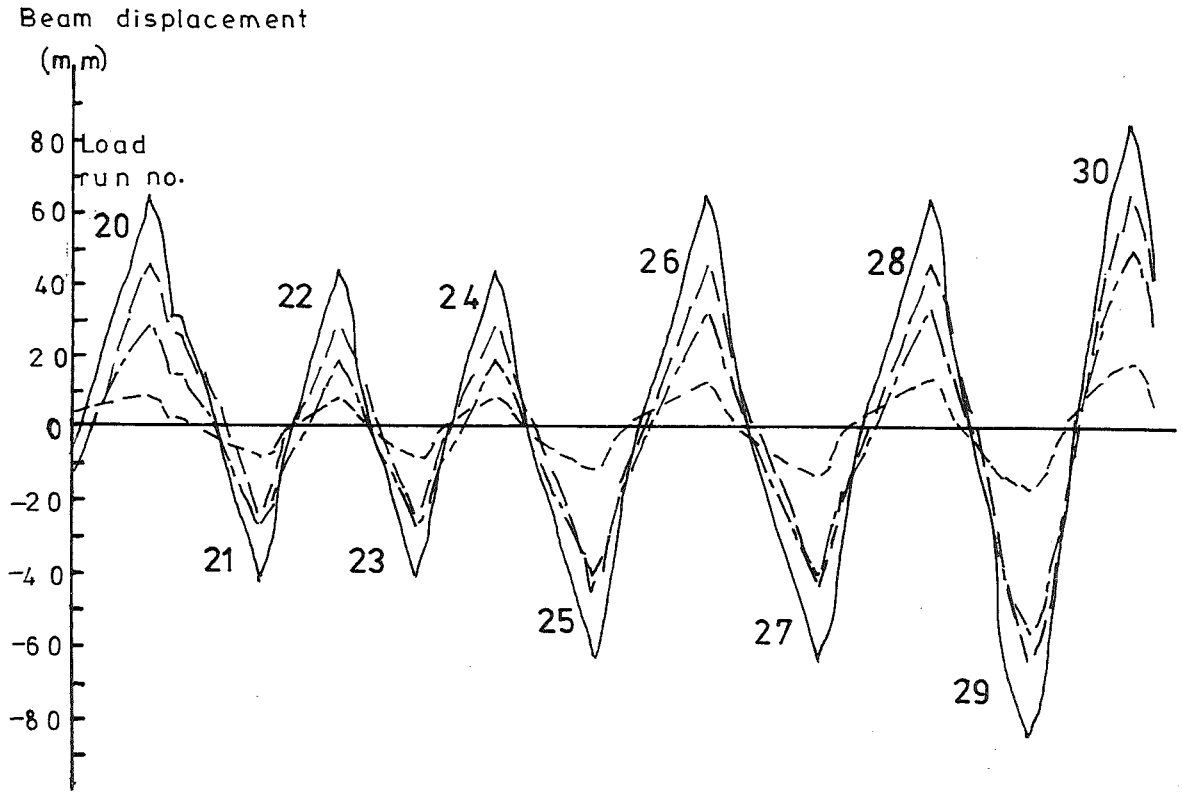

FIG.5.12 :(CONTD.) COMPONENTS OF BEAM END DISPLACEMENT FOR WESTERN BEAM

significant as yielding spread along the beam steel away from the column face. As a proportion of the total this component was a maximum in load run 17 when it comprised 25% of the total. During test Bl3B the contribution of rotation in second gauge length to the total displacement diminished due to the greater contribution at this stage of joint shear deformation and slip.

As noted with respect to the previous tests, the displacements due to rotation within the beam lagged behind the displacement due to joint deformation because of the more elastic nature of the latter component, i.e. the residual joint deformation was much smaller than the residual beam rotation at zero load at the end of a load run. The joint deformation conformed to the sense of the loading much earlier in a load run than did the beam rotation. This behaviour is emphasized by the negative component of displacement due to beam rotation observed in load run 15. The tendency of the beam rotation to lag behind the joint deformation was not so marked in test Bl3B where the joint behaviour was less elastic, with more extensive cracking and some yielding.

Measurements were also taken in this test of shear deformations in the beam hinges, utilizing the specially lengthened Demec gauge used to measure joint shear deformation (see Section 2.6). Since interference with the beam rotation yokes made the use of this instrument awkward and time consuming, a continuous record of these displacements was not made, with most measurements being taken at maximum displacement only. For this reason they are not included in Fig. 5.12 but the results taken at maximum displacement are listed in Table 5.2. The lengths of beam over which these measurements were taken correspond approximately to the rotation gauge lengths shown in Fig. 2.13, but the inner shear gauge length extended 30 mm inside the column face in order to include the shear displacements along the face crack, while the outer shear gauge length was correspondingly larger than the outer rotation gauge length to allow the same instrument to be used for all of the measurements.

The results show that from comprising about 1% of the total beam end displacements in the initial elastic cycles, the contribution of beam shear displacement rapidly increased when yielding of the beam flexural reinforcement occurred, causing wide flexural cracks to open. During test Bl3A the proportion of total beam displacement due to the measured shear displacement reached a maximum for a major cycle in load run 20, when 11.8% of the total was attained. However, in load run 15, where less than the previous maximum displacement was applied, the contribution of beam shear

TABLE 5.2 : BEAM SHEAR DISPLACEMENTS

Load Run No.	Western Beam				Eastern Beam			
	$\Delta_{\gamma b1}$ (i) (mm)	$\Delta_{\gamma b2}$ (ii) (mm)	$\frac{\Delta_{\gamma b1}}{\Delta_B}$ (iii)	$\frac{\Delta_{\gamma b2}}{\Delta_B}$	$\Delta_{\gamma b1}$ (mm)	$\Delta_{\gamma b2}$ (mm)	$\frac{\Delta_{\gamma b1}}{\Delta_B}$	$\frac{\Delta_{\gamma b2}}{\Delta_B}$
1	-0.05	-0.09	0.007	0.012	0.07	0.11	0.008	0.013
2	0.02	0.07	0.003	0.009	-0.05	-0.08	0.006	0.009
3	-0.05	-0.09	0.006	0.011	0.07	0.12	0.008	0.013
4	0.02	0.08	0.003	0.010	-0.06	-0.07	0.006	0.007
5	-0.49	-0.16	0.023	0.008	0.46	0.17	0.021	0.008
6	0.65	0.15	0.030	0.007	-0.64	-0.12	0.029	0.005
7	-0.92	-0.17	0.043	0.008	0.84	0.18	0.039	0.008
8	0.69	0.11	0.032	0.005	-0.71	-0.13	0.033	0.006
9	-0.48	-0.11	0.061	0.014	0.47	0.12	0.060	0.015
10	0.26	0.04	0.031	0.005	-0.30	-0.03	0.036	0.004
11	-1.96	-0.39	0.046	0.009	1.77	0.75	0.042	0.018
12	1.86	0.80	0.044	0.019	-1.86	-0.62	0.043	0.014
13	-2.52	-1.01	0.059	0.024	2.47	1.05	0.059	0.025
14	2.40	1.19	0.056	0.028	-2.35	-1.18	0.054	0.027
15	-2.21	-0.27	0.275	0.034	2.18	0.17	0.277	0.022
16	-1.11	0.14	-0.101	0.013	-0.43	-0.40	0.041	0.038
17	-3.59	-1.93	0.056	0.030	3.43	2.14	0.055	0.034
18	3.68	2.76	0.058	0.044	-3.68	-2.23	0.057	0.034
19	-4.35	-2.75	0.068	0.043	4.12	2.65	0.066	0.042
20	4.20	3.64	0.066	0.057	-4.09	-3.25	0.063	0.050
21	-4.64	-2.85	0.108	0.066	4.30	2.83	0.102	0.067
22	3.87	3.07	0.091	0.072	-3.90	-2.69	0.089	0.062
23	-4.63	-2.86	0.108	0.067	4.25	2.90	0.101	0.069
24	3.87	3.09	0.091	0.073	-3.94	-2.70	0.090	0.062
25	-5.08	-3.42	0.080	0.054	4.62	3.54	0.073	0.056
26	4.46	3.75	0.070	0.059	-4.65	-3.41	0.072	0.053
27	-5.19	-3.45	0.081	0.054	4.70	3.60	0.075	0.057
28	4.49	3.75	0.071	0.060	-4.74	-3.39	0.073	0.052
29	-5.63	-3.88	0.066	0.046	5.15	4.07	0.061	0.048
30	5.30	4.35	0.063	0.052	-5.50	-4.01	0.064	0.047

(i) $\Delta_{\gamma b1}$ = shear displacement of beam from 27 mm inside column to 280 mm along beam from column face

(ii) $\Delta_{\gamma b2}$ = shear displacement of beam between 280 mm and 580 mm along beam from column face

(iii) Δ_B = total beam end displacement

displacement was much greater. This occurred because flexural cracks were still open, and the shear stiffness of the beams was consequently less. This observation was confirmed by other readings taken at small total displacements which showed that beam shear displacement was the major component at the beginning of each load run. In the reversed load run 16 the residual beam rotation caused the major component of beam end displacement as noted above, and the contribution of beam shear displacement was consequently less.

In the first two cycles of test Bl3B the total displacement was again less than the previous maximum, and the shear displacement was proportionately large at 15 to 17% of the total. In subsequent cycles with greater total displacements, the shear displacement again increased due to further degradation of the sliding shear mechanism, but it was somewhat less as a proportion of the total beam displacement at maximum displacements due to the closing of flexural cracks at full load.

5.3.2 Rotational and Curvature Ductility Factors

Tables 5.3a and 5.3b list the rotations, ϕ_{bl}, measured in the d/2 gauge length adjacent to the column face for the Western and Eastern beams respectively, along with the curvatures derived from strain readings from the outer beam bars. The rotations given include the effects of yield penetration into the joint, and of bar slip where it occurred, but the effect of joint shear rotation has been subtracted. The curvatures listed as ϕ_1 are those measured at 76 mm from the column face, which was the closest available position to the face, while the curvatures ϕ_{max} are the maximum values of curvatures measured at intervals of 102 mm for 686 mm along the beam from the face. The length $l_{\phi max}$ was the distance from the column face at which maximum curvature was observed. The values given may be compared to the effective depth of the beam, $d = 560$ mm. All curvatures are average values measured over a 102 mm gauge length. For both rotation and curvature, ductility factors were calculated with respect to experimental yield values extrapolated from the appropriate observations in load run 1 as described in Section 2.7.

Measured rotation values increased throughout the test, largely due to the increasing influence of yield penetration and slip. The maximum rotational ductility factors were observed in load runs 29 and 30, whereas the curvature ductility factor, which was not affected by slip, reached a maximum value in load run 11. The net difference between strains in the top and bottom bars was greatest at this stage because closing of cracks under compression was maximum due to limited sliding shear

TABLE 5.3a : BEAM ROTATIONAL AND CURVATURE DUCTILITIES - BEAM WEST

Load Run No.	μ	θ_{bl} rad.x10^{4}	$\frac{\theta_{bl}}{\theta_{by}}$	ϕ_l rad/mm x10^{6}	ϕ_{max} rad/mm x10^{6}	$^{1}\phi_{max}$ mm	$\frac{\phi_l}{\phi_y}$	$\frac{\phi_{max}}{\phi_y}$
5	2.0	-51.7]	3.50	-17.07	-17.07	76	4.08	4.08
6		53.07	3.59	20.06	20.06	76	4.80	4.80
7		-49.34	3.34	-21.92	-21.92	76	5.24	5.24
8		49.79	3.37	15.63	15.63	76	3.74	3.74
9	0.75	-5.60	0.38	1.264	-3.209	279	-0.30	0.77
10		23.17	1.57	6.801	6.801	76	1.63	1.63
11	4.0	-129.50	8.77	-31.56	-47.33	178	7.55	11.32
12		104.90	7.10	27.55	31.33	178	6.59	7.50
13		-101.07	6.84	-26.70	-27.37	279	6.39	6.55
14		85.61	5.80	23.71	23.71	76	5.67	5.67
15	0.75	3.21	-0.22	5.60	- 2.67	483	-1.34	0.64
16		26.23	1.78	10.34	10.34	76	2.47	2.47
17	6.0	-149.94	10.15	-39.96	-39.96	76	9.56	9.56
18		107.54	7.28	30.66	34.90	483	7.34	8.35
19		-143.37	9.71	-33.70	-33.70	76	8.06	8.06
20		97.08	6.57	24.55	28.19	584	5.87	6.74
21	4.0	-88.95	6.02	-10.61	-11.09	178	2.54	2.65
22		48.14	3.26	7.02	18.47	584	1.68	4.42
23		-89.87	6.09	-9.55	-10.12	178	2.28	2.42
24		48.48	3.28	6.12	18.12	584	1.47	4.34
25	6.0	-138.38	9.37	-20.70	-22.30	178	4.95	5.34
26		96.60	6.54	14.34	16.50	584	3.34	3.95
27		-140.06	9.48	-16.54	-19.40	178	3.96	4.64
28		96.51	6.53	10.56	14.31	584	2.53	3.42
29	8.0	-190.61	12.91	-21.13	-29.25	178	5.06	7.00
30		151.36	10.25	10.04	17.37	178	2.40	4.16

TABLE 5.3b : BEAM ROTATIONAL AND CURVATURE DUCTILITIES - BEAM EAST

Load Run No.	μ	θ_{bl} rad. x 10^4	$\frac{\theta_{bl}}{\theta_y}$	ϕ_l rad./mm x 10^6	ϕ_{max} rad./mm x 10^6	$l_{\phi max}$ mm	$\frac{\phi_l}{\phi_y}$	$\frac{\phi_{max}}{\phi_y}$
5	2.0	59.96	3.86	16.79	16.79	76	4.02	4.02
6		-56.62	3.83	-21.19	-21.19	76	5.07	5.07
7		52.50	3.55	20.31	20.31	76	4.86	4.86
8		-53.46	3.62	-19.99	-19.99	76	4.78	4.78
9	0.75	9.67	0.66	-3.22	3.49	279	-0.77	0.84
10		-22.25	1.51	-9.05	-9.05	76	2.17	2.17
11	4.0	123.86	8.39	29.72	43.05	178	7.11	10.30
12		-146.64	9.93	-26.07	-35.01	178	6.24	8.38
13		94.38	6.39	27.63	27.63	76	6.61	6.61
14		-127.60	8.64	-24.90	-24.90	76	5.96	5.96
15	0.75	-20.14	-1.36	-3.84	3.19	483	-0.92	0.76
16		-45.65	3.09	-9.01	-12.55	279	2.15	3.00
17	6.0	133.53	9.04	36.56	38.06	381	8.75	9.11
18		-172.11	11.66	-39.66	-39.66	76	9.49	9.49
19		110.30	7.47	26.88	30.06	178	6.43	7.19
20		-146.56	9.92	-32.92	-32.92	76	7.88	7.88
21	4.0	65.72	4.45	4.22	8.25	483	1.01	1.97
22		-89.22	6.04	-16.42	-16.68	279	3.93	3.99
23		71.89	4.87	3.10	7.56	483	0.74	1.81
24		-88.77	6.01	-15.32	-16.11	279	3.67	3.85
25	6.0	119.75	8.11	13.89	19.21	178	3.32	4.60
26		-134.01	9.08	-24.45	-24.45	76	5.85	5.85
27		121.56	8.23	9.94	16.57	178	2.38	3.96
28		-134.70	9.12	-20.71	-21.69	279	4.96	5.19
29	8.0	171.84	11.64	15.54	26.47	178	3.72	6.33
30		-184.30	12.48	-20.63	-26.84	279	4.94	6.42

displacements along the cracks, while tensile strains were limited by entry into the strain hardening range.

In the early stages of the test the rotational ductility factor was less than the curvature ductility factor due to the integral nature of the rotation measurement, and the non-uniform curvature distribution along the beams. Curvature measured at a particular section was likely to be greater than the average value given by the rotation measurement. However in later cycles, and especially during test B13B the influence of yield penetration and slip on the rotation readings resulted in the apparent rotational ductility factor exceeding the curvature ductility factor.

The position of maximum beam curvature, which was initially observed to be at the strain reading closest to the column face, varied considerably along the length of the beam during the larger inelastic cycles (that is for displacement ductility factors larger than 4). This variation occurred because of the varying influences of diagonal beam cracking, strain history of the beam flexural reinforcing at various locations, and slip of the beam bars in the plastic hinge region.

In load run 9 the rotational ductility factor was relatively small, while in load run 15 the value was negative. The same behaviour was noted with respect to the curvature, ϕ_1 , at 76 mm from the column face. As explained in Section 5.3.1 this occurred because of the lag of beam rotations behind the applied loads and the total beam end displacements.

5.3.3 Beam Reinforcement Strain Profiles

Strain profiles measured from the outer bars in each layer of beam reinforcement are shown for selected load runs in Figs. 5.13 to 5.17. The strains were measured over gauge lengths of 102 mm, and the values plotted are the mean of those recorded on the two faces of the beam. Strains in the outer layers of bars were recorded at each increment of loading, while those in the inner layers were measured at more widely spaced increments only.

Fig. 5.13 shows that after yield strain was first exceeded in the vicinity of the column face, cycling to displacement ductility factor of two caused yield strain to extend for about 150 mm along each beam and to penetrate into the joint to within perhaps 150 mm from the column centre-line. When displacements were applied to displacement ductility factor of four (Fig. 5.14), yielding spread for over 400 mm along the beams away from the column face, while yield strain penetrated into the joint to within less than 100 mm from the column centreline. When a displacement

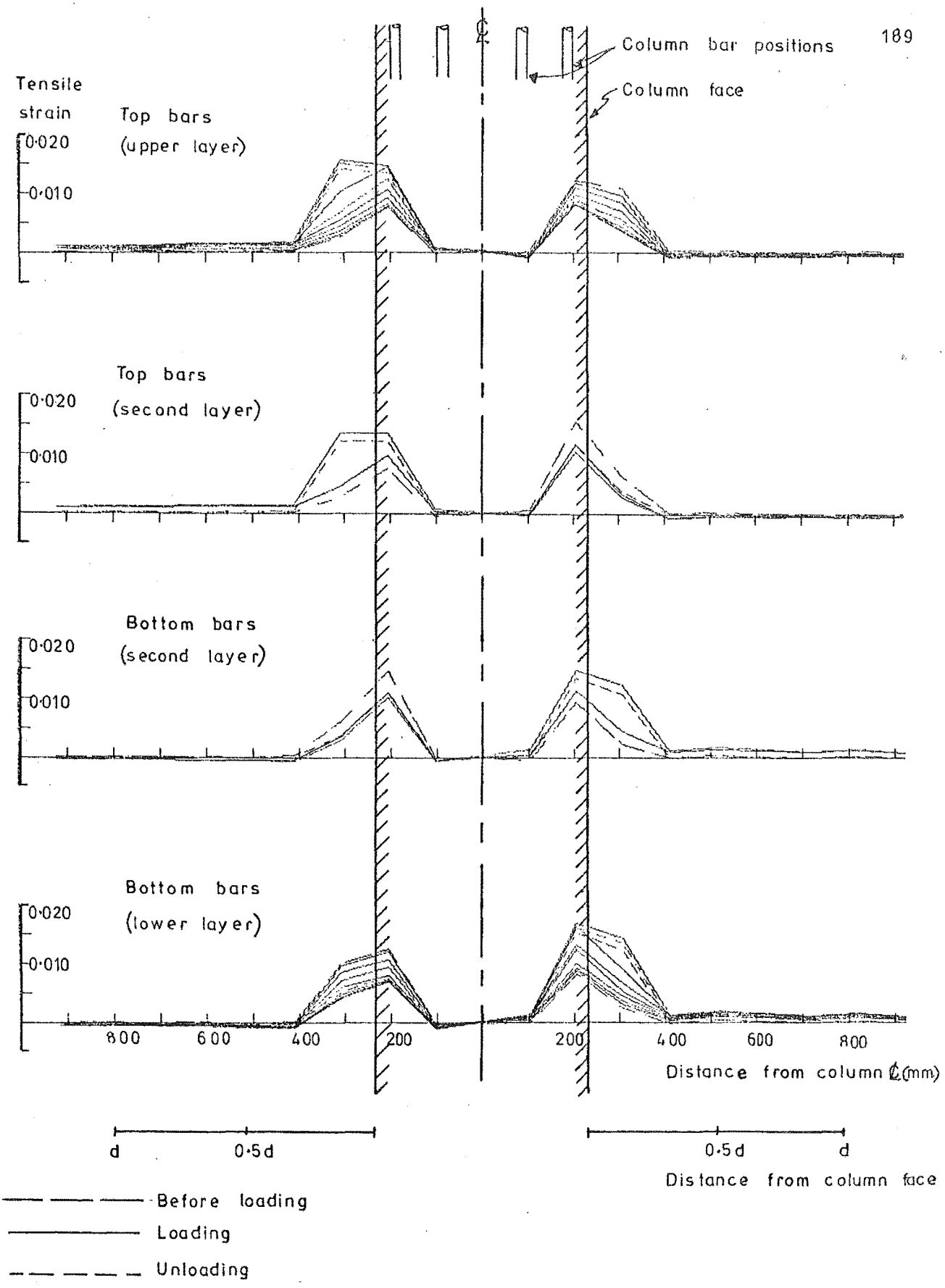

FIG.5. 13 :BEAM BAR STRAINS, LOAD RUN 7

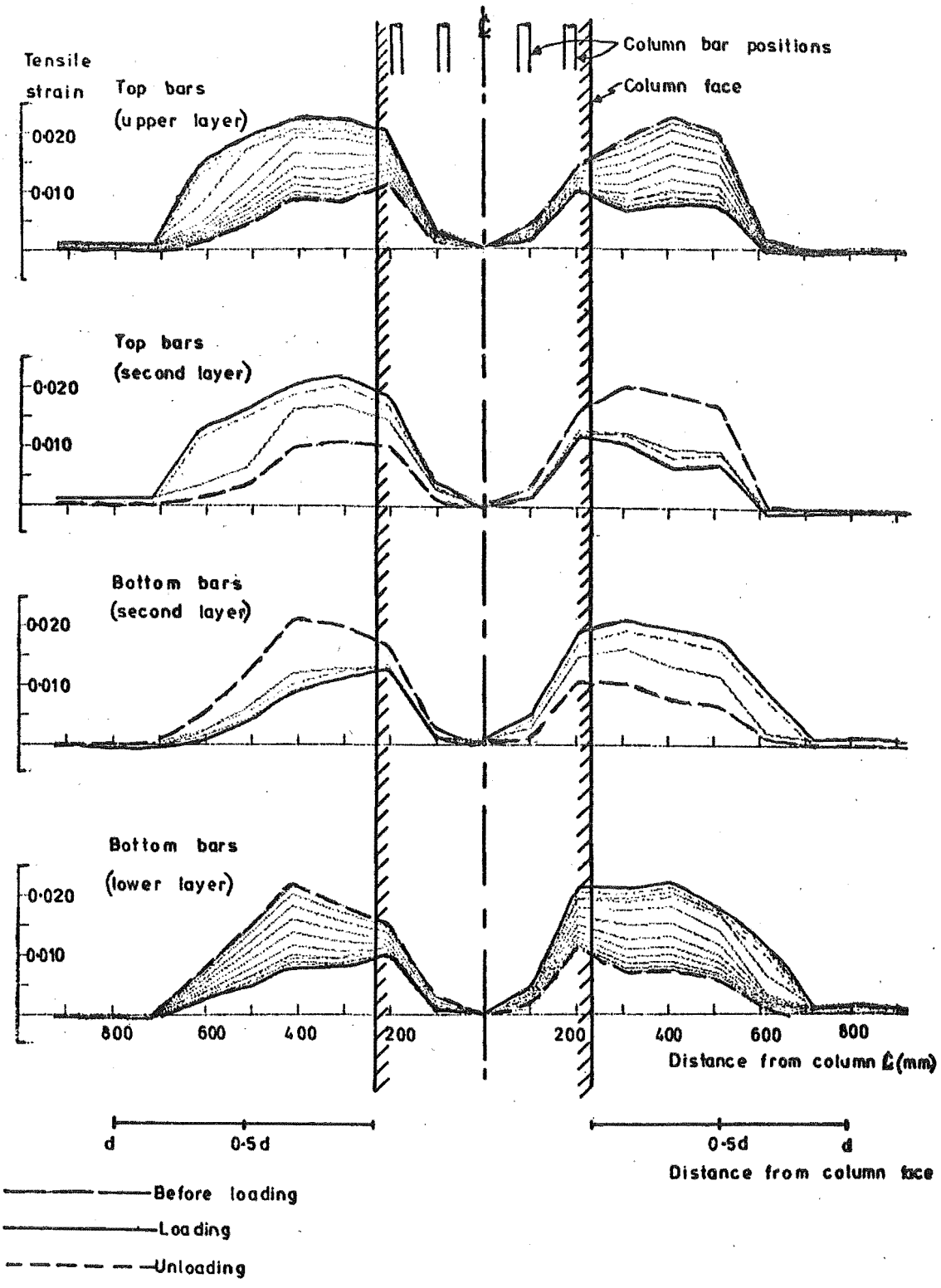

FIG.5.14 :BEAM BAR STRAINS, LOAD RUN 13

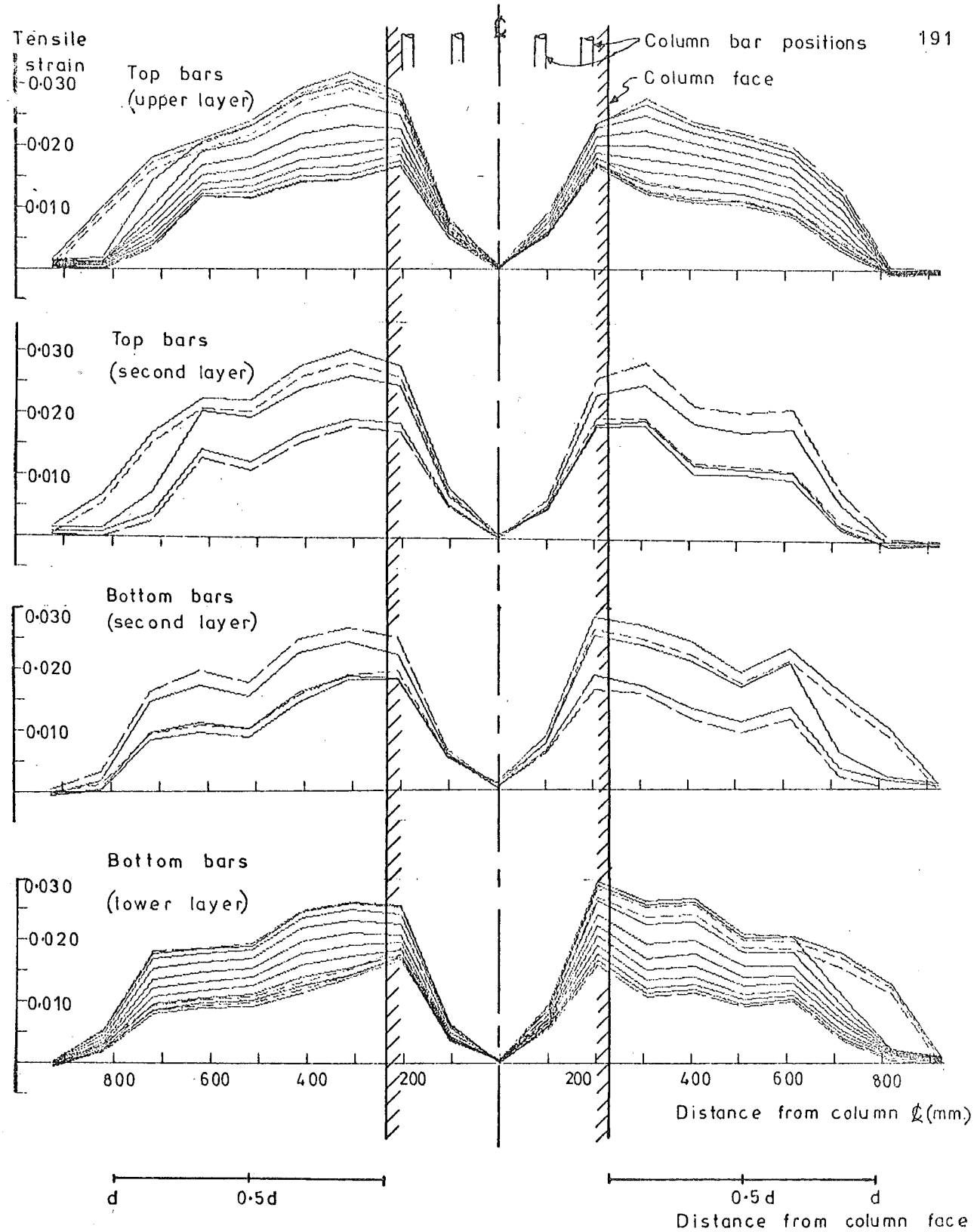

FIG.5.15 :BEAM BAR STRAINS, LOAD RUN 19

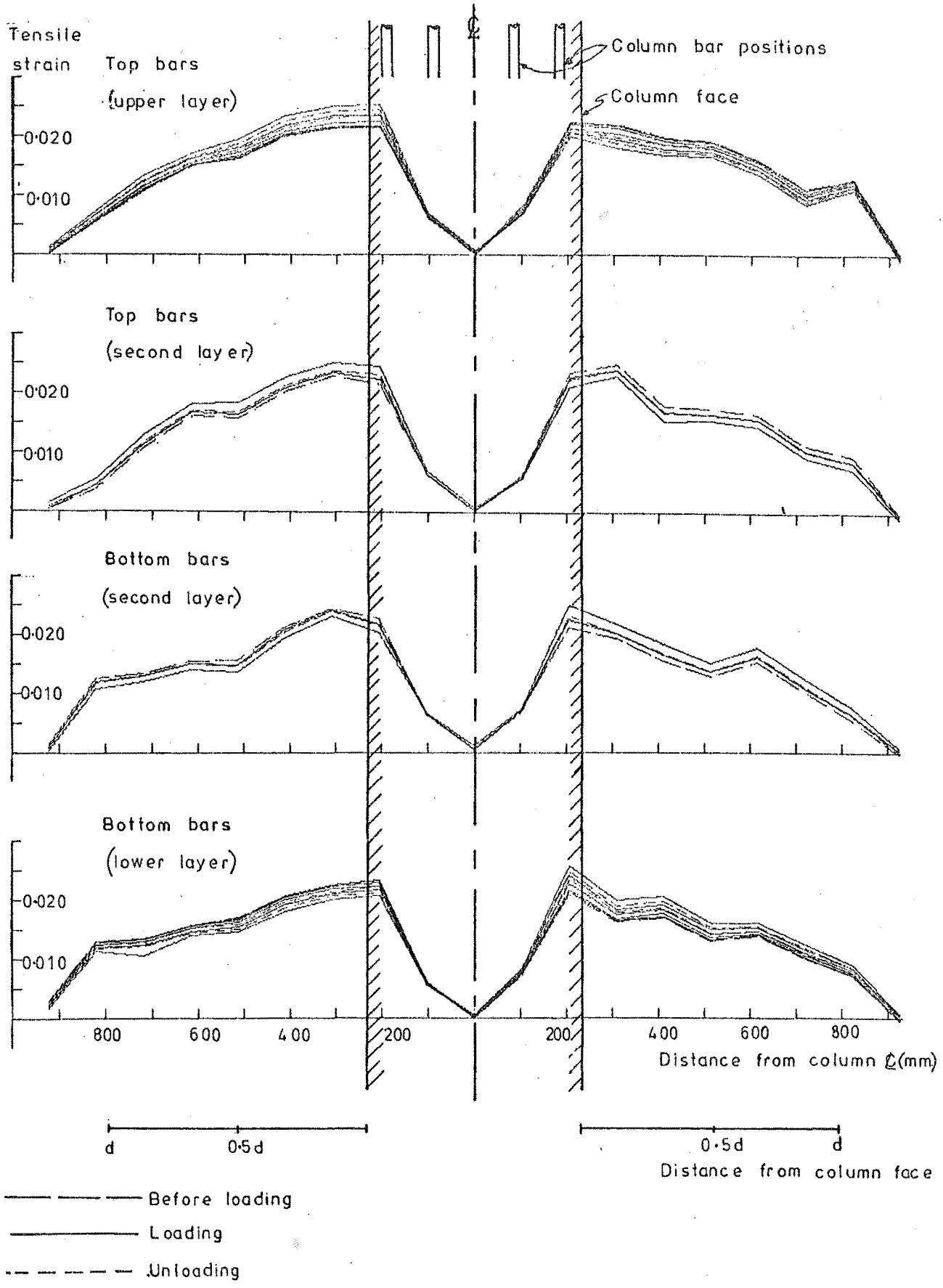

FIG.5.16 :BEAM BAR STRAINS, LOAD RUN 23

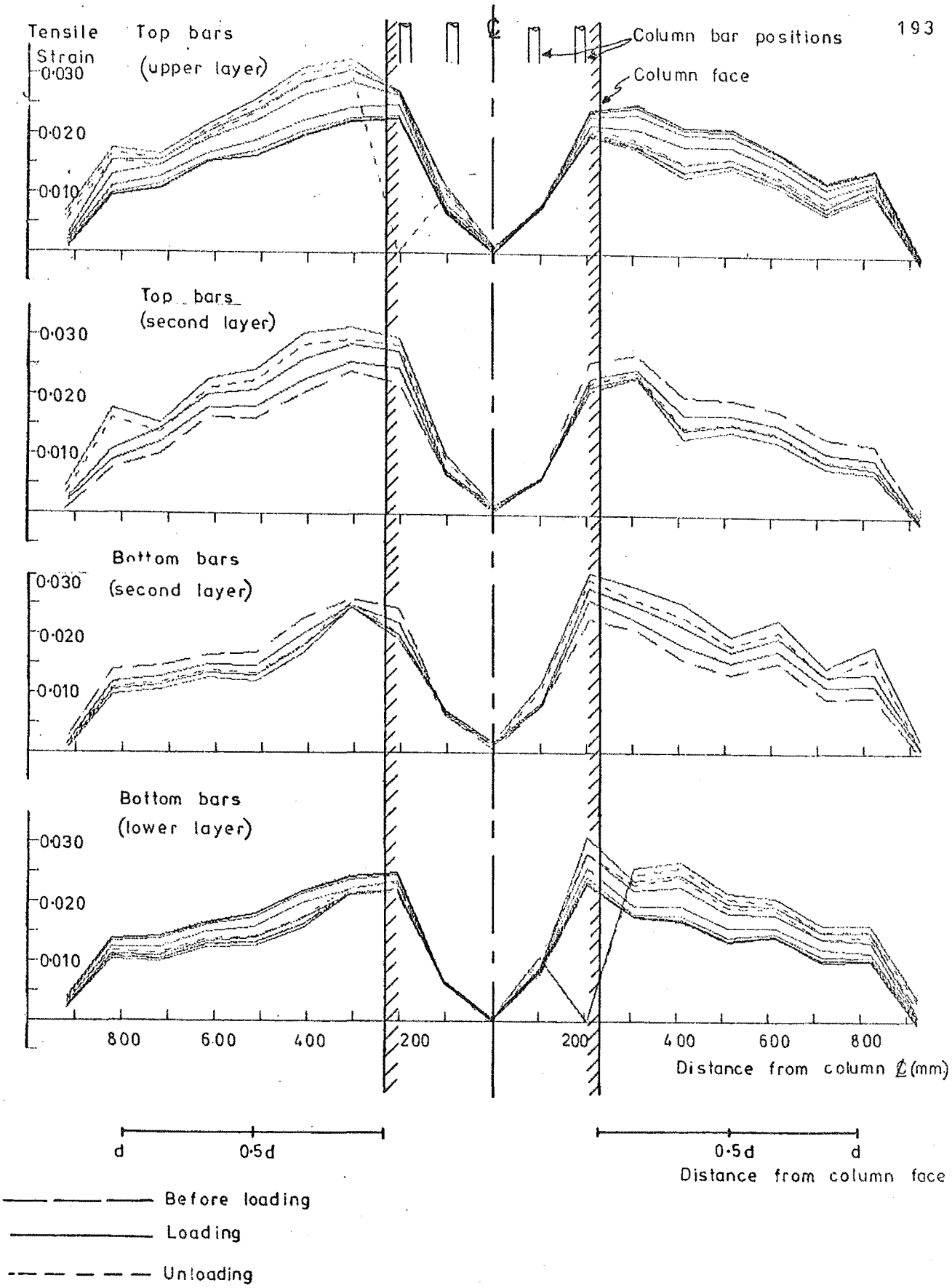

FIG. 5.17 : BEAM BAR STRAINS, LOAD RUN 29

ductility factor of six was imposed (Fig. 5.15) yield strain was exceeded for over 600 mm along the beams away from the column face, while yield penetration into the joint again increased slightly, possibly to within 50 mm of the column centreline. Because the Demec strain gauges used to obtain the strain readings had a gauge length of 102 mm, which is a relatively large proportion of the total column breadth of 457 mm, it is impossible to determine more exactly the extent of yield penetration at any stage.

When the column axial load was reduced for test B13B the pattern of strain distribution did not change immediately because the applied displacements and loads were smaller in the initial cycles. Comparison of Fig. 5.16 with Fig. 5.14 shows that the differences between the strains measured at zero load and at maximum displacement in load runs to the same ductility factor were much less in test B13B,where other sources of beam end displacement were more significant than plastic beam rotation, as explained in Section 5.3.1. When a displacement ductility factor of six was again applied, yield strain spread further along the beams to about 700 mm away from the column face, due probably to the strengthening of the beams closer to the column caused by strain-aging. In the final cycle to displacement ductility factor of eight (Fig. 5.17) the extent of yield strain in the beams again increased, while the bars commenced to slip through the joint as yield penetration occurred throughout the available anchorage length. Since the slippage caused some Demec studs to come into bearing against the sides of their holes in the cover concrete, some readings were invalidated at this stage, and the plot is therefore incomplete.

From load run 11 onwards, strains were observed in excess of the strain-hardening strain of 0.020. This was reflected in the loads recorded at maximum displacements, which from this stage onwards were in excess of the theoretical ultimate loads based on steel stress not greater than the yield strength (see Table 5.1).

As noted with respect to the test of unit B12, all layers of beam reinforcing underwent similar changes in strain during any given load run, implying that the total steel content of the symmetrically reinforced beams was efficiently utilized for energy dissipation.

5.3.4 Beam Reinforcement Stresses

Stress-strain histories computed for the top two layers of beam reinforcing steel at a section 76 mm away from the column face in the Western beam are presented in Figs. 5.18 and 5.19. As in the other units

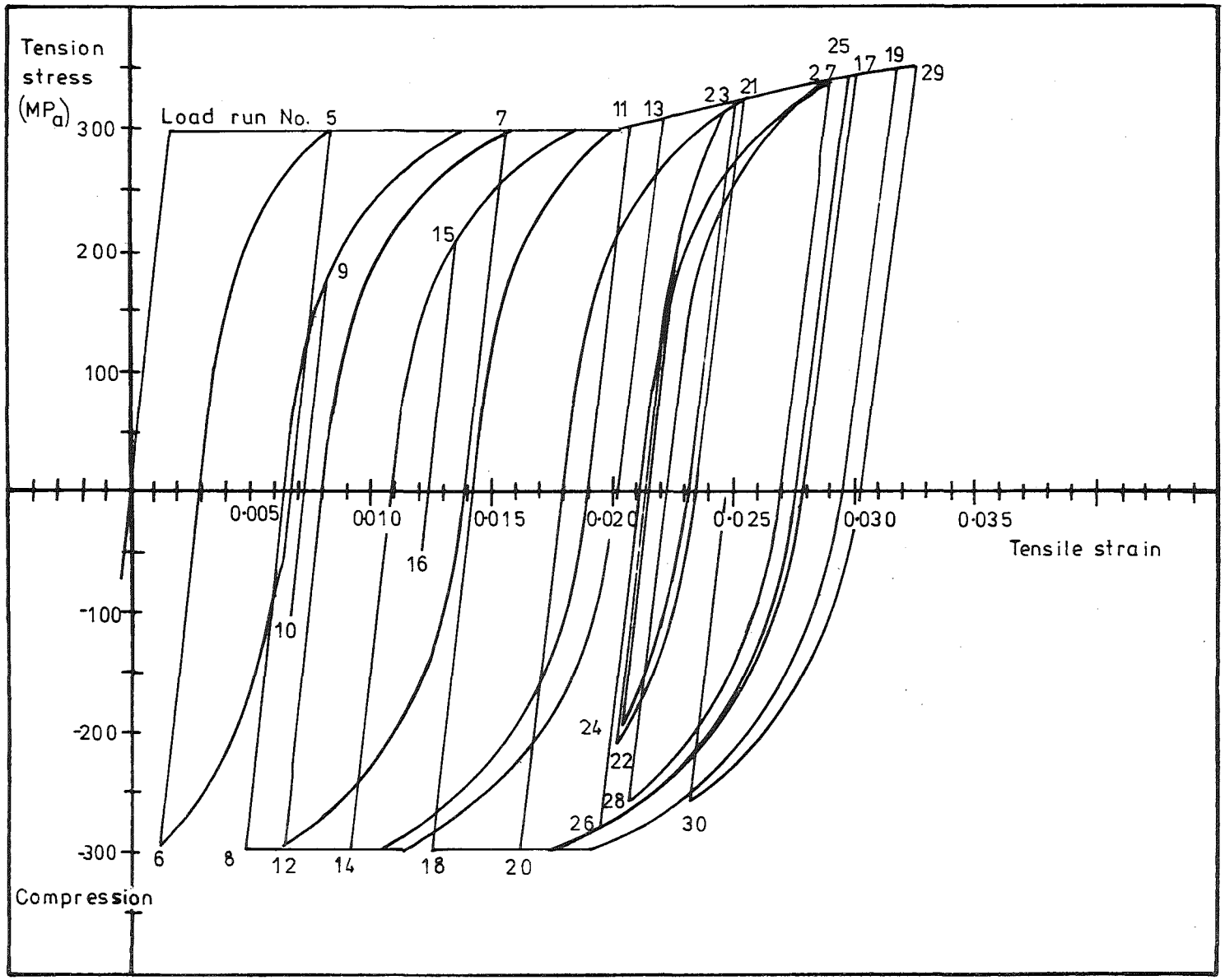

FIG.5.18 :STRESS-STRAIN HISTORY FOR UPPER LAYER OF BEAM TOP STEEL AT 76 MM. AWAY FROM COLUMN FACE IN WESTERN BEAM

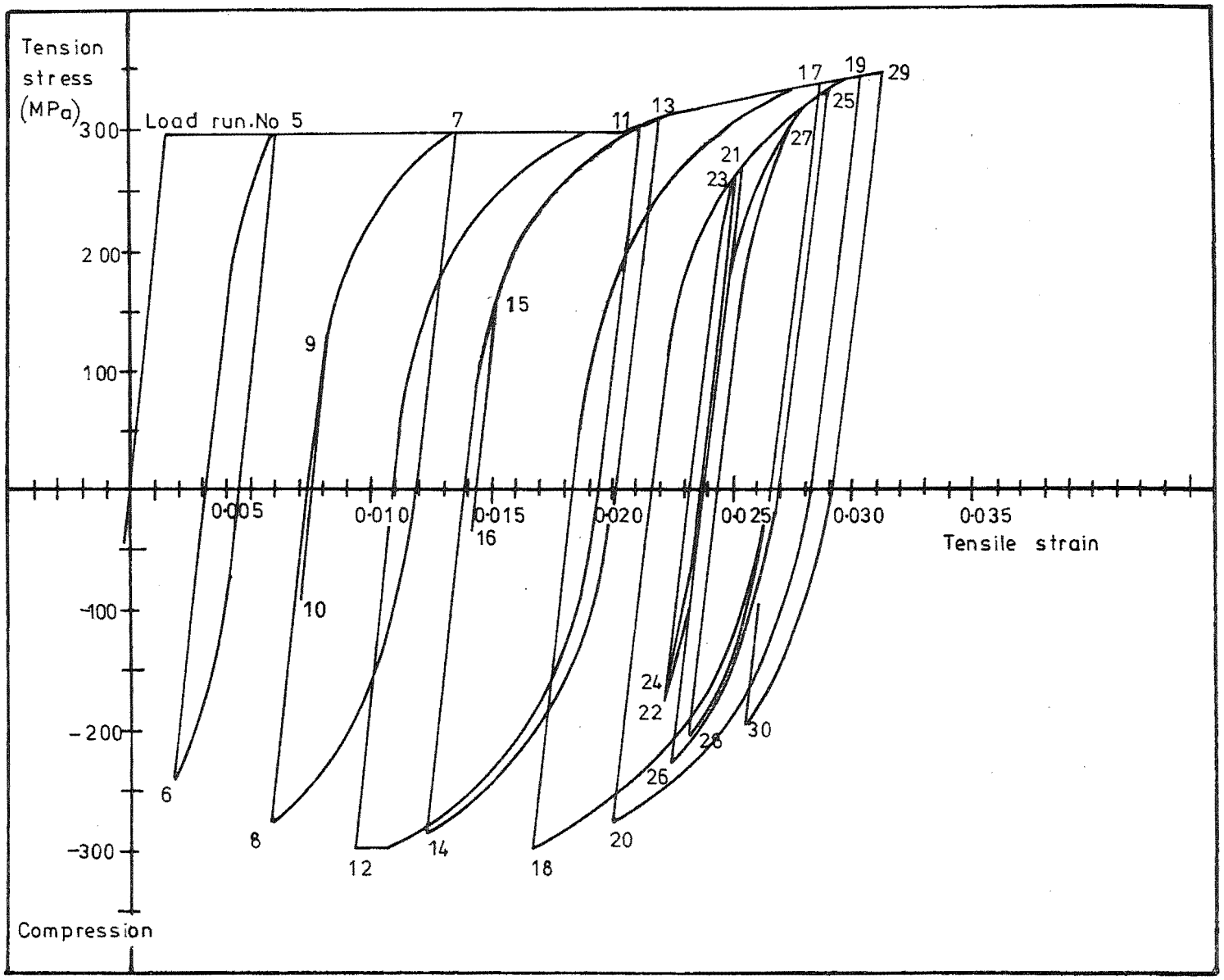

FIG.5.19:STRESS-STRAIN HISTORY FOR SECOND LAYER OF BEAM TOP STEEL AT 76 MM. AWAY FROM COLUMN FACE IN WESTERN BEAM

these results were derived using the experimentally obtained strain histories as input for a computer program for analysis of the reversed stress response of the steel, including the Bauschinger effect. The results computed for the bottom reinforcement were very similar to those presented for the top reinforcement.

Equilibrium checks were carried out using the computed stress results for both beams. Force balances between top and bottom reinforcement could not be obtained in the symmetrically reinforced section, since a small proportion of the necessary compression was resisted by the beam concrete in all cases. Checking the internal moment of resistance against the external moment applied by the beam end loads and the beam self weight indicated that stresses were underestimated once the strain-hardening range was entered. The concrete compression force was assumed to act at the level of the outer layer of compression reinforcement since, as explained in Section 3.3.4, it could not be located with any certainty. The average underestimate of the section moment during the major load runs of test B13A was 3%, while in test B13B the average discrepancy increased to 6%. The phenomenon of strain-aging was again thought to be responsible for the errors since the preliminary tests, described in Section 2.4.2, showed that the mild steel used in the units displayed strengthening due to strain-aging in the same range as the discrepancies noted above. However, in load runs 21 to 24, for which the calculations also showed a significant underestimate of section moment, the maximum stresses did not reach the stress envelope. In this case the strain-aging phenomenon could not account for the error. Since these results were obtained from the rising part of the curve, they are more sensitive to small errors in the experimental strain readings than those from cycles where the maximum stresses are on the envelope. This factor could explain the errors noted in these cycles.

Areas enclosed by the loops of the stress-strain curves represent the relative amounts of energy dissipated by the steel at the particular location during given cycles. Examination of the curves in Figs. 5.18 and 5.19 reveals that the second layer of bars dissipated slightly less energy than the top layer in most cycles. The energy dissipated by both layers of bars during test B13B was significantly less than that dissipated during the equivalent cycles of test B13A. This observation is reflected in the reduced area of the beam end load vs. displacement curves in test B13B due to the increased participation of low energy-dissipating modes of displacement, as discussed in Section 5.2. The longer plastic

hinge zone in test B13B may also have contributed to the reduced energy dissipation per unit length of bar apparent in the stress-strain histories.

Distributions of stress along beam bars in the joint area at the maximum displacement of major load runs are shown in Figs. 5.20 to 5.23. The stresses at each gauge point were computed from similar analyses to those shown in Figs. 5.18 and 5.19.

The difference between monotonic and cyclic loading conditions is clearly shown by the change in stress gradient across the joint between load run 5 and the subsequent load runs. The steeper stress gradient observed under cyclic loading implies a more severe bond requirement, which increased in severity as more cycles were applied with increasing ductility demand. The smaller loads applied in load runs 21 to 24 led to a smaller bond requirement over these cycles (Fig. 5.22) because the maximum stresses were lower, especially for the second layer of bars. In the remaining cycles of test B13B the increased yield penetration under the combination of reduced axial load and full beam end loads caused higher tensile stresses at the column centreline, and consequently increased bond requirement and eventual slip failure. An indication of the impending slip failure is given in Fig. 5.23 by the reduction of steel compression stresses in the beams at the column face as further load cycles are applied. This behaviour contrasts with the situation in Fig. 5.21, where with bond strength still maintained the reinforcement at the column face carried more compression during the repeated cycle than in the initial cycle.

The uniform bond stresses associated with the steepest stress gradients in Figs. 5.20 to 5.23 are shown for each layer of beam reinforcement in Fig. 5.24. The bond stresses were approximately equal for all bars until load run 25 when the situation of the bottom steel became more critical. The reason for this difference is not clear.

The level of bond stress sustained across the centre of the joint was significantly greater than the ultimate levels implied by the equations of ACI 318-77, Section 12.2, for development of bars in tension, but the high levels of stress could not be sustained indefinitely when the bond environment was changed by the reduction in axial load. The benefit of heavy axial load with respect to bond performance appeared to be in limiting the extent of yield penetration under cyclic loading, rather than in allowing a greater level of bond stress to be sustained.

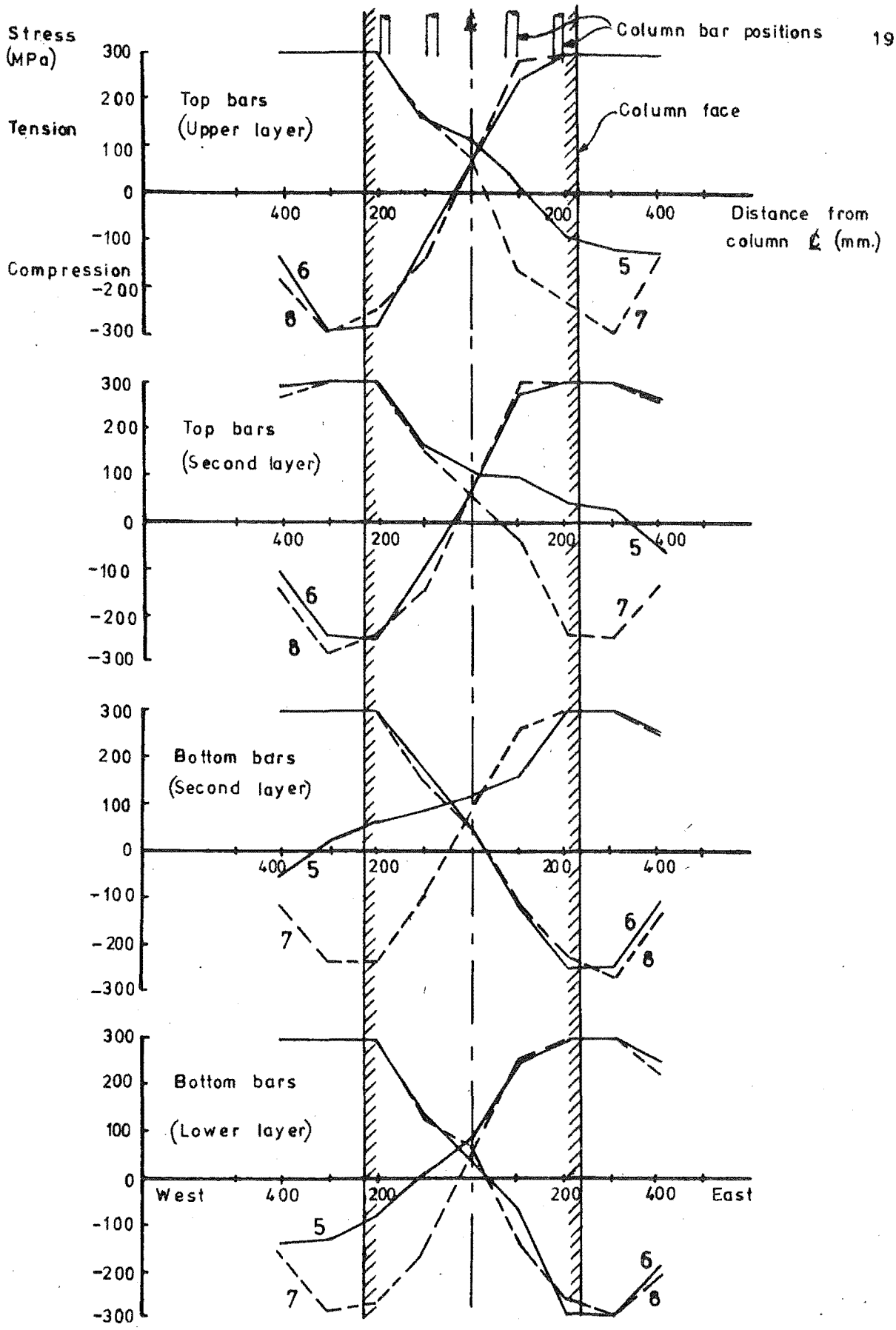

FIG·5.20 :BEAM STEEL STRESSES ACROSS JOINT, LOAD RUNS 5 TO 8

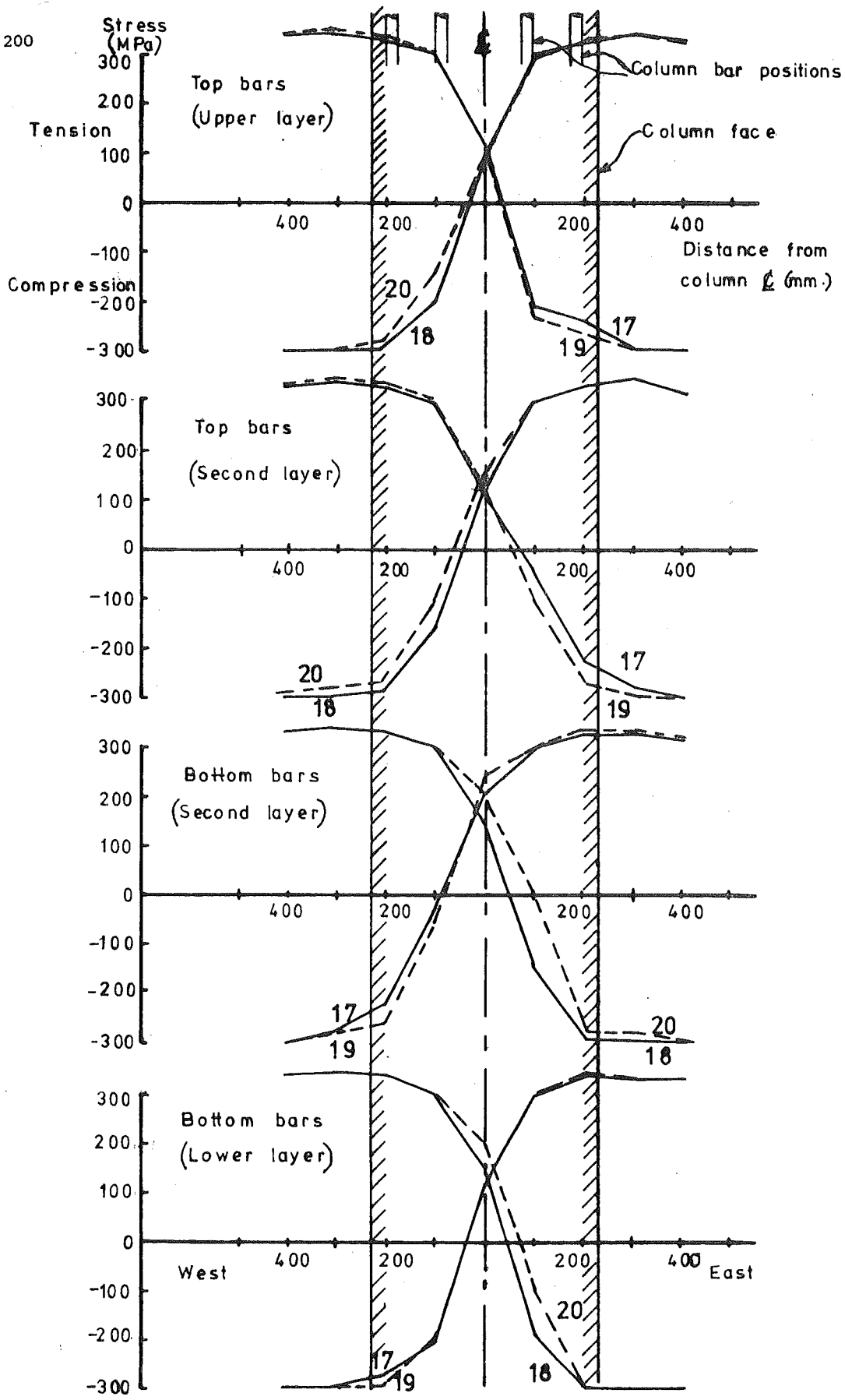

FIG.5.21 :BEAM STEEL STRESSES ACROSS JOINT, LOAD RUNS 17 TO 20

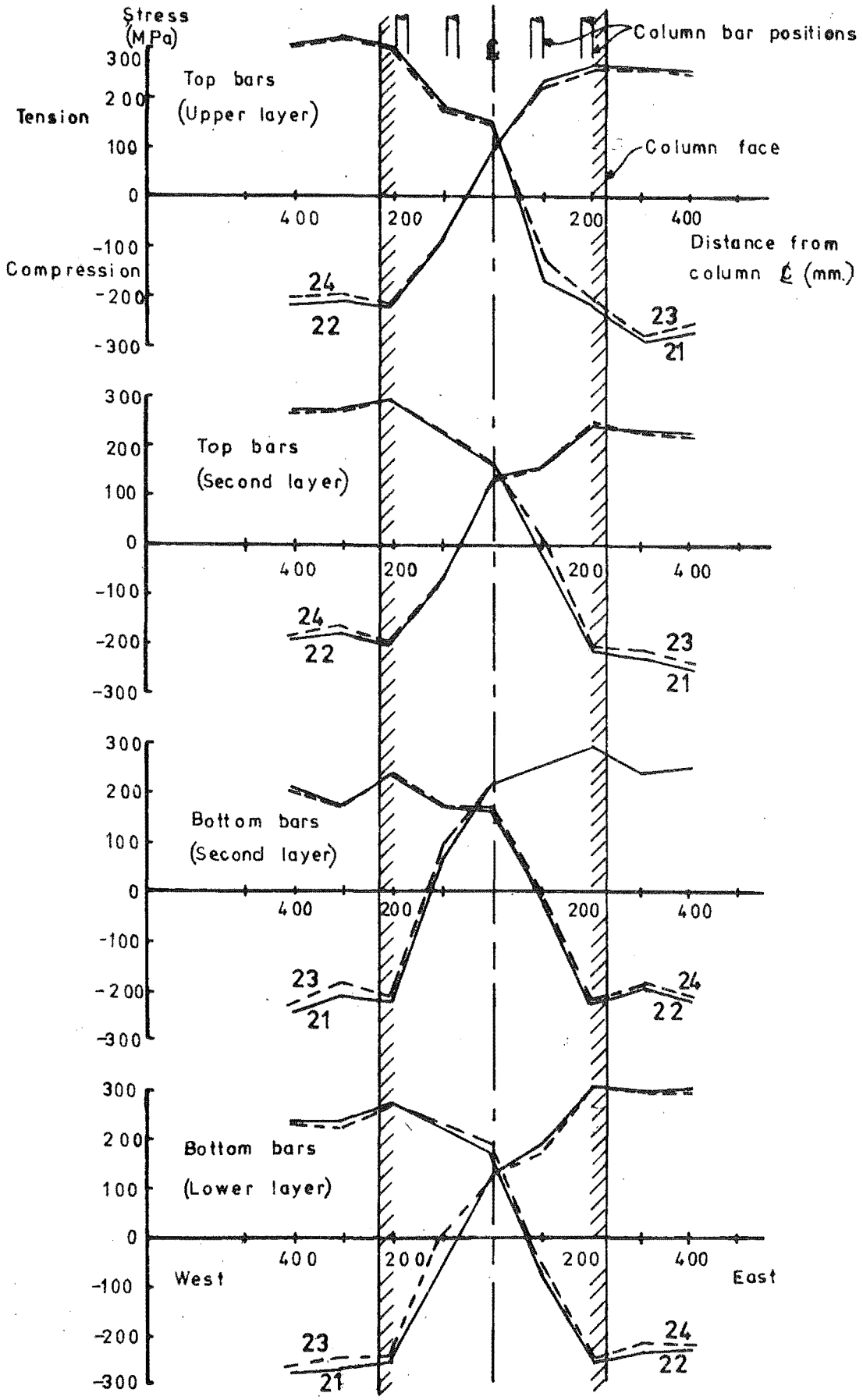

FIG.5.22 : BEAM STEEL STRESSES ACROSS JOINT, LOAD RUNS 21 TO 24

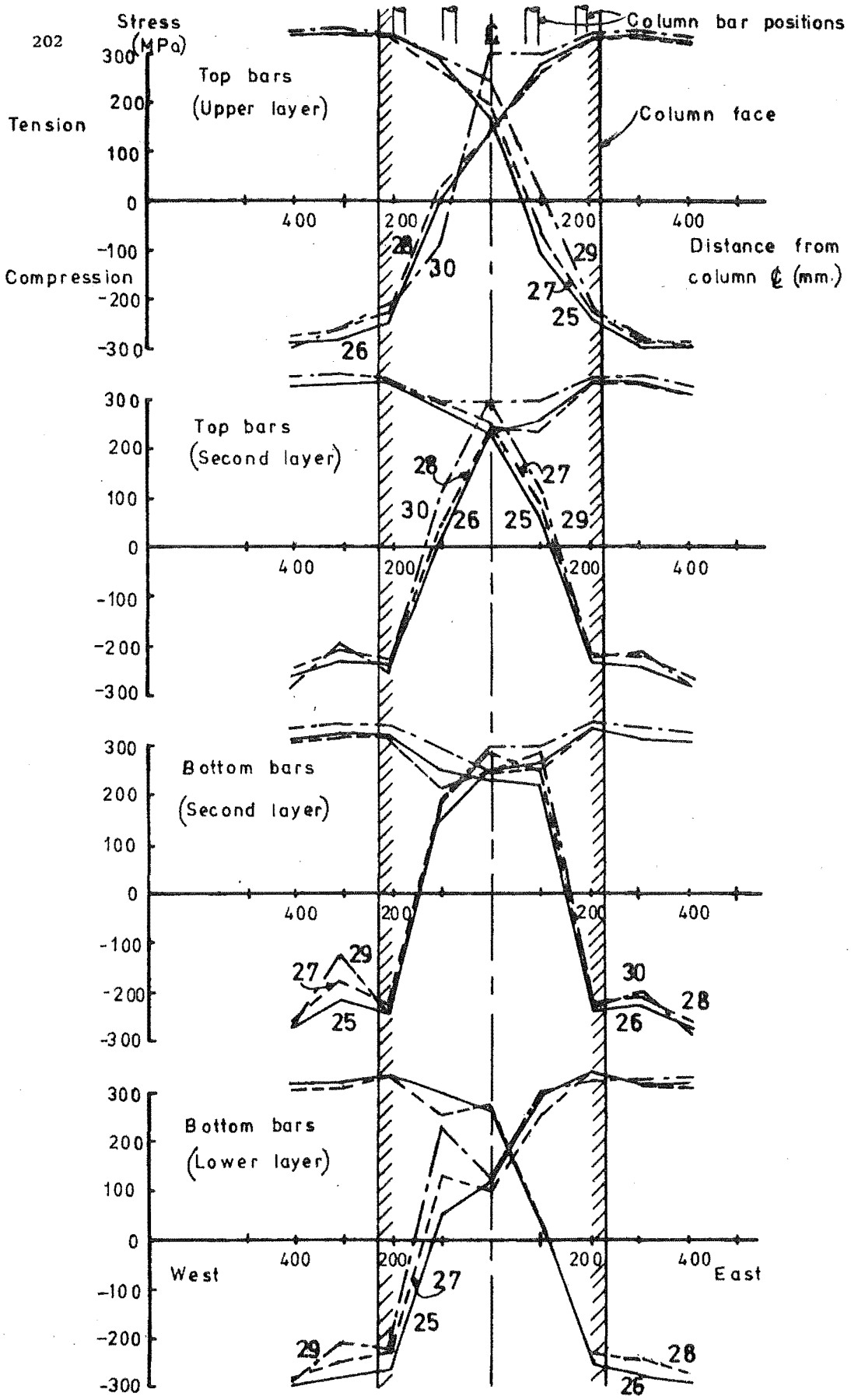

FIG.5.23 : BEAM STEEL STRESSES ACROSS JOINT, LOAD RUNS 25 TO 30

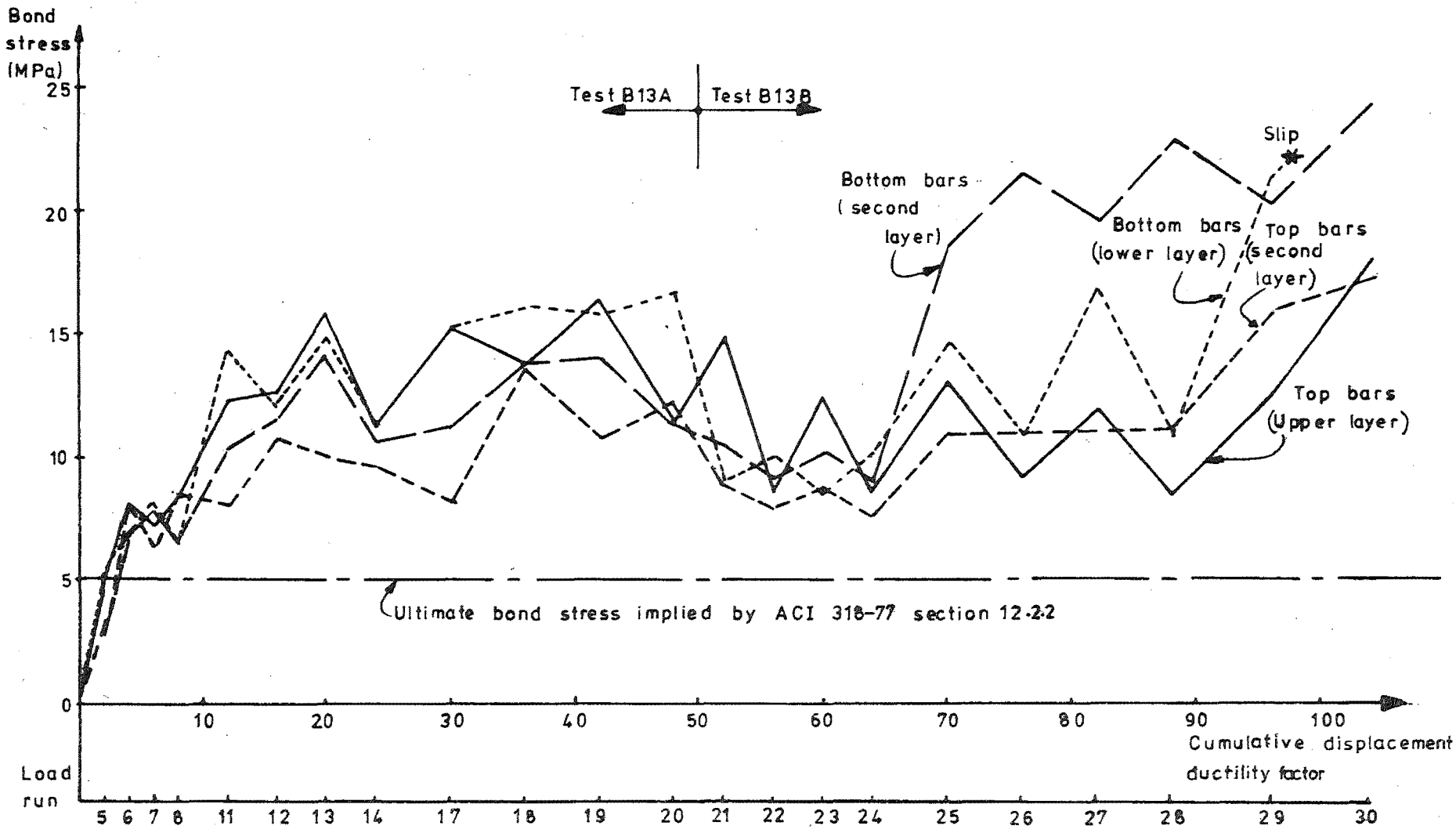

FIG.5.24: BOND STRESSES IN BEAM BARS ACROSS JOINT

5.3.5 Beam Shear Resistance

Strains were measured at the mid-depth of every third set of beam stirrups throughout the test. As in the previous tests the holes formed in the cover concrete around the Demec studs acted as crack initiators (see Figs. 5.1 to 5.5), so that the data obtained was probably somewhat unrepresentative. Possibly additional distortion of the readings could have occurred during the later cycles when shear sliding of adjacent blocks of concrete could have caused bending of the stirrups. However the results indicated that an unfavourable pattern of diagonal cracking could lead to relatively large local strains in the stirrups, compared to those predicted by a conventional 45° truss mechanism, even where no contribution to shear resistance from the concrete is assumed.

As noted in Section 5.3.1, shear deformation in the beam plastic hinge region was measured in this test and was found to cause substantial proportions of the total beam end displacements, particularly in repeated cycles where the flexural cracks remained open across the beam throughout the early part of the cycle. The favourable conditions for the occurrence of sliding shear deformation, as a result of the tendency for well distributed flexural cracks around the longitudinal bars to combine into larger more widely spaced cracks in the mid-depth of the beam, was again noted.

Since the beam was identical to that used in test B12, some comparison was possible between the approximate visual measurements of shear deformation along the flexural cracks made in test B12 and the more exact measurements taken in this test. Comparison showed, as expected, that the visual measurement underestimated the total shear displacement, with the amount of discrepancy ranging from 10% to 50% at various stages of the test.

5.4 Column Behaviour

Strains measured from the column reinforcement in the South face of the column at various stages of the test are shown in Figs. 5.25 to 5.27. The expected compression dominated behaviour of the column during test B13A is clearly shown, but the measured strains implied that the reinforcement at the levels of the beam top and bottom faces was carrying much more load than was predicted by theory, assuming a parabolic stress-strain relationship for the concrete up to the cylinder strength at a strain of 0.002. The reason for this may have been a transverse strain gradient across the column indicated by strain reading from Demec points

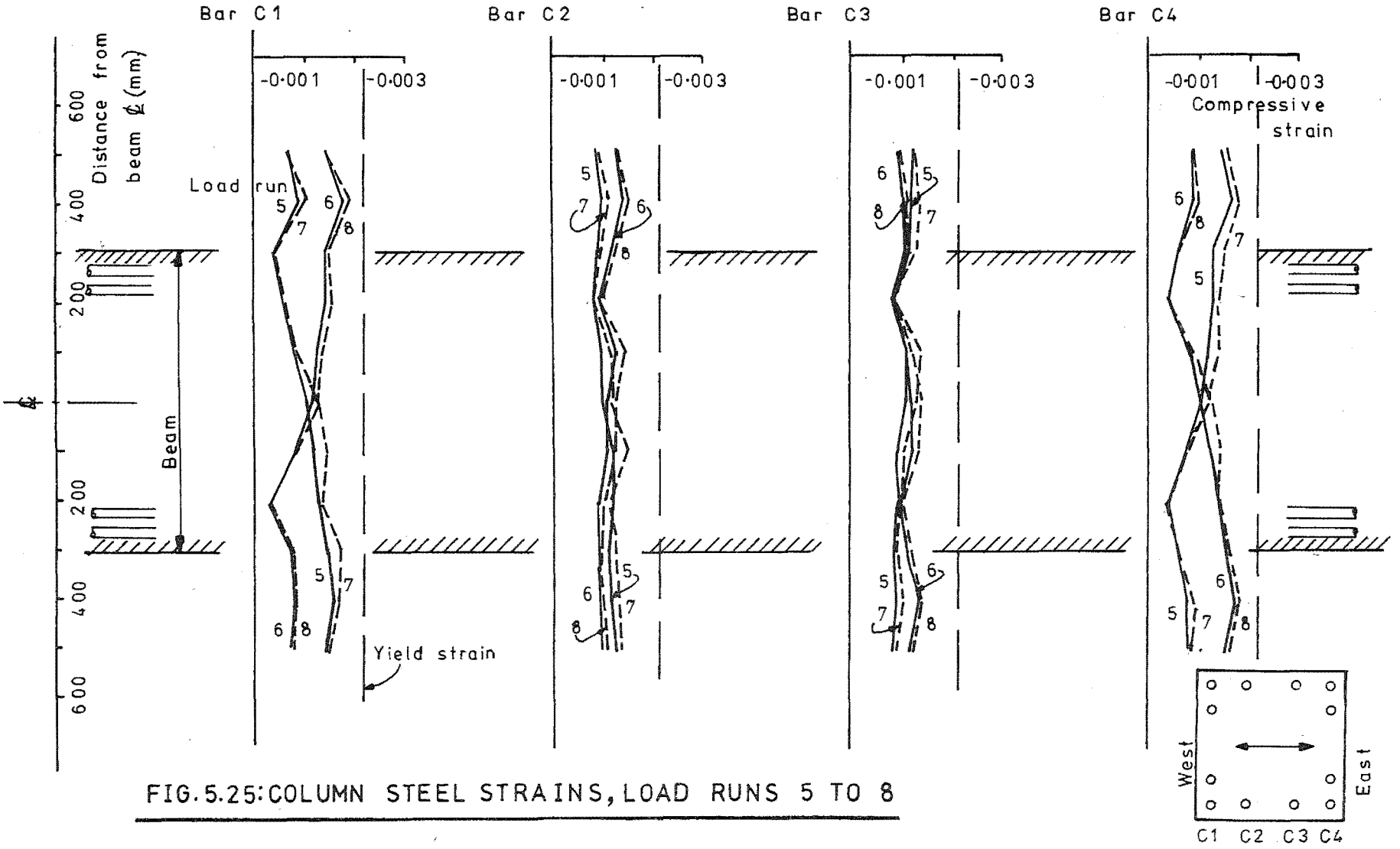

FIG. 5.25: COLUMN STEEL STRAINS, LOAD RUNS 5 TO 8

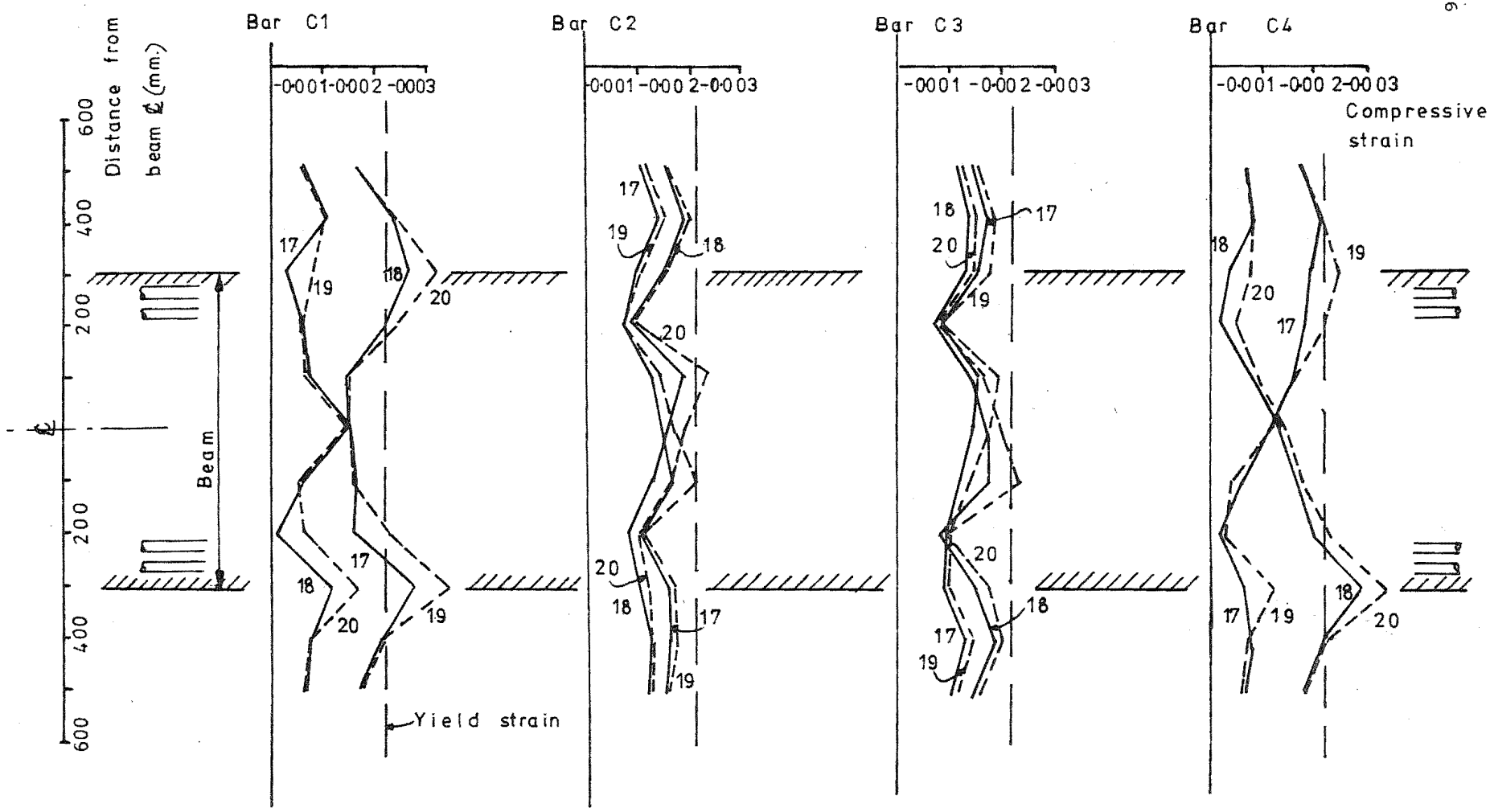

FIG.5.26 :COLUMN STEEL STRAINS , LOAD RUNS 17 TO 20

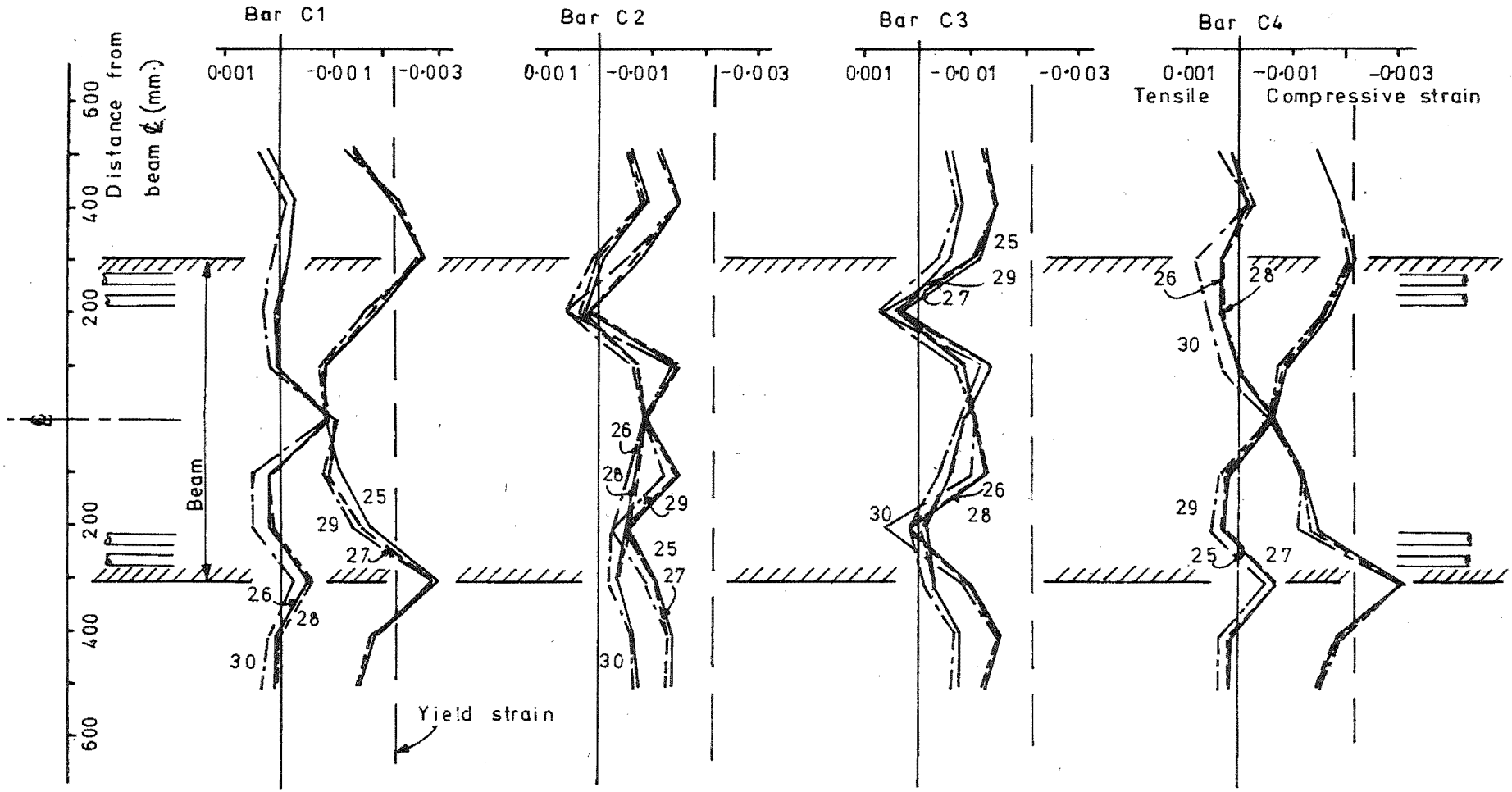

FIG.5.27 : COLUMN STEEL STRAINS, LOAD RUNS 25 TO 30

fixed to the concrete surface on both faces of the column. These readings indicated that the concrete was under significantly greater compressive strain on the South face, from which the steel strain readings were taken, than on the North face. This strain gradient may have been due either to a significant gradation of concrete properties across the column section resulting from the unit being poured on the flat, or to some initial eccentricity in the application of the axial load. These sources of eccentricity could have been accentuated by the longitudinal cracking observed at the ends of the column due to inadequate confinement provided under the end bearing plates by which load was transferred from the test rig. A further contributory cause could have been the concentration of holes in the cover concrete for Demec studs and Pfender gauge readings (see Section 2.6),which was much greater in the South face of the column, and which would have resulted in slightly unsymmetrical section properties in the transverse direction. Calculation of the section properties at the level of a set of four Demec holes to the column bars in the South face indicated that the column centroid at this section was displaced 1.5 mm from that at a section having complete cover.

Analysis of the strain readings taken from the surface before lateral load was applied showed that if the strain gradient was solely due to eccentricity of load application then this eccentricity would be about 11 mm from the column centreline. It is considered most unlikely, due to the method of construction, that the bearing plate could have been misplaced on the column end section by more than about 4 mm, so the likeliest explanation would be that the error arose due to an adverse combination of the reasons outlined above.

Thus the mean compression strain in all the column reinforcement was probably slightly less than shown in the strain profiles, with the magnitude of the discrepancy varying through the test, depending on the proportion of total load carried by the reinforcement at any particular stage. Up to load run 14 the behaviour of the column bars was predictable (see Fig. 5.25) with a gradual strain gradient down the depth of the joint. However in the vicinity of the inner bars C2 and C3 diagonal cracking was induced by bond and shear stresses, and the strain profiles for these bars consequently 'bulged' somewhat over the mid-depth of the joint as the bars were required to carry more compression, because the concrete was weakened by the cracking. No disruption of the column strains at the level of the beam reinforcement due to the influence of large bond stresses was apparent in this test, presumably because the bursting effects of bond

forces were adequately confined by the presence of heavy axial load.

In load runs 17 to 20 (Fig. 5.26) the strain in the corner bars C1 and C4 exceeded the yield strain in compression at the levels of the beam top and bottom faces. The reason for this is apparent from the photographs (Fig. 5.3) which show that the corners of the joint not confined by the beam had begun to spall off at this stage. This is especially apparent at the lower right hand corner of Fig. 5.3, which shows the North face of the column, but the phenomenon was evident at all four corners of the South face, from which the reinforcement strains were recorded.

During test B13B the total compression carried by the reinforcement was reduced as expected, but similar patterns to those observed in test B13A were apparent, with large compressive strains recorded in the corner bars at the level of the beam top and bottom faces due to the loss of the joint corners, while the inner bars and to a lesser extent the corner bars carried a 'bulge' of compression strain over the mid-depth of the joint due to the weakening of the joint concrete by diagonal cracking.

Calculation of the input of the column reinforcement and concrete forces to the joint as vertical joint shear is carried out in Section 5.5.4.

5.5 Joint Behaviour

5.5.1 Joint Cracking

The large axial load applied in this test has a very noticeable effect on the pattern of joint cracking, as shown in the photographs (Figs. 5.1 to 5.5). During the initial elastic cycles no cracking at all was observed in the joint panel, but when inelastic cycles were applied diagonal cracks appeared in the vicinity of the inner column bars, due to the local concentrations of diagonal tension stresses arising from the combination of bond and shear resistance. The cracks were inclined at angles to the horizontal significantly steeper than the joint diagonal, because of the influence of the axial load on the directions of principal stresses.

In the later cycles of test B13A the diagonal cracks extended, but were still concentrated around the inner column bars. The maximum crack width observed in the joint panel was 0.30 mm, with recovery up to 0.10 mm when the beam end loads were removed. Because of the step in member breadth at the column face, the cover concrete to the joint was not confined at the corners of the column section, and began to spall off at the levels

of the beam top and bottom faces under the influence of the heavy diagonal compression, commencing at load run 17. However, no separation of the concrete cover over the remainder of the joint panel could be detected.

When the column load was reduced for test B13B the joint cracking became more extensive, even under reduced applied shear, as shown in Fig. 5.4. The inclination of the new diagonal cracks was not as steep as in the first part of the test,approaching the joint diagonal angle. By the end of the test joint cracking was very extensive, but the well distributed pattern did not degenerate to concentration in a single crack. Maximum crack widths had increased by the final cycle to 0.60 mm, closing up to 0.25 mm at zero load, while all four corners of the joint cover were separated from the joint core on both faces of the column. Separation of cover over the remainder of the joint panel was difficult to determine, but it was not likely that more than 10% of the joint cover had separated by the end of the test.

5.5.2 Joint Deformation

As expected from the limited cracking of the joint panel in test B13A, the deformation of the joint was much smaller than was observed in the previous tests. The fine cracks and the absence of sliding displacement along the cracks resulted in joint deformation causing only 8 to 12% of the total beam end displacements during test B13A. When the axial load was reduced for test B13B, the joint underwent significantly more cracking and some yielding of joint shear reinforcement was observed. These factors resulted in greater joint deformations, and the consequent components of beam end displacement ranged between 20 and 25% of the totals.

Although joint deformation was possibly elastic in character throughout test B13A, the occurrence of limited tie yielding in test B13B caused significant residual joint deformations at zero load, showing the effect of inelastic response of the joint.

5.5.3 Strains in Stirrup Legs of Joint Reinforcement

The distribution of strains measured in the stirrup legs of the horizontal joint reinforcement at various stages of test B13A is given in Fig. 5.28. The strains increased as the test progressed and the displacement ductility demand increased, but they were generally well below yield level. However, as in the previous tests the distributions of strain down the depth of the joint were not uniform, and the inner stirrup legs again carried substantially more strain than the outer legs, while

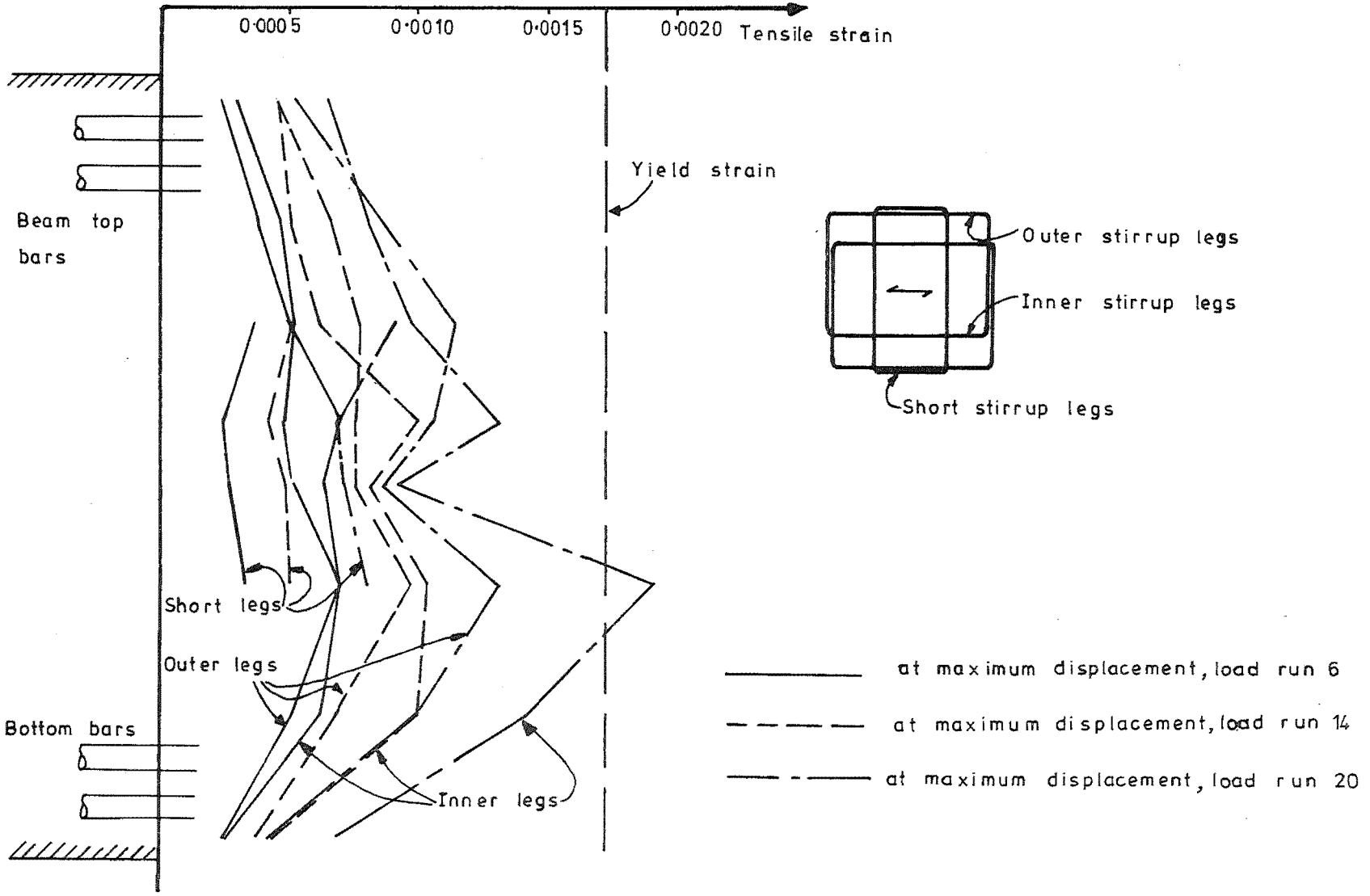

FIG·5·28: DEVELOPMENT OF STRAINS IN STIRRUP LEGS OF JOINT REINFORCEMENT-TEST B13A

the long stirrup legs carried more than the short legs.

Fig. 5.29 shows the further development of strains in the stirrup legs during test B13B. The strains followed a similar pattern to that observed in test B13A, but were considerably increased throughout the depth of the joint with strains greater than yield strain observed in three inner stirrup legs in load run 30, the maximum strain being 3.29 times yield strain.

Envelopes of strains recorded in the stirrup legs in both parts of the test are presented in Fig. 5.30. The difference in the amount of yielding observed in the two tests is clearly shown. Whereas strain greater than yield strain was recorded at only one location during test B13A, the reduced axial load in test B13B caused joint reinforcement to yield in three different locations in the inner stirrup legs, while strains in the outer legs also approached yield level.

Fig. 5.31 shows strains recorded at intervals of 100 mm along the outer stirrup legs of certain tie sets during selected load runs. A distinct strain gradient along the tie legs, as observed in the previous tests, was not obvious in this case, due to the steeper diagonal cracks formed in the joint with the heavy axial load. The maximum strain tended instead to occur at the column centreline due to the greater crack density in this region.

A history of the strain measured in a long inner stirrup leg of a joint tie set at the mid-depth of the joint plotted against the applied horizontal joint shear is presented in Fig. 5.32. The plot shows that during the initial elastic cycles the strain was virtually unchanged from that recorded under the application of column axial load only, this being due to the confining action of the joint reinforcement. This behaviour was consistent with the absence of joint cracks during the elastic cycles.

When joint cracks first appeared in load run 5, additional strain accrued in the tie, with very little of the additional strain being recovered at zero load. The same behaviour occurred in the reversed load run 6, while in the remaining cycles of test B13A the strain at maximum displacement increased, but substantial elastic recovery occurred.

During test B13B the reduced stiffness of the joint in shear due to the additional diagonal cracking is shown by the reduced slope of the shear versus strain curves. Maximum strain in the tie increased and yield

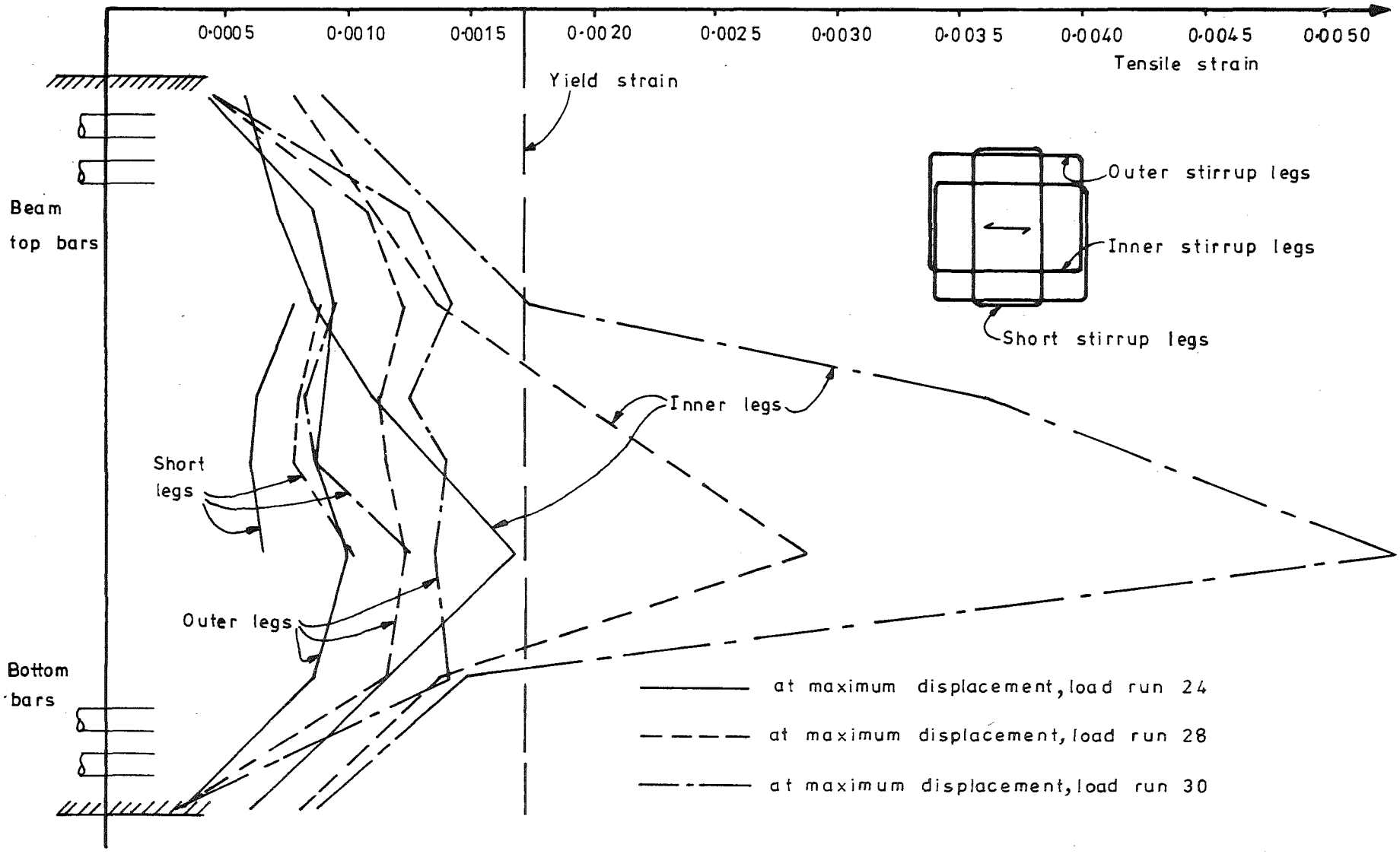

FIG·5·29: DEVELOPMENT OF STRAINS IN STIRRUP LEGS OF JOINT REINFORCEMENT - TEST B13B

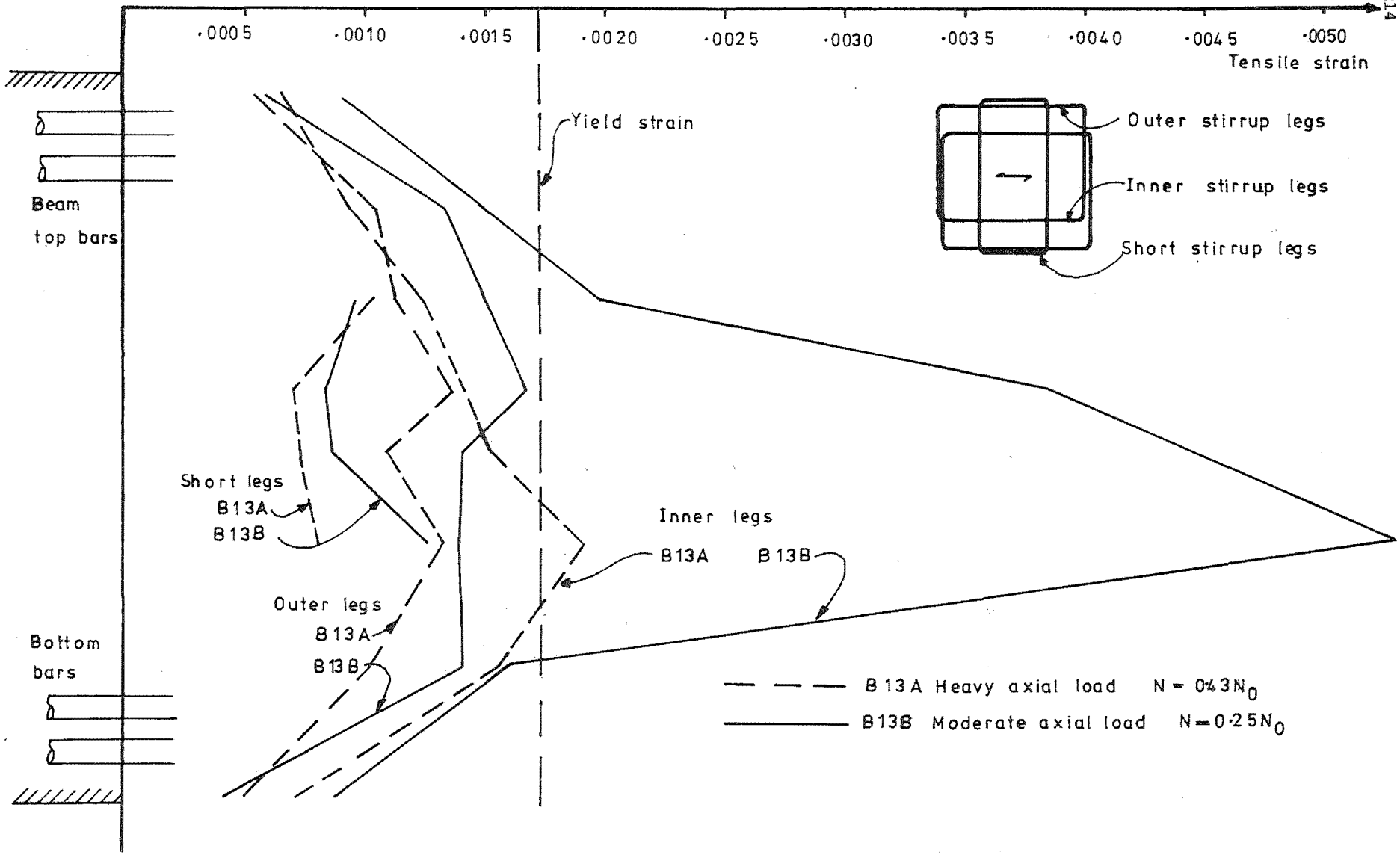

FIG.5.30 :ENVELOPE OF STRAINS IN STIRRUP LEGS OF JOINT REINFORCEMENT

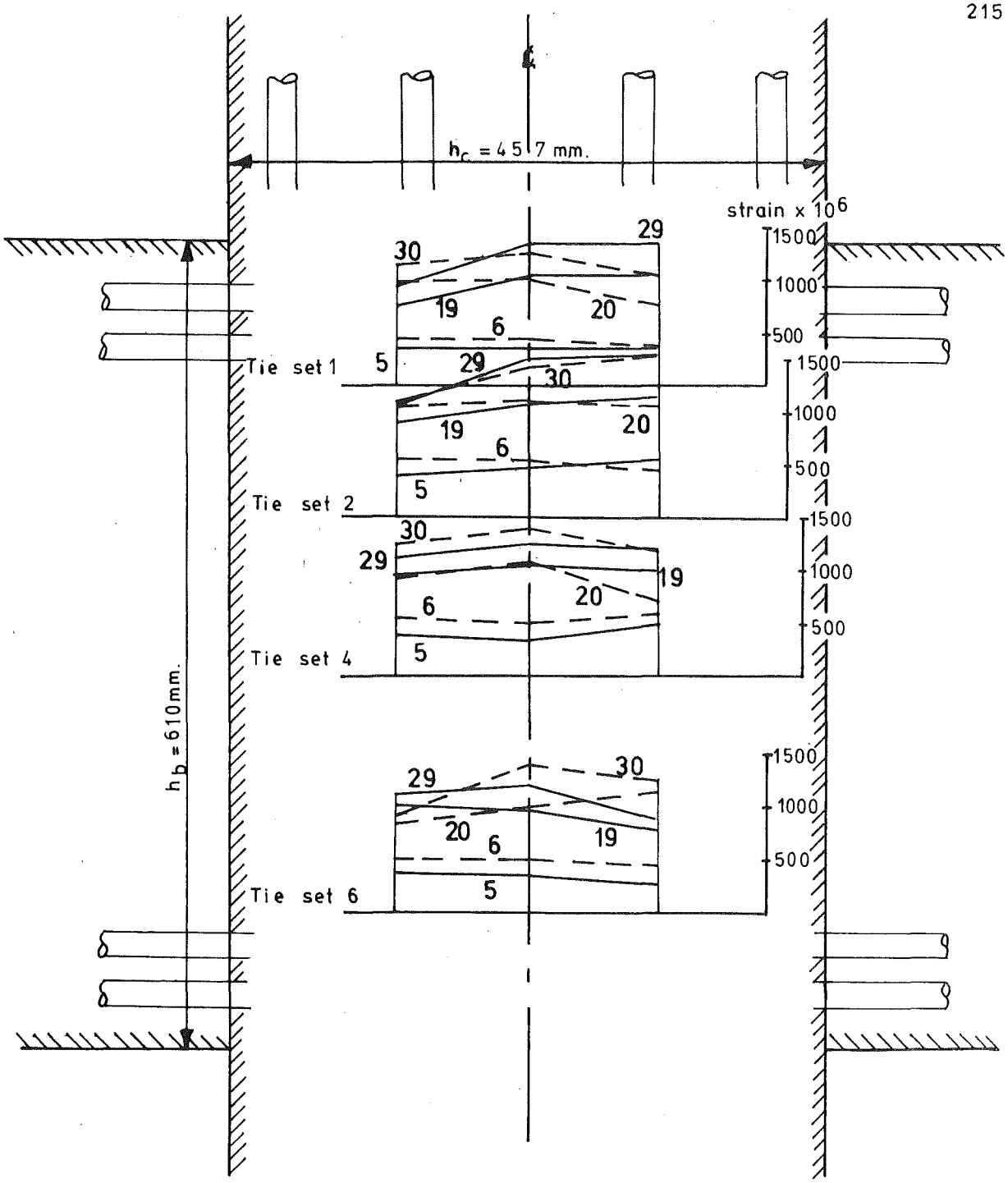

FIG.5.31 :STRAINS ALONG OUTER STIRRUP LEGS OF JOINT REINFORCEMENT IN SELECTED LOAD RUNS

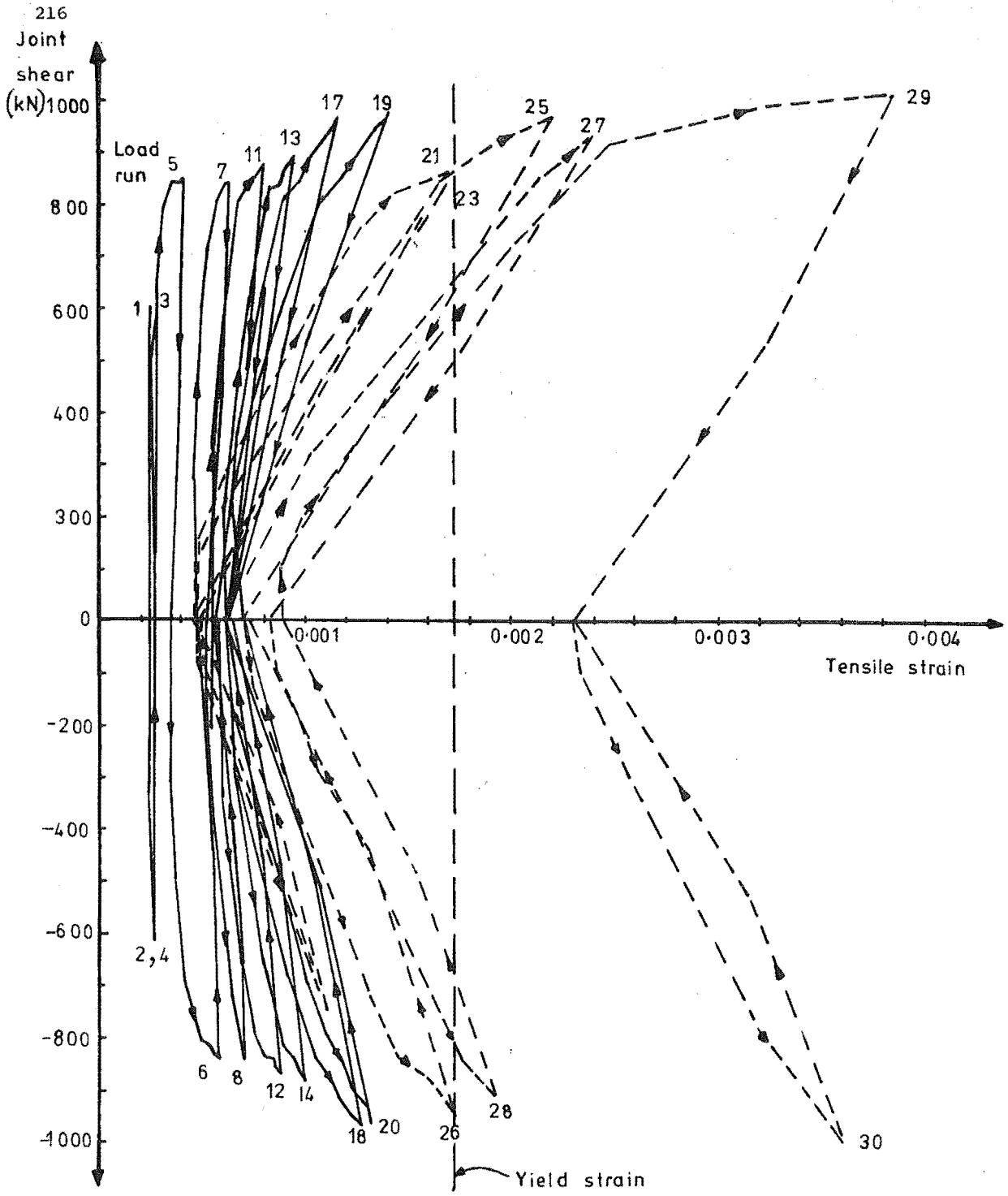

FIG.5.32:STRAIN HISTORY FOR LONG INNER STIRRUP LEG OF TIE AT MID-DEPTH OF JOINT

strain was eventually exceeded under both positive and negative applied shear. The residual strain at zero shear also increased gradually as the test progressed, until the tie underwent much more severe yielding in load run 29, with a consequently large residual strain. Joint tie yielding was shown to be an inefficient means of dissipating energy under cyclic loading, since the reversed loading did not reverse the direction of straining, and the next loop (load run 30) consequently enclosed relatively little area.

5.5.4 Mechanism of Joint Shear Resistance

The strains measured in the stirrup legs of the joint reinforcing were converted to bar forces and summed over the depth of the joint to give the appropriate components of resistance to horizontal joint shear supplied by the long and short stirrup legs at the maximum displacement of the major cycles. The contribution of the joint concrete to horizontal joint shear resistance was then taken as the difference between the applied joint shear and the resistance calculated as supplied by the joint reinforcing. These values are listed in Table 5.4, and are presented in histogram form in Fig. 5.33 for test Bl3A and in Fig. 5.34 for test Bl3B.

During the initial elastic cycles, when there was no joint cracking, the joint concrete was able to resist 70 to 75% of the total horizontal joint shear input, but this proportion diminished as inelastic cycles were imposed until only 15% of the total horizontal shear was resisted by the concrete in load run 20. During test Bl3B the reduction in column axial load caused a further decrease in the horizontal shear resistance provided by the concrete mechanism. The proportion of the total horizontal shear resisted by the joint concrete mechanism varied between zero and 8%. As in the test of unit Bl2 the short stirrup legs of joint reinforcement were found to carry a significant proportion of the total horizontal shear, varying between 5 and 12% in test Bl3A, and between 11 and 15% in test Bl3B, but as expected the major component of resistance in the later stages was provided by the long stirrup legs of the joint reinforcing.

For comparison, the design case is also shown in Figs. 5.33 and 5.34. Although the shear assigned to the concrete for design purposes was arbitrarily decided at 25% of the total input, comparison with the test results over load runs 17 to 20 shows that this was a good estimate. The resistance required of the joint reinforcing, as shown in Fig. 5.34 for test Bl3B, on the other hand clearly exceeded the design case and yielding of the joint reinforcement occurred as a result. However, it should be pointed out once again that the total ductility demand made on

TABLE 5.4 : MECHANISM OF RESISTANCE TO JOINT SHEAR

Load Run No.	V_{jh} (kN)	V_{sh1} (kN)	$\frac{V_{sh1}}{V_{jh}}$	V_{sh2} (kN)	$\frac{V_{sh2}}{V_{jh}}$	V_{ch} (kN)	$\frac{V_{ch}}{V_{jh}}$	V_{jv} (kN)	$\tan\beta_T$	$\tan\beta_C$
1	601.8	126.7	0.211	31.9	0.053	443.2	0.736	2156.6	3.584	3.660
2	611.5	130.3	0.213	24.2	0.040	457.0	0.747	2105.3	3.443	3.513
3	612.9	142.0	0.232	33.3	0.054	437.6	0.714	2109.7	3.442	3.561
4	609.0	130.9	0.215	24.8	0.041	453.3	0.744	2028.5	3.331	3.357
5	848.3	257.2	0.303	41.7	0.049	549.4	0.648	2201.3	2.595	2.774
6	840.1	313.0	0.373	42.4	0.050	484.7	0.577	2055.2	2.446	2.635
7	840.1	358.3	0.426	48.4	0.058	433.4	0.516	2178.0	2.593	2.944
8	840.1	347.1	0.413	46.2	0.055	446.8	0.532	2012.4	2.395	2.675
11	882.7	420.5	0.476	54.7	0.062	407.5	0.462	2204.1	2.497	2.803
12	872.0	435.8	0.494	60.9	0.069	386.0	0.437	2018.5	2.315	2.474
13	895.1	506.4	0.566	66.2	0.074	322.5	0.360	2210.8	2.470	2.818
14	882.5	496.7	0.563	74.5	0.084	311.3	0.353	1992.1	2.257	2.451
17	971.6	628.9	0.647	85.5	0.088	257.2	0.265	2183.3	2.247	2.498
18	967.6	654.1	0.676	110.1	0.114	203.5	0.210	2095.3	2.165	2.440
19	978.1	748.3	0.765	102.6	0.105	127.2	0.130	2143.9	2.192	2.451
20	962.7	700.1	0.727	118.3	0.123	144.3	0.150	2045.9	2.125	2.395
21	873.4	773.1	0.885	100.3	0.115	0.0	0.0	1616.7	1.851	2.075
22	749.9	604.5	0.806	102.5	0.137	42.9	0.057	1183.6	1.578	1.751
23	843.3	737.0	0.874	94.2	0.112	12.1	0.014	1587.6	1.883	2.196
24	743.7	585.0	0.787	100.4	0.135	58.3	0.078	1172.2	1.576	1.745
25	974.3	845.0	0.867	113.5	0.116	15.8	0.016	1898.7	1.949	2.291
26	952.0	752.6	0.791	137.2	0.144	62.2	0.065	1798.2	1.889	2.214
27	934.9	822.7	0.880	113.3	0.120	0.0	0.0	1907.9	2.041	2.474
28	910.4	744.6	0.818	132.1	0.145	33.7	0.037	1769.4	1.944	2.342
29	1014.9	883.8	0.871	126.8	0.125	4.3	0.004	2094.4	2.064	2.558
30	1004.9	845.8	0.842	146.9	0.146	12.2	0.012	2093.4	2.083	2.774

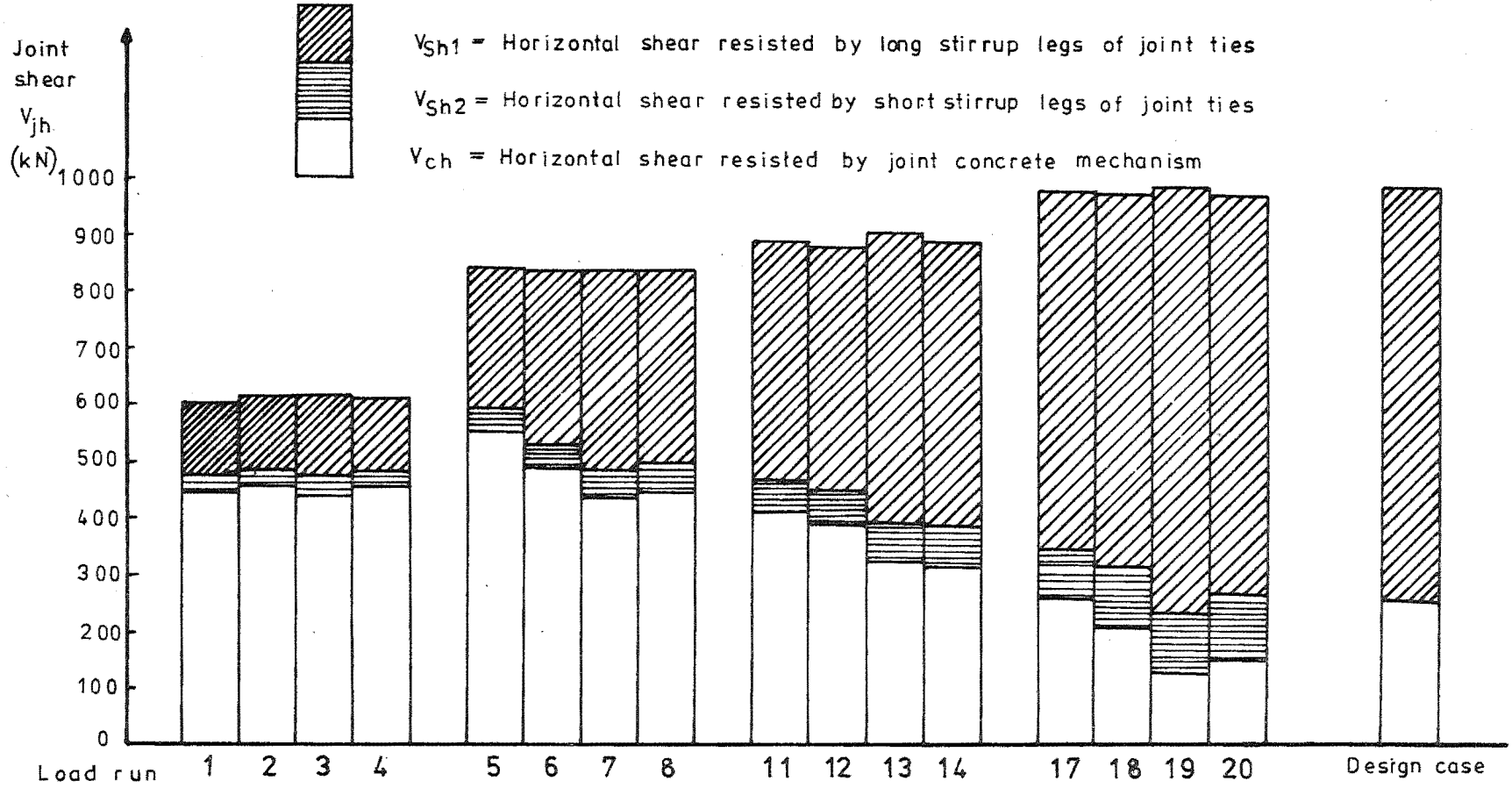

FIG.5.33: MODE OF RESISTANCE TO HORIZONTAL JOINT SHEAR (B13A)

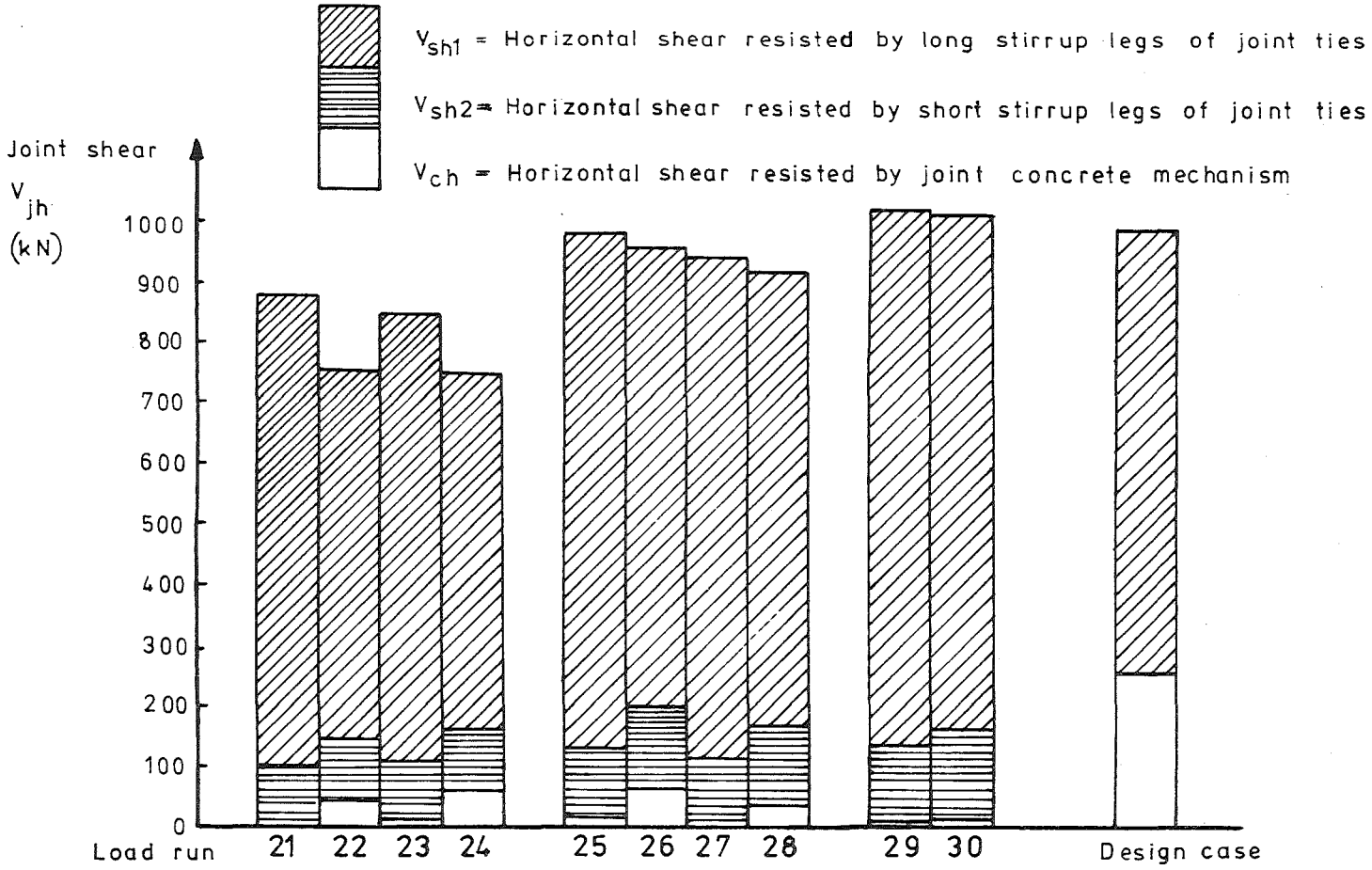

FIG.5.34: MODE OF RESISTANCE TO HORIZONTAL JOINT SHEAR (B13B)

the unit by the completion of the test was excessive, and the results of the final cycles should therefore be treated with some caution.

Table 5.4 also lists values for the applied vertical joint shear V_{jv}, and the tangents of the angle of applied joint shear β_T (= $\tan^{-1} V_{jv}/V_{jh}$), and of the inclination β_C to the horizontal of the line between the centroids of concrete compression in the column sections above and below the joint. The tangents of these angles are also shown in Fig. 5.35. The derivation of these values was explained in Section 3.5.4. In the uncracked state of the joint in the initial load cycles the angle of resistance of the concrete strut, β_C was very steep. This occurred because the low moment to axial load ratio in the column meant that the eccentricity of the centre of concrete compression from the column centre-line was small, and the strut joining these centres above and below the joint was therefore steeply inclined.

When greater loads were applied in the inelastic cycles the angle of resistance decreased somewhat as the position of the centre of concrete compression in the column moved outward from the column centreline. The angles of resistance remained fairly constant throughout the inelastic cycles of test Bl3A, but in test Bl3B the angle of resistance decreased to almost the joint diagonal angle β_J because the vertical shear input V_{jv} was reduced with the lower axial load. This was reflected in the angle of cracking in the joint panel, which also approached the joint diagonal angle in test Bl3B (see Figs. 5.4, 5.5), the cracking being caused by diagonal tension stresses at right angles to the inclined compression struts.

No account has been taken in these calculations of the errors in the column bar strain readings pointed out in Section 5.4. Since extra compression was noted in all column bars, values computed for vertical joint shear will not be greatly affected. However, reduced compression forces in the column reinforcement would increase the concrete compression force, hence requiring a slightly smaller lever arm and consequently a slightly steeper angle between the centres of compression above and below the joint. Thus the values given for β_C in Table 5.4 may be slightly low, but it is unlikely that the error was very large.

5.5.5 Strains in Transverse Tie Legs of Joint Reinforcement

Fig. 5.36 shows an envelope of the maximum strains measured in the transverse tie legs of the joint reinforcement during the two parts of the test. Strains everywhere within the depth of the joint were

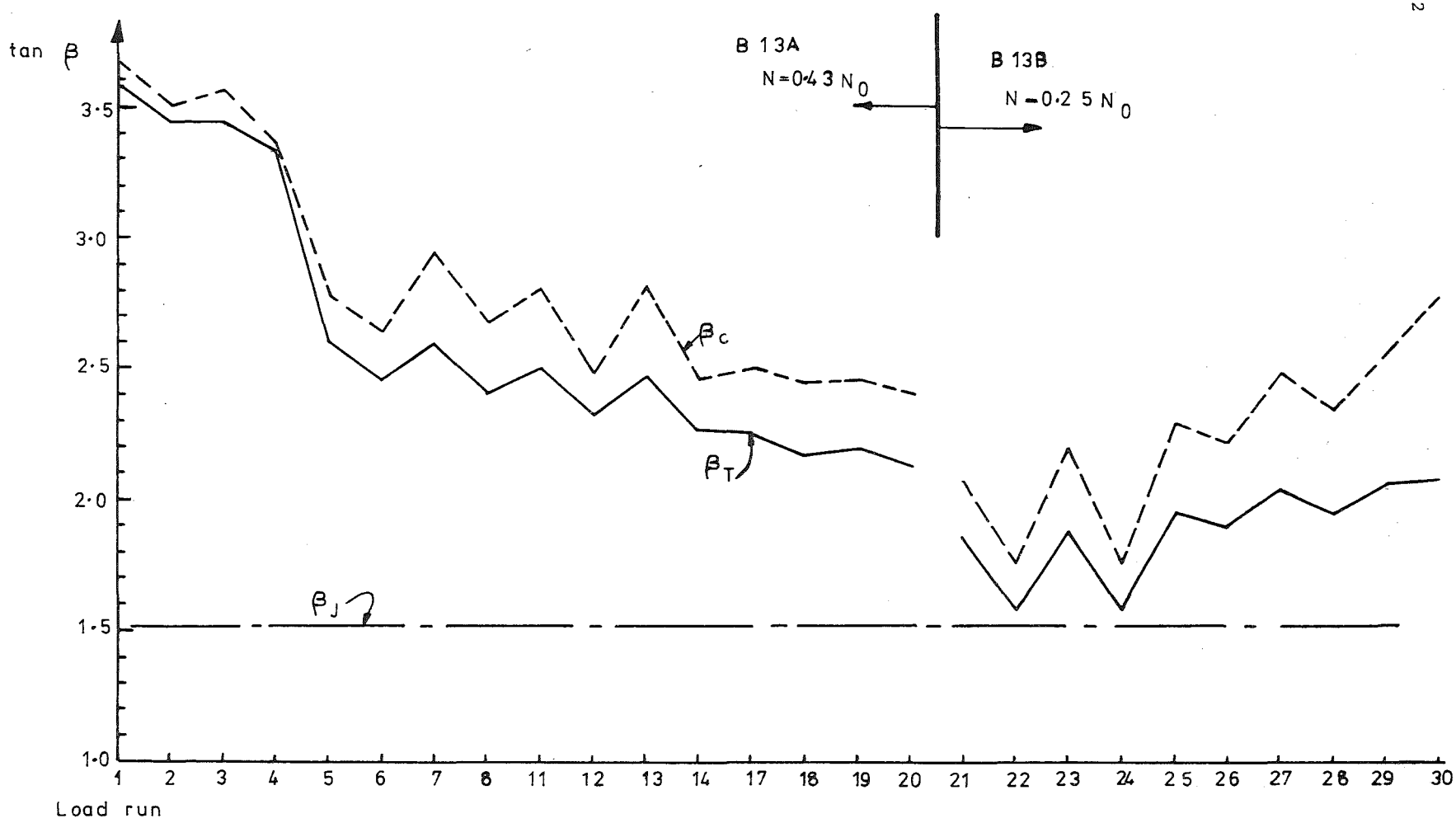

FIG.5.35 : ANGLE OF RESISTANCE TO JOINT SHEAR

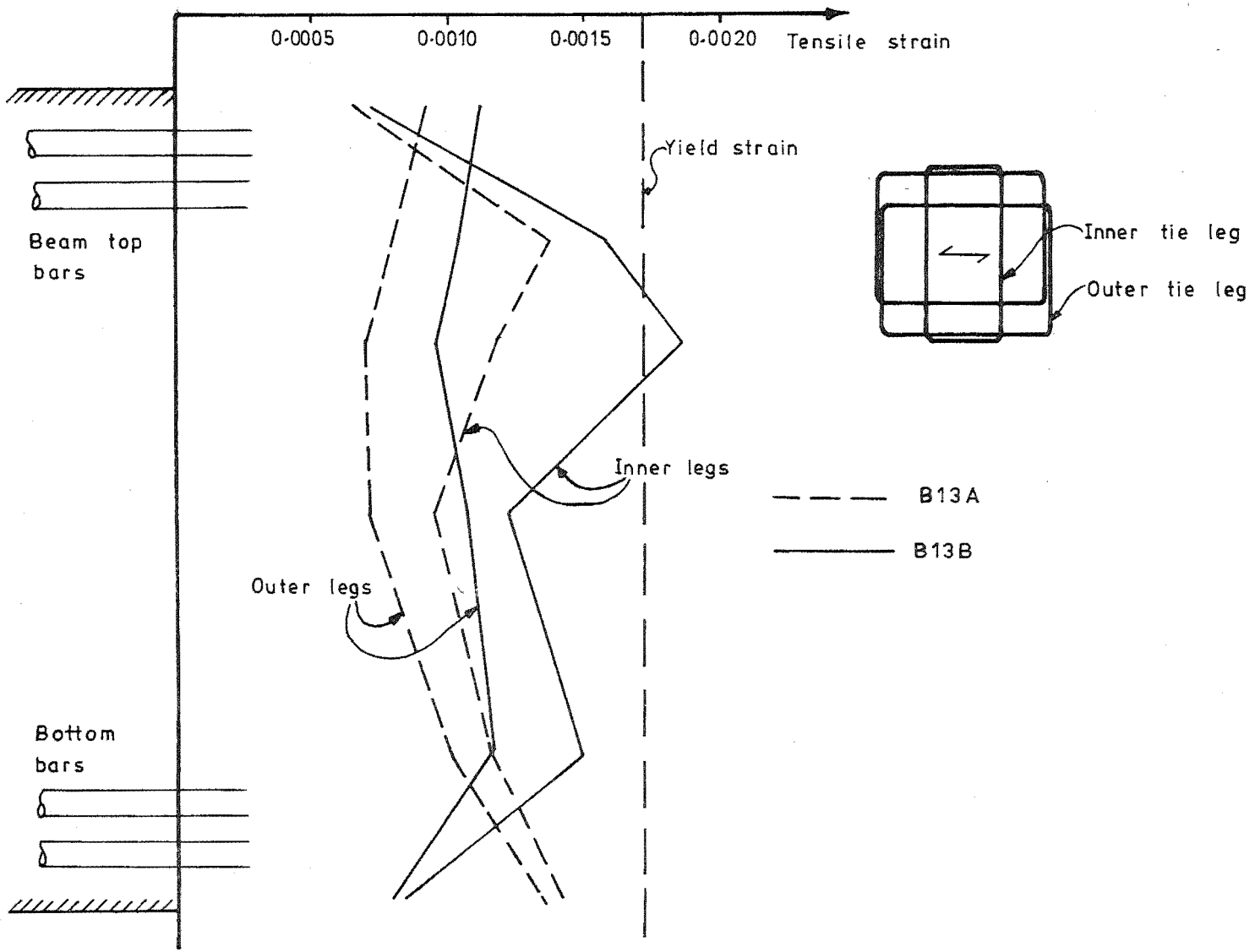

FIG.5·36 :ENVELOPE OF STRAINS IN TRANSVERSE TIE LEGS OF JOINT REINFORCEMENT

greater in test B13B than in test B13A, in spite of the lower axial load applied in the second test. Presumably this occurred because the more extensive diagonal cracking in test B13B reduced the stiffness of the concrete in the joint, thus allowing a greater tendency for lateral expansion under axial compression. The consequent strains included a measurement of strain 8% in excess of yield strain in one strain gauge position, showing that perhaps the degree of diagonal cracking and yielding in the stirrup legs of the joint reinforcing was excessive, considering the level of axial load.

Strains were fairly uniform throughout the depth of the joint, showing that confinement of the diagonal compression struts was as important as confinement of the bond forces from the beam reinforcement in this case. This contrasts with the situation noted in the test of unit B12, where confinement of the bond forces was the primary function of the transverse tie legs. Over the depth of the joint the inner tie legs carried more strain than the outer legs in both parts of the test, because the inner legs were in a more favourable location to confine the compression strut as it crossed the joint diagonally than were the outer legs.

5.6 Summary

The performance of the test unit B13 under severe cyclic loading was very good. During test B13A, in which the column axial load was very heavy, the response was entirely satisfactory with bond strength of the beam flexural bars maintained across the centre of the joint, and shear cracking and deformation of the joint panel limited. This resulted in most of the post-elastic deformation being supplied by plastic straining of the beam flexural reinforcing, with consequently full load-displacement loops and efficient energy dissipation. The only unfavourable aspect of the response was the reduction in net column seismic shear carried caused by the P-delta effect in the column, which was quite severe in the response of the test unit. However the axial load applied to the column was much heavier than the average value that would be carried by the columns of a complete frame, and the P-delta effect for the complete structure would therefore be much less significant than was observed in the response of the test unit. When the column axial load was reduced for test B13B the response was not as ideal, with more extensive joint cracking and some yielding of joint reinforcement leading to greater deformation within the joint and less effective energy dissipation. In the final cycle of the

test the anchorage of the beam flexural bars across the column centreline failed, and slippage of the bars across the joint resulted. However by this stage the unit had undergone eleven full cycles to displacement ductility factor of two or greater, with a total cumulative displacement ductility of 104, which is considered to be somewhat excessive for this type of structure. For this reason not too much attention should be paid to the slip failure. As in the previous tests strain-hardening and strain-aging of the beam flexural steel caused beam end loads to be applied significantly greater than the ideal ultimate strengths of the beams. In this test the maximum overstrength was 24% in the final cycle, but as noted with respect to the previous tests this need not be considered unrepresentative,since actual material properties in a prototype structure may result in a less favourable combination of initial strengths than was the case in the test unit.

The test results showed that the presence of a constant heavy axial load did allow satisfactory joint performance to be achieved when joint reinforcement was reduced, compared to that shown by the previous tests to be necessary in a joint with low axial load. However, the likelihood of a constant axial load ot the magnitude employed in this test being imposed on a prototype joint under actual earthquake loading is not very great. The results from the second part of the test, where the column load was smaller, show that a lower limit of axial load will be critical in defining the joint response, while a cyclic pattern of axial loading may provide an even more severe response. If a joint is softened by cracking and possible yielding under a lower level of axial load, it may not subsequently carry a heavier axial load as efficiently as was observed in this test.

The improved bond conditions provided for the beam flexural bars by the heavy axial load in test Bl3A allowed the concrete compression strut mechanism to carry sufficient joint shear to justify the reduction in joint reinforcing content. Reduction of the data showed that the strut acted at a steep angle to the horizontal, and since the vertical shear input was large, a significant proportion of the horizontal joint shear introduced by bond near the column centreline could be carried by the concrete strut mechanism alone. This is the reason why the joint reinforcement was relatively lightly stressed in the first part of the test. In test Bl3B the strut acted at a smaller angle to the horizontal, but the changed location of the centres of concrete compression meant that the reduced vertical shear could not pick up enough horizontal shear

from bond to allow an effective concrete strut mechanism to function. Virtually all the horizontal shear was therefore imposed on the steel truss mechanism, leading eventually to the yielding of joint reinforcement observed in the final cycles.

The arbitrary allocation of 25% of the joint shear resistance to the joint concrete made in the design of this unit proved to be correct, or possibly slightly conservative for test B13A, with heavy axial load of $0.50f'_cA_g$, but slightly non-conservative for test B13B with reduced axial load of $0.29f'_cA_g$.

CHAPTER 6

SUMMARY OF PLANE FRAME TEST SERIES

6.1 Comparison of Test Results

6.1.1 General

Three tests on interior beam-column joint units from plane frames were carried out as described in the previous three chapters. The principal test variables and some highlights of the results are summarised in Table 6.1. The third test B13 was carried out in two parts, B13A and B13B, under different levels of column axial load as shown in the table.

Performance of all units was satisfactory although slip of beam bars through the joint compromised the response of units B11 and B12 to some extent during the final cycles of the tests. Some yielding of joint reinforcement was observed in all tests, but since the total strengths of the joint shear transfer mechanisms were not exceeded the overall response was not seriously affected. Heavy axial load was shown to be beneficial to the performance of the joint with unit B13 responding satisfactorily in spite of a lower joint reinforcement content than was used in the other units.

6.1.2 Joint Flexibility

The relative flexibilities of the joint panels of the individual test units were indicated by the proportion of the total beam end displacements caused by joint deformation only at any stage. These proportions, as determined at the maximum displacement of each major load run throughout each test, are shown in Fig. 6.1. The flexibility of the joint in units B11 and B12 was satisfactory, while in test B13A the significance of joint deformation was even less, as expected from the much less extensive cracking observed on the joint panel. However, in test B13B the combination of joint reinforcement content and the reduced column axial load allowed extensive joint cracking and more significant yielding of joint reinforcement to occur. This caused the joint to respond in a more flexible manner as shown in Fig. 6.1.

In the initial inelastic cycles (load runs 5 to 8) the applied displacement ductility factor was only two, and at this low displacement ductility factor the joint core deformation made a significant contribution to the total beam end deflections in all tests, although the joint core remained in the elastic range. In later cycles to greater displacement

TABLE 6.1 : MAJOR TEST VARIABLES AND RESULTS

Unit	B11	B12	B13A	B13B
Beam Top Reinforcement	8/D19	6/D19	6/D19	
Bottom Reinforcement	4/D19	6/D19	6/D19	
Joint Reinforcement	8 sets x 3/R12.7 ties	8 sets x 3/R12.7 ties	6 sets x 3/R12.7 ties	
Column axial load N (kN)	311	311	2890	1677
$N/f'_c A_g$ (design properties)	0.054	0.054	0.501	0.290
Maximum imposed beam end displacement ductility factor μ_{max} (see Section 2.7.1)	6.0	6.0	6.0	8.0
Total imposed cumulative displacement ductility factor $\Sigma\mu$	60.0	60.0	48.0	104.0
Maximum overstrength V_{col}/V_u	1.152	1.169	1.163	1.206
measured in load run	18	18	19	29
Maximum beam curvature ductility factor	12.60	13.03	11.32	7.00
measured in load run	11	11	11	29
Cumulative beam displacement ductility factor, $\Sigma\mu$, at which significant slip of beam bars across joint first occurred	28	28	-	94
Maximum crack width measured in joint panel (mm)	0.60	0.60	0.30	0.60
Cumulative beam displacement ductility factor, $\Sigma\mu$, at which yielding of joint reinforcement was first observed	20	36	48	-
Cumulative plastic strain in joint ties $\Sigma\varepsilon_{pl} \times 10^6$ (see Section 6.1.3)	840	80	185	8590

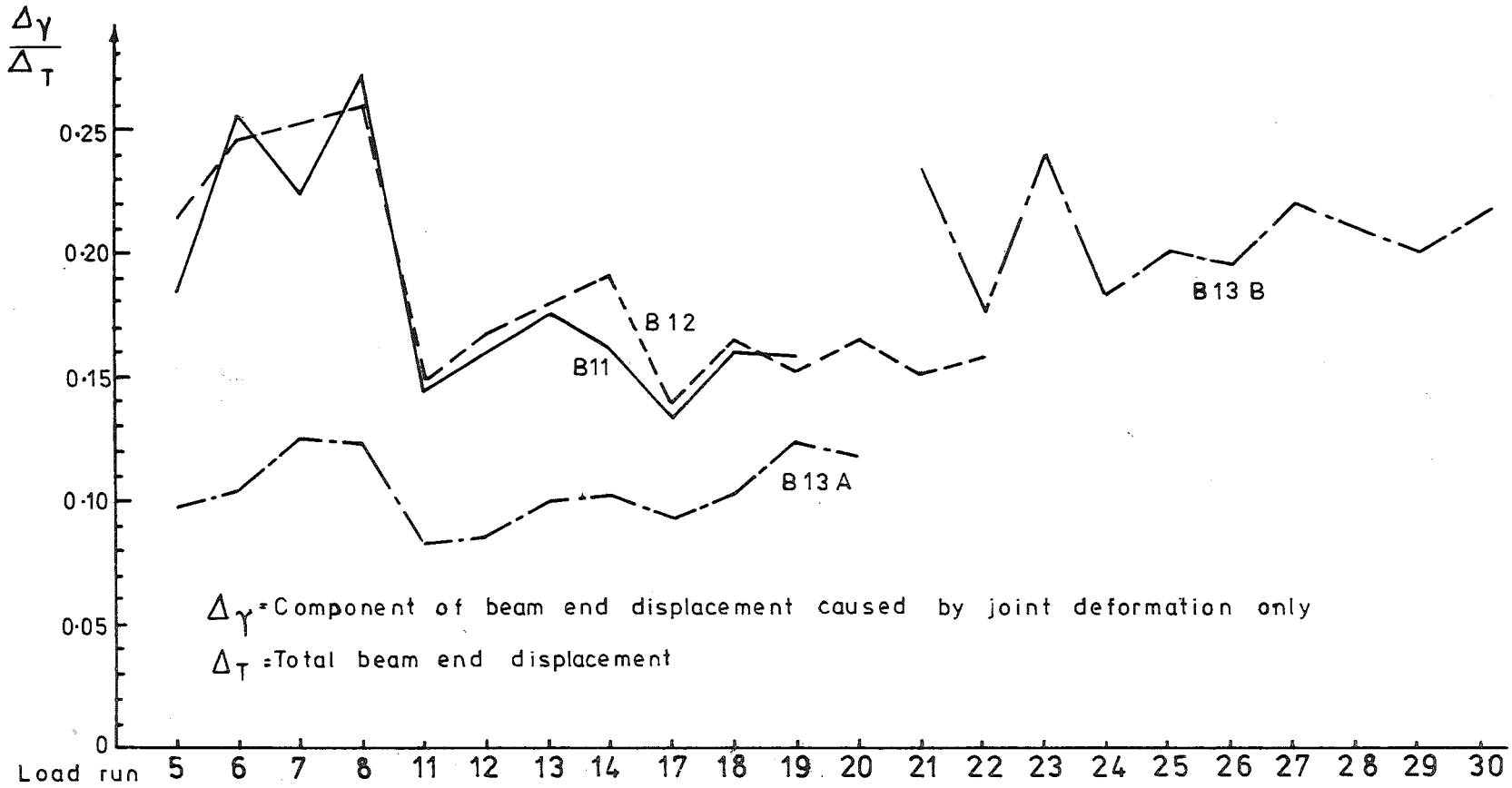

FIG.6.1 : COMPARISON OF JOINT DEFORMATIONS

ductility factors the joint cores were still responding in a basically elastic manner, with most of the inelastic deformation occurring in the beam plastic hinges. Since the loads did not increase much when greater displacement ductility factors were applied, the contribution of joint deformation to total beam end displacement decreased as a proportion.

In the case of units B11 and B12 severe slippage of beam bars through the joint from load run 17 onwards lead to some relief on the demand on other modes of displacement, including joint core deformation.

6.1.3 Strains in Horizontal Joint Shear Reinforcement

Envelopes of strain measured in the inner stirrup legs of joint reinforcement are presented in Fig. 6.2. The strains measured in outer legs of joint shear reinforcing followed similar patterns to those in the inner legs, but were rather smaller in magnitude, with yield strain never exceeded. Yield strain was exceeded in the inner legs at some stage during all the tests, but the extent of yielding recorded in tests B11, B12, and B13A was not considered to be serious (see Fig. 6.2). The yielding measured in test B13B was more significant, but the total cumulative displacement ductility applied during this test was more than would be likely to be required of a single element of a multi-degree of freedom structure in an actual earthquake, so that the yielding may not in fact be representative of prototype response.

The distributions of strain show that units B12 and B13, which had symmetrically reinforced beams, produced greatest strains in the mid-depth of the joint. However for unit B11, which had a ratio of top reinforcement to bottom reinforcement of two to one, the greatest strains tended to occur towards the top of the joint, where the total horizontal shear input was introduced by bond from the beam reinforcing, because flexural cracks never closed in the top of the beam.

A quantitative assessment of the total amount of yielding in the joint reinforcing in each test is given by the cumulative plastic strain $\Sigma\varepsilon_{pl}$ listed in Table 6.1. This quantity gives the strains in excess of yield strain measured in individual tie legs, summed over all the joint ties over the complete loading history for each test.

6.1.4 Horizontal Joint Shear Resisted by the Concrete Mechanism

Fig. 6.3 shows the proportion of the horizontal input shear resisted by the joint concrete mechanism at maximum displacement of each major load run during each test. It was assumed that since the direction of joint cracking was always the same as or steeper than the lines between

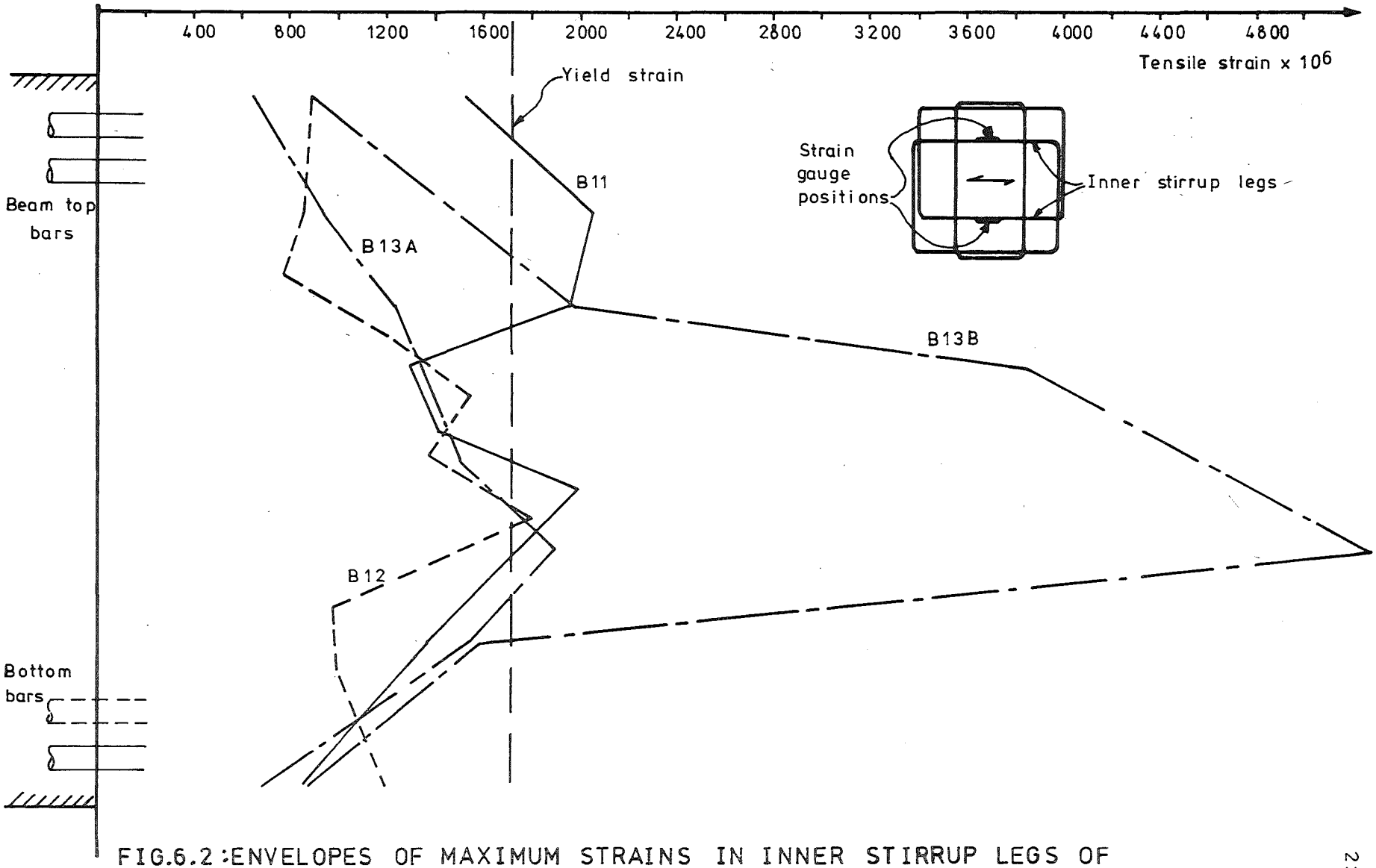

FIG.6.2 : ENVELOPES OF MAXIMUM STRAINS IN INNER STIRRUP LEGS OF JOINT REINFORCEMENT

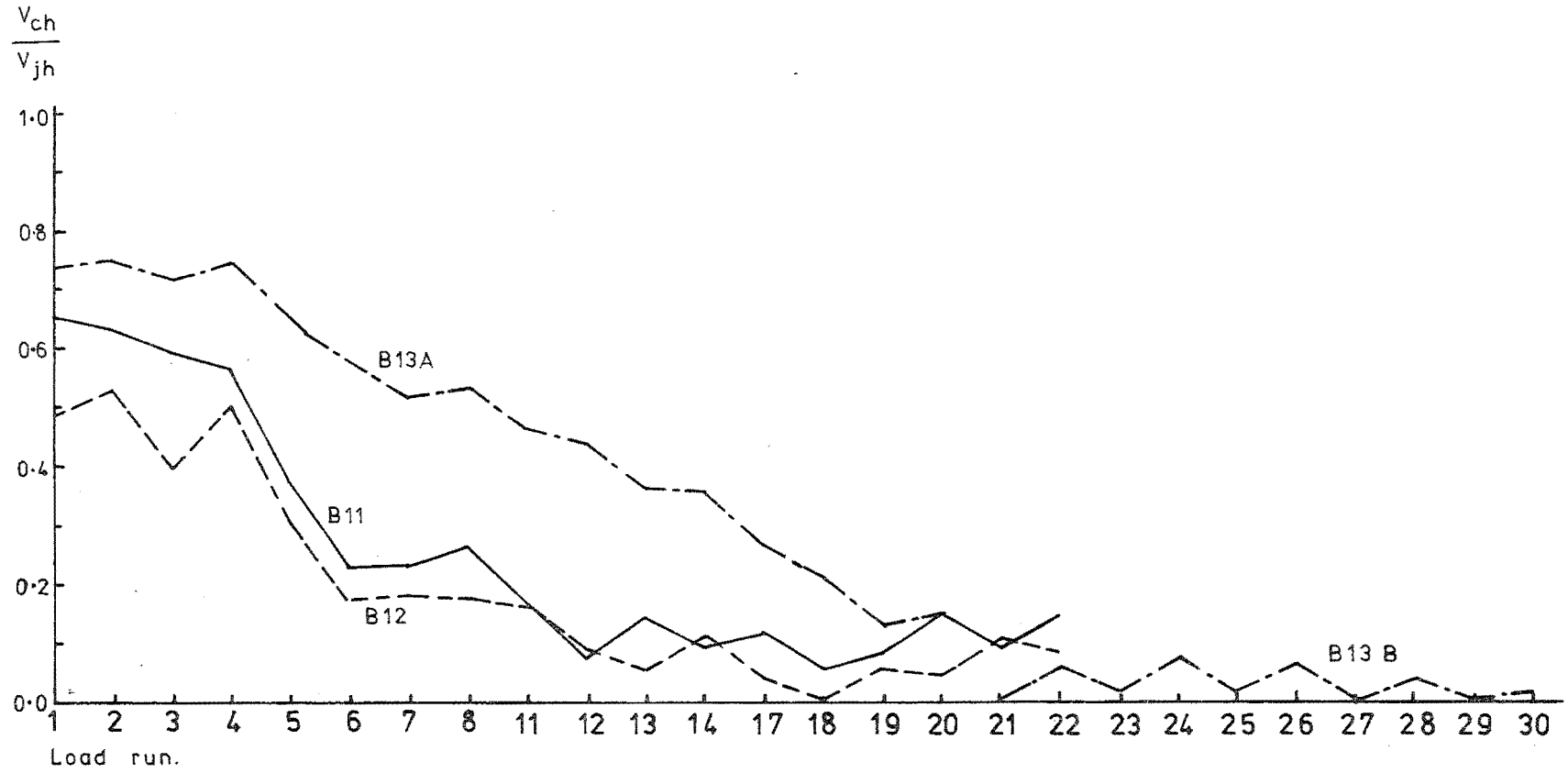

FIG.6.3: PROPORTION OF HORIZONTAL JOINT SHEAR RESISTED BY JOINT CONCRETE MECHANISM

diagonally opposite corners of the joint panel, then the horizontal shear resisted by the joint shear reinforcing could be calculated by summing the stirrup leg forces obtained from strain measurements over the depth of the joint. The shear resisted by the concrete mechanism was then obtained by subtracting this value from the total horizontal input shear. The figure shows that the concrete mechanism could resist a significant proportion of the horizontal joint shear in the initial elastic cycles, and in load run 5, which represented the case of monotonic loading. However, the contribution of joint concrete to horizontal shear resistance decreased dramatically as inelastic cyclic loading was applied. As explained further in Section 6.4 the penetration of yield strain in the beam flexural bars towards the centre of the column diminished the efficiency of the concrete shear transfer mechanism. The heavy column load applied in test B13A preserved the bond strength of the beam bars across the centreline of the joint, and this resulted in significantly more shear being resisted by the joint concrete mechanism in this case. By load run 17 the joint concrete mechanism in unit B13 was still resisting sufficient horizontal shear to justify the arbitrary allocation of 25% of the total joint shear resistance to this mechanism which was made for the design of this unit. This may be compared to the response of units B11 and B12, to which light axial load only was applied. The joint concrete mechanism resisted very little horizontal shear in these units by load run 17, which was also consistent with the design assumptions, which allocated zero resistance to the joint concrete mechanisms for these two units.

When the column axial load on unit B13 was reduced to $0.290f'_cA_g$ for test B13B, the joint concrete shear resisting mechanism deteriorated as shown in Fig. 6.3, and this is reflected in the increased joint flexibility shown in Fig. 6.1, and in the greater strains measured in the stirrup legs of joint reinforcement as shown in Fig. 6.2. The arbitrary design assumptions made for the design of the joint horizontal reinforcement was evidently inadequate for this case of axial loading.

6.2 Comparison With Other Test Results

6.2.1 Test of Blakeley, Megget and Priestley

A summary of a variety of tests carried out on beam-column joint units by various workers was given in Section 1.2. Certain results of these tests may be compared with the results reported here. The most interesting comparison is that between units B11 and B12 and the interior joint tested by Blakeley et al[17], which was in most respects approximately a 3/2 scale

enlargement of the present units, with a beam reinforcement configuration intermediate between those of units B11 and B12. The most notable point of contrast in the results is that whereas beam reinforcement was observed to slip across the joint core in both units B11 and B12, the beam bars did not slip across the joint core in the interior joint unit of Blakeley et al. This difference in behaviour occurred in spite of units B11 and B12 and the unit of Blakeley et al having similar axial load levels and identical ratios of column depth to beam bar diameter, h_c/d_b, while a greater displacement ductility factor (up to $\mu = 8.0$) was applied to the unit of Blakeley et al than units B11 and B12 ($\mu = 6.0$). Various explanations may be advanced to account for this difference in behaviour. Perhaps the chief amongst these might be the relatively smaller loads applied to the unit of Blakeley et al. The maximum column shear applied was only about 10% greater than that associated with the development of ideal ultimate flexural strengths in the two beams, while the actual yield strength of the beam flexural bars was the nominal strength of 275 MPa. This compared with a maximum overstrength of 16% in tests B11 and B12, and an actual yield strength of the flexural bars of 298 MPa. The reason for the smaller overstrength observed in the test of Blakeley et al was the much shorter time-scale over which this test was conducted, thus eliminating the strain-aging effect. Other factors which might have influenced the improved bond characteristics of the beam bars include the greater cylinder strength of the concrete (48 MPa compared to 35 MPa for B11 and B12), the presence of six vertical column bars in each column face (compared with four bars in B11 and B12), and the reduced flexibility of the joint panel due to greater joint reinforcing content. The behaviour of the joint panel and the joint shear reinforcing was very similar to that observed in the present tests, with the majority of the horizontal joint shear resisted by joint reinforcing, although the joint stiffness was somewhat greater.

6.2.2 Tests of Irvine and Fenwick

Comparison may also be made with the test results reported by Irvine and Fenwick[18]. Units 1 and 3 from this test series represented conventional joints, and severe slippage of beam reinforcement across the joint occurred in both cases. The h_c/d_b ratio for unit 1 was 15, which was clearly insufficient, but the ratio used in unit 3 was 25, which was slightly greater than the value of 24 appropriate to units B11 and B12, so that unit 3 might have been expected to respond at least as well as B11 and B12. However, it was noted by Irvine and Fenwick that the beam bars in unit 3 slipped as a group. This phenomenon was not apparent in the present tests, where it was shown by exposing the bars of unit B12

after the test was completed (see Fig. 4.17) that bond failure occurred for the bars individually, in spite of the relatively close groupings of bars in each corner of the beam section. Possibly the group bond failure noted in Irvine and Fenwick's tests occurred because of a scale effect in the smaller test units, or the absence of intermediate column bars may have adversely affected the bond performance of the beam bars. It is felt that the behaviour of the bigger test units with intermediate column bars included is more relevant to the response of full-scale prototype structures.

6.2.3 Tests of Uzumeri and Seckin

Uzumeri and Seckin in a recent report[22] concluded from the results of a series of tests on plane frame exterior joints that column axial load level has a negligible effect on joint shear strength, which is somewhat in contrast to the conclusions drawn from the present test series. Examination of the results published earlier by these authors[21], with regard to the more heavily loaded unit (Specimen 6), reveals that significant yielding of joint reinforcement occurred during this test resulting in degradation of stiffness and reduced efficiency of energy dissipation. The more recent paper does not describe yielding of joint reinforcement in the more lightly loaded unit, but it might be inferred from the similar shapes of the respective load-displacement curves that similar amounts of yielding occurred in the joints of both units. Inclusion of intermediate column bars allowed the joint truss mechanisms to continue to respond effectively even after yielding of the ties, so that the strength of the units at maximum displacement was not impaired by the yielding of the joint reinforcement. However it is felt that the degree of plasticity observed in the joints of both of these units was undesirable, and hence that the results cannot demonstrate the influence of column axial load on joint strength from the design point of view.

6.2.4 Other Tests

Most of the other test results described in Section 1.2 are of limited value for the purposes of correlation with the results of the present series, because inadequate strength in shear or in anchorage led to premature failure. This type of response is inappropriate either to the present tests or to desirable prototype behaviour.

6.3 Comparison with Published Recommendations for Joint Design

It was noted in Section 1.3 that the resistance of beam-column joint cores to shear in the horizontal direction may be considered as being supplied by two principal mechanisms. The first mechanism involves shear resisted by a diagonal compression strut across the joint core and requires some confining reinforcement only in the joint core. The horizontal joint shear resisted by this mechanism is often described as the shear, V_{ch}, resisted by the joint concrete, although the mechanism involved is quite different from that associated with the shear resistance of concrete in flexural members. To resist the remaining horizontal joint shear, V_{sh}, a truss mechanism which involves both horizontal and vertical joint reinforcement is necessary. For design, the quantities V_{ch} and V_{sh} must be evaluated so that the necessary reinforcing for a particular joint can be detailed. Recently published recommendations for joint design include equations by means of which this may be achieved. Table 6.2 gives a comparison of values of V_{sh} and V_{ch} determined from the test results, against the values used for design of the test units, and against values calculated using the appropriate equations from the 'Recommendations for Design of Beam-Column Joints in Monolithic Reinforced Concrete Structures' by the ACI-ASCE Committee 352[7], and from the draft New Zealand Concrete Code[5].

The design of the test units was based on the nominal material strengths, and strength reduction factor of $\phi_j = 0.85$ was used. All other values listed in Table 6.2 were calculated using actual material properties, with $\phi_j = 1.0$, since strengths and loads were known exactly.

The ACI-ASCE Recommendations give as the basic equation for the shear strength of joint concrete

$$V_{ch} = 0.3\beta\gamma\sqrt{f'_c}\left(1 + 0.3N_u/A_g\right).\ [b'.d_c] \qquad (6\text{-}1)$$

but $V_{ch} \leq {}^2/_3\ V_{jh}$

where β = 1.4 for Type 1 joints (no ductility requirement)
= 1.0 for Type 2 joints (ductility required in the adjacent beam plastic hinges)

γ = 1.4 if the joint is confined by beams in the transverse direction
= 1.0 otherwise.

f'_c = compressive strength of the concrete, MPa

N_u = minimum compressive axial load, N

A_g = gross cross-sectional area of column, mm^2

TABLE 6.2 : RESISTANCE TO JOINT SHEAR PREDICTED BY PUBLISHED RECOMMENDATIONS

Unit		B11	B12	B13A	B13B
f'_c (MPa)		35.9	34.6	31.4	
N_u (kN)		311	311	2890	1677
Design horizontal shear strengths (see Section 2.1)	V_{jh} (i)	979	979	979	
	V_{sh}	968	968	726	
	V_{ch}	11	11	253	
Horizontal shear strengths predicted by ACI-ASCE 352 Recommendations[7]	V_{sh}	1133	1239	885	885
	V_{ch}	322	316	301	301
	V_{jh}	1455	1555	1186	1186
	V'_{ch} (ii)	387	380	652 (iii)	555
	V'_{jh}	1520	1619	1537	1440
Horizontal shear strengths predicted by DZ3101 [5]	V_{sh}	1386	1386	1040	1040
	V_{ch}	0	0	385	260
	V_{jh}	1386	1386	1425	1300
Experimental horizontal shear strength results (load run 6)	V_{sh}	630	693	355	707 (iv)
	V_{ch}	188	147	485	43
	V_{jh}	818	840	840	750
Experimental horizontal shear strength results (load run 18)	V_{sh}	911	982	764	993 (v)
	V_{ch}	54	0	204	12
	V_{jh}	965	982	968	1005
Vertical shear strengths predicted by DZ3101[5]	V_{sv}	655	654	616	616
	V_{cv}	1036	1033	1817	1493
	V_{jv}	1691	1687	2433	2109

Notes: i) All shear force values in kN

ii) V'_{ch} = horizontal shear strength of joint concrete mechanism as calculated by Eq. (6-1) assuming N_u to be at the known value applied in test. $V'_{jh} = V_{sh} + V'_{ch}$.

iii) Limited by $V_{ch} < 2/3\ V_{jh}$.

iv) Load run 22.

v) Load run 30.

b' = effective width of joint to outside of ties, mm

d_c = effective depth of column, mm

V_{jh} = total applied joint horizontal shear.

It is suggested in the Recommendations that for Type 2 joints under earthquake attack the column axial load may be poorly defined, and should therefore be taken as zero. V_{ch} is therefore listed in Table 6.2 both as calculated with this assumption, and with the assumption that N_u is known to be at the level used in the tests.

The equation given in the Recommendations for the horizontal shear resisted by joint reinforcing

$$V_{sh} = \frac{A_v . f_{yh} . d_c}{s} \qquad (6\text{-}2)$$

where A_v = area of shear reinforcement within the distance s, mm^2

f_{yh} = yield strength of joint horizontal reinforcement, MPa

s = spacing between sets of joint reinforcement, mm.

The equations given in the Draft New Zealand Concrete Code for the horizontal shear strength of joints in plane frames are

$$V_{ch} = 0.25 \left(1 + \frac{f'_c}{25} \right) \sqrt{\frac{N_u}{A_g} - \frac{f'_c}{10}} \; [b_j . h_c] \qquad (6\text{-}3)$$

and $V_{ch} = 0$ if $N_u/A_g \leq f'_c/10$

and $V_{sh} = A_{jh} . f_{yh}$ (6-4)

where b_j = effective joint width (mm)
(= overall column width b_c in this case)

h_c = overall depth of column, mm

A_{jh} = effective total area of horizontal joint reinforcement crossing the joint diagonal.

Values of joint horizontal shear strength calculated using equations (6-1) to (6-4) are compared in Table 6.2 to the values derived from the test data at the maximum displacement of load run 6 (first inelastic reversal), and at load run 18 (after reasonably severe cyclic loading, first cycle to displacement ductility factor of six). As explained earlier (Section 3.5.4) experimental values of V_{sh} were calculated by summing forces derived from strain measurements in the individual stirrup legs over the depth of the joint, assuming the critical surface to be always inclined to the horizontal at an angle at least equal to that of the joint diagonal. It was noted in the tests that this assumption was always validated by the

observed angle of joint cracking during post-elastic loading. Values of V_{ch} were then obtained as the difference between the applied horizontal shear, V_{jh}, and the derived values of V_{sh}. Note that whereas equation (6-4) given by the Draft New Zealand Concrete Code for V_{sh} implies a comparable assumption for the angle of joint cracking, the equation (6-2) given in the ACI-ASCE Recommendations implies joint cracking at 45° to the horizontal.

Obviously the full strength of the joint horizontal reinforcement was not mobilised in any of the tests, but in all cases some limited yielding occurred in joint reinforcement, and it is considered that the design procedure (see Section 2.1), which was in general accordance with that suggested in the Draft New Zealand Code, resulted in efficient design. The joint reinforcing was not required to undergo large inelastic strains, but the available strength of the joint was fully utilized under severe cyclic loading. The diminution in the horizontal shear resisted by the concrete mechanism, as shown in Fig. 6.3, suggests that the values determined in load run 18 would give a good indication of the resistance which may be expected from this mechanism after severe seismic loading. Thus the zero recommendation given in the Draft New Zealand Concrete Code for joints with light axial loads (as in units B11 and B12) is quite realistic. The values for V_{ch} given in the ACI-ASCE Recommendations are optimistic in these cases, although the different assumption for the position of the critical joint surface leads to a conservative estimate for V_{sh}. However as mentioned above this assumption does not relate well to the experimental evidence, and it could lead to non-conservative results for joints in which the column depth exceeds the beam depth.

For the case where heavy axial load is applied to the joint (test B13A), the ACI-ASCE Recommendations are again optimistic if the known axial load is used in the equation for V_{ch}. If the axial load is taken to be zero as suggested for Type 2 joints, the value derived for V_{ch} is reasonable. However it seems rather illogical that the joint design procedure should assume that a designer cannot estimate the limits on the axial load acting on a given joint, although he must make some such assessment for the purposes of column design. The Draft New Zealand Code recommendations in this case give a value of V_{ch} intermediate between those determined at load runs 6 and 18.

It is apparent that the values of V_{ch} reached in test B13B are much less than predicted by either recommendation. However as pointed out previously the total ductility demand imposed on this unit during the

tests was considered to be excessive, and hence the bond conditions for the beam bars in particular were unrealistic. Thus it is considered that this result is not very relevant to actual structural performance, and may therefore be discarded.

Table 6.2 also gives values for the vertical shears resisted by joint concrete and reinforcement mechanisms, V_{cv} and V_{sv} respectively. These quantities were calculated using the appropriate equations from the Draft New Zealand Concrete Code, as follows:

$$V_{cv} = \frac{A_{sc}}{A'_{sc}} \frac{V_{jv}}{2} \left(1 + \frac{N_u}{0.6A_g f'_c}\right) \qquad (6\text{-}5)$$

where A_{sc} = lesser area of column flexural steel in tensile or compressive face at the joint (mm^2)

A'_{sc} = greater area of column flexural steel in tensile or compressive face at joint (mm^2)

V_{jv} = total vertical shear force across the joint

and $V_{sv} = A_{jv}.f_{yv}$ (6-6)

where A_{jv} = total area of vertical joint reinforcement (mm^2)
(= area of 4/D22.2 intermediate column bars in this case)

f_{yv} = yield strength of vertical joint reinforcement.

The ACI-ASCE Recommendations make no provision for resistance to vertical joint shear.

No exact results could be derived from the test data to check these equations. However strains measured in the intermediate column bars of units B11 and B12 during the tests (see Figs.3.30,4.24) were substantially below yield, while in test B13A the intermediate column bars were in compression throughout the test (see Fig. 5.26). Since the actual applied vertical shears were up 2100 kN it is apparent that values of V_{cv} of up to 1600 kN in tests B11 and B12 and up to 2100 kN in test B13A, were available throughout the tests, so that equation (6-5) may be somewhat conservative.

Possible modifications to equations (6-3) and (6-5) are suggested in Section 6.6.

6.4 Comparison with Postulated Mechanism of Resistance

A postulated mechanism of resistance to joint shear was outlined in Section 1.3. In the proposed mechanism part of the input joint shear was resisted by the joint concrete acting as a direct diagonal strut, and part of the shear was resisted by joint reinforcement acting as a truss. During the analysis of the test results for each unit the horizontal shear

resisted by joint core reinforcing, V_{sh}, was determined at the maximum displacement of each load run by summing the individual stirrup leg forces down the full depth of the joint, as described in Chapters 3 to 5. The horizontal shear resisted by joint concrete mechanism, V_{ch}, was then determined by subtraction. The proportions V_{ch}/V_{jh} at maximum displacement of each load run are shown in Fig. 6.3.

According to the postulated mode of joint concrete shear resistance for joints carrying little or no column axial load, the direct concrete strut acts between the concrete compression forces in the flexural members (see Fig. 1.4). This implies that very little horizontal shear will be resisted by the joint concrete mechanism once cyclic loading in the inelastic range has commenced, due to the permanently open flexural cracks and the consequently small compression forces carried by the beam concrete. This prediction was substantiated in the tests of units B11 and B12 by the difference noted in the proportions V_{ch}/V_{jh} determined in load runs 1 to 4, the initial elastic cycles, and load run 5, which represented monotonic inelastic conditions, as compared to the proportions calculated in the subsequent load runs, where cyclic inelastic conditions prevailed.

In the case of unit B11, where the beam reinforcing configuration was unsymmetrical, significant compression was carried by the concrete in the bottom of the beam, but none in the top. The shape of the strain distributions measured in the joint reinforcing down the depth of the joint indicated that in this case a composite mechanism operated whereby some shear resistance was transferred from a direct concrete strut at the bottom of the joint to the steel truss towards the top of the joint.

It was further postulated in Section 1.3 that when significant axial compression is applied to the joint sufficient bond forces might be acquired from the beam bars to provide a horizontal component for the direct concrete strut, even under cyclic inelastic conditions. This prediction was verified by test B13A, where significant proportions of the horizontal joint shear were found to be resisted by joint concrete during inelastic cycles, although the proportion decreased throughout the test as penetration of yield strain in the beam bars into the joint core increased.
In test B13B the reduction in column axial load shifted the centre of concrete compression in the column sections above and below the joint core so that much less horizontal shear could be picked up from the beam bar bond forces to form an effective diagonal strut. This resulted in the much lower proportions of joint horizontal shear resisted by the joint

concrete mechanism in this test, as shown in Fig. 6.3.

From these results it appears that the crucial factors in promoting effective shear resistance by the joint concrete are the column axial load level and the extent of beam reinforcement yield penetration into the joint. In all cases of significant cyclic loading it is likely that some yield penetration will occur, while concrete compression forces in the beam plastic hinges will be small at the level of at least one of the principal reinforcement areas. However if a significant part of the concrete compression force in the column can act with bond forces from the central length of beam flexural steel over which bond is still effective, then a valid direct diagonal strut mechanism may be formed. The various possibilities are illustrated in Fig. 6.4, in which the actions in the column and joint reinforcing are omitted in order to show clearly the action of the concrete direct strut mechanism.

A small increase in the horizontal shear resisted by the joint concrete mechanism was noted in the final stages of tests B11 and B12. This was caused by the onset of severe slippage of the beam bars across the joint, resulting in some compression again being carried by beam concrete at the column face, so that to a small extent the situation illustrated in Fig. 6.4(a) again applied. However, the slip failure is not a desirable design objective and the concrete contribution at this stage is not therefore significant.

The balance of the horizontal joint shear was resisted by horizontal joint reinforcement. It was postulated in Section 1.3 that this would be achieved by a truss mechanism involving joint ties as horizontal members, column bars and column axial load (in excess of that required for the concrete mechanism) as vertical members, and diagonal concrete struts as inclined members. The test results showed that the majority of the horizontal shear was resisted by this truss mechanism, especially in tests B11 and B12, where the column load level was small. Although the extensive instrumentation used was able to define the horizontal actions in the joint reinforcement quite precisely, the vertical actions were less well verified. However, measurements of strain from the column bars within the joint showed that tensions additional to those corresponding to a linear strain gradient across the joint were present in the intermediate column bars in tests B11 and B12, and these were attributed to the vertical action of the truss. During test B13, additional compression strains were noted in the column bars, and this was considered to be due to the weakening of the surrounding joint concrete by diagonal cracking, which required the column bars to

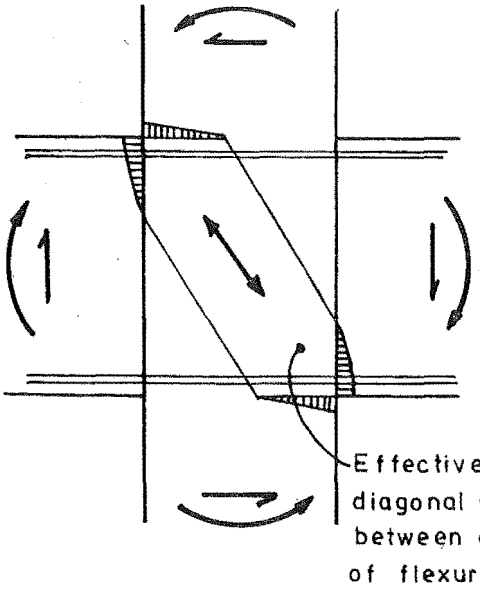

(a) Zero column load, elastic or monotonic inelastic loading

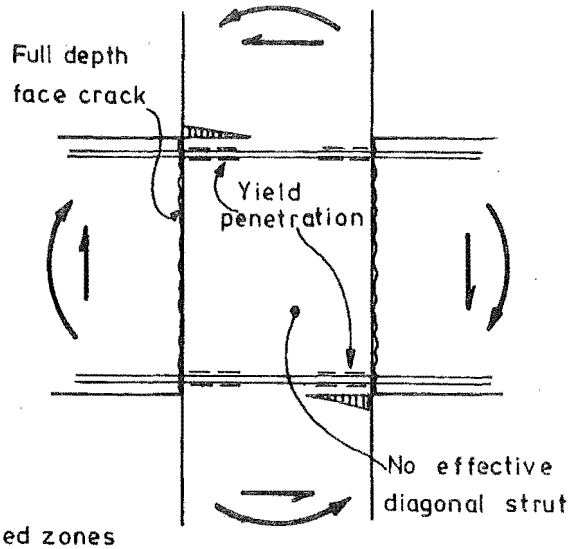

(b) Zero column load, cyclic inelastic loading

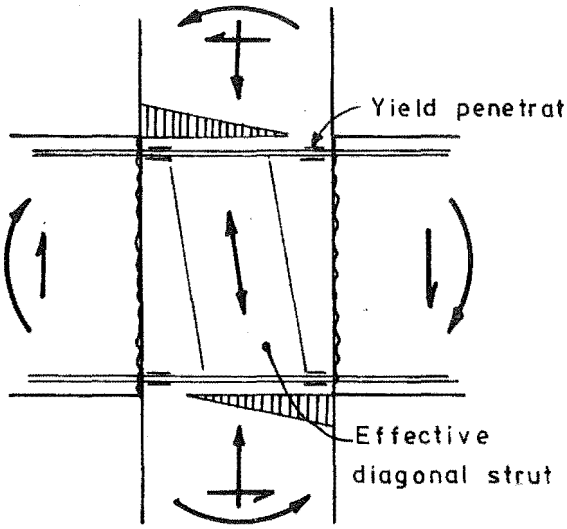

(c) Significant column load, limited yield penetration, cyclic inelastic loading

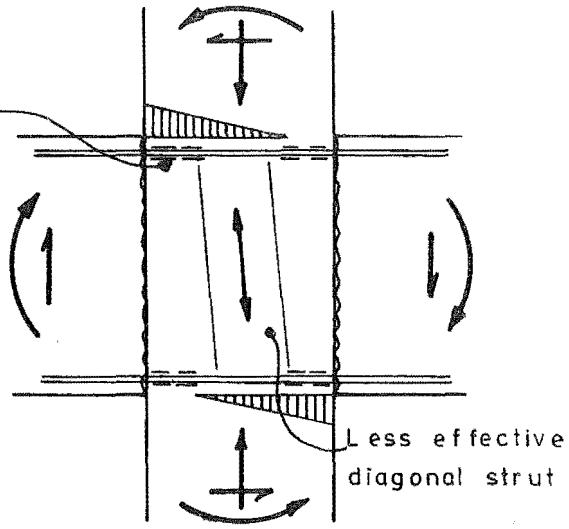

(d) Significant column load, increased yield penetration, cyclic inelastic loading

FIG.6.4: OPERATION OF DIRECT CONCRETE STRUT MECHANISM FOR SHEAR TRANSFER UNDER VARIOUS CONDITIONS

carry more of the compressive load. In this case it is apparent that most of the vertical component of the truss mechanism was applied by the concrete. In all cases, calculations show that the reinforcement alone was insufficient to carry the applied vertical joint shear, so that participation of the concrete in resisting vertical joint shear had to be sustained at significant levels throughout the tests. This was possible due to the absence of wide flexural cracks in the column, since the column reinforcement did not yield. This allowed significant concrete compression forces to be carried by the concrete in the column sections immediately above and below the joint, at all stages of each test.

Relationships between horizontal and vertical shears were calculated at all stages of the tests (see Figs. 3.36 , 4.29 , 5.35). It was concluded that the angle of resistance to joint shear followed the angle of inclined cracking quite closely. Diagonal cracks were observed at inclinations approximately equal to that of the joint diagonal in tests B11, B12 and B13B, but they developed at a much steeper angle in test B13A.

6.5 Effect of Joint Performance on Overall Structural Response of Frames

The performance of the joints of a framed structure under earthquake attack is likely to have some influence on the overall response of the structure. For example these tests showed that the flexibility of the joints was quite significant, accounting for up to 27% of the total deformation of the beam-column unit, as shown in Fig. 6.1. This observation contrasts with the conventional design practice of assuming joint panels to be infinitely rigid for the purposes of analysis under lateral loading.

A prominent aspect of the response of all the test units was the phenomenon of stiffness degradation, which was caused by a variety of factors including joint cracking, sliding shear displacement in the beam plastic hinges, penetration of yielding of the beam reinforcement into the joint core, and in some cases slippage of the beam bars across the joint core. These factors are discussed in detail in the individual test reports in Chapters 3 to 5. As a result of the degradation of stiffness under cyclic loading, the efficiency of energy dissipation was also much less than might be predicted by assuming an idealised bilinear-elastic load displacement response. The comparative efficiency in energy dissipation for each test unit during each major load run is given in Fig. 6.5. The actual energy dissipated in each load run was taken as the area under

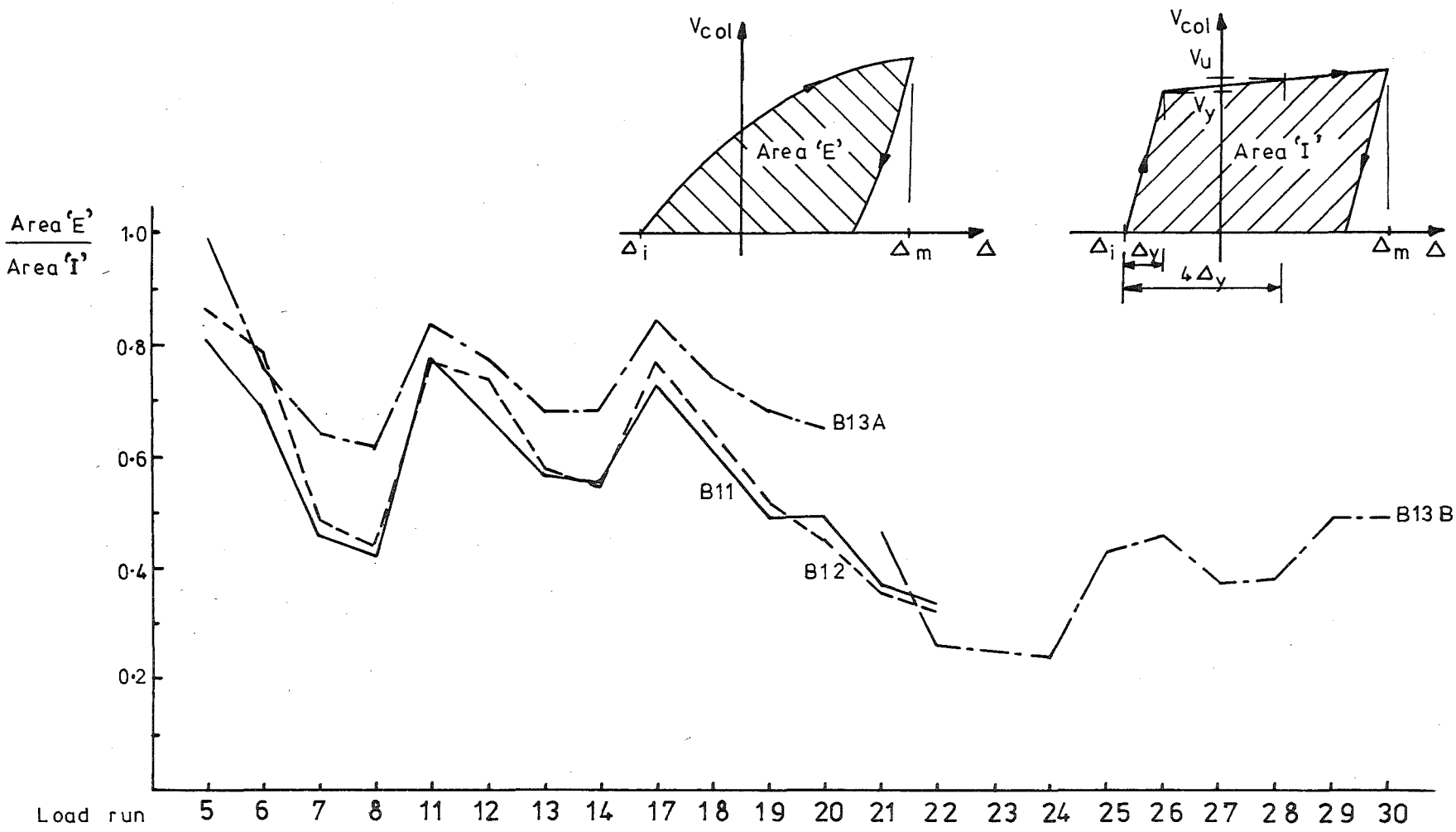

FIG.6.5:COMPARISON OF EFFICIENCY OF ENERGY DISSIPATION

a curve giving the measured relationship between column shear and storey sidesway displacement, without any correction having been applied for the 'P-delta' effect. This was compared to the energy indicated by the area under a bilinear curve fitted between the measured initial displacement Δ_i and the measured maximum displacement Δ_m, as shown in Fig. 6.5. The initial slope of this idealised curve was given by

$$k_e = \frac{V_y}{\Delta_y} \qquad (6\text{-}7)$$

where V_y is the column shear at which yield strain was calculated to be first attained in all the beam tension reinforcing, and Δ_y is the experimental yield displacement, extrapolated from the measurements taken in load run 1, as explained in Section 2.7. The slope, k_1 of the second or strainhardening part of the idealised curve was derived by assuming that the ideal flexural strength of the unit, V_u, was obtained at a displacement ductility factor of four.

Thus
$$k_1 = \frac{V_u - V_y}{3\Delta_y} \qquad (6\text{-}8)$$

where V_u is the column shear corresponding to the beam end loads P_u necessary to cause the ideal ultimate flexural strength to be attained in the beams at the column face, where steel stress does not exceed the (actual) yield strength, and maximum concrete strain in compression is 0.003. The stiffness on unloading was again taken to be k_e.

It is apparent from Fig. 6.5 that the efficiency in energy dissipation in the tests was much less than in the ideal case, although unit B13A, to which the heaviest axial load was applied, showed the best response. In all test units the efficiency of energy dissipation decreased during repeated cycles at a given ductility factor. The loss of energy dissipation capability implies that if the earthquake motion continues with the same or a greater level of input energy as that which caused a particular level of ductility to be imposed in a given location, then the ductility demand at that section will increase. Alternatively the energy may be dissipated at some other location in the structure, redistribution of load occurring as a result of the reduced stiffness at the original location. The reduced stiffness will also affect the response of the structure to the earthquake.

Attempts have been made by several researchers to perform time-history dynamic analyses of structures under earthquake attack taking the

degrading stiffness phenomenon into account. The first major effort in this direction was made by Clough [37] who reported analyses of single degree of freedom structures using the load-displacement relationships shown in Figs. 6.6(a) and (b). Various combinations of earthquake acceleration record, building period, damping, building strength, and strain hardening properties were employed, and comparison was made with the response of the equivalent elasto-plastic or bilinear system. The conclusion drawn from Clough's study was that the difference in ductility demand computed for the two types of load-displacement response was not very great, except for buildings of very short periods ($T < 0.6$ sec.), for which the degrading stiffness system required greater ductility. Apart from this rather broad trend of the results, no straightforward correlation of the responses of the degrading stiffness systems to those of systems having conventional (non-degrading) properties could be established.

Obviously the results of a single degree of freedom analysis must be treated with some caution when one seeks to apply them to a multi-degree-of-freedom structure such as a multistorey frame building. Chopra and Kan [38] provided some additional results which go some way to rectify this situation. The analyses which they reported were performed using Clough's bilinear degrading stiffness model (Fig. 6.6(b)) as the storey shear-sidesway relationship from an 8-storey shear building. Again the results were compared with those obtained from analysis of the equivalent bilinear hysteresis system, using buildings with fundamental periods of 2.0 seconds and 0.5 seconds. Similar trends were observed to those noted in Clough's study, although the authors point out that particular conclusions drawn from the single degree of freedom analysis cannot be accurately extrapolated to the multi-degree-of-freedom system. Again no simple or consistent relationships between the ductility demands computed for conventional bilinear and degrading hysteresis systems was apparent, although the effect of degrading stiffness was greater for the stiffer building ($T = 0.5$ secs) than for the more flexible building ($T = 2.0$ secs), The authors suggest that the changes in ductility requirements due to degrading stiffness are generally less than those associated with the variation from one earthquake record to another of similar intensity. A caution is also sounded to the effect that more refined analyses than that reported would be necessary to define precisely the local member ductility requirements, which cannot be extracted from an analysis in which only storey drift is modelled at each level.

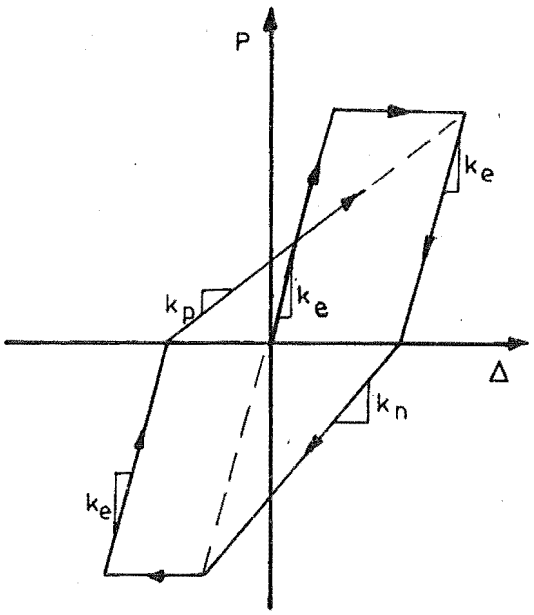

(a) Clough's ordinary degrading stiffness model[37]

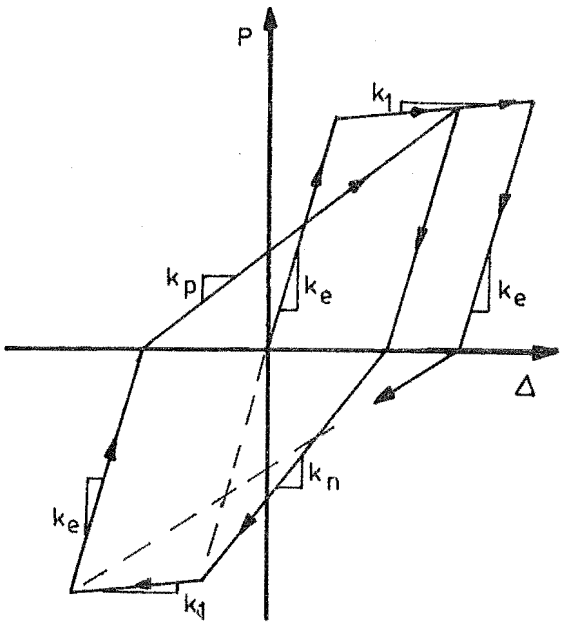

(b) Clough's bilinear degrading stiffness model[37]

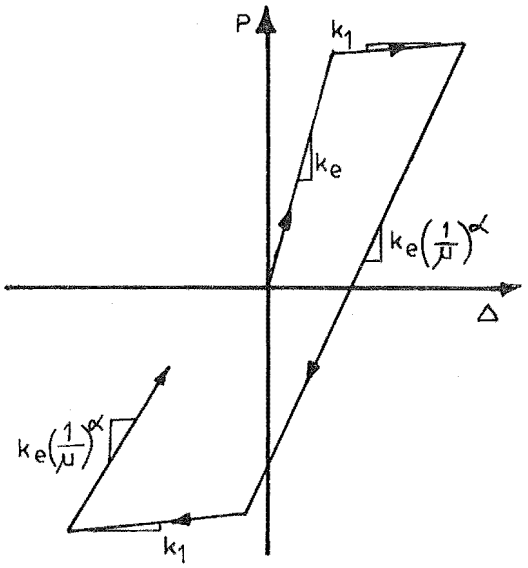

(c) Imbeault and Nielsen's degrading bilinear model[39]

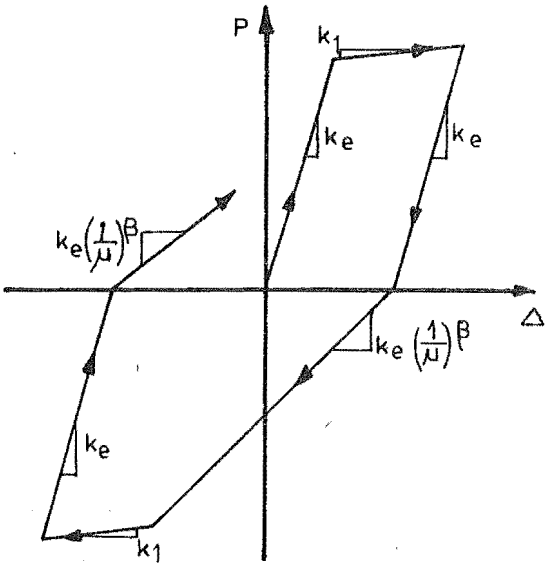

(d) Anderson and Townsend's degrading trilinear model[40]

FIG·6·6 : VARIOUS DEGRADING STIFFNESS MODELS PROPOSED FOR REINFORCED CONCRETE MEMBERS

An alternative approach to the modelling of the degrading stiffness characteristic was presented by Imbeault and Nielsen[39], who utilized a moment-curvature relationship in which the curve shape was basically bilinear, as shown in Fig. 6.6(c). The strain hardening stiffness k_1 was unchanged throughout the loading history, but the instantaneous 'elastic' stiffness was reduced, depending on the extent of previous yielding, so that

$$k = k_e \left(\frac{1}{\mu}\right)^{\alpha} \qquad (6\text{-}9)$$

where μ = current maximum ductility factor and $0.5 < \alpha < 0.6$.

Although this model is much easier to handle computationally than Clough's model, it does not represent the actual response of the structure as effectively, since the change in stiffness observed on reversal of load is not included in the model.

An extention of this approach was given by Anderson and Townsend[40] who described analyses conducted using various moment-rotation models. As well as the conventional bilinear hysteresis model and Imbeault and Nielsens' degrading bilinear model, a degrading trilinear model was defined as shown in Fig. 6.6(d). For this model the unloading stiffness and the strain hardening stiffness were unchanged, but the reloading stiffness was reduced in all post-yield situations.

$$k = k_e \left(\frac{1}{\mu}\right)^{\beta} \qquad (6\text{-}10)$$

where $\beta = 1.5$.

An additional model, described as the 'degrading trilinear connection' model, was also employed in which all stiffnesses defined for the previous model were divided by four to account for overall stiffness reduction due to joint deformation, beam bar slip, etc. This model was applied only over the beam plastic hinge length, whereas the others were applied to the members as a whole. The results of the analyses indicated that the definitions of both these trilinear load-displacement relationships were too severe, because positive and negative loading stiffness were not differentiated between. Hence the models cannot represent accurately any but very poorly designed structures in which chronic joint deformation and bar slip occur.

From this discussion of some published analyses it is apparent that the best available results from which conclusions might be drawn regarding overall structural response due to degrading stiffness are those

presented by Chopra and Kan. These results indicate that the ductility demand at any given location would not differ greatly from that required of a structure having conventional bilinear hysteresis characteristics. The reason that this occurs in the analyses is that once yield has occurred in the degrading stiffness model, energy is dissipated in all subsequent reversals of loading, whereas in the bilinear model energy is dissipated only when yield load is reached in either direction. This factor tends to compensate for the reduced energy dissipation achieved in major cycles by the degrading stiffness model, and is probably reasonably consistent with the actual structural response.

It seems likely, therefore, that the loss of stiffness of the beam-column joint assembly due to joint cracking and deformation, beam shear displacement, and beam steel yield penetration, would not have a very severe effect on the overall response of the structure. If severe stiffness degradation due to slip of beam bars across the joint is encountered, however, the ductility demand may increase significantly. It is unlikely that the ability of a beam-column assembly to attain full load at maximum displacement under these circumstances will be compromised, unless the compressed concrete in the beam crushes and reduces the effective beam cross-section. This possibility arises because the 'compression' reinforcement in either beam would be carrying near full yield load in tension from the beam at the opposite face of the column due to the loss of anchorage. Thus the concrete alone could be required to carry twice the compression force calculated assuming the beam to be singly reinforced. Clearly this situation is undesirable in terms of ductile beam plastic hinge behaviour, for which significant effective compression reinforcement is required. The effect on the energy dissipation capability of the affected joint would also be severe, since the load-displacement loops would enclose virtually no area over a wide range of displacement, because the assembly could resist very little load until the cracks closed up and the required compression forces were developed in the beam concrete. However it must be remembered that the occurrence of beam bar slippage represents an extreme response, which is unlikely to be encountered in joints designed in accordance with the recommendations outlined in this chapter. In a frame having several bays, the likelihood of severe slippage occurring simultaneously in all joints of a given bent must be remote, while redistribution of load laterally to other bents will tend to protect a frame weakened by such slippage failure. In a frame having only two bays it may be prudent for

the designer to pay particularly generous attention to the anchorage of the beam reinforcing in the exterior columns.

A further qualification needs to be stated with respect to the overall structural response of a frame. The effect of the chosen loading sequence and the validity of that sequence in relation to the actual response must be considered. From computer-based time-history analyses such as those mentioned above, and from certain trends in the experimental data, it seems likely that even perfectly symmetrical structures are likely to respond assymetrically to earthquake ground motions. It was noted in the tests that response tended to be stiffer in the direction of first yielding than in the direction of reversed loading, and reports on dynamic analyses[6] frequently note the occurrence of permanent set, with oscillation about an off-centre point on the load-displacement relationship after the initial yield excursion. The effect on the performance of the test unit of such off-centre oscillations is difficult to assess, although the total cumulative displacement ductility factors applied lend some confidence that the results will be conservative. In test B13 the heavy axial loads caused significant P-delta effects in the net column shear versus storey sway relationships, and this phenomenon could tend to exaggerate the problem of assymetrical response. Experimental studies comparing the response of similar test units to symmetrical and assymetrical cyclic loading sequences would be very useful to clarify this point.

6.6 Recommendations for the Design of Interior Beam-Column Joints in Plane Frames

6.6.1 Bond Strength of Beam Bars Across the Joint

As a simple design rule to reduce the likelihood of slippage failure of beam flexural bars across the joint under seismic loading, a limit may be placed on the ratio of the overall column depth to the maximum beam bar diameter, h_c/d_b. From the results of the present tests and of earlier tests[17,19], a minimum value of 25 appears to be appropriate for this ratio for Grade 275 deformed steel bars. For higher strength bars the ratio should be increased.

While other parameters such as the concrete strength and the absolute value of the column depth are also expected to have some effect on the resistance of beam bars to slippage failure, insufficient evidence is available at present to justify any more complicated design rule than that described above.

The results of test B11 showed that where beams are not symmetrically reinforced, and the larger area of reinforcement includes at least two layers of bars, then the bond requirement for bars in an inner layer of the larger area of reinforcement is less than that for bars in the outer layer, or for bars in the smaller area of reinforcement. Thus these inner layer bars could be of larger diameter than is required to meet the requirements given above, although the designer may not always wish to mix bar sizes, since the likelihood of construction errors may be increased.

6.6.2 Determination of Actions on the Joint Core

As described in Section 1.3, the horizontal shear, V_{jh}, applied to a beam-column joint may be calculated from the maximum likely overstrength of the beam flexural bars, less the shear in the column above.

$$V_{jh} = (A_{sb} + A_{st}) . \alpha . f_y - V_{col} \qquad (6\text{-}11)$$

where A_{st} = area of top reinforcement
A_{sb} = area of bottom reinforcement
α = overstrength factor
f_y = specified yield strength of beam reinforcement
V_{col} = column shear.

A value of the overstrength factor $\alpha = 1.25$ is commonly used for steel bars of Grade 275 in New Zealand[5,8] and this value was used in the design of the present test units. During the course of the tests strain hardening of beam reinforcing steel occurred when displacements were applied to a ductility factor of four, and strain hardening combined with the actual yield strength of the bars caused the total horizontal shear inputs in some cases to exceed slightly the design input shear calculated in accordance with Eq. (6 11). In normal circumstances this overload would be accommodated by the use of the strength reduction factor ϕ_j, and by the likely overstrength of the joint reinforcement. Nevertheless designers should be aware that the use of an overstrength factor of $\alpha = 1.25$ for Grade 275 steel does not preclude the possibility that the design joint shear may be exceeded under severe seismic loading. It is desirable that designers should know the actual properties of the particular beam steel to be used as exactly as possible when the design of the joint is undertaken.

The vertical joint shear V_{jv} to be considered for design of the joint may be derived from consideration of the forces in the column sections when appropriate actions are applied to the joint to produce the design horizontal shear.

6.6.3 Resistance of the Joint to Horizontal Shear

For design purposes the resistance to the horizontal joint shear, V_{jh}, may be allocated to the concrete direct strut mechanism, V_{ch}, and to the truss mechanism, V_{sh}, for which joint reinforcement is required:

$$V_{jh} = \phi_j(V_{sh} + V_{ch}) \qquad (6\text{-}12)$$

It is common practice in the strength design of reinforced structures to apply a strength reduction factor ϕ to the ideal strength, to allow for defects in workmanship or materials, approximations in design equations, and the consequences of the particular mode of failure. A value of $\phi_j = 0.85$ is considered to be reasonable for joint design.

Discussion of the postulated mechanisms of joint shear resistance in Sections 1.3 and 6.4 showed that compressive loads must be carried by the joint concrete diagonally across the joint panel in both principal mechanisms of resistance. The diagonal concrete struts required across the joint for the concrete direct strut mechanism and for the truss mechanism are shown in Figs. 1.4 and 1.5 respectively. To guard against compressive failure of the diagonal struts it is necessary to impose limits on the total horizontal shear force which may be applied to the joint. The draft New Zealand Concrete Design Code[5] requires that

$$V_{jh} < 1.5\phi_j\sqrt{f'_c} \cdot b_j \cdot h_c \qquad (6\text{-}13)$$

while the recommendations of ACI-ASCE Committee 352[7] provide that

$$V_{jh} < 1.66\phi_j\sqrt{f'_c} \cdot b' \cdot d_c \qquad (6\text{-}14)$$

For columns within reasonable dimensional limitations (less than 1600 mm square, with cover to centroid of longitudinal bars 50 mm), the smaller area over which the limiting stress is considered in Eq. (6-14) results in a slightly smaller maximum value for V_{jh} than is obtained from Eq. (6-13). Since some separation of the joint cover was observed during the tests, an equation such as Eq. (6-14) which is based on the core area of the joint, rather than on the gross area, may give a limit for the strength of joints which is more consistent with experimental evidence.

Since neither the present test series nor many others have included joints which failed in compression, it is impossible to comment from a basis of experience on the limits given in Eqs. (6-13) and (6-14). However both equations will give rise to maximum diagonal compression stresses substantially less than the cylinder strength of the concrete, and this is in accordance with test observations. Fig. 3.4, for example, shows extensive diagonal cracking in both directions in the joint panel after the application of severe cyclic loading, and this would undoubtedly result in considerably reduced strength in diagonal compression.

The presence of significant column axial loads may be expected to cause greater compressive stresses in the joint core. However the presence of heavy axial load also reduces the extent of diagonal cracking in the joint panel (see Fig. 5.3), and this should mean that more compressive strength is available in this case. Hence the column axial load need not be considered as a parameter affecting Eqs. (6-13) and (6-14) in the general case. However, if there is likely to be a wide range of axial loads applied to the column, the joint could be extensively cracked under light axial load, and then be required to carry greater compressive stresses under heavy axial load. In this situation the designer would be wise to take a lower value for the limiting horizontal shear force.

In all cases transverse confining reinforcement should be placed through the joint at a similar density to that required in potential plastic hinges elsewhere in the columns[5,7].

6.6.4 Resistance of the Concrete Direct Strut Mechanism to Horizontal Joint Shear

It was shown in Section 6.3 that Eq.(6-1) for the horizontal shear resistance of the joint concrete mechanism, given in the recommendations of ACI-ASCE Committee 352[7], did not reflect the performance of the test units very accurately. By contrast Eq. (6-3), given in the draft New Zealand Concrete Design Code[5], predicted the resistance of the test units quite reasonably. Consequently an equation of similar form to Eq. (6-3) is proposed for design.

However, inspection of Eq. (6-3) reveals an anomaly insofar as the influence of concrete strength, f'_c, on the strength of the joint concrete mechanism is concerned. The concrete cylinder strength has no direct influence on the strength of the concrete direct strut mechanism, which depends largely on the presence of suitable boundary conditions.

The joint shears must be introduced to the joint core so as to allow suitable end reactions to the diagonal strut to be obtained. The concrete strength thus has some influence on the effectiveness of the mechanism, because stronger concrete will result in greater bond strength for the flexural bars across the joint. This will result in more bond forces from the bars being introduced closer to the corners of the joint panel, which provides more effective end conditions for the direct strut. This improvement is not always reflected by Eq. (6-3).

Therefore it is suggested that the strength of the concrete direct strut mechanism may be more effectively stated as:

$$V_{ch} = 0.25\left(1 + \frac{f'_c}{25}\right)\sqrt{\frac{N_u}{A_g} - 2.5}\left(b_j \cdot h_c\right) \qquad (6\text{-}15)$$

where the constants 25 and 2.5 have the units of MPa,

and $V_{ch} = 0$

if $\frac{N_u}{A_g} \leq 2.5$ MPa.

This equation results in a value of 396 kN for the predicted strength of the joint concrete mechanism in test unit B13A. Table 6.2 shows that this compares well with the values observed in the test.

Fig. 6.4 shows conditions by means of which the effectiveness of the concrete direct strut mechanism may be enhanced. It is apparent that if penetration of beam bar strains in excess of yield strain into the joint core can be reduced, then the resistance of the joint concrete mechanism to horizontal shear may be expected to increase. Thus it is possible that a parameter reflecting this should be included in an equation for the evaluation of V_{ch}. The obvious parameter to use for this purpose is the ratio h_c/b_d of column depth to beam bar diameter. However, since no test results are available pertaining to test units with values of the h_c/d_b ratio greater than the minimum value suggested in Section 6.6.1, it is impossible to evaluate the quantitative effect of this parameter on the resistance of the concrete mechanism.

6.6.5 Design of Joint Horizontal Shear Reinforcement

Joint reinforcement must be provided to resist the shear not carried by the concrete mechanism. The usual form of horizontal joint reinforcement provided consists of stirrup ties enclosing the column longitudinal bars. The truss mechanism by means of which this reinforcement

is postulated to resist horizontal shear is illustrated in Fig. 1.5. It was noted in the test that the angle of diagonal cracking in the joint panel under cyclic inelastic loading was always equal to or greater than the inclination of the joint diagonal. Thus it is recommended that the horizontal shear resistance of joint reinforcement may be given by the sum of forces in ties crossing a potential diagonal crack, as stated in Eq. (6-4)

$$V_{sh} = A_{sh} \cdot f_{yh} \qquad (6\text{-}4)$$

Short tie legs were shown to make some contribution to the resistance of horizontal joint shear, but they were not loaded as effectively as the tie legs which extended over the full depth of the joint. The draft New Zealand Code[5] recommends that ties should be of a length in the shear direction of at least one-third the column depth, h_c, to be considered effective. However since the short tie legs in the test units were slightly longer than $h_c/3$ and not fully effective, it is recommended that a sliding scale of tie leg effectivemess should be used. Tie legs may be assumed to be ineffective if shorter than $h_c/4$, and to increase from half effectiveness at $h_c/4$ to full effectiveness at a length of $h_c/2$.

The effective area of tie legs of length ℓ and gross cross-sectional area A_b is then given by:

$$\left.\begin{array}{ll} \text{If } \ell \leq h_c/4 & A_{eff} = 0 \\ \text{If } h_c/4 < \ell < h_c/2 & A_{eff} = A_b(4\ell - h_c)/h_c \\ \text{If } \ell \geq h_c/2 & A_{eff} = A_b \end{array}\right\} \qquad (6\text{-}16)$$

Note, however, that where tie legs do not cross the critical diagonal plane, they cannot be included in the effective joint shear reinforcement, regardless of their length. This tends to render short ties placed close to the beam flexural bars ineffective in the calculation of joint horizontal shear resistance.

The effective area of tie legs oriented at an angle to the shear direction, such as in diamond or octagonal shaped ties, may be taken as

$$A_{eff} = A_b \cdot \cos\alpha \qquad (6\text{-}17)$$

where α = angle in plan between the centreline of the tie and the centreline of the beam.

6.6.6 Resistance to Vertical Joint Shear

It is apparent from the mode of operation of the postulated mechanisms of joint shear resistance, that where yielding of column bars is prevented or very limited, then part of the applied vertical shear can always be resisted by the joint concrete. This occurs because in this situation forces can be transferred by bond from the column flexural reinforcement throughout the depth of the joint, while a significant compression force occurs in the column concrete at all stages of loading. Where the concrete direct strut is ineffective in transferring horizontal shear, the joint concrete can still be effective in resisting vertical shear by supplying appropriate reactions to the truss mechanism. This situation is recognised in the draft New Zealand Concrete Design Code[5]. Eq. (6-5) implies that half the applied vertical shear may be assigned to the joint concrete in joints for which the column axial load is zero. Table 6.2 shows that the equation is somewhat conservative. Park and Yeoh[41] have proposed that the factor 0.5 should be increased to 0.6, based on available test results, and the present test results would support this change. It is suggested that the design equation may then be given as

$$V_{cv} = 0.6 \frac{A_{sc}}{A'_{sc}} \left(1 + \frac{N_u}{20A_g}\right) \qquad (6\text{-}18)$$

where the constant 20 has the units MPa.

As in the derivation of Eq. (6-15) the term giving the effect of the axial load intensity is now not normalized with respect to the concrete cylinder strength, since it seems unlikely that increased concrete strength will reduce the resistance of joint concrete to vertical shear.

Vertical joint reinforcing may be designed according to Eq. (6-6) to carry the remaining vertical shear. However in the light of test results it is considered necessary that a minimum of one intermediate column bar should be included in the relevant faces of all joints to ensure efficient response.

6.7 Response of Exterior Joints in Plane Frames

6.7.1 Mechanisms of Shear Resistance

In some respects the shear resistance of exterior beam-column joints in plane frames subject to seismic loading may be expected to be somewhat superior to that of interior joints. The same basic mechanisms of shear resistance as have been postulated for interior joints will apply to

exterior joints, but the mode of introduction of the input forces to the joint core will differ slightly, as shown in Fig. 6.7. Assuming that, in accordance with recent practice[5,7], the beam flexural bars are terminated in hooked anchorages, either within the column core or in a separate anchorage block located beyond the outer face of the column, then it is apparent that significant forces are available in the right direction and position at the root of the hook to provide appropriate end conditions for the operation of a direct concrete strut across the joint. However the conditions at the diagonally opposite corner of the joint panel may not be so favourable. If the beam is assymetrically reinforced, with a greater area of top reinforcement than of bottom reinforcement, then under loading producing positive bending in the beam there will be no compression force in the concrete at the top of the beam after cyclic inelastic loading. This occurs because the yield force of the bottom bars in tension is insufficient to yield the top bars in compression, so that the cracks in the top of the beam can never close, and hence the concrete can carry very little compression. The end conditions for development of a direct diagonal strut are thus poor at the upper corner (as shown in Fig. 6.7(b)), unless the presence of significant column axial load means that suitable horizontal forces can be transferred by bond from the top bars within the compressed depth of the column section above the joints.

Under negative moment loading, on the other hand, the bottom reinforcement is insufficient to carry all the compression necessary when tensile yielding of the top bars occurs. Thus some compression will be carried by the beam concrete when full negative moment is applied, and this provides a suitable end reaction for a diagonal strut (as shown in Fig. 6.7(a)). The response of an exterior joint for which the beam is assymetrically reinforced may therefore be expected to be better than that of a similar interior joint, because the presence of adequate anchorage hooks implies that suitable end conditions for the action of the direct diagonal strut are always available at both outer corners of the joint panel, and to a limited extent at one (bottom) inner corner. In an interior joint, one (top) end of a possible diagonal strut will always have unsuitable end conditions after cyclic loading in the inelastic range, as was observed in the test of unit B11. Thus it is suggested that for exterior joints with adequate anchorage for the beam flexural reinforcement, the joint horizontal reinforcement may be designed on the basis outlined for interior joints in Section 6.6, considering only the lesser of the two possible design shear forces, i.e. the lesser of the shears resulting

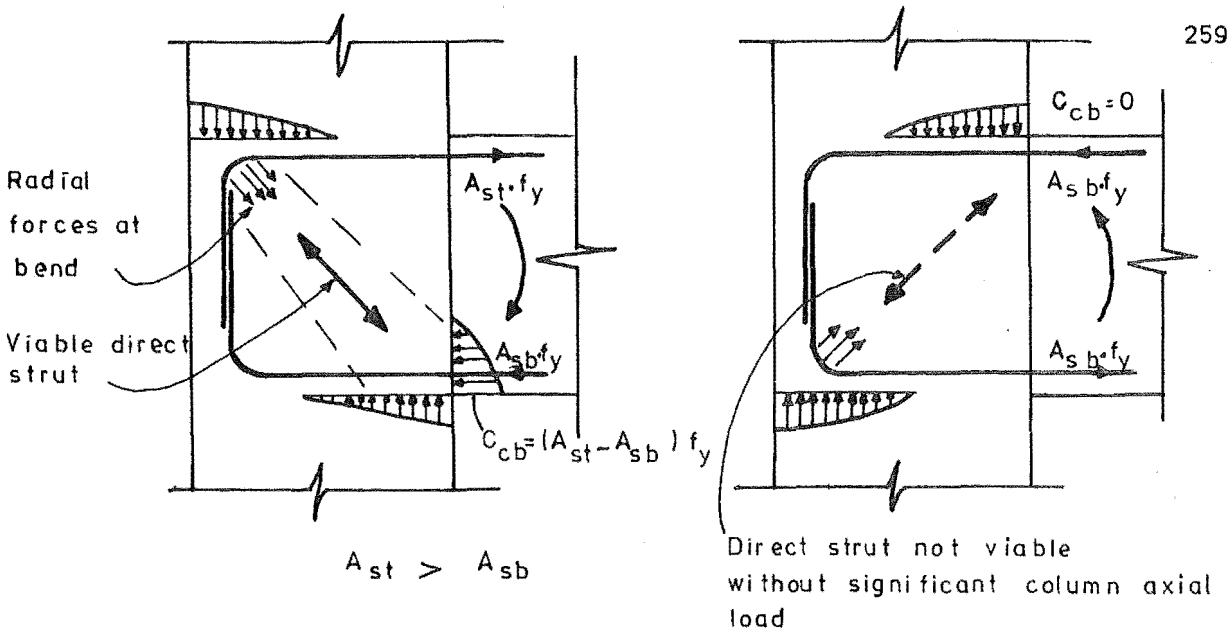

(a) Negative bending load. (b) Positive bending load

FIG.6.7 : DIRECT CONCRETE STRUT MECHANISM FOR SHEAR RESISTANCE IN EXTERIOR JOINTS

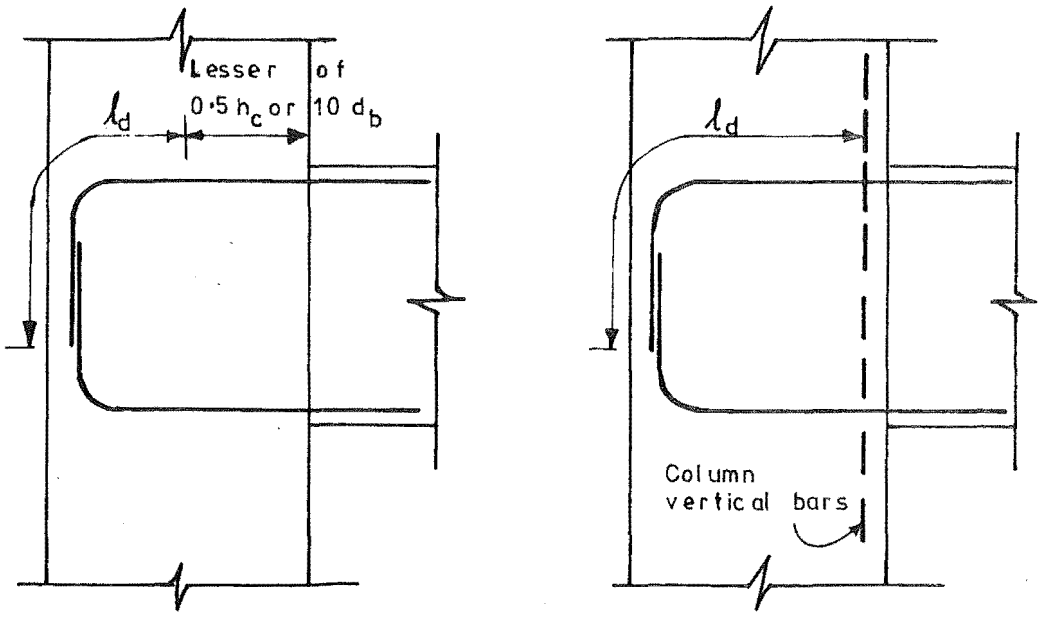

(a) According to NewZealand Draft Concrete Code

(b) Recommendations of ACI-ASCE Committee 352

FIG.6.8 : RECOMMENDATIONS FOR ANCHORAGE OF BEAM FLEXURAL BARS AT EXTERIOR JOINTS

from either positive or negative bending moment. The direct concrete strut shown in Fig. 6.7(a) is available to carry the remaining shear arising from the (reversed) larger moment. Note, however, that the maximum total horizontal shear which may be applied to an exterior joint is still limited by Eq. (6-14).

The column axial load will tend to vary much more widely in exterior columns than in interior columns, and it is important that the minimum axial load should be carefully evaluated for use in Eq. (6-15).

For design to resist vertical joint shear, the situation of an exterior joint is similar to that of an interior joint, and similar procedures may be followed for design as described in Section 6.6.6.

6.7.2 Requirements for Anchorage of Beam Flexural Reinforcement in Exterior Joints

Requirements for the anchorage of beam flexural bars at exterior joints are given in both sets of recommendations for joint design quoted earlier (Section 6.3). The draft New Zealand Concrete Design Code[5], in accordance with observed test results for exterior beam-column joints under cyclic loading[15,17], requires that the development length, l_d, for beam flexural bars should be taken from the centreline of the column, or from $10d_b$ inside the inner column face, whichever provides the smaller lead-in distance. The recommendations of ACI-ASCE Committee 352[7], on the other hand, suggest the development length may be taken from the line of the outermost layer of column bars. These two situations are illustrated in Fig. 6.8.

The draft New Zealand Code also makes a more conservative assessment of the stress, f_h, able to be developed by a standard 90° hook than does the American recommendation. The draft New Zealand Code gives the expression

$$f_h = 30\sqrt{f'_c} \qquad (6\text{-}19)$$

while the ACI-ASCE recommendations give

$$f_h = 60(1 - 0.012d_b)\sqrt{f'_c} \qquad (6\text{-}20)$$

for bars in joints having light confinement only. For bars in more heavily confined joints, a 30% increase is permitted in the stress given in Eq. (6-19), while increases of either 40% or 80% are permitted in the stress given in Eq. (6-20). The approach of ACI-ASCE Committee 352

appears to be based on the results of tests[30], which did not include reversed cyclic loading, and it appears that the recommendations may not therefore be entirely appropriate for joints in frames subject to seismic attack.

6.8 Joints Without Adjacent Plastic Hinges

As noted in Section 1.4.6, it has recently been suggested[8] that some advantages may accrue from beams being detailed so that beam plastic hinges cannot form immediately adjacent to the joint. The shear resistance of the concrete direct strut mechanism in such joints might be substantially increased relative to that of conventional joints. Bull[28] has tested possible details for relocated beam plastic hinges, while Birss[29] tested two beam-column joint units similar to units B12 and B13 of the present series, in order to establish the response of joints for which the beams remained in the elastic range adjacent to the joint.

The beams of Birss's units B1 and B2 contained approximately 25% more flexural reinforcement than the beams of units B12 and B13, but the horizontal joint reinforcement used in unit B1 was only 50% of that used in unit B12, while unit B2 contained only 17.5% of the horizontal joint reinforcement used in unit B13. The units were similar in other respects with the column axial loads applied to units B1 and B2 corresponding to those applied to units B12 and B13 respectively.

Birss's units were loaded cyclically up to loads equal to or greater than the maximum loads applied in the present series, but strains in the beam sections adjacent to the column were less than yield strain at all times. (This was possible because of the greater flexural reinforcement content of the 'elastic' units). Observation of the condition of the joint panels and measurements of the joint reinforcement strains showed that under these circumstances the strength of the joint was adequate to resist the imposed shear throughout six full cycles of loading. Measurements from the outer stirrup legs only of joint ties indicated maximum strains of about 55% of yield strain for both unit B1 (low axial load) and unit B2 (heavy axial load). This showed conclusively that the concrete direct strut mechanisms were much more effective in resisting horizontal joint shear than was the case for units B12 and B13, where similar loads were applied, but where inelastic rotation of the beam plastic hinges adjacent to the column faces occurred.

Subsequent inelastic loading of Birss's test units showed, as expected, that the joints were inadequately reinforced for this type of loading, and joint failures occurred.

These results suggest that relocation of beam plastic hinges may provide a useful solution to the problem of providing sufficient joint strength to resist seismic actions, particularly since closely spaced joint ties are difficult to place on site. Even if the same total weight of reinforcement is required to force the plastic hinge to form at an appropriate distance away from the column face, savings should result from the easier fabrication of joints of this type.

The satisfactory response of Birss's units under elastic loading, and their subsequent failure under inelastic loading, lends further validity to the mechanisms of joint shear resistance described with respect to the present test series (Section 6.4), since these mechanisms would predict this response, as described by Paulay, Park and Priestley[8].

CHAPTER 7

TEST OF SPACE FRAME UNIT B21

7.1 INTRODUCTION

7.1.1 Design

The summary given in Section 1.2 of tests reported on beam-column joints stated that while many tests have been carried out in recent years on joints from plane frames, there is a conspicuous absence of test results pertaining to joints from space frames. Some researchers[10,24] have included transverse beam stubs in their test units in order to simulate the effect of transverse beams, but since the stubs were not loaded concurrently with the main beams in any of these tests, the enhancement of joint performance generally noted cannot be regarded as having very valid application to prototype response under seismic loading. For this reason a complete interior beam-column joint test unit, taken from a space frame, was included in the present test series, and the test rig was designed to allow simultaneous loading of all four beams.

For purposes of comparison, the space frame test unit B21 was made similar to plane frame unit B13, and the same heavy column axial load of 2890 kN ($0.50f'_cA_g$) was applied during the test. As shown in Fig. 7.1, the beam in the East-West direction was reinforced similarly to that of unit B13, except that as the stock of imperial size (No. 6 or D19) bars used for the plane frame units was insufficient, the main flexural reinforcement was composed of bars of the nearest metric size (D20). The different bars meant that the theoretical strengths of the East-West beams were 7% greater than those of the beams in unit B13. The beam in the North-South direction contained the same quantity of reinforcing steel as the East-West beam, but the bars were placed at a reduced internal lever arm to allow for the cross-over of bars at the joint. Thus the design joint shear input from both beams was similar, but the moment input to the column from the North-South beams was less than that from the East-West beams. The column flexural reinforcing steel was increased to four D28 and eight D24 bars (ρ_t = 2.9%), to enable it to carry the biaxial bending moments resulting from concurrent loading of the beams.

The mechanism of resistance postulated in Section 1.4 for beam-column joints under skew loading implied that more joint reinforcement might be required for this case than for unidirectional loading. However the

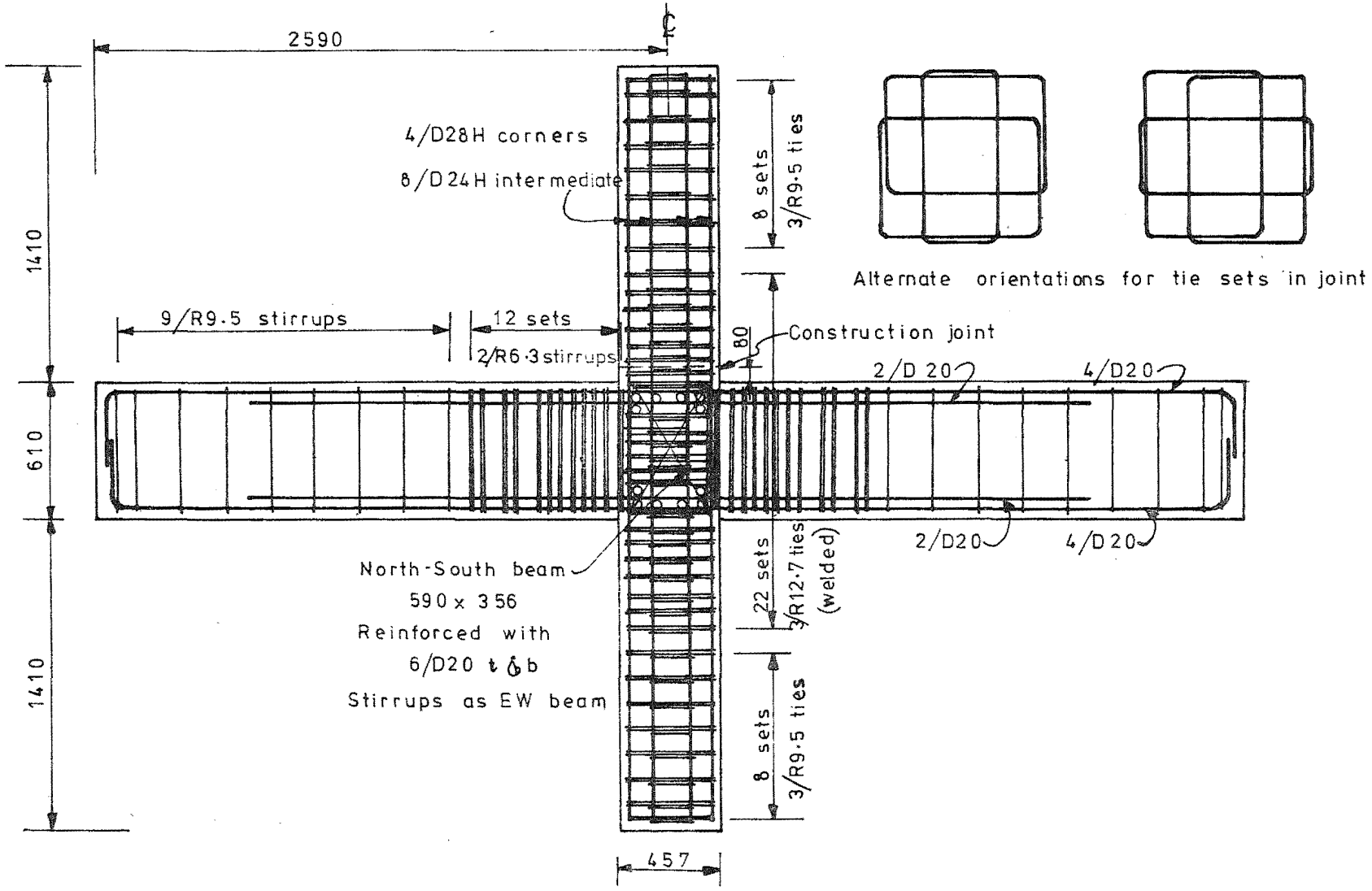

FIG. 7. 1 TEST UNIT B21-REINFORCING FOR EAST-WEST BEAM

strength of the joint concrete shear resisting mechanism in the skew loading case could not be well defined from unsupported theoretical studies and extrapolation from the plane frame test results. It can be argued that the presence of beams on all four column faces might tend to maintain the integrity of the concrete diagonal strut mechanism during cyclic loading, and that this may compensate to some extent for the increased joint shear force, and the diagonal direction of action resulting from concurrent loading. Hence, the same joint reinforcement was used in the space frame unit as in plane frame unit B13, except that the orientation of tie sets within the joint was alternated as shown in Fig. 7.1, so that the response in the two directions would be as nearly equal as possible.

7.1.2 Construction and Materials

Because the finished test unit was too heavy to lift with the overhead crane in the laboratory, and because of the awkward shape of the unit, it was decided to cast the unit with the column in the vertical position in the test rig,so that no lifting would be necessary before testing. Concrete was placed in two pours, a construction joint being made across the column section at 80 mm above the beam top surface. The reinforcing cage assmbled in the mould prior to Pour 1 and Pour 2 is shown in Figs. 7.2(a) and 7.2(b) respectively. Pour 2 was made 10 days after Pour 1.

Material properties for the test unit are summarised in Tables 7.1 and 7.2. Since the test was again expected to take several weeks to complete, the strain aging properties of the D20 reinforcing steel were checked as described in Section 2.5 with respect to the D19 bars used in the plane frame test units. Similar results were obtained, with increases for up to 10% in bar strength being observed in the strain-hardening range due to strain-aging.

Member strengths and properties for the unit are given in Table 7.3. The shear V_{sh} resisted by joint reinforcing under skew loading was calculated on the basis of a critical diagonal plane across the joint similar to that shown in Fig. 1.7. As in the plane frame tests the horizontal shears imposed on the joint during the test exceeded those given in Table 7.3 for actual material properties, because of strain-hardening and strain-aging of the beam reinforcing steel, but the design values were never exceeded.

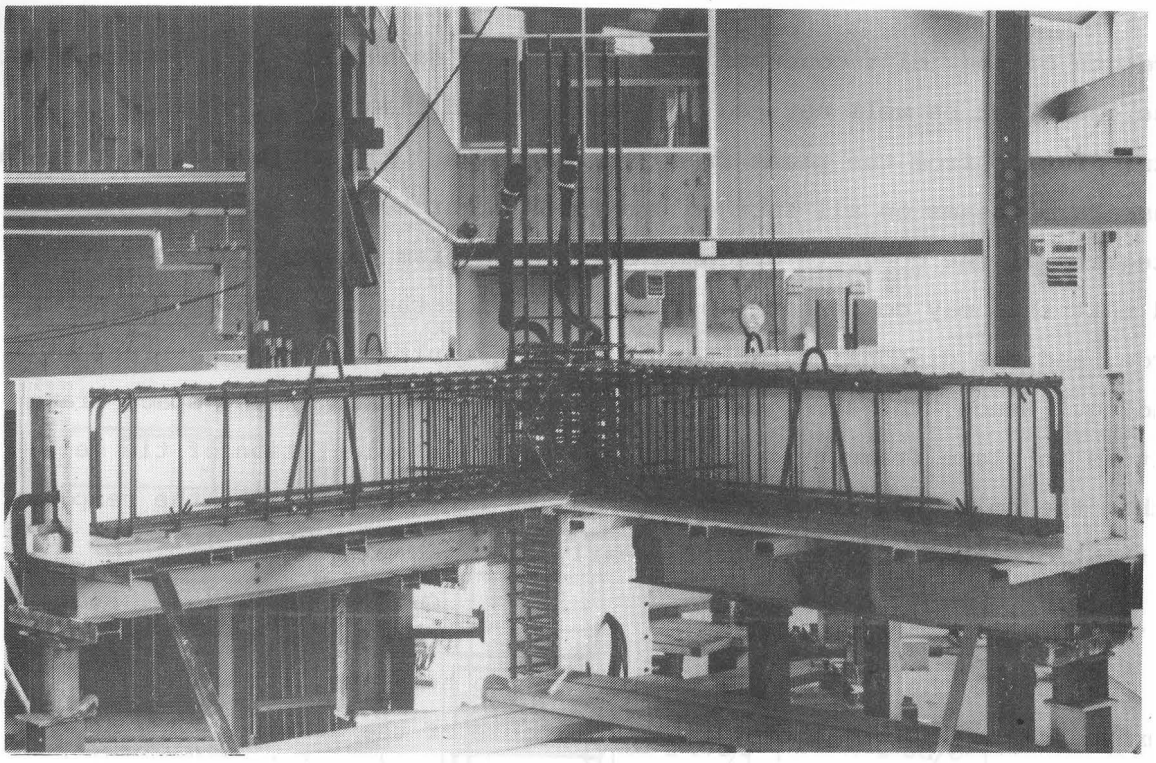

(a) BEFORE POUR 1

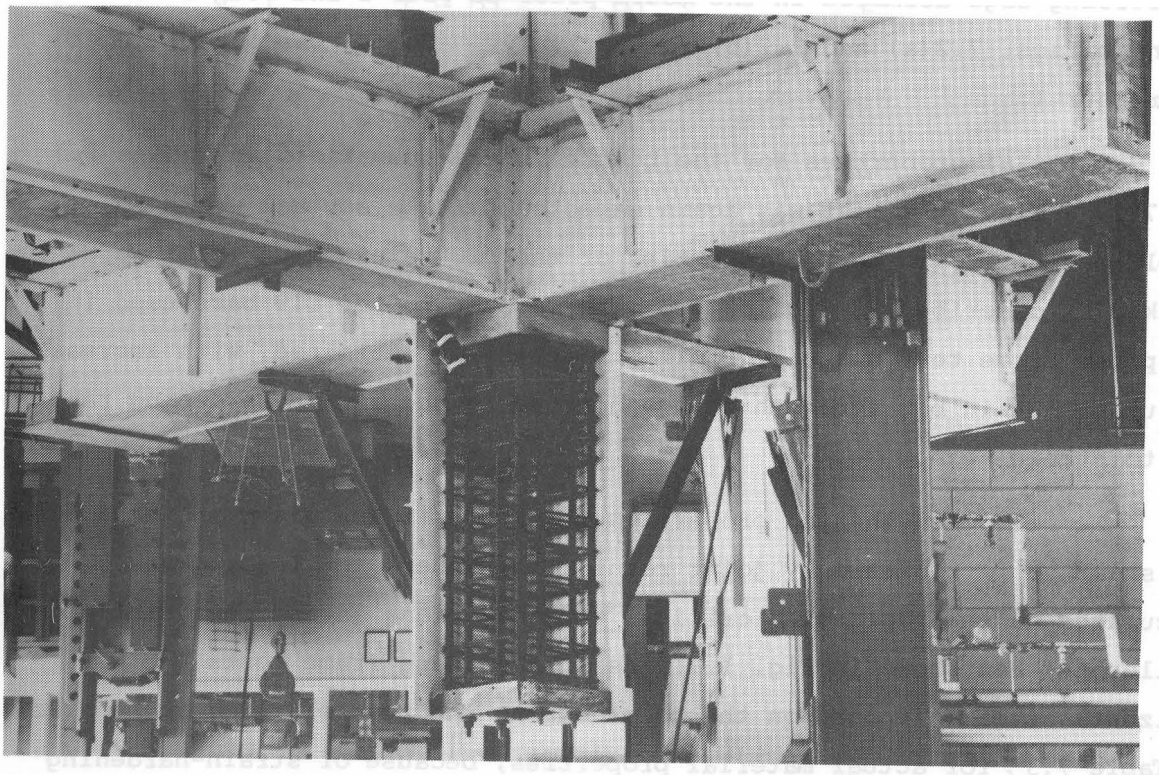

(b) BEFORE POUR 2

FIG·7.2 : REINFORCING CAGE IN MOULD FOR TEST UNIT B 21

Table 7.1 : Properties of Reinforcing Steel

Bar	D20 Grade 275	R12.7 Grade 275	R9.5 Grade 275	R6.35 Grade 275	D24 Grade 380	D28 Grade 380
f_y (MPa)	286.0	336.2	337.9	329.2	411.3	399.1
f_u (MPa)	462.2	447.6	468.5	429.9	716.3	681.2
$\frac{\varepsilon_{sh}}{\varepsilon_y}$	11.03	10.84	Not measured		2.22	2.78

Table 7.2 : Properties of Concrete

	Pour 1	Pour 2
Slump (mm)	100	80
f'_c 28 days (MPa)	33.02	32.81
Age at test (days)	93	83
f'_c at test (MPa)	34.75	37.16
ε_o	0.0021	0.0022

TABLE 7.3 : BEAM, COLUMN, AND JOINT PROPERTIES AND THEORETICAL STRENGTHS*

	Direction	East-West	North-South	Skew
	Beam top bars	6/D20	6/D20	
	d_T (mm)	555	516	
	ρ_T	0.0095	0.0103	
	ρ_T/ρ_b	0.193	0.207	
	Beam bottom bars	6/D20	6/D20	
	d_B (mm)	568	536	
	ρ_B	0.0095	0.0099	
	ρ_B/ρ_b	0.193	0.199	
	P_y (up) (kN)	129.62	123.86	
	P_y (down) (kN)	116.72	107.83	
	P_u (up) (kN)	138.50	133.79	
	P_u (down) (kN)	125.60	116.29	
	Column Bars	4/D28H	4/D24H	
	ρ_t	0.029		
	N_{col} (kN)	2890		
Based on actual material properties	N_{col}/N_b	1.071		
	N_{col}/N_o	0.342		
	$N_{col}/f'_c A_g$	0.398		
Based on design material properties	N_{col}/N'_b	1.204		
	N_{col}/N'_o	0.409		
	$N_{col}/(f'_c A_g)$	0.501		
	Joint Reinforcement 6 sets x 3 ties R12.7 ($\frac{1}{2}$"ϕ)			
	A_{vj} (mm^2)	3096	3096	
Based on actual material properties	V_{jh} (kN)	899.2	909.8	1279.1
	v_{jh} (MPa)	5.54	5.60	8.83
	$v_{jh}/\sqrt{f'_c}$	0.94	0.95	1.50
	V_{sh} (kN)	883.7	883.7	624.9
	V_{ch} (kN)	15.5	26.1	654.2
Based on design material properties	V'_{jh} (kN)	1084.6	1097.5	1543.0
	v'_{jh} (MPa)	6.68	6.76	10.65
	$v'_{jh}/\sqrt{f'_c}$	1.27	1.29	2.03
	V'_{sh} (kN)	725.9	725.9	513.3
	V'_{ch} (kN)	358.7	371.6	1029.7

* See notes on page 269.

Notes to Table 7.3

d_B = effective depth for bottom bars

d_T = effective depth for top bars

$\rho_T = \frac{A_{ST}}{b.d}$ = top reinforcement content of beam

$\rho_B = \frac{A_{SB}}{b.d}$ = bottom reinforcement content of beam

ρ_b = reinforcement content to cause balanced failure of beam

P_y = calculated beam end load to cause the measured yield strain to be attained in all beam tension reinforcement at the column face

P_u = calculated beam end load to cause ultimate flexural strength of beam section to be attained at column face, assuming steel stress does not exceed the measured yield strength, maximum concrete strain = 0.003

$\rho_t = \frac{A_{st}}{b.h}$ = total reinforcement content of column section

N_{col} = axial load applied to column (compression)

N_b = calculated axial load to cause balanced failure of column, i.e., concrete reaching maximum strain of 0.003, simultaneously with tension reinforcement reaching yield strain

$N_o = 0.85f'_c A_g + A_{st} f_y$ = calculated ultimate axial load capacity of column

f'_c = cylinder crushing strength of concrete

A_g = gross area of column section

A_{vj} = total area of joint reinforcement in the shear direction

V_{jh} = joint horizontal shear

v_{jh} = average nominal shear stress on joint core

V_{sh} = horizontal joint shear resisted by joint reinforcement mechanism

V_{ch} = horizontal joint shear resisted by joint concrete mechanism

7.1.3 Test Rig

As explained in Section 2.3, the test rig used for the plane frame test series was designed to allow the beam loading systems in the two principal directions to operate independently of each other and of the column axial loading system. Fig. 7.3 gives an overall view of the test set-up for the space frame test, showing the two beam loading systems (Fig. 2.7) assembled at 45° to the column axial loading system (Fig. 2.6).

7.1.4 Instrumentation

Loads applied to the test unit were measured by calibrated load cells as described in Section 2.6. The column axial load was monitored at the jacking point, while beam end loads were measured at the point of application to the unit. As in the plane frame tests, one load cell output from each beam was recorded directly using a Budd Strain Indicator, and a second output was used to drive the Y-axis of an X-Y recorder. The X-axis of each plotted was driven by a Linear Variable Displacement Transducer (L.V.D.T.) fixed to measure the appropriate beam end displacement, so that continuous traces of beam end load versus displacement were available for all four beams throughout the test.

A total of fifty-four dial gauges were used to measure beam and column displacements and beam rotations, the distribution of dial gauges in each principal direction being similar to that shown in Fig. 2.13 for the plane frame units. Towards the end of the test four additional dial gauges were placed to measure the horizontal displacements of the beams as explained in Section 7.5.1 below.

Strains in the outer beam flexural bars and stirrups were measured using Demec strain gauges (see Section 2.6), but in this case the presence of the transverse beams meant that strains from beam bars passing through the joint could not be obtained by this means. The nearest strain readings to the column obtained by Demec gauges were taken at 76 mm from the column face for each beam. Further strain readings were taken by the Demec strain gauges from Demec points fixed to the surface of the beam and column concrete.

Because of the restricted access for mechanical strain gauges in this test electrical resistance strain gauges were used more extensively than in the plane frame tests. A total of eighty-eight electrical resistance gauges were used to monitor strains in beam reinforcing bars within the joint, column bars, and joint stirrup-ties, as shown in Fig. 7.4. The

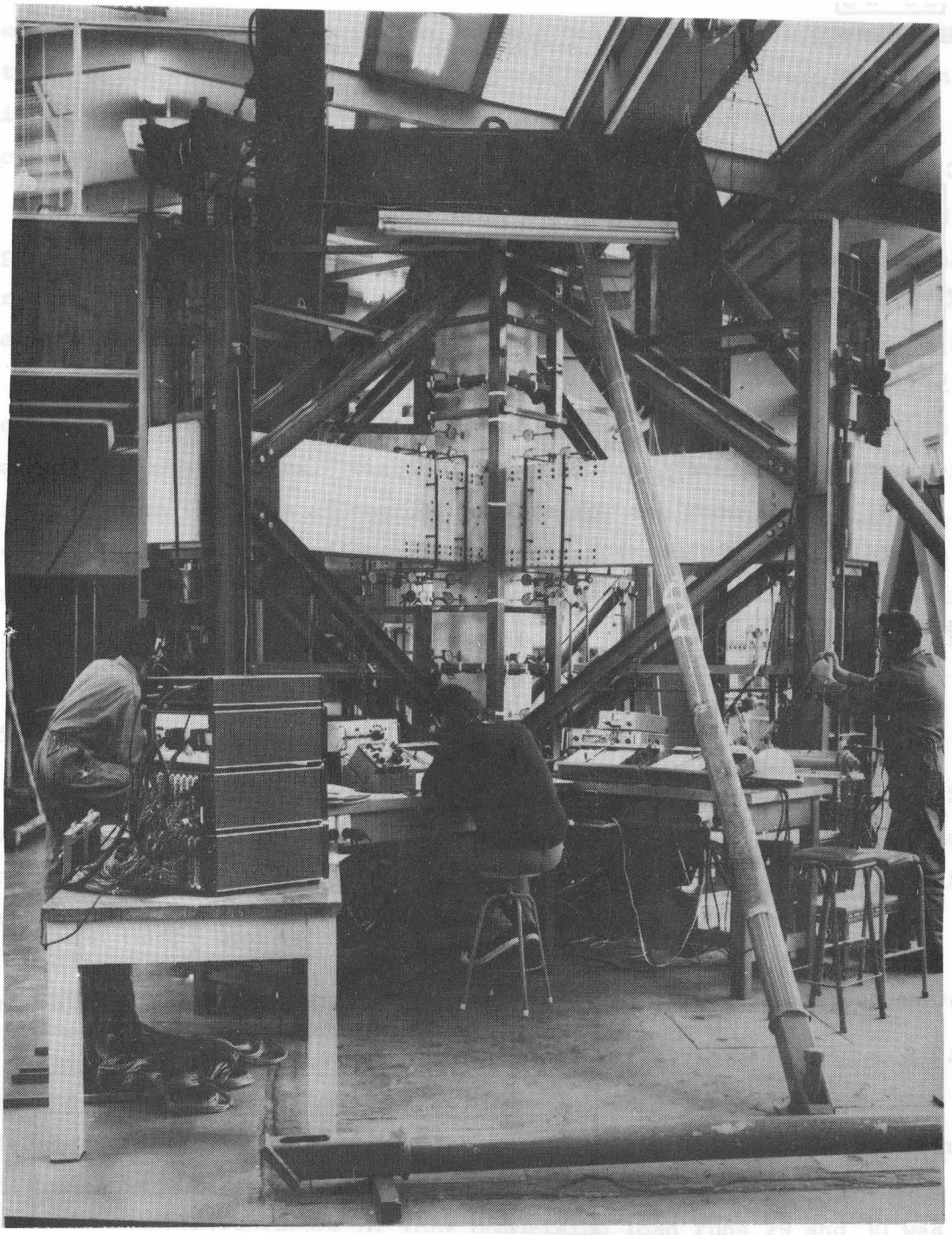

FIG.7.3 : TEST UNIT B 21 UNDER TEST

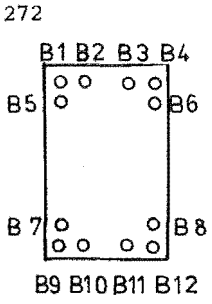

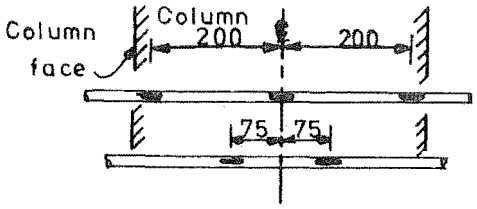

East-West beam . North-South beam.

B1, B4	B9, B12
B5, B6	B7, B8

(a) Beam bar strain gauge positions

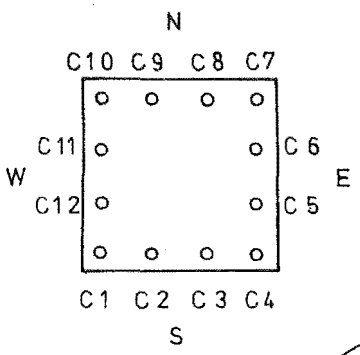

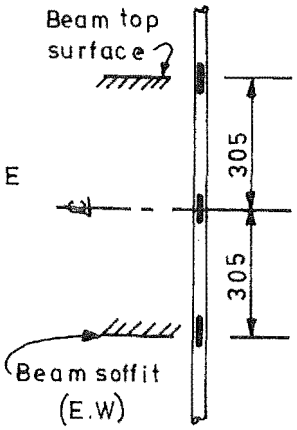

Strain gauged bars

D28 H	C1, C4, C7, C10
D24 H	C8, C11, C12

(b) Column bar strain gauge positions

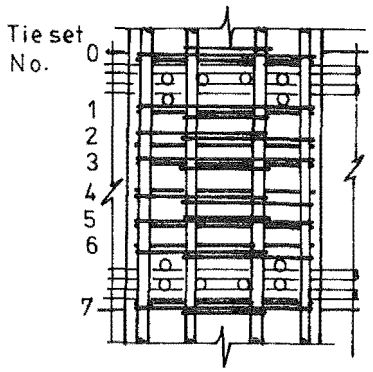

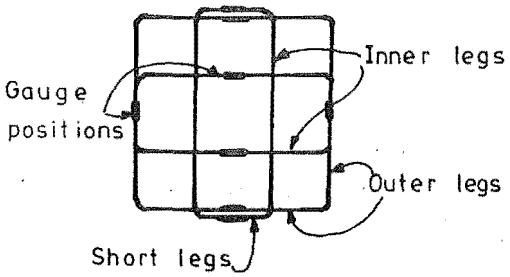

Strain gauge code

42 S = tie set 4

tie no 2

(from top of set)

South leg of tie

Tie Set No	Strain gauges on Inner legs	Outer legs	Short legs
0	01E, 02N	02W, 02N	
1	11N, 13E	11S, 11W, 12W	
2	21E, 23N	21W, 21S, 22S	23E
3	31N, 33W	31E, 32E, 31S	33N
4	41N, 43W	42S, 43S, 43E	41W
5	51E, 52N	52S, 52W, 53W	
6	61S, 62E	62W, 62N, 63N	
7	72N, 73E	71W, 72W, 72S	73S

(c) Joint tie strain gauge positions

FIG.7.4 :LOCATION OF ELECTRICAL RESISTANCE STRAIN GAUGES

total number of strain gauge leads had to be minimised so that the effective area of column concrete would not be too greatly reduced. Hence only top or bottom beam bars were strain gauged across the joint for each beam, and only seven of the twelve column bars were instrumented. All leads were routed out of the joint core region via the column above or below. Details of strain gauge installation and water-proofing procedures were given in Section 2.6. Strain gauge results for this test were recorded on a 200-channel Solartron Data Recorder.

In order to make comparisons with the joint deformations measured in the plane frame tests it was desired to make some measurements of diagonal deformation across the joint. Since the modified Demec gauge used for the plane frame tests was not suitable for this test, four 12 mm travel L.V.D.T's were mounted on studs at the upper corners of the joint in the East-West direction, the cores being fixed to 3 mm diameter rods attached to studs at the opposite lower corners. Diagonal holes of 8 mm internal diameter were provided through the beam at the column face for the rods to move in. Because of the congestion of instrumentation in the joint region this shear deformation of the joint could be measured in the East-West direction only. No measurements of shear deformation of the beams were taken in this test.

7.1.5 Cyclic Loading Sequence

The cyclic loading sequence used in this test is shown in Fig. 7.5. An experimental yield deflection was determined in the initial elastic load run in each direction (load run 1 for the East-West beam, and load run 15 for the North-South beam) as described in Section 2.7.1, and these were used to define the displacement ductility factors in terms of which the subsequent inelastic cycles were controlled.

The test was conducted in several parts. Initially the East-West beams, and then the North-South beams, were loaded separately up to displacement ductility factors of four in a similar cyclic loading pattern to that used in the plane frame tests. A further single cycle to a displacement ductility factor of four comprising load runs 29 and 30 was then applied in the East-West direction only, so that the effectiveness of the confinement provided by the transverse (North-South) beam to the joint core could be assessed both before and after cyclic loading of the transverse beam.

Two-directional or skew loading of the test unit commenced at load run 31 with loads applied initially in the NW-SE direction, then in the

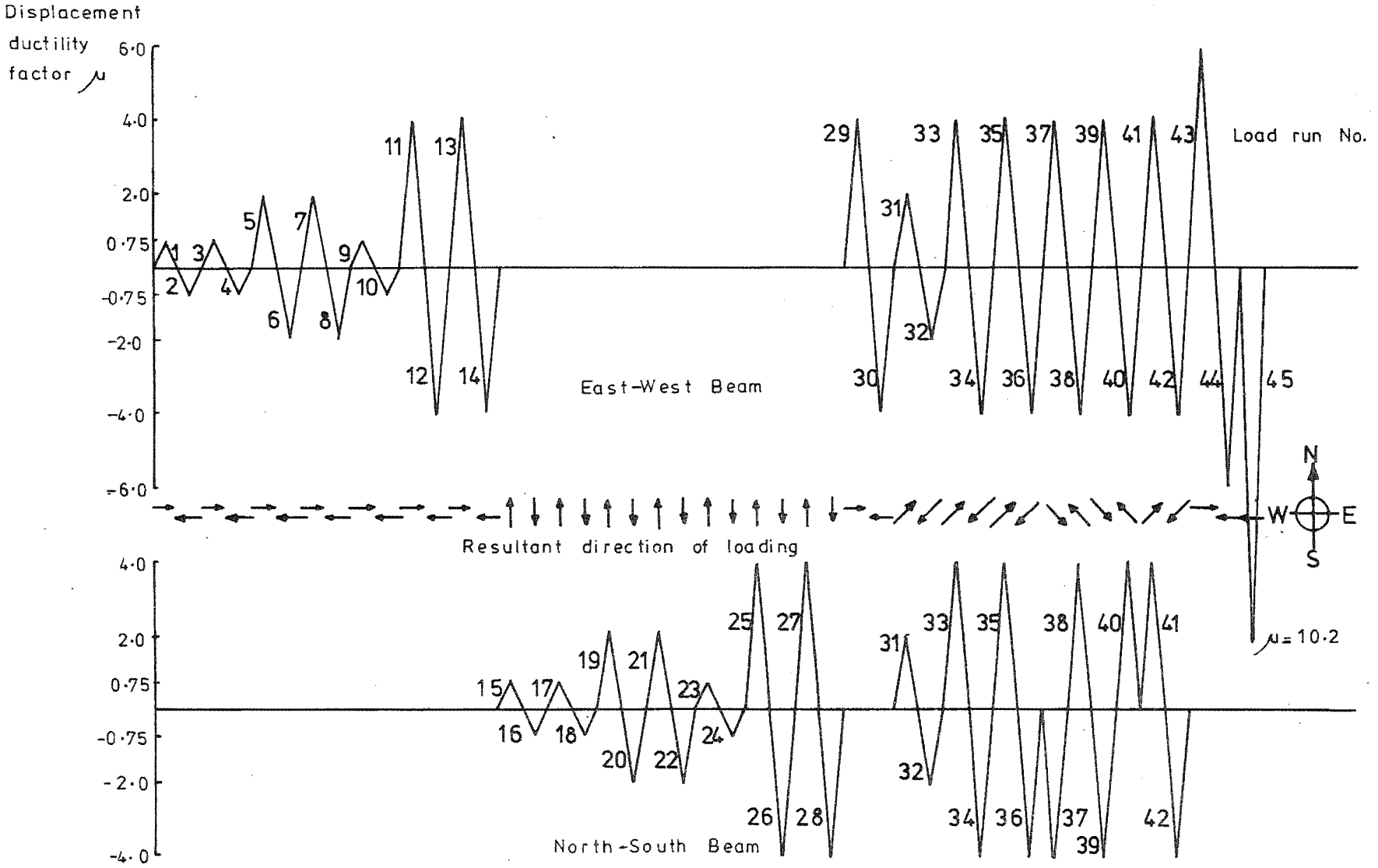

FIG.7.5 :CYCLIC LOADING SEQUENCE

NE-SW direction, and then a further cycle in the NW-SE direction. Where the direction of skew loading was changed by 90° (eg. between load runs 36 and 37), this was achieved by maintaining the reversed cyclic loading pattern on the East-West beams, while reapplying loads to the North-South beams in the sense of the preceding load run. During the two-directional loading cycles the maximum displacement ductility factor applied in each direction was four, since it was felt that this represented an adequately severe level of ductility demand for the case of simultaneous loading in the two directions, in relation to the displacement ductility factor of six which was normally imposed as a maximum in the plane frame tests.

At the conclusion of the skew loading cycles, the East-West beams only were loaded up to a displacement ductility factor of six, in order to determine the effect of the previously applied severe concurrent loading on the unidirectional response. Finally a single load run to a displacement ductility factor of 10.2 was imposed on the East-West beams in an endeavour to fail the unit under monotonic loading. However the displacements were limited by the presence of dial gauge stands beneath the beams, with the result that the unit could not be failed.

7.2 Test Unit Response

7.2.1 General

The outcome of the test was satisfactory in that the simultaneous two-directional loading did not overtax the strength of the joint even though only unidirectional loading was considered in the design. Skew loading did cause larger joint deformations and more yielding of joint reinforcing than was observed under unidirectional loading. However, the reserve strength of the joint concrete shear resisting mechanism allowed the unit to maintain its integrity throughout a large number of inelastic cycles.

The condition of the unit at various stages of the test is shown in the photographs (Figs. 7.6 to 7.9). The photographs were taken in the South-East quadrant of the test unit, showing the Southern beam on the left, and the Eastern beam on the right. Cracks have been marked with felt-tip pens to show their positions more clearly. The pattern of flexural and diagonal tension cracking in the beams was similar to that observed in the plane frame tests, but the condition of the joint was indicated only at the exposed corners of the column down the depth of the beams. Cracking was observed at these corners throughout the unidirectional

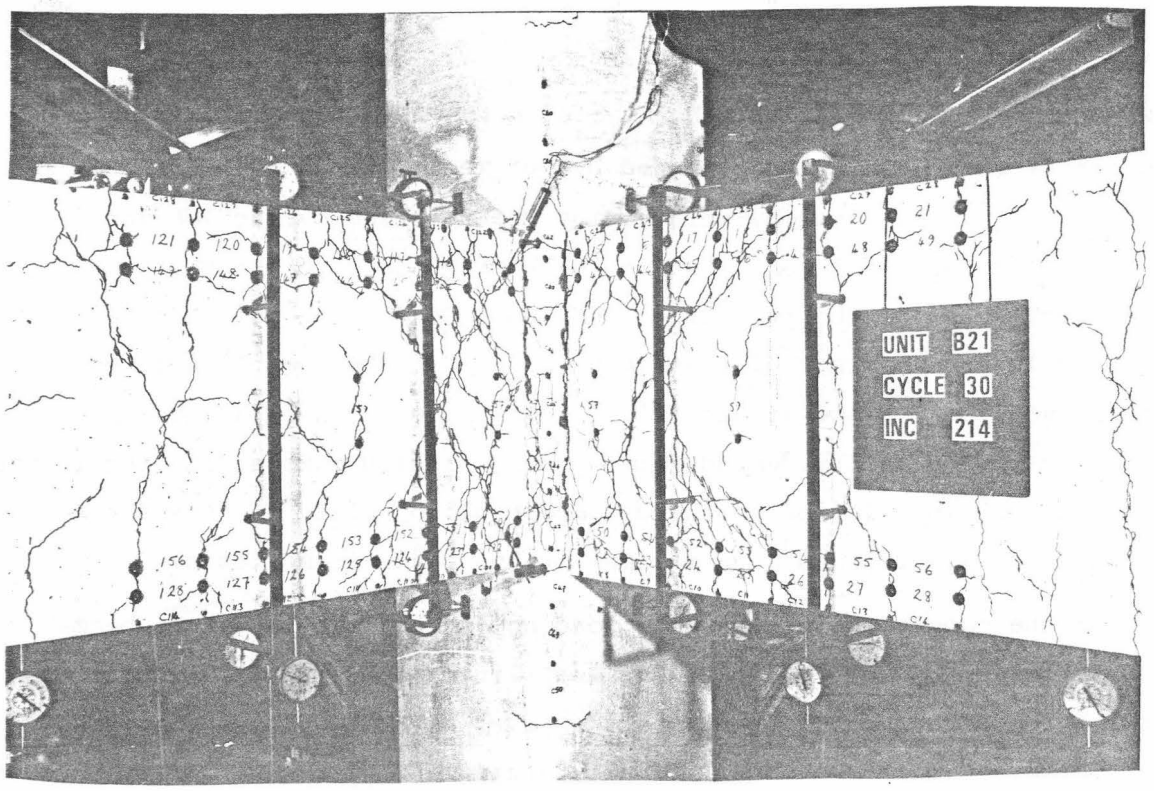

FIG.7.6: TEST UNIT AT MAX. DISPLACEMENT, LOAD RUN 30 (FINAL UNI-DIRECTIONAL RUN, μ = 4.0)

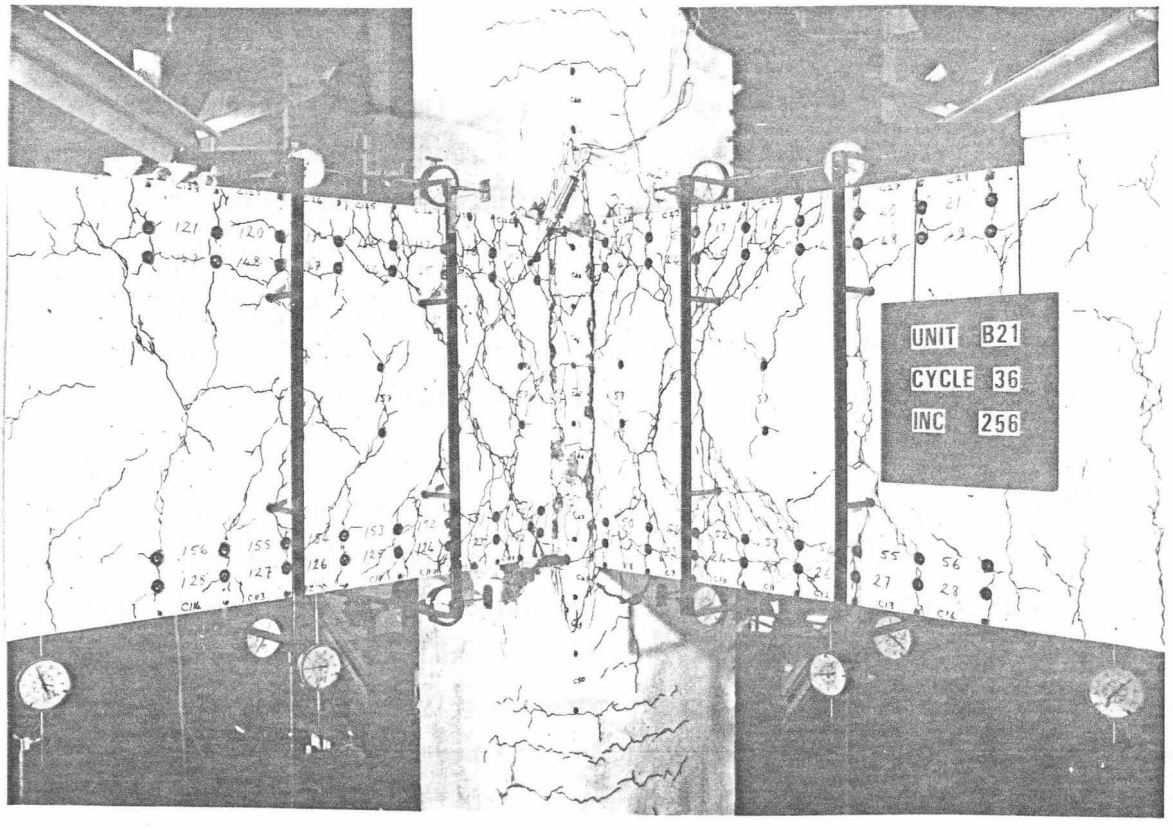

FIG.7.7: TEST UNIT AT MAX. DISPLACEMENT, LOAD RUN 36 (SKEW LOADING IN ONE DIAGONAL DIRECTION ONLY, μ = 4.0)

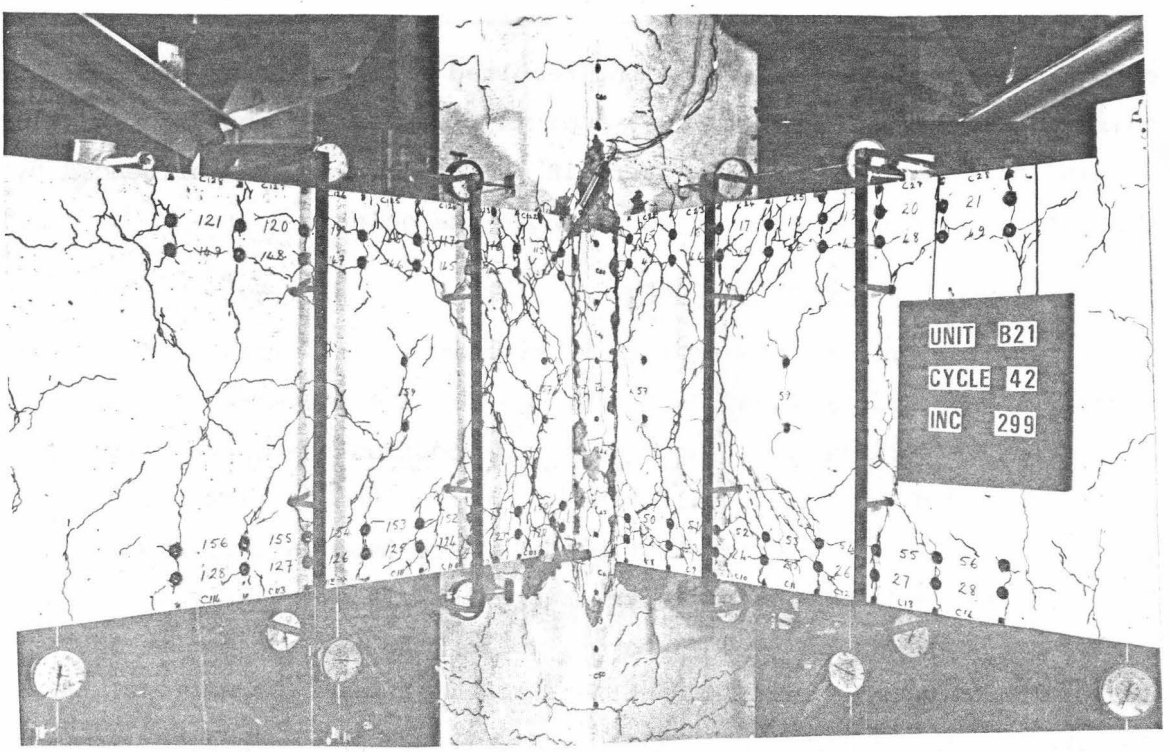

FIG.7.8: TEST UNIT AT MAX. DISPLACEMENT, LOAD RUN 42 (FINAL SKEW LOADING RUN, $\mu = 4.0$)

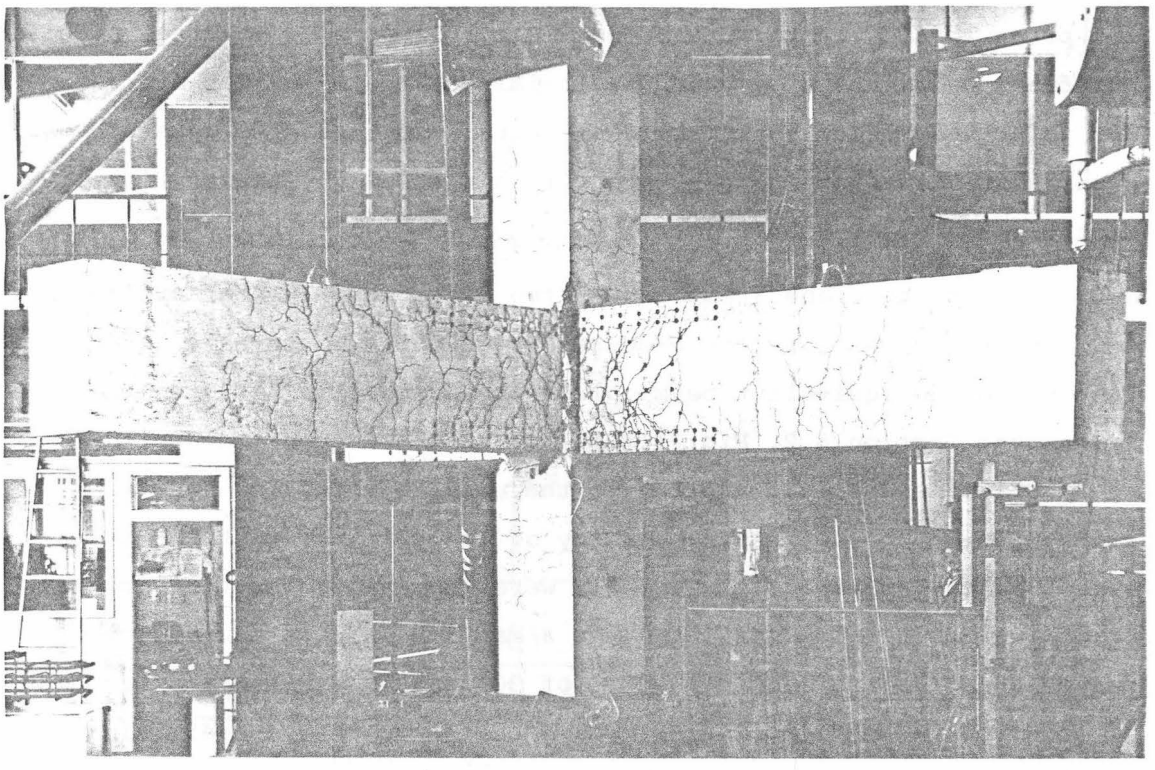

FIG.7.9: TEST UNIT AT COMPLETION OF TEST (μ=10.2 EAST-WEST, $\mu = 4.0$ NORTH-SOUTH)

cycles (Fig. 7.6), and skew loading resulted in spalling of the cover in this locality (Figs. 7.7 to 7.9). Column cracking was observed under skew loading only, and the crack pattern in the column was not influenced by the construction joint located at 80 mm above the joint.

7.2.2 Load-Displacement Response

The response of the test unit is shown in the plots of column shear versus storey sway in Figs. 7.10 and 7.11 for the East-West and North-South directions respectively. These were derived from the appropriate beam end loads and displacements allowing for the column P-delta effect as described in the plane frame test reports (see Section 3.2). As shown in Fig. 7.5 the unit was loaded in the East-West direction only in the load runs 1 to 14, 29 to 30, and 43 to 45, while load was applied in the North-South direction only in load runs 15 to 28. Shears and deflections shown for skew loading runs in Figs. 7.10 and 7.11 are the components measured in the principal (i.e. East-West and North-South) directions, not the resultant effects.

Relatively little stiffness degradation was observed during the first series of unidirectional loading runs in both principal directions, although the initial elastic stiffness in the North-South direction was about 5% less than that in the East-West direction due to (a) the smaller effective beam depth, and (b) the more flexible nature of the joint due to the prior loading of the transverse beam. Under skew loading, significant stiffness degradation occurred due mainly to the more flexible response of the joint under skew loading. Some degradation was also caused by sliding shear displacement in the beam plastic hinges and by penetration of yielding of the beam bars into the joint.

As in the plane frame tests, the measured column shears were modified to account for the P-delta effect which would have affected the response of an equivalent beam-column subassembly in an actual building frame (see Section 3.2, Fig. 1.10). As in the response of unit B13, the heavy column axial load applied to the unit resulted in significant reductions in the net shear capacity of the unit due to the P-delta effect as the applied displacements were increased. In the East-West direction the P-delta effect caused a maximum calculated reduction in column shear during cyclic loading of 30% at the maximum displacement of load runs 43 and 44, with a 47% reduction in load run 45. In the North-South direction, where the maximum displacements were less than those imposed in the East-West direction, the maximum calculated reduction in column shear was 28% in load run 42. However, the strengthening of the

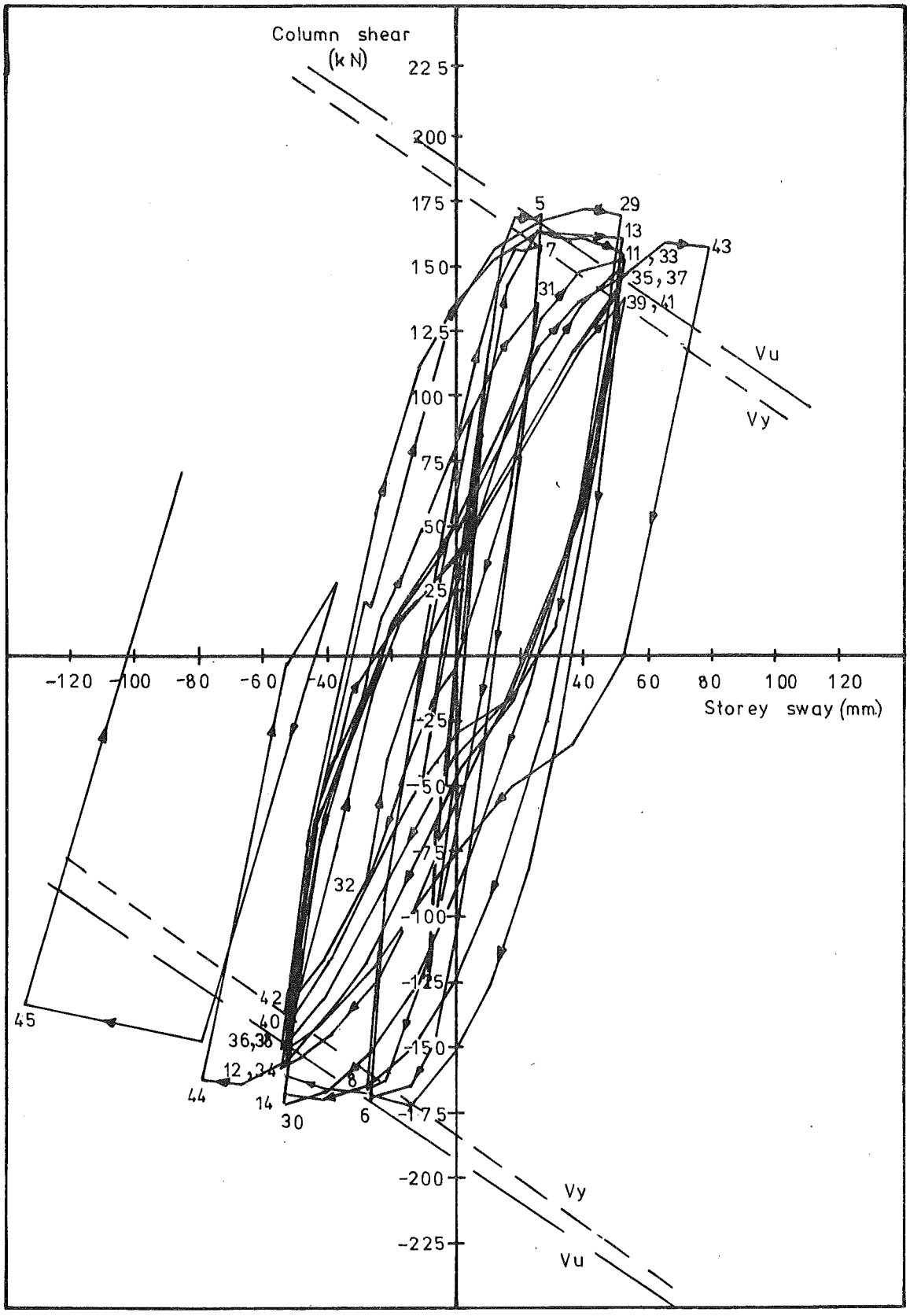

FIG. 7.10 : COLUMN SHEAR - STOREY SWAY RESPONSE IN EAST-WEST DIRECTION

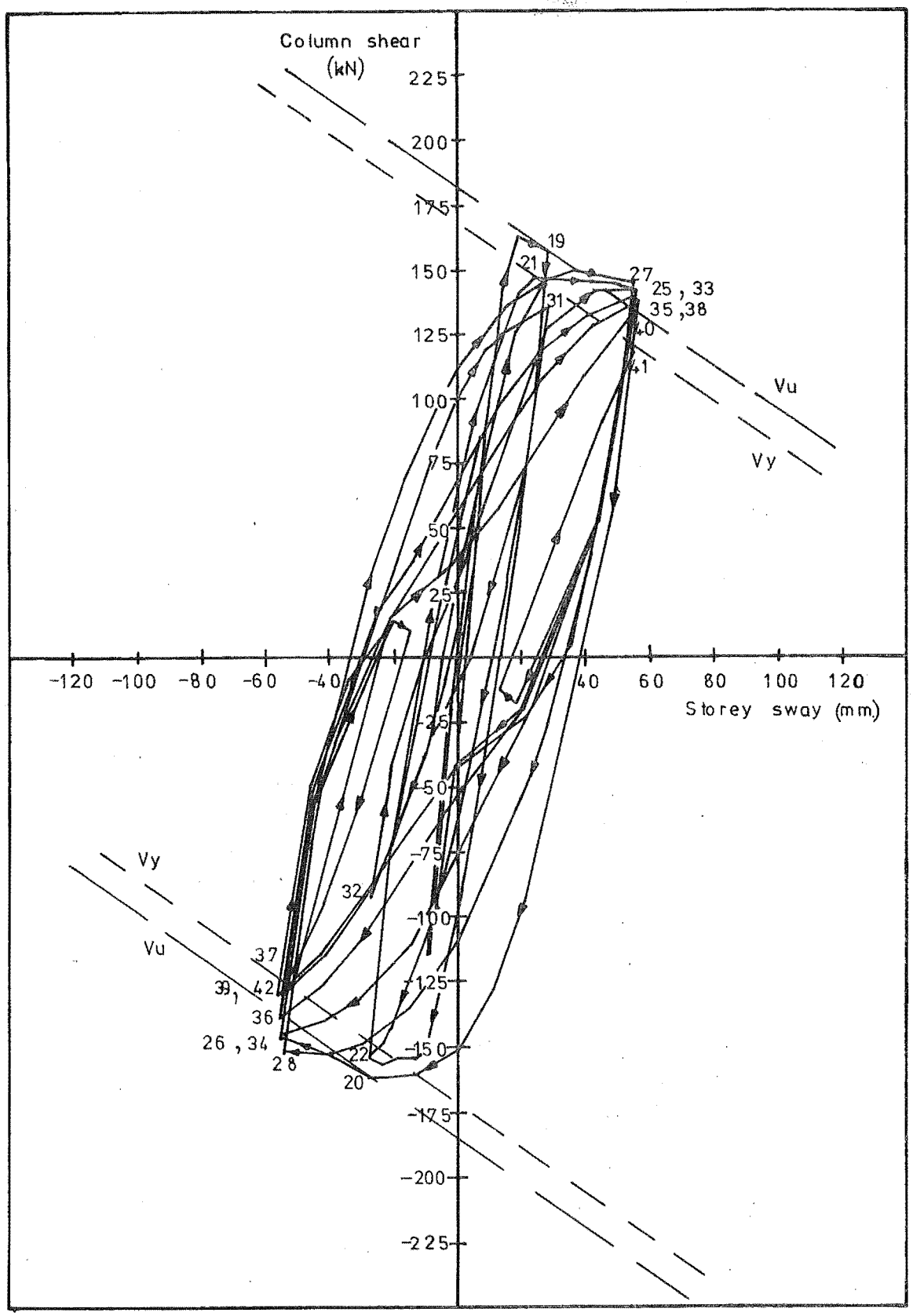

FIG. 7. 11 :COLUMN SHEAR-STOREY SWAY RESPONSE IN NORTH-SOUTH DIRECTION

beams caused by strain-hardening and strain-aging of the flexural reinforcing steel compensated for most of the column shear reduction due to the P-delta moments.

Beam end loads at maximum displacement are listed in Tables 7.4a and 7.4b for the East-West and North-South beams respectively. The influence of strain-aging on the test results is shown by the increased loads measured for the East-West beams in load runs 29 and 30, compared to those in load runs 11 to 14. A fault occurred in the data-logging equipment between load runs 25 and 26 which took over three weeks to repair, so that the total time between load runs 14 and 29 was about six weeks. This was reflected in the relatively large loads observed in load runs 29 and 30.

In the first cycle of skew loading (load runs 31 and 32) the reduced stiffness and the smaller displacement ductility demand ($\mu = 2.0$) resulted in lower loads, but in subsequent skew loading cycles to $\mu = 4.0$ the full ultimate strength of the beams was exceeded. As the number of cycles increased and the direction of loading was changed the strength available at $\mu = 4.0$ decreased, so that at the maximum displacement of load run 42 the average proportion of ideal ultimate strength attained in the four beams was only 95%, compared to the 106% attained in load run 33. However, since the total cumulative displacement ductility demand on the beams by this stage of the test was 76 for the East-West beams, and 68 for the North-South beams, this relatively small degradation in strength was considered quite acceptable.

Where loading was reapplied in the same sense as in the previous load run (that is repeated instead of reversed, in load runs 37 and 41 in the North-South direction - see Fig. 7.5), the existing residual deflection was initially reduced. This occurred because the East-West beams only were loaded in the initial stages of the load run and no loads were applied to the North-South beams until the displacements of all beams in the senses required for the new direction of loading were equal, by which stage the East-West beams were carrying substantial loads. When the repeated loads were applied to the North and South beams it was found that the stiffness in the North-South direction was much greater than that observed under reversed loading, and the loads attained by these beams were about 95% of those attained in the preceding load run. In this situation cracks in the compressed faces of the beams did not have to be closed up due to tensile yielding of the reinforcement in the preceding load run, and this allowed a much stiffer response than that observed

TABLE 7.4a : WEST AND EAST BEAM END LOADS

Load Run No.	μ	Beam West			Beam East		
		P (kN)	P/P_y	P/P_u	P (kN)	P/P_y	P/P_u
1	0.75	-84.94	0.728	0.676	93.71	0.723	0.677
2		83.39	0.643	0.602	-96.83	0.830	0.771
3		-83.91	0.719	0.668	95.01	0.733	0.686
4		94.15	0.726	0.680	-84.61	0.725	0.674
5	2.0	-128.66	1.102	1.024	140.49	1.084	1.014
6		136.99	1.057	0.989	-122.57	1.050	0.976
7		-122.39	1.049	0.974	130.76	1.009	0.944
8		131.65	1.016	0.951	-124.15	1.064	0.988
9	0.75	-77.67	0.665	0.618	94.23	0.727	0.680
10		43.47	0.335	0.314	-30.26	0.259	0.241
11	4.0	-133.37	1.143	1.062	144.53	1.115	1.044
12		146.26	1.126	1.056	-132.53	1.135	1.055
13		-136.97	1.173	1.091	150.57	1.162	1.087
14		149.34	1.152	1.078	-139.76	1.197	1.113
29	4.0	-143.04	1.225	1.139	156.73	1.209	1.132
30		153.28	1.183	1.107	-141.09	1.209	1.123
31	2.0	-102.47	0.878	0.816	120.78	0.932	0.872
32		79.70	0.615	0.575	-68.37	0.586	0.544
33	4.0	-133.90	1.147	1.066	144.31	1.113	1.042
34		144.56	1.115	1.044	-132.68	1.137	1.056
35		-128.80	1.103	1.025	146.16	1.128	1.055
36		140.02	1.080	1.011	-127.40	1.091	1.014
37	4.0	-125.87	1.078	1.002	141.36	1.091	1.021
38		139.13	1.073	1.005	-128.08	1.097	1.020
39		-120.73	1.034	0.961	138.17	1.066	0.998
40		133.99	1.034	0.967	-120.10	1.029	0.956
41	4.0	-116.18	0.995	0.925	141.89	1.095	1.024
42		135.20	1.043	0.976	-113.10	0.969	0.901
43	6.0	-147.72	1.266	1.176	166.72	1.286	1.204
44		160.22	1.236	1.157	-151.21	1.295	1.204

TABLE 7.4b : NORTH AND SOUTH BEAM END LOADS

Load Run No.	μ	Beam North			Beam South		
		P (kN)	P/P_y	P/P_u	P (kN)	P/P_y	P/P_u
15	0.75	-90.52	0.839	0.778	90.06	0.727	0.673
16		89.84	0.725	0.672	-77.69	0.721	0.668
17		-78.59	0.729	0.676	90.59	0.731	0.677
18		90.02	0.727	0.673	-78.77	0.730	0.677
19	2.0	-115.75	1.073	0.995	135.09	1.091	1.010
20		128.70	1.039	0.962	-112.90	1.047	0.971
21		-109.59	1.016	0.942	129.12	1.042	0.965
22		125.77	1.015	0.940	-114.34	1.060	0.983
23	0.75	-66.30	0.615	0.570	82.75	0.668	0.619
24		39.27	0.317	0.293	-28.60	0.265	0.246
25	4.0	-124.34	1.153	1.069	139.79	1.129	1.045
26		139.04	1.123	1.039	-123.86	1.149	1.065
27		-125.13	1.160	1.076	143.96	1.162	1.076
28		142.29	1.149	1.064	-127.94	1.187	1.100
31	2.0	-103.22	0.957	0.888	120.83	0.976	0.903
32		83.82	0.677	0.626	-75.62	0.701	0.650
33	4.0	-125.74	1.166	1.081	140.03	1.131	1.047
34		138.85	1.121	1.038	-123.68	1.147	1.064
35		-123.74	1.148	1.064	138.10	1.115	1.032
36		134.97	1.090	1.009	-118.78	1.102	1.021
37	4.0	127.02	1.026	0.949	-111.90	1.036	0.962
38		-122.26	1.134	1.051	138.48	1.118	1.035
39		127.80	1.032	0.955	-113.18	1.050	0.973
40		-115.48	1.071	0.993	131.19	1.059	0.981
41	4.0	-106.90	0.991	0.919	125.65	1.014	0.939
42		130.30	1.052	0.974	-113.21	1.050	0.974

Note: 1) For definition of terms refer to Table 3.1.

2) Values of P_y, P_u are listed in Table 7.3.

under reversed loading. It is possible that the joint also responded more stiffly under repeated loading than under reversed loading, but this could not be verified due to the lack of instrumentation for joint deformation in the North-South direction.

When unidirectional loading was imposed on the East-West beams to displacement ductility factor of six in load runs 43 and 44, the ideal ultimate strengths were again exceeded by considerable margins, although the stiffness was reduced compared to that observed in the earlier East-West cycles. The loss of stiffness was due primarily to the effect of skew loading on the flexibility of the joint and the column.

7.3 Beam Behaviour

7.3.1 Rotational and Curvature Ductility Factors

Values of beam rotation, θ_b , measured over a 280 mm gauge length from the column face, and of beam curvature, ϕ , derived from strain readings in the reinforcing bars at the maximum displacements of the post-elastic cycles, are listed in Tables 7.5a, 7.5b, 7.5c and 7.5d for the four beams, together with ductility factors based on experimental yield rotations and curvatures extrapolated from the appropriate measurements in load runs 1 and 15. The curvature ϕ_1 was that observed at 76 mm from the column face, while ϕ_{max} was the maximum value of curvature observed at intervals of 102 mm in the plastic hinge up to 690 mm away from the column face. The length $l_{\phi max}$ was the distance from the column face to the position at which the maximum curvature was observed.

Up to load run 14 the ductility factors obtained for the East-West beams were similar to those measured in test B13. The influence of joint shear distortion on the apparent values of θ_{b1} , the beam rotation adjacent to the column face, was allowed for in the values listed for the East and West beams, where joint deformation was measured, but not for the North and South beams, where no such measurement was made. Hence the apparent rotations measured in the North and South beams were greater than those in the corresponding cycles for the East and West beams, although the ductility values were similar, since the experimental yield rotations were also greater for the North and South beams. The curvature values measured in the North and South beams were also greater than those in the East and West beams, because of the smaller lever arm between the outer layers of reinforcing in these beams. However the curvature ductility factors observed were similar for corresponding load runs in the two directions.

TABLE 7.5a : ROTATIONAL AND CURVATURE DUCTILITY FACTORS - BEAM WEST

Load Run No.	μ	θ_{bl} rad x 10^4	$\frac{\theta_{bl}}{\theta_y}$	ϕ_l rad/mm x 10^6	ϕ_{max} rad/mm x 10^6	$^l\phi_{max}$ mm	$\frac{\phi_l}{\phi_y}$	$\frac{\phi_{max}}{\phi_y}$
5	2.0	-46.13	3.11	-11.70	-11.70	76	3.57	3.57
6		54.77	3.69	18.72	18.72	76	5.71	5.71
7		-44.94	3.03	-19.75	-19.75	76	6.03	6.03
8		54.91	3.70	20.69	20.69	76	6.32	6.32
9	0.75	-0.75	0.05	4.19	-3.12	178	-1.28	0.95
10		25.72	1.73	10.40	10.40	76	3.18	3.18
11	4.0	-108.61	7.32	-22.70	-41.14	178	6.93	12.56
12		120.43	8.12	27.54	33.56	279	8.41	10.24
13		-85.66	5.77	-22.47	-27.98	381	6.86	8.54
14		109.32	7.37	25.43	25.43	76	7.76	7.76
29	4.0	-66.25	4.46	-16.23	-19.18	483	4.95	5.86
30		99.01	6.67	20.91	20.91	76	6.38	6.38
31	2.0	-8.67	0.58	0.16	-4.70	483	-0.05	1.44
32		55.40	3.73	9.89	9.89	76	3.02	3.02
33	4.0	-60.05	4.05	-10.22	-12.93	483	3.12	3.95
34		92.92	6.26	15.88	15.88	76	4.85	4.85
35		-56.29	3.79	-8.07	-11.31	483	2.46	3.45
36		87.33	5.89	14.36	14.36	76	4.38	4.38
37	4.0	-55.26	3.72	-7.68	-10.51	483	2.32	3.21
38		87.76	5.91	14.12	14.12	76	4.31	4.31
39		-51.55	3.47	-6.39	-9.67	483	1.95	2.95
40		84.72	5.71	12.67	12.67	76	3.87	3.87
41	4.0	-51.27	3.45	-5.42	-9.08	483	1.66	2.77
42		86.02	5.80	12.17	12.17	76	3.72	3.72
43	6.0	-88.86	5.99	-16.08	-24.66	483	4.91	7.53
44		108.78	7.33	18.08	18.55	483	5.52	5.66

TABLE 7.5b : ROTATIONAL AND CURVATURE DUCTILITY FACTORS - BEAM EAST

Load Run No.	μ	θ_{bl} rad x 10^4	$\frac{\theta_{bl}}{\theta_{by}}$	ϕ_l rad/mm x 10^6	ϕ_{max} rad/mm x 10^6	$l_{\phi max}$ mm	$\frac{\phi_l}{\phi_y}$	$\frac{\phi_{max}}{\phi_y}$
5	2.0	59.26	3.99	13.31	13.31	76	4.06	4.06
6		-50.57	3.41	-19.35	-19.35	76	5.91	5.91
7		58.72	3.96	25.65	25.65	76	7.80	7.80
8		-47.69	3.21	-16.31	-16.31	76	4.98	4.98
9	0.75	-1.68	-0.11	-0.72	4.13	178	0.22	1.26
10		-17.32	1.17	-5.68	-5.68	76	1.73	1.73
11	4.0	142.34	9.59	27.67	41.01	178	8.45	12.52
12		-118.86	8.01	-25.75	-34.13	178	7.86	10.42
13		112.82	7.60	27.58	31.54	381	8.42	9.63
14		-99.09	6.68	-24.40	-25.81	178	7.45	7.88
29	4.0	86.73	5.84	20.02	20.02	76	6.11	6.11
30		-81.29	5.48	-18.84	-19.37	178	5.75	5.91
31	2.0	27.96	1.88	3.43	8.36	483	1.05	2.55
32		-36.44	2.47	-6.94	-8.84	178	2.12	2.70
33	4.0	78.42	5.28	14.33	14.33	76	4.37	4.37
34		-70.48	4.75	-13.24	-14.84	178	4.04	4.53
35		75.58	5.09	12.80	12.80	76	3.91	3.91
36		-65.02	4.38	-11.68	-13.33	178	3.57	4.07
37	4.0	73.50	4.95	11.99	11.99	76	3.66	3.66
38		-66.24	4.46	-11.63	-12.21	483	3.55	3.73
39		71.37	4.81	10.13	11.52	483	3.09	3.52
40		-60.96	4.11	-9.76	-10.49	178	2.98	3.20
41	4.0	81.32	5.48	11.53	12.02	483	3.52	3.67
42		-52.95	3.57	-8.27	-8.43	178	2.53	2.58
43	6.0	129.15	8.70	23.79	24.09	483	7.26	7.35
44		-82.01	5.53	-17.56	-17.79	178	5.36	5.43

TABLE 7.5c : ROTATIONAL AND CURVATURE DUCTILITY FACTORS - BEAM NORTH

Load Run No.	μ	θ_{bl} rad x 10^6	$\frac{\theta_{bl}}{\theta_y}$	ϕ_l rad/mm x 10^6	ϕ_{max} rad/mm x 10^6	$^l\phi_{max}$ mm	$\frac{\phi_l}{\phi_y}$	$\frac{\phi_{max}}{\phi_y}$
19	2.0	-53.33	3.16	-14.84	-14.84	76	4.01	4.01
20		57.33	3.40	11.46	11.46	76	3.09	3.09
21		-52.67	3.12	-23.17	-23.17	76	6.26	6.26
22		55.33	3.28	8.24	14.41	178	2.22	3.89
23	0.75	-7.33	0.44	-6.39	-6.39	76	1.73	1.73
24		23.67	1.40	-0.19	8.93	178	-0.05	2.41
25	4.0	-137.67	8.15	-39.04	-41.09	178	10.54	11.09
26		133.00	7.88	25.23	39.10	279	6.81	10.56
27		-78.33	4.64	-21.29	-27.58	381	5.75	7.45
28		128.67	7.62	22.63	26.67	279	6.11	7.20
31	2.0	-14.00	0.83	-4.08	-4.78	483	1.10	1.29
32		69.67	4.13	8.86	14.31	279	2.39	3.86
33	4.0	-72.67	4.30	-14.97	-15.13	178	4.03	4.09
34		123.67	7.32	17.21	20.74	279	4.65	5.60
35		-74.33	4.40	-13.41	-14.40	178	3.62	3.89
36		121.67	7.21	15.73	19.21	279	4.25	5.19
37	4.0	122.33	7.24	16.75	18.63	279	4.52	5.03
38		-72.00	4.26	-12.01	-12.34	178	3.24	3.33
39		116.00	6.87	12.40	16.02	279	3.35	4.33
40		-69.33	4.11	-10.40	-10.92	178	2.81	2.95
41	4.0	-75.00	4.44	-10.19	-10.67	178	2.75	2.88
42		119.67	7.09	12.64	16.47	279	3.41	4.45

TABLE 7.5d : ROTATIONAL AND CURVATURE DUCTILITY FACTORS - BEAM SOUTH

Load Run No.	μ	θ_{bl} rad x 10^4	$\frac{\theta_{bl}}{\theta_{by}}$	ϕ_l rad/mm x 10^6	ϕ_l rad/mm x 10^6	$^l\phi$ max mm	$\frac{\phi_l}{\phi_y}$	$\frac{\phi_{max}}{\phi_y}$
19	2.0	53.33	3.16	9.54	9.54	76	2.58	2.58
20		-52.00	3.08	-20.40	-20.40	76	5.51	5.51
21		54.00	3.20	19.50	19.50	76	5.27	5.27
22		-49.33	2.92	-18.73	-18.73	76	5.06	5.06
23	0.75	11.67	0.69	- 2.47	3.57	178	-0.67	0.96
24		-20.00	1.18	- 9.25	- 9.25	76	2.50	2.50
25	4.0	131.33	7.78	31.41	44.09	178	8.48	11.90
26		-88.33	5.23	-21.75	-33.70	178	5.87	9.10
27		132.00	7.82	24.96	25.44	178	6.74	6.87
28		-78.00	4.62	-22.61	-26.79	178	6.10	7.23
31	2.0	66.00	3.97	6.10	6.10	76	1.65	1.65
32		-21.00	1.24	-8.14	-11.46	178	2.20	3.09
33	4.0	120.00	7.11	16.67	17.30	178	4.50	4.67
34		-72.33	4.28	-17.06	-19.25	178	4.61	5.20
35		113.00	6.69	14.09	15.30	178	3.80	4.13
36		-70.00	4.15	-15.06	-16.79	178	4.07	4.53
37	4.0	-73.33	4.34	-16.48	-16.48	76	4.45	4.45
38		111.67	6.61	13.56	14.58	178	3.66	3.94
39		-71.33	4.22	-13.20	-13.20	76	3.56	3.56
40		109.67	6.49	11.36	12.66	178	3.07	3.42
41	4.0	114.67	6.79	10.89	12.41	178	2.94	3.35
42		-70.67	4.19	-11.48	-12.63	178	3.10	3.41

In load runs 29 and 30 where unidirectional loading in the East-West direction was repeated after loading in the transverse direction (see Fig. 7.5), the rotational and curvature ductility demands were significantly less than in the previous East-West cycles because of the increased flexibility of the joint caused by transverse loading. When skew loading was applied the rotational and curvature demand decreased due to increased joint deformation. The apparent rotational ductility factor also became greater than the curvature ductility factor at this stage due to increased yield penetration and slip of beam bars within the joint. As in the plane frame tests, slip of beam bars increased the apparent rotation because of the method of obtaining this measurement. Summation of curvature values over the rotational gauge length for the East-West beams showed that during load runs 5 to 8 and 11 to 14 the sum of curvatures accounted for an average of 65% of the measured rotations, whereas during load runs 33 to 42 calculation showed that an average of 45% of the apparent rotation was caused by curvature in the plastic hinge, with the remainder caused by yield penetration and slip of beam bars. In this test no curvature measurement was available closer than 76 mm to the column face, and the value obtained at this point was therefore assumed to be applicable up to the face. The calculations were therefore somewhat less accurate than those made in the plane frame tests, where a value of curvature was available 25 mm inside the column face. Nonetheless it is considered that the calculations were sufficient to show that yield penetration was more significant during skew loading than during unidirectional loading. This was caused partly by the column and joint cracking under skew loading, and partly by progressive attrition of bond strength as the number of cycles increased.

The position of maximum curvature within the plastic hinges varied from one beam to another but at constant levels of displacement demand (i.e. $\mu = 4.0$) the maximum curvature tended to recur in the same position for loading of the same sense for each beam. This was as expected since the crack pattern in the beams did not vary much during successive cycles.

7.3.2 Components of Beam End Displacement

The components of beam end displacement determined for the Western beam throughout the test are shown in Fig. 7.12. The components of beam displacement measured for the Eastern beam were similar, but joint deformation was measured in the East-West direction only and hence the resulting component of beam end displacement could not be determined for the North

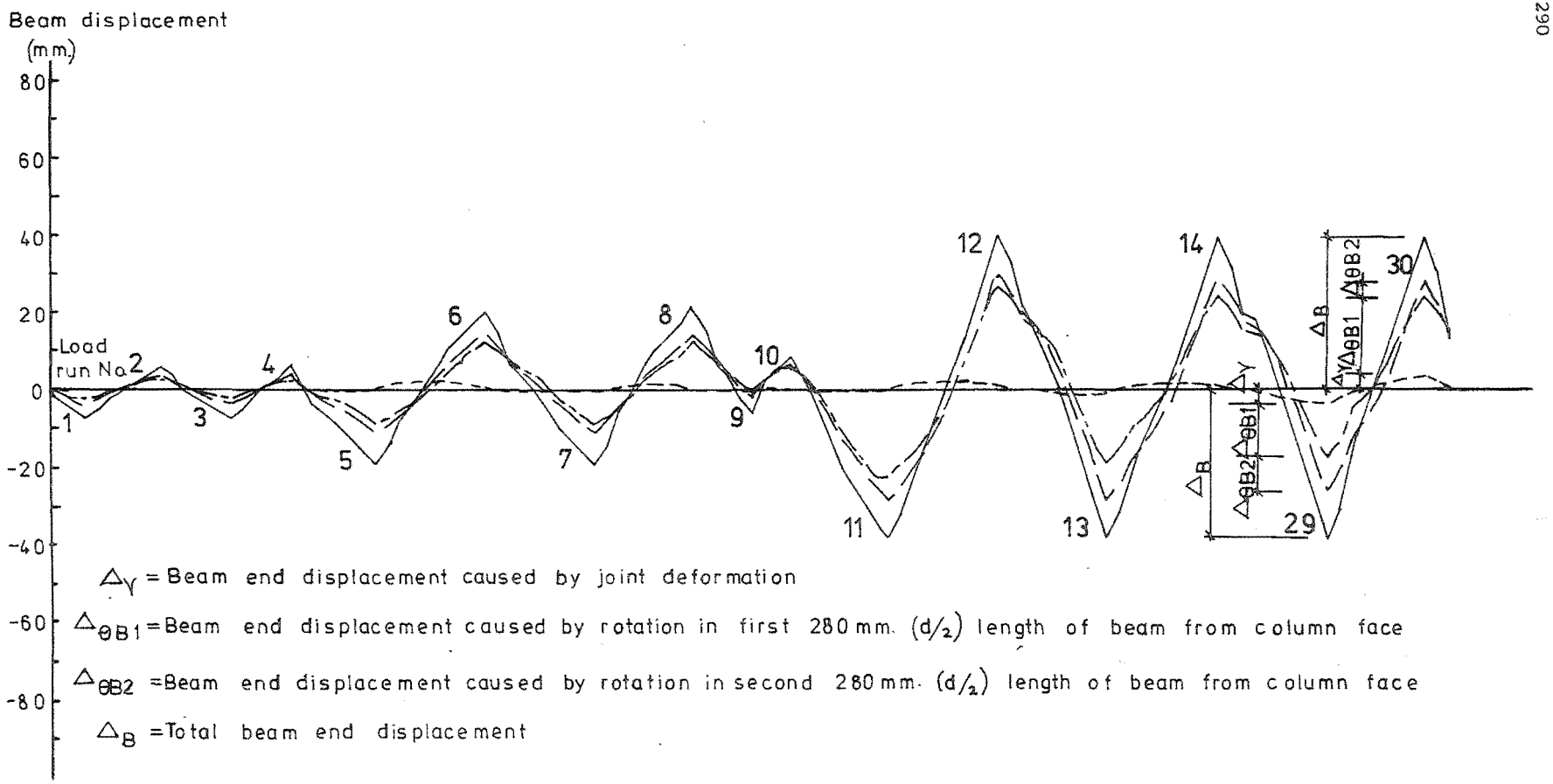

FIG. 7.12a: COMPONENTS OF BEAM END DISPLACEMENT FOR WESTERN BEAM

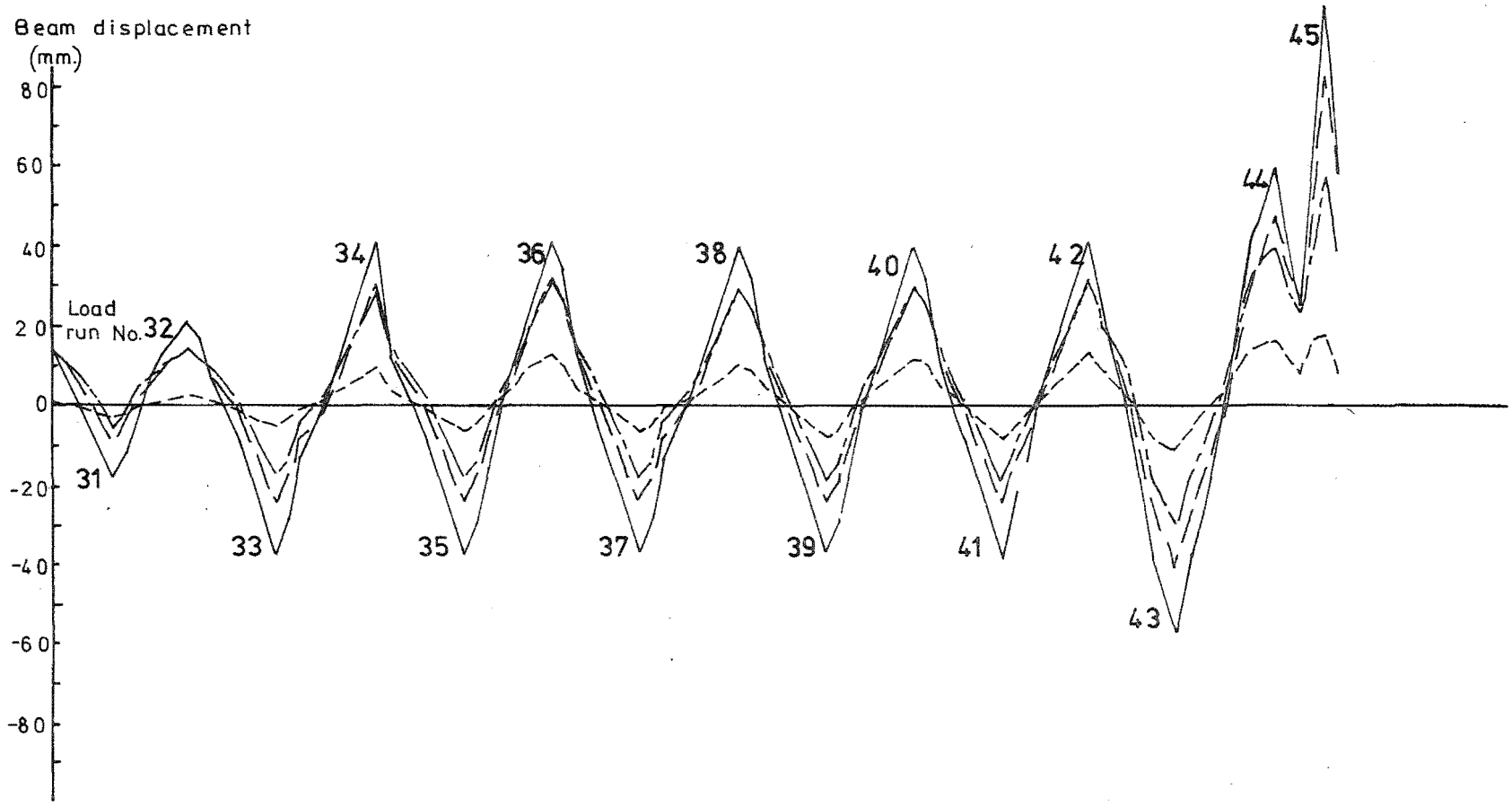

FIG. 7. 12b: COMPONENTS OF BEAM END DISPLACEMENT FOR WESTERN BEAM

and South beams.

Fig. 7.12 shows that, as found in the plane frame test results, beam rotation in the first 280 mm gauge length away from the column face, θ_{b1}, caused the major component of beam displacement throughout the test. Rotation in the second 280 mm gauge length, θ_{b2}, caused relatively small components of the beam end displacements until load run 43 when the imposition of a beam displacement ductility factor of six caused yield strain in the beam flexural reinforcing to spread further along the beam; the rotation in the second gauge length then became more significant.

Joint deformation caused only about 3% of the total beam end displacements up to load run 14, while the as-yet unloaded transverse beam was providing maximum confinement to the joint. However, after loading of the North-South beam, the joint deformations measured at the maximum displacements of the repeated cycle under East-West loading (load runs 29 and 30, see Fig. 7.5) caused 9% of the total beam displacements. During the major cycles of skew loading (load runs 33 to 42) the results indicated that joint deformation caused an average of 23% of the maximum displacements, the proportion increasing slightly as the number of cycles increased. At the maximum displacements of the final cycle of unidirectional loading (load runs 43 and 44) the average proportion of beam end displacement caused by joint deformation was 22%, showing that skew loading had had a severe effect on the joint flexibility under unidirectional loading.

It is considered likely that the transverse beams interfered to some extent with the diagonal rods used to transfer the diagonal deformations of the joint to the LVDT's by means of which the joint distortion was measured. Hence it is unlikely that the joint deformations recorded were very accurate, but the differences in the recorded joint deformations before and after loading of the transverse beams, and before, during, and after skew loading, were sufficiently pronounced that their usefulness in describing the joint response was not prejudiced. The tendencies indicated by the joint deformation readings were corroborated by the results obtained from the electrical resistance strain gauges on the joint reinforcement. The correlation between joint shear deformation and joint reinforcement strains was clearly shown in the plane frame tests.

7.3.3 Strains in Beam Flexural Reinforcing

As explained in Section 7.1.4, the strains in the beam bars through the joint could not be obtained by Demec gauges as was done in the plane frame tests, and electrical resistance strain gauges were employed to

partly compensate for this lack of information (see Fig. 7.4). However, to avoid undue congestion of lead wires and loss of bond of the bars, the number of strain gauges used was limited, and when some penetration of yield strain into the joint occurred some gauges were lost due to differential movement between the bars and the surrounding concrete. Consequently the record of strains in beam bars across the joint was relatively sparse compared to those obtained in the plane frame tests. However, the gauges fixed to the top layer of bars of the East-West beam at the column centreline functioned throughout the test, and these gauges indicated that yield penetration did not reach the column centreline at any stage.

The strain results obtained at each increment of load runs 13, 35, and 41 for the East-West beams are presented in Figs. 7.13, 7.14, and 7.15 respectively. The strains plotted for each layer of bars were the mean values of those measured in the outer two bars in each layer. Although the results obtained across the joint were insufficient to show the extent of yield penetration at the various stages, the figures are still useful in showing the extent of plastic straining produced during each load run, for all of which the maximum displacement ductility factor was four. Fig. 7.13 shows that during load run 13, when unidirectional loading had been applied in the East-West direction only (see Fig. 7.5), the amount of plastic strain induced in the reinforcing in the plastic hinges was much greater than that shown in Figs. 7.14 and 7.15 for load runs 35 and 41, when both beams were being loaded simultaneously. The difference between the strains observed before loading and at maximum load in the latter cases was much less than for unidirectional loading runs. This was due to the greater joint flexibility under skew loading and was reflected in the loss of stiffness and energy absorbing capacity indicated on the load-displacement graphs (Fig. 7.10) for the skew loading cycles compared to the unidirectional cycles. It was also shown in the greater rotational and curvature ductility demands for the earlier load runs, listed in Tables 7.4a to d.

7.3.4 Beam Reinforcement Stresses

The available strain results obtained from beam reinforcing steel throughout the test were converted to stresses using the cyclic stress-strain analysis described previously with respect to the plane frame test results (see Section 3.3.4). Stress-strain curves produced by these analyses are shown in Figs. 7.16 and 7.17 for bars in the top layer of reinforcing at 76 mm from the column face for the West and North beams respectively. The decrease in effective energy dissipation at these

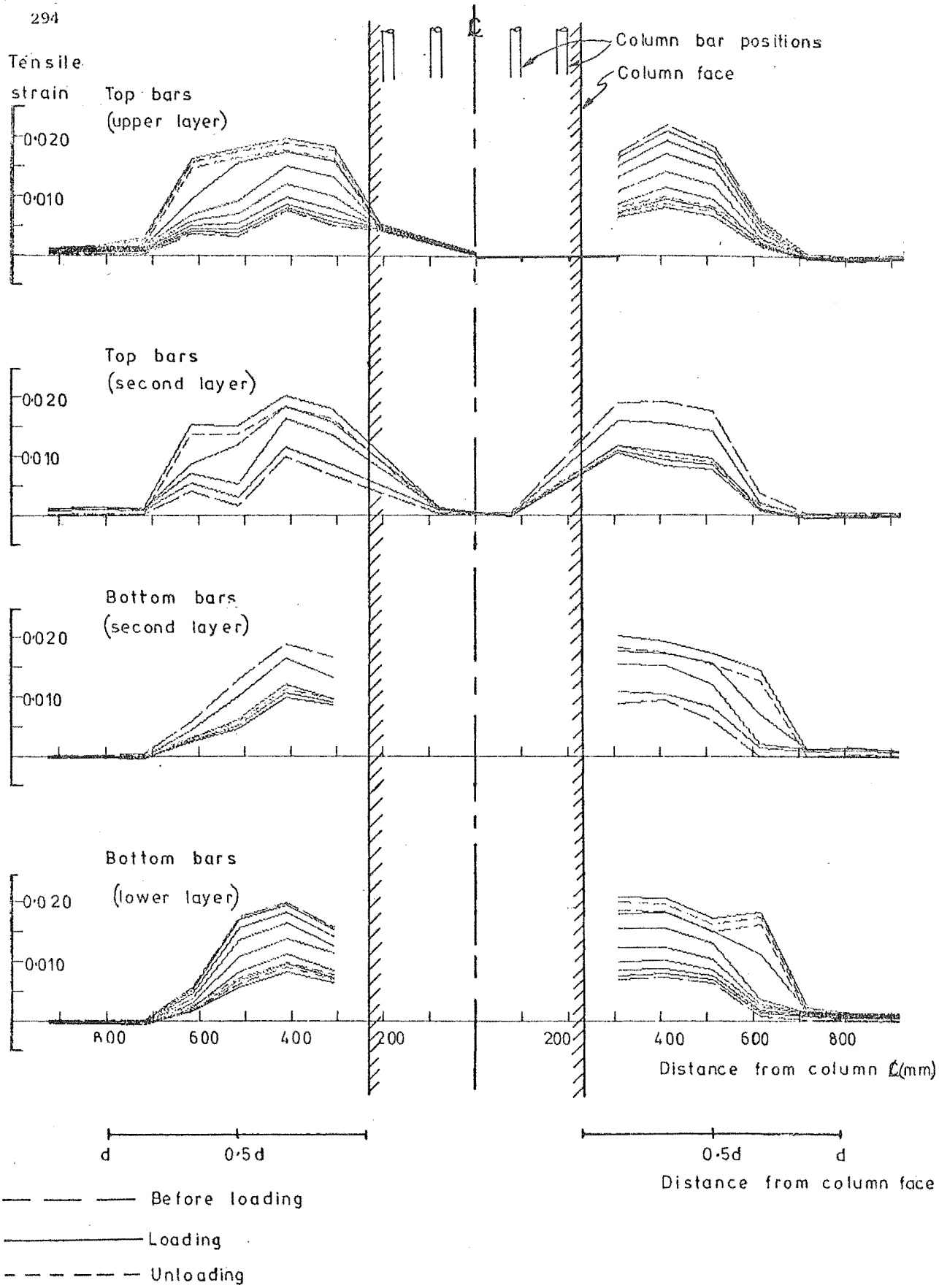

FIG.7.13 : BEAM BAR STRAINS, EAST-WEST BEAM, LOAD RUN 13

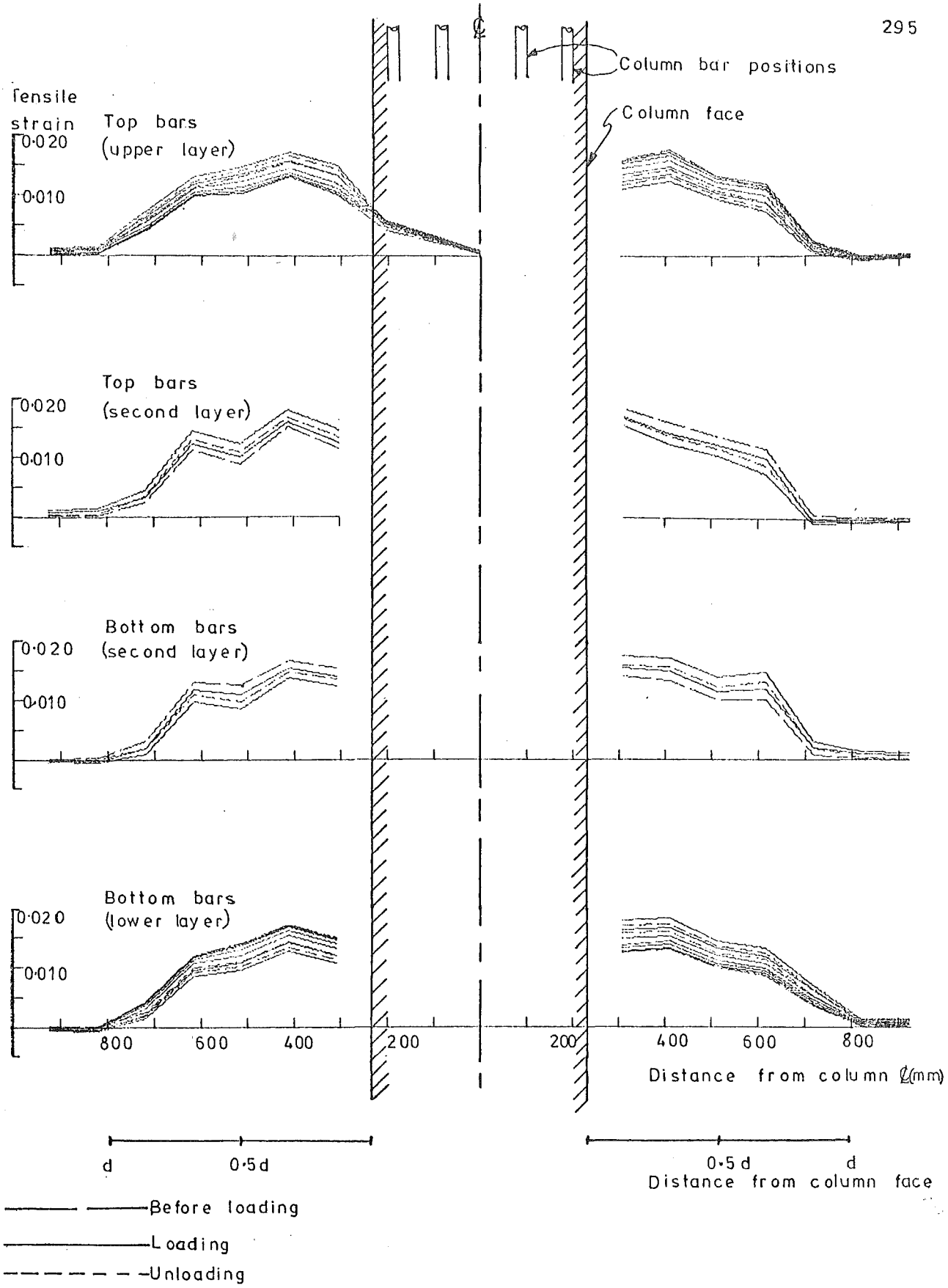

FIG.7.14 : BEAM BAR STRAINS, EAST-WEST BEAM, LOAD RUN 35

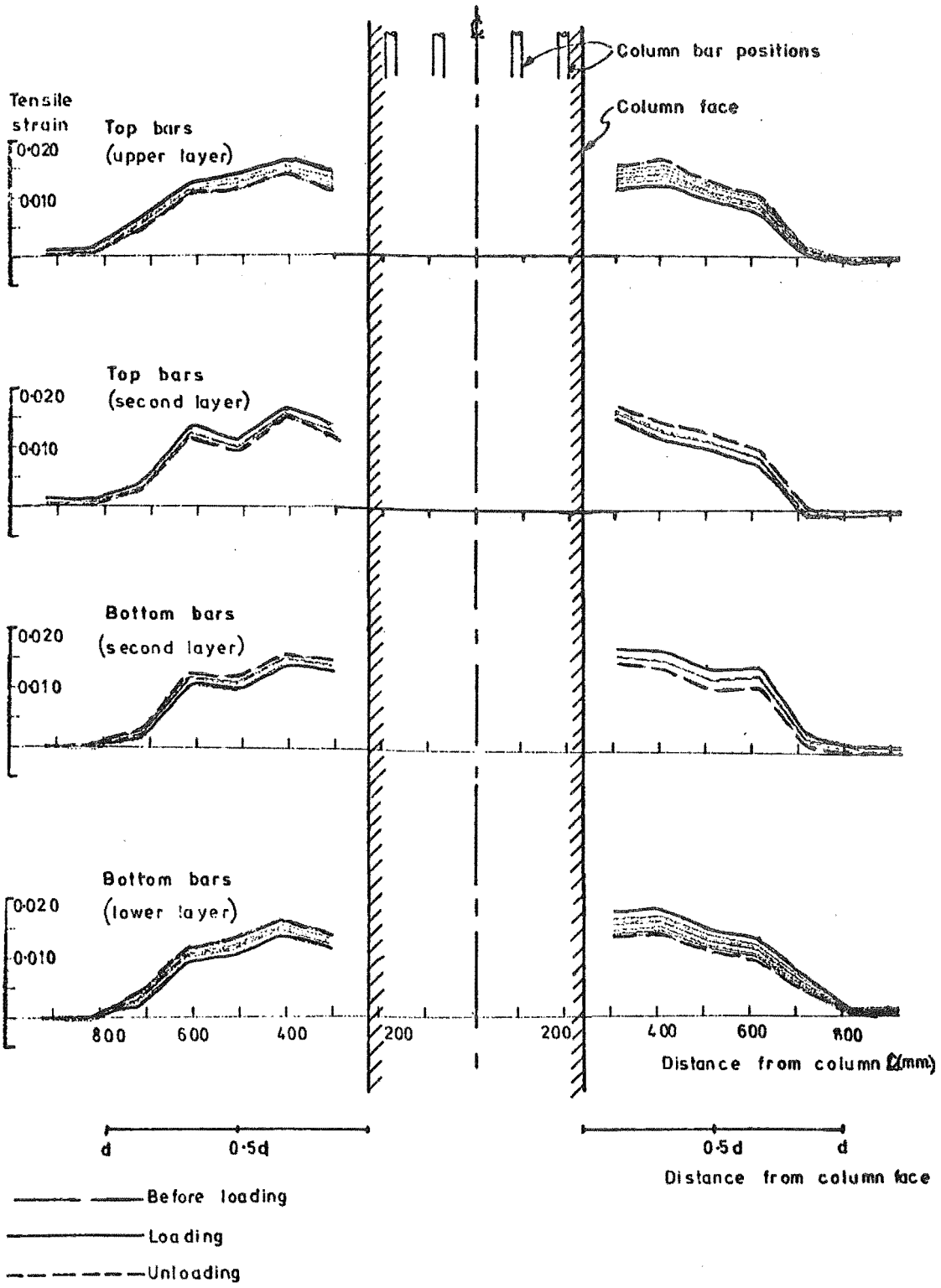

FIG. 7. 15 : BEAM BAR STRAINS, EAST-WEST BEAM, LOAD RUN 41

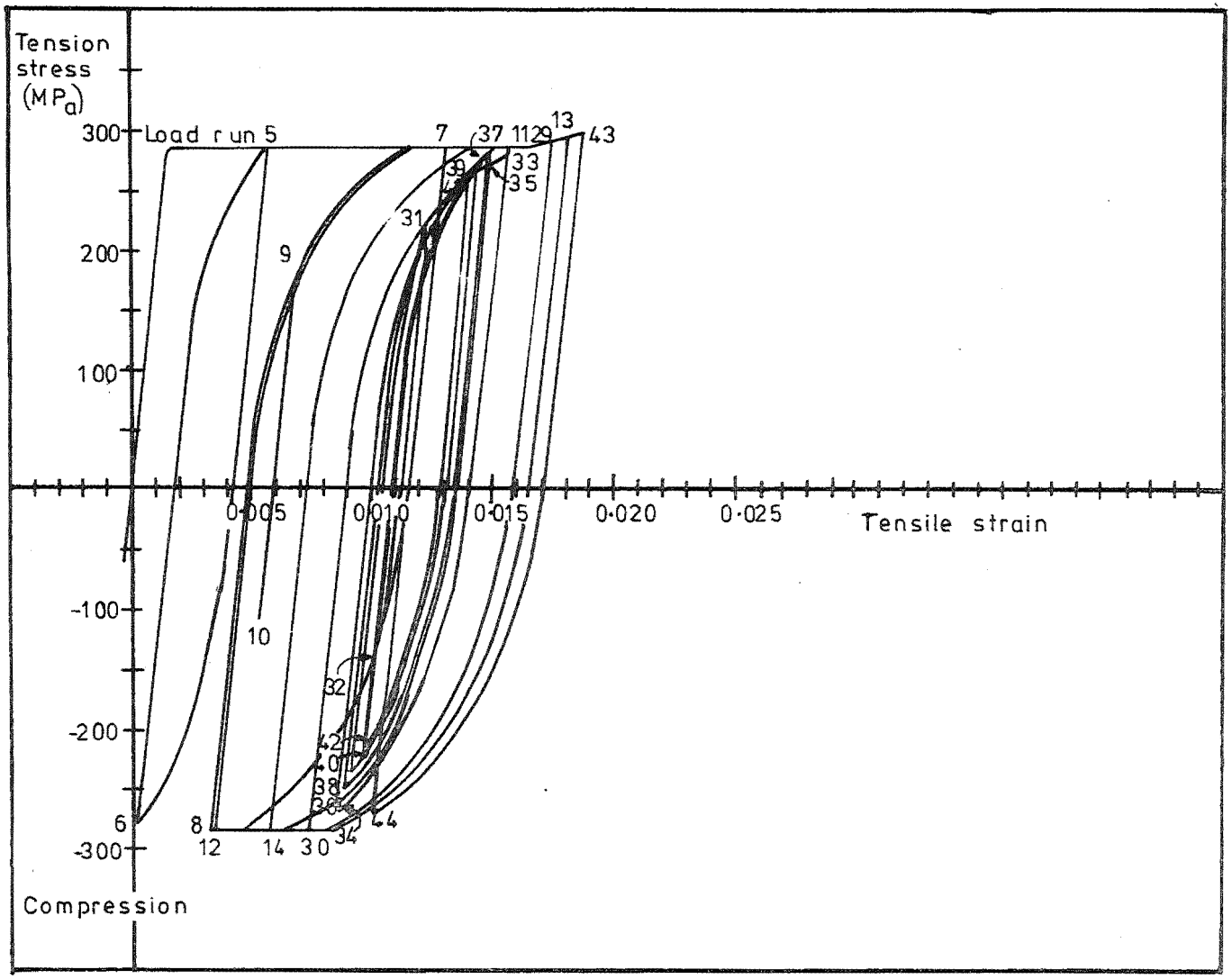

FIG. 7.16 : STRESS-STRAIN HISTORY FOR UPPER LAYER OF TOP REINFORCING IN EAST-WEST BEAM AT 76 MM. FROM WEST COLUMN FACE

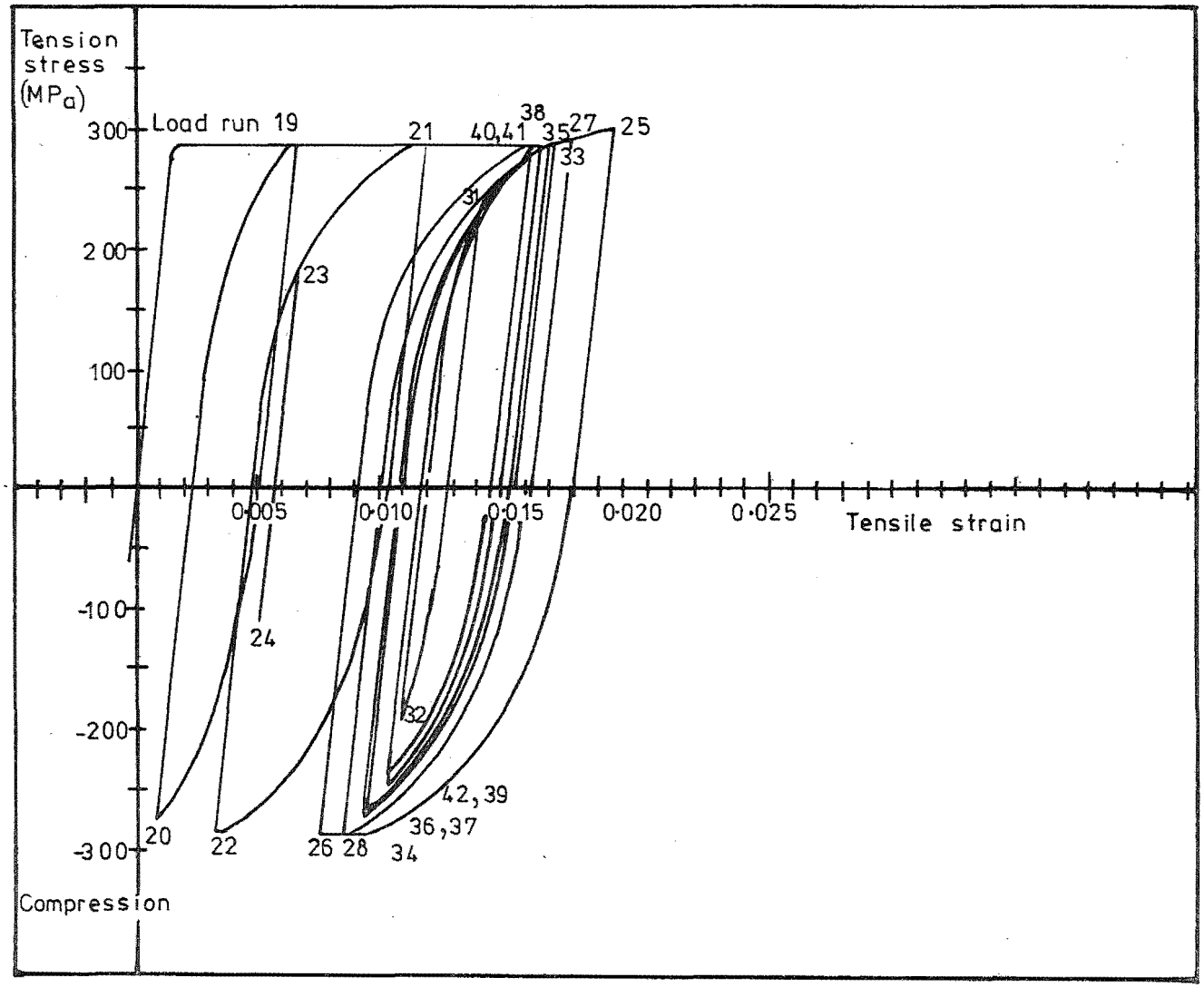

FIG.7.17 :STRESS-STRAIN HISTORY FOR UPPER LAYER OF TOP REINFORCING IN NORTH-SOUTH BEAM 76 MM. FROM NORTH COLUMN FACE

locations when skew loading was applied is shown by the smaller area enclosed by the stress-strain loops for each cycle from load run 31 to load run 42. As noted elsewhere this occurred due to reduced joint stiffness under skew loading.

Equilibrium checks were carried out using the stress results for all bars at this first available section from the column face. The resulting internal moments were compared with the external moments applied by the beam end loads at the maximum displacement of each load run, together with those due to dead load. As in the plane frame tests it was found that the derived stress results underestimated the required internal moments of equilibrium, in this case by an average of 8%. The discrepancy between applied and calculated internal moments tended to increase with time once the strain-hardening range was attained, due to the effects of strain-aging of the steel. However, it may be noted that in some cases under skew loading the calculated stresses did not in fact reach the envelope curve, implying that either the basic cyclic stress-strain algorithm used in the analysis underestimated the stresses, or that the strain data was inaccurate in some of these cases. Small errors from either of these sources could have caused the observed differences to the resulting stress.

Since the strains in flexural bars through the joint were monitored by means of electrical resistance strain gauges which became inoperative as yield penetration and slip occurred, stress profiles across the joint could not be calculated throughout the test, as was done for the plane frame test units. However, up to load run 30 some results were available, and bond stresses calculated from the steepest slope of the resulting stress profiles are shown in Fig. 7.18 for the various layers of bars. Comparison with Fig. 5.24 shows that the bond stresses derived for unidirectional loading in this test were significantly less than those derived at corresponding stages of the plane frame tests. Part of the difference was due to the fact that the average bond stresses for this test were calculated from bar stresses computed at the ends of a 'bond gauge length' between adjacent strain-monitoring points of 200 mm for outer bars and 150 mm for inner bars, as compared to the bond gauge length of 100 mm used in the plane frame calculations. However, careful study of the data from both tests on the basis of a 200 mm bond gauge length showed that bond stresses were significantly less in the space frame test unit under unidirectional loading than in the plane frame unit, although not by as much as first inspection of Figs. 5.24 and 7.18 might suggest.

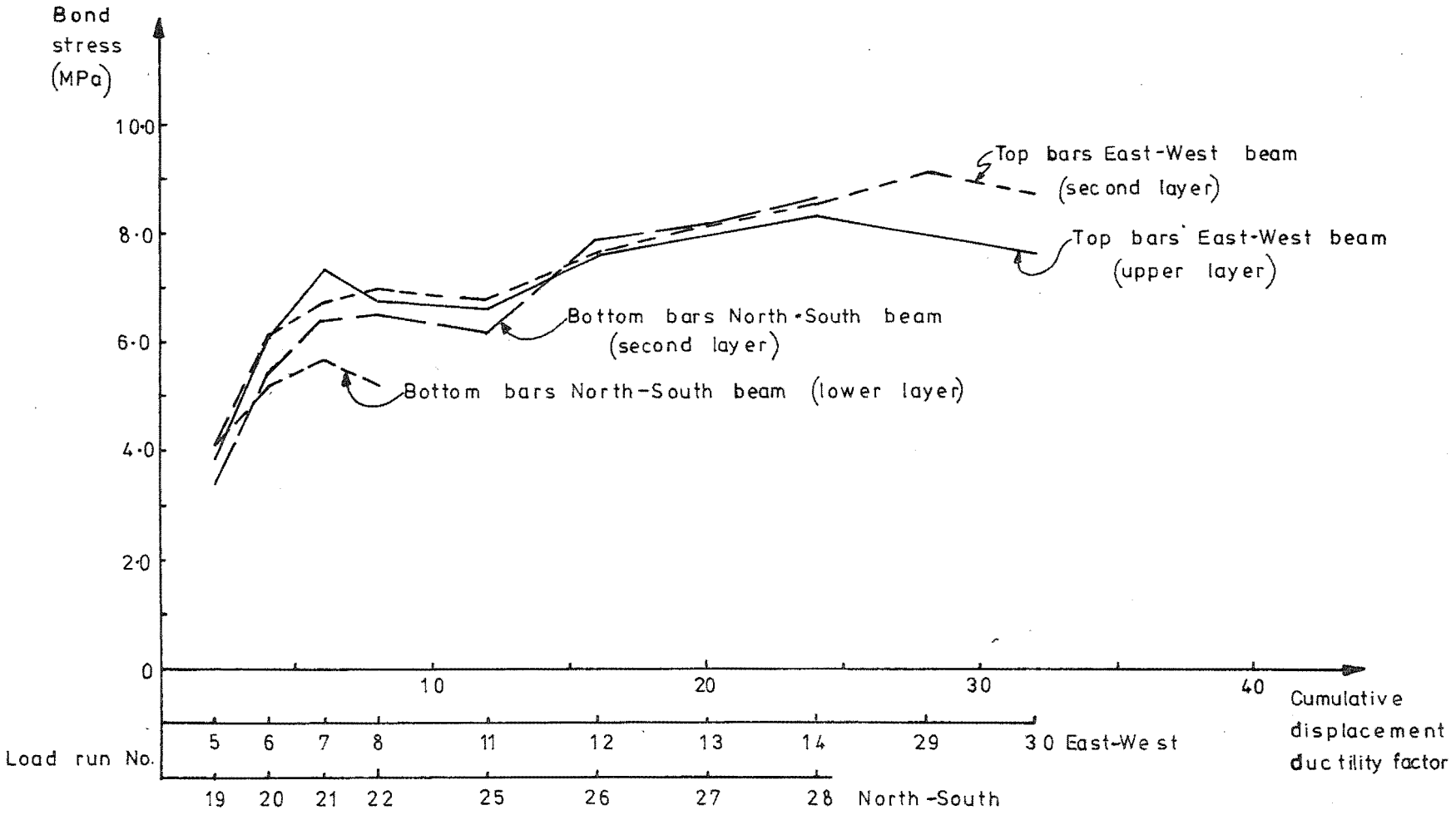

FIG.7.18 :BOND STRESSES IN BEAM BARS ACROSS JOINT

The bond stresses were similar for the bars in the beams in the two directions after similar amounts of loading, in spite of the fact that the transverse beams had already been loaded before the North-South beams were loaded, whereas in the case of the East-West beams the transverse beams had not been loaded. This result suggests that (independent) loading of the transverse beam had little effect on the development of bond stresses of the flexural bars across the joint. This conclusion is supported by small increases in the bond stresses calculated for the bars of the East-West beam in load runs 29 and 30, compared to those derived for load runs 11 to 14.

Most of the strain gauges on the beam flexural bars were lost soon after skew loading of the test unit was imposed. Hence bond stresses could not be calculated for the bars during this part of the test, but it seems that yield penetration increased at this stage, and the resulting bond stresses would therefore have been greater than those calculated for unidirectional loading.

7.3.5 Beam Shear Behaviour

Demec strain gauges were used to monitor strains at the mid-depth of every third beam stirrup in the plastic hinge region of each beam. Similar results were obtained to those in the plane frame test B13, with the results again distorted somewhat by the presence of the Demec holes, which acted as diagonal crack initiators.

Sliding shear displacement along the flexural cracks again contributed to degrading stiffness of the unit, but no measurements of this displacement were taken in this test. It is expected that the results obtained in test B13 would be applicable, where shear displacement in the beams was found to comprise 5 to 6% of the total beam end displacements at a displacement ductility factor of four.

7.4 Column Behaviour

The response of the column was monitored throughout the test by electrical resistance strain gauges fixed to seven out of the twelve vertical bars at the levels of the upper and lower beam surfaces and at the mid-depth of the joint, as shown in Fig. 7.4. During the course of the test seven of these twenty-one gauges ceased to function due to short-circuiting or other problems, so that the record obtained towards the end of the test was less complete than was desirable.

Because the strain was measured at only three points on each bar the profiles obtained were not as extensive as those obtained for the plane frame units, where a full record of strain from 250 mm above the joint to 250 mm below was obtained at intervals of 100 mm using Demec strain gauges on the bars in the South face only. However, the strains recorded at the levels of the beam top and bottom surfaces during unidirectional loading may be usefully compared with those measured in the test of Unit B13. In the present test strains across the West face of the column were measured for four different bars (C1, C10, C11, and C12 - see Fig. 7.4), while two bars (C4 and C7) were instrumented in the Eastern face. The compressive strains obtained were consistent across the breadth of the column during loading in the East-West direction, and distinctly smaller than those recorded for unit B13 at corresponding stages. As discussed in Section 5.4, it was considered that the compressive strains recorded from the bars in the South face of unit B13 were exagerrated by various effects,and these results confirm that view. When the North-South beam was loaded, three gauges (on bars C7, C8 and C10) were available in the North face of the column, and two (on bars C1 and C4) in the South face, and the strain results obtained were consistent, both across the breadth of the column,and in comparison with those measured under East-West loading.

The column bar strains measured at the maximum displacement of load runs 33 to 36 are shown in Fig. 7.19, and those for load runs 37 to 40 in Fig. 7.20. Strains at the three instrumented sections (top, mid-depth, and bottom of beam levels) were plotted along the column diagonal parallel to the direction of loading (i.e. perpendicular to the neutral axis).

Where two strain gauges were available to measure strain in any location the mean of those results was plotted. The theoretical strain values plotted for comparison were calculated using the column moments caused by the ideal beam ultimate loads P_u (see Table 7.3a) applied to each beam, and the actual material properties for the column. It is apparent that the measured strains differed considerably from the theoretical values, although the agreement was better during load runs 33 to 36 than in the later cycles. This was probably due to the spalling of the column corners over the depth of the joint, as shown in the photographs (Figs. 7.7 and 7.8). The strain distributions in Figs. 7.19 and 7.20 show that the corner bars C1, C4, C7 and C10 carried greater compressive strains than predicted theoretically, assuming the full column section to be effective. The strains measured at mid-depth of the joint also showed greater compressive strains in the corner bars.

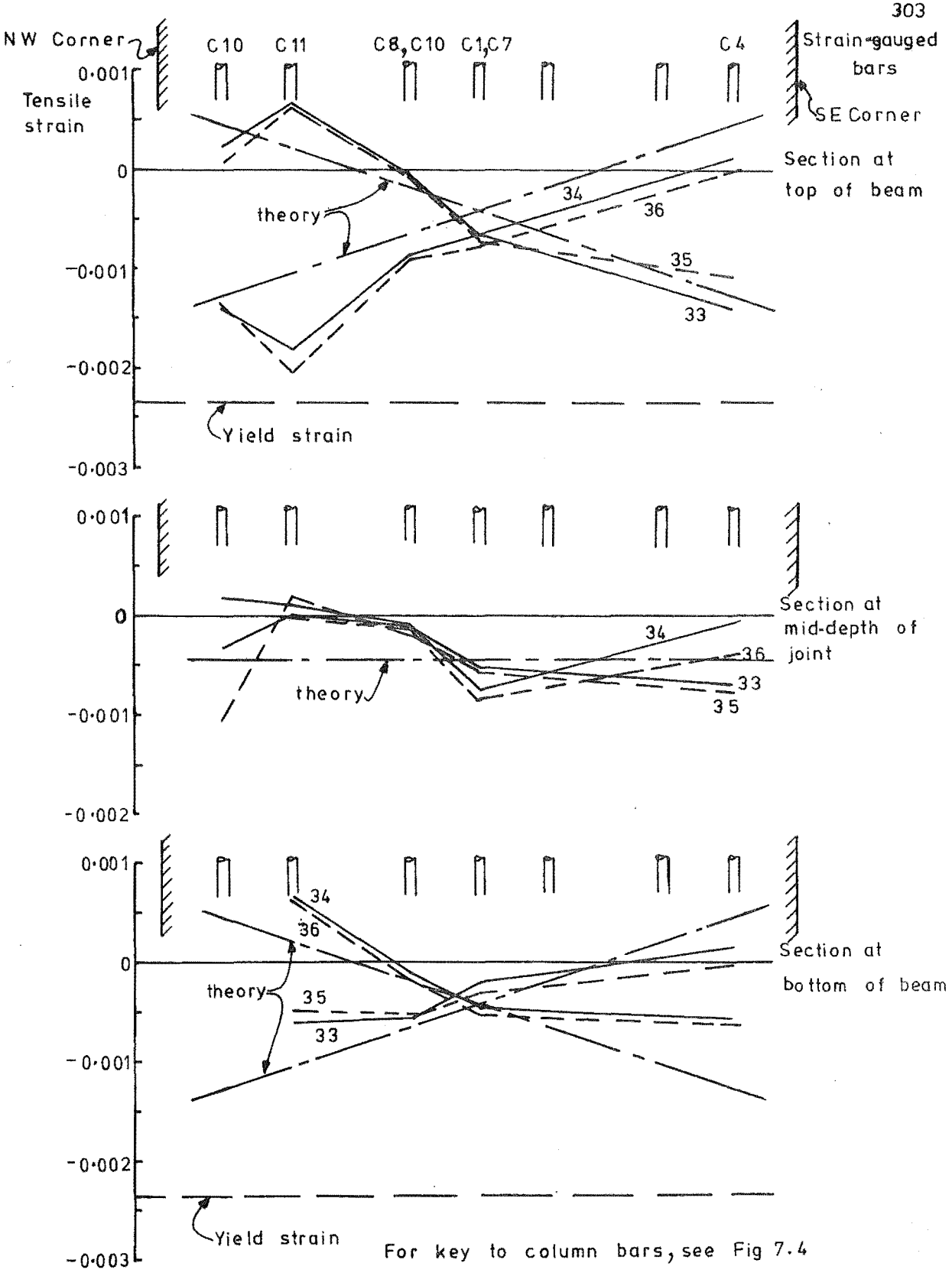

FIG. 7.19 : COLUMN BAR STRAINS, LOAD RUNS 33 TO 36

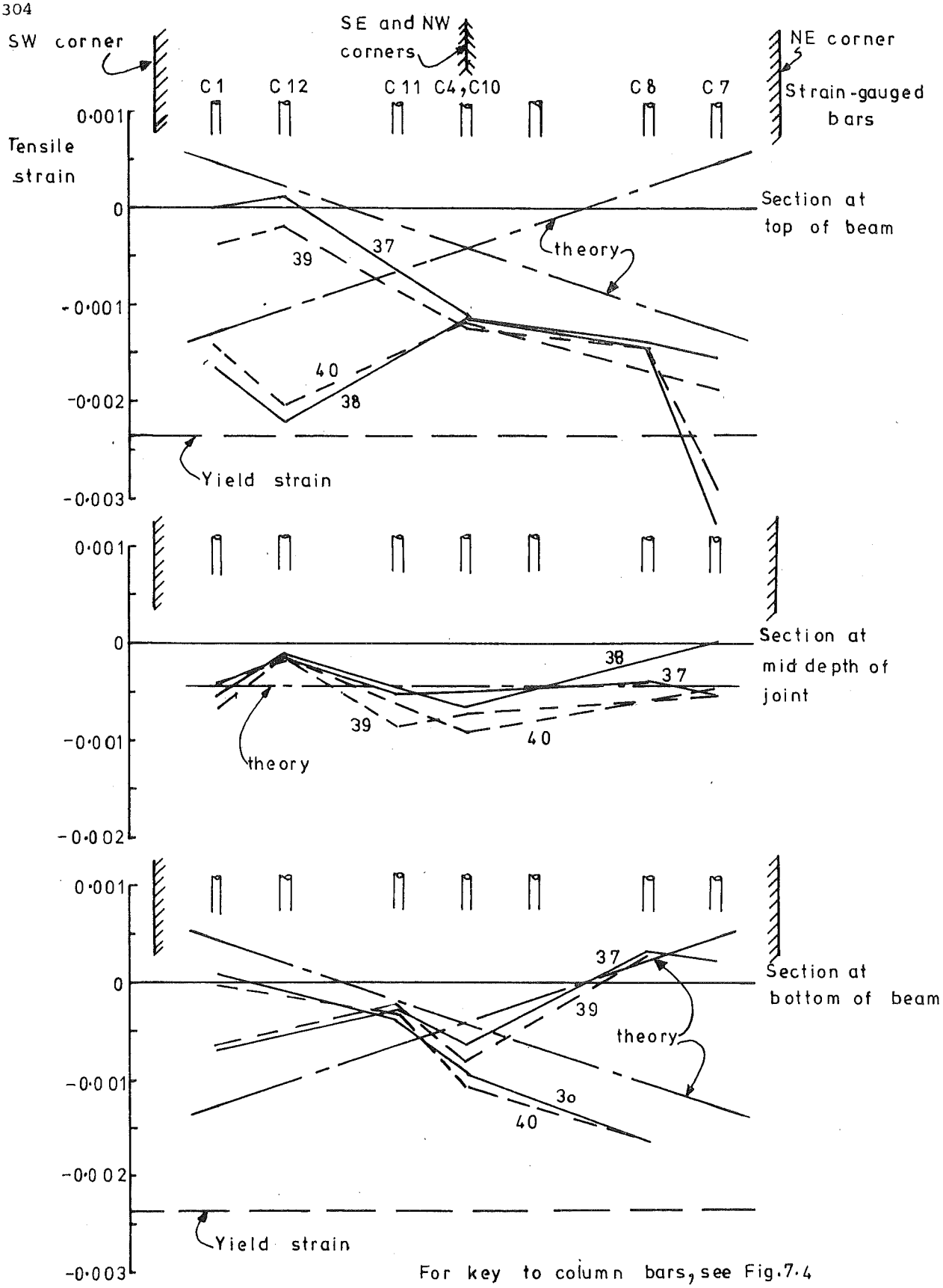

FIG.7.20 : COLUMN BAR STRAINS, LOAD RUNS 37 TO 40

From load run 41 onwards the column strain results obtained were too sparse to allow any worthwhile comparisons to be made with the preceding cycles.

7.5 Joint Behaviour

7.5.1 Joint Cracking and Deformation

The extent of cracking in the joint could not be seen during the test due to the presence of members on all four faces. The only visual indication of the condition of the joint was given by the exposed corners of the column down the depth of the joint. As the photographs (Figs. 7.6 to 7.9) show, these corners cracked under unidirectional loading, and spalled under skew loading.

As described in Section 7.3.1, the shear deformation of the joint was measured in the East-West direction, although no measurement could be made in the North-South direction. The results showed the joint deformation under unidirectional loading to be greater after loading of the transverse beam, while skew loading further increased the joint flexibility.

It was noticed during the skew loading part of the test that some horizontal distortion of the joint was also occurring. This was first noted as significant differences in the apparent strains measured from the beam flexural bars in opposite sides of each beam, together with a tendency for the beam ends to move sidesways against the test rig. From load run 40 onwards the horizontal movement of the beams was measured by dial gauges fixed at about 1200 mm away from the column face for each beam. The measurements taken indicate that the beams were displaced as shown in Fig. 7.21. The direction of the horizontal displacements of the beams changed between load runs 40 and 41 following the change in the direction of loading, with loads applied in the NE-SW direction in load run 40 and in the NW-SE direction in load runs 41 and 42 (see Fig.7.5). As expected there was no change in the sense of the observed deformations between load runs 41 and 42, since load was applied in the same direction in both these load runs. Since no zero readings were obtained for these displacements, the absolute values of deflection shown in Fig. 7.21 cannot be given, but the maximum difference in deflection observed between load runs 40 and 41 was 6 mm.

During the subsequent unidirectional load runs (43 and 44) very little horizontal movement of the beams was observed, showing clearly that it was the skew loading that caused this behaviour.

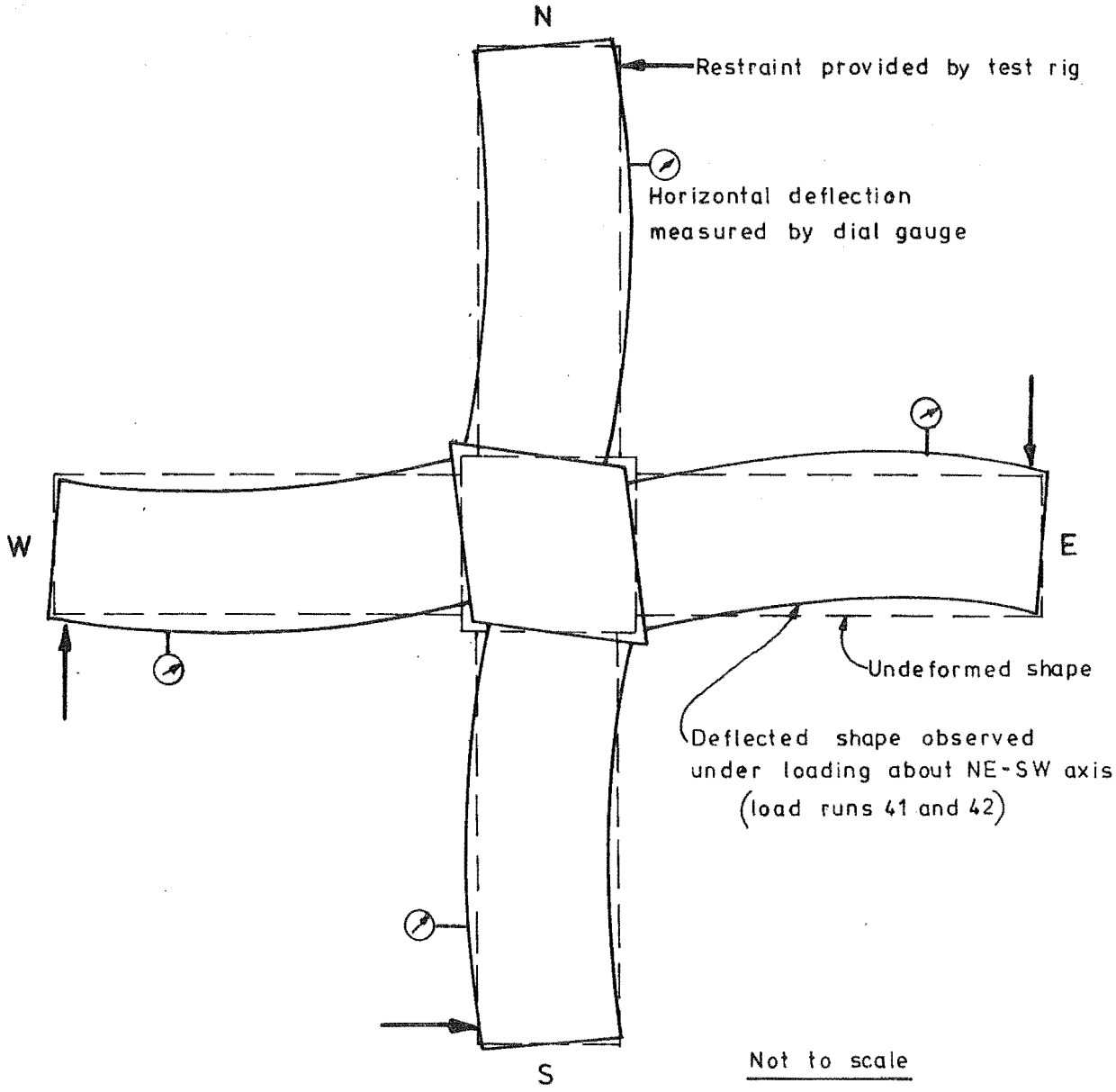

FIG. 7. 21: PLAN VIEW OF TEST UNIT SHOWING HORIZONTAL DEFORMATION UNDER SKEW LOADING

The observed deformations implied a biaxial bending condition in the beams of the test unit. This could have occurred due to bond conditions for beam flexural bars within the joint being relatively better[26] at diagonally opposite corners of each beam section due to the greater compressive stresses near the corresponding edges of the column above and below the joint, caused by the biaxial bending of the column, as shown somewhat schematically in Fig. 7.22. Consideration of the expected stress distributions in the column under biaxial bending shows that expected areas of higher bond strength for beam bars due to higher concrete compressive stresses in the vicinity would have resulted in assymetrical response of the beams consistent with the observed deformations.

Note that the occurrence of biaxial bending in the beams would also be consistent with the suggestion made in Section 1.4 that local stress concentrations would be required at the beam-column interfaces to provide suitable end conditions for a concrete diagonal strut to act diagonally across the joint core under skew loading.

In a prototype structure the slab would at least partially restrain the beams against the type of deformation observed in the test, where no slab was included. Thus it seems possible that the reaction of the slab on the beam might provide additional confinement to the joint under skew loading, thus increasing its strength compared to that observed in the test unit. In the test, the test rig provided some lateral restraint to the beams at the points of loading, but obviously no restraint was available over the remainder of the length of the beams, and the joint deformation was therefore basically unrestricted.

7.5.2 Strains in Joint Horizontal Reinforcement

Envelopes of strains measured at various stages of the test in the joint horizontal ties are given in Fig. 7.23 for the inner legs of ties, and in Fig. 7.24 for the outer legs. Because load was applied to the joint in both principal directions the tie legs cannot be characterised as stirrup legs (primarily resisting the applied shear), or as transverse tie legs (primarily providing confinement to the joint core), as was done in the plane frame test reports. The results are therefore presented simply in terms of strains measured in the tie legs parallel to the East and West faces of the joint, and those in tie legs parallel to the North and South faces. When the East and West beams only were loaded (load runs 1 to 14, 29 to 30, and 43 to 44), the North and South legs were acting as stirrup legs while the East and West legs acted as confining ties. When the North and South beams only were loaded (load runs 15 to 28), the North and South

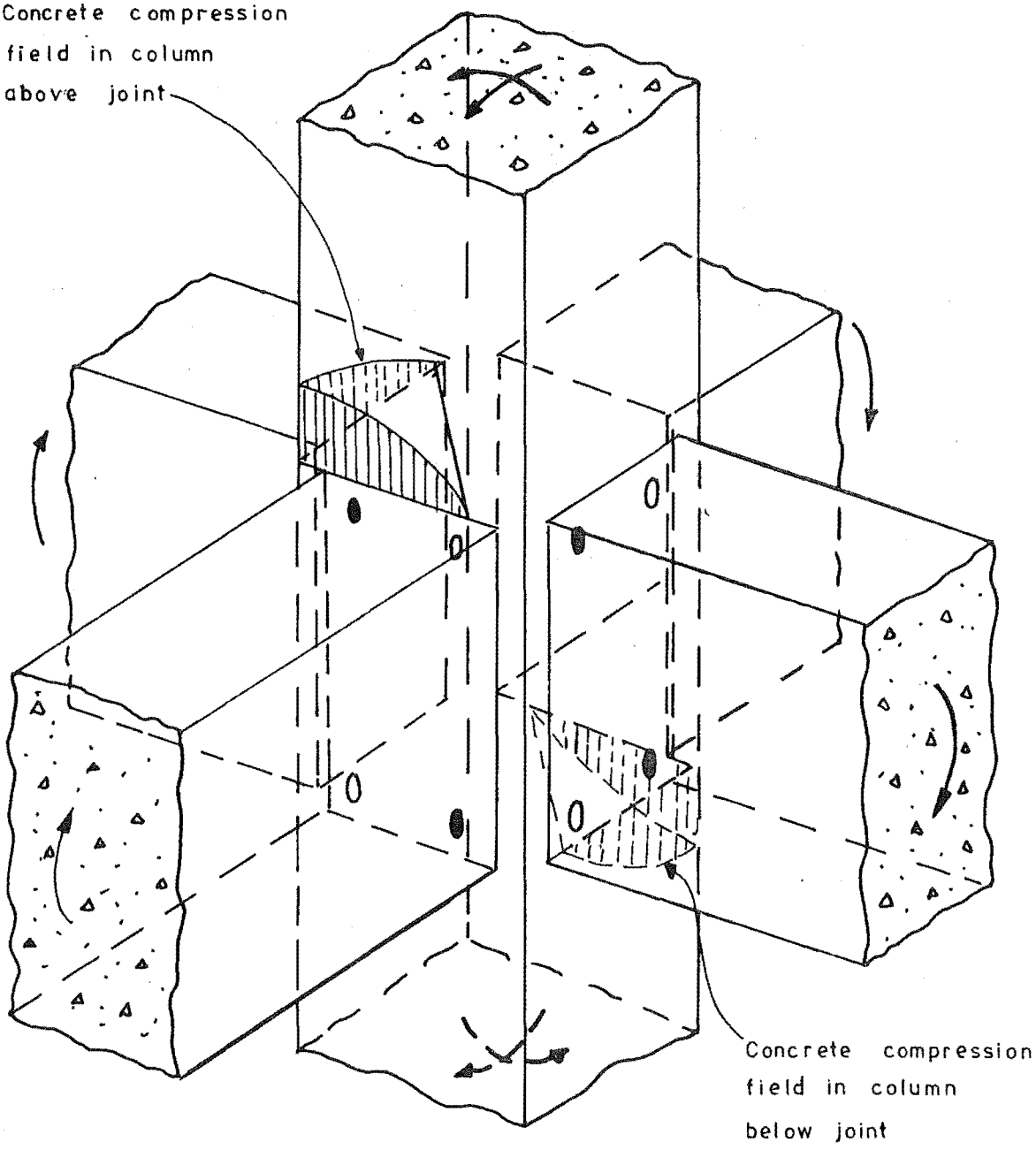

FIG·7·22: POSSIBLE SOURCE OF OBSERVED HORIZONTAL BEAM DEFORMATIONS

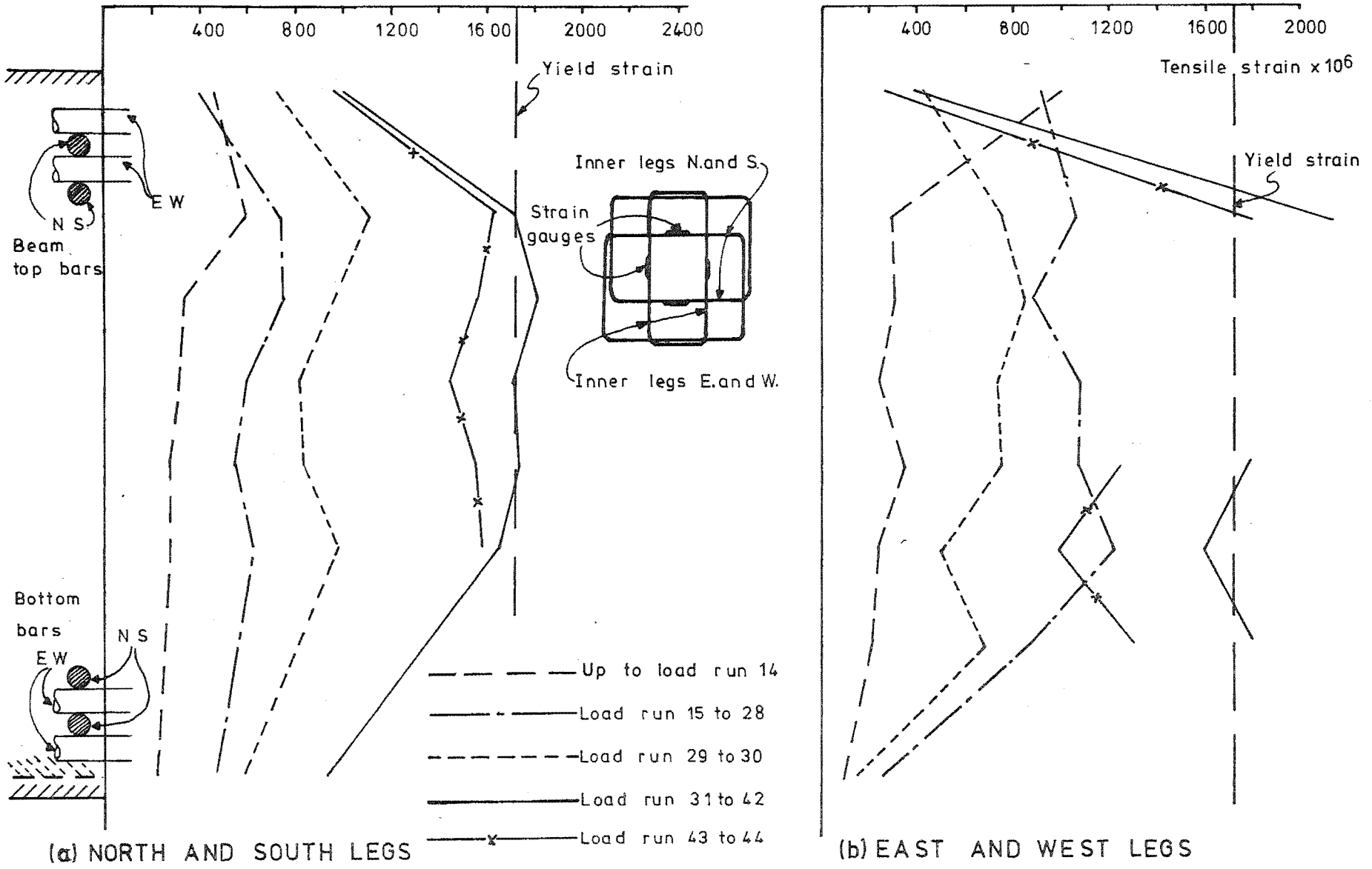

FIG. 7.23 : ENVELOPES OF STRAIN IN INNER LEGS OF JOINT REINFORCING

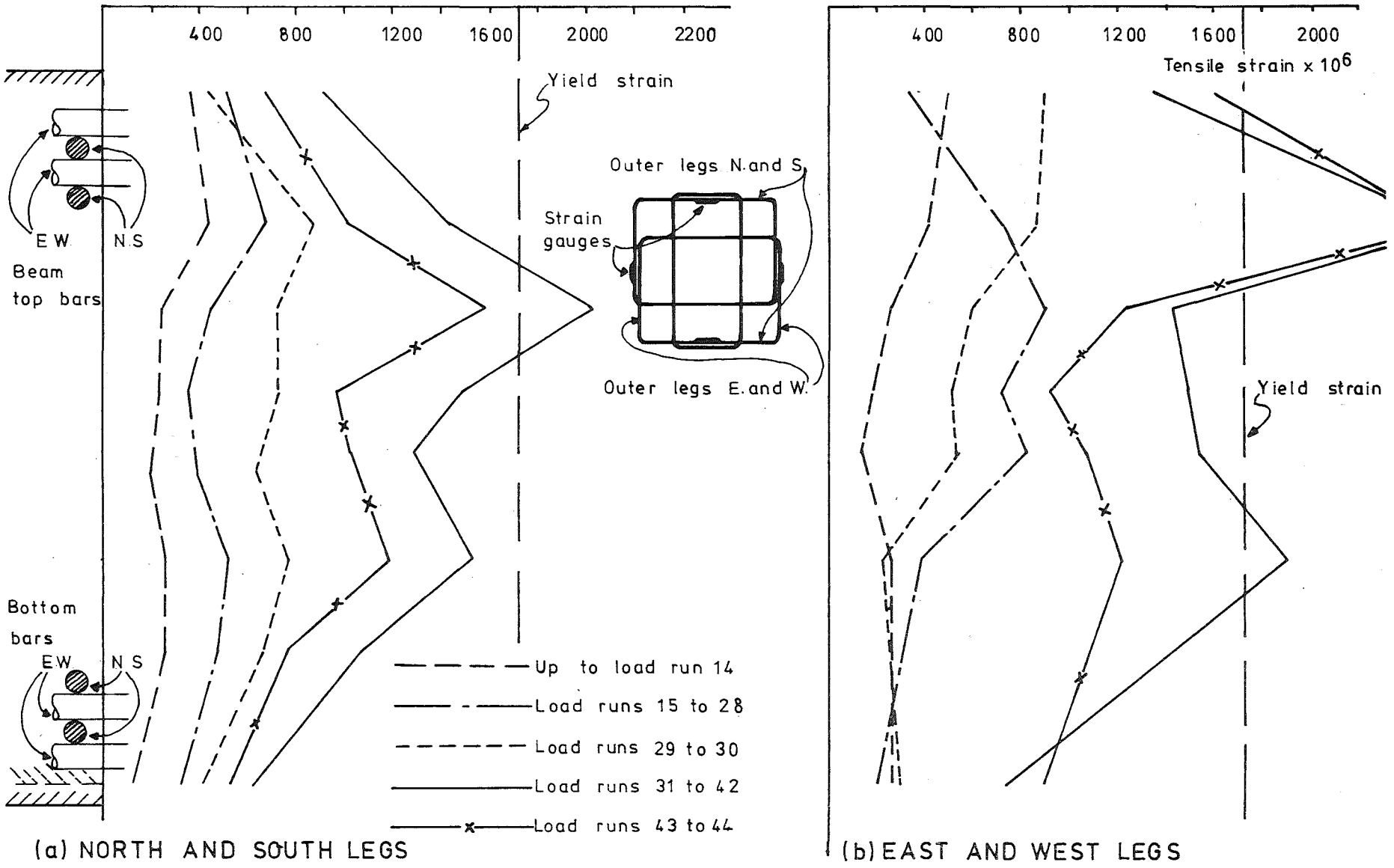

FIG. 7. 24 : ENVELOPES OF STRAIN IN OUTER LEGS OF JOINT REINFORCING

legs provided confinement, and the East and West legs acted as stirrups. When all beams were loaded simultaneously (load runs 31 to 42), all tie legs contributed to both shear resistance and confinement. As in other locations, some of the strain gauges fixed to joint reinforcing were lost as the test progressed, so that the results obtained in the final stages were incomplete.

The envelopes of strain up to load run 30 show clearly that the joint concrete was significantly less effective in resisting horizontal shear due to unidirectional loading after loading of the transverse beam. Similarly confining ties were required to carry greater strains after the transverse beam had been loaded inelastically. This is shown by the greater strains measured in both directions in load runs 15 to 28 as compared to those observed during load runs 1 to 14. In the repeated East-West cycle (load runs 29 and 30, see Fig. 7.5), the strains observed in the North and South (stirrup) legs again increased compared to those measured up to load run 28, but the strains in the East and West (confining tie) legs were less than those observed in load runs 15 to 28, although they were greater than those in load runs 1 to 14. This shows that, as expected from the plane frame test results, the strains due to confining action were less than those required in the shear-resisting direction.

The envelopes given for strains under skew loading (load runs 31 to 42) show that this was the critical loading on the joint. Up to load run 30 the maximum strain observed was 70% of yield strain, while the majority of strains were less than 50% of yield strain. During skew loading yield strain was exceeded in eight different locations, and this yielding was reflected in the increased joint deformations noted during these cycles. Although significant stiffness degradation occurred as a result of the yielding, together with small degradations in the measured strength at constant displacement levels, the loading program was considered to be quite severe, and the response of the joint was therefore satisfactory. The strains measured in outer legs of joint ties were quite close to those in inner legs, in contrast to the plane frame test results, where outer legs of joint ties carried significantly less strain than the inner legs throughout the loading history.

A history of strain measured in a particular tie leg versus the horizontal joint shear applied by the East-West beam is given in Fig. 7.25. The tie leg for which the history is given was the inner North leg closest to the mid-depth of joint (41N in Fig. 7.4), i.e. the corresponding position to that for which a strain history was given in Fig. 5.32 for plane frame

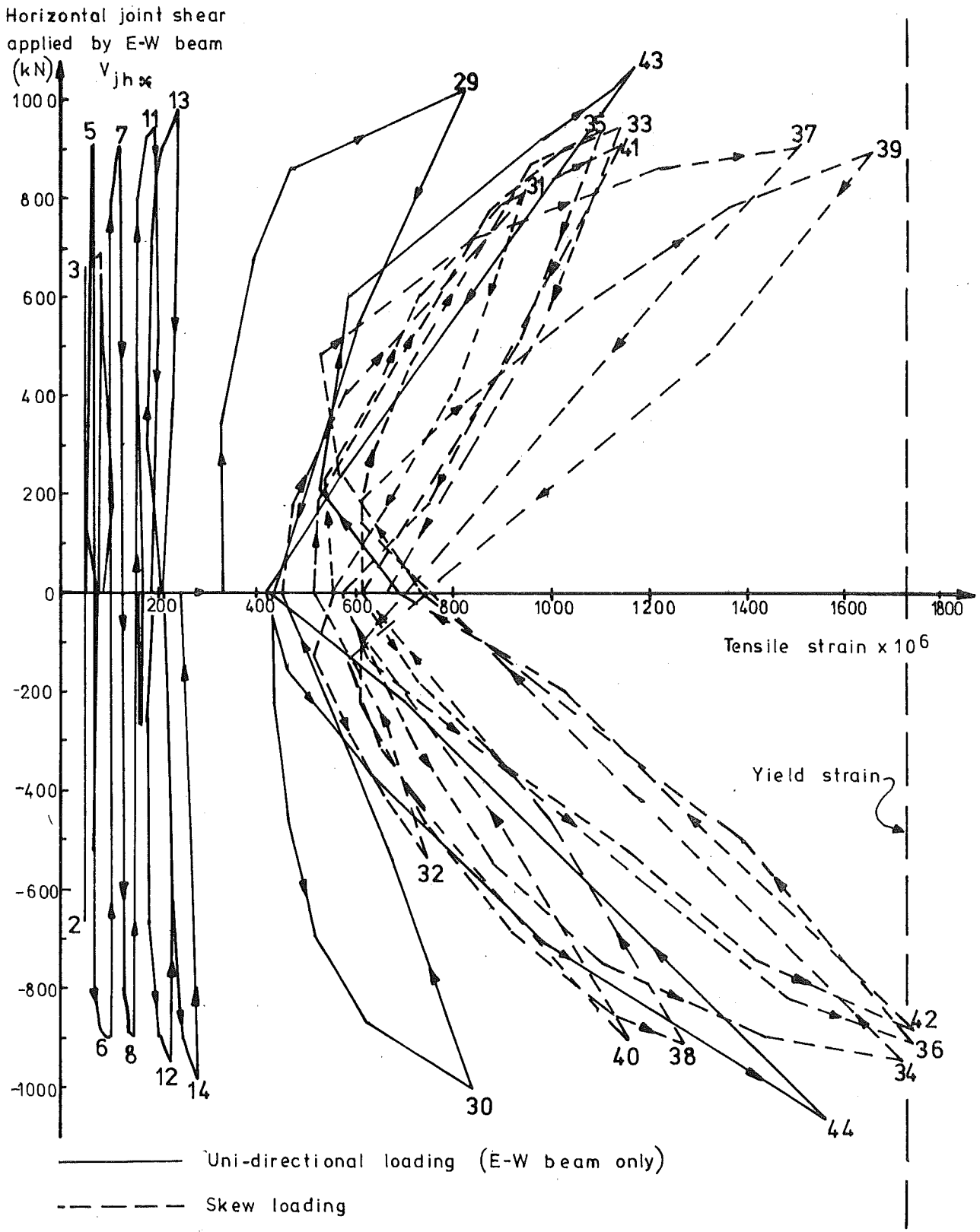

FIG.7.25: HISTORY OF STRAIN vs. JOINT HORIZONTAL SHEAR FOR INNER NORTH LEG OF TIE SET 3

unit B13. During the first unidirectional loading cycles the observed strains were quite small, although progressive increases in strain were noted with each load run. During the repeated cycle of loading in the East-West direction (load runs 29 and 30), the strains imposed on the tie leg and the hysteresis displayed by the shear versus strain loops were much greater than in the earlier cycles. This again demonstrates the reduced effectiveness of the transverse beam in enhancing the joint strength by confinement after transverse loading had been applied.

Under skew loading the strain in the tie leg again increased substantially. Note that the shear plotted as ordinate in Fig. 7.25 was the East-West component of horizontal joint shear only, not the resultant horizontal joint shear which acted diagonally across the joint. The magnitude of strains observed during this part of the test depended on the direction of loading. During load runs 31 to 36 and 41 to 42 where load was applied in the NW-SE direction, tie leg 41N developed significantly greater strains under negative joint shear (even-numbered load runs) than under positive shear. However, when the joint shear acted in the NE-SW direction during load runs 37 to 40, the greatest strains were observed under positive shear (odd-numbered load runs). Measurements of strain in other ties also showed this tendency, showing that the position of the critical surfaces within the joint changed as the direction of horizontal shear was changed.

In load runs 43 and 44 the absence of load on the transverse beams meant that the strains were smaller than noted during skew loading, in spite of the larger component of shear in the East-West direction. The residual strains remaining at zero load also decreased following unidirectional loading, showing that this caused less severe distortion of the joint than did skew loading.

7.5.3 Mechanism of Resistance to Joint Shear

Following the procedure used in analysing the plane frame test results, the participation of various modes of resistance to the horizontal joint shear was assessed from the test data, and the results of these calculations for the maximum displacement of each major load run are listed in Table 7.6, and presented graphically in Fig. 7.26. During the unidirectional load cycles the horizontal joint shear resisted by joint reinforcing was calculated for East-West loading as the sum of tie forces between the outermost layers of beam bars, for the North and South tie legs,

TABLE 7.6: RESISTANCE TO JOINT SHEAR

Load Run No.	V_{jh} (kN)	V_{shl} (kN)	$\frac{V_{shl}}{V_{jh}}$	V_{ch} (kN)	$\frac{V_{ch}}{V_{jh}}$	V_{jv} (kN)	$\tan\beta_T$	$\tan\beta_C$
1	652.2	50.6	0.078	601.6	0.922	2487.5	3.814	4.320
2	662.2	51.5	0.078	610.8	0.922	2365.7	3.572	4.054
3	652.8	30.3	0.046	622.5	0.954	2376.1	3.640	4.117
4	652.5	38.4	0.059	614.1	0.941	2387.6	3.659	4.023
5	916.6	43.3	0.047	873.3	0.953	2487.4	2.714	2.818
6	899.2	74.7	0.083	824.5	0.917	2520.9	2.804	3.011
7	899.2	77.3	0.086	821.9	0.914	2458.2	2.734	3.082
8	899.2	108.6	0.121	790.6	0.879	2487.2	2.766	3.046
11	946.6	127.3	0.135	819.3	0.865	2495.0	2.636	2.818
12	949.2	157.0	0.165	792.2	0.835	2511.5	2.646	2.803
13	979.1	147.8	0.151	831.2	0.849	2478.9	2.532	2.703
14	985.1	186.0	0.189	799.1	0.811	2514.6	2.553	2.703
15	712.6	118.1	0.166	594.5	0.834	2194.9	3.080	3.430
16	657.7	115.0	0.175	542.7	0.825	2192.7	3.334	3.662
17	664.3	113.6	0.171	550.7	0.829	2173.9	3.273	3.634
18	662.9	116.9	0.176	546.0	0.824	2186.7	3.299	3.634
19	918.6	191.8	0.209	726.9	0.791	2291.9	2.495	2.577
20	909.8	249.1	0.274	660.7	0.726	2277.1	2.503	2.661
21	909.8	252.9	0.278	656.9	0.722	2359.0	2.593	2.815
22	909.8	288.4	0.317	621.4	0.683	2311.3	2.540	2.767
25	961.7	331.4	0.345	630.3	0.655	2350.8	2.444	2.563
26	957.3	458.7	0.479	498.6	0.521	2475.9	2.586	2.676
27	979.0	422.4	0.431	556.6	0.569	2375.8	2.427	2.577
28	984.3	504.2	0.512	480.1	0.488	2413.7	2.452	2.577
29	1020.8	464.2	0.455	556.7	0.545	2396.8	2.348	2.486
30	1002.6	459.6	0.458	543.0	0.542	2330.4	2.324	2.417
31	1197.9	366.5	0.306	831.4	0.694	2283.4	1.906	2.238
32	827.2	261.1	0.316	566.1	0.684	1922.0	2.323	2.689
33	1354.7	471.2	0.348	883.5	0.652	2612.3	1.928	2.056
34	1343.6	536.1	0.399	807.5	0.601	2530.3	1.883	1.968
35	1335.8	483.2	0.362	852.6	0.638	2500.3	1.872	1.953
36	1296.9	529.6	0.408	767.3	0.592	2447.9	1.887	1.953
37	1099.9	529.6	0.481	570.3	0.519	2357.7	2.143	2.048
38	1315.0	586.2	0.446	728.8	0.554	1873.1	1.424	1.391
39	1279.2	527.5	0.412	751.7	0.588	2188.6	1.711	1.846
40	1279.2	542.4	0.424	736.8	0.576	1824.2	1.426	1.430
41	1282.7	481.5	0.375	801.2	0.625	1693.4	1.320	1.368
42	1269.4	515.5	0.406	753.9	0.594	1829.2	1.441	1.446
43	1070.0	678.0	0.634	392.0	0.366	1796.5	1.679	1.642
44	1061.4	686.2	0.647	375.2	0.353	1682.1	1.585	1.501

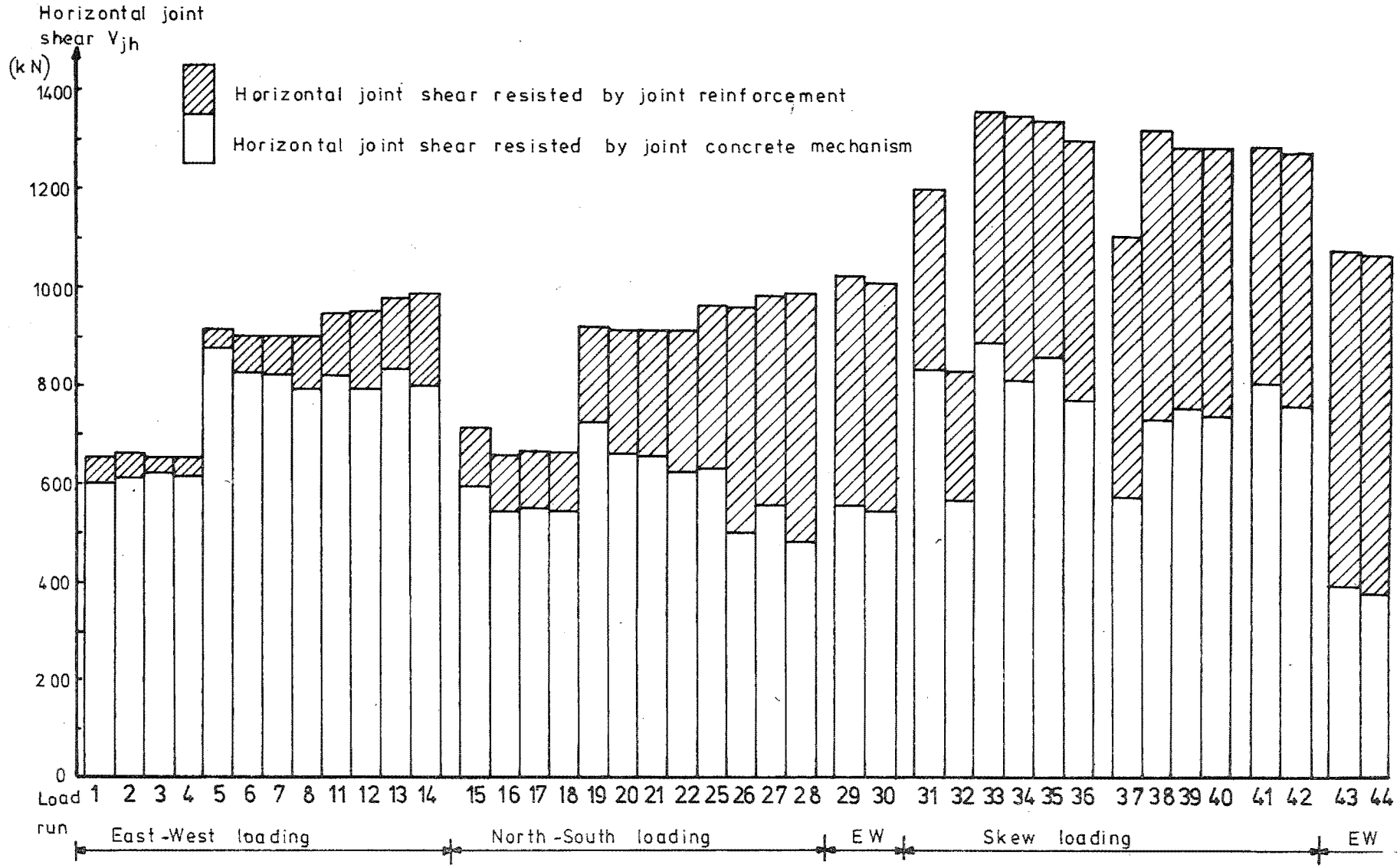

FIG.7.26 :MODE OF RESISTANCE TO HORIZONTAL JOINT SHEAR

and for North-South loading as the sum of forces in the East and West tie legs between the outermost layers of beam bars. No accurate assessment of forces in the short tie legs was possible in this test since only one strain gauge for loading in the East-West direction and two strain gauges for the North-South direction were available to measure these forces. However, these three gauges did indicate that the relationship of strains in short tie legs to those in long legs was similar to that observed in test B13. Hence the relationship of shears resisted by short tie legs would be expected to have been similar for the two tests. However, due to the lack of precise information, the shear resistance provided by short tie legs is not included in either Table 7.6 or Fig. 7.26.

The effect of loading the transverse beam is again clearly shown by the difference in the proportions of horizontal shear resisted by the joint concrete mechanism during the first cycles of loading in the East-West direction and in the cycles of loading in the North-South direction, or in the repeated East-West cycle. The joint concrete mechanism resisted over 80% of the applied horizontal joint shear up to load run 14, but the corresponding proportion in load runs 29 and 30 was only 55%.

It was shown in Section 1.3 (see Fig. 1.8) that a critical plane for a joint carrying skew shear crosses only half of the tie legs in each principal direction. The effective tie forces under skew loading were therefore assessed on this basis, and summed vectorially to give the resultant shear resisted by the joint horizontal reinforcement in these cycles.

$$V_{sh} = \left((\Sigma A_s f_s)^2_{EW} + (\Sigma A_s f_s)^2_{NS} \right)^{\frac{1}{2}} \quad \ldots \quad (7\text{-}1)$$

The resultant horizontal joint shear was derived from its two components:

$$V_{jh} = \left(V_{jh_{EW}}^2 + V_{jh_{NS}}^2 \right)^{\frac{1}{2}} \quad \ldots \quad (7\text{-}2)$$

The skew shear resisted by the joint concrete mechanism was then obtained by subtraction

$$V_{ch} = V_{jh} - V_{sh} \quad \ldots \quad (7\text{-}3)$$

The results of these calculations, plotted in Fig. 7.26, show that in spite of the high strains carried by joint reinforcing during skew loading (Figs. 7.23 and 7.24) the joint concrete mechanism was required to resist

large horizontal shears. It is apparent that the concrete direct strut mechanism was able to provide the necessary shear strength and to maintain it throughout the six full cycles of skew loading. This suggests that the mechanism of resistance of joint concrete to skew shear permitted greater shears to be carried in this case than in the plane frame situation. Although the imposition of greater displacement ductility factors simultaneously on both beams would undoubtedly have taxed the joint more severely, it is considered most unlikely that a loading sequence of greater severity than was actually applied would be encountered in a prototype structure under actual earthquake attack.

The response in load runs 43 and 44 showed a reduction of 20% in the proportion of joint horizontal shear resisted by the joint concrete mechanism when compared to that observed in the cycle before skew loading was applied (load runs 29 and 30), but this decrease was considered acceptable in view of the total cumulative ductility requirement at this stage of the test.

The inclination of the applied joint shear β_T, and the angle of resistance of the concrete strut mechanism β_C, were calculated for the unidirectional loading runs as for the plane frame tests (see Section 3.5.4). For the skew loading runs the vertical joint shear, V_{jv}, was calculated by assessing all the vertical forces acting to one side of a vertical cut taken down the plan diagonal of the joint parallel to the neutral axis in the column section under the imposed biaxial bending. Column bar forces in the column sections above and below the joint were calculated from bar strains determined either directly as experimental data, or by linear interpolation between adjacent values where no strain results were available for particular layers of bars. The concrete compression force for each case was then calculated as the sum of the bar tension forces and the axial load. The inclination of the applied joint shear was then given by

$$\tan\beta_T = \frac{V_{jv}}{V_{jh}} \qquad \ldots \quad (7\text{-}4)$$

where V_{jh} is given by Equation(7-2) above.

The position of the centroid of concrete compression $\bar{x}_c$, in the column sections above and below the joint was then determined by considering moment equilibrium between the external loads and the internal forces about the diagonal of the column section. The inclination of the concrete

struts under skew loading was then given by

$$\tan\beta_C = \frac{d - d'}{h_c \sec 45° - \bar{x}_{ct} - \bar{x}_{cb}} \quad \ldots \quad (7\text{-}5)$$

where d - d' was the average internal lever arm for the two beam sections, and h_c was the column depth.

Values of $\tan\beta_T$ and $\tan\beta_C$ calculated at the maximum displacement of each major load run are listed in Table 7.6 and shown in Fig. 7.27. Except in the initial elastic cycles in each direction the two angles were similar at all stages of the test, showing that the concept of a concrete strut acting between centroids of column concrete compression has equal validity for skew loading to that demonstrated for unidirectional loading in the plane frame tests and in the early part of this test.

The angle of the joint diagonal β_J appropriate to each direction of loading varied because of the different depths at which beam bars were placed in the two directions, while in the skew loading case the joint diagonal angle was that between the opposite corner bars of the column in the top and bottom of the joint. As expected, the joint shear resistance was obtained at a smaller angle under skew loading, but in all cases the angle of resistance was significantly steeper than the appropriate joint diagonal angle, due to the larger neutral axis depth in the column than in the beam.

7.6 Summary and Recommendations

The response of the space frame unit B21 tested under severe unidirectional and skew loading was satisfactory. Although the joint was designed to resist the actions resulting from plane frame action only, the performance under several cycles of skew loading in both diagonal directions was considered adequate. Yielding of joint ties occurred, but as in the plane frame tests the extent of yielding was limited, while the effect of joint tie yielding on the overall response of the unit was not severe. Some stiffness degradation was apparent as a result of the greater joint flexibility under skew loading, but the beam strengths attained at a constant level of displacement did not diminish greatly. The final cycle of the test showed that the unidirectional strength was not prejudiced by severe skew loading although the stiffness was reduced. The only visible damage to the joint was spalling of the exposed column corners, while the strain results indicated that yield penetration of beam bars into the

FIG. 7.27 : ANGLE OF RESISTANCE TO JOINT SHEAR

joint core may have increased as a result of skew loading, although the available data was not comprehensive in this respect, so that no definite conclusion can be drawn on this point.

Reduction of the test data showed that joint shear caused by skew loading was carried by similar mechanisms to those mobilized under unidirectional loading. The inclination of the applied joint shear was close to that of the line between the centroids of column compression in the column sections above and below the joint during both unidirectional and skew loading, showing that a concrete strut acting between these points was available to carry the shear not resisted by the joint reinforcement.

The test results showed clearly that no enhancement of the strength of space frame joints can be assumed due to the confining action of the beams on all faces of the joint, as suggested in the Recommendations of ACI-ASCE Committee 352[7]. Prior cyclic loading of the transverse beam diminished the effectiveness of the confinement which was initially available, while skew loading in any case imposed more severe demands on the joint than did unidirectional loading.

Horizontal deformations of the beams were observed during skew loading of the test unit, and it is considered possible that restraint of this deformation by the slab in a prototype structure may provide some enhancement of strength against skew shear.

The design of a multistoreyed space frame subject to earthquake attack must allow for the probability that full strength of the beam plastic hinges may be attained in both directions simultaneously at any given joint at some instant of the loading history. However, it seems unlikely that this situation will recur in many cycles, especially for a large frame having many redundancies. The test result showed that unidirectional joint design provided satisfactory response to cyclic skew loading throughout a loading sequence which was considered to adequately exceed probable demands during actual seismic loading.

Since there are no other test results for space frame joints available to verify or extend the conclusions from the present test, any recommendations based upon this result must be made with an element of caution. It is evident that further tests are necessary to examine the response of edge and corner joints of space frames (see Fig. 1.2), together with the effect on space frame joint response of other parameters such as the column axial load level, which was shown in the earlier tests

to be significant with respect to plane frame joint response. Varying the geometric parameters, such as the column aspect ratio, h_{cx}/h_{cy}, and the joint aspect ratios, h_{bx}/h_{cx} and h_{by}/h_{cy}, would provide further useful information. The effect of the slab on joint response could be shown by comparative testing of suitable test units.

However, for the present, the clearly satisfactory test result reported in this chapter leads to the recommendation that concurrency need not be considered in the design of space frame joints to resist skew seismic loading. That is, the design should be based only on the requirements for resistance to plane frame action considered separately in each principal direction.

CHAPTER 8

STRENGTH OF COLUMNS IN BIAXIAL BENDING

8.1 Introduction

Concurrent development of the beam plastic hinges in the two principal directions of a multistoreyed space frame due to seismic loading will cause skew shears on the beam-column joints, and biaxial bending of the columns. An experimental study of the response of a space frame joint to skew shear was reported in Chapter 7, and in this chapter an analytical study of the strength of columns under biaxial bending is described.

The loads applied to the column in the space frame test were limited by the beam flexural strengths, and the column was deliberately designed to possess greater strength than required to resist this moment input. Hence the column was not failed in bending, and the test results were not useful in assessing biaxial bending strength. However several series of test results are available pertaining to the strength of columns under biaxial bending [42, 43, 44, 45], and these have been used to verify the analytical results.

Obviously when biaxial bending of columns occurs, it is likely to impose the maximum strength demand on the column section, so that it may be considered that accurate design for this effect will be necessary for economy. However it has been suggested[46] that columns designed to resist amplified uniaxial actions only will possess sufficient biaxial bending strength to resist any likely load combination arising from concurrent response.

Design of regular multistoreyed framed structures to resist seismic attack can normally be satisfactorily achieved by considering equivalent static lateral loads applied to the structure[1,2] to determine the strength required at the selected plastic hinge locations. Regular framed structures are normally designed so that plastic hinges will form in the beams (see Fig. 1.1). The philosophy of capacity design then requires the strength at other locations to exceed the demands likely to be imposed by the development of the flexural overstrength at the beam plastic hinges.

Inelastic dynamic analyses of structures under earthquake loading[6] have shown that the dynamic response of frames may be quite different from the elastic behaviour under static lateral loading, due to the effects of higher modes of vibration and of plastic behaviour. In particular the

deformation of the columns may be such that the points of contraflexure do not occur close to the midheight, as is the usual pattern resulting from static lateral loading. The moment input from the beam plastic hinges at a particular joint will not therefore be shared equally between the columns above and below the joint, with a consequently much higher flexural demand on one or other of the column sections.

This phenomenon may be allowed for in design by the application of a dynamic magnification factor ω to the beam input moments for column design, as suggested in the report of the New Zealand National Society for Earthquake Engineering Discussion Group on Ductile Moment Resisting Frames[46]. Since higher mode effects tend to be more dominant in more flexible buildings, the value suggested in the above report for the dynamic magnification factor in plane frames, based on the results of computer analyses of typical framed structures, is

$$\omega_p = 0.6T_1 + 0.85 \qquad (8\text{-}1)$$

$$\text{but } 1.2 < \omega_p < 1.8$$

where T_1 = fundamental period of the building in seconds.

It is further suggested in the report that column design in space frames may be facilitated by modification of the dynamic magnification factor for unidirectional loading, omitting any specific design for biaxial bending due to concurrent loading. The dynamic magnification factor for the case of space frames

$$\omega_s = 0.5T_1 + 1.10 \qquad (8\text{-}2)$$

$$\text{but } 1.5 < \omega_s < 1.9$$

The magnified beam moment inputs are combined with axial loads derived from the sum of beam shears in the storeys above. A more conservative assessment of the axial load is made in the case of compression dominated columns, where overloads could cause unsafe conditions, whereas for axial loads less than the balanced failure load of a column, an increase in the compressive load increases the available flexural strength. For columns with low compressive loads or axial tension, a higher likelihood of column yielding can be tolerated, due to the greater ductility available to columns in this situation[3]. The likelihood of the critical axial load, which tends to be associated with first mode response, occurring simultaneously with the critical moments in both directions, is considered to be low,

since the moments are associated with higher mode response. Hence the difference between the dynamic magnification factors given in Eqs. (8-1) and (8-2) were judged to provide sufficient additional strength for space frame columns to resist any likely combination of loads arising from skew response of the building.

The intention of this chapter is to assess the validity of this approach for the design of columns of space frames and to provide design aids for biaxial bending where this is a necessary design task.

8.2 Review of Approaches for Determining the Flexural Strength of Columns with Biaxial Bending

The 'exact' analysis or design of reinforced concrete sections to carry bending moment about both principal axes plus axial compression is a difficult problem because the combination of all three actions represents a point on a failure surface which cannot be readily defined mathematically. Fig. 8.1 shows that for a section having given dimensions, reinforcing content, and material properties, and subject to either M_{ux} or M_{uy}, together with axial load N_u, the strength is represented by a single interaction curve in the appropriate plane. When bending is applied about both axes the failure condition at a given level of axial load is given by the contour between the points on the uniaxial curves. Since the strength of columns in uniaxial bending is relatively well defined, and is readily available to designers by means of design charts[47], a common approach to biaxial design has been to attempt to define the shape of these contours[48]. However the shape of the contours varies with the axial load level, and depends also on other parameters, such as the reinforcing content, concrete strength, and the section aspect ratio. Hence this method cannot readily be made accurate over a wide range of possible variables, and conservative values inevitably result in many design approximations.

Meek[49] suggested that if the bending strength of a column section could be determined for bending in the direction of a section diagonal, as well as in the two principal directions, the interaction curve could be conservatively approximated by two straight lines between the three known points as shown in Fig. 8.2. Following this approach to the problem Weber[50] derived design charts for square columns loaded along a diagonal, and proposed that the strength (or the required reinforcement) at other angles of loading could be obtained by linear interpolation between the values from the diagonal charts and uniaxial charts.

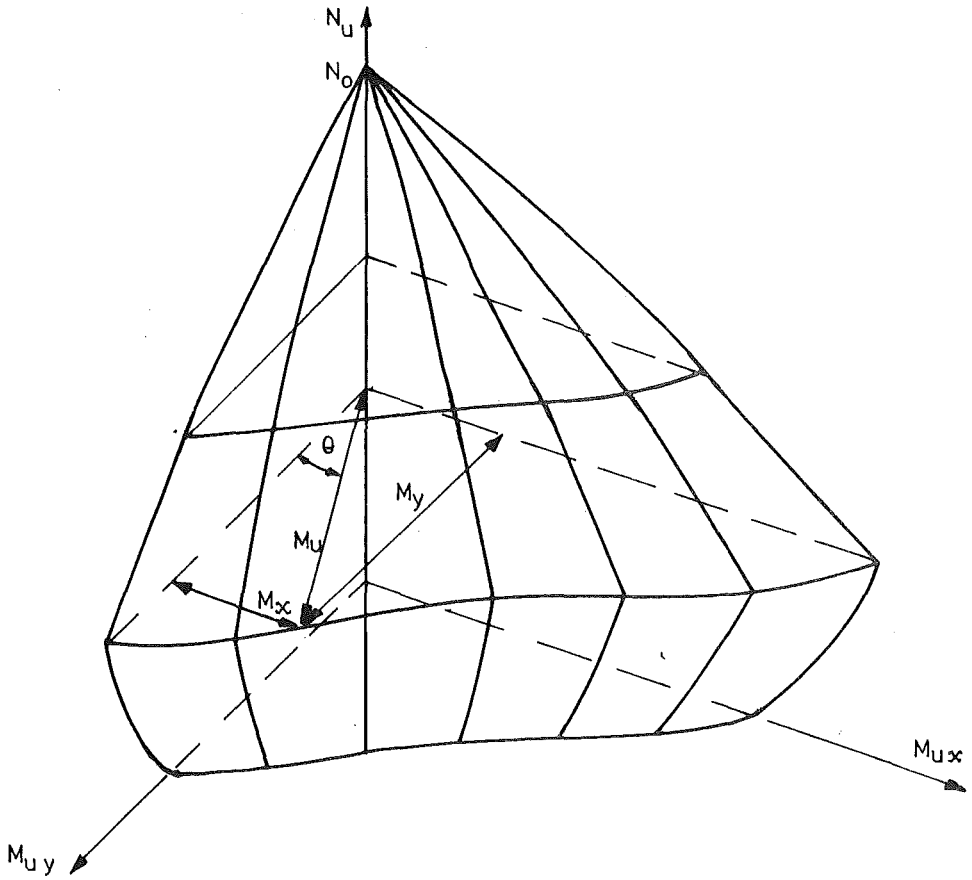

FIG.8.1:FAILURE SURFACE FOR COLUMN UNDER BIAXIAL BENDING

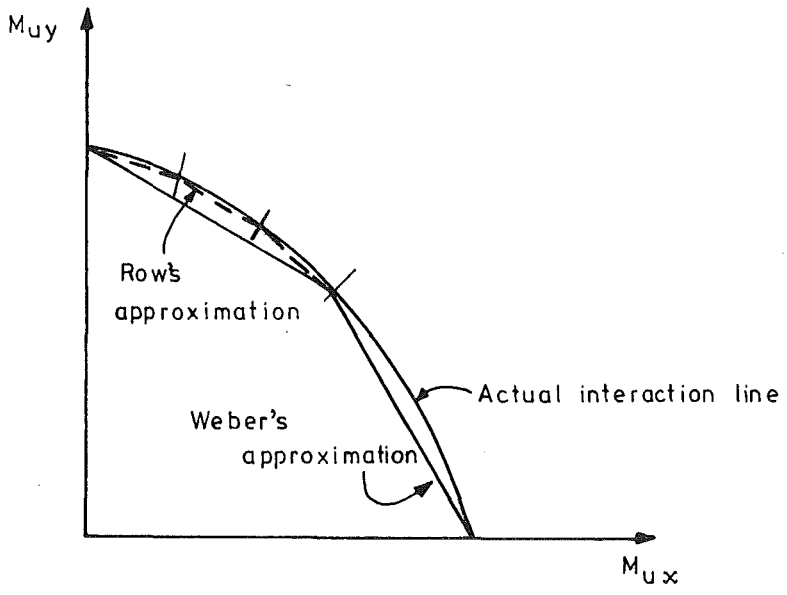

FIG.8.2:APPROXIMATIONS TO THE BIAXIAL BENDING INTERACTION LINE FOR COLUMN WITH CONSTANT AXIAL LOAD

This approach was refined by Row[51], who developed design charts for bending about three different inclined axes, thus giving a much closer representation to the actual biaxial bending strength contour as shown in Fig. 8.2. Row used the dimensionless parameters suggested by Moran[52] to allow the charts to be used for rectangular sections of any aspect ratio, which makes them much more widely applicable in design.

8.3 Stress-Strain Relationships for Concrete

8.3.1 Introduction

The design charts of Weber[50] were produced using the conventional ACI compressive rectangular stress block and extreme fibre strain[4] to represent the concrete actions in the column. However tests on overreinforced beams with triangular compression zones[53] have shown that the ACI rectangular stress block and extreme fibre strain gave conservative results. This tendency could be expected to be more apparent in columns. Row's[51] analysis for biaxial column bending were carried out using a curvilinear stress-strain curve for concrete in compression but this curve may also have been too conservative[3]. In the present study various alternatives for the concrete stress-strain relationship were studied, and comparisons were made to establish the most useful ones.

8.3.2 Equivalent Rectangular Stress-Block

The equivalent rectangular stress block recommended by the ACI Code[4] for the design of flexural members is based on extensive test results[54]. The stress distribution assumed in the compressed part of the section is shown in Fig. 8.3(a). The maximum concrete compressive strain is 0.003, and the uniform stress across the depth of the stress block is $0.85f'_c$, where f'_c is the cylinder crushing strength of the concrete. The proportion of the neutral axis depth over which uniform stress is assumed depends on the concrete strength.

If $f'_c < 27.6$ MPa (4,000 psi)

$$\beta_1 = 0.85$$

$f'_c > 27.6$ MPa

$$\beta_1 = 0.85 - \frac{f'_c - 27.6}{6.9} \times 0.05 \qquad (8\text{-}3)$$

The equivalent rectangular stress block is a design and analysis tool which has been shown[54] to predict very closely the strength of reinforced concrete beams and columns under uniaxial loading, since it is experimentally based on a rectangular compressed area of concrete.

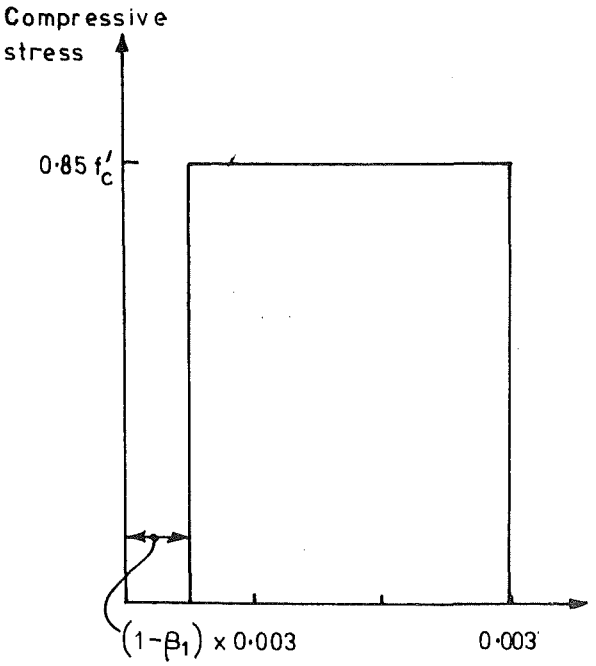

(a) ACI Rectangular stress block[4]

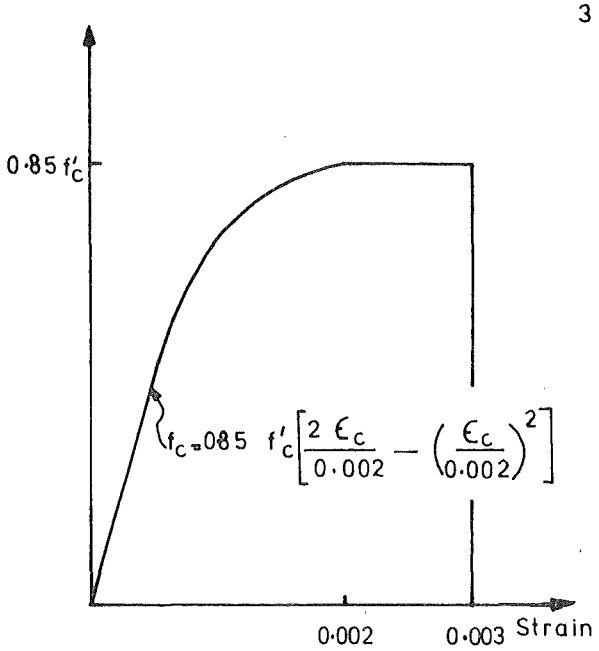

(b) Row's Curvilinear stress-strain curve[51]

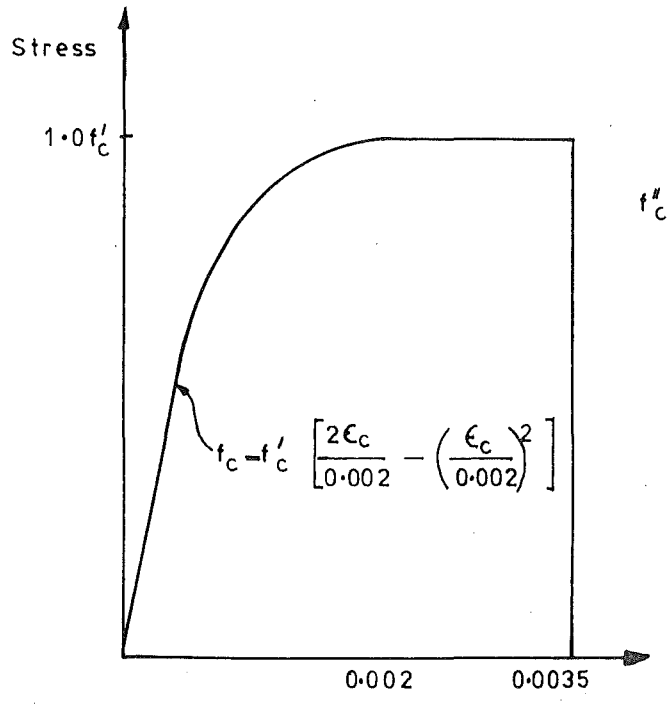

(c) CEB-FIP Curvilinear stress-strain strain curve (short term loading)[55]

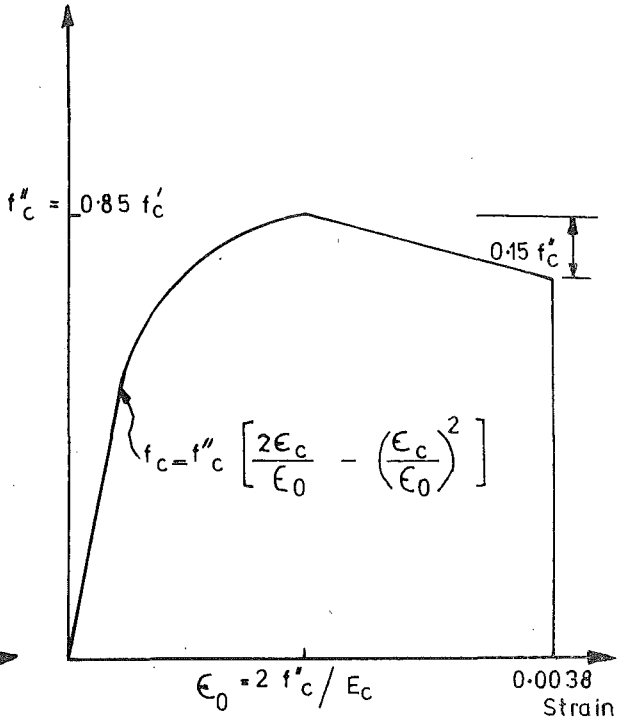

$E_c = 12410 + 460\ f''_c\ (MPa)$

(d) Hognestad's Curvilinear stress-strain curve[56]

FIG.8.3:STRESS-STRAIN CURVES FOR CONCRETE IN FLEXURE

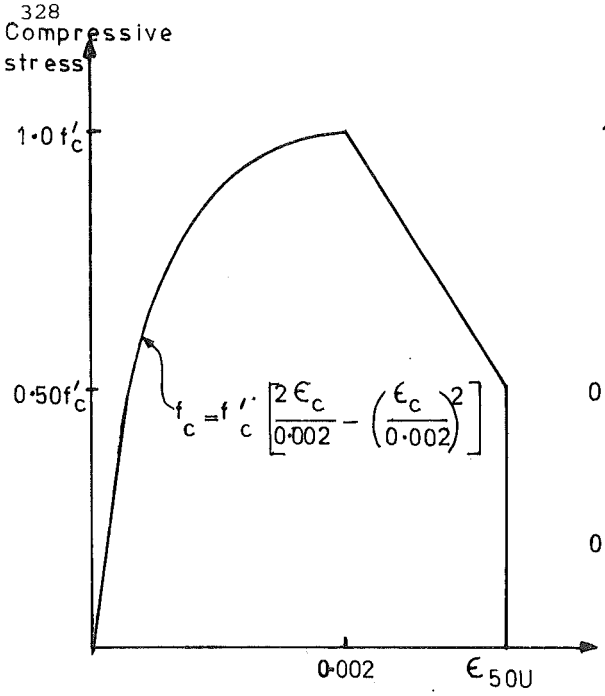

$$\epsilon_{50U} = \frac{3{\cdot}0 + f'_c / 3{\cdot}45}{145\, f'_c - 1000}$$

(e) Kent & Park's stress-strain curve for unconfined concrete[57]

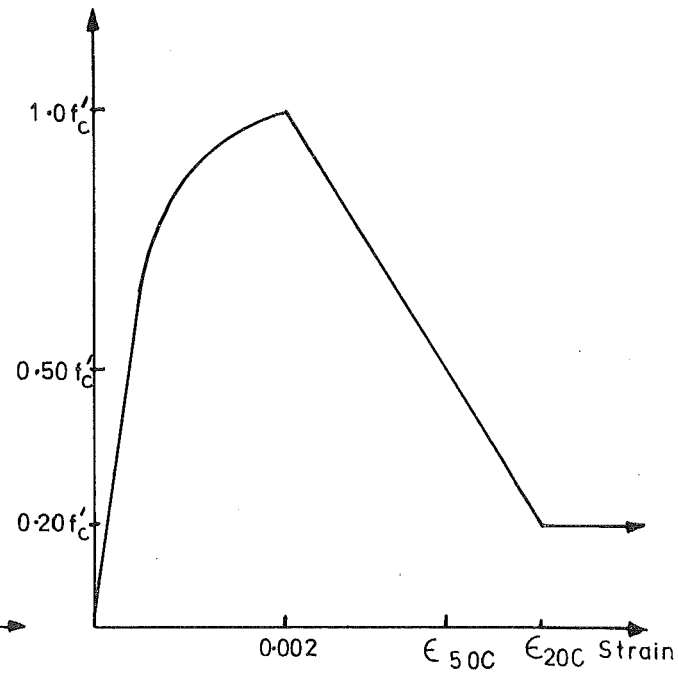

$$\epsilon_{50C} = \epsilon_{50U} + \frac{3}{4}\rho_s \sqrt{\frac{b''}{s_h}}$$

(f) Kent & Park's stress-strain curve for confined concrete[57]

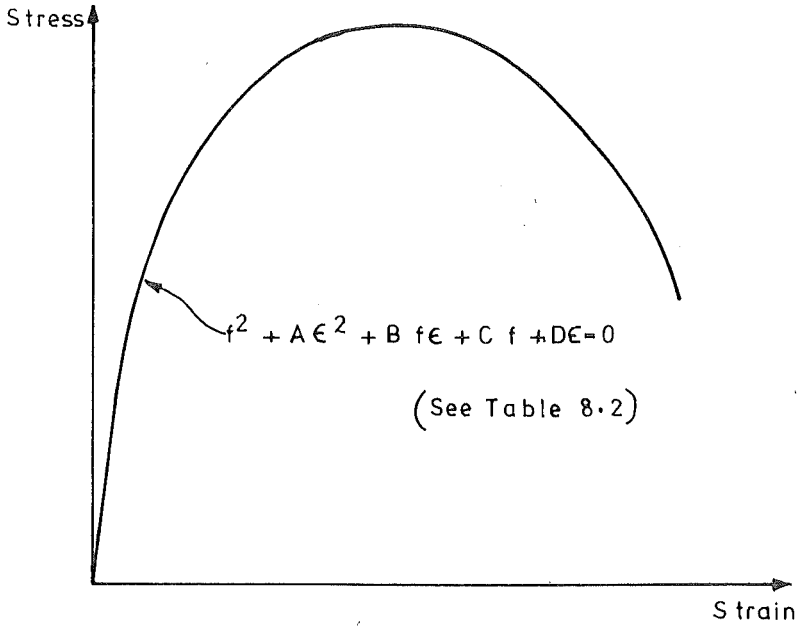

(g) Quadratic stress-strain curve of Kriz & Lee[60]

FIG.8.3(contd): STRESS-STRAIN CURVES FOR CONCRETE IN FLEXURE

However the validity of this approach for biaxial bending, in which the compressed area of concrete is not rectangular, is somewhat less well defined. The maximum compressive strain at the extreme fibre of a triangular compression zone at the maximum moment capacity, for instance, will normally be significantly greater than the value of 0.003 assumed by the conventional stress block. This study will attempt to establish alternative parameters for a rectangular stress block for use in biaxial column bending analysis.

8.3.3 Parabolic-Linear Stress-Strain Relationships

A common assumption for the shape of the concrete flexural stress-strain curve consists of a parabolic curve up to the strain ε_o at which maximum stress is first attained, together with a linear branch either continuing at constant stress, or descending to some smaller stress at a specified maximum strain. Four such curves are shown in Fig. 8.3(b)-(e) (51, 55, 56, 57). Curves for which the linear branch is maintained at constant stress give a more idealised representation of the actual behaviour, although they are easier to handle computationally. Curves with descending linear branches give a more accurate representation of the actual behaviour of concrete in flexure, but the possibility arises that the maximum moment carried by a given section with a given neutral axis position may not occur when the maximum permissible strain is attained at the extreme compression fibre, but rather at some smaller strain. Thus in analysing sections using this type of stress-strain relationship it is necessary to search iteratively for that extreme fibre strain which corresponds to maximum moment being carried. To maintain a similar magnitude of total concrete compressive force over the compressed areas of flexural members having a given strain gradient, the maximum strain and neutral axis depth for curves having a linear descending branch are typically greater than those for which constant stress is maintained.

The parameters for the stress-strain curves shown in Fig. 8.3(b)-(e) are listed in Table 8.1, together with comparisons of the concrete compressive forces predicted by these curves under a linear strain gradient in various situations. The concrete forces derived using the parabolic-linear stress-strain curves are compared to the forces derived using the ACI rectangular stress block, either with the same strain gradient (i.e. the same curvature) or with the same depth of compression. These comparisons were obtained by integrating over a rectangular compressed area (relating to uniaxial bending), or over a triangular compressed area (relating to biaxial bending), for concrete strengths of 25 MPa and 40 MPa.

TABLE 8.1 : COMPARISON OF PARABOLIC-LINEAR STRESS-STRAIN CURVES WITH ACI RECTANGULAR STRESS BLOCK

Stress Strain Curve			Row[51]	CEB-FIP Code[55]	Hognestad[56]	Kent & Park[57] (unconfined)
Maximum stress			$0.85f'_c$	$1.0f'_c$	$0.85f'_c$	$1.0f'_c$
Strain at maximum stress ε_o			0.002	0.002	$1.70f'_c/E_c$	0.002
Maximum strain			0.003	0.0035	0.0038	$\frac{3.0 + f'_c/3.45}{145f'_c - 1000}$
Stress at maximum strain			$0.85f'_c$	$1.0f'_c$	$0.723f'_c$	$0.50f'_c$
f'_c = 25 MPa	Assuming equal strain gradient	F_i/F_{ACI} □	0.915	1.307	1.167	1.274
		F_i/F_{ACI} Δ	0.872	1.493	1.496	1.826
	Assuming equal neutral axis depth	F_i/F_{ACI} □	0.915	1.120	0.921	0.979
		F_i/F_{ACI} Δ	0.872	1.097	0.932	1.079
f'_c = 40 MPa	Assuming equal strain gradient	F_i/F_{ACI} □	1.023	1.462	1.247	1.091
		F_i/F_{ACI} Δ	1.090	1.867	1.714	1.284
	Assuming equal neutral axis depth	F_i/F_{ACI} □	1.023	1.253	0.985	1.076
		F_i/F_{ACI} Δ	1.090	1.372	1.068	1.250

F_i = concrete compressive force in assumed stress block

F_{ACI} = concrete compressive force in ACI rectangular stress block

□ for rectangular compressed area

Δ for triangular compressed area

The comparisons show that Row's curve (Fig. 8.3(b)) definitely gives a more conservative (smaller) assessment of the concrete forces than the other relationships. However the extent to which the strength of a section under biaxial bending predicted using the various stress-strain curves is influenced by the different compressive forces calculated in Table 8.1 for constant strain gradient or constant compressed depth may be expected to vary in a complex manner, depending on the section geometry, the loading, and the reinforcing content. For sections carrying a heavy axial load the compressed area will be trapezoidal in shape, and the appropriate force properties will be intermediate between those listed in Table 8.1 for triangular or rectangular compressed areas. Thus realistic comparison of the various stress-strain curves can only be made by comparing the moments computed using each relationship for a range of typical section properties.

8.3.4 Stress-Strain Curve for Confined Concrete

Tests[57,58] have shown that although confinement of concrete by small to moderate quantities of lateral reinforcement in the form of rectangular hoops makes little difference to the maximum stress attained by concrete in flexure, the slope of the falling branch of the stress-strain curve is affected by the presence of confinement reinforcing. In order to assess the influence of this behaviour on the biaxial bending strength of columns, the stress-strain relationship proposed by Kent and Park[57], and shown in Fig. 8.3(f), was used in the analysis. This curve comprises a parabolic portion up to the maximum stress $1.0f'_c$ at strain $\varepsilon_o = 0.002$, and a linear descending branch whose slope depends on the content and spacing of the lateral reinforcing.

i.e. for $\varepsilon_c < 0.002$

$$f_c = f'_c \left[\frac{2\varepsilon_c}{0.002} - \left(\frac{\varepsilon_c}{0.002} \right)^2 \right] \qquad (8\text{-}4)$$

for $0.002 \leq \varepsilon_c \leq \varepsilon_{20c}$

$$f_c = f'_c \left[1 - Z\,(\varepsilon_c - 0.002) \right] \qquad (8\text{-}5)$$

where $$Z = \frac{0.5}{\varepsilon_{50u} + \varepsilon_{50h} - 0.002} \qquad (8\text{-}6)$$

$$\varepsilon_{50u} = \frac{3.0 + f'_c/3.45}{145f'_c - 1000} \qquad (8\text{-}7)$$

and $$\varepsilon_{50h} = 0.75\rho_s \sqrt{\frac{b''}{s_h}} \qquad (8\text{-}8)$$

where f'_c = concrete cylinder strength in MPa, ρ_s = ratio of volume of lateral reinforcement to volume of concrete core measured to outside of hoops, b" = width of confined core measured to the outside of hoops, and s_h = spacing of hoops. The cover concrete is assumed to follow the same stress-strain curve as the confined core until the descending branch of the curve has fallen to $0.5f'_c$, at which stage it spalls and carries no further load. Once the stress in the core has fallen to 20% of the maximum stress, the confined core is assumed to be able to sustain this stress indefinitely. For strength calculations it is not likely that this branch of the curve will be mobilized. As the maximum strain which may be carried is not limited, it is necessary to find for each neutral axis position for a given section the extreme fibre strain and the resulting stress distribution which will maximize the moment carried by the section.

An alternative approach to the stress-strain relationship for confined concrete was proposed by Sargin et al[59], who suggested a polynomial equation. Coefficients for this equation were determined on the basis of experimental results in terms of the lateral reinforcing content and other parameters. However for the purposes of this study the relationship was much too complex to deal with in the required manner, and only the relationship of Kent and Park was used.

8.3.5 Quadratic Stress-Strain Relationship

To give a reference assessment of concrete flexural stress-strain behaviour, which other cases might be compared with, the quadratic functions derived by Kriz and Lee[60] from the data of Hognestad et al[54] were utilized for some of the analyses performed.

These functions have the form

$$f^2 + A\varepsilon^2 + Bf\varepsilon + Cf + D\varepsilon = 0 \qquad (8\text{-}9)$$

where the coefficients A, B, C, D depend on the concrete cylinder strength, as listed in Table 8.2.

Values of the maximum proportion of the cylinder strength attained for each curve, and the strain at which this occurs, are also listed in Table 8.2. Although these values are not in fact necessary to define the curves represented by the coefficients given in the table, they are included so as to give a general idea of the peak values of the curves.

The quadratic stress-strain function was assumed to be equally valid in relation to triangular or trapezoidal compression zones as for the rectangular compression zones from which the curves were derived.

TABLE 8.2: COEFFICIENTS FOR QUADRATIC STRESS-STRAIN RELATIONSHIP

Concrete strength f'_c (MPa) (lb/in^2)	6.9 (1000)	13.8 (2000)	20.7 (3000)	27.6 (4000)	34.5 (5000)	41.5 (6000)
A	-3.348	-40.19	-163.2	-547.2	-1633	-2677
B	-40.19	-17.59	-23.68	-24.96	-8.246	26.06
C	- 8.701	-22.69	-46.55	-98.32	-216.6	-304.3
D	83.00	385.5	1073	2709	6551	9503
Strain at maximum stress ε_o	0.00176	0.00174	0.00181	0.00187	0.00192	0.00196
Maximum stress f_{max}/f'_c	1.053	1.011	0.985	0.965	0.952	0.940

$$f^2 + A\varepsilon^2 + Bf\varepsilon + cf + D\varepsilon = 0$$

where f = concrete stress in MPa

ε = concrete strain x 1000

The maximum strain is not specified, and it is necessary to search for the extreme fibre strain which results in the maximum moment being carried in any given situation.

8.4 Analysis for Biaxial Bending

8.4.1 Assumptions

The analyses carried out in this study used equations derived in accordance with the following assumptions:

1) Strain at any location was directly proportional to the distance from the neutral axis.

2) Stress in reinforcement at strains less than the yield strain ε_y was directly proportional to the strain

$$f_s = E_s \cdot \varepsilon_s \qquad (8\text{-}10)$$

where E_s was Young's Modulus for the steel. For strains greater than the yield strain, the stress in the reinforcement was constant and equal to the yield strength, f_y. For reinforcement in the compression zone the net steel stress was taken as $(f_s - f_c)$, where f_c was the concrete stress at the particular location. This allowed for the concrete displacement by the reinforcement. No strain hardening of the steel has been considered.

3) Various assumptions have been used for stress-strain behaviour of the concrete as discussed in Section 8.3. However in all cases the tensile strength of the concrete has been neglected.

4) The total reinforcement content of the section was divided for purposes of computation into N_s discrete elements of equal area, with one quarter of the total reinforcing placed adjacent to each face of the column.

5) In most cases the concrete section was divided into a grid of N_c discrete rectangular elements of equal area. The stress over each element was assumed constant and equal to the value computed using the strain at the centroid of the element. When considering uniaxial loading the division of the section was reduced to a series of strips, each extending the full width of the section parallel to the neutral axis, and constant stress across the strip was again assumed. Where a rectangular stress block was used to represent the concrete actions, the concrete actions were determined analytically, and numerical integration over the grid of elements or strips was not required.

6) No strength reduction factor was applied to the computed results.

8.4.2 Equilibrium Equations

Where a numerical integration approach is used according to assumptions 4) and 5) above, the equilibrium equations for a column section may be shown to be:

$$\frac{N_u}{f'_c bh} = \frac{1}{N_c} \sum_{i=1}^{N_c} \alpha_i + \frac{\rho_T}{N_s . f'_c} \sum_{j=1}^{N_s} f_{sj} \qquad (8\text{-}11)$$

$$m_x = \frac{M_{ux}}{f'_c bh^2} = \frac{-1}{N_c} \sum_{i=1}^{N_c} \alpha_i . y_i - \frac{\rho_T}{N_s . f'_c} \sum_{j=1}^{N_s} f_{sj} . Y_j \qquad (8\text{-}12)$$

and $$m_y = \frac{M_{uy}}{f'_c b^2 h} = \frac{1}{N_c} \sum_{i=1}^{N_c} \alpha_i . X_i + \frac{\rho_T}{N_s . f'_c} \sum_{i=1}^{N_s} f_{sj} . X_j \qquad (8\text{-}13)$$

where N_u = column axial load

M_{ux}, M_{uy} = ultimate moments about X and Y axes

f'_c = cylinder strength of concrete

b, h = column width and overall depth

α_i = proportion of f'_c carried by the ith concrete element

$\rho_T = \frac{A_{ST}}{bh}$ = reinforcing content of the section

f_{sj} = steel stress in the jth steel element

$X_i = \frac{x_i}{b}$, $Y_i = \frac{y_i}{h}$

x_i, y_i = coordinates of the ith concrete element, and

m_x, m_y may be defined as specific moments in each direction.

The derivation of these equations is given in Appendix A, together with the corresponding equations for the analytical solution for the rectangular stress block case.

To define the failure curve for biaxial bending of a rectangular section, it is necessary that the aspect ratio h/b should be included in the parameter describing the angle of loading, since the conditions associated with fixed angles of loading will vary depending on the aspect ratio. The loading direction is therefore expressed as

$$\frac{M_{uy}}{M_{ux}} = K \frac{b}{h} \qquad (8\text{-}14)$$

or $$\frac{m_y}{m_x} = K \qquad (8\text{-}15)$$

which is independent of b and h. The quantity $\theta = \tan^{-1}K$ may be thought of as the specific angle of loading. When $K = 1$ the failure load is applied along the diagonal, while $K = 0$ implies bending about the X-axis only, and $K = \infty$ implies bending about the Y-axis only. The reinforcing bars in a rectangular section are placed at lever arms of f.b in the X direction, and g.h in the Y-direction. For a section in which f = g = constant, the failure surface may be defined by conditions at K values between zero and unity, since in a particular case the axis about which the largest specific moment occurs may be arbitrarily termed the X-axis. When $f \neq g$ this procedure cannot be followed and K values over the full range between zero and infinity must be considered.

In order to produce convenient design charts values of $\frac{P_u}{f'_c bh}$ may be plotted against m_θ where

$$m_\theta = \sqrt{m_x^2 + m_y^2} \qquad (8\text{-}16)$$

for suitable values of K.

Since $K = m_y/m_x$

then $$m_\theta = m_x\sqrt{1 + K^2} \qquad (8\text{-}17)$$

or $$m_\theta = m_y \sqrt{1 + \left(\frac{1}{K}\right)^2} \qquad (8\text{-}18)$$

8.4.3 Computer Program

In order to assess the validity of various stress-strain assumptions for the concrete in columns under biaxial bending, a computer program was written to produce column design charts for biaxial bending, or to compare the moment values obtained using different stress-strain curves. A brief description of the program and a listing is given in Appendix B.

8.5 Results

8.5.1 Data

The analyses carried out in this study were based on columns having reinforcement of yield strength 380 MPa, which is the grade of high strength steel normally used in columns for multistoreyed buildings in New Zealand. A modulus of elasticity for steel of 200 000 MPa was used, and concrete strengths of 25 MPa and 35 MPa were considered. Since it was desired to assess the contribution of concrete compression forces to the biaxial bending strength in the various cases for comparative analyses, the moment contributed by the reinforcement was reduced by carrying out most analyses

with f = g = 0.7, which is the lowest relative lever arm likely to occur in columns of a prototype multistoreyed structure.

Most analyses were carried out with the section divided into 400 discrete concrete elements (20 divisions in each direction). Some analyses were done using a finer mesh of elements to check the accuracy of the 20 x 20 grid, but variations in the computed results were small (generally less than 1%). The 20 x 20 grid was considered to give optimum results in terms of accuracy and computational effort. All analyses were carried out with reinforcement located in forty discrete positions around the perimeter. This allocation is considered to give accurate results for columns containing eight or more bars, but would be slightly conservative for a four-bar column. Reinforcing contents of 1%, 3%, and 5% were considered for comparative analyses, and moment results were only considered to be relevant at axial load levels of less than $0.60f'_cA_g$.

8.5.2 Comparative Analyses

Fig. 8.4 shows the moments calculated using the ACI equivalent rectangular stress block (Fig. 8.3(a))as a proportion of the moments calculated at the same axial load level using the quadratic stress-strain function (Fig. 8.3(g)), for columns with reinforcing of yield strength f_y = 380 MPa, concrete strength f'_c = 25 MPa, and relative lever arms f = g = 0.7. Comparisons are shown for reinforcing contents of 1%, 3% and 5%, and at values of K = 0.0, 0.268, 0.577, and 1.0, corresponding to specific angles of loading of 0°, 15°, 30° and 45°.

The comparisons show that under uniaxial loading (K = 0.0), the moment results calculated using the two approaches to the determination of the concrete force were similar up to axial load levels of $0.60f'_cA_g$. At higher levels of axial load the two results diverge, but this part of the moment-axial load relationship is of little interest since no columns will be designed for this level of axial load. For biaxial bending the ACI rectangular stress block underestimated the moment strength throughout the relevant range of axial load, especially for the higher reinforcing contents. For loading only along the section diagonal (K = 1.0), the moments strengths predicted using the ACI stress block in a column having 1% of reinforcing averaged 5.3% less than those computed using the quadratic function up to axial loads of $0.60f'_cA_g$. The corresponding reductions for columns with reinforcing contents of 3% and 5% were 8.9% and 11.4% respectively. These reductions in the calculated strengths may be compared to average underestimates of between 4.8% and 3.2% for

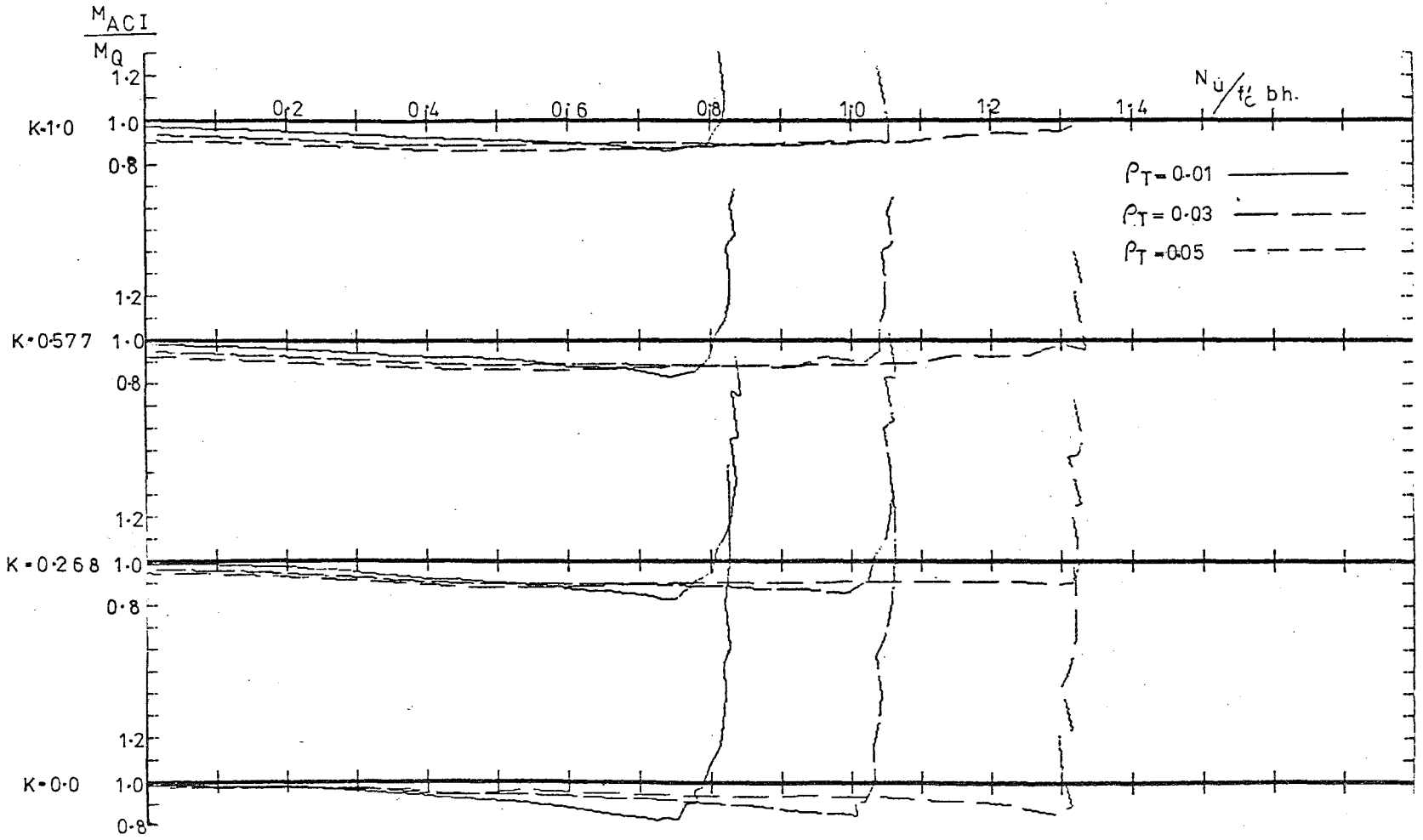

FIG.8.4 : COMPARISON OF MOMENTS CALCULATED USING ACI STRESS BLOCK AND QUADRATIC STRESS-STRAIN FUNCTION

uniaxial loading. This shows clearly that the ACI rectangular stress block is conservative for biaxial bending analysis.

Inspection of the results at intermediate angles of loading (K = 0.268 and K = 0.577) shows that although the differences in the computed moments are not as great as for loading along the diagonal, the discrepancies are closer to those obtained for diagonal loading than for uniaxial loading. This occurs because the compressed area in any biaxial bending situation is triangular or trapezoidal in shape and the results may therefore be expected to differ significantly from those pertaining to uniaxial bending, where the compressed area is rectangular.

Similar trends were shown in a corresponding analysis with f_y = 380 MPa, f = g = 0.7, and f'_c increased to 35 MPa. In this case the average difference in the moments predicted by the ACI method and the quadratic stress-strain function was less than 1% for uniaxial loading at axial loads up to $0.60f'_cA_g$. While agreement was also good for diagonal loading in lightly reinforced columns (ρ_T = 1%), the average reductions in predicted strength for more heavily reinforced columns were greater at 3.8% and 6.1% for columns having ρ_T = 3% and 5% respectively. Repetition of the analyses with f = g = 0.9 showed as expected that the same trends were followed, but that the differences in the computed results were not as great as for f = g = 0.7, since the reinforcement then provided a greater proportion of the total moment resistance, and this was not affected by the choice of concrete stress-strain behaviour.

8.5.3 Parameters for an Alternative Rectangular Stress Block for Biaxial Bending

The results obtained using the quadratic function (Eq. (8-9)) to represent the concrete stress-strain curve showed that the maximum concrete strain at the extreme compressive fibre over the relevant range of axial load intensity (0 - $0.6f'_cA_g$) under biaxial bending was significantly greater than the value of 0.003 used for the conventional ACI rectangular stress block. This has also been noted in test reports[53]. Study of the analytical results suggested a relationship of the form

$$\varepsilon_{cmax} = 0.006(1 - 0.01f'_c) \qquad (8\text{-}18)$$

but $0.003 < \varepsilon_{cmax} < 0.005$

where f'_c = cylinder strength of concrete in MPa.

This relationship was used to define one parameter for an alternative rectangular stress block to be used in biaxial bending analyses. So that results would be consistent with those calculated for uniaxial loading using the conventional ACI stress block it was necessary that the proportion of the cylinder strength maintained across the rectangular stress block should be the same in both cases (i.e. $\alpha = 0.85$). This implied that both stress block assumptions (i.e. conventional ACI, and proposed biaxial stress block) would predict the same ultimate axial load strength without moment, N_o, for a given column section.

Having thus fixed the proportion of the cylinder strength to comprise the uniform stress over the stress block, any necessary adjustment to the stress block may be made by altering the parameter β_1, the proportion of the neutral axis depth over which uniform stress is to be assumed. This was determined by running comparative analyses of the moment results, M_R, calculated using rectangular stress blocks having a range of values β_1 from 0.66 up to 0.84, with the maximum strain given by Eq. (8-18). Each of these results was compared to the appropriate value obtained using the quadratic strain function, M_Q, for loading along the section diagonal ($K = 1.0$). The mean of the ratio of moments obtained for axial loads up to $0.60f'_c A_g$ in each case is shown in Fig. 8.5 for concrete cylinder strengths of 25 MPa and 35 MPa, with steel yield strength of 380 MPa, and $f = g = 0.7$ in both cases. The figure shows that a value of $\beta_1 = 0.75$ would give a good agreement in both cases, with the calculated ratios of $\bar{M}_R/\bar{M}_Q$ then being similar to those obtained by comparing results derived using the conventional ACI stress block to the quadratic function results for uniaxial loading. This value was therefore adopted and the resulting stress block is shown in Fig. 8.6. Results of analyses performed with $f = g = 0.9$ showed the proposed stress block to be equally valid in this case.

The choice of a constant value for $\beta_1 = 0.75$ irrespective of concrete strength differs from the value given for this parameter in the conventional ACI stress block (Fig. 8.3(a), Eq. (8-3)). However the reduction in maximum fibre strain with concrete strength given in Eq. (8-18) reduces the available concrete force for the proposed stress block in a similar manner to the reduction in concrete force given by the reduction in β_1 with concrete strength in Eq. (8-3), together with constant maximum fibre strain, for the ACI stress block. The proposed approach offers the advantage that forces contributed by the column reinforcement are more accurately assessed due to the more accurate extreme fibre strain used in the calculation.

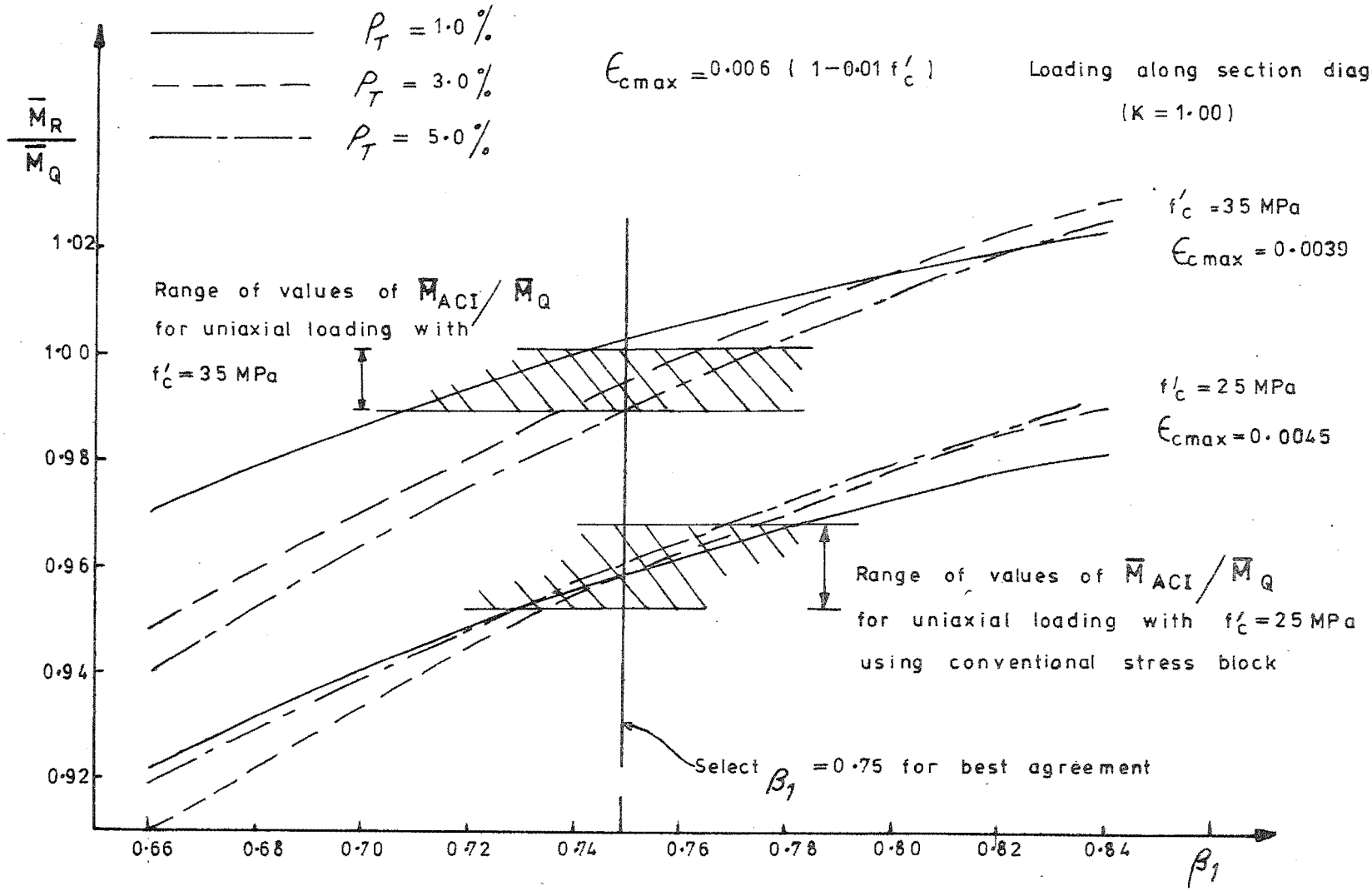

FIG·8·5 : SELECTION OF PARAMETER β_1 FOR ALTERNATIVE BIAXIAL RECTANGULAR STRESS BLOCK

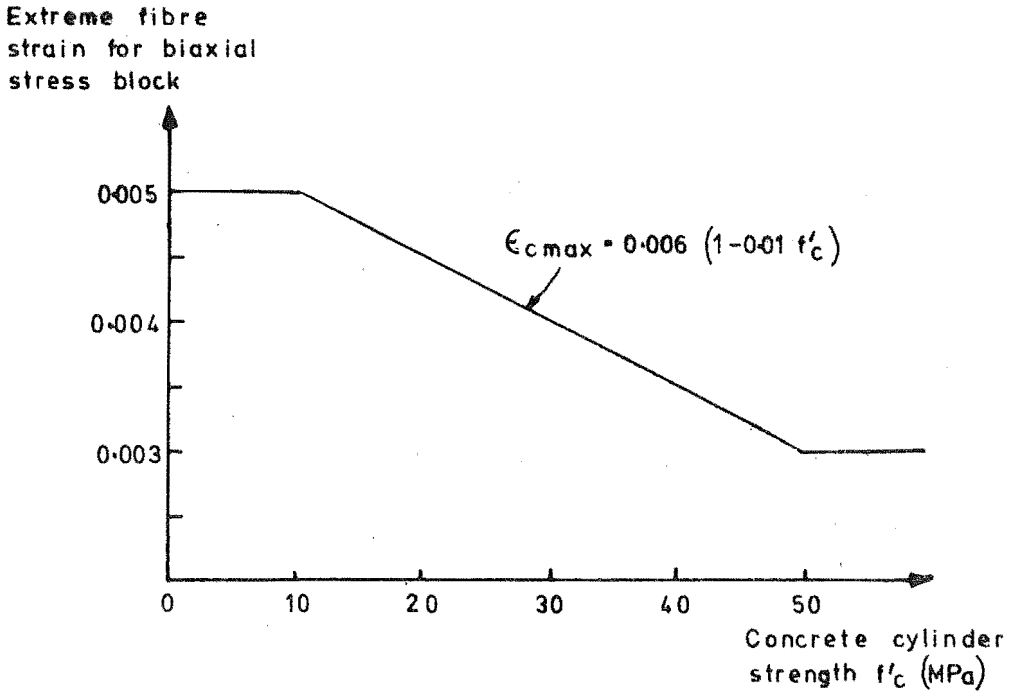

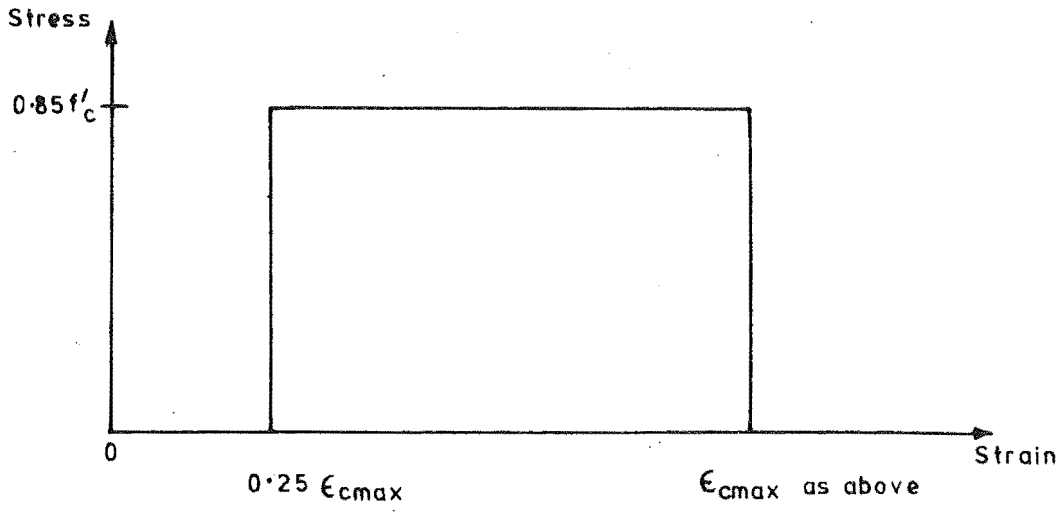

FIG.8.6 :ALTERNATIVE RECTANGULAR STRESS BLOCK FOR BIAXIAL BENDING

8.5.4 Comparison with Test Results

Column properties and parameters and experimental failure loads pertaining to columns tested in biaxial bending by various investigators [42, 43, 44, 45] are listed in Table 8-3, together with the failure loads calculated analytically using the conventional ACI stress block, and the proposed alternative stress block. The relative eccentricity of loading e_x/b (or e_y/h) at which failure was observed in each test was used to define a point on the interaction curve calculated for each test unit, and this gave the computed failure load in each case, as illustrated in Fig. 8.7 for Ramamurthy's unit A1. Comparison of analytical and test results shows that the concrete stress block proposed for biaxial column bending has validity over a wide range of parameters, although as expected the predicted strengths are conservative for columns having four bars only. For the columns having more than four bars the mean ratio of predicted to experimental failure loads is 0.981 using the proposed alternative stress block, while the mean ratio using the ACI stress block is 0.957. While the difference in the accuracy of the two methods is not large on the average, the scatter of results for the proposed stress block is rather less than for the ACI block. This is shown by the standard deviation of 0.045 over 16 values of the ratio of predicted to experimental failure loads for the proposed stress block, as compared to the standard deviation of 0.082 for the 16 results computed using the ACI stress block.

8.5.5 Design Charts

Typical design charts produced by the computer program using the proposed alternative rectangular stress block (Fig. 8.6) for biaxial bending, and the conventional ACI stress block (Fig. 8.3(a)) for uniaxial bending, are shown in Figs. 8.8 to 8.10. Note that these charts do not incorporate a strength reduction factor, ϕ.

Where f = g a single chart such as Fig. 8.8 or Fig. 8.9 may be used. In this case the axis about which the greatest specific moment is applied is taken as the X-axis, and the value of $K = m_y/m_x$ will therefore always be less than or equal to unity. Linear interpolation between the reinforcement requirements obtained from the two quadrants with K values closest to the required value will give the necessary value of reinforcement content ρ_T.

If for example the design moments are such that K = 0.35 and $\theta = \tan^{-1} K = 19.3°$, then interpolation is required between the quadrants for K = 0.268 (θ = 15°) and K = 0.577 (θ = 30°). Suppose the quadrant for K = 0.268 gives $\rho_T = 0.021$, and the quadrant for K = 0.577 gives

TABLE 8.3 : COMPARISON OF EXPERIMENTAL AND COMPUTED RESULTS FOR BIAXIAL BENDING STRENGTH

Test Unit	Column Size h x b (mm)	Column Bars	ρ_T	f_y (MPa)	f'_c (MPa)	f	g	TEST			Computed using conventional ACI stress block		Computed using proposed stress block	
								$K = \frac{e_x.h}{e_y.b}$	$\frac{e_x}{b}$	$\frac{N_u}{f'_c bh}$	$\frac{N_u}{f'_c.bh}$	$\frac{N_u(\text{analysis})}{N_u(\text{test})}$	$\frac{N_u}{f'_c.bh}$	$\frac{N_u(\text{analysis})}{N_u(\text{test})}$
Anderson & Lee [42]														
SC1,6	102 x 102	4-$\frac{1}{4}$" ϕ	0.012	246.8	37.5	0.625	0.625	1.00	0.785	0.0572 (i)	0.0542	0.948	0.0532	0.930
SC2,7	102 x 102	4-$\frac{5}{16}$" ϕ	0.019	270.3	37.5	0.625	0.625	1.00	0.767	0.0845	0.0769	0.910	0.0762	0.903
SC3,8	102 x 102	4-$\frac{3}{8}$" ϕ	0.028	277.2	37.5	0.625	0.625	1.00	0.764	0.1110	0.0960	0.865	0.0962	0.867
SC4,9	102 x 102	4-$\frac{1}{2}$" ϕ	0.049	315.1	37.5	0.625	0.625	1.00	0.758	0.1598	0.1392	0.871	0.1425	0.892
Bresler [43]														
B5	203 x 152	4-#5	0.026	368.9	22.1	0.417	0.563	1.00	0.50	0.2083	0.1912	0.918	0.1916	0.920
B6	203 x 152	4-#5	0.026	368.9	25.5	0.417	0.563	1.00	1.00	0.0957	0.0844	0.882	0.0928	0.970
B7	203 x 152	4-#5	0.026	368.9	24.1	0.417	0.563	2.00	0.50	0.1250	0.1212	0.970	0.1157	0.926
B8	203 x 152	4-#5	0.026	368.9	24.8	0.417	0.563	0.50	1.00	0.1389	0.1108	0.797	0.1250	0.900
								Mean for 4-bar columns				0.895		0.914
Ramamurthy [44]														
A1	203 x 203	8-#4	0.025	291.9	46.8 (ii)	0.750	0.750	0.268	0.435	0.2920	0.2930	1.003	0.2949	1.010
A2	203 x 203	8-#4	0.025	291.9	51.5	0.750	0.750	0.268	0.625	0.1862	0.1739	0.934	0.1805	0.970
A3	203 x 203	8-#4	0.025	291.9	49.6	0.750	0.750	0.268	0.625	0.1845	0.1739	0.942	0.1805	0.979
A10	203 x 203	8-#4	0.025	291.9	49.9	0.750	0.750	0.577	0.438	0.2247	0.2284	1.017	0.2345	1.043
A12	203 x 203	8-#4	0.025	291.9	44.7	0.750	0.750	0.577	0.875	0.0922	0.0994	1.078	0.0914	0.991

TABLE 8.3 (CONTINUED)

Test Unit	Column Size h x b (mm)	Column Bars	ρ_T	f_y (MPa)	f'_c (MPa)	f	g	TEST $K = \frac{e_x.h}{e_y.b}$	TEST $\frac{e_x}{b}$	TEST $\frac{N_u}{f'_c bh}$	Computed using conventional ACI stress block $\frac{N_u}{f'_c.bh}$	Computed using conventional ACI stress block $\frac{N_u(\text{analysis})}{N_u(\text{test})}$	Computed using proposed stress block $\frac{N_u}{f'_c.bh}$	Computed using proposed stress block $\frac{N_u(\text{analysis})}{N_u(\text{test})}$
Ramamurthy	(Contd)													
B6	203 x 203	8-#5	0.038	322.6	27.6	0.750	0.750	1.00	0.318	0.4399	0.4211	0.957	0.4287	0.975
B7	203 x 203	8-#5	0.038	322.6	29.5	0.750	0.750	1.00	0.354	0.4240	0.3661	0.864	0.3916	0.924
B8	203 x 203	8-#5	0.038	322.6	34.1	0.750	0.750	1.00	0.500	0.2624	0.2333	0.889	0.2720	1.037
E1	305 x 152	8-#5	0.034	322.6	23.5	0.600	0.900	1.00	0.373	0.4266	0.3720	0.872	0.3920	0.919
E2	305 x 152	8-#5	0.034	322.6	21.4	0.600	0.900	1.00	0.500	0.3131	0.2876	0.919	0.2928	0.935
F1	229 x 152	8-#4	0.029	291.9	29.3	0.550	0.700	0.402	0.242	0.5382	0.5713	1.062	0.5884	1.086
Hsu[45]														
H1	108 x 108	8-#3	0.049	306.8	29.1	0.618	0.618	0.833	0.765	0.1781	0.1920	1.078	0.1935	1.086
U1	102 x 102	9-D5	0.027 (iii)	503.3	26.9	0.608	0.608	0.714	0.875	0.1536	0.1404	0.914	0.1447	0.942
U2	102 x 102	9-D5	0.027	503.3	26.2	0.608	0.608	0.857	0.875	0.1429	0.1306	0.914	0.1389	0.973
U3	102 x 102	9-D5	0.027	503.3	26.8	0.608	0.608	1.00	0.875	0.1284	0.1190	0.927	0.1263	0.984
U4	102 x 102	9-D5	0.027	503.3	26.4	0.608	0.608	1.00	0.500	0.2334	0.2132	0.914	0.2263	0.970
						Mean for columns with more than 4 bars -						0.964		0.989

Notes: i) Values of N_u(test) for Anderson & Lee tests are mean of two results

ii) f'_c for Ramamurthy's tests taken as $0.90 f_{cu}$

iii) Hsu columns series U include 1 bar placed at centre of column. This has been assumed half as effective as perimeter bars for calculation of equivalent ρ_T

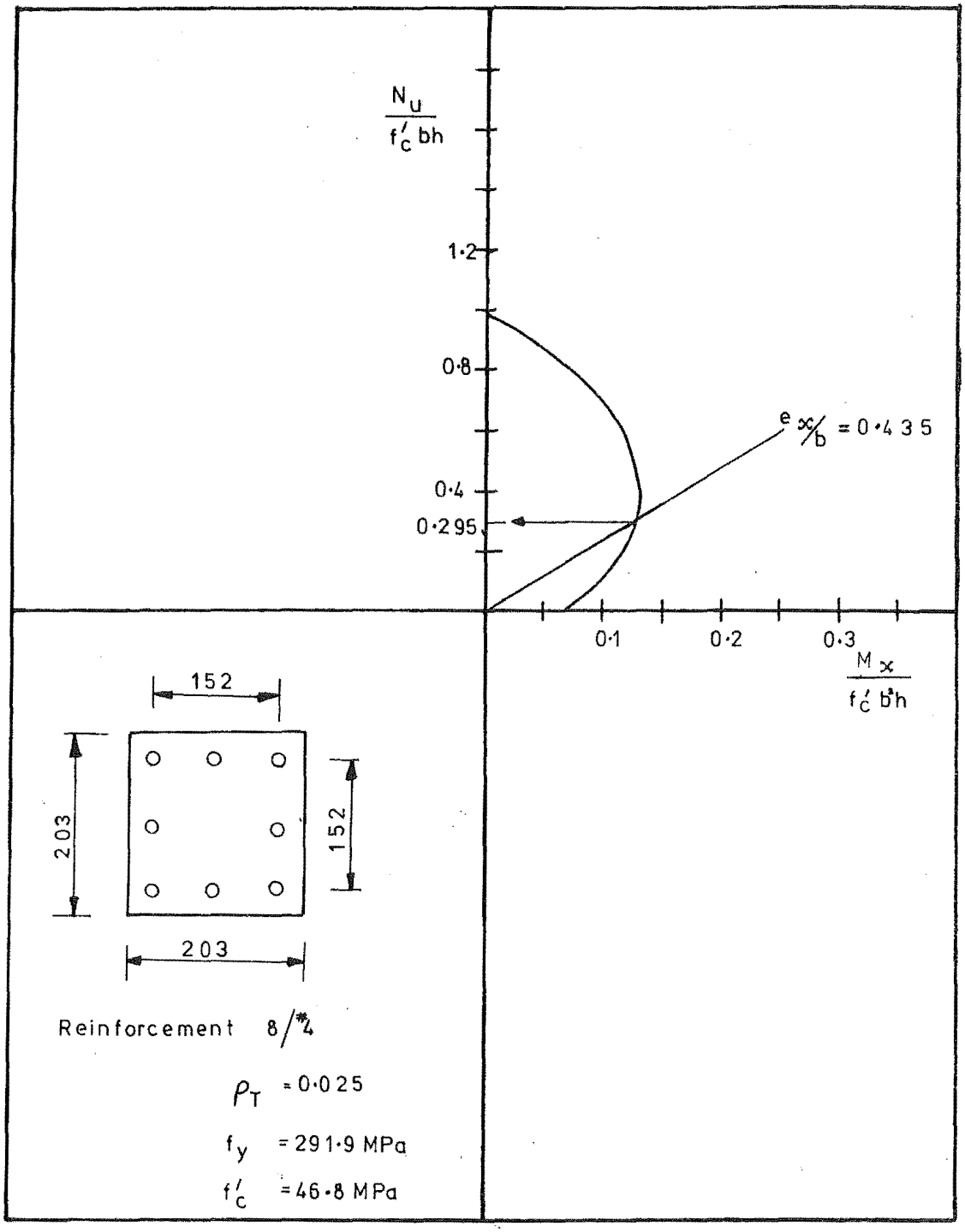

FIG.8.7:DERIVATION OF COMPUTED FAILURE LOAD FOR RAMAMURTHY'S TEST UNIT A1

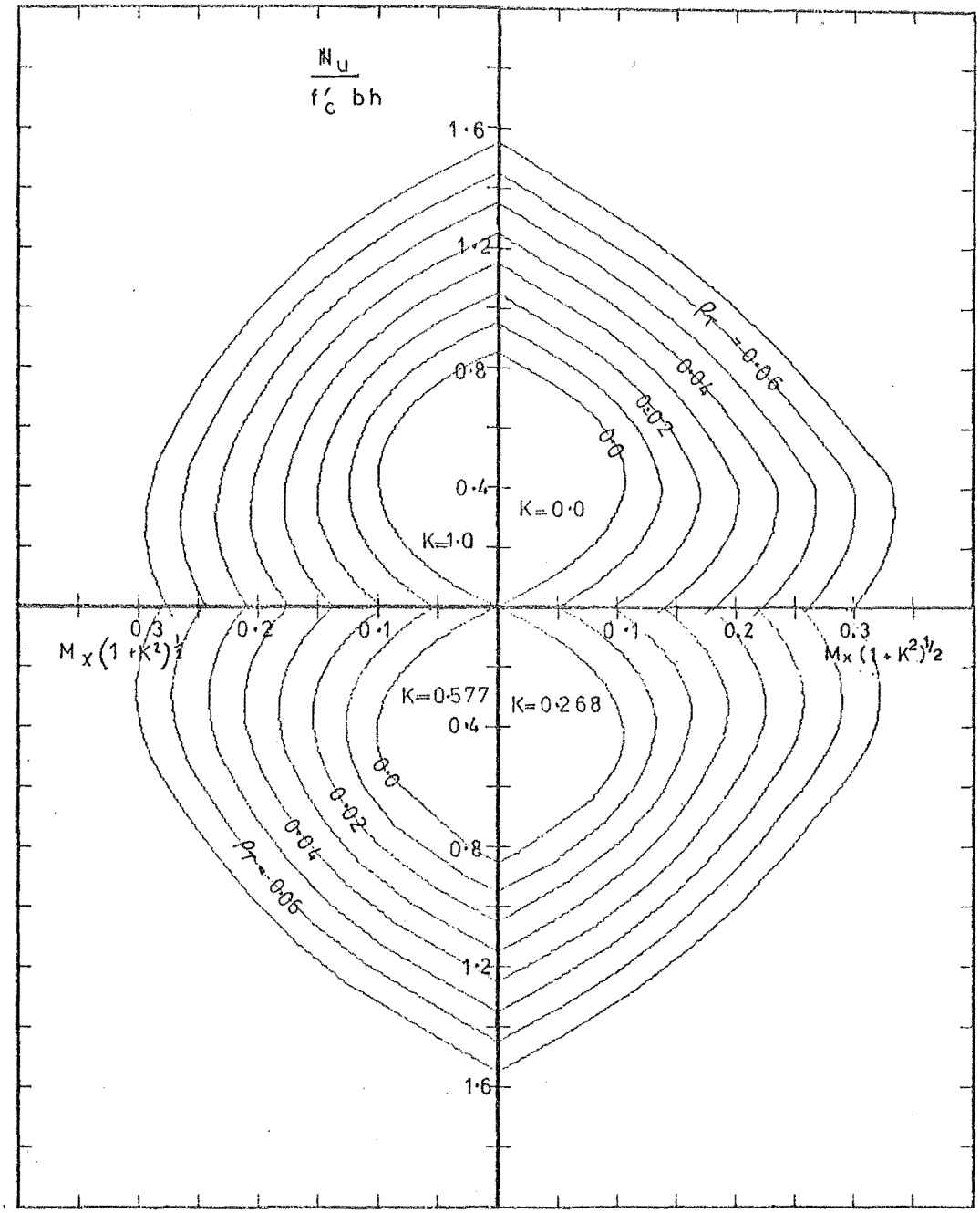

FIG.8·8: COLUMN BIAXIAL BENDING DESIGN CHART

f_y = 380 MPa , f'_c = 35 MPa , f-g = 0·9

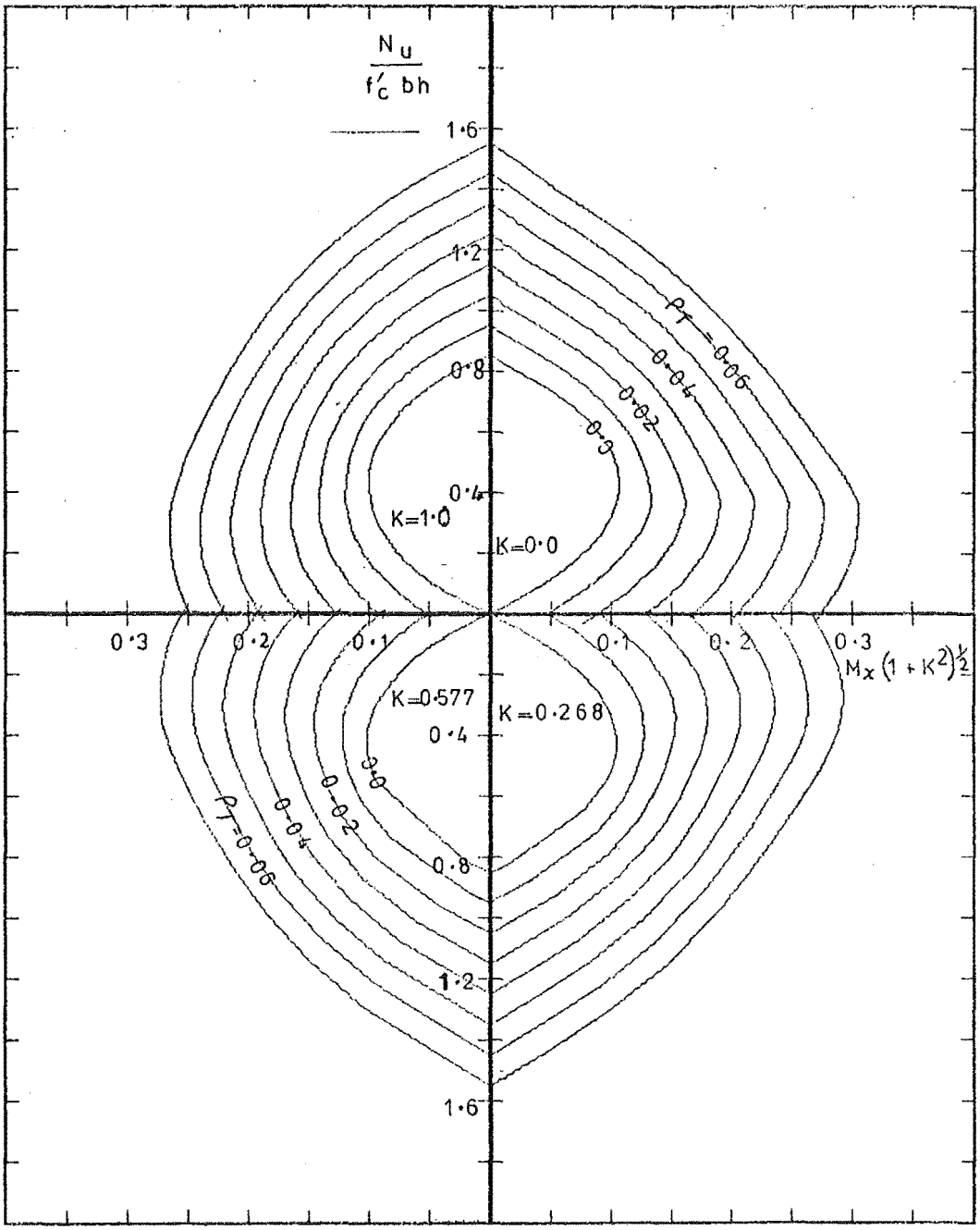

FIG·8·9 : COLUMN BIAXIAL BENDING DESIGN CHART

f_y=380 MPa , f'_c=35 MPa, f = g = 0·8

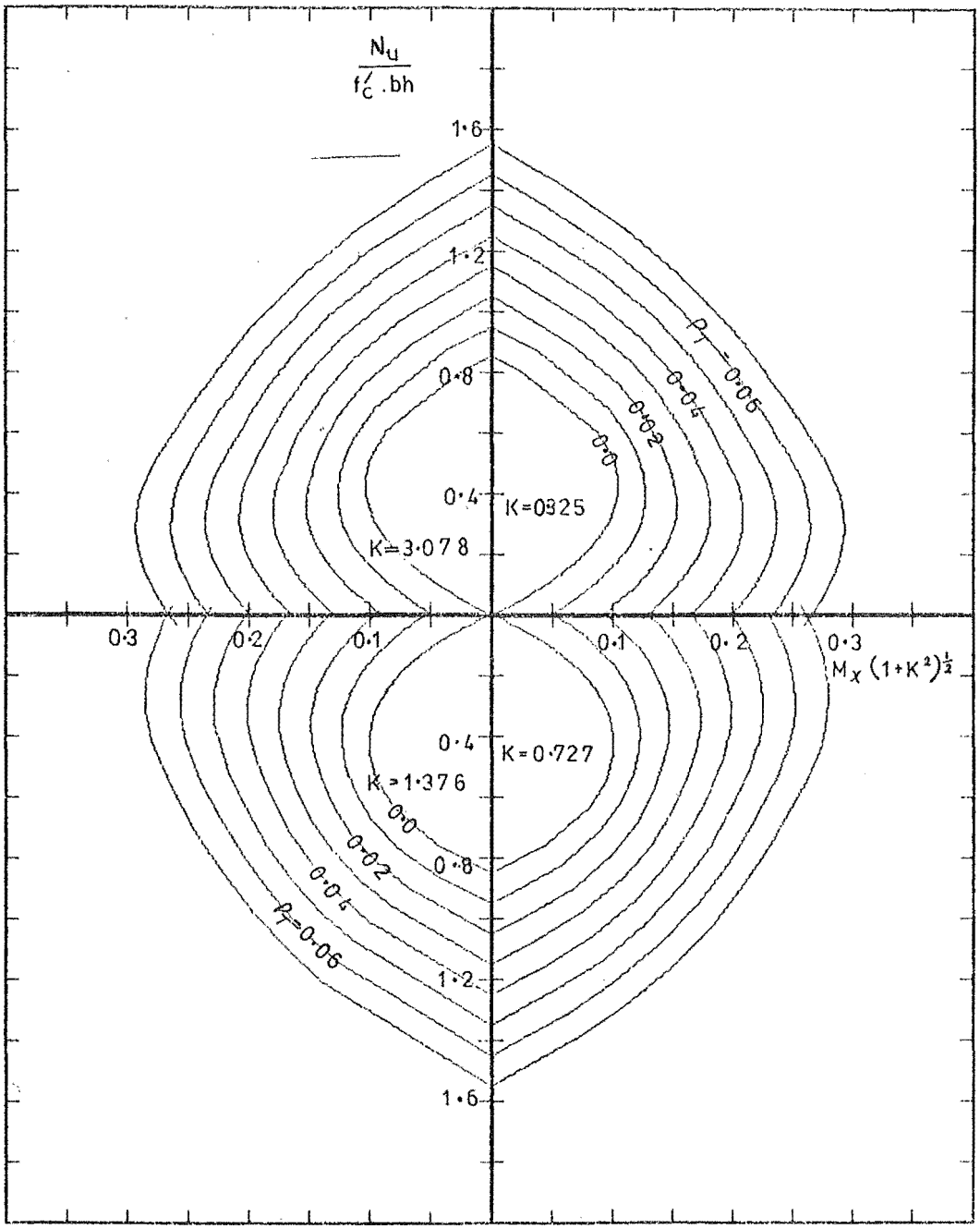

FIG.8·10 : COLUMN BIAXIAL BENDING DESIGN CHART

$f_y = 380$ MPa $f'_c = 35$ MPa $f = 0{\cdot}9$ $g = 0{\cdot}8$

$\rho_T = 0.025$. Then the required reinforcement for K = 0.35 is

$$\rho_T = 0.021 + \frac{19.3 - 15}{30 - 15}(0.025 - 0.021)$$

$$= 0.022$$

Where $f \neq g$ a chart of the form in Fig. 8.10 is required. In this case the X-axis cannot be arbitrarily defined, and K can therefore take any value between zero and infinity. However the appropriate charts derived for f = g can still be used at K = 0 since bending about the X-axis is independent of f, and also for $K = \infty$, since bending about the Y-axis is independent of g. The interpolation with respect to θ may then be done between any of the four cases given in the chart for $f \neq g$, and between the extreme values of $\theta = 0°$ or 90° using the appropriate chart for f = g.

8.5.6 Ratio of Biaxial Bending Strength to Uniaxial Strength for Columns

Fig. 8.11 shows the reduction in the moment capacity about a principal axis of a reinforced concrete column caused by concurrent bending about the other axis for columns having reinforcement of yield strength 380 MPa, concrete of cylinder strength 35 MPa, and f = g = 0.7 or f = g = 0.9. The biaxial bending strengths were computed at K values of 0.3, 0.6, 0.8 and 1.0 using the alternative biaxial stress block (Fig. 8.6), while the uniaxial strengths M_{uxo} were calculated using the conventional ACI stress block. The figures show that for loading along the section diagonal (K = 1.0) the uniaxial strength of a column may be reduced by up to 40%, whereas for loading at a specific angle of 22.5° (K = 0.414) the reduction will be 15% or less. Reduction of the uniaxial strength due to concurrent loading is less with smaller reinforcement contents, and with smaller axial loads, throughout the range of loading angles. Similar results may be shown for columns with other material strengths and section properties.

Fig. 8.12 shows the reduction in unidirectional moment strength due to loading along a section diagonal as a function of the column axial load intensity for various section parameters. The strength reduction is greatest in all cases for axial loads in the range of $0.30A_g.f'_c$ to $0.40A_g.f'_c$, and more heavily reinforced sections show a greater reduction in strength as a result of skew loading than do lightly reinforced sections. The concrete strength and the relative lever arm at which the reinforcement is placed have little effect on the strength reduction.

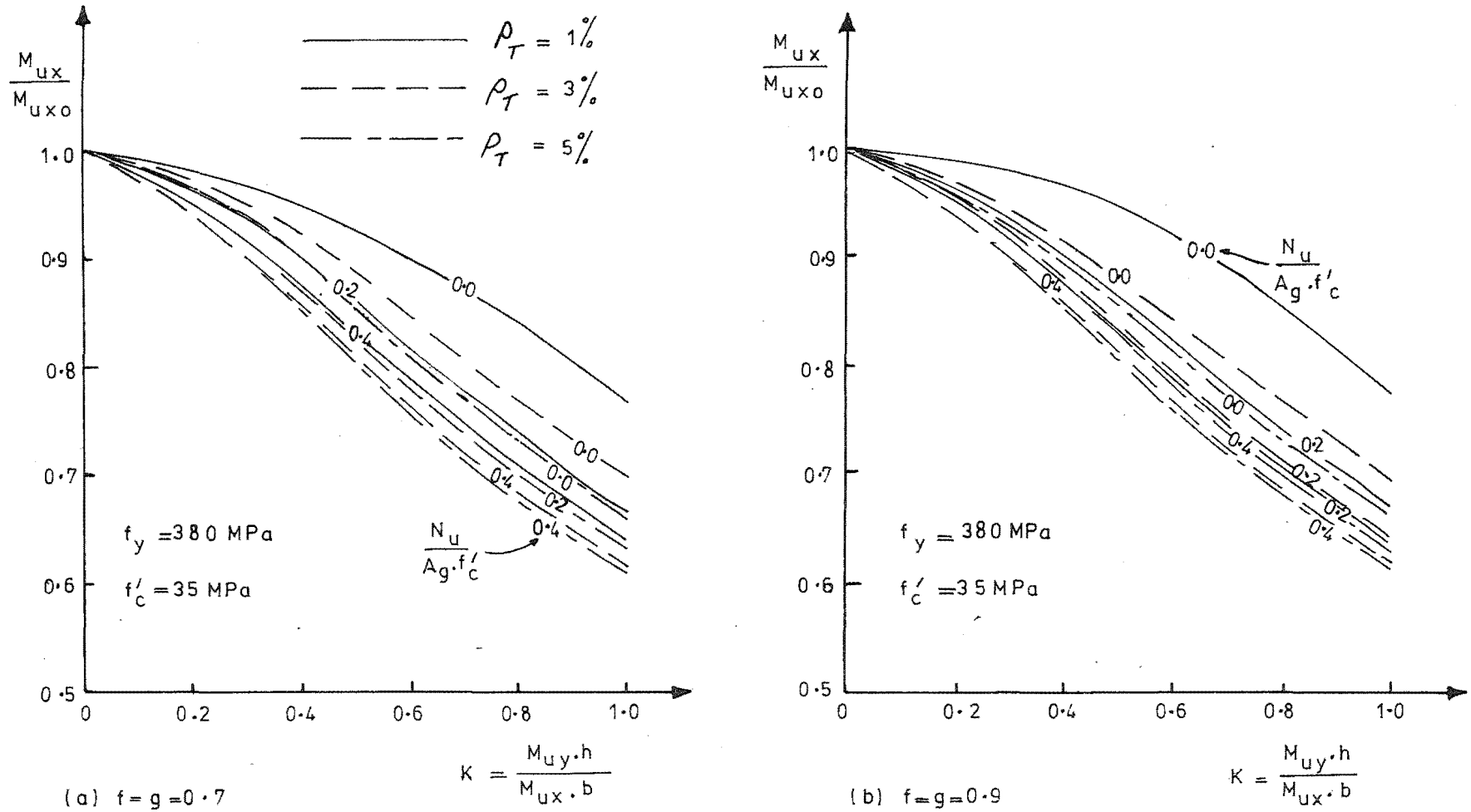

FIG.8·11 : REDUCTION IN UNIAXIAL STRENGTH OF COLUMNS DUE TO BIAXIAL BENDING

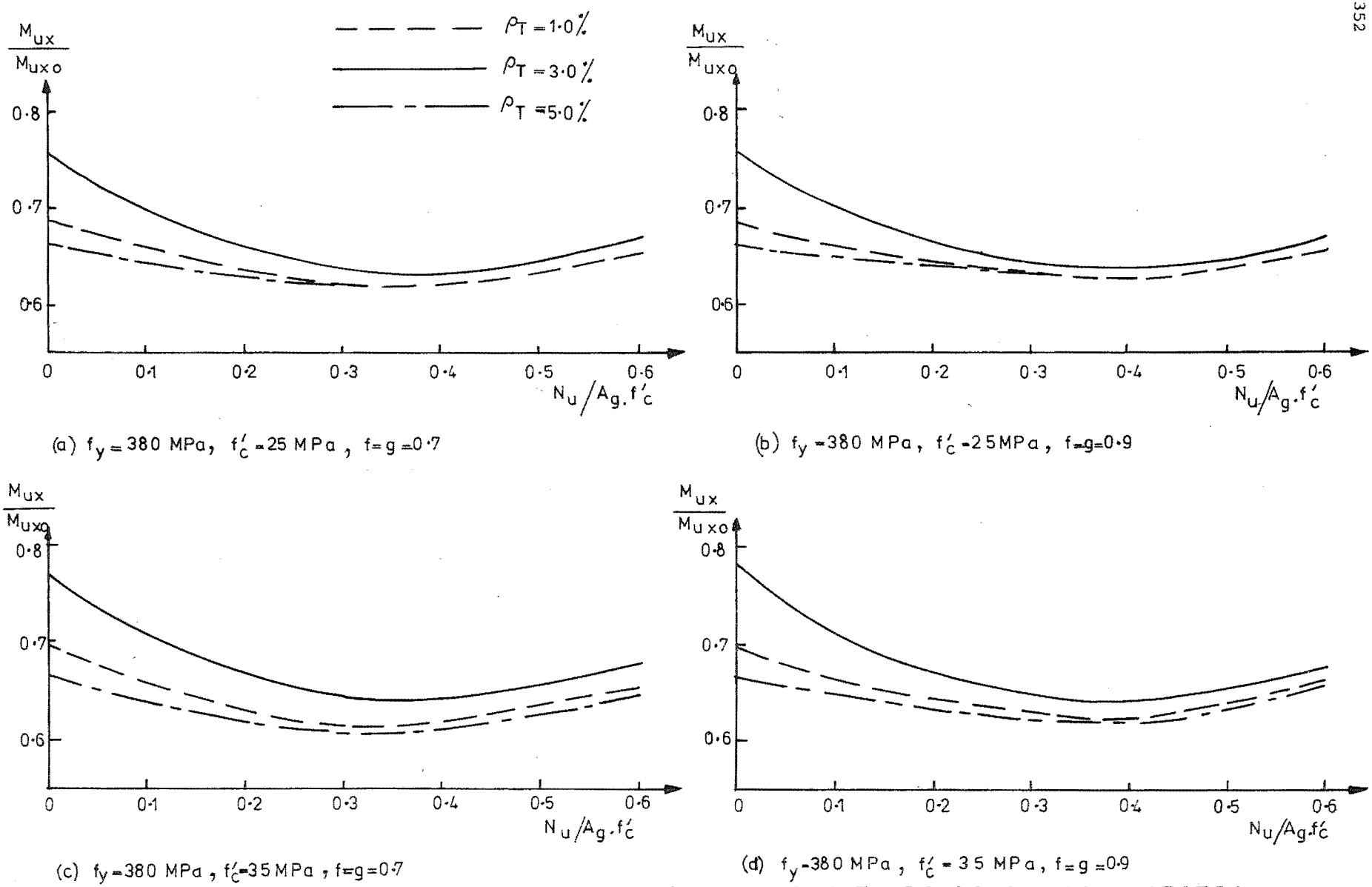

FIG. 8.12 : REDUCTION IN UNIAXIAL MOMENT STRENGTH DUE TO BENDING ALONG SECTION DIAGONAL (K=1·00)

It is apparent that for a column under biaxial bending due to loading applied along the section diagonal, the moment strength about a principal axis may be reduced by up to 40%. When the relative eccentricity of loading is greater in the direction of one principal axis than in the other, then the reduction in strength is less severe. Inspection of the limits to Eqs. (8-1) and (8-2), for the dynamic magnification factors[46], ω_p and ω_s, for column design moments in plane frames and space frames respectively, shows that for a stiff building ($T_1 < 0.6$ secs) the ratio of ω_s/ω_p is 1.25, while for a flexible building ($T_1 > 1.6$ secs), the ratio of 1.06. Applying these multipliers to the minimum ratios of uniaxial strength under skew loading to that under planar loading, given in Fig. 8.11, results in the envelopes given in Fig. 8.13 for the strength of biaxial bending of columns designed to resist magnified uniaxial bending moments only. Fig. 8.13 shows that a space frame column in a stiff building may carry biaxial bending moments at specific angles of loading of up to about 30° without overtaxing the section. Alternatively up to 75% of the maximum uniaxial column input moments in each direction may be carried concurrently without causing overload. Should some other load combination be imposed on the column, corresponding to a point in the shaded area in Fig. 8.13, then yielding of column reinforcing will occur. However as mentioned in Section 8.1, this will occur only if an extreme case of axial load is imposed in conjunction with the biaxial bending case, and this is unlikely because the critical moments and the critical axial loads tend to be associated with different types of dynamic building response.

For more flexible buildings the strength under biaxial bending of the columns may be reduced further relative to the uniaxial demand, since the structure will be highly redundant (typically 15 or more storeys for $T_1 > 1.6$ secs), and the likelihood of all critical actions occurring simultaneously is further reduced.

The probable actions on a column section are further reduced by the effects of stiffness degradation on the moment input from the beams, together with the low probability of dynamic magnification of column moments occurring simultaneously in the two directions at a given location. Thus it is clear that while the design approach of using magnified uniaxial moments for column design does not provide absolute protection to columns with respect to the possibility of yielding under biaxial bending, the likelihood of such overloads is small, and should be acceptable in most design situations. In cases where specific design for biaxial bending must be undertaken then design charts of the type shown in Figs. 8.8 to 8.10 provide a suitable means to achieve this.

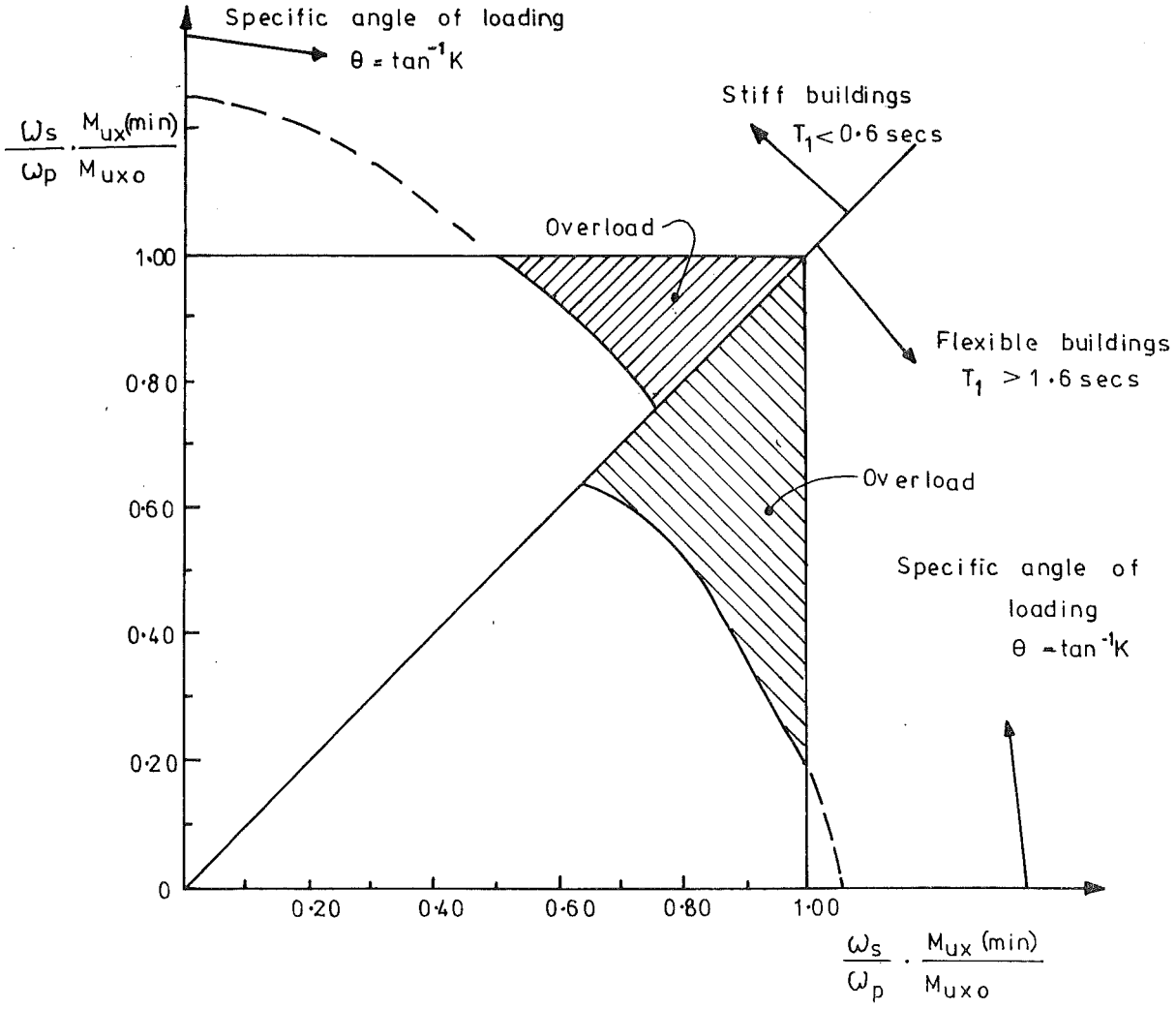

FIG.8.13: STRENGTH OF COLUMNS DESIGNED FOR MAGNIFIED UNIAXIAL MOMENTS SUBJECT TO BIAXIAL BENDING

CHAPTER 9

CONCLUSIONS

9.1 Summary of Research Findings

The principal part of the research reported in this thesis has been the testing under cyclic loading, simulating earthquake loading, of three reinforced concrete beam-column joint assemblies from plane frames, and one from a space frame. The plane frame test results showed that beam-column joints can be designed so that plastic deformation under seismic loading is restricted to the beam plastic hinges. Some stiffness degradation was observed under cyclic inelastic loading, but this was not considered likely to seriously affect the overall response of prototype structures to seismic loading. The test units to which small column axial loads were applied displayed a secondary failure towards the end of each test when the beam flexural reinforcing bars slipped through the joint core. This slip resulted in more serious stiffness degradation, with consequent loss of energy dissipating capacity.

The results obtained from the tests were shown to be consistent with the mechanisms of joint shear resistance postulated in Chapter 1. According to these postulates, the applied joint shear is resisted partly by a concrete compression strut acting between diagonally opposite corners of the joint core, and partly by a truss which requires horizontal and vertical joint core reinforcement. For the concrete strut mechanism to be effective suitable boundary conditions must be available to allow significant shear to be introduced at or near the corners of the joint core. After cyclic loading causing plastic hinging in the beams at the column faces the presence of full depth cracks in the beams means that suitable boundary conditions occur only for joint cores carrying heavy column axial loads. In this case it was postulated that a greater depth of the concrete compression zone in the column sections would enable part of the bond force from the beam bars to combine with vertical forces from the column to allow a compression strut to develop between the corners of the joint core, even though no concrete compression forces were available in the beams. This behaviour was well illustrated in the tests, where the joint core of the test unit carrying heavy column axial load performed much better than those of the units with low axial loads. This better behaviour occurred in spite of the fact that the unit to which heavy axial load was applied had less horizontal joint core reinforcement. The response of the test units to cyclic elastic and monotonic inelastic

loading was also consistent with the proposed mechanisms. In both cases the presence of beam concrete compressive forces caused favourable end conditions for the concrete compressive strut mechanism, and this was reflected by the low strains measured in joint core horizontal reinforcement during these parts of each test. As soon as reversed cyclic inelastic loading was applied, however, the joint core tie strains increased, and the concrete mechanism became much less effective.

Following the success of the postulated mechanisms, for transferring forces across the joint core, in predicting the response of the plane frame test units to cyclic loading in the inelastic range, the provisions of present codes were critically examined. Recommendations for the design of beam column joint cores subject to seismic loading are made in Chapter 6.

Consideration of the end conditions for the joint core concrete compression strut has led to the proposal[8] that efficient operation of the strut could be maintained by the use of 'elastic' joints, in which the beam plastic hinges are located at some distance away from the column faces. Tests conducted by Birss[27], in parallel with the present series, have shown that this concept has considerable merit. If the beam sections adjacent to the column faces remain in the elastic range, the joint core concrete strut mechanism continues to resist substantial shear throughout cyclic loading, and the necessary joint core shear reinforcement can be reduced considerably.

The testing of a space frame beam-column joint assembly, to which loads were applied concurrently in both principal directions, allowed the response of space frame joints to be related to that of plane frame joints with more confidence than previously. The test results showed that the space frame joint, which was designed for plane frame actions only, possessed adequate strength under severe concurrent loading. On the basis of this admittedly limited evidence from a single test, it was recommended that plane frame actions need only be considered for the design of space frame joint cores.

The mechanisms of shear resistance in space frame joints under concurrent loading were postulated to be similar to those identified in plane frame joints under unidirectional loading. The reasons for the more efficient performance of the space frame joint core were not precisely clear from the test results. The end conditions for the concrete compression strut in this case were indeterminate, and local stress redistributions in this vicinity may have enhanced the strength of the mechanism in some ill-defined manner.

The response of space frames to seismic actions was also examined in an analytical study of the strength of reinforced concrete columns subject to combined biaxial bending and axial load. The effect of the choice of the stress-strain curve for concrete on the computed flexural strength of columns in biaxial bending was studied in some detail. It was concluded that the conventional ACI rectangular concrete compressive stress block with a maximum concrete fibre strain of 0.003 does not give reliable results for columns in biaxial bending when the axial load is significant, and an alternative rectangular concrete compressive stress block, incorporating a larger extreme fibre concrete strain, was proposed for use in this case.

The effect of biaxial bending on the flexural strength of columns in each principal direction was also investigated. Computed results showed that the reduction in flexural strength about one principal axis due to bending about the other principal axis, was greatest for loading along a diagonal, and for axial loads close to the balanced failure load. Paulay[46] has suggested that concurrent seismic load effects might be allowed for in regular frames by using a greater moment magnification factor for space frame columns than for plane frame columns, and then designing for the resulting magnified uniaxial moments only. This approach to the design of space frame columns was shown to provide adequate flexural strength in the typical cases that were studied, with tolerably remote possibilities of column yielding occurring under the most adverse combination of possible load conditions. Such yield excursions could be expected to be limited in extent and brief in duration, and should not cause significant distress to the response of the structure as a whole.

9.2 Suggestions for Further Research

Although the understanding of the response of beam-column joint cores to seismic loading has recently been considerably improved, it is apparent that further testing of joint units would provide additional clarification. Further test results would allow the postulated mechanisms of resistance to joint shear to be refined, with consequent further improvements to the design procedures.

On the basis of the results of the present study it is suggested that for conventional beam-column joints with beam plastic hinges located next to the column faces, particular benefit might be gained by examining more closely the relationship between the bond strength of beam flexural reinforcing across the joint core, and the horizontal shear strength of

the joint core concrete strut mechanism. The variation in column axial load level used in the present study has partly shown this relationship. However column axial load is expected to influence the joint concrete mechanism irrespective of its effect on beam bar bond strength, because of the deeper concrete compression zone in the column sections above and below the joint. Thus the influence of beam bar bond strength on the strength of the concrete joint core mechanism would be better shown by the variation of a parameter which does not significantly effect the depth of column concrete in compression. A suitable parameter would appear to be the ratio of column depth to beam bar diameter. Further test results arising from the variation of this parameter could be most valuable.

The concept of 'elastic' joints, which are designed so that beam plastic hinges form away from the column faces, appears to provide a promising solution to the problem of congested joint core reinforcing, but test results appropriate to this type of joint are limited to date. Relevant parameters for further experimental programs could include the distance at which the plastic hinges are located from the column faces, the method of reinforcing the hinges and the joint core, and the column axial load level.

It was suggested in the present study that concurrent seismic load actions could be ignored in the design of space frame joint cores. This recommendation was based on the single test result reported herein. Obviously more test results pertaining to space frames would be desirable to give more weight to this suggestion, although the complexity of space frame joint testing presents difficulties. In particular, results for space frame joints with low column axial loads, and for edge and corner joints of space frames, would provide very significant information. Testing of space frame joints presents some problems in deriving an appropriate cyclic loading sequence for the beams in the two directions, and the effect on performance of variations in the imposed loading sequence should be determined experimentally.

In the beam-column joint tests, the effect of the slab, which in the prototype structure is usually constructed to act monolithically with the beams, was not included due to practical difficulties in construction and testing. For completeness it would be desirable to compare the behaviour of joints with and without slabs included in the test specimen.

The approach to the design and analysis of columns subject to biaxial bending and axial load, given in Chapter 8, could be refined and proved in

greater depth, over a wider range of concrete and reinforcement strengths. Due to limited time only the more common cases of columns were considered in the present study, but for general application of the approach, a more widely ranging study is desirable.

Due to the nature of the materials, and to the variations of seismic loading possible, the response of reinforced concrete frames covering all possible variations cannot be investigated. However the current design approach of restricting inelastic deformations to desired plastic hinge locations, utilising the philosophy of capacity design, provides a sound basis for the seismic design of buildings. Better understanding of joint core behaviour will allow designers to detail this critical area of frames more effectively and economically, and further research in this field will thus be well justified.

APPENDIX A

DERIVATION OF EQUILIBRIUM EQUATIONS FOR COLUMNS UNDER BIAXIAL BENDING

A.1 : Numerical Integration Approach

Using concrete stress-strain relationships other than the rectangular stress block, the obvious means of evaluating column actions when biaxial bending is applied is to integrate numerically over a grid of concrete elements, and over a set of discrete reinforcing positions distributed around the section perimeter. Since the rectangular stress block approach involves a step function, the numerical integration technique may not be sufficiently sensitive, and an analytic solution is more appropriate, as detailed in Section A.2.

Considering the strain diagram in Fig. A.1, the strain $\varepsilon(x,y)$ at any point in a column section may be expressed in terms of the neutral axis position, the maximum compressive strain, ε_{cmax}, and the coordinates (x,y) of the point from the principal axes of the section

$$\frac{\varepsilon(x,y)}{k_y.h - h/2 - (b/2 - x)\cot\phi - y} = \frac{\varepsilon_{cmax}}{k_y.h} \qquad (A\text{-}1)$$

$$\text{However} \quad \cot\phi = \frac{k_y.h}{k_x.b} \qquad (A\text{-}2)$$

$\therefore$ Equation (A-1) becomes

$$\varepsilon(x,y) = \varepsilon_{cmax}\left(1 - \frac{1}{2k_y} - \frac{1}{2k_x} - \frac{y}{k_y.h} + \frac{x}{k_x.b}\right) \qquad (A\text{-}3)$$

The concrete stress at any point may be expressed as

$$f'_c = \alpha_i.f'_c \qquad (A\text{-}4)$$

where α_i is a function of the strain in the ith concrete element, depending on the chosen stress-strain relationship (see Section 8.3), and f'_c is the cylinder strength of the concrete. Numerical integration may be carried out using the mid-point method[61] over a grid of $N_x \times N_y = N_c$ elements in the total section. The total concrete force P_c, taken positive for compression, is then

$$P_c = \sum_{i=1}^{N_c} \alpha_i.f'_c \cdot \frac{b}{N_x} \cdot \frac{h}{N_y} \qquad (A\text{-}5)$$

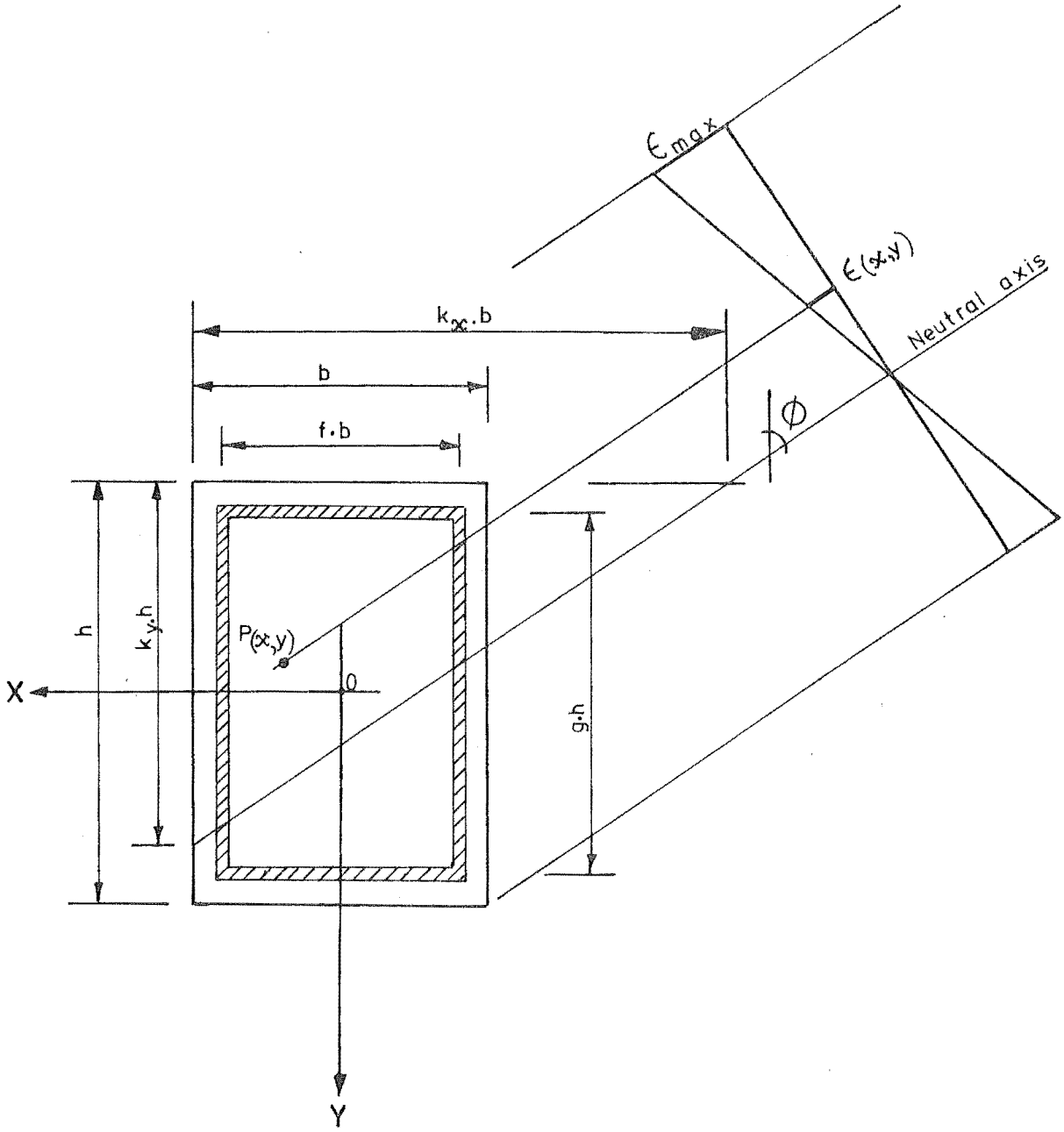

FIG. A.1 : STRAIN PROFILE FOR COLUMN SECTION UNDER BIAXIAL BENDING

The moments about the X and Y axes may be found by multiplying the elemental forces by the appropriate y and x coordinates, and integrating, the sign of the moments being given by the right hand screw rule

$$M_{cx} = - \sum_{i=1}^{N_c} \alpha_i \cdot f'_c \cdot \frac{b}{N_x} \cdot \frac{h}{N_y} \cdot y_i \qquad \text{(A-6)}$$

$$M_{cy} = \sum_{i=1}^{N_c} \alpha_i \cdot f'_c \cdot \frac{b}{N_x} \cdot \frac{h}{N_y} \cdot x_i \qquad \text{(A-7)}$$

Now if the steel stress of the jth steel element is f_{sj}, and the area of each element is $A_j = \frac{A_T}{N_S}$ where A_T is the total area of reinforcement, and N_S is the number of discrete steel elements, then the total steel force is

$$P_S = \frac{A_T}{N_S} \sum_{j=1}^{N_s} \cdot f_{sj} \qquad \text{(A-8)}$$

and the corresponding moments are

$$M_{sx} = - \frac{A_T}{N_S} \sum_{j=1}^{N_s} f_{sj} \cdot y_j \qquad \text{(A-9)}$$

$$M_{sy} = \frac{A_T}{N_S} \sum_{j=1}^{N_s} f_{sj} \cdot x_j \qquad \text{(A-10)}$$

Utilising the following dimensionless forms:

$$X = {}^{x}/_{b} \qquad \text{(A-11)}$$

$$Y = {}^{y}/_{h} \qquad \text{(A-12)}$$

$$\rho_T = {}^{A_T}/_{b.h} \qquad \text{(A-13)}$$

Equation (A-3) becomes

$$\varepsilon(x,y) = \varepsilon_{cmax} \left(1 - \frac{1}{2k_y} - \frac{1}{2k_x} - \frac{Y}{k_y} + \frac{X}{k_x}\right) \qquad \text{(A-14)}$$

and the total column axial load N_u is

$$N_u = P_c + P_s = \frac{b.h.f'_c}{N_c} \sum_{i=1}^{N_c} \alpha_i + \frac{A_T}{N_S} \sum_{j=1}^{N_s} f_{sj} \qquad \text{(A-15)}$$

or

$$\frac{N_u}{f'_c.bh} = \frac{1}{N_c} \sum_{i=1}^{N_c} \alpha_i + \frac{\rho_T}{N_s.f'_c} \sum_{j=1}^{N_s} f_{sj} \qquad (8\text{-}11)$$

Similarly

$$M_{ux} = M_{cx} + M_{sx} = -\frac{f'_c.bh^2}{N_c} \sum_{i=1}^{N_c} \alpha_i.y_i - \frac{A_T}{N_S}.h. \sum_{j=1}^{N_s} f_{sj}.y_j \qquad (A\text{-}16)$$

or

$$\frac{M_{ux}}{f'_c bh^2} = -\frac{1}{N_c} \sum_{i=1}^{N_c} \alpha_i y_i - \frac{\rho_T}{N_S.f'_c} \sum_{j=1}^{N_s} f_{sj}.y_j \qquad (8\text{-}12)$$

Also

$$\frac{M_{uy}}{f'_c b^2 h} = \frac{1}{N_c} \sum_{i=1}^{N_c} \alpha_i X_i + \frac{\rho_T}{N_S.f'_c} \sum_{j=1}^{N_s} f_{sj}.X_j \qquad (8\text{-}13)$$

The right hand sides of Eqs. (A-14), (8-11), (8-12) and (8-13) are this independent of b and h, and a general solution is provided.

A.2 : Analytic Solution for Concrete Actions Using A Rectangular Stress Block

If the concrete actions in a column section are to be represented by a rectangular stress block of the form shown in Fig. A.2(a), then an analytic solution is available. Various cases for the location of the neutral axis must be considered as shown in Fig. A.2(b) to (f).

Case 1) Where $\beta_1 k_x.b < b$ (A-17)

and $\beta_1 k_y.h < h$ (A-18)

Then the area over which the uniform stress $\alpha.f'_c$ acts is triangular in shape, and the concrete compression force is

$$P_c = P_{c1} = \frac{\beta_1.k_x.b.\beta_1 k_y.h}{2}.\alpha.f'_c \qquad (A\text{-}19)$$

or

$$\frac{P_c}{f'_c.bh} = \frac{\beta_1^2 k_x.k_y}{2}.\alpha \qquad (A\text{-}20)$$

and the moments are

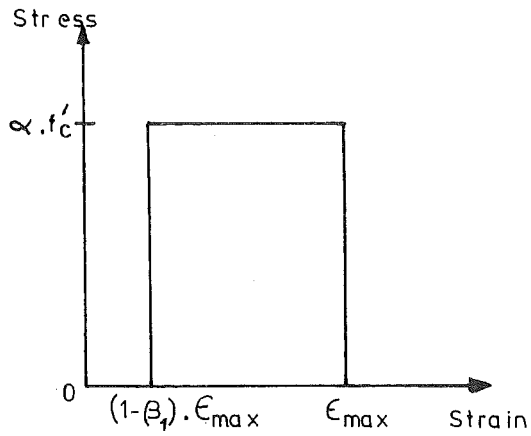

(a) Concrete stress strain relationship

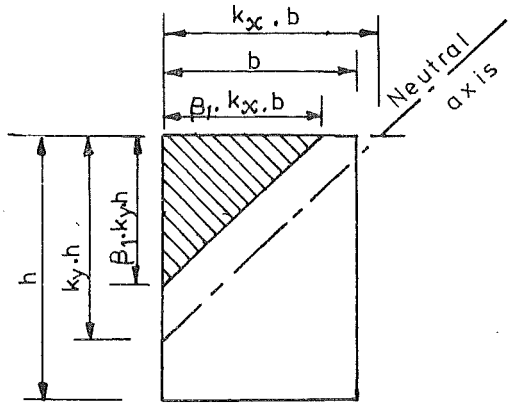

(b) Case 1 : Triangular compressed area

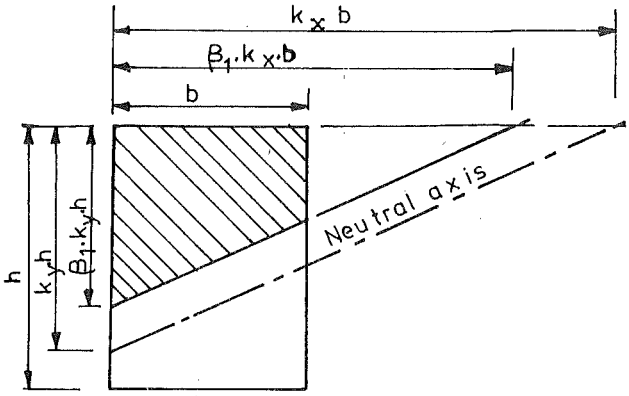

(c) Case 2 : Trapezoidal compressed area

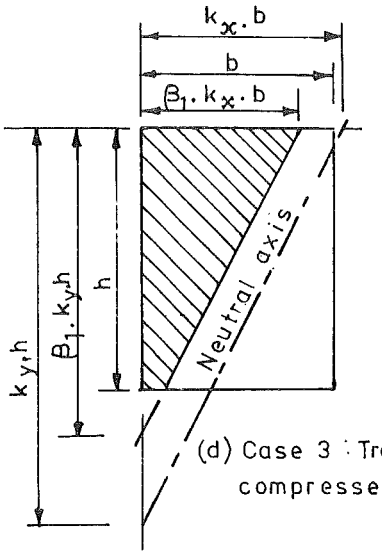

(d) Case 3 : Trapezoidal compressed area

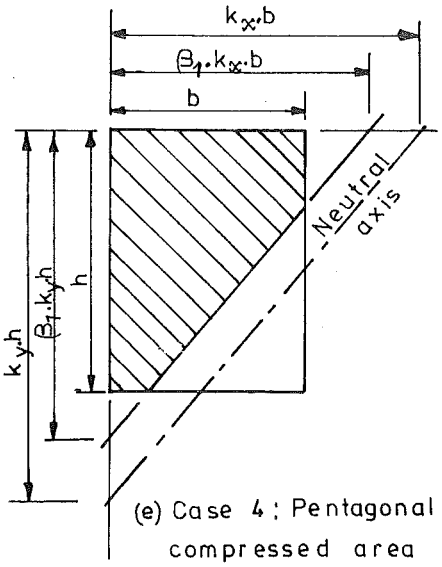

(e) Case 4 ; Pentagonal compressed area

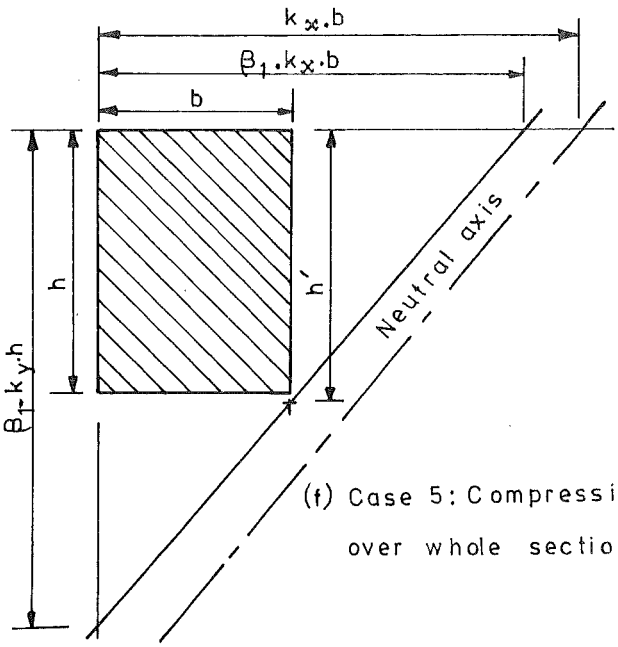

(f) Case 5: Compression over whole section

FIG.A.2: RECTANGULAR STRESS BLOCK IN COLUMN UNDER BIAXIAL BENDING

$$M_{cx} = P_{c1}\left(0.5h - \frac{\beta_1.k_y.h}{3}\right) \quad \text{(A-21)}$$

or $$m_{cx1} = \frac{M_{cx}}{f'_c bh^2} = \frac{P_{c1}}{f'_c bh}\left(0.5 - \frac{\beta_1.k_y}{3}\right) \quad \text{(A-22)}$$

Similarly

$$m_{cy1} = \frac{M_{cy}}{f'_c b^2 h} = \frac{P_{c1}}{f'_c.bh}\left(0.5 - \frac{\beta_1.k_x}{3}\right) \quad \text{(A-23)}$$

Case 2) Where $\beta_1.k_x.b > b$ (A-24)

and $\beta_1.k_y.h < h$ (A-25)

The area over which the uniform stress $\alpha.f'_c$ acts is trapezoidal, and the actions are most conveniently evaluated by considering the differences between the two triangles:

The concrete force arising from the 'negative' triangle is

$$P_{c2} = \frac{(\beta_1.k_x.b - b)}{2} \cdot \frac{(\beta_1.k_x.b - b)}{\beta_1 k_x b} \cdot \beta_1.k_y h.\alpha.f'_c \quad \text{(A-26)}$$

The net concrete force is

$$P_c = P_{c1} - P_{c2} \quad \text{(A-27)}$$

Thus from Eqs. (A-19) and (A-27)

$$\frac{P_c}{f'_c.bh} = \frac{\beta_1 k_x.k_y}{2} \cdot \alpha - \frac{(\beta_1 k_x - 1)^2}{2} \frac{k_y}{k_x} \cdot \alpha \quad \text{(A-28)}$$

The moments caused by the 'negative' concrete triangle are

$$M_{cx2} = P_{c2}\left(0.5h - \frac{\beta_1 k_x - 1}{3k_x}.k_y.h\right) \quad \text{(A-29)}$$

which may be reduced to

$$m_{cx2} = \frac{M_{cx2}}{f'_c bh^2} = \frac{P_{c2}}{f'_c bh}\left(0.5 - (\beta_1 k_x - 1).k_y/3k_x\right) \quad \text{(A-30)}$$

while $$m_{cy2} = \frac{M_{cy2}}{f'_c b^2 h} = \frac{P_{c2}}{f'_c.bh}\left(0.5 + (\beta_1 k_x - 1)/3\right) \quad \text{(A-31)}$$

The total actions are then

$$\frac{M_{cx}}{f'_c bh^2} = m_{cx1} - m_{cx2} \qquad \text{(A-32)}$$

$$\frac{M_{cy}}{f'_c . b^2 h} = m_{cy1} + m_{cy2} \qquad \text{(A-33)}$$

Case 3) Where $\beta_1 . k_x . b < b$ (A-34)

and $\beta_1 . k_y , h > h$ (A-35)

The stressed area is similar to that considered in Case 2, and the same arguments apply.

The 'negative' concrete force is

$$P_{c3} = \frac{\beta_1 . k_y . h - h}{2} \cdot \frac{\beta_1 . k_y . h - h}{\beta_1 . k_y . h} \cdot \beta_1 . k_x . b . \alpha . f'_c \qquad \text{(A-36)}$$

and the net concrete force is

$$\frac{P_c}{f'_c bh} = \frac{\beta_1^2 k_x . k_y}{2} . \alpha . - (\beta_1 k_y - 1)^2 \frac{k_x}{k_y} . \frac{\alpha}{2} \qquad \text{(A-37)}$$

The specific moments due to the negative concrete force are

$$m_{cx3} = \frac{P_{c3}}{f'_c bh} \left(0.5 + \frac{\beta_1 . k_y - 1}{3}\right) \qquad \text{(A-38)}$$

and $$m_{cy3} = \frac{P_{c3}}{f'_c bh} \left(0.5 - (\beta_1 . k_y - 1) k_x / 3 k_y\right) \qquad \text{(A-39)}$$

so that the net actions are

$$\frac{M_{cx}}{f'_c bh^2} = m_{cx1} + m_{cx3} \qquad \text{(A-40)}$$

$$\frac{M_{cy}}{f'_c b^2 h} = m_{cy1} - m_{cy3} \qquad \text{(A-41)}$$

Case 4) Where $\beta_1 . k_x . b > b$ (A-42)

and $\beta_1 . k_y . h > h$ (A-43)

The area over which the uniform stress $\alpha f'_c$ acts is pentagonal, and the two negative stress triangles considered separately in Cases 2 and 3 must be included.

Thus $$P_c = P_{c1} - P_{c2} - P_{c3} \quad \text{(A-44)}$$

or $$\frac{P_c}{f'_c bh} = \frac{\beta_1^2 k_x . k_y}{2} . \alpha - (\beta_1 . k_x - 1)^2 \frac{k_y}{k_x} . \frac{\alpha}{2} - (\beta_1 . k_y - 1)^2 \frac{k_x}{k_y} . \frac{\alpha}{2}$$

(A-45)

and $$\frac{M_{cx}}{f'_c bh^2} = m_{cx1} - m_{cx2} + m_{cx3} \quad \text{(A-46)}$$

$$\frac{M_{cy}}{f'_c b^2 h} = m_{cy1} + m_{cy2} - m_{cy3} \quad \text{(A-47)}$$

Case 5) occurs when the complete section carries the uniform compressive stress $\alpha f'_c$ as shown in Fig. A.2(f). This will occur when the distance h' in the figure exceeds the column depth h

Now $$h' = \frac{\beta_1 . k_y . h \ (\beta_1 . k_x . b - b)}{\beta_1 k_x b.} \quad \text{(A-48)}$$

Therefore the condition for this case to occur is

$$h' > h \quad \text{(A-49)}$$

or $$\frac{\beta_1 . k_y . h \ (\beta_1 . k_x . b - b)}{\beta_1 . k_x . b} > h \quad \text{(A-50)}$$

This inequality reduces to

$$\frac{k_y (\beta_1 . k_x - 1)}{k_x} > 1 \quad \text{(A-51)}$$

which may be rearranged to give

$$\frac{1}{\beta_1 . k_x} + \frac{1}{\beta_1 . k_y} > 1 \quad \text{(A-52)}$$

In this situation

$$P_c = \alpha . f'_c . b . h \quad \text{(A-53)}$$

or $$\frac{P_c}{f'_c bh} = \alpha \quad \text{(A-54)}$$

and $$M_{cx} = M_{cy} = 0 \quad \text{(A-55)}$$

The actions due to the reinforcement may be evaluated by numerical integration as previously (using the appropriate parts of Eqs. (8-11), (8-12) and (8-13)),and added to the above analytic results for the concrete actions.

APPENDIX B

COMPUTER PROGRAM

B.1 : Program Description

A listing of the biaxial column bending analysis program is given below in Section B.2. The program was written in FORTRAN IV for the Burroughs B6718 computer, and graphical output was obtained using the Calcomp X-Y plotter.

If the analysis option DESIGN is set, the program produces biaxial bending charts as desired, while if the analysis option COMPARE is set, comparisons of the moment strengths calculated using different stress-strain assumptions for concrete may be obtained.

After input of initial data the subroutine BIPLOT is called to set up the required plots. The subroutines RBLOCK, PARLIN, TRIARM, or QUADRC are then called to determine the initial parameters for the required stress-strain curve. Certain stress-strain curves of such type are available intrinsically within the program (see Section 8.3, Fig. 8.3), or alternatively curves of the same form may be used with the parameters read in as data.

The subroutine GEN is called to calculate coordinates for the elemental concrete grid and steel tube, and the interaction curve is then determined for each value of reinforcing content ρ_T. The neutral axis depth is set by fixed increments in one direction (k_y), and the neutral axis depth in the other direction (k_y) is determined by iteration using the secant method[61], until the direction of the resultant internal moments agrees with the prescribed loading direction. When the analysis option DESIGN is set, the interaction curve is plotted on the design chart. When the analysis option is COMPARE, the results for the first stress-strain curve type are stored, and the moment results for subsequent cases are divided by the stored values. The output in this case may be either printed or plotted (or both).

```
C     BIAXIAL COLUMN BENDING ANALYSIS PROGRAM
C
C     OPTION = DESIGN PRODUCES DESIGN CHARTS USING THE CHOSEN
C                    CONCRETE STRESS-STRAIN RELATIONSHIP
C
C     OPTION = COMPARE GIVES COMPARISON OF MOMENTS CALCULATED USING
C                    VARIOUS CONCRETE STRESS-STRAIN RELATIONSHIPS
C
C     ****************************************************************



      DIMENSION PLAB(6),PTV(8),FKV(4),CSV(7),ISV(7),P(60),PE(60),
     1 IDIV(32),PISAVE(60,32),PEISAV(60,32),PPLOT(60),PEPLOT(60),
     2 IS1(4),IS2(4),CSTV(4)
      COMMON/CORD1/CX(50,50)/CORD2/CY(50,50)/CORD3/SX(100),SY(100)
      COMMON/CALCPM/XM,YM,PU,XK,YK,FY,FC,YMS,PT
      DATA DESIGN,COMPAR,END/6HDESIGN,6HCOMPAR,3HEND/,BLANK/6H      /
      DATA CSV/3HACI,5HDGRON,6HCEBFIP,6HHOGNES,6HKPUNCF,6HKPCUNF,
     1         6HKRZLEE/,ISV/1,4*2,3,4/
      DATA CSTV/6HRBLOCK,6HPARLIN,6HTRIARM,6HQUADRC/
      DATA IS1/1,1,-1,-1/,IS2/1,-1,-1,1/
      DATA XXC,YYC / 0.125,0.50 /,STEP,TEST /0.2,0.002 /
C
    5 READ(5,501)OPTION
C
      IF(OPTION.EQ.END) GO TO 450
      READ(5,502)FY,YMS,F,G,FC,ICG,ISG,NOC,IPRINT,IPLOT,PLAB
      IF(OPTION.EQ.COMPAR) GO TO 10
      WRITE(6,601)

      WRITE(6,603) FY,YMS,F,G,FC,ICG,ICG,ISG,PLAB
      IOPT=1
      READ(5,503)PTI,PTINC,NPT
      DO 6 I=1,NPT
    6 PTV(I)=(I-1)*PTINC+PTI
      WRITE(6,605) NPT,PTINC,PTI
      GO TO 16
C
   10 WRITE(6,602)
      WRITE(6,603) FY,YMS,F,G,FC,ICG,ICG,ISG,PLAB
      IOPT=2
      READ(5,506)PTV
      DO 12 I=2,8
      IF(PTV(I).EQ.0.) GO TO 14
   12 CONTINUE
   14 NPT=I-1
      WRITE(6,606)(PTV(I),I=1,NPT)
C
   16 READ(5,508)FKV
      DO 18 I=2,4
      IF(FKV(I).EQ.0.) GO TO 19
   18 CONTINUE
   19 NK=I-1
      WRITE(6,608)(FKV(I),I=1,NK)
C
C     ANALYZE ONE CASE AT A TIME
C
      DO 400 IC=1,NOC
      READ(5,510) CSTYPE,CSNAME
      IF(CSTYPE.NE.BLANK) GO TO 25
      DO 20 I=1,7
      IF(CSNAME.EQ.CSV(I)) ITYPE=ISV(I)
   20 CONTINUE
      GO TO 30
   25 DO 28 I=1,4
      IF(CSTYPE.EQ.CSTV(I)) ITYPE=I
   28 CONTINUE
   30 IF(ITYPE.EQ.0) GO TO 350
C
      IF(IC.EQ.1) CSNAMD=CSNAME


      IF(IOPT.EQ.1.OR.IC.GE.2)CALL BIPLOT(IOPT,IPLOT,CSNAME,
     1 CSNAMD,PLAB,NK)
C
C     CALL APPROPRIATE SUBROUTINE TO CALCULATE STRESS-BLOCK PARAMETERS
C
      GO TO (31,32,33,34)ITYPE
   31 CALL RBLOCK(1,CSNAME,ISG)
      GO TO 38
   32 CALL PARLIN(1,CSNAME,ICG,ISG)
      GO TO 38
   33 CALL TRIARM(1,CSNAME,ICG,ISG,F,G)
      GO TO 38
   34 CALL QUADRC(1,CSNAME,ICG,ISG)
   38 CONTINUE
C
      DO 300 IK=1,NK
      FK=FKV(IK)
      IFK=FK*1000
      YOR=1.5*IK
      IX=IS1(IK)*25+30
      IF(FK.LE.1.0) GO TO 45
      IF((FK-1.)*(FKL-1.)*IKK.GT.0.)GO TO 46
      FK=1.0/FK
      FDUM=F
      F=G
      G=FDUM
   45 CALL GEN(F,G,ICG,ISG)
      IKK=1
   46 FKL=FK
      RMOOR=SQRT(FK*FK+1.)
C
      DO 250 IP=1,NPT
      PT=PTV(IP)
      IP1=(IK-1)*NPT+IP
      NLINE=40-IP*10
      NGAP=35*NLINE
C
C     CALL APPROPRIATE SUBROUTINE TO CALCULATE PO
C
      GO TO (51,52,53,54)ITYPE
   51 CALL RBLOCK(2,CSNAME,ISG)
      GO TO 58
   52 CALL PARLIN(2,CSNAME,ICG,ISG)
      GO TO 58
   53 CALL TRIARM(2,CSNAME,ICG,ISG,F,G)
      GO TO 58
   54 CALL QUADRC(2,CSNAME,ICG,ISG)
C
   58 P(1)=PU
      PE(1)=0.
C
C     SET YK BY FIXED INCREMENTS AND ITERATE ON XK BY SECANT METHOD
C     SO THAT DIRECTION OF INTERNAL MOMENT=DIRECTION OF APPLIED LOAD
C        (NO ITERATION NECESSARY FOR UNIAXIAL CASE)
C
      WRITE(6,620)CSNAME,PT,FK
      IF(IPRINT.GT.0) WRITE(6,621)
      RO=0.
      I=2
      YK=2.3
      IF(FK.EQ.0.) GO TO 60
      YK=YK*FK
      IF(YK.LT.1.5) YK=1.5
C
   60 CONTINUE
      NIT=0
      IF(FK.LT.0.01) GO TO 64
      XK=YK/FK*(1.0-RO)*XK+RO
      K=0
      XKL=0.
      RO=1.0
      GO TO 65
   64 XK=1.0E6
   65 IF(XK.LE.0.) XK=XKL/2.0
      NIT=NIT+1
   70 GO TO (71,72,73,74)ITYPE
```

```
   71 CALL RBLOCK(3,CSNAME,ISG)
      GO TO 76
   72 CALL PARLIN(3,CSNAME,ICG,ISG)
      GO TO 76
   73 CALL TRIARM(3,CSNAME,ICG,ISG,F,G)
      GO TO 76
   74 CALL QUADRC(3,CSNAME,ICG,ISG)
C
   76 IF(FK.LT.0.01) GO TO 100
      IF(XM.NE.0.) GO TO 80
      IF(PU*PT.EQ.0.) GO TO 99
      DM=YK/FK
      GO TO 82
   80 DM=YM/XM-FK
      IF(NIT.GT.30) GO TO 99
   82 ADM=ABS(DM)
      IF(ADM.LE.TEST)GO TO 99
      XKST=XK
      IF(K.EQ.1)GO TO 95
   94 XK=SIGN(STEP,DM)+XK
      K=1
      GO TO 98
   95 IF(ABS(DML-DM).LT.TEST) GO TO 94
      XK=(DML*XK-DM*XKL)/(DML-DM)
   97 CONTINUE
      IF(ADML.LT.ADM) GO TO 65
   98 XKL=XKST
      DML=DM
      ADML=ADM
      GO TO 65
C
   99 CONTINUE
      IF(NIT.GT.29) R0=0.
  100 P(I)=PU
      PE(I)=R*UDK*XM
      IF(IPRINT.EQ.2) WRITE(6,625)XK,YK,XM,YM,PU,NIT
      IF(PU.LT.0.)GO TO 140
      I=I+1
      IF(YK.LT.0.04)GO TO 130
      YK=YK-0.03
      IF(YK.GT.1.1)YK=YK-0.07
      GO TO 60
  130 I=I-1
C
  140 IF(IOPT.EQ.1)GO TO 170
C
      IF(IC.GE.2)GO TO 143
C
CC    STORE DIVISOR VALUES FOR COMPARISON PLOTS
C
      IDIV(IP1)=I
      DO 142 II=1,I
      P1SAV(II,IP1)=P(II)
  142 PE1SAV(II,IP1)=PE(II)
      GO TO 180
C
CC    DIVIDE BY STORED VALUES
C
  143 IGO=2
      INO=IDIV(IP1)
      PEM1=0.
      IM1=0
      DO 148 ID=2,INO
      IN=ID-1
      PE1DIV=PE1SAV(ID,IP1)
      PTEST=P1SAV(ID,IP1)
      PPLOT(IN)=PTEST
      IF(PE1DIV.EQ.0.)GO TO 150
      DO 144 IG=IGO,I
      IF(PTEST-P(IG)) 144,145,146
  144 CONTINUE
      GO TO 151
  145 PEPLOT(IN)=PE(IG)/PE1DIV
      GO TO 147
  146 ALPHA=(P(IG-1)-PTEST)/(P(IG-1)-P(IG))
      PEPLOT(IN)=((1.-ALPHA)*PE(IG-1)+PE(IG)*ALPHA)/PE1DIV
  147 IGO=IG
      IF(PTEST.GT.0.6) GO TO 148
      PEM1=PEPLOT(IN)+PEM1
      IM1=IM1+1
      GO TO 148
  148 GO TO 148
  150 PEPLOT(ID)=1.0
  148 CONTINUE
  151 INO=ID-2
C
      IF(IPRINT.GT.0) WRITE(6,602)CSNAME,CSNAMD,((PPLOT(I),
     1                PEPLOT(I)),I=1,INO)
      PEM1=PEM1/IM1
      WRITE(6,650) CSNAME,CSNAMD,PEM1
      IF(IPLOT.EQ.0) GO TO 180
      IF(IP.EQ.1)CALL ALINE(PPLOT,PEPLOT,INO,0.,YOR,0.2,0.625)
      IF(IP.GT.1)CALL ALINED(PPLOT,PEPLOT,INO,0.,YOR,0.2,0.625,
     1NLINE,NGAP)
      GO TO 180
C
  170 XX=XXO*IS1(IK)
      IF(IPLOT.EQ.0) GO TO 180
      YY=YYO*IS2(IK)
      CALL ALINE(PE,P,I,0.,0.,XX,YY)
  180 NIT=0
  250 CONTINUE
C
      IF(IPLOT.LT.2) GO TO 300
      IF(IOPT.GT.1)GO TO 280
      IY=IS2(IK)*20-10
      CALL ASCA(IX,IY,100,100,IFK,0,1,1,2)
      GO TO 300
  280 IF(IC.LT.2) GO TO 300
      IY=IK*160-85
      CALL ASCA(-120,IY,100,100,IFK,0,1,1,2)
  300 CONTINUE
C
      IF(IOPT.GT.1.AND.IC.EQ.1) GO TO 400
      IF(IPLOT.GT.0) CALL AEND
      GO TO 400
  350 WRITE(6,680)CSTYPE
  400 CONTINUE
      GO TO 5
C
  450 WRITE(6,690)
      STOP
C
  501 FORMAT(A6)
  502 FORMAT(5F10.2,5X,5I5/6A6)
  503 FORMAT(2F10.4,I5)
  506 FORMAT(8F10.4)
  508 FORMAT(4F10.4)
  510 FORMAT(A6,4X,A6)
C
  601 FORMAT(40X,'REINFORCED CONCRETE COLUMN BIAXIAL BENDING ANALYSIS'//
     1 53X,'TO PRODUCE DESIGN CHARTS'//53X,21(1H*))
  602 FORMAT(20X,'REINFORCED CONCRETE COLUMN BIAXIAL BENDING ANALYSIS'//
     1 20X,'TO COMPARE BIAXIAL BENDING STRENGTHS USING DIFFERENT CONCRE'
     2,'TE STRESS-STRAIN RELATIONSHIPS'//54X,20(1H*))
  603 FORMAT(//20X,'COLUMN SECTION PROPERTIES ='//30X,'REINFORCING'
     1 ,' STEEL - YIELD STRENGTH',36X,F10.2,' MPA.'/48X,'= MODULUS'
     2 ,' OF ELASTICITY',29X,F10.1,' MPA.'//30X,'PROPORTION OF COLUMN'
     3 ,' DEPTH AT WHICH REINFORCING IS PLACED =F (X DIRN.)',F10.3/88X,
     4 '=G (Y DIRN.)',F10.3//30X,'CONCRETE CYLINDER STRENGTH',44X,
     5 F10.2,' MPA.'///20X,'ANALYSIS CARRIED OUT USING CONCRETE GRID',
     6 I5,' X',I3/47X,'REINFORCING STEEL AT',I3,' DISCRETE LOCATIONS',
     7 ' DIVIDED EQUALLY'/71X,'AMONGST THE FOUR FACES'//10X,'LABEL ',
     8 'FOR PLOT ='/30X,6A6//10X,100(1H*)///)
  605 FORMAT(//20X,'RUN',I2,' VALUES OF REINFORCING RATIO (RHO)',
     1 'IN INCREMENTS OF',F6.3,' FROM INITIAL VALUE',F6.3)
  606 FORMAT(//20X,'RUN FOR VALUES OF REINFORCING RATIO (RHO)',
     1 /30X,'= ',8(F6.3,','))
  608 FORMAT(///20X,'RUN FOR TANGENT OF SPECIFIC ANGLE OF LOADING (K)',
     1 /30X,'= ',4(F6.3,',')///1X,120(1H*)////)
  620 FORMAT(///1X,6(1H*),'RESULTS CALCULATED FOR STRESS-BLOCK ',A6,
     1 ' WITH RHO=',F6.3,' AT K=',F6.3,1X,6(1H*))
  621 FORMAT(/11X,'XK',14X,'YK',14X,'XM',14X,'YM',14X,'PU',7X,'NIT')
  625 FORMAT(1X,5(1PE16.3),0PI6)
```

```
  650 FORMAT(10(1H=),'MEAN VALUE OF M(',A6,')/M(',A6,' UP TO ',
     1 'PU/FC,BH= ,60 =',F8,3/)
  662 FORMAT(///3X,'PU/FC,BH',4X,'M(',A6,')/M(',A6,')'/
     1 60(1X,F10,3,7X,F10,3/))
  680 FORMAT(///3X,12(1H*),'INVALID STRESS-STRAIN TYPE=',A6,1X,
     1 12(1H*))
  690 FORMAT(///1X,'DATA TERMINATED BY END CARD')
C
      END
```

```
      SUBROUTINE GEN(F,G,ICGRID,ISGRID)
C
C     GENERATES CO-ORDINATES OF ELEMENTAL CONCRETE GRID AND OF
C     DISCRETE STEEL REINFORCING POSITIONS
C
      COMMON/CORD1/CX(50,50)/CORD2/CY(50,50)/CORD3/SX(100),SY(100)
C
      A=0,
      IS1=ISGRID/4
      DIV=(1,*1,/IS1)/2,
      DO 40 I=1,IS1
      SX(I)=(DIV-A/IS1)*F
      SY(I)=-,5*G
      SX(I+IS1)=SX(I)
      SY(I+IS1)=-SY(I)
      SY(I+IS1*2)=(DIV-A/IS1)*G
      SX(I+IS1*2)=,5*F
      SX(I+IS1*3)=-SX(I+IS1*2)
      SY(I+IS1*3)=SY(I+IS1*2)
   40 A=A+1,0
C
      DO 70 I=1,ICGRID
      DO 60 J=1,ICGRID
      CX(I,J)=0,5-(I-0,5)/ICGRID
   60 CY(I,J)=(J-0,5)/ICGRID-0,5
   70 CONTINUE
C
      RETURN
      END
```

```
      SUBROUTINE BIPLOT(IOPT,IPLOT,CSN1,CSN2,PLAB,NK)
C
      DIMENSION PLAB(6),CSLAB1(1),CSLAB2(1),YLINE(2),RLABK(1),
     1 RLABPU(2),RLABM(1)
      DATA RLABK,RLABPU,RLABM/1HK,8HPU/FC,BH,3HM$*/
C
      IF(IPLOT,EQ,0)RETURN
      CSLAB1(1)=CSN1
      IF(IOPT,GT,1)GO TO 100
C
C     SET UP PLOT FOR DESIGN CHART
C
      CALL AINIT(700)
      CALL AORIG(10,10)
      CALL ABCX(0,0,8,10,40,40,2)
      CALL ABCX(0,400,8,10,40,40,2)
      CALL ABCX(320,0,8,10,40,40,2)
      CALL ABCX(320,400,8,10,40,40,2)
      CALL ALAB(100,850,PLAB,36,1,2)
      IF(IPLOT,LT,2) GO TO 50
C
      CALL ASCA(265,315,0,-80,4,4,4,1,2)
      CALL ASCA(265,475,0,80,4,4,4,1,2)
      CALL ALAB(230,760,RLABPU,8,1,2)
      CALL ASCA(200,385,-80,0,10,10,3,1,2)
      CALL ASCA(360,385,80,0,10,10,3,1,2)
      CALL ALAB(615,380,RLABM,3,1,2)
      CALL ALAB(500,850,CSLAB1,6,1,2)
   50 CALL AORIG(330,410)
      RETURN
C
C     SET UP PLOT FOR COMPARISON OF BIAXIAL-MOMENTS
C
  100 CALL AINIT(1100)
      CSLAB2(1)=CSN2
      CALL AORIG(120,210)
      CALL ABCX(0,0,18,5,50,16,2)
      CALL ABCX(0,80,18,10,50,16,2)
      CALL ABCX(0,240,18,10,50,16,2)
      CALL ABCX(0,400,18,10,50,16,2)
      CALL ABCX(0,560,18,5,50,16,2)
      CALL ALAB(140,700,PLAB,36,1,2)
      CALL ALAB(-90,670,RLABM,1,1,2)
      CALL ALAB(-90,645,RLABM,1,1,2)
      CALL ALAB(-80,665,CSLAB1,6,1,2)
      CALL ALAB(-80,640,CSLAB2,6,1,2)
      CALL ALINEX(-90,70,YLINE,2,-6,6,1,0)
      IF(IPLOT,LT,2)RETURN
C
      IYK=NK*160-60
      CALL ALAB(-90,IYK,RLABK,1,1,2)
      CALL ALAB(810,20,RLABPU,8,1,2)
      CALL ALAB(810,610,RLABPU,8,1,2)
      CALL ASCA(160,5,200,0,4,4,4,1,2)
      CALL ASCA(160,625,200,0,4,4,4,1,2)
      DO 10 I=1,4
      IY=I*160-149
      CALL ASCA(-55,IY,0,32,6,2,5,1,2)
   10 CONTINUE
      RETURN
C
      END
```

```
      SUBROUTINE RBLOCK(ICALL,CSNAME,ISG)
C
C     CALCULATES SPECIFIC MOMENT AND AXIAL LOAD FOR COLUMN
C     WITH GIVEN NEUTRAL AXIS DEPTH ASSUMING ACI-TYPE RECTANGULAR
C     STRESS BLOCK FOR CONCRETE
C
C
C     PFC=PROPORTION OF F'C OVER DEPTH OF STRESS BLOCK
C     EMAX=MAXIMUM CONCRETE STRAIN AT ULTIMATE LOAD
C     BETA1=PROPORTION OF N.A. DEPTH OVER WHICH UNIFORM STRESS
C     IS ASSUMED
C
      COMMON/CORD1/CX(50,50)/CORD2/CY(50,50)/CORD3/SX(100),SY(100)
      COMMON/CALCPM/XM,YM,PU,XK,YK,FY,FC,YMS,PT
      COMMON/RBHOLD/EBETA,EY,FCC,PC,BETA1,VA,PFC,EMAX
      DATA ACI/3HACI/
C
      GO TO(10,20,30)ICALL
C
C     CALCULATE INITIAL PARAMETERS
C
   10 IF(CSNAME.NE.ACI)GO TO 15
      BETA1=0.85
      EMAX=0.003
      PFC=0.85
      IF(FC.GT.27.6)BETA1=0.85-(FC-27.6)/138.
      GO TO 18
   15 READ(5,501)PFC,BETA1,EMAX
   18 WRITE(6,601)CSNAME,PFC,BETA1,EMAX
      EBETA=(1.-BETA1)*EMAX
      EY=FY/YMS
      FCC=PFC*FC
      GO TO 200
C
C     CALCULATE PO
C
   20 PU=(FY/FC-PFC)*PT+PFC
      VA=PT/(FC*ISG)
      GO TO 200
C
C     CALCULATE PU,XM,YM FOR GIVEN XK AND YK
C               = CONCRETE ACTIONS
C
   30 BXK=BETA1*XK
      BYK=BETA1*YK
      IF(AXK.LT.0.9E06) GO TO 44
      IF(BYK.GE.1.) BYK=1.
      PU=PFC*BYK
      XM=(1.-BYK)/2.*PU
      YM=0.
      GO TO 110
   44 IF(1./BXK+1./BYK.GT.1.) GO TO 70
      PU=PFC
      XM=0.
      YM=0.
      GO TO 110
   70 PU=BXK*BYK*PFC/2.
      XM=(1.5-BYK)/3.*PU
      YM=(1.5-BXK)/3.*PU
      IF(BXK.LE.1.) GO TO 75
      AXK=BXK-1.
      AYK=BYK*AXK/BXK
      P1=AXK*AYK*PFC/2.
      XM=(AYK-1.5)/3.*P1+XM
      YM= (AXK+1.5)/3.*P1+YM
      PU=PU+P1
   75 IF(BYK.LE.1.) GO TO 110
      CYK=BYK-1.
      CXK=BXK*CYK/BYK
      P2=CXK*CYK*PFC/2.
      PU=PU+P2
      XM= (CYK+1.5)/3.*P2+XM
      YM=(CXK-1.5)/3.*P2+YM
C
C               = STEEL ACTIONS
C
  110 CMULT=-XK/YK
      CADD=CMULT/2.+XK-0.5
      EBAR=EMAX/XK
      DO 120 I=1,ISG
      EXY=(SY(I)*CMULT+SX(I)+CADD)*EBAR
      FS=EXY*YMS
      IF(EXY.GE.EY) FS=FY
      IF(EXY.GE.EBETA) FS=FS-FCC
      IF(EXY.LE.-EY) FS=-FY
      SP=FS*VA
      PU=SP+PU
      XM=-SY(I)*SP+XM
  120 YM=SX(I)*SP+YM
C
  200 RETURN
C
  501 FORMAT(3F10.3)
  601 FORMAT(//10X,10(1H*),' PARAMETERS FOR RECTANGULAR CONCRETE ',
     1 'STRESS BLOCK ',A6,1X,10(1H*)//15X,'PROPORTION OF FC OVER DEPTH',
     2 ' OF STRESS BLOCK',18X,F8.3/15X,'PROPORTION OF N.A. DEPTH OVER ',
     3 'WHICH UNIFORM STRESS IS ASSUMED',F8.3/15X,'MAXIMUM ',
     4 'COMPRESSIVE STRAIN FOR CONCRETE',23X,F8.4//10X,77(1H*)///)
C
      END
```

```
      SUBROUTINE PARLIN(ICALL,CSNAME,ICG,ISG)
C
C     CALC. M AND P FOR COLUMN GIVEN N.A. DEPTH ASSUMING
C     PARABOLIC-STRAIGHT CONCRETE STRESS-BLOCK AS E.G
C     D.G.ROW(1973) AND CEB-FIP CODE                                    35
C
C     PFC=MAX. CONCRETE STRESS AS PROPORTION OF F'C
C     EO=STRAIN AT TRANSITION FROM PARABOLIC TO LINEAR
C     EMAX=MAX. STRAIN IN CONCRETE                                      36
C     PFC2=PROPORTION OF PFC MAINTAINED AT EMAX
C
      COMMON/CORD1/CX(50,50)/CORD2/CY(50,50)/CORD3/SX(100),SY(100)
      COMMON/CALCPM/XM,YM,PU,XK,YK,FY,FC,YMS,PT
      COMMON/PLHOLD/PFC,EO,EMAX,PFCM,EY,VA,FCC,FCC2,EST
      DATA ROW,CEB,HOG,RKPU/5HDGROW,6HCEBFIP,6HHOGNES,6HKPUNCF/
C
      GO TO(10,20,30)ICALL
      CALCULATE INITIAL PARAMETERS
C           - INTRINSIC CURVES ARE D.G.ROW(1973),CEB-FIP CODE(1970) C
C             E.HOGNESTAD(1951),AND KENT-PARK UNCONFINED CONCRETE
C             E.HOGNESTAD(1951),KENT-PARK UNCONFINED CONCRETE CURVE
C             E.HOGNESTAD(1951),KENT-PARK UNCONFINED CONCRETE(1971)
C
   10 PFC=0.85
      EO=0.002
      EMAX=0.003
      PFCM=1.0
      IF(CSNAME.EQ.ROW)GO TO 15
      IF(CSNAME.NE.CEB)GO TO 12
      PFC=1.0                                                           60
      EMAX=0.0035                                                       70
      GO TO 15
   12 IF(CSNAME.NE.HOG)GO TO 13
      FCC=PFC*FC                                                        80
      EC=FCC*460+12410.                                                 C
      EO=FCC*2./EC
      EMAX=0.0038
      PFCM=0.85
      GO TO 15
   13 IF(CSNAME.NE.RKPU) GO TO 14
      PFC=1.0                                                           94
      EMAX=(FC/3.45+3.)/(FC*145.-1000.)
      PFCM=0.5                                                          96
      GO TO 15
   14 READ(5,501)PFC,EO,PFCM,EMAX
   15 WRITE(6,601)CSNAME,PFC,EO,PFCM,EMAX
      FCC=PFC*FC
      EY=FY/YMS
      FCC=PFC*FC
      FCC2=FCC*(1.-PFCM)/(EO-EMAX)
      RETURN
C
C     CALCULATE PO (AT EITHER EY OR EO)                                 130
C                                                                       140
   20 IF(PFCM.EQ.1.0)GO TO 22
      IF(EO.GE.EY)GO TO 25
      P2=(EO*YMS/FC-PFC)*PT+PFC
   22 FFC=PFCM*PFC                                                      120
      FFO=(PFC-FFC)*(EMAX-EY)/(EMAX-EO)+FFC                             C
      PU=(FY/FC-FFO)*PT+FFO
      IF(P2.LT.PU)GO TO 27                                              C
      PU=P2
      EST=EY                                                            101
      GO TO 29
   25 PU=(FY/FC-PFC)*PT+PFC
   27 EST=EO
   29 IF(PFCM.EQ.1.0)EST=EMAX
      VA=PT/(FC*ISG)
      RETURN
C
C     ITERATE ON THE EXTREME FIBRE STRAIN (EM) TO MAXIMIZE XM           103
C                                                                       100
   30 IC2=ICG
      PC=PFC/ICG
      IF(XK.GE.0.9E6)IC2=1
      PC=PC/IC2
      PC2=PC*(1.-PFCM)/(EO-EMAX)
      CMULT=-XK/YK
      CADD=CMULT/2.+XK-0.5
      XM=0.
      K=1
      EM=EST*(IK*K/30.+1.0)
      IF(EM.LE.EMAX) GO TO 36
      K=0
      EM=EMAX                                                           36
      XML1=XML
      XML=XM
      EL2=EL1
      EL1=EL
      EL=EM
      IK=IK+1
      PU=0.
      XM=0.
      YM=0.
      EBAR=EM/XK

      DO 60 I=1,IC2
      I1=1
      IF(IC2.EQ.1)I1=ICG+1
      DO 60 J=1,ICG
      EXY=(CY(I,J)*CMULT+CX(I1,J)+CADD)*EBAR
      IF(EXY.LT.0.) GO TO 80
      RA=(EO-EXY)/EO
      IF (RA.GT.0.) GO TO 60
      P=(EXY-EO)*PC2+PC
      GO TO 70
   60 P=(-RA*RA+1.)*PC                                                  60
   70 PU=PU+P                                                           70
      XM=-CY(I,J)*P+XM
      YM=CX(I1,J)*P+YM
   80 CONTINUE

      DO 120 I=1,ISG
      EXY=(SY(I)*CMULT+SX(I)+CADD)*EBAR
      IF(EXY.LE.EO) GO TO 94
      SBAR=(EXY-EO)*FCC2+FCC
      GO TO 96
   94 RA=(EO-EXY)/EO                                                    94
      SBAR=(-RA*RA+1.)*FCC
   96 IF(EXY.GE.EY) FS=FY                                               96
      FS=FS-SBAR
      FS=EXY*YMS
      IF (EXY.LT.0.) GO TO 130
      RA=(EO-EXY)/EO
      SBAR =FCC
      IF(RA.GT.0.)SBAR=(-RA*RA+1.)*SBAR
      IF(EXY.GE.EY)FS=FY
      FS=FS-SBAR
      GO TO 140
  130 IF(EXY.LE.-EY)FS=-FY                                              130
  140 SP=FS*VA                                                          140
      PU=SP+PU
      XM=-SY(I)*SP+XM
      YM=SX(I)*SP+YM
  120 CONTINUE

      IF(PFCM.EQ.1.0) RETURN

      IF(K)103,110,101
      IF(XM.GT.XML)GO TO 35                                             101
      IF(IK.GT.2) GO TO 100
      K=1
      HOLDXM=XM
      XM=XML
      XML=HOLDXM
      EL=EL1
      EL1=EM
      GO TO 35
  103 IF(XM.GT.XML) GO TO 35                                            103
      K=0                                                               100
      IF(XML1.GT.XM) GO TO 105
      IF(XML1.EQ.XM) EL=(EL+EL2)/2.0
      GO TO 115
```

```
  105 IF(XML.GT.XML1) GO TO 106
      EL=EL2                                                            C
      XM=XML1                                                           C
      GO TO 115                                                         C
  106 XM=XML                                                            C
      XML=XML1                                                          C
      EL=EL1                                                            C
      EL1=EL2                                                           C
      GO TO 115                                                         C
  110 IF(XM.LE.0.) GO TO 112                                            C
      IF(ABS(XM-XML)/XM.LT.0.0005) GO TO 150                            C
  112 IF(XML1.GT.XML) GO TO 114                                         C
      IF(XML1.EQ.XM) EL=(EL+EL2)/2.0                                    C
      GO TO 115                                                         C
  114 EL1=EL2                                                           C
      XML=XML1                                                          C
  115 EM=(EL+EL1)/2.0                                                   C
      GO TO 36                                                          C
  150 IF(ABS(EL-EL1).GT.0.0001) GO TO 112                               C
      EST=EM                                                            C
      RETURN                                                            C
C                                                                       C
  501 FORMAT(4F10.4)
  601 FORMAT(//10X,10(1H*),' PARAMETERS FOR CONCRETE STRESS-STRAIN ',
     1 'RELATIONSHIP ',A6,1X,10(1H*)//15X,'PARABOLIC UP TO MAXIMUM ',
     2 'STRESS',F6.3,'FC AT STRAIN',F7.4//15X,'LINEAR DESCENDING ',
     3 'DOWN TO',F6.3,' OF MAXIMUM STRESS AT STRAIN',F7.4//10X,79(1H*)//
     4 )
      END
```

```
      SUBROUTINE TRIARM(ICALL,CSNAME,ICG,ISG,F,G)

C     CALC. P AND M FOR COLUMN GIVEN N.A. DEPTH ASSUMING
C     STRESS-STRAIN CURVE SIMILAR TO THAT PROPOSED
C     FOR CONFINED CONCRETE BY KENT AND PARK (1971)

C     PFC,E0 AS DEFINED IN PARLIN
C     EC2=STRAIN AT WHICH LINEAR DESCENDING BRANCH OF CURVE ENDS
C     PFC2=PROPORTION OF PFC*FC MAINTAINED AT STRAIN GREATER
C     THAN EC2
C     EMU=STRAIN AT WHICH UNCONFINED COVER CONCRETE SPALLS

      COMMON/CORD1/CX(50,50)/CORD2/CY(50,50)/CORD3/SX(100),SY(100)
      COMMON/CALCPM/XM,YM,PU,XK,YK,FY,FC,YMS,PT
      COMMON/THRHOLD/E0,PFC,EC2,PFC2,Z,EY,VA,EST
      DATA RKPCON/6HRKPCON/

      GO TO (10,20,30,40)ICALL

C      CALCULATE INITIAL PARAMETERS (KENT-PARK IS INTRINSIC)

   10 IF(CSNAME.NE.RKPCON) GO TO 15
      READ(5,501)RHOS,BCORE,SHOOP
      E0=0.002
      PFC=1.0
      PFC2=0.2
      EMU=0.004
      E50H=SQRT(BCORE/SHOOP)*RHOS*0.75
      PFC2=PFC2*PFC
      E50U=(0.002*FC+0.0207)/(FC-6.9)
      Z=0.5/(E50U+E50H-E0)
      EC2=(PFC-PFC2)/Z+E0
      EY=FY/YMS
      GO TO 18
   15 READ(5,502)PFC,E0,PFC2,EC2,EMU
      Z=(PFC-PFC2)/(EC2-E0)
   18 WRITE(6,601)CSNAME,PFC,E0,PFC2,EC2,EMU
      RETURN

C     CALCULATE PU (AT EITHER EY OR E0)

   20 IF(E0.GE.EY) GO TO 28
      P2=(E0*YMS-PFC)*PT/FC+PFC
      PFC=(E0-EY)*Z+PFC
      PU=(FY-PFC)*PT/FC+PFC
      IF(P2.LT.PU) GO TO 29
      PU=P2
      EST=EY
      GO TO 29
   28 PU=(FY-PFC)*PT/FC+PFC
      EST=E0
   29 VA=PT/(FC*ISG)
      RETURN

C     ITERATE ON THE EXTREME FIBRE STRAIN (EM) TO MAXIMIZE XM

   30 IC2=ICG
      IF(XK.GE.1.0E6) IC2=1
      IPC=IC2*ICG
      CMULT=-XK/YK
      CADD=CMULT/2.+XK-0.5
      XM=0.
      K=1
   32 EM=EST*(1K*K/30.+1.0)
   34 XML1=XML
      XML=XM
      EL2=EL1
      EL1=EL
      EL=EM
      IK=IK+1
      PU=0.
      XM=0.
      YM=0.
      PS=0.
      XS=0.
      YS=0.
```

```
      EBAR=EM/XK
C
      DO 80 I=1,IC2
      II=I
      IF(IC2.EQ.1) II=ICG+1
      DO 80 J=1,ICG
      EXY=(CY(I,J)*CMULT+CX(II,J)+CADD)*EBAR
      IF(EXY.LE.0.) GO TO 60
      IF(EXY.GT.E0) GO TO 60
      RA=(E0-EXY)/E0
      P=(-RA*RA+1.)*PFC
      GO TO 75
   60 IF(ABS(CY(I,J)).GT.G/2.) GO TO 65
      IF(ABS(CX(II,J)).GT.F/2.) GO TO 65
   62 P=(E0-EXY)*Z+PFC
      IF(EXY.GT.E2C) P=PFC2
      IF(IC2.EQ.1.AND.EXY.GT.EMU) P=P*F
      GO TO 75
   65 IF(EXY-EMU) 62,62,80
   75 PU=PU+P
      XM=-CY(I,J)*P+XM
      YM=CX(II,J)*P+YM
   80 CONTINUE
C
C     COMPRESSION STEEL ASSUMED WITHIN CONFINED CORE
C
      DO 120 I=1,ISG
      EXY=(SY(I)*CMULT+SX(I)+CADD)*EBAR
      FS=EXY*YMS
      IF(EXY.LT.0.) GO TO 130
      IF(EXY.GE.EY) FS=FY
      IF(EXY.GT.E0) GO TO 125
      RA=(E0-EXY)/E0
      SBAR=(-RA*RA+1.)*PFC
      GO TO 128
  125 SBAR=(E0-EXY)*Z+PFC
      IF(EXY.GT.E2C) SBAR=PFC2
  128 FS=-SBAR*FC+FS
      GO TO 140
  130 IF(EXY.LE.-EY) FS=-FY
  140 PS=PS+FS
      XS=-SY(I)*FS+XS
      YS=SX(I)*FS+YS
  120 CONTINUE
      PU=PS*VA+PU/IPC
      XM=XS*VA+XM/IPC
      YM=YS*VA+YM/IPC
C
      IF(K)103,110,101
  101 IF(XM.GT.XML) GO TO 32
      IF(IK.GT.2) GO TO 100
      K=1
      HOLDXM=XM
      XM=XML
      XML=HOLDXM
      EL=EL1
      EL1=EM
      GO TO 32
  103 IF(XM.GT.XML) GO TO 32
  100 K=0
      IF(XML1.GT.XM) GO TO 105
      IF(XML1.EQ.XM) EL=(EL+EL2)/2.0
      GO TO 115
  105 IF(XML.GT.XML1) GO TO 106
      EL=EL2
      XM=XML1
      GO TO 115
  106 XM=XML
      XML=XML1
      EL=EL1
      EL1=EL2
      GO TO 115
  110 IF(XM.LE.0.) GO TO 112
      IF(ABS(XM-XML)/XM.LT.0.0005) GO TO 150
  112 IF(XML1.GT.XML) GO TO 114
      IF(XML1.EQ.XM) EL=(EL+EL2)/2.0
      GO TO 115
  114 EL1=EL2
      XML=XML1
  115 EM=(EL+EL1)/2.0
      GO TO 34
  150 IF(ABS(EL-EL1).GT.0.0001) GO TO 112
      EST=EM
   40 RETURN
C
  501 FORMAT(3F10.4)
  502 FORMAT(5F10.4)
  601 FORMAT(//10X,10(1H*),' PARAMETERS FOR CONFINED CONCRETE ',
     1 'STRESS-STRAIN RELATIONSHIP ',A6,1X,10(1H*)//15X,'PARABOLIC',
     2 ' UP TO MAXIMUM STRESS',F6.3,'FC AT STRAIN',F7.4//15X,
     3 'LINEAR DESCENDING DOWN TO CONSTANT STRESS',F6.3,'FC ',
     4 'FROM STRAIN',F7.4,' ONWARDS'//15X,'COVER CONCRETE SPALLS ',
     5 'AT STRAIN',F7.4//10X,88(1H*)///)
      END
```

```
      SUBROUTINE QUADRC(ICALL,CSNAME,ICG,ISG)
C
C     CALC. M AND P FOR GIVEN N.A. POSITION ASSUMING QUADRATIC
C     STRESS-STRAIN CURVE FOR CONCRETE IN FLEXURE AS KRIZ AND LEE (1960)
C
      DIMENSION AV(6),BV(6),CV(6),DV(6)
      COMMON/CORD1/CX(50,50)/CORD2/CY(50,50)/CORD3/SX(100),SY(100)
      COMMON/CALCPM/XM,YM,PU,XK,YK,FY,FC,YMS,PT
      COMMON/CHOLD/A,B,C,D,VA,EST,EY
      DATA CONST/4730./
      DATA AV/-0.07042,-0.8454,-3.434,-11.51,-34.35,-56.31/
      DATA BV/-1.421,-2.552,-3.434,-3.62,-1.196,3.780/
      DATA CV/-1.262,-3.291,-6.751,-14.26,-31.41,-44.13/
      DATA DV/1.746,6.109,22.58,56.99,137.8,199.9/
      DATA RKRZLE/6HKRZLEE/
C
      YMSQ=YMS/1000.
      GO TO (10,20,30,40)ICALL
C
C     INTERPULATE FOR QUADRATIC COEFFICIENTS'
C
   10 IF(CSNAME.NE.RKRZLE)GO TO 15
      IFC=FC/6.89475
      ALPHA=FC/6.89475-IFC
      BETA=1.-ALPHA
      IFC1=IFC+1
      A=(AV(IFC1)*ALPHA+AV(IFC)*BETA)*47.53764
      B=(BV(IFC1)*ALPHA+BV(IFC)*BETA)*6.89475
      C=(CV(IFC1)*ALPHA+CV(IFC)*BETA)*6.89475
      D=(DV(IFC1)*ALPHA+DV(IFC)*BETA)*47.53764
      GO TO 17
   15 READ(5,501)A,B,C,D
   17 EY=FY/YMSQ
      EST=1.0
      WRITE(6,601)CSNAME,A,B,C,D
      RETURN
C
C     CALCULATE PO(ITERATE ON E)
C
   20 E=EST
   21 IF(IK.GT.0)E=2*EL-EL1
   22 PL1=PL
      PL=P
      EL2=EL1
      EL1=EL
      EL=E
      IK=IK+1
      BB=(B+E*C)/2.
      CC=(A+E*D)*E
      EFC=-SQRT(BB*BB-CC)-BB
      FS=E*YMSQ
      IF(E.GT.EY)FS=FY
      P=(FS-EFC)*PT/FC+EFC/FC
      IF(K.NE.0)GO TO 25
      IF(P.GT.PL)GO TO 21
      K=1
      IF(PL1.GT.P)EL=EL2
      IF(PL1.EQ.P)EL1=(EL1+EL2)/2.0
   25 DP1=P-PL
      IF(ABS(DP1)/P.LT.0.001)GO TO 28
   26 IF(PL1.GT.PL)EL1=EL2
      IF(PL1.EQ.PL)EL=(EL+EL2)/2.0
      E=(EL+EL1)/2.0
      GO TO 22
   28 IF(ABS(EL-EL1).GT.0.2)GO TO 26
      EST=E
      PU=P
      VA=PT/(FC*ISG)
      RETURN
C
C     ITERATE ON THE EXTREME FIBRE STRAIN (EM) TO MAXIMIZE XM
C
   30 IC2=ICG
      IF(XK.GE.1.0E06) IC2=1
      DPC=ICG-IC2*FC
      CMULT=-XK/YK
      CADD= XK+CMULT/2.-0.5
      XM=0.
      K=1
      EM=EST*(1K*K/30.+1.0)
      XML1=XML
      XML=XM
      EL2=EL1
      EL1=EL
      EL=EM
      IK=IK+1
      PU=0.
      XM=0.
      YM=0.
      PS=0.
      XS=0.
      YS=0.
      EBAR=EM/XK
C
      DO 80 I=1,IC2
      I1=1
       IF(IC2.EQ.1) I1=ICG+1
      DO 80 J=1,ICG
      EXY=(CY(I,J)*CMULT+CX(I1,J)+CADD)*EBAR
      IF(EXY.LE.0.) GO TO 80
      BB=(B*EXY+C)/2.
      CC=(A*EXY+D)*EXY
      P=-SQRT(BB*BB-CC)-BB
      PU=PU+P
      XM=-CY(I,J)*P+XM
      YM=CX(I1,J)*P+YM
   80 CONTINUE
C
      DO 120 I=1,ISG
      EXY=(SY(I)*CMULT+SX(I)+CADD)*EBAR
      FS=EXY*YMSQ
      IF(EXY.LT.0.)GO TO 130
      BB=(B*EXY+C)/2.
      CC=(A*EXY+D)*EXY
      SBAR=-SQRT(BB*BB-CC)-BB
      IF(EXY.GE.EY)FS=FY
      FS=FS-SBAR
      GO TO 140
  130 IF(EXY.LE.-EY)FS=-FY
  140 PS=PS+FS
      XS=-SY(I)*FS+XS
      YS=SX(I)*FS+YS
  120 CONTINUE
      PU=PS*VA+PU/DPC
      XM=XS*VA+XM/DPC
      YM=YS*VA+YM/DPC
C
      IF(K) 103,110,101
  101 IF(XM.GT.XML) GO TO 32
      IF(IK.GT.2)GO TO 100
      K=1
      HOLDXM=XM
      XM=XML
      XML=HOLDXM
      EL=EL1
      EL1=EM
      GO TO 32
  103 IF(XM.GT.XML) GO TO 32
      K=0
      IF(XML1.GT.XM)GO TO 105
      IF(XML1.EQ.XM)EL1=(EL1+EL2)/2.0
      GO TO 115
  105 IF(XML.GT.XML1) GO TO 106
      EL=EL2
      XM=XML1
      GO TO 115
  106 XM=XML
      XML=XML1
      EL=EL1
      EL1=EL2
      GO TO 115
  100 IF(XM.LE.0.) GO TO 112
```

```
      IF(ABS(XM-XML)/XM.LT.0.0005) GO TO 150
  112 IF(XML1.GT.XML)GO TO 114
      IF(XML1.EQ.XML) EL=(EL+EL2)/2.0
      GO TO 115
  114 EL1=EL2
  116 XML=XML1
  115 EM=(EL+EL1)/2.0
      GO TO 34
  150 IF(ABS(EL-EL1).GT.0.2)GO TO 112
      EST=EM
   40 RETURN
C
  501 FORMAT(4F10.3)
  601 FORMAT(//10X,10(1H*),' COEFFICIENTS FOR QUADRATIC STRESS-',
     1 'STRAIN RELATIONSHIP ',A6,1X,10(1H*)//15X,'F**F = A*E**E ',/
     2 '+ B*E**E + C*F + D*E = 0'//20X,'WHERE F = STRESS IN MPA,'/
     3 26X,'E = STRAIN X 1000'/26X,'A =',F8.3/26X,'B =',F8.3/26X,
     4 'C =',F8.3/26X, 'D =',F8.3//10X,82(1H*)///)
C
      END
```